General Disclaimer

One or more of the Following Statements may affect this Document

- This document has been reproduced from the best copy furnished by the organizational source. It is being released in the interest of making available as much information as possible.

- This document may contain data, which exceeds the sheet parameters. It was furnished in this condition by the organizational source and is the best copy available.

- This document may contain tone-on-tone or color graphs, charts and/or pictures, which have been reproduced in black and white.

- This document is paginated as submitted by the original source.

- Portions of this document are not fully legible due to the historical nature of some of the material. However, it is the best reproduction available from the original submission.

Produced by the NASA Center for Aerospace Information (CASI)

NASA CR-170457

E83-10128
CR-170457

"Made available under NASA sponsorship in the interest of early and wide dissemination of Earth Resources Survey Program information and without liability for any use made thereof."

MSS-D

MULTISPECTRAL SCANNER

FINAL REPORT

APRIL 1982

DEC 1982
RECEIVED
NASA STI FACILITY
ACCESS DEPT.

Prepared for
GODDARD SPACE FLIGHT CENTER
Greenbelt, Maryland 20771

(E83-10128) MSS D MULTISPECTRAL SCANNER SYSTEM Final Report, Apr. 1978 - Nov. 1981 (Hughes Aircraft Co.) 502 p HC A22/MF A01 CSCL 05B
N83-15797
Unclas
G3/43 00128

HUGHES

HUGHES AIRCRAFT COMPANY
SPACE AND COMMUNICATIONS GROUP
EL SEGUNDO, CALIFORNIA

SCG 820015R

ORIGINAL PAGE IS
OF POOR QUALITY

TECHNICAL REPORT STANDARD TITLE PAGE

1. Report No.	2. Government Accession No.	3. Recipient's Catalog No.
MSS D Multispectral Scanner System - Final Report		5. Report Date April 1982
		6. Performing Organization Code Hughes 44-00
7. Author(s) A.M. Lauletta, R.L. Johnson, K.L. Brinkman		8. Performing Organization Report No. E1966
9. Performing Organization Name and Address Hughes Aircraft Company Space and Communications Group P.O. Box 92919 Airport Station Los Angeles, CA 90009		10. Work Unit No. —
		11. Contract or Grant No. NAS5-25050
12. Sponsoring Agency Name and Address Goddard Space Flight Center Greenbelt, Maryland 20771		13. Type of Report and Period Covered Final April 78 — November 81
		14. Sponsoring Agency Code —

15. Supplementary Notes

16. Abstract

This report summarizes the development and acceptance testing of the 4-band Multispectral Scanners to be flown on Landsat-D and Landsat-D' earth resources satellites. Emphasis is placed on the acceptance test phase of the program. Test history and acceptance test algorithms are discussed. Trend data of all the key performance parameters are included and discussed separately for each of the two Multispectral Scanner instruments. Anomalies encountered and their resolutions are presented.

17. Key Words (Selected by Author(s))	18. Distribution Statement
Landsat, Multispectral Scanner, remote sensing, acceptance tests, satellite sensors, earth resources	Unlimited

19. Security Classif. (of this report)	20. Security Classif. (of this page)	21. No. of Pages	22. Price*
Unclassified		525	

*For sale by the Clearinghouse for Federal Scientific and Technical Information, Springfield, Virginia 22151.

HS 248-0010-0867

MULTISPECTRAL SCANNER

FINAL REPORT

APRIL 1982

ORIGINAL PAGE IS
OF POOR QUALITY

Prepared for
GODDARD SPACE FLIGHT CENTER
Greenbelt, Maryland 20771

Contract No. NAS 5-25050

Hughes Ref No. E1966

HUGHES

HUGHES AIRCRAFT COMPANY
SPACE AND COMMUNICATIONS GROUP
EL SEGUNDO, CALIFORNIA

CONTENTS

			Page
1.	INTRODUCTION		
	1.1	Program Background and History	1-1
	1.2	Program Plan and Objectives	1-3
2.	SUMMARY		
	2.1	Development	2-1
	2.2	System Performance Summary	2-3
	2.2.1	Signal-to-Noise Ratio	2-3
	2.2.2	Signal Correction (DCC, DBB)	2-4
	2.2.3	Square Wave Response (MTF)	2-5
	2.2.4	Scan Precision Parameters	2-5
3.	SYSTEM REQUIREMENTS		
	3.1	Comparative Specifications	3-1
	3.1.1	Resolution	3-1
	3.1.2	Instantaneous Fields of View	3-2
	3.1.3	Scan Mirror Assembly	3-2
	3.1.4	Geometric Fidelity	3-3
	3.1.5	Scanner Modulation Transfer Function	3-3
	3.1.6	Signal-to-Noise	3-5
	3.1.7	Vibration	3-5
	3.1.8	Mass Properties	3-11
	3.1.9	Power	3-13
	3.1.10	Commands	3-15
	3.1.11	Telemetry	3-18
	3.1.12	Backup Start-of-Scan Monitor Pulse	3-20
	3.2	Requirements Verification	3-20
	3.3	Mass Properties	3-20
	3.4	System Eccentricities	3-29
4.	MSS-D SYSTEM TEST		
	4.1	Test Philosophy	4-1
	4.2	Test Types	4-3
	4.3	System Test Approach	4-3
	4.4	System Test Flow Diagram	4-5
5.	TEST CONFIGURATIONS		
	5.1	Performance Testing	5-1
	5.2	Alignment	5-1
	5.3	System Radiometric Calibration	5-3
	5.4	Collimator Transfer Calibration	5-3
	5.5	EMI/EMC Testing	5-3
	5.6	Vibration Testing	5-3
	5.7	Acoustic Testing	5-3
	5.8	Thermal-Vacuum Testing	5-5
	5.9	Special System Tests	5-5

6. DATA REDUCTION SYSTEM
6.1 Introduction 6-1
6.2 DRS Development 6-1
6.2.1 MSS-C 6-1
6.2.2 Modifications for MSS-D 6-3
6.3 MSS-D DRS Configuration 6-5
6.3.1 Hardware 6-5
6.3.2 Software 6-7
6.4 Algorithms 6-13
6.4.1 Signal-to-Noise Ratio 6-13
6.4.2 COSL, DCC, and DBB 6-16
6.4.3 Square Wave Response (MTF) 6-22
6.4.4 Mean Line Length, Line Length Variation, and Scan-to-Scan Repeatability 6-26
6.4.5 Cross-Axis Repeatability 6-31
6.5 Off-Line Analysis 6-33

7. PROTOFLIGHT ACCEPTANCE TEST RESULTS
7.1 Introduction 7-1
7.2 Protoflight Test History 7-2
7.3 Signal-to-Noise Performance Evaluation 7-28
7.3.1 Introduction 7-28
7.3.2 Noise Model Description 7-28
7.3.3 Performance 7-35
7.3.4 Temperature Sensitivity 7-36
7.3.5 Summary Assessment 7-36
7.4 Corrected Signal Level 7-48
7.4.1 Introduction 7-48
7.4.2 Average Signal Level Performance History 7-49
7.4.3 System Gain Performance History 7-53
7.4.4 Corrected Signal Level Performance History 7-79
7.5 Modulation Transfer Function 7-96
7.5.1 Introduction 7-96
7.5.2 MTF Model Description 7-96
7.5.3 Protoflight MTF Performance 7-106
7.6 Scan Precision Parameters 7-111
7.6.1 Introduction 7-111
7.6.2 Mean Line Length 7-114
7.6.3 Line Length Variation 7-115
7.6.4 Scan Repeatability 7-118
7.6.5 Cross-Axis Repeatability 7-118

8. PROTOFLIGHT PICTURE ANALYSIS
8.1 Ground Processing Equipment 8-1
8.1.1 Qualification Test Picture Content 8-2
8.1.2 Picture Quality Rating 8-7
8.1.3 EMI Noise Evaluation 8-9
8.1.4 Performance History During Acceptance Test 8-9
8.1.5 GPE Anomalies 8-11

	8.2	Video Processor and Image Recorder Picture Evaluation	8-11
		8.2.1 VPIR Picture Format	8-11
		8.2.2 VPIR Picture Quality Rating	8-12
		8.2.3 EMI Noise Evaluation	8-16
		8.2.4 Performance History During Acceptance Test	8-16
9.	PROTOFLIGHT SPECIAL PROBLEMS		
	9.1	Flex Pivot Failure	9-1
		9.1.1 Summary	9-1
		9.1.2 Analysis and Test Program	9-3
	9.2	Shutter Synchronizer Anomaly	9-18
	9.3	DC Restore Problem	9-23
	9.4	Video Cable Noise	9-31
	9.5	Channel 9 Gain Variation	9-45
	9.6	Mission Black-White Code	9-52
10.	FLIGHT MODEL (F-1) ACCEPTANCE TEST RESULTS		
	10.1	Introduction	10-1
	10.2	F-1 Flight Test History	10-3
	10.3	Signal-to-Noise Performance Evaluation	10-15
		10.3.1 Introduction	10-15
		10.3.2 F-1 Noise Estimation Results	10-15
		10.3.3 Performance	10-15
		10.3.4 Summary Assessment	10-31
	10.4	Corrected Signal Level	10-31
		10.4.1 Introduction	10-31
		10.4.2 Average Signal Level Performance History	10-31
		10.4.3 System Gain Performance History	10-34
		10.4.4 Corrected Signal Level Performance History	10-59
	10.5	Modulation Transfer Function	10-96
		10.5.1 Introduction	10-96
		10.5.2 F-1 MTF Measurements	10-96
	10.6	Scan Precision Parameters	10-103
		10.6.1 Introduction	10-103
		10.6.2 Mean Line Length	10-103
		10.6.3 Line Length Variation	10-105
		10.6.4 Scan Repeatability (SRO)	10-109
		10.6.5 Cross-axis Repeatability	10-109
11.	FLIGHT MODEL PICTURE ANALYSIS		
	11.1	Ground Processing Equipment Pictures	11-1
		11.1.1 Picture Quality Rating	11-1
		11.1.2 EMI Noise Evaluation	11-3
		11.1.3 Performance History During Acceptance Test	11-3

11.2 VPIR Pictures 11-4
11.2.1 VPIR Picture Quality Rating 11-4
11.2.2 EMI Noise Evaluation 11-4
11.2.3 Performance History During Acceptance Test 11-4

12. F-1 SPECIAL PROBLEMS
12.1 Scan Mirror Subharmonic Operation, 3/4 Mode 12-1
12.2 Fiber Optics Plate 12-39
12.3 Flex Pivot Corrosion 12-89

ILLUSTRATIONS

		Page
1-1	1978 Master Phasing Schedule - Five Band MSS-D	1-2
1-2	Revised Master Phasing Schedule - Four Band MSS-D	1-4
1-3	Four Band Multispecral Scanner MSS-D	1-6
1-4	Actual Master Phasing Schedule	1-7
1-5	MSS-D Program Historical Events	1-8
3-1	Protoflight Center-of-Gravity Location	3-28
3-2	F-1 Calibration Wedge Pinhole	3-30
4-1	Unit/Subsystem Integration and Test	4-2
4-2	Engineering Model Test Sequence	4-6
4-3	Protoflight and Flight Model Test Sequence	4-8
5-1	MSS-D in System Performance Test Configuration	5-2
5-2	MSS-D Alignment Configuration	5-2
5-3	System Radiometric Calibration	5-4
5-4	EMI/EMC Test Configuration	5-6
5-5	Vibration Test Configuration	5-6
5-6	Acoustic Test Configuration	5-7
5-7	Thermal-Vacuum Test Configuration	5-7
5-8	Relative Spectral Response Test Configuration	5-8
6-1	MSS-D Data Reduction System	6-6
6-2	Data Reduction System Software	6-8
6-3	Collimator Chevron Pattern Reticle Dimension	6-30
6-4	Typical Chevron Pattern System Response	6-30
6-5	F-1 Calibration Stability During Thermal-Vacuum Testing	6-36
6-6	Shading Correlation - Channel 11	6-38
6-7	Radiance Correlation - Bands 1 and 4	6-38
6-8	Band 1 Average Collimator Radiance - F-1 in Thermal-Vacuum	6-40
6-9	Collimator Shading Versus Temperature - Channel 11	6-40
7-1	Protoflight Test Sequence	7-8
7-2	Protoflight Acoustic Test Setup	7-16
7-3	Acoustic Spectrum Microphone Average	7-18
7-4	Protoflight Thermal-Vacuum Temperature Profile	7-19
7-5	Signal-to-Noise Ratio Model	7-29
7-6	Noise Model Estimation Accuracy	7-30
7-7	Protoflight Noise Model Coefficient History	7-33
7-8	Noise Measurements During Protoflight System Test - Linear/Low Gain Mode	7-37
7-9	Noise Measurements During Protoflight System Test - Compression/Low Gain Mode	7-39
7-10	Noise Measurements During Protoflight System Test - Linear/High Gain Mode	7-40
7-11	Noise Measurements During Protoflight System Test - Compression/High Gain Mode	7-41
7-12	Noise Temperature Sensitivity - Channel 9	7-42
7-13	Noise Temperature Sensitivity - Channel 11	7-44
7-14	Noise Temperature Sensitivity - Channel 12	7-46

7-15	Protoflight Average Signal Level - Linear/Low Gain Mode	7-51
7-16	Protoflight Gain History - Linear/Low Gain Mode	7-57
7-17	Protoflight Average Gains Versus Temperature - Linear/Low Gain Mode	7-70
7-18	Protoflight Channel Gain with Temperature Dependence Removed - Linear/Low Gain Mode	7-78
7-19	Protoflight COSL Performance - Linear/Low Gain Mode	7-80
7-20	Protoflight Band Average COSL Performance - Linear/Low Gain Mode	7-83
7-21	Protoflight Mean-Normalized COSL Performance - Linear/Low Gain Mode	7-89
7-22	Internal Calibration System - Apparent Radiance Versus Temperature	7-95
7-23	Filter Response as a Function of Temperature	7-101
7-24	Estimated MSS-D MTF	7-102
7-25	MSS-C and MSS-D Square Wave Response	7-104
7-26	Temperature Effects on MTF	7-105
7-27	Protoflight MTF Performance	7-107
7-28	Protoflight Nominal MTF Versus Temperature	7-110
7-29	Protoflight Mean Line Length	7-114
7-30	Protoflight VLL Performance After Flex Pivot Replacement	7-115
7-31	Protoflight VLL Performance (Pre/Post Vibration)	7-116
7-32	Protoflight Scan Repeatability Performance	7-119
7-33	Protoflight Cross-Axis Repeatability Performance	7-119
8-1	Ground Processing Equipment Block Diagram	8-2
8-2	Ground Processing Equipment	8-3
8-3	GPE Picture Content from Qualification Test Patterns	8-4
8-4	Ground Processor Print Format	8-5
8-5	GPE Individual Band Picture Format	8-6
8-6	Video Processor and Demultiplexer	8-10
8-7	Image Recorder, Front View	8-12
8-8	Typical Test Photo Format (Mode 2)	8-13
8-9	Channel Scanning Sequence Mode 2, Picture Format	8-14
9-1	Engineering Model Scan Mirror Assembly Accelerometer Locations	9-4
9-2	Flex Pivot	9-5
9-3	Load Distribution on MSS Scan Mirror	9-5
9-4	Load Conditions for Nastram Model	9-6
9-5	Identification of Finite Elements on Flex Pivot Webs	9-7
9-6	Flex Pivot Webs Stress Distribution	9-8
9-7	Fatigue Cycling Test Results	9-14
9-8	ASD Curves of Scan Mirror Response During Qualification Acoustic Test	9-16
9-9	Broken Photodiode Lead in Shutter Preamplifier	9-18
9-10	MSS-D Shutter Position Sensing Method	9-19
9-11	Shutter Monitor Preamplifer Schematic Diagram	9-20
9-12	DC Restore Problem	9-22

9-13	MSS-D Band 4 Photodiode Signal Processing Block Diagram	9-24
9-14	DC Restore Pulses and Resulting DC Restore Waveforms	9-26
9-15	Protoflight Preamplifier Output Pulses	9-28
9-16	Protoflight dc Restore Waveforms with 3.9K Resistor	9-30
9-17	Video Cable, Interface Specification Configuration (EO1724A)	9-32
9-18	Video Cable, EO2061A Configuration	9-33
9-19	Video Cable Initial Configuration	9-34
9-20	EO1747A Configuration	9-36
9-21	Protoflight Channel Analog Switch Transient Connected to Laboratory Tester	9-40
9-22	Engineering Model Channel 15 Analog Switch Transient Connected to Laboratory Tester	9-40
9-23	Protoflight Analog Switch Transient Connected to Scanner at SBRC	9-40
9-24	Multiplexer Input Wave Shapes with Series Resistors in Place	9-41
9-25	Multiplexer Input Wave Shapes with Shunt Capacitor Added	9-41
9-26	Scanner Amplifier Output and Multiplexer Input Wave Shapes with Cable	9-42
9-27	Scanner Amplifier Output and Multiplexer Input Wave Shapes with RG 173, Coaxial Cable	9-42
9-28	P/N 78622 Configuration	9-44
9-29	Spectrum of Analog Video Noise with 78622 Cable	9-45
9-30	Band 2 Gain History	9-47
9-31	Band 2, System B, Integrating Sphere Calibration	9-50
9-32	Channel 9 Gain Versus PMT Noise	9-51
10-1	F-1 Test Sequence	10-2
10-2	F-1 Acoustic Test Spectrum	10-8
10-3	Acoustic Test Setup	10-8
10-4	F-1 Thermal-Vacuum Temperature Profile	10-13
10-5	F-1 Acoustic Test Spectrum	10-14
10-6	Penalty Acoustic Test Spectrum	10-14
10-7	Noise Model Coefficient History	10-21
10-8	Noise Measurements During F-1 System Test - Linear/Low Gain Mode	10-23
10-9	Noise Measurements During F-1 System Test - Compression/Low Gain Mode	10-25
10-10	Noise Measurements During F-1 System Test - Linear/High Gain Mode	10-27
10-11	Noise Measurements During F-1 System Test - Compression/High Gain Mode	10-28
10-12	F-1 Average Signal Level - Linear/Low Gain Mode	10-32
10-13	F-1 F-1 Gain History - Linear/Low Gain Mode	10-36
10-14	F-1 Average Gains Versus Temperature - Linear/Low Gain Mode	10-50

10-15	F-1 Channel Gain with Temperature Dependence Removed - Linear/Low Gain Mode	10-58
10-16	F-1 COSL Performance - Linear/Low Gain Mode	10-60
10-17	F-1 COSL Performance in Ambient	10-63
10-18	F-1 COSL Performance in Thermal-Vacuum	10-68
10-19	F-1 Band Average COSL Performance - Linear/Low Gain Mode	10-79
10-20	F-1 Mean-Normalized COSL Performance - Linear/Low Gain Mode	10-84
10-21	F-1 Thermal-Vacuum Temperature Profile	10-88
10-22	F-1 MTF Performance	10-97
10-23	Nominal MTFs Versus Temperature	10-102
10-24	F-1 Mean Line Length Performance	10-104
10-25	F-1 Line Length Variation (VLL) Performance	10-104
10-26	Line Length Variation History	10-108
10-27	F-1 Scan Repeatability Performance	10-110
10-28	F-1 Cross-Axis Repeatability Performance	10-110

TABLES

		Page
1-1	On-Orbit MSS Instruments	1-3
2-1	Key System Requirements	2-2
3-1	Verification Matrix	3-21
3-2	Mass Properties Summary	3-28
4-1	Standard Orbits	4-4
4-2	Standard Data Sets	4-4
4-3	System Performance Parameters	4-6
4-4	System Radiometric Calibration Test Configuration	4-7
6-1	System (Collimator/Scanner) Configuration for Signal-to-Noise Data Sets	6-15
6-2	System Configuration for Data Sets 4, 5, and 6	6-23
6-3	System Configuration for Data Set 0	6-28
6-4	Line Length Decoding Example	6-28
6-5	System Configuration for Data Set 7	6-30
7-1	Protoflight Reference Orbits	7-3
7-2	EMI/EMC Tests	7-9
7-3	MSS-D Vibration Test Levels	7-12
7-4	Anomaly List from Vibration Test	7-14
7-5	Protoflight MSS-D Test Chronology	7-21
7-6	Noise Model/Parameter Estimates	7-32
7-7	Protoflight Model Extrapolated Signal-to-Noise Performance	7-32
7-8	Approximate Maximum Noise Permissible Without Violating Specification	7-35
7-9	Protoflight Nominal Gain Performance	7-65
7-10	Gain Change/^{o}C	7-69
7-11	DCC Specification Violations Before Recalibration	7-93
7-12	DCC Specification Violations After Recalibration	7-94
7-13	MSS Telescope Modulation Transfer Function, $M_T(\nu)$	7-98
7-14	MSS Scan Aperture Modulation Transfer Function, $M_D(\nu)$	7-101
7-15	MSS Presample Filter MTF, $M_F(\nu)$	7-101
7-16	MTF Performance Summary	7-112
8-1	GPE/VPIR Picture Rating Scale	8-7
8-2	Protoflight GPE Evaluation Summary	8-8
8-3	GPE Conducted Susceptibility Test (CS01) Results	8-9
8-4	Protoflight VPIR Evaluation Summary	8-15
8-5	VPIR Conducted Susceptibility Test Results	8-16
9-1	Random Vibration Levels, All Axes	9-2
9-2	Scanner Acoustic Noise Levels	9-2
9-3	MSS Maximum Stress from 1 g Load, 1.6 lbf	9-9
9-4	MSS Vibration and Acoustic rms Accelerations Comparison	9-10
9-5	MSS Flex Pivots Maximum, Minimum, and Best Estimates of Stress Levels	9-10
9-6	Estimated Time to Fatigue Failure Summary	9-17

9-7	Summary of dc Restore Trigger Margins	9-31
9-8	MSS-D Engineering Model Multiplexer Test Data	9-37
9-9	MSS-D Protoflight Multiplexer Test Data	9-38
10-1	Flight Reference Orbits	10-4
10-2	EMI/EMC Tests	10-11
10-3	F-1 Vibration Test Sinusoidal Vibration Level	10-11
10-4	MSS-D F-1 Test Chronology	10-16
10-5	Flight Model Extrapolated STN Performance	10-30
10-6	Approximate Maximum Noise Permissible Without Violating Specification	10-30
10-7	F-1 Nominal Gain Performance	10-44
10-8	Gain Change/^{o}C	10-59
10-9	Summary of DCC Violations	10-90
10-10	F-1 DCC Violations by Band and Temperature	10-95
10-11	F-1 Acceptance Test MTF Performance Summary	10-100
10-12	Events Surrounding VLL Anomaly	10-106
10-13	Data Used to Generate Figure 10-26	10-111
11-1	GPE/VPIR Picture Rating Scale	11-2
11-2	GPE Evaluation Summary	11-2
11-3	GPE Conducted Susceptibility Test Results	11-4
11-4	VPIR Evaluation Summary	11-4
11-5	VPIR Conducted Susceptibility Test Results	11-6

GLOSSARY

AMLC	asynchronous multiline controller
ANL	average noise level
ASL	average signal level
ASP	active scan period
ASPT	abbreviated system performance test
BTE	bench test equipment
CCD	collimator calibration diagnostic program
COSL	corrected signal level
CPU	central processing unit
CRT	cathode ray tube
CSPT	complete system performance test
CXAXO	cross-axis repeatability
DBB	deviation band-to-band
DCC	deviation channel-to-channel
DPP	deviation peak-to-peak
DRS	data reduction system (computer)
DSN	deviation signal to noise
ECR	engineering change requirement
EM	engineering model
EMC	electromagnetic compatibility
EMI	electromagnetic interference
EO	engineering order
F-1	flight model
GPE	ground processing equipment
IR	image recorder
LOS	line-of-sight
MLL	mean line length/active scan period
MMS	Multimission Modular Spacecraft
MSS	Multispectral Scanner
MTF	modulation transfer function (abbreviation used to denote square wave response)
MUX	multiplexer
NDF	neutral density filter
OASPL	overall acoustic sound pressure level
PF	protoflight
PMT	photomultiplier tube
PROM	programmable read-only memory
QL	quantum level
RIU	remote interface unit
RSE	receiving site equipment
SAPT	system ambient performance test
SBRC	Santa Barbara Research Center
SMA	scan mirror assembly
SMP	scan monitor pulse
S/N	serial number
SOC	system option controller
SON	sequential orbit mumber
SRO	scan repeatability
SSL	Space Simulation Laboratory
STN	signal-to-noise

STNO	signal-to-noise ratio (output)
STR	special test request
STS	scanner test set
STU	self-test unit
TDRSS	Tracking and Data Relay Satellite System
TM	Thematic Mapper
UFD	user file directory
URC	unit record controller
VLL	line length variation
VP	video processor
VPIR	pictures made with the video processor working in conjunction with the image recorder

1. INTRODUCTION

This final report, submitted in accordance with Article XXVII of Contract NAS 5-25050, documents the development of the Multispectral Scanner System for Landsat D as conducted by the Hughes Aircraft Company. The first six sections describe the overall program, the technical requirements, and MSS-D performance against those requirements, and the development of the software and test equipment required for system performance evaluation.

The protoflight model and F-1 model test history, performance data, and data analysis through ambient and environmental tests are described in Sections 7 through 12. Specific problems encountered with system noise, flex pivots, shutter synchronizer circuits, and others are described, along with the corrective actions and verifications.

1.1 PROGRAM BACKGROUND AND HISTORY

The Multispectral Scanner System (MSS) was designed and developed on a NASA contract starting in 1969. Several contracts followed which resulted in the development, launch, and operation of three systems, on Landsat 1 (originally ERTS), Landsat 2, and Landsat 3. MSS-3 (Landsat 3) was the first five-band system built and launched, the first two systems being four-band instruments similar to the present MSS-D. All three instruments were launched aboard a Nimbus class spacecraft built by General Electric Company for NASA (see Table 1-1). These systems initiated the now worldwide earth resources activity.

In the 1970's NASA developed plans for a second generation system to provide improved earth resources technology for the 1980's and beyond. A new spacecraft design was conceived utilizing the multimission modular concept with TDRSS and shuttle compatibility. The spacecraft would be optimized for earth resources data, include a sophisticated second generation instrument, the Thematic Mapper, and fly at a lower orbit (705 km compared to 919 km for MSS 1 through 3). It was also decided that continuation of MSS data was required to complete current earth resources programs as well as to provide a transition period for the Thematic Mapper. The new earth resources program was designated Landsat D.

Hughes prepared a proposal for the MSS-D system and submitted it to NASA/GSFC early in 1978. A letter of contract was issued 29 March 1978 to proceed with MSS-D development. The contract was definitized and negotiations were completed on 31 July 1978.

ORIGINAL PAGE IS
OF POOR QUALITY

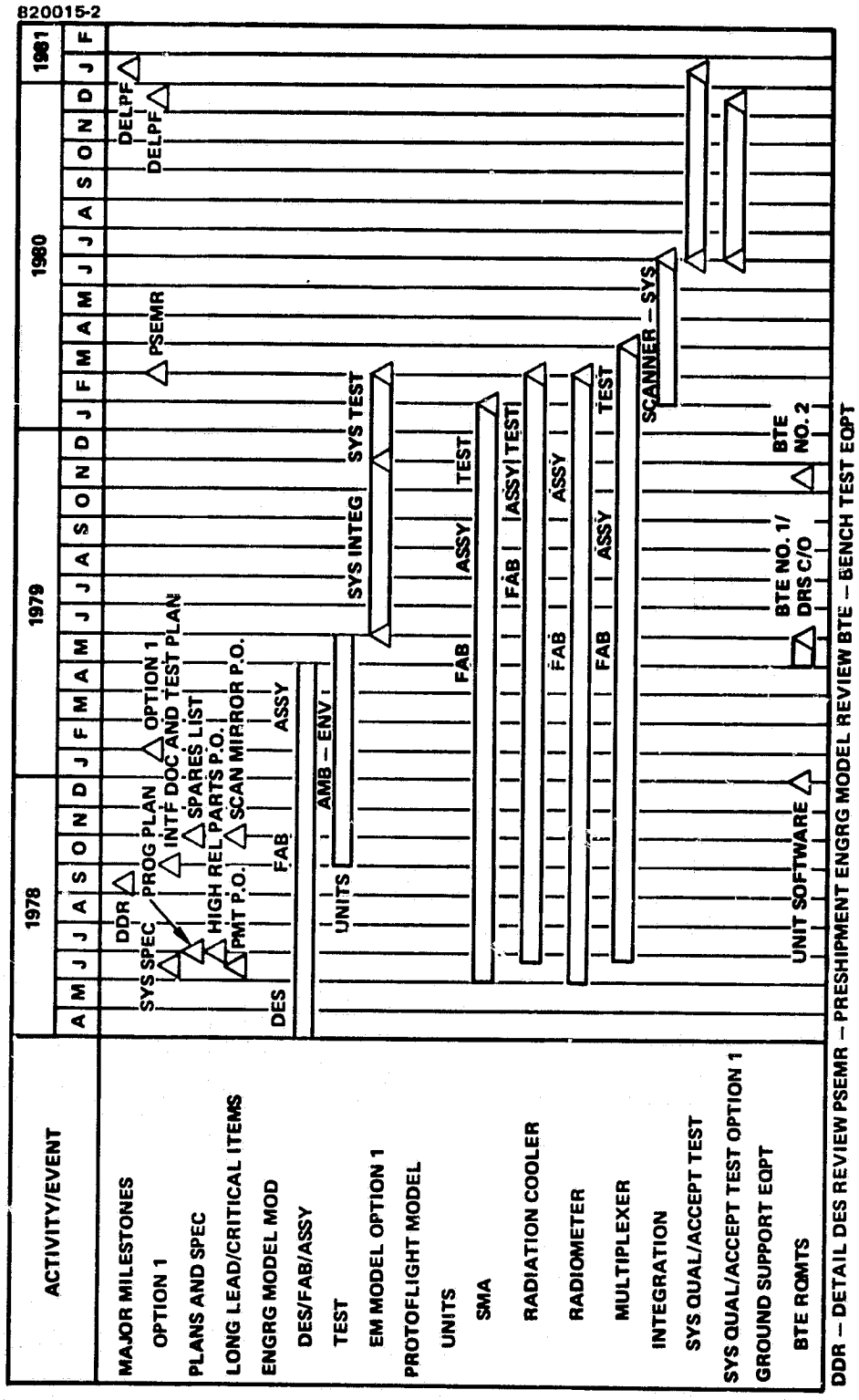

FIGURE 1-1. 1978 MASTER PHASING SCHEDULE – FIVE BAND MSS-D

TABLE 1-1. ON-ORBIT MSS INSTRUMENTS

Instrument	Launched
MSS-1 (four-band)	23 July 1972
MSS-2 (four-band)	25 January 1975
MSS-3 (five-band)	5 March 1978

An earlier long lead study contract was completed in March 1978 to help develop the design and aid the long lead activities prior to program go-ahead. A study report was issued for these activities under a separate contract.

1.2 PROGRAM PLAN AND OBJECTIVES

The initial plan for the MSS-D program is summarized in Figure 1-1. The plan included the development of a five-band protoflight model to be delivered in January 1981. An option was included to integrate and environmentally test the engineering model units from June 1979 through January 1980. These tests, if accomplished on the engineering model system, would reduce the test time required on the protoflight model, thereby providing an earlier protoflight model delivery (December 1980). This option was not exercised, but a compromise engineering model system assembly and test program was eventually agreed to.

After difficulties were encountered in orbit with the fifth band on MSS-3, NASA decided to delete this band on MSS-D. On 22 September 1978 a contract modification was issued deleting the requirement for the fifth band.

Early in 1979 Hughes submitted a proposal to NASA/GSFC to add another flight system, designated the F-1 model, to the contract to act as a backup for Landsat D. Go-ahead was received on 1 April 1979 to add the development of the F-1 model to the current contract. The revised plan is shown in Figure 1-2. The protoflight and F-1 models would both be four-band systems as shown in Figure 1-3. The protoflight model delivery was scheduled for 24 December 1980 and the F-1 model 1 July 1981. The plan also included the revised engineering model assembly and test program, and became the baseline for all program operations. The actual schedule performance achieved is shown in Figure 1-4.

The principal tasks for the MSS-D program and, therefore, the primary objectives of the program were as follows:

Design

1) MSS 1 through 3 would be used as baseline design; for user compatibility, data rates and formats kept the same for MSS-D

2) Baseline design modified for the lower orbit

3) Interface compatibility with new Landsat D spacecraft provided; different power system, telemetry, command, and redundancy scheme

4) Design improvements over earlier MSS incorporated

5) Bench test equipment redesigned and upgraded

ORIGINAL PAGE IS
OF POOR QUALITY

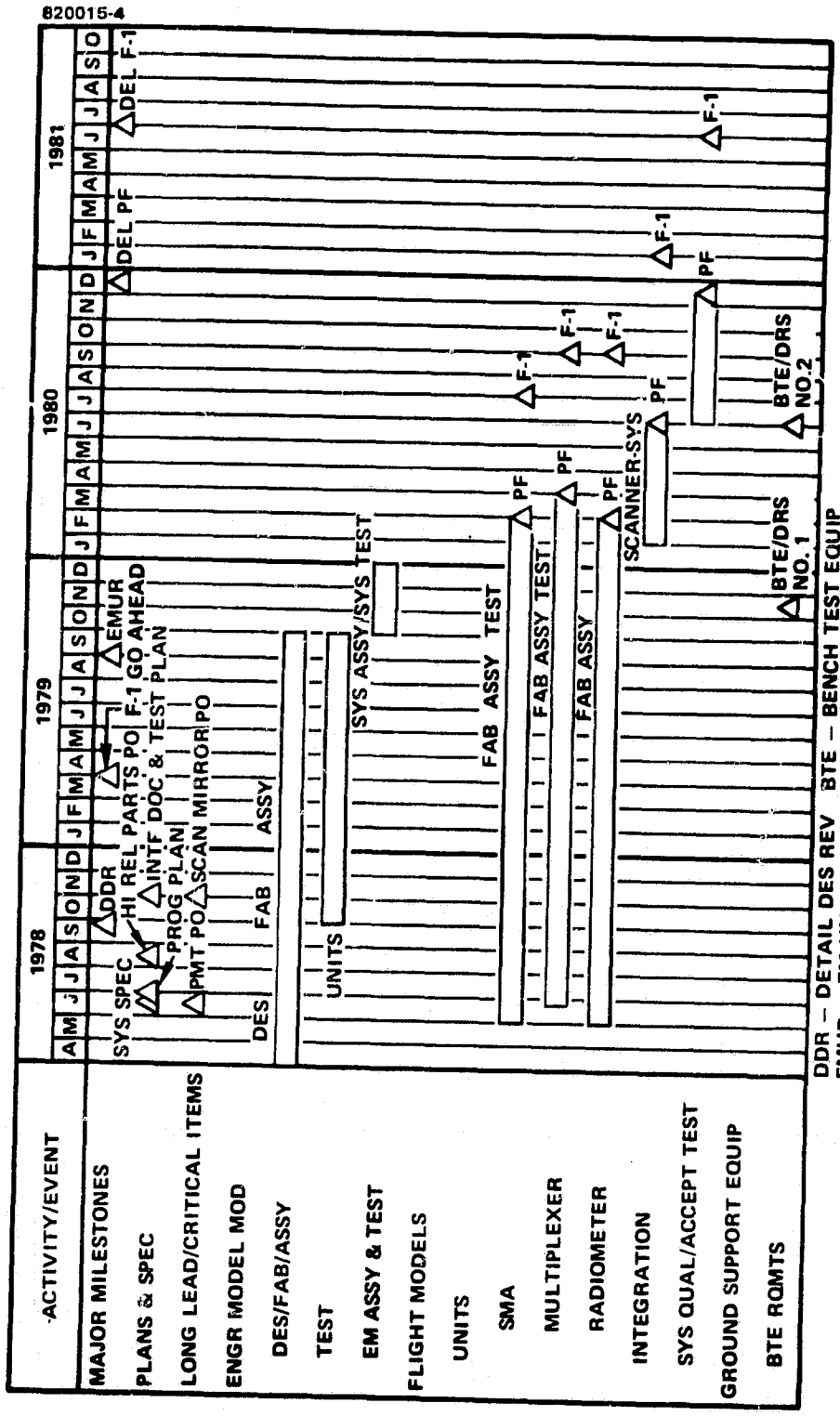

FIGURE 1-2. REVISED MASTER PHASING SCHEDULE – FOUR BAND MSS-D

Development Tests

1) Breadboards

   a) Primary power supply - added unit for spacecraft compatibility

   b) Selected circuits - command and telemetry functions and circuits which underwent major revisions

2) Engineering models

   a) Modified engineering model scan mirror assembly

   b) Modified engineering model multiplexer

   c) Partially modified scanner (no optics or detector changes incorporated)

   d) Engineering model system assembled and electrically tested

3) Life tests

   a) Scan monitor laser diode

   b) Scan mirror assembly dampers

Qualification Tests

1) Units/components

   a) Laser diodes

   b) Photodiodes

   c) Primary power supply

   d) Scan mirror assembly electronics

   e) Multiplexer

2) System

   a) Protoflight model

All of these principal tasks were completed over the course of the program.

A timeline of the key program historical events from the beginning of the program through completion of the F-1 model system is presented in Figure 1-5.

This report completes the final deliverables as defined in the contract. The remaining effort is to provide support at the direction of NASA/GSFC for pre- and post-launch activities for the protoflight and F-1 models.

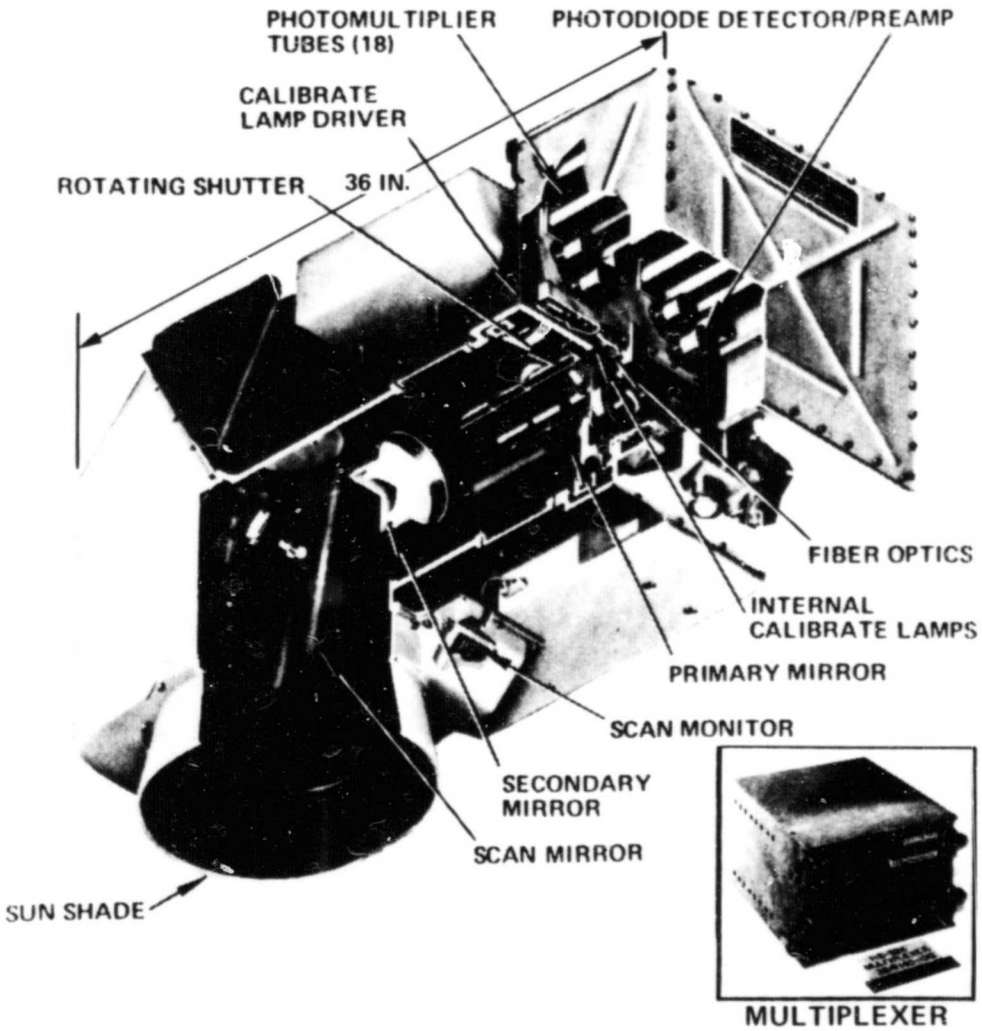

820015-3

MSS-D SYSTEM CHARACTERISTICS

LENGTH – 36 IN.
WEIGHT – 65 KG (143 LB)
POWER CONSUMPTION – 85 W (NORMAL OPERATION)

SPECTRAL BANDS (μM)	DETECTOR TYPE	NO. DETECTORS
0.5 – 0.6	PHOTOMULTIPLIER TUBES	6
0.6 – 0.7	PHOTOMULTIPLIER TUBES	6
0.7 – 0.8	PHOTOMULTIPLIER TUBES	6
0.8 – 1.1	Si PHOTODIODES	6

SCAN FREQUENCY	13.52 Hz
SCAN EFFICIENCY	45%
TELESCOPE	9 IN. APERTURE RITCHEY-CHRÉTIEN
PICTURE SIZE	185 x 185 KM
DATA RATE	15 MBPS
IFOV (SQUARE)	BANDS 1-4 = 117.2 μRAD (83 M)
IN FLIGHT CALIBRATION	ALL BANDS
SAMPLE QUANTIZATION	6 BITS
CUSTOMER:	NASA
APPLICATION:	LANDSAT-D

FIGURE 1-3. FOUR BAND MULTISPECTRAL SCANNER MSS-D

ORIGINAL PAGE IS OF POOR QUALITY

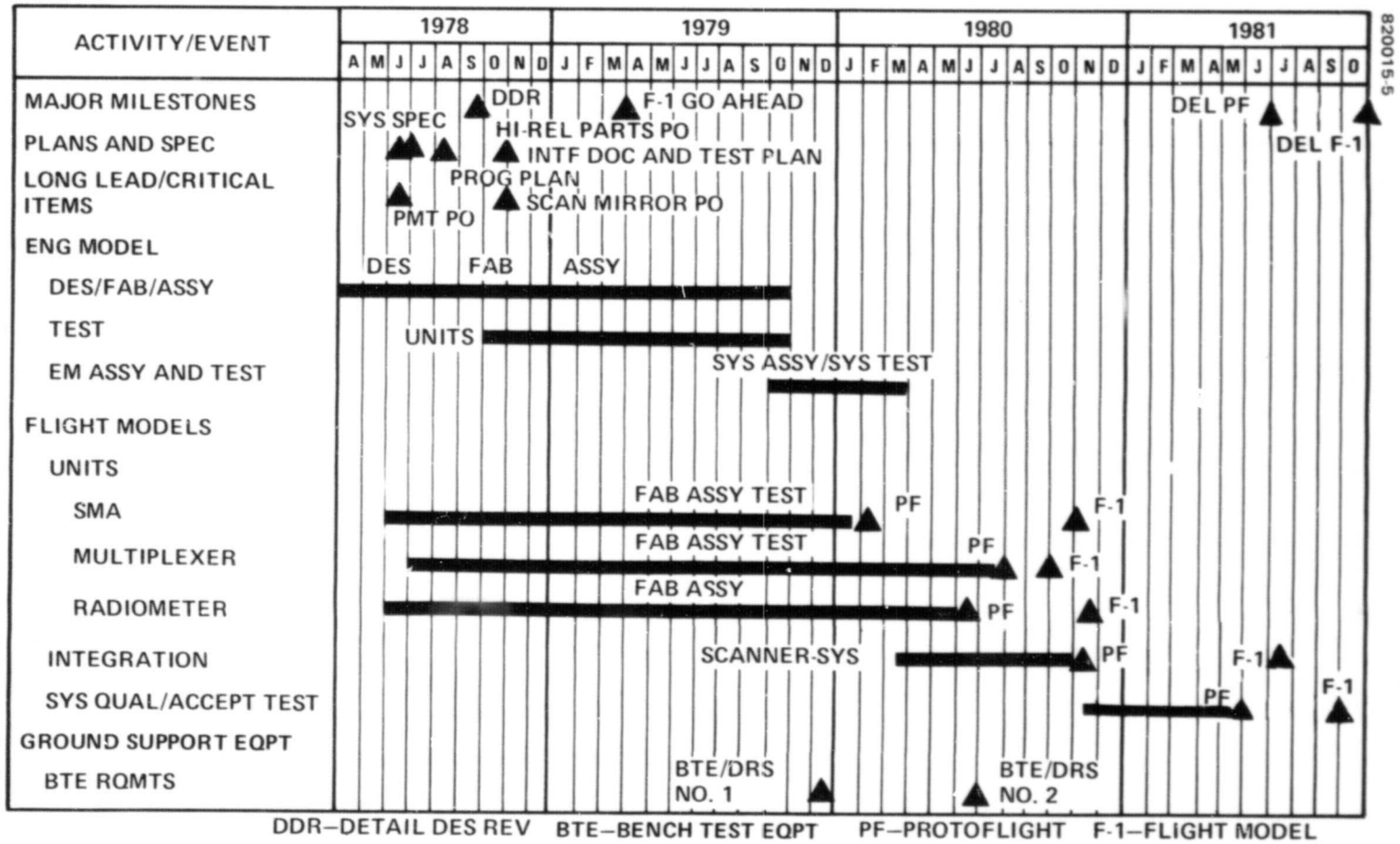

FIGURE 1-4. ACTUAL MASTER PHASING SCHEDULE

ORIGINAL PAGE IS OF POOR QUALITY

ORIGINAL PAGE IS
OF POOR QUALITY

820015-6

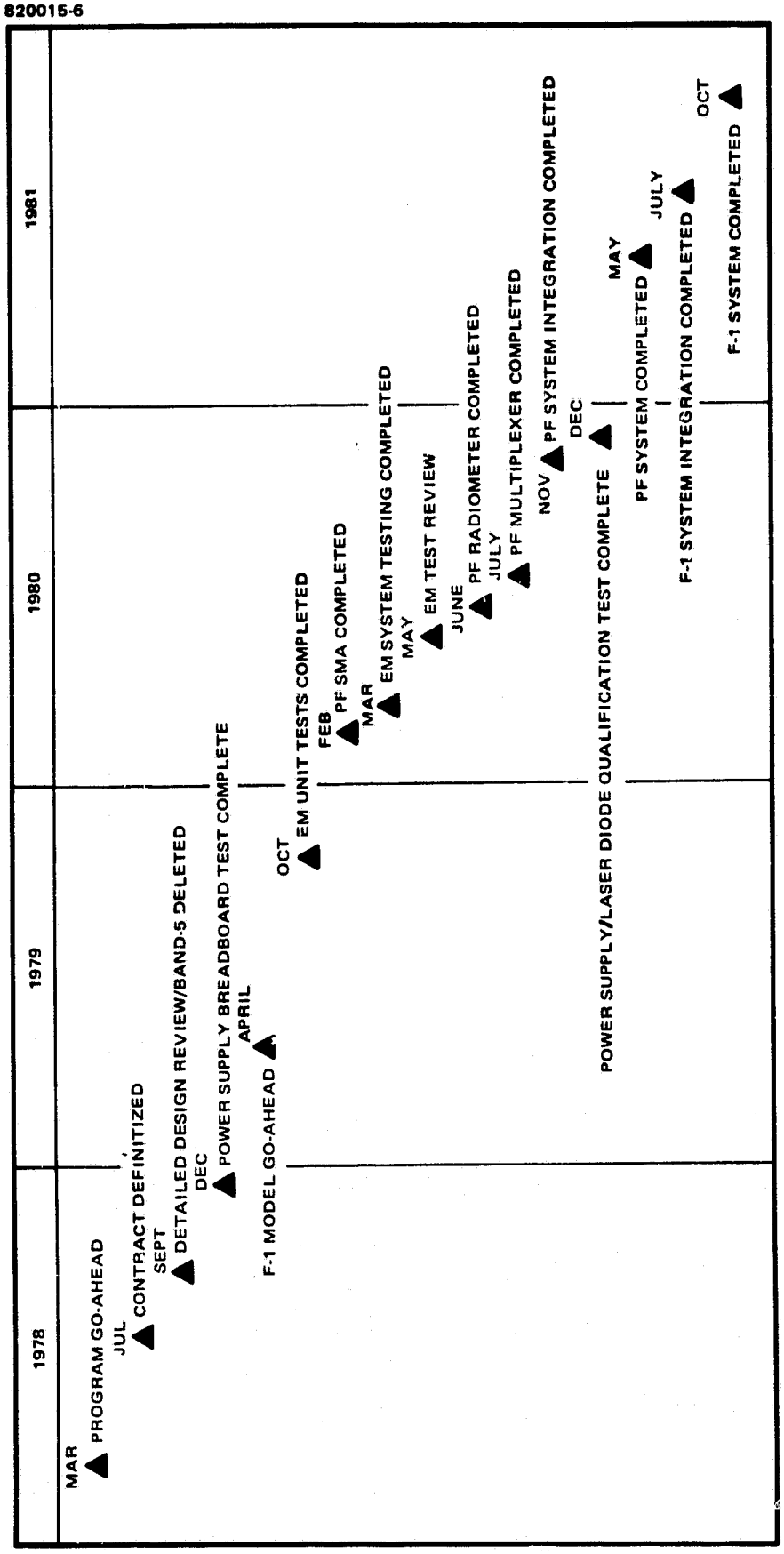

FIGURE 1-5. MSS-D PROGRAM HISTORICAL EVENTS

2. SUMMARY

2.1 DEVELOPMENT

The MSS-D program has been a technical success. The challenges to overcome in the execution of the program were: 1) to adapt the previous design to the new orbital altitude and modified spacecraft interfaces of Landsat D; 2) to correct mutually agreed upon design deficiencies of the former flight systems; and 3) to streamline and upgrade the analysis capabilities of the test hardware and software so that system performance evaluation could be completed rapidly and with unambiguous results. All three challenges have been met successfully.

Modifying the design to meet the new interface requirements of the Landsat D mission was the most comprehensive effort. To operate from the Landsat D orbital altitude of 705 km, rather than the former altitude of 919 km, implied an increase of scan angle and a re-layout of the focal plane array geometry. In modifying the scan mirror assembly for the larger angle, a control loop instability resurfaced which had caused problems back in 1971. After additional tests on the engineering model, flight hardware, and simulations of the scan mirror control loop, a stable operating point was selected for the flight hardware. All the telemetry and command circuitry was completely redesigned for the Landsat D spacecraft interfaces. The redesign was straightforward, but involved extensive rewiring and re-layout of circuit boards throughout MSS-D. The primary power supply was a completely new addition to MSS-D. To make room for its addition, the existing radiometer power supply was repackaged and moved from its location in the electronics box to the aft optics area where the detectors and high voltage power supplies are located. The function of the primary power supply is to take the positive polarity unregulated bus voltages of Landsat D and scale them into negative polarity regulated voltages required by the rest of the MSS electronics. Although the development effort associated with the new power supply was painful and accounted for significant schedule delays during the integration phase of the program, the resulting power system is now debugged and was trouble-free during the system test phase of the program.

Several changes were made to the former MSS design to correct known problems. A timing problem existed in the multiplexer analog-to-digital converter which caused it to make an occasional one bit error in conversion. A change was implemented to fix this problem, and tests were performed to verify the fix. The scan monitor, which is used to start video out of the multiplexer at the beginning of each scan line and as a primary reference for scan mirror position, was very sensitive to angular misalignments on previous MSS instruments. The light sources in the scan monitor assemblies had been 1970 vintage GaAs light emitting diodes. The scan monitor was desensitized to mechanical misalignments, and more modern GaAs light emitting diodes were procured having a much longer expected mean time to failure. Additional backup capability was designed

TABLE 2-1. KEY SYSTEM REQUIREMENTS

Characteristic	Specification				Protoflight				Flight-1				Reference Section
Instantaneous FOV	117.2 μrad x 117.2 μrad, nominal				116 μrad X 119 μrad				116 μrad X 119 μrad				
Square wave response	>36%, 102 μrad bars				0.38 < SWR < 0.53				0.40 < SWR < 0.53				7.5.3; 10.5.3
Active scan period, ms	32.75 ±1.25				32.5 ± 0.5*				32.3 ± 0.3*				7.6.2; 10.6.2
Line length variation, μrad	≤42 rms				29.4 max*				22.9 max*				7.6.3; 10.6.3
Scan repeatability, μrad	≤24 rms				8 ± 5*				6 ± 3*				7.6.4; 10.6.4
Cross-scan motion, μrad	≤33				2.3 max*				3.6 max*				7.6.5; 10.6.5
Forward scan angle, mr	260 ± 1				260.3				260.1				
Scan nonlinearity, %	≤+2.4, −5				+1.41, −3.21				+1.63, −4.50				
Registration, %	≤15 of IFOV				<10				<12				
Deviation channel to channel (DCC), %	≤2 p-p				>2 at 10°C ≥ temperature ≥ 30°C				>2 at 10°C ≥ temperature ≥ 30°C occasionally > 2 at 15°C and 20°C				7.4.4; 10.4.4
Deviation band to band (DBB), %	≤3p-p				<3				<3				7.4.4; 10.4.4
Operating range, °C	20 ± 15				Confirmed in thermal-vacuum				Confirmed in thermal-vacuum				
Survival range, °C	20 ± 20				Confirmed in thermal-vacuum				Not verified				
	Band 1	Band 2	Band 3	Band 4	Band 1	Band 2	Band 3	Band 4	Band 1	Band 2	Band 3	Band 4	
Signal to noise ratio — System A													7.3.2, 10.3.2
Linear mode													
64 QL, low gain	89.1	72.9	49.8	108	127.2	107.5	97.9	150.3	125.1	108.4	101.4	162.4	
high gain	58.7	45.8	N/A	N/A	84.4	71.5	N/A	N/A	92.3	72.1	N/A	N/A	
32 QL, low gain	54.3	46.4	33.5	54	79.1	66.1	59.6	75.1	71.8	66.9	64.4	81.2	
high gain	38.7	31.0	N/A	N/A	57.8	48.1	N/A	N/A	59.2	48.8	N/A	N/A	
Compression mode													
64 QL, low gain	110.3	94.8	68.8	N/A	168.9	137.6	125.7	N/A	150.9	140.9	134.1	N/A	
high gain	79.4	63.8	N/A	N/A	118.1	98.2	N/A	N/A	120.5	99.7	N/A	N/A	
32 QL, low gain	59.1	51.9	38.9	N/A	86.9	72.2	64.6	N/A	75.5	73.1	71.9	N/A	
high gain	44.4	36.2	N/A	N/A	68.4	56.2	N/A	N/A	66.7	57.1	N/A	N/A	
Signal to noise ratio — System B													7.3.2, 10.3.2
Linear mode													
64 QL, low gain	89.1	72.9	49.8	108	130.1	111.7	98.9	146.8	131.2	106.6	88.0	170.7	
high gain	58.7	45.8	N/A	N/A	85.8	74.6	N/A	N/A	99.0	71.7	N/A	N/A	
32 QL, low gain	54.3	46.4	33.5	54	81.2	67.5	60.9	73.4	73.4	65.7	53.0	85.3	
high gain	38.7	31.0	N/A	N/A	58.8	49.1	N/A	N/A	61.1	48.9	N/A	N/A	
Compression mode													
64 QL, low gain	110.3	94.8	68.8	N/A	171.5	139.5	137.7	N/A	152.8	134.6	118.0	N/A	
high gain	79.4	63.8	N/A	N/A	119.7	101.1	N/A	N/A	125.7	97.6	N/A	N/A	
32 QL, low gain	59.1	51.9	38.9	N/A	89.4	73.1	66.2	N/A	76.3	71.9	57.0	N/A	
high gain	44.4	36.2	N/A	N/A	69.6	56.2	N/A	N/A	66.9	57.7	N/A	N/A	

*Measured in thermal-vacuum (5° to 35°C)

ORIGINAL PAGE IS
OF POOR QUALITY

into the multiplexer to assure no loss of video data in the unlikely event of a failure of the scan monitor assembly. During the assembly of the video buffer amplifier cards, another defect was found in the design which made the bandpass of the video electronics dependent on the gain setting (high or low) of the buffer amplifiers. The correction of this defect showed up in the system test results as improved margin over earlier systems in square wave response.

Because of improvements made in the test hardware and software, data analysis and performance evaluation were more timely and revealing of system performance than formerly. A considerable effort was expended to make the computer algorithms fault tolerant so as not to bring testing to a halt in the presence of erroneous data. The computer hardware capability was upgraded to allow large off-line programs to be brought on-line to the Prime 300 test computer. Algorithms that could produce ambiguous or erroneous results under some conditions were modified or replaced. We were thus cognizant of genuine flight hardware anomalies in near real time and spent little time chasing "ghosts" of flight hardware problems which later turned out to be algorithm faults in disguise. The net result is a high degree of confidence in the accuracy and completeness of the test results summarized in 2.2 and reported in detail in the remainder of this final report.

2.2 SYSTEM PERFORMANCE SUMMARY

The MSS-D protoflight (PF) and flight (F-1) model both performed satisfactorily throughout system acceptance testing. Table 2-1 gives the key performance parameters for these systems. Some out-of-specification performance was observed, but none which would prohibit either of the MSS-D systems from operating satisfactorily in orbit. The following paragraphs discuss each of the performance parameters in turn, emphasizing those features of the test results which are particularly noteworthy. A more detailed discussion of system performance is given in Section 7 for the protoflight and in Section 10 for the flight model.

The parameters of particular importance for MSS-D system performance evaluation are signal-to-noise ratio (STN), corrected signal level (COSL), with its related specified performance parameters deviation channel-to-channel (DCC) and deviation band-to-band (DBB), square wave response (called here MTF) and the scan precision parameters, line-to-line variation (VLL), scan repeatability (SRO), and cross-axis repeatability (CXAXO).

2.2.1 Signal-to-Noise Ratio

Values of STN presented in Table 2-1 represent the best estimate of the nominal STN performance of each instrument at the specified radiance levels. These numbers are based on data taken during scanner calibration runs against the GSFC-furnished integrating sphere. The numbers displayed have been extrapolated to the specified radiance levels using the noise model discussed in 7.3.2. These data are considered to be more representative of scanner performance than those measured during acceptance testing using the test collimator for the following reasons:

1) The presence of test cable and other test equipment induced noise during the regular (collimator) orbits tends to mask the scanner's true performance.

2) The presence of collimator light output variations due to collimator source spatial nonuniformities and power supply instabilities tends to corrupt the scanner noise performance with collimator (test equipment) noise.

Reruns of the data using a collimator noise estimation algorithm helped significantly to eliminate the errors in STN estimates. Since the integrating sphere is presumed to have a spatially uniform output, its use eliminates concern over spatial nonuniformities and, for that reason, its use for STN estimation is preferred over data taken with the collimator.

The degree to which the test equipment introduced noise into the measured data is discussed in 7.3 and 10.3. These sections provide a detailed discussion of MSS-D signal-to-noise ratio acceptance test performance.

2.2.2 Signal Correction (DCC, DBB)

Since the individual gains of each of the channels in a band are different for the same set of environmental conditions (e.g., temperature, pressure) and each channel has its own characteristic behavior as a function of these conditions, all of the channels in a band must be normalized (corrected) to a common signal level so that ground processing equipment pictures of a spatially uniform source appear unstriped. The concept of the corrected signal level was developed on earlier MSSs to provide a quantitative means of assessing the capability of the internal calibration system to supply the gain and offset estimates required to perform this normalization.

Deviation channel to channel is the parameter which provides the necessary assessment of "de-striping" performance. It is defined as the percentage difference peak-to-peak of the individual COSL for all channels in a band relative to the band average COSL for that band. The specification for this parameter is that it be less than 2 percent. Measured performance which exceeds this specification and is not traceable to test equipment problems is an indication of inadequate gain correction capability of the internal calibration system.

Both the MSS-D protoflight and flight models exhibited a number of out-of-specification values of DCC, especially during thermal-vacuum testing at temperature extremes. The number of out-of-specification measurements under these circumstances can be reduced if calibration at the various temperature plateaus is permitted, as was done on MSS 1, 2, and 3. The success of this calibration-at-temperature is dependent on the stability of the corrected signal levels at a fixed temperature level and the repeatability of the corrected signal levels on return to that temperature. In some of the earlier MSS scanners, the calibration was repeated even on return to a temperature level previously attained.

The stability and repeatability of the COSLs for the MSS-D protoflight and F-1 were sufficiently good that reprocessing of the data with calibration at the temperature plateaus significantly reduced the number of out-of-specification cases. Even channels which exhibited very deviant behavior were brought into specification by this process (see 7.4 and 10.4).

As with earlier instruments, it will be necessary to perform system calibration close to the operating temperature of the instrument to ensure DCC performance within specifications.

Deviation band-to-band is the peak-to-peak spread in the ratio of the geometric mean of COSL across all six channels in a band relative to the value of this mean at the time of calibration. It is required to be less than 3 percent of the ratio of the mean of the band average COSLs to that mean obtained at calibration. No out-of-specification DBB performance was observed during normal acceptance testing of either instrument.

The complete history of signal correction performance during MSS-D acceptance testing is given in 7.4 and 10.4. DCC and DBB performance history is presented, and the results of reprocessing with calibration at temperature are described in detail. Gain versus temperature plots for all channels are provided for both instruments.

2.2.3 Square Wave Response (MTF)

In this report the square wave response is referred to as MTF, an abbreviation normally reserved for modulation transfer function. The reasons for this are historical with MSS programs, the earlier programs having been specified in terms of modulation transfer function rather than square wave response.

In MSS-D the specification states that system response to a rectilinear bar reticle pattern corresponding to a half-wave resolution at the earth's surface of 235 feet, be less than or equal to 0.36, at operating temperatures between 10° and 30°C. A specification relief of 20 percent (i.e., MTF $\leq$0.29) was permitted at temperatures above and below those temperature boundaries (35° and 5°C, respectively). The MTF performance versus specifications for both systems was excellent. In only two cases did the MTF drop below 0.36 and these occurred during MSS-D protoflight testing. The first below-specification performance occurred prior to thermal-vacuum testing and was traced to a problem in the test collimator. The second was not a violation of specification since it occurred at 0°C, at which temperature no specification requirement was imposed. Even this case did not result in values 20 percent below specification. In both cases channel 21 was involved. This channel was consistently 12 percent lower than other channels in band 4. This lower performance, as well as the spreading of other channels in other bands, is the result of the unavailability of sufficiently precise capacitors in the Approved Parts List; these capacitors were used to trim the poles of the Butterworth filter, which participates in establishing the MTF.

The MTF performance throughout thermal-vacuum testing for both systems was well within the boundaries of theoretical predictability. The MTF versus temperature behavior was very repeatable and indicated that the MTF for the protoflight scanner peaked at 20°C, while that of the F-1 scanner peaked at greater than 30°C. The temperature slope at the low temperature end was not sufficiently steep to cause out-of-specification performance. The MTF performance is discussed in detail for both MSS-D scanners in 7.5 and 10.5.

2.2.4 Scan Precision Parameters (VLL, SRO, CXAXO)

The scan repeatability parameters were well behaved during acceptance testing on both the protoflight and flight models with only a few exceptions. Cross-axis repeatability was always well within the specification of 33 μrad. As Table 2-1 indicates, the value of the parameter for both instruments was nominally 2 μrad. Scan repeatability was never in jeopardy of exceeding its specification of 24 μrad, being typically 6 to 8 μrad. The only cases of out-of-specification scan repeatability performance noted

ORIGINAL PAGE IS
OF POOR QUALITY

throughout acceptance testing on either instrument were observed during the reprocessing of data from tape at the time of the flex pivot failure in the protoflight. Even during this time with a broken or damaged flex pivot, the SRO was rarely out-of-specification.

The only scan parameter which exhibited out-of-specification performance in both instruments was the line length variation. VLL is typically higher in an ambient pressure environment than in vacuum as a result of aerodynamic loading of the scanning mirror. During normal operation at ambient pressure, the VLL attains values in the low to middle 30's (μrad). A drop to values of 10 to 20 μrad is typical in vacuum.

The measured out-of-specification VLL performance observed in the two instruments was different. During MSS-D protoflight testing the system exhibited anomalously high values during the initial prethermal-vacuum endbell testing. These tests were the first series of tests following the vibration testing during which the flex pivots failed. High VLL values were an indication of the flex pivot failure, but the indication was not a strong one since even after flex pivot failure the instrument exhibited intermittent in specification VLL performance. No further VLL anomalies were observed in protoflight testing using the replacement flex pivots.

The VLL performance for the flight model scanner was essentially without incident throughout acceptance testing with the original set of flex pivots. With this system configuration the MSS-D flight model exhibited higher values than the protoflight at ambient pressure but dropped to lower values than the protoflight in vacuum. The pivots were replaced with new ones after the system had completed thermal-vacuum testing. This system with the new pivots exhibited out-of-specification performance in the complete system performance tests (CSPTs) which followed. An extended "run-in" test of the bumpers with these pivots was performed, but even the initial test data taken during run-in showed the system to have ambient performance within specification. Subsequent testing at General Electric has failed to exhibit a recurrence of the problem. It is believed that the cause was a poor electrical connection which was corrected on the mating and re-mating of connectors during investigations of the problem. It is anticipated that the VLL performance in vacuum will remain within specification.

A detailed discussion of these performance parameters throughout acceptance testing is given in 7.6 and 10.6.

3. SYSTEM REQUIREMENTS

3.1 COMPARATIVE SPECIFICATIONS

The Multispectral Scanner System was initially designed as a four band scanner system with provisions for retrofit capability to make it a five band system. The first three spacecraft used for Landsat were similar in design to the Nimbus spacecraft, utilizing Nimbus type power, command, telemetry and thermal control systems. Landsat-D uses the Multimission Modular Spacecraft (MMS) rather than the Nimbus type spacecraft, with resulting interface changes, and a different orbital altitude. The effects of these changes on MSS-D can best be assessed by comparative evaluations of the MSS-C (SS31324-001) and MSS-D (SS32238-001) system specifications. Paragraph differences that relate only to the fifth band on MSS-C are ignored.

3.1.1 Resolution

MSS-C

3.1.1.1.4 Resolution. Bars as small as 0.075 mr across in the direction of scan shall be discernible at light intensity levels compatible with the signal to noise values specified in 3.1.1.1.17 herein and the modulation transfer function specified in 3.1.1.11 herein in Bands 1 to 4. Similar observables in areas as small as 0.26 mr across shall be discernible in Band 5.

MSS-D

3.1.1.1.4 Resolution. Bars as small as 0.102 mr across in the direction of scan shall be discernible at light intensity levels compatible with the signal to noise ratios specified in 3.1.1.1.17 and the modulation transfer function specified in 3.1.1.1.11.

Comment

This difference in system resolution is the result of changes made when the orbital altitude was revised. The degradation of the angular resolution is mostly compensated for by the reduction in spacecraft altitude.

ORIGINAL PAGE IS
OF POOR QUALITY

3.1.2 Instantaneous Fields of View

MSS-C

3.1.1.1.5 Instantaneous Fields of View. The nominal instantaneous fields of view (IFOV) shall be 0.086 mr for Bands 1 to 4 . . . .

MSS-D

3.1.1.1.5 Instantaneous Fields of View. The nominal instantaneous fields of view (IFOV) shall be 117.2 μr by 117.2 μr for Bands 1 to 4.

Comment

In order to preserve the video data formats and data rates for compatibility with existing ground stations, the MSS-D width of pictures was kept the same as that for MSS-C: 185 km. The size of the IFOV projected on the ground, or ground resolution, grew from 79 m to 82 m. This change in ground resolution, in conjunction with the change in orbital altitude from 919 km to 750 km, resulted in the specified change in IFOV. Contiguous coverage from scan line to scan line was thus maintained.

3.1.3 Scan Mirror Assembly

MSS-C

3.1.1.1.8 Scan Mirror Assembly. Sensor ground coverage perpendicular to the satellite track shall be accomplished by means of a flat scanning mirror oriented at 45 degrees with respect to the scene which scans about the X-axis. The following parameters define this scan mirror assembly system:

a. Scan frequency	13.62 Hz ± 0.01 percent
b. Scan angle across scene	11.60 ± 0.05 degrees

MSS-D

3.1.1.1.8 Scan Mirror Assembly. Sensor cross-track ground coverage shall be accomplished by means of a flat scanning mirror, oriented at 45° with respect to the scene, which scans about the X-axis as defined in Figure 3 (page 20). The following parameters define the scan mirror assembly function characteristics:

a. Scan frequency	13.62 Hz ±0.01 percent
b. Scan angle across scene	14.90 ± 0.06°

Comment

The timing of the scan mirror activity stayed constant with the change in orbit. The only difference is the angle of scan across the scene, which increased as a function of the change in altitude to maintain the 185 km scene width.

3.1.4 Geometric Fidelity

MSS-C

3.1.1.1.9 Geometric Fidelity. Geometric fidelity shall be defined by:

e. Scan nonlinearity	For the linear portion of the forward scan, the repeatable scan rate shall not deviate more than +2, -4.3 percent from the mean scan rate.

MSS-D

3.1.1.1.9 Geometric Fidelity. Geometric fidelity shall be defined by:

e. Scan nonlinearity	For the linear portion of the forward scan, the repeatable scan rate shall not deviate more than +2.4, -5.0 percent from the mean scan rate.

Comment

The reason for the change in scan linearity is the spring constant of the flexure pivots and the moment of inertia of the mirror. The flexure pivots are the same type as used in previous scanners. Their spring constant did not change, but the scan angle did, with a resultant increase in pivot torque, which in turn results in greater scan nonlinearity. The scan mirror was reduced in inertia in scaling the scan mirror for MSS-D. Both effects, increased scan angle and reduced inertia, increase the scan nonlinearity.

3.1.5 Scanner Modulation Transfer Function

MSS-C

3.1.1.1.11 Scanner Modulation Transfer Function (Along Scan Direction). A response greater than 29 percent at the sinusoidal spatial frequency corresponding to 0.075 mr bars shall be provided in Bands 1 through 4. A response greater than 29 percent at the sinusoidal spatial frequency corresponding to 0.26 mr bars shall be provided in Band 5. These responses shall be degraded by approximately 20 percent at spacecraft temperatures of 5° and $35^{o}C$ (nonoperational temperature extremes).

ORIGINAL PAGE IS
OF POOR QUALITY

MSS-D

3.1.1.1.11 Scanner Modulation Transfer Function (Along Scan Direction). The response shall be greater than 36 percent at the square wave spatial frequency corresponding to 0.102 mr bars. The response may be degraded by approximately 20 percent at spacecraft temperatures of 5° and $35^{o}C$ (nonoperational temperature extremes).

Comment

The scan aperture was increased by more than 1.303 to 1 in order to prevent underlap of adjacent scans in the cross scan (orbit velocity vector) direction (ground resolution change from 79 m to 82 m). Since the scan aperture inside dimension is the primary factor determining the theoretical MTF, the specified MTF performance level was also corrected.

The MTF contribution of the scan aperture is

$$\mathrm{MTF} = \frac{\sin \frac{\pi \nu}{\nu_o}}{\frac{\pi \nu}{\nu_o}}$$

where ν is the spatial frequency of the sinusoidal bar pattern and ν_o is the spatial frequency of period $1/\alpha$, where

α = angular dimension of the scanning aperture

α MSS–C = 80×10^{-6}

α MSS–D = 111×10^{-6}

For a sinusoidal bar pattern of bar width 225 feet or spatial period of 450 feet, the ratio of scanning aperture MTF MSS-D to MSS-C is:

$$\frac{\mathrm{MTF}_{\alpha_2}}{\mathrm{MTF}_{\alpha_1}} = \frac{\sin\left(\frac{\pi 5184}{9009}\right) \Big/ \left(\frac{\pi 5184}{9009}\right)}{\sin\left(\frac{\pi 6697}{12500}\right) \Big/ \left(\frac{\pi 6697}{12500}\right)}$$

$$= \frac{0.5376}{0.590} = 0.911$$

The specified MTF at 225 feet should be reduced to

MTF = 0.35 x 0.911 = 0.32 (square bar)

Similarly, for a bar pattern of 235 feet, the specified MTF should be

MTF = 0.385 x 0.929 = 0.36 (square bar)

3.1.6 Signal to Noise Ratio

MSS-C

3.1.1.4.2 Signal to Noise. The rms noise relative to peak signal versus input signals for the scanner and multiplexer shall be according to Table 2, when the multiplexer samples are in the linear mode. When the multiplexer compresses signals from Bands 1, 2 and 3, the signal/noise shall be that shown in Table 3.

MSS-D

3.1.1.4.2 Minimum Signal-to-Noise Ratio. The peak signal-to-rms noise ratios for the scanner and multiplexer shall be according to Table II, when the multiplexer samples are in the linear mode. When the multiplexer compresses signals from Bands 1, 2 and 3, the signal/noise shall be that shown in Table III.

Comment

The change in orbital altitude increased the IFOV, which provided more radiant energy to the detectors. The result was an improvement in signal level and a consequent improvement in the expected signal to noise ratio.

3.1.7 Vibration

MSS-C

3.1.2.4.4 Vibration. The qualification and flight acceptance vibration levels for the MSS units, as mounted in the spacecraft are given in Tables 4 and 5. The units shall not suffer any detrimental effects by exposure to the specified levels. These vibration levels are to be considered as applied separately along the mutually orthogonal axes at the attachment fittings. The axis directions are the same as those specified for moments of inertia in Figures 2 and 3.

MSS-D

3.1.2.4.4 Vibration. The qualification and flight acceptance vibration levels for the MSS units, as mounted in the spacecraft, are given in Table IV. The units shall not suffer any permanent detrimental effects by exposure, in the launch mode, to the specified levels. These vibration levels are to be considered as applied separately along the mutually

ORIGINAL PAGE IS
OF POOR QUALITY

TABLE 2. LINEAR MODE

	Band			
	1	2	3	4
High Radiance Level:				
Minimum Scanner S/N Output	80	62	40	89
MSS System S/N Output (after D/A conversion)	71	57	38	77
1/2 High Radiance Level:				
Minimum Scanner S/N Output	56	43	28	44
MSS System S/N Output (after D/A conversion)	45	38	26	38

MSS-C

TABLE II. LINEAR MODE SIGNAL TO NOISE RATIO

	Band			
	1	2	3	4
High radiance level:				
Minimum scanner S/N output	124	94	66	188
MSS system S/N output*	89	73	50	104
1/2 high radiance level:				
Minimum scanner S/N output	87	66	41	102
MSS system S/N output*	54	46	33	54

*After D/A conversion

MSS-D

ORIGINAL PAGE IS
OF POOR QUALITY

TABLE 3. COMPRESSION MODE

	Band		
	1	2	3
High Radiance Level:			
Minimum Scanner S/N Output	80	62	40
MSS System S/N Output (after D/A conversion)	61	51	36
1/2 High Radiance Level:			
Minimum Scanner S/N Output	56	43	28
MSS System S/N Output (after D/A conversion)	40	33	25

MSS-C

TABLE III. COMPRESSION MODE SIGNAL TO NOISE RATIO

	Band		
	1	2	3
High radiance level:			
Minimum scanner S/N output	124	94	66
MSS system S/N output*	75	65	47
1/2 high radiance level:			
Minimum scanner S/N output	87	66	41
MSS system S/N output*	43	38	30

*After D/A conversion (Decompression)

NOTE: All S/N values in these tables may be reduced by approximately 15% at spacecraft temperatures of 5° and 35°C.

MSS-D

ORIGINAL PAGE IS
OF POOR QUALITY

TABLE 4. QUALIFICATION VIBRATION LEVELS

Scanner Only: Sinusoidal		
Axes	Frequency Range (Hz)	Amplitude (g's 0-to-peak ±10 percent)
Thrust	5-15	*
	15-50	6.0
	50-90	11.0
	90-2000	5.0
Lateral	5-12.5	*
	12.5-30	3.8
	30-50	7.5
	50-2000	5.0
*Exposure limited to 0.5 inch, double amplitude. Sweep rate: 2 octaves/minute.		
Random		
Axes	Frequency Range (Hz)	Power Spectral Density
All	20-300	Increasing at a rate of 4 dB/octave ±3 dB to 0.09 g^2/Hz at 300 Hz
	300-2000	0.09 g^2/Hz with a tolerance of ±3 dB
Test duration: 4 minutes, each axis		Overall: 12.8 g rms ±10 percent
Multiplexer Only: Sinusoidal		
Axes	Frequency Range (Hz)	Amplitude (g's 0-to-peak ±10 percent)
All	5-17	0.5 (inch, double amplitude)
	17-200	7.5
	200-2000	5.0
Sweep rate: 2 octaves/minute		
Random		
Axes	Frequency Range (Hz)	Power Spectral Density
All	20-2000	0.09 g^2/Hz with a tolerance of ±3 dB, 13.4 g rms ±10 percent
Test duration: 4 minutes each axis.		

ORIGINAL PAGE IS
OF POOR QUALITY

TABLE IV. VIBRATION LEVELS

A. SINUSOIDAL VIBRATION LEVELS (Scanner and Multiplexer)				
Axis	Frequency (Hz)	Protoflight Level	Flight Level	Sweep Rate (Oct/Min)
Thrust	5 to 50	7.5 g*	5.0 g*	4
	50 to 100	3.0 g	2.0 g	
Lateral	5 to 50	5.25 g*	3.5 g*	4
	50 to 100	3.0 g	2.0 g	
*Exposure limited to 0.50 inch double amplitude (12.7 mm).				

B. RANDOM VIBRATION LEVELS (Multiplexer Only)		
Multiplexer Qualification Levels		
Axes	Frequency Range (Hz)	Power Spectral Density
All	20 to 2000	0.09 g^2/Hz with a tolerance of ±3 dB, 13.4 g rms ±10 percent
Test duration: 1 minute each axis		
Multiplexer Flight Levels		
Axis	Frequency Range (Hz)	Power Spectral Density
All	20 to 2000	0.04 g^2/Hz with a tolerance of ±3 dB, 8.9 g rms ±10 percent
Test duration: 1 minute each axis		

MSS-D

ORIGINAL PAGE IS
OF POOR QUALITY

TABLE 5. FLIGHT ACCEPTANCE VIBRATION LEVELS

Scanner Only: Sinusoidal		
Axes	Frequency Range (Hz)	Amplitude (g's 0-to-peak ±10 percent)
Thrust	5-15	*
	15-50	4.0
	50-90	7.3
	90-2000	3.3
Lateral	5-12.5	*
	12.5-30	2.5
	30-50	5.0
	50-2000	3.3
*Exposure limited to 0.33 inch, double amplitude. Sweep rate: 4 octaves/minute		
Random		
Axes	Frequency Range (Hz)	Power Spectral Density
All	20-300	Increasing at a rate of 4 dB/octave ±3 dB to 0.04 g^2/Hz at 300 Hz
	300-2000	0.04 g^2/Hz with a tolerance of ±3 dB
Test duration: 2 minutes each axis		Overall: 8.5 g rms ±10 percent
Multiplexer Only: Sinusoidal		
Axes	Frequency Range (Hz)	Amplitude (g's 0-to-peak ±10 percent)
All	5-14	0.5 (inch, double amplitude)
	14-200	5.0
	200-2000	3.3
Sweep rate: 4 octaves/minute		
Random		
Axes	Frequency Range (Hz)	Power Spectral Density
All	20-2000	0.04 g^2/Hz with a tolerance of ±3 dB, 8.9 g rms ±10 percent
Test duration: 2 minutes each axis		

orthogonal axes at the attachment fittings. The axis directions are the same as those specified for moments of inertia in Figures 3 and 4. During this test, the MSS flight system shall be operated in the normal launch mode. A low-level survey from 5 Hz to 2000 Hz shall be performed in each axis prior to full level application at 1/2 g p-p for vibration, and 6 dB below nominal SPL for acoustic noise. All test data shall be recorded on magnetic tape suitable for data reduction and analysis.

3.1.2.4.4.1 Acoustic Noise. The MSS scanner only, shall be placed in a reverberant test chamber and exposed to an induced vibration in accordance with the acoustic spectrum specified in Table V.

3.1.2.4.6 Acceleration. The MSS flight system, when operating in the launch mode, shall survive the acceleration levels shown in Table VI.

Comment

With the change in spacecraft, a change in vibration specifications was required even though the booster is the same. The change of spacecraft caused a thrust axis change in addition to the change in applied levels and frequencies.

A structural overload in random vibration testing at qualification levels caused a change from random vibration testing to acoustic testing. Acceleration was done by analysis.

3.1.8 Mass Properties

MSS-C

3.2.1.3 Mass Properties. Maximum weights and center of gravity locations for the scanner and multiplexer shall be as shown in their respective interface control drawings 3241120-400 and 3241140-400. The maximum allowable weights of the units are as follows:

Scanner	140.0 pounds
Multiplexer	7.5 pounds
Total allowable weight	147.5 pounds

MSS-D

3.2.1.3 Mass Properties. Maximum weights and center of gravity locations for the scanner and multiplexer shall be as shown in their respective interface control drawings, 361720-400 and 3617140-400. The moment-of-inertia about one principal axis shall be measured. Calculations shall be

ORIGINAL PAGE IS
OF POOR QUALITY

MSS-C

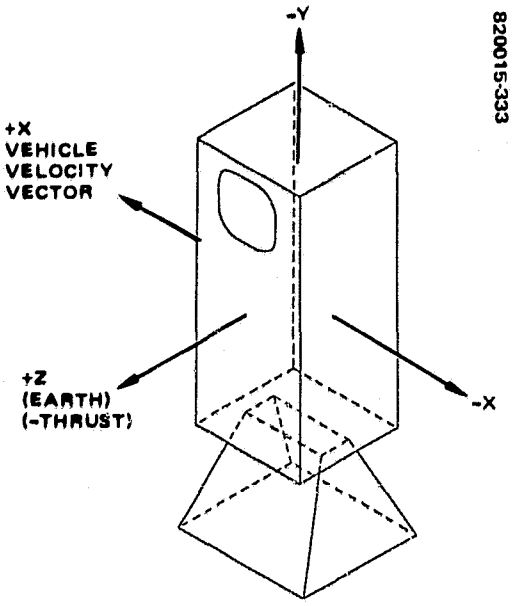

FIGURE 2. SCANNER AXES

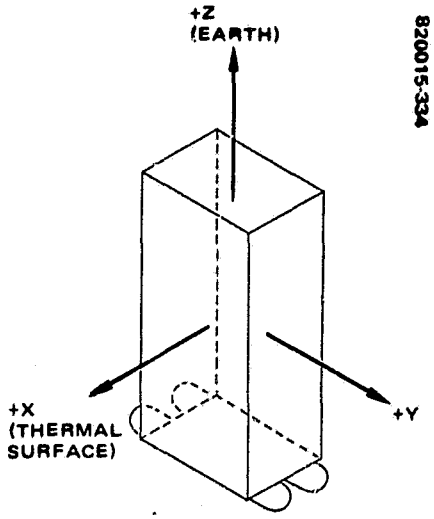

FIGURE 3. MULTIPLEXER AXES

MSS-D

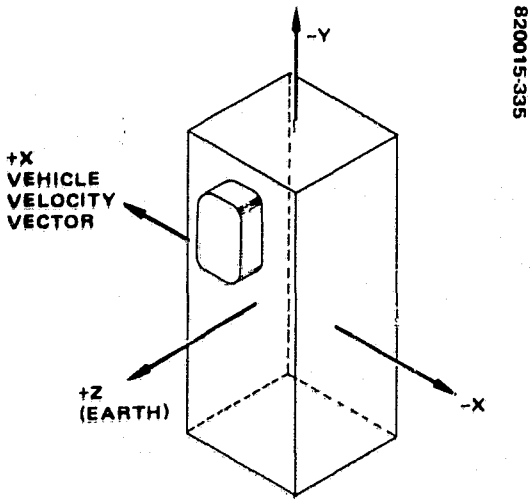

FIGURE 3. SCANNER AXES

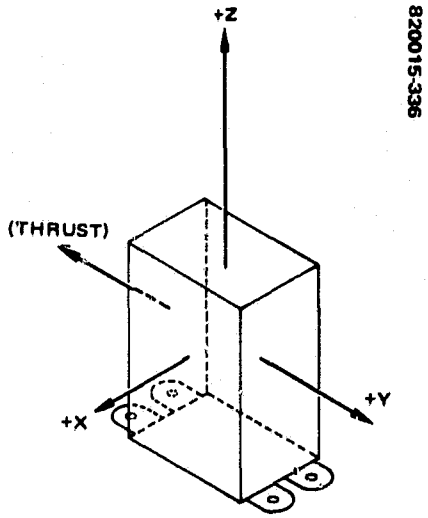

FIGURE 4. MULTIPLEXER AXES

provided for all three principal axes and their cross-products. The maximum allowable weights are as follows:

Radiometer	106 lb
Scan mirror assembly	20 lb
Scanner total	126 lb
Multiplexer	6.5 lb
Contingency	10.5 lb
MSS system total	143 lb

Comment

The weight allowance for the MSS-C scanner includes the fifth band. The original four band scanners weighed approximately 106 pounds including the scan mirror assembly; the MSS-D four band scanners weigh approximately 116 pounds including the scan mirror assembly. The principal difference in weight from the former to the latter is the additional power conditioning electronics required to condition Landsat-D unregulated spacecraft bus. The Nimbus spacecraft provided regulated power to MSS.

3.1.9 Power

MSS-C

3.2.2 Electrical Requirements

3.2.2.1 Spacecraft Power Subsystem Interface. The spacecraft power subsystem shall provide the basic power to the MSS flight subsystem.

3.2.2.1.1 Voltage. The voltage supplied to the scanner by the spacecraft power subystem shall be as follows:

a.	Regulated	-24.5, -0.5, +0.7 vdc
b.	Unregulated	-26 to -39 vdc

3.2.2.1.2 Current. The current supplied to the MSS subsystem by the spacecraft power subsystem at the nominal voltage shall be as follows:

a.	Regulated	2.1 amps, average
b.	Unregulated, radiation cooler (outgas mode)	1.0 amp
c.	Unregulated, Scan Mirror	0.60 amp, average

ORIGINAL PAGE IS
OF POOR QUALITY

TABLE V. ACOUSTIC NOISE LEVELS
(Scanner Only)

Center Frequency (Hz)		Sound Pressure Level dB*				Test Tolerance dB
		Acceptance		Protoflight		
One-Third Octave	Octave	One-Third Octave	Octave	One-Third Octave	Octave	
25 32 40	32	119 120 121	125	122 123 124	128	+3, –6
50 63 80	63	123 124 124	128	126 127 127	131	+3, –3
100 125 160	125	127 129 131	134	130 132 134	137	+3, –3
200 250 315	250	130 132 134	137	133 134 137	140	+3, –3
400 500 730	500	134 139 134	141	137 142 136	144	+3, –3
800 1,000 1,250	1,000	131 129 129	134	134 132 130	137	+3, –3
1,600 2,000 2,500	2,000	127 126 124	131	130 129 127	134	+3, –3
3,150 4,000 5,000	4,000	124 122 122	127	127 125 125	130	+3, –6
6,300 8,000 10,000	8,000	120 118 118	124	123 121 121	127	+3, –6
Overall		144		147		+3, –1

Notes: *Reference level: 0 dB = 20 $\mu N/m^2$
Test Duration: 1 minute

MSS-D

TABLE VI. PROTOFLIGHT ACCELERATION LEVELS (1 minute each axis)

Acceleration Level, g*		Acceleration Level, g**	
Thrust	Lateral	Thrust	Lateral
16.8	3.0 Z axis	22.4	4.0 Z axis
16.8	3.0 Y axis	22.4	4.0 Y axis
*For Test: Thrust and lateral accelerations must be applied simultaneously.		**For Analysis: Above accelerations must be used.	

MSS-D

MSS-D

3.2.2 Electrical Requirements

3.2.2.1 Spacecraft Power Subsystem Interface. The spacecraft power subsystem will provide fully redundant power to the MSS flight subsystem via redundant power supply lines.

3.2.2.1.1 Voltage. The voltage supplied to the scanner by the spacecraft power subsystem will be +28 ± 7 volts dc.

3.2.2.1.2 Current. The current required by the MSS system from the spacecraft power subystem at +28 volts dc shall not exceed:

a.	Unregulated normal operation	3 A average
b.	Standby	0.11A

Comment

MSS was originally designed for a Nimbus power bus, which included a regulated -24.5 volt bus (-24.0 volts to -25.2 volts), as well as unregulated -26 volts to -39 volts power. Only the scan mirror electronics and the outgas heater used the unregulated spacecraft bus. Landsat-D has only a positive unregulated power bus, which can vary from +22 volts to +35 volts. Allowing for a 1 volt drop in the spacecraft harness, MSS-D is designed to operate from +21 volts to +35 volts. This bus voltage change required a new approach to power conditioning. A primary power supply has been incorporated into the MSS-D hardware which operates from the Landsat-D unregulated bus and provides power to the MSS-D subsystems. The power increase in MSS-D is largely the overhead of this new power conditioning unit.

3.1.10 Commands

MSS-C

3.2.2.2 Spacecraft Command Subsystem Interface. The MSS flight subsystem shall be designed to receive commands from the spacecraft command subsystem.

3.2.2.2.1 Command Pulse. The basic command pulse characteristics are as follows:

a.	Command pulse amplitude	-23.5 ±1.0 volt
b.	Command pulse width	40 ±5 ms
c.	Maximum load current	220 ma
d.	Source impedance system On/Off commands	30 ±5 ohms, each line

ORIGINAL PAGE IS
OF POOR QUALITY

TABLE 8. COMMAND PULSE CHARACTERISTICS

A. Matrix Output		
State	Voltage	Impedance
Energized	−23.5 ± 1.0 volt	30 ± 5 ohms
Deenergized	−1.0 ± 1.0 volt	>30 K ohms
B. Matrix Output		
State	Voltage	Impedance
Energized	−0.5 ± 0.5 volt	30 ± 5 ohms
Deenergized	−24.5 ± 1.0 volt	>30 K ohms

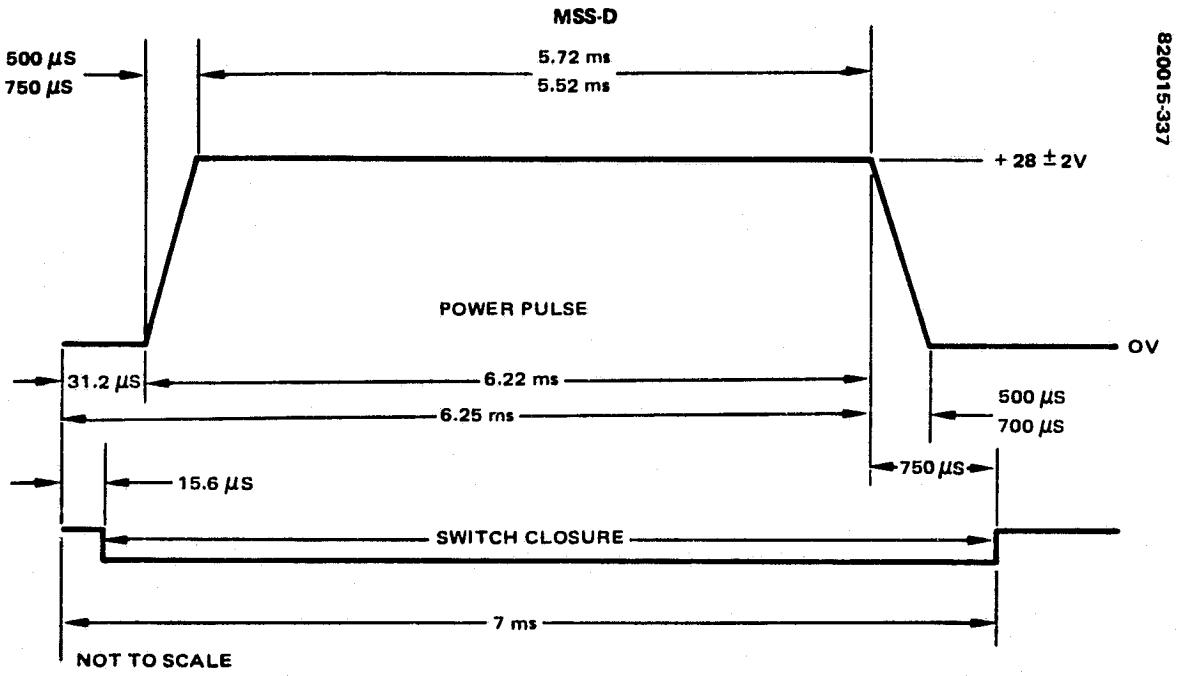

FIGURE 6. COMMAND PULSE TIMING

The matrix A and matrix B are shown in Table 8.

MSS-D

3.2.2.2 Spacecraft Command Subsystem Interface. The MSS flight system shall be designed to receive commands from the spacecraft RIU.

3.2.2.2.1 Discrete Commands. The MSS flight system shall require not more than 62 redundant discrete commands for proper operation. These commands will be provided by redundant RIUs. The signal characteristics are as follows:

a) Switch Closure Outputs - The discrete commands are single-ended transistor switch signals. The switch is an open collector output that is normally open. A command or TM word from the CU causes the switch to connect the output to signal ground. Since the RIU is power strobed, the MSS must complete the switching transistor collector circuit, e.g., by providing a pull-up resistor from the switch signal to the MSS positive power supply voltage and to the MSS logic circuitry. These signals have the following characteristics:

V_{oh}(inactive state)	Typical +5.0 Vdc +30.0 Vdc max.
I_{oh} (inactive state)	300 μA max @30 Vdc
V_{ol}(active state)	0.5 Vdc max @20.0 mA
Discrete commands	200 mA, max
Discrete command enable duration	See Figure 6.

b) Command Pulses - Three individually switched +28 volt dc pulses, dc isolated from the unregulated +28 volt dc power source, shall be used to drive the MSS command relays. One of the three switched pulses is grouped with 32 discrete commands such that signal return is connected to the pulse source through any one of the even numbered transistor switch closures (assumes commands are numbered 0 to 63.) The second of the three pulses is similarly grouped with the first 24 of the 32 odd numbered commands. The third pulse is grouped with the remaining eight odd numbered commands. Note that only 62 commands are available to the user (MSS). Signal return shall be connected directly to the pulse source through a selected discrete command switch closure. The circuit is capable of surviving a short circuit to ground on the

output for an indefinite time. The pulse has the following characteristics:

V_o (inactive state)	0.5 Vdc maximum
V_o (active state)	28 ± 2 Vdc nominal
Source impedance	$\leq 100\ \Omega$
Current drive capability	200 mA minimum
Pulse duration	6.5 to 7.0 ms
Number of outputs	3

Comment

MSS-C has a matrix command system and the associated matrix decoding network to route the received command pulse to the appropriate relay. MSS-D has individual command lines coming from the spacecraft to actuate individual relays. Extensive rewiring on MSS-D was necessary to accommodate the new command philosophy. The change in pulse length from 40 ms on MSS-C to 6.5 ms on MSS-D necessitated the building of pulse stretchers to develop a high enough energy pulse to actuate the high current relays in the primary power supplies.

3.1.11 Telemetry

MSS-C

3.2.2.3 Spacecraft Telemetry Subsystem Interface. The MSS flight subsystem shall be designed to provide outputs to the spacecraft telemetry subsystem.

3.2.2.3.1 Telemetry Outputs. The characteristics of the telemetry outputs shall be as follows:

a. Analog

(1)	Range	0 to -6.375 vdc
(2)	Output impedance	10 K ohms maximum (to maintain accuracy)
(3)	Load impedance	1 M ohm sampling. 10 M ohm nonsampling
(4)	Resolution	25 mv

b. Digital (single bit words)

(1)	OFF condition	-0.5 ±0.5 vdc
(2)	ON condition	-7.5 ±2.5 vdc
(3)	Output impedance - ON	1 M ohm, maximum
(4)	Output impedance - OFF	50 K ohm, maximum

MSS-D

3.2.2.3 Spacecraft Telemetry Subsystem Interface. The MSS flight system shall be designed to provide outputs to the spacecraft telemetry subsystem.

3.2.2.3.1 Telemetry Outputs. The characteristics of the telemetry outputs shall be as follows:

a) Analog

(1)	Range	0 to +5.12 Vdc
(2)	Source impedance	5 kΩ max
(3)	Load impedance	≥10 MΩ , nonsampling
(4)	Resolution (RIU)	8 bits

b) Digital (bilevel signals)

(1)	OFF condition	-1 to +1.5 Vdc
(2)	ON condition	+3.5 to +15 Vdc
(3)	Source impedance	5 kΩ max
(4)	Load impedance	≥10 MΩ, nonsampling

c) Conditioned analog

(1)	Range	0 to +5.12 Vdc
(2)	Source impedance	5 kΩ max
(3)	Sampling pulse	1 mA ±5μA (from RIU)
(4)	Sampling pulse duration	61.0 μsec max
(5)	Load impedance	≥10 MΩ, nonsampling

Comment

The telemetry design of MSS-D was almost completely changed from that of MSS-C. The polarity, source impedance, and scale factor of the bilevel and analog channels changed. The temperature telemetry was simplified by taking advantage of the spacecraft telemetry subsystem to provide the power source to excite the thermistors. The most challenging redesign was to determine simple methods to invert the polarity of the analog functions which had been derived directly from the voltage sources they were monitoring.

3.1.12 Backup Start-of-Scan Monitor Pulses

MSS-C

No requirement.

MSS-D

3.2.2.4.1 Backup Start-of-Scan Monitor Pulses. When the scan monitor OFF command is executed, the multiplexer will insert a substitute start-of-scan pulse at the nominal location of the scan monitor-generated start-of-scan pulse, 11.4 ms after beginning of preamble. If the multiplexer fails to receive a start-of-scan pulse when the scan monitor is ON, the multiplexer will insert a pseudo start-of-scan 18.4 ms after the beginning of preamble.

Comment

Hughes selected a commandable backup SMP-I. With this design concept when the scan monitor is on, the multiplexer operates as it did in former MSS models; i.e., if SMP-I from the scanner is not detected by the multiplexer, a pseudo SMP-I signal is put into the data stream 7 ms after the nominal SMP-I. If the scan monitor is commanded OFF, a substitute SMP-I signal is inserted in the data stream by the multiplexer at the nominal location of the scanner generated SMP-I, so that when the scan monitor is off, there will be nominally no loss of video data.

3.2 REQUIREMENTS VERIFICATION

Both the MSS-D protoflight and F-1 met the requirements of the NASA System Specification GSFC 430-D-205, Rev B, with few exceptions. The performance with respect to key parameters for both flight instruments is summarized in Table 2-1; and Table 3-1 gives a detailed requirements verification matrix including a cross reference to other MSS-D documents containing more detailed information about the verification of individual parameters.

3.3 MASS PROPERTIES

A mass model of the MSS-D scanner was constructed to predict weight, center of gravity, moments of inertia, and products of inertia. Actual weight, center of gravity, and two moments of inertia were measured on both the protoflight and flight model MSS

TABLE 3-1. VERIFICATION MATRIX

Test Requirements GSFC Specification 430-D-205, Rev. B	Reports/Remarks
3.1 Performance. The MSS system shall consist of a scanner and multiplexer.	Meets
The scanner shall be designed to operate in four spectral bands from 0.5 to 1.1 μm	Meets
The multiplexer shall process the scanner video data into a single bit stream suitable for modulating a broadband transmitter.	Meets
The MSS system shall be designed for a minimum in-orbit operational lifetime of one year, with a design goal of two years.	Meets
It shall meet all performance requirements in orbit.	TBD
It shall meet all performance requirements in a 1g field in air or vacuum.	Meets
It shall be designed for use on Landsat-D	Meets
3.1.1.1.1 Spectral Bands. The scanner shall operate in four spectral bands as defined below:	Meets,
a. Band 1 0.5 to 0.6 micormeters	Spectral Response, HS 248-6312, 7/24/80; and HS 248-6677, 6/10/81
b. Band 2 0.6 to 0.7 micrometers	
c. Band 3 0.7 to 0.8 micrometers	
d. Band 4 0.8 to 1.1 micrometers	
3.1.1.1.2 Detectors.	
Band 1 6 photomultiplier tubes	Meets
Band 2 6 photomultiplier tubes	
Band 3 6 photomultiplier tubes	
Band 4 6 silicon photodiodes	
3.1.1.1.3 Radiance/Signal Range. The scanner shall provide signals which are accurately related to radiance values in each spectral band. The maximum radiance levels are:	Meets;

	Maximum Radiance, mW/cm^2 - ster	Scanner Video Output (Low Gain) at Max Radiance
a. Band 1	2.48	4.0 V 5%
b. Band 2	2.00	4.0 V 5%
c. Band 3	1.76	4.0 V 5%
d. Band 4	4.60	4.0 V 5%

Gain and Offset Test Results, HS 248-6333, dated 8/5/80; and HS 248-6777, dated 10/14/81

3.1.1.1.4 Square Wave Response (Modulation Transfer Function). A response greater than 36 percent at the square wave spatial frequency corresponding to 102 μr bars, shall be provided. The response shall be degraded by approximately 20% at spacecraft temperatures of 5° and 35°C.	Meets; System Tests, Data Set 4, 5/81 and 9/81
3.1.1.1.5 IFOV. The nominal instantaneous fields of view (IFOV) shall be 117.2 μr for Bands 1 to 4.	MSS-D Fiber Optics, HS 248-0037, dated 1/12/78 and HS 248-0010-0611, p 2-6, dated 5/81; HS 248-0010-0604, 10/81
3.1.1.1.6 Field Stops. The field stops for bands 1 to 4 shall consist of square fiber optics, arranged in a 4 x 6 matrix. Each band shall use six optical fibers and six uncooled detectors.	Meets
3.1.1.1.7 Optical System. A two-element reflective optical system shall be used	Meets, Ritchey-Crétien design

ORIGINAL PAGE IS OF POOR QUALITY

Table 3-1 (continued)

Test Requirements GSFC Specification 430-D-205, Rev. B	Reports/Remarks
3.1.1.1.8 Scan Mirror Assembly. The following parameters define the scan mirror assembly functional characteristics: a. Scan frequency — 13.62 Hz ±0.01% b. Scan angle across scene — 14.90 ±0.06° c. Timing format — Figure 3.1.1.1.8-1 (GSFC 430-D-205, p 10) d. Active scan period — 31.5 ms, minimum; 34.0 ms, maximum	Meets; Test procedure 32238-021; Multiplexer Acceptance Test, HS 248-1087 dated 2/2/81, and HS 248-1139, dated 12/2/80 Meets, by design Scan Mirror Acceptance Test, HS 248-0810-2, dated 4/81, and HS 248-1023-2, dated 10/81
3.1.1.1.9 Geometric Fidelity. Geometric fidelity shall be defined by: b. Line length variation — 42 μr rms over 100 scans. d. Scan repeatability — Scan angle versus time repeatable within 24 μr, rms, over 100 scans e. Scan nonlinearity — For the linear portion of the forward scan, the repeatable scan rate shall not deviate more than +2.4, -5.0% from the mean scan rate f. Cross-scan motion — The center to center spacing between line groups (6 lines) shall not vary from nominal by more than 33 μr (1 σ). Systematic linearity shall be within ±200 μr (peak error)	Meets; System Test Data 5/81, data set 0, data set 1 System Test Data 9/81, data set 0, data set 1
3.1.1.1.10 Scan Monitor. An indication of beginning of scan, center of scan, and end of scan shall be provided by pulses from the scanner to the multiplexer on a single output over the temperature range specified in 3.1.2.3.1.	Meets; STRs HS 248-1126-26, dated 2/20/81, and HS 248-1126-32, dated 3/2/81; HS 248-0010-0804, dated 10/81 (p 2-27) Meets,
3.1.1.1.11 Optical Filter Characteristics 1) Absolute Transmission — for each band shall be 70% minimum at the peak of the spectral response characteristics. 2) Spectral Flatness — shall be maintained to ±5% over the central 70% bandwidth region for bands 1, 3, and 4; ±7.5% for band 2. 3) Half-Power Points — the half-power transmission points (50% of peak transmission) shall be within ±0.01 μm of the spectral end point (band edge) designated in 3.1.1.1.1. 4) Band Edge Slope — the wavelength between 5% absolute and 50% of peak transmission shall be less than 0.02 μm on the short wave side for Bands 1 to 3, and on the long wave side 0.04 μm for Band 1, 0.045 μm for Band 2, and 0.05 μm for Band 3. Band 4 shall be 0.035 μm on the short wave side, and will have no slope requirements for the long wave side. 5) Spurious Response — Response outside the 5% points shall not exceed 5% of the in-band spectral response for a solar equivalent input over the wavelength interval from 0.4 to 0.8 μm.	Spectral Filter Analysis, HS 248-6455, dated 11/30/80 HS 248-6598-1, dated 6/9/81
3.1.1.1.12 Butterworth Filter. The response between 1 kHz and 100 kHz in Bands 1 to 3, and between 1 kHz and 60 kHz in Band 4, shall conform to the response of the ideal 3-pole Butterworth filter with a pole frequency of 42.3 kHz within ±11% frequency deviation or ±0.5 dB amplitude variation, whichever is greater.	Meets; Photodiode Preamp Analysis, HS 248-6098, 2/26/80
3.1.1.1.13 Lamp Calibration System (Bands 1-4). The scanner shall have internal redundant calibration lamps and a continuous neutral density filter (calibration wedge) to introduce a calibration wedge output into the video data stream of Bands 1 through 4 at the end of every other active scan period. The neutral density filter shall provide a continuous monotonically decreasing attenuation with a maximum to minimum transmission ratio of not less than 55.	Meets; Internal Calibration System NDF, HS 248-6454, dated 11/13/80 and HS 248-1404, dated 8/12/81
3.1.1.1.17 Short Term Uniformity of Channel Response. The MSS system output shall not vary more than ±1 percent of full scale throughout the scan for a constant radiance input.	Meets.
3.1.1.1.18 Selectable Gain Levels. A one-step commandable gain change by a factor of three shall be provided in Bands 1 and 2.	Meets; Dwg. 49107; System Test Data, 5/81 and 9/81
3.1.1.1.19 Witness Mirror. A witness mirror shall be mounted on the cover plate attached to the earth-side of the scanner housing.	Meets
3.1.1.1.20 Purge. A single fitting shall be placed in the scanner housing to purge the telescope and aft housing area with nitrogen. The purge fitting shall be located such that it is readily accessible when the MSS is installed in the spacecraft.	Meets

ORIGINAL PAGE IS OF POOR QUALITY

Table 3-1 (continued)

Test Requirements GSFC Specification 430-D-205, Rev. B	Reports/Remarks
3.1.1.3.1 Signal Processing. The multiplexer shall sample all video channels and encode them into a single binary bit stream. Sampling of each line shall be initiated by the scan monitor line start pulse, supplied by the scanner.	Meets
3.1.1.3.2 Timing Signals. The multiplexer shall process the three scan monitor pulses to a resolution of 400 nsec. Transmission of the midscan pulse shall be selectable by ground command.	Meets
3.1.1.3.3 Spacecraft Time Code. The multiplexer shall incorporate the spacecraft time code into the output data format. Timing and inout characteristics shall be as described in Figure 3.1.1.3.3-1 (GSFC 430-D-205).	Meets; STR 1126-33, dated 3/2/81; HS 248-0010-0804, dated 10/81
3.1.1.3.4 Sampling Rate. The output bit rate shall be 135 x 2^{13} times the mirror scan frequency. The sampling rate in each channel of bands 1 to 4 shall be not less than 1.4 samples per IFOV.	Meets; Multiplexer Acceptance Tests, HS 248-1087, dated 2/2/81, and HS 248-1139, dated 12/2/80
3.1.1.3.5 Clocking Reference. The multiplexer's internal clock shall provide a timing reference with a long-term stability of not less than 1 part in 10^4.	Meets; Multiplexer Acceptance Tests, HS 248-1087, dated 2/2/81, and HS 248-1327, dated 5/22/81; and HS 248-1139, dated 12/2/80
3.1.1.3.6 Data Transition Density. The format of the encoded data and coding and timing information shall be identical with the formats used in MSS-C.	Meets; System Test Data, May 1981 and September 1981
3.1.1.3.7 Input Switch Protection. The multiplexer shall not be damaged by the application of voltages in the range of ±28 volts for 30 seconds and ±15 volts continuously to an input switch.	Partially meets; request for waiver W045, 5/22/81
3.1.1.3.8 Quantization. Each sample shall be encoded into a 6-bit word.	Meets; drawing 3248111
3.1.1.3.9 Signal Processing Modes. The multiplexer shall provide both a linear and a signal compression mode of processing for the video signal in Bands 1, 2, and 3. The two modes shall be selected by ground commands.	Meets; Drawing 3248051 and System Test Data, May 1981 and September 1981
3.1.1.3.10 Encoded Data Accuracy. The MUX shall convert the video data in the frequency range of dc to 42.3 kHz into 6-bit digital words. The output shall be within ±130 mV ± 1/2 LSB of the nonlinear transfer function value for input voltage levels of 2, 1, 0.5 volts and 0.25 volts and ± 4.5 volts and ± 45 mV ± 1/2 LSB of the transfer function value for input voltage levels of 0 and 4 volts. The output shall be repeatable within ±15 mV ±1/2 LSB, for any multiplexer, at the input voltage levels of 4, 2, 1, 0.5 V 0.25 V, and 0 volts	Meets; Multiplexer Acceptance Tests, HS 248-1087, dated 2/2/81, and HS 248-1139, dated 12/2/80
3.1.1.3.11 Sampling Sequence. The multiplexer sampling sequence shall be as shown below:	Meets; Multiplexer Acceptance Tests, HS 248-1087, dated 2/2/81 and HS 248-1139, dated 12/2/80

MNFS	1A	2A	1B	2B	...	1F	2F	3A	4A	3B	4B	...	3F	4F
5A	1A	2A	1B	2B	...	1F	2F	3A	4A	3B	4B	...	3F	4F
5B	1A	2A	1B	2B	...	1F	2F	3A	4A	3B	4B	...	3F	4F
$\overline{\text{MNFS}}$	1A	2A	1B	2B	...	1F	2F	3A	4A	3B	4B	...	3F	4F
5A	1A	2A	1B	2B	...	1F	2F	3A	4A	3B	4B	...	3F	4F
5B	1A	2A	1B	2B	...	1F	2F	3A	4A	3B	4B	...	3F	4F

ORIGINAL PAGE IS OF POOR QUALITY

Table 3-1 (continued)

Test Requirements GSFC Specification 430-D-205, Rev. B	Reports/Remarks
3.1.1.3.12 Shutter Synchronization Signal. The multiplexer shall provide to the scanner a shutter synchronization signal which shall consist of a pair of complementary current source outputs.	Meets; STR HS 248-1126-19, dated 2/14/81
3.1.1.3.13 Pseudo SMP-1. The timing of the MUX-generated beginning of scan scan monitor pulse shall occur no later than 3 ms after the normal time of occurrence of SMP-1.	Meets; Multiplexer Acceptance Tests, HS 248-1087, dated 2/2/81 and HS 248-1139, dated 12/2/80
3.1.1.4.1 Registration. Registration for identical points on maps produced from each spectral band shall be maintained within 15 percent of an IFOV, both along and across the orbit track.	Meets; Band-to-Band Registration, HS 248-6605, 4/3/81 and HS 248-6756, 8/10/81
3.1.1.4.2 Signal-to-Noise Ratio.	

LINEAR MODE PEAK SIGNAL TO RMS NOISE RATIO

	Band			
	1	2	3	4
High radiance level: MSS system S/N output*	89	73	50	104
1/2 high radiance level: MSS system S/N output*	54	46	33	54

*After D/A conversion

COMPRESSION MODE PEAK SIGNAL TO RMS NOISE RATIO

	Band		
	1	2	3
High radiance level: MSS system S/N output*	75	65	47
1/2 high radiance level: MSS system S/N output*	43	38	30

*After D/A conversion (decompression)

NOTE: All S/N values in these tables may be reduced approximately 15 percent at spacecraft temperatures of 5° and 35°C.

ORIGINAL PAGE IS OF POOR QUALITY

Meets (mostly);

TV System Test Data 5/9/81 – 5/19/81, dated 5/28/81; and 9/8/81 – 9/21/81, HS 248-1438, dated 9/24/81 occasional out-of-specification conditions in channels 1, 2, 3, 7, 9, 11, and 19; see FR 5120, 5123, 5124, 4126, 5127, 2490, 5132, 5135, and 5142. HS 248-1328, dated 5/28/81 and HS 248-1438, dated 9/24/81

Table 3-1 (continued)

Test Requirements GSFC Specification 430-D-205, Rev. B	Reports/Remarks
3.1.1.4.4 Internal Calibration Accuracy. After sun calibration, for a period of 54 minutes beginning 3 minutes after turnon, the calibrate wedge output shall provide the means to calibrate gains and offset values for Bands 1 through 4 (see 3.1.1.1.2) within the relative accuracies stated below. The amplitude range of the calibration signal in the low gain mode shall vary from a maximum of greater than 3.5 volts to a minimum of less than 0.5 volt, and in the high gain (Bands 1 and 2 only) mode from a maximum of greater than 4.0 volts to a minimum of less than 2.0 volts.	Meets: Test Procedures 16794 (SBRC, 11/10/80 16894 (SBRC), 11/7/80 16895 (SBRC), 11/10/80
a. Channel to channel (within a band) (1) Ratio of gains between channels: 2.0 percent peak-to-peak (2) Offset difference between channels: ±15 mV	System Test Data, May 1981 and September 1981
b. Band-to-Band (1) Ratio of band average gain (average of 6 channels) between bands: 3.0 percent peak to peak (2) Band average offset (average of 6 channels) between bands: ±30 mV	
c. Stability of any channel (1) Gain change: ±2.0 percent over the 54 minute period (2) Offset change: ±12 mV over the 54 minute period	
3.1.2.1 Maintainability-Interchangeability. Maintainability and interchangeability shall be provided for in both the MSS and the ground equipment. No special tools shall be required for mounting or disassembly.	Meets
3.1.2.2 Useful Life. The useful life of the MSS system shall be a minimum of 1 year in orbit with a design goal of 2 years, at an average 1/3 orbital duty cycle.	TBD
3.1.2.3.1 Thermal. The MSS system shall meet the requirements of the specification when operating with the spacecraft mounting and radiative interface at 20°C ±10°C, and shall not suffer any permanent degradation when operated with the spacecraft mounting and radiative interface at 20°C ±20°C.	Meets: T/V Test 5/9/81 — 5/19/81, HS 248-1328, dated 5/28/81, and T/V Test 9/81, HS 248-1438, dated 9/24/81
3.1.2.4.2 Pressure. The MSS shall not suffer any detrimental effects from exposure to ambient pressures from 1 atmosphere to 10^{-10} Torr for the design life of the equipment and shall meet all requirements of the specification when operating in ambient pressures of 1 atmosphere or 10^{-5} Torr, or less.	Meets; T/V Test 5/9/81 — 5/19/81, HS 248-1328, dated 5/28/81, and 9/8/81—9/21/81, HS 248-1438, dated 9/24/81
3.1.2.4.3 Humidity. The MSS shall not suffer any detrimental effects from exposure to an atmosphere having 0 to 60% RH over the temperature range from 0° to 40°C.	Meets, by design
3.1.2.5 Natural Radiation. The MSS shall operate within specification for 12 months with a design goal of 24 months when exposed to worst-case radiation levels expected at 705 km altitude during 1980-1990.	Meets, by design
3.1.2.6 Transportability. The MSS shall be transportable in any attitude, at temperatures between 0° and 40°C; relative humidity shall be maintained below 60%.	Meets, by design
3.1.2.7 Human Performance. Full consideration shall be given to human engineering requirements, wherever possible.	Meets, by design
3.1.2.8 Safety. The MSS equipment shall be designed to ensure maximum safety to personnel and equipment.	Meets, by design
3.2.1.1 Mechanical Interface. Lift-off weight of the MSS shall be minimized. It shall not exceed 143 lbs. Weight and center of gravity shall be measured and reported. Moment-of-inertia about one principal axis shall be measured; calculations shall be provided for all three principal axes and their cross-products.	Meets; 122.3 lbs Protoflight; 121.2 lbs. F-1 MSS-D Mass Properties, HS 248-1337, dated 6/8/81 and HS 248-1459, dated 10/15/81
3.2.1.3 Interface Documentation. An interface specification document as well as interface control drawings and schematics shall be provided. A 3-stage system for release of interface information, shall be provided.	Meets; IF 32238-005, drawing 3617120-400, drawing 3617140-400
3.2.2.1 Spacecraft Power. The MSS shall operate from the 28 V bus, provided by the Landsat-D spacecraft. Power consumption shall not exceed 85 W — operational average (over one scan cycle); 3 W — stand-by power	Meets: Operational 80 W Stand-by 1 W

ORIGINAL PAGE IS OF POOR QUALITY

Table 3-1 (continued)

Test Requirements GSFC Specification 430-D-205, Rev. B	Reports/Remarks
3.2.2.2 Command Interface. The MSS shall be designed to operate with a redundant Remote Interface Unit (RIU) system.	Meets
3.2.2.2.1 Command Functions. The MSS shall, as a minimum, use the following commands: MSS — On/Off Each band — On/Off Gain — Bands 1 and 2 Low and High Gain SMA and MUX — Normal/Inhibit Electronics — On/Off Multiplexer — Linear/Compression	Meets; IF 32238-005, Table IV; System Test Data, May 1981 and September 1981
3.2.2.3 Telemetry Interface. The MSS shall provide telemetry for evaluation of instrument status. Critical telemetry points shall be available full-time. Telemetry outputs shall not be damaged by shorting to bus, ground, or other telemetry points, nor shall MSS performance be affected. Telemetry shall be compatible with and stay within the capability of one RIU (and expander unit).	Meets; IF 32238-005; System Test Data, May 1981 and September 1981
3.2.2.4 Test Points. Test points shall be provided, as required, to determine MSS status and to permit instrument alignment.	Meets
Test points shall be short-circuit protected; MSS shall function with any test point shorted to bus, ground, or another test point.	See request for waiver No. W046, dated 5/22/81
4.1 R&QA. MSS reliability and quality assurance shall be in accordance with GSFC 430-D-330A, 5/78	Meets; Product Assurance Plan, HS 248-0034, dated May 1978
4.2.1 Test Plan. A test plan shall be generated to define the alignment, calibration, and tests to be performed on the major elements, as well as the fully assembled MSS.	Meets; System Test Plan, 3617000-600A, dated September 1979.
4.2.2 Calibration. Calibration of all appropriate MSS system performance parameters shall be performed.	Meets
4.2.3 Pictorial Displays. The MSS output shall have negligible coherent noise in all four bands for all values of radiance, including zero.	Meets; System Test Data, May 1981 and September 1981
4.2.4 Test Procedure. Test procedures shall be provided for each test phase, including step-by-step instructions for alignment, calibration, or test, outlined in the Test Plan.	Meets
4.3 Environmental Testing. Environmental testing of MSS shall be performed in accordance with GSFC 430-D-340B, 5/78.	Meets; Vibration: Mux—Sine & Random, see OCHR Scanner—Sine only HS 248-1180, 2/12/81 and HS 248-1433, 9/21/81 Acoustic: Scanner only—HS 248-1319, 5/19/81 and HS 248-1423, 9/3/81 EMI: HS 248-1213, dated 3/13/81; and HS 248-1414, dated 8/26/81 Thermal/Vacuum: System T/V Test Data, May 9-19, 1981 and September 8-21, 1981 Acceleration: HS 248-6656, dated 5/18/81

ORIGINAL PAGE IS OF POOR QUALITY

Table 3-1 (continued)

Test Requirements GSFC Specification 430-D-205, Rev. B	Reports/Remarks
5.1 Handling. A specification shall be prepared for handling, packaging, and delivery of the MSS. The specification shall provide for a safe environment for the instrument.	Meets; Handling, Moving, and Transportation Procedure, TP 32238-100, dated 9/30/80
5.2 Shipping Container: Each MSS shall be packaged in a resuable container.	Meets
6. Program Reviews. Program reviews will be as specified in the contract schedule.	Meets

ORIGINAL PAGE IS OF POOR QUALITY

ORIGINAL PAGE IS
OF POOR QUALITY

TABLE 3-2. MASS PROPERTIES SUMMARY

System	Weight, lb	Center of Gravity, in			Moments of Inertia, lb-in^2			Products of Inertia, lb-in^2		
		$\bar{X}$	$\bar{Y}$	$\bar{Z}$	I_{xx}	I_{yy}	I_{zz}	I_{xy}	I_{xz}	I_{yz}
Scanner, calculated	122.4	+0.41	+11.64	+0.08	12,600	4,900	11,700	-300	-90	500
Protoflight, measured										
Scanner	116.2	+1.70	+11.28	-1.70	12,800		12,500			
Multiplexer	5.5									
Total	121.7									
Flight-1, measured										
Scanner	115.0	+1.61	+11.32	-1.72	12,700		12,300			
Multiplexer	5.6									
Total	120.6									

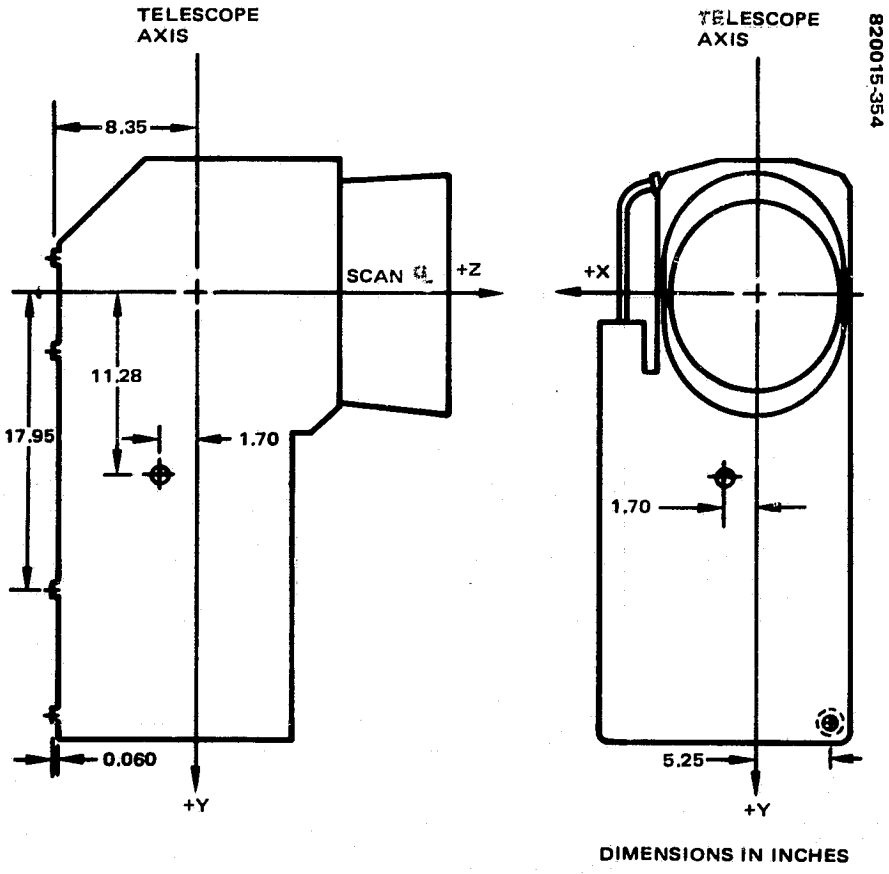

FIGURE 3-1. PROTOFLIGHT CENTER-OF-GRAVITY LOCATION

ORIGINAL PAGE IS
OF POOR QUALITY

scanners. For the multiplexers only the actual weights of the flight hardware were taken.

The results of the mass properties analysis and tests are summerized in Table 3-2. The center of gravity location for the protoflight is shown in Figure 3-1 together with the reference coordinate frame used for the measurements. The set of coordinates in the figure is identical to that in the interface control drawing, 3617120-400. The auxiliary dimensions on the figure establish the location of the coordinate reference frame with respect to the MSS mounting interface plane. The moments of inertia given in Table 3-2 are for a coordinate system whose origin is at the center of gravity and whose axes are parallel to the coordinates of Figure 3-1.

3.4 SYSTEM ECCENTRICITIES

During development and testing, three peculiarities of system behavior, which will show up in the video data stream, were noted. These peculiarities are discussed here in hopes of reducing confusion later if these effects are recognized in the Landsat data stream.

The first of these peculiarities has to do with the format of the black and white codes put out by the multiplexer to mark midscan and endscan. In the serial video data stream these codes are 100 words of black (level 0), followed by 100 words of white (level 63), and appear in the demultiplexed data stream as 4 words of black followed by 4 words of white in each video channel. On previous multispectral scanners the words immediately preceding and following the 200 words of black and white were normal video words. On MSS-D the words preceding the black and white code are normal, but the one word in the serial data stream immediately following the last word of white is a mixed word. Its most significant three bits are white and its least significant three bits are video. It usually comes out as level 56 (111000) and appears randomly in each demuxed video channel with a probability of 1/25. This peculiarity was introduced into the multiplexer analog-to-digital converter by a design change to correct a previously existing problem.

A second peculiarity of the design also involves the analog-to-digital converter in the multiplexer. When a video level less than 1/8 scale (001000 in the digital output) is input to the multiplexer, it will infrequently encode this output as exactly a 1/8 scale output, a level 8 output. This peculiarity was present and noted in MSS multiplexers predating MSS-D. An investigation was performed on the engineering model multiplexer to isolate the source of the fault. The fault was found in the storage registers downstream of the comparators in the A/D converter. The specific cause of the fault is a negative ringing overshoot on the clock pulse line to these storage registers causing one of the J-K flip-flops in the register to end up in an incorrect state. A temporary fix, which clipped off the negative overshoots on the clock pulses, was installed on the engineering model, and it was shown to eliminate the problem. Because of the benign nature of the anomaly and the cost and schedules implications for installing and testing the fix on the flight hardware, it was not retrofitted with the change. Tests on the two flight units indicated that the anomaly occurred with a lower frequency on the unit on Landsat-D, S/N 003 multiplexer, than on the unit slated to go on Landsat-D', S/N 002 multiplexer.

ORIGINAL PAGE IS
OF POOR QUALITY

The third peculiarity, which will be evident is the MSS-D video data stream, has to do with the structure of the internal calibration signal present in every other line of MSS video data. The calibration signal is produced by passing the neutral density filter between the internal light source and the inputs to the detectors in the focal plane of the system. The light intensity seen by the detectors is a decaying exponential in time. The neutral density filters used on MSS-D to generate the calibration exponential have several small pinholes in the filter material which cause local irregularities in the calibration exponential. The most pronounced of these irregularities is in band 4 of the F-1 instrument. Shown in Figure 3-2, taken from the F-1 Radiometric Calibration and Alignment Handbook, is a plot of the calibration words from channel 20 (band 4, channel 2) used by Hughes during testing of the F-1 instrument. The 20 words plotted are the average value of every 24th word from the calibration wedge selected from a portion of the exponential to cover the dynamic range of the instrument. Note that word number 9 displays the effect of the pinhole by having a several percent higher value of radiance than would be predicted by the overall shape of the curve.

The effect of a pinhole is different for each MSS channel calibration signal. Because of the location of the neutral density filter in the internal calibration optical train, each channel senses a slightly different area of the neutral density filter as it sweeps by in front of the focal plane. Because of the way in which the neutral density filter is scanned across the focal plane, the effects of a pinhole tend to be similar for every channel in a spectral band and vary rapidly from one band to the next. Although the nonuniformities introduced by the pinholes are time invariant and hence the calibration data from the affected words are valid, the using community might find it more convenient to select their calibration information from words on the smoother part of the exponential curves. A more complete survey of the nature of the internal calibration curves is found in the MSS Calibration and Alignment Handbooks.

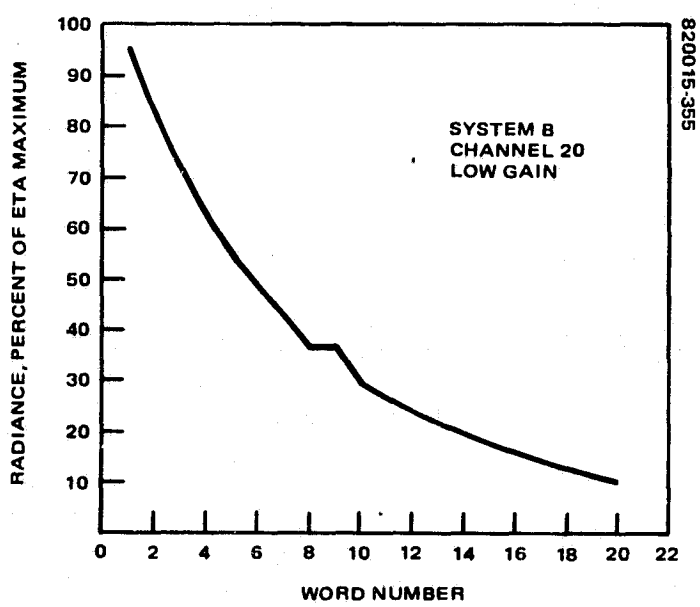

FIGURE 3-2. F-1 CALIBRATION WEDGE PINHOLE

ORIGINAL PAGE IS
OF POOR QUALITY

4. MSS-D SYSTEM TEST

4.1 TEST PHILOSOPHY

The MSS-D test philosophy was based on the MSS-C Test Program Plan. The MSS-C test plan was used as a baseline document; deviations from the MSS-C baseline were incorporated as required to accommodate changes from the MSS-C design and to include environmental constraints introduced by the Landsat D spacecraft design and the new family of launch vehicles. An engineering model development program and a protoflight qualification program were proposed to develop and prove new designs and to qualify the system for operation in the new environments. No structural or packaging design changes were incorporated into the system to accommodate changes in the launch loads; therefore, the MSS-D protoflight qualification test program was planned to closely parallel the earlier MSS-1 prototype qualification test program, and the MSS-D F-1 flight acceptance program was planned to closely parallel the MSS-2 flight acceptance test program.

This same test philosophy was carried through to the unit/subsystem levels of testing. Unit level testing of the scan mirror assembly consisted of performance tests at ambient, high, and low temperatures. The multiplexer unit level tests consisted of performance tests at ambient, high, and low temperatures and a complete qualification or acceptance level vibration test. The radiometer received no environmental tests at unit level. Performance tests were conducted on the radiometer under ambient temperature and pressure conditions to verify unit performance characteristics and unit interface requirements.

With the exception of the multiplexer vibration tests, all formal environmental tests were conducted at the scanner or system level of assembly. Since during its lifetime the system could be expected to operate in adverse electromagnetic interference (EMI), vacuum, and thermal conditions, performance criteria were included in these environmental exposures. During the dynamic environments of acoustic and vibration, the system was powered, but the pass/fail criteria for the dynamic environments were that the system survive without damage and with no performance degradation.

ORIGINAL PAGE IS
OF POOR QUALITY

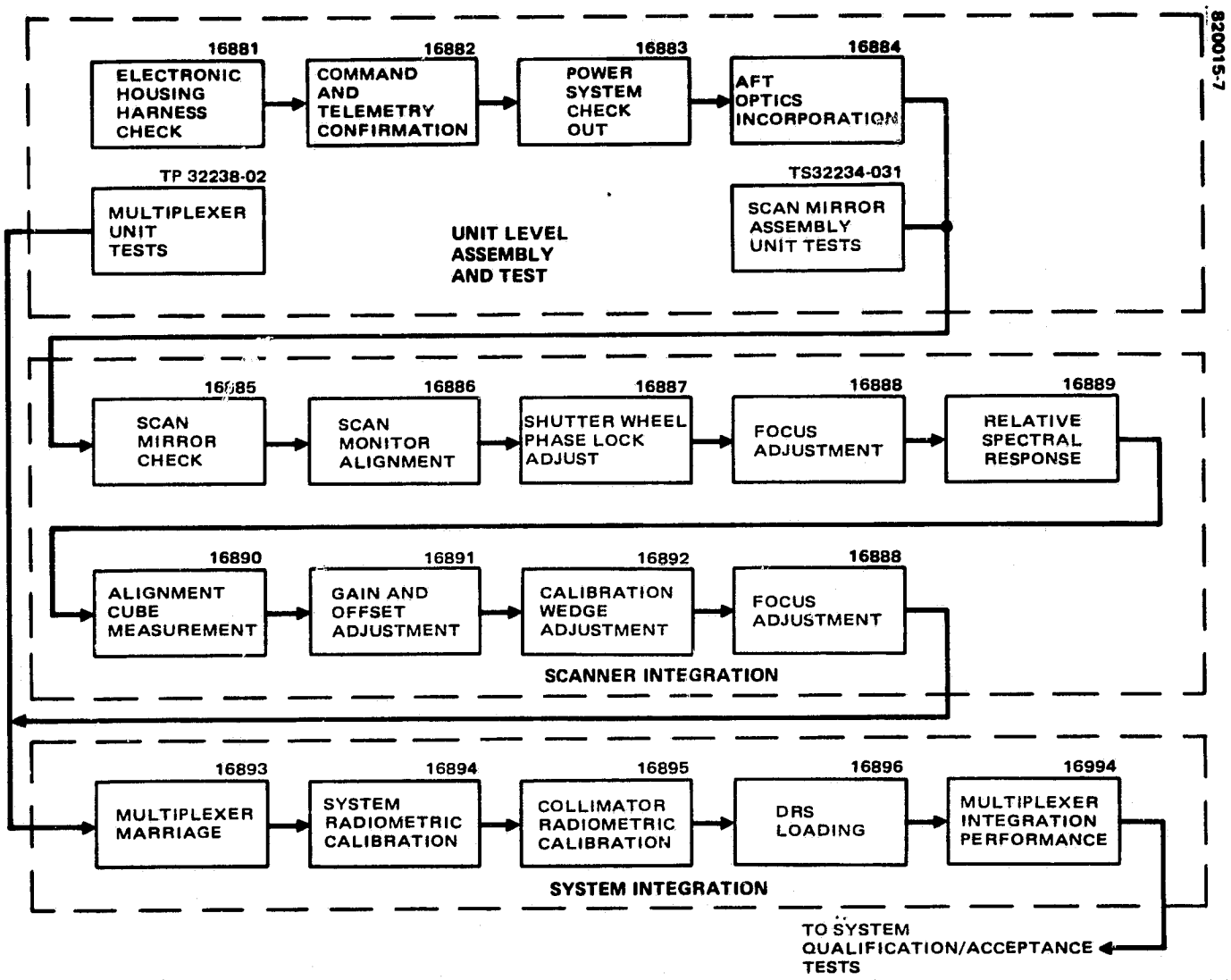

FIGURE 4-1. UNIT/SUBSYSTEM INTEGRATION AND TEST

ORIGINAL PAGE IS
OF POOR QUALITY

4.2 TEST TYPES

Development Tests

Developmental tests were conducted on component and unit level hardware for which new designs were required because of new spacecraft interfaces in telemetry, command, or power, or because of new operational constraints, i.e., lower orbital altitude. The developmental tests were less formal than the qualification or acceptance tests and were conducted for engineering evaluation of the new or changed design concepts. Except for the flex pivot tests, which were conducted on the engineering model scan mirror assembly mounted in the structural test model, most system level development tests were confined to peformance tests which verified unit performance in the system configuration.

Integration Tests

Integration tests included adjustments, alignments, functional tests, and performance tests. These tests were conducted in accordance with formal released and controlled procedures, under the surveillance of Quality Assurance personnel, during and subsequent to the assembly of lower level assemblies into units, subsystems, and systems. The integration tests verified that the higher level assemblies had been properly integrated. Figure 4-1 shows the integration and test flow associated with the radiometer unit assembly, the scanner subsystem integration, and the MSS-D system integration.

Protoflight Qualification/Acceptance Tests

Protoflight qualification/acceptance tests were conducted to verify the design adequacy of the protoflight system, to demonstrate a minimum level of equipment capability, and to disclose workmanship defects in time to permit correction prior to the end use of the MSS-D system. The tests were designed to verify survivability of the system in the environmental stresses predicted for shipment, handling, launch, ascent, and orbit, and to evaluate system performance in selected operating modes, under launch, ascent and on-orbit environmental stresses. The actual test conditions were intended to be more severe than predicted operating conditions to provide assurance of disclosing any design weaknesses, thus compensating to some extent for the statistical limitations of a small sample size. These conditions, however, were not intended to be severe enough to exceed reasonable safety margins or to excite unrealistic modes of failure. Since the protoflight was intended to be a flight model as well as a qualification test model, the environmental test levels were full qualification levels and were applied only for acceptance test durations.

4.3 SYSTEM TEST APPROACH

The MSS performance tests changed only in details throughout the years since the qualification tests of the first MSS prototype. The approach then and during the MSS-D program was to organize the tests into time-based units approximating a normal orbital period, about 99 minutes, referred to as "standard orbits." As in normal operations on orbit, the system was constrained to an approximate one-third active duty cycle, that is, about 33 minutes "on" for data acquisition and about 66 minutes "off."

ORIGINAL PAGE IS
OF POOR QUALITY

TABLE 4-1. STANDARD ORBITS

Standard Orbit	Test Mode	Primary Power Supply	Shutter Monitor Source	Scan Monitor Source	PMT High Voltage Supplies	Calibration Lamp	Simulated Spacecraft, Bus, Vdc	Multiplexer Output Line
1	A	A	A	A	A	A	28.0 ±0.5	4
2	B	B	B	B	B	B	28.0 ±0.5	4
3	A Low	A	A	A	A	A	21.5 ±0.5	1
4	B Low	B	B	B	B	B	21.5 ±0.5	1
5	A High	A	A	A	A	A	34.5 ±0.5	2
6	B High	B	B	B	B	B	34.5 ±0.5	2
7	AB	A	A	A	B	A	28.0 ±0.5	3
8	BA	B	B	B	A	B	28.0 ±0.5	3

Abbreviated system performance test – standard orbits 1, 2, 7, and 8.
Complete system performance test – standard orbits 1 through 8.

TABLE 4-2. STANDARD DATA SETS

Data Set	Collimator			Multiplexer Mode/Scanner Gain Selection	Data Reduction Procedure	System Parameters Evaluated
	Neutral Density Filter, %	MTF Reticle Position	Flooding Lamp			
0	50	Open	Off	Linear/Low	2	Scan repeatability, line length variation, mean line length
7	50	Chevron	Off	Linear/Low	4	Cross-axis jitter
1	50	Open	Off	Linear/Low	1	Signal level, noise, signal-to-noise ratio, 20 level calibration wedge, corrected signal level, deviation band to band (DBB), deviation channel to channel (DCC)
6	50	650′	Off	Linear/Low	3	MTF, MTF signal level, MTF noise
5	50	450′	Off	Linear/Low	3	MTF, MTF signal level, MTF noise
4	50	236′	Off	Linear/Low	3	MTF, MTF signal level, MTF noise
22	10	Open	Off	Linear/High	1	Signal level, noise, signal-to-noise ratio, 20 level calibration wedge, corrected signal level, DBB, DCC
23	10	Open	Off	Compression/ High	1	Signal level, noise, signal-to-noise ratio, 20 level calibration wedge, corrected signal level, DBB, DCC
3	50	Open	Off	Compression/ Low	1	Signal level, noise, signal-to-noise ratio, 20 level calibration wedge, corrected signal level, DBB, DCC
24	Opaque	Open	On	Linear/Low	1	Average signal level, channels 1 to 12*
25	Opaque	Open	On	Linear/Low	1	Average signal level, channels 13 to 24*
16	25	450′	On	Compression/ High	None	Ground processing equipment (GPE) picture

*Accumulation of data for collimator calibration.

ORIGINAL PAGE IS
OF POOR QUALITY

Implementation of this simulated orbital testing resulted in establishment of the standard orbits and standard data sets, the standard orbit made up of a series of standard data sets. In general, the standard orbit defines the flight hardware configuration, i.e., ON/OFF configuration of redundant functions within the MSS (A or B), bus voltage levels, and the multiplexer output lines to be used for data collection. The standard data set defines the test equipment configuration, the scanner gain selection for bands 1 and 2 (high or low), the multiplexer mode (linear or compression), and the data reduction procedure for automated data reduction. The data reduction procedure defines the calculations to be performed in the data reduction system computer on a specific set of data to provide an output in terms of the system performance parameters, of interest. Each standard orbit is designed to evaluate all system performance parameters, and the standard data sets are tailored for the particular parameter to be measured.

Table 4-1 lists and defines standard orbits 1 through 8. These eight orbits comprise the complete system performance test. The abbreviated system performance test consists of standard orbits 1, 2, 7, and 8. Other standard orbits not described in Table 4-1, but used extensively throughout the test program, are 13, 14, 15, and 16, which comprise the system radiometric calibration test and are run against the integrating sphere. Orbits 27 and 28, which are run against the collimator during the collimator transfer calibration, are used to derive calibration coefficients for the collimator to be used in standard data reduction procedures.

Table 4-2 lists and defines the standard data sets and the sequence in which they are run during each standard orbit. In addition, the required data reduction procedure and the system performance parameters which are evaluated are listed for each data set.

Table 4-3 lists the performance parameters measured during the system performance test. Evaluation of these performance parameters establishes the operating characteristics of the MSS system.

Table 4-4 presents the system and test equipment configurations during the system radiometric calibration test orbits 13, 14, 15, and 16.

4.4 SYSTEM TEST FLOW DIAGRAM

Throughout the MSS-D program the planned test sequence was somewhat fluid in that new tests were proposed and in some cases incorporated into the sequence to augment or replace originally planned tests. Figure 4-2 is the planned engineering model test sequence. Initially the engineering model was to have been upgraded so that even the EMI/electromagnetic compatibility (EMC) tests could be conducted on it. The engineering model test program was planned as a method to get early engineering verification of new designs in the power supplies, the remote interface unit/scanner interfaces in command and telemetry, and the new two-bounce scan monitor. System integration and testing of the engineering model was totally eliminated from the MSS-D program, but was finally reinstated in a greatly reduced form. Some of the greatest value of the engineering model tests lay in the early checkout of the bench test equipment interfaces, data reduction software, and system performance test procedures, as well as verification of the redesigned scan monitor and the power, command, and telemetry interfaces.

ORIGINAL PAGE IS
OF POOR QUALITY

TABLE 4-3. SYSTEM PERFORMANCE PARAMETERS

1)	Signal-to-noise ratio (STN)
2)	Square wave response (MTF)
3)	Deviation band to band (DBB)
4)	Deviation channel to channel (DCC)
5)	Mean line length (MLL)
6)	Variation in line length (VLL)
7)	Scan repeatability (SRO)
8)	Cross-axis repeatability (CXAXO)

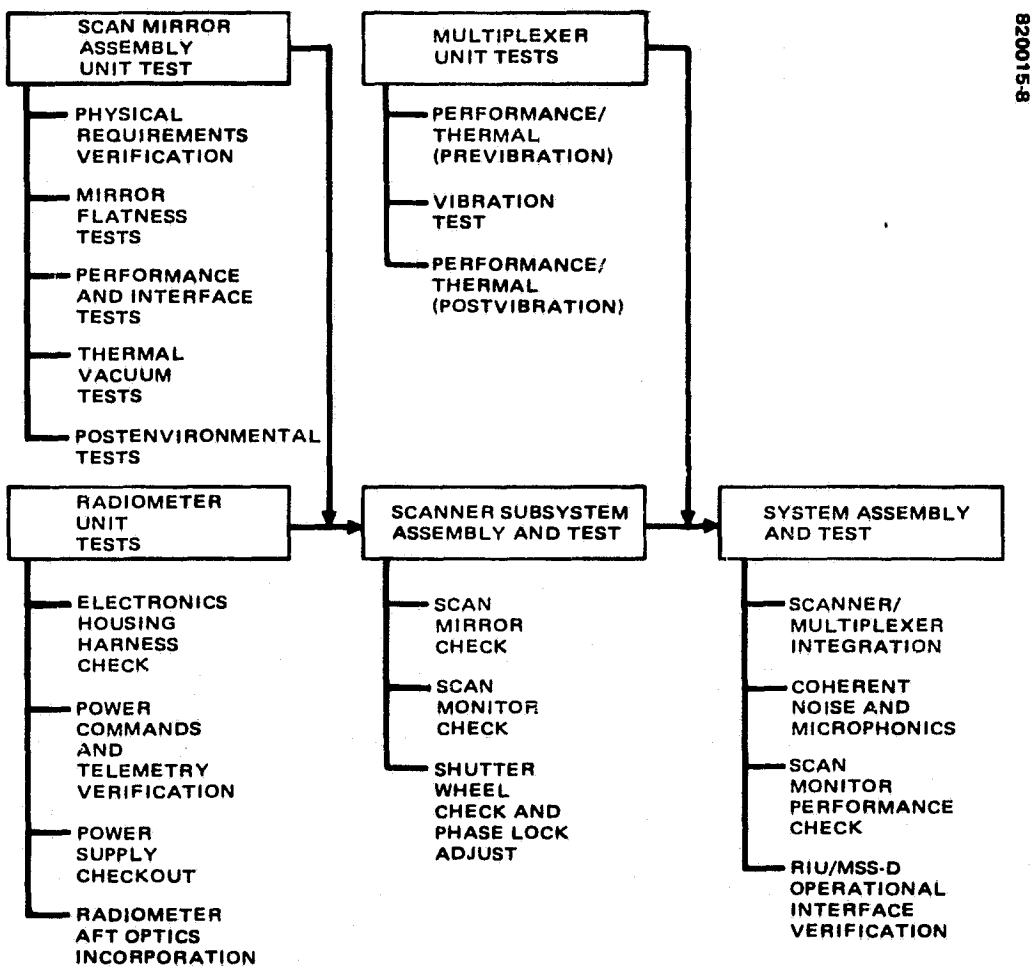

FIGURE 4-2. ENGINEERING MODEL TEST SEQUENCE

TABLE 4-4. SYSTEM RADIOMETRIC CALIBRATION TEST CONFIGURATION

Test Mode	Test Sequence Type	Data Set	Integrating Sphere Lamps	Multiplexer Mode/ Scanner Gain Selection	Data Reduction System Input Data	System Parameters Evaluated	Pictures		Remarks
							VPIR	GPE	
Alignment	—	—	6	Linear/Low	—	—	No	No	No video data taken
Conditioning	—	—	6	Linear/Low	—	—	No	*	Only continuous video tape made
Standard orbits 13 and 14									
Orbit 13 — Mode A	H1	100	12	Linear/Low	Video pulse and 20 level calibration wedge for channels 1—6	1 signal level, noise, STN ratio, 20 level calibration wedge	No	*	Video data mag tape required
Orbit 14 — Mode B									
	H1	101	12	Compression/Low	Same as above	Same as above	No	*	Same as above
	H1	106	6	Linear/Low	Video pulse and 20 level calibration wedge for channels 1—12	Same as above	No	*	Same as above
	H1	107	6	Compression/Low	Same as above	Same as above	No	*	Same as above
	H1	108	5	Linear/Low	Same as above	Same as above	No	*	Same as above
	H1	109	5	Compression/Low	Same as above	Same as above	No	*	Same as above
	H1	112	4	Linear/Low	Video pulse and 20 level calibration wedge for channels 1—18	Same as above	Yes	*	Same as above
	H1	113	4	Compression/Low	Same as above	Same as above	Yes	*	Same as above
Standard orbits 15 and 16									
Orbit 15 — Mode A	H2	114	3	Linear/Low	Video pulse and 20 level calibration wedge for channels 1—24 (100 pulses)	1 signal level, noise, STN ratio, 20 level calibration wedge	Yes	*	Video data mag tape required
Orbit 16 — Mode B									
	H2	116	3	Linear/High	Same as above	Same as above	No	*	Same as above
	H2	117	3	Compression/High	Same as above	Same as above	No	*	Same as above
	H2	115	3	Compression/Low	Same as above	Same as above	No	*	Same as above
	H2	118	2	Linear/Low	Same as above	Same as above	No	*	Same as above
	H2	120	2	Linear/High	Same as above	Same as above	No	*	Same as above
	H2	121	2	Compression/High	Same as above	Same as above	No	*	Same as above
	H2	119	2	Compression/Low	Same as above	Same as above	No	*	Same as above
	H2	122	1	Linear/Low	Same as above	Same as above	No	*	Same as above
	H2	124	1	Linear/High	Same as above	Same as above	No	*	Same as above
	H2	125	1	Compression/High	Same as above	Same as above	No	*	Same as above
	H2	123	1	Compression/Low	Same as above	Same as above	No	*	Same as above

*Optional

ORIGINAL PAGE IS
OF POOR QUALITY

ORIGINAL PAGE IS
OF POOR QUALITY

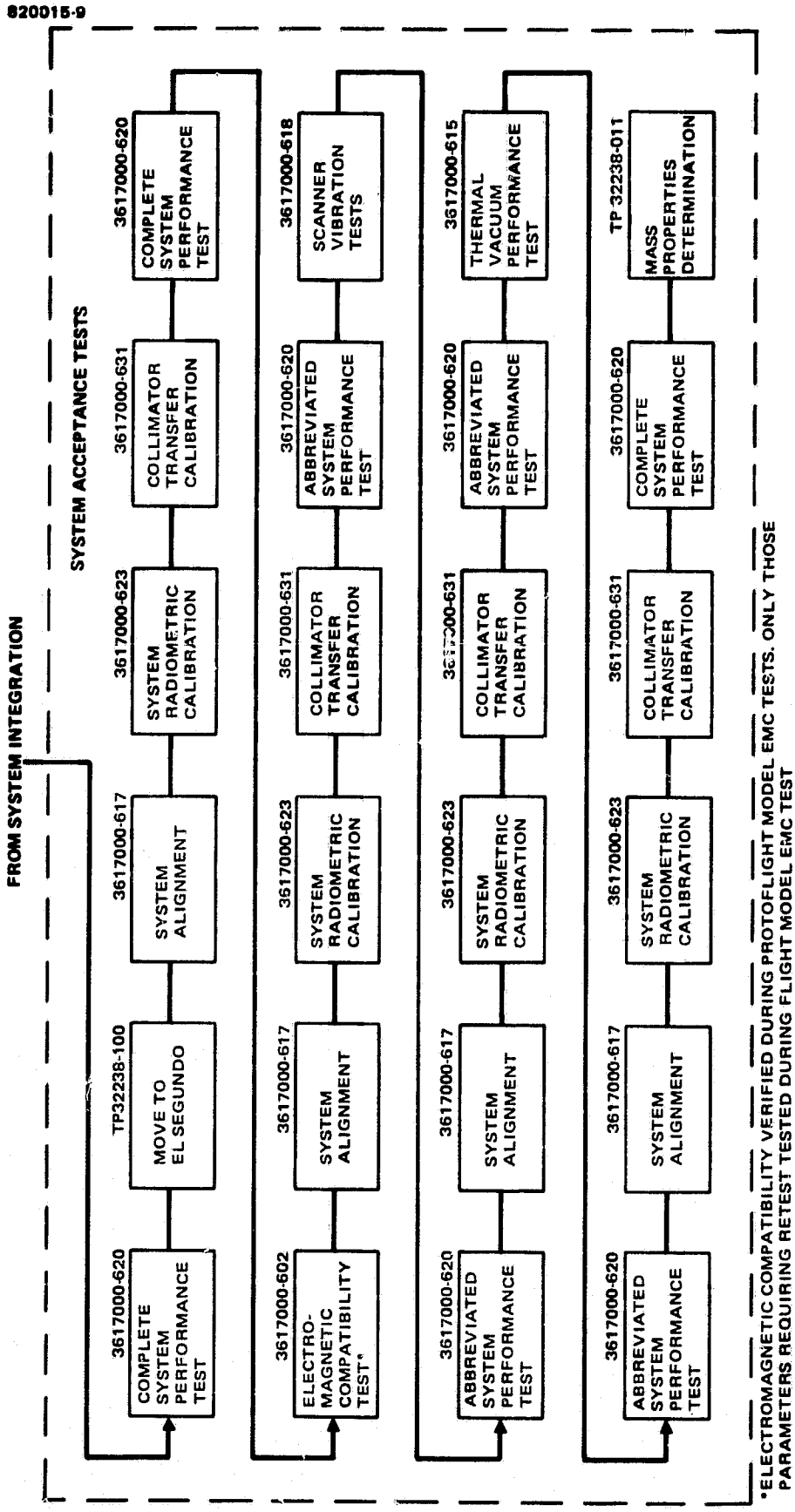

FIGURE 4-3. PROTOFLIGHT AND FLIGHT MODEL PLANNED TEST SEQUENCE

Baseline planning indicated the protoflight and the F-1 models should undergo the same test sequence, with only the individual tests modified to reflect either qualification or flight acceptance environmental levels. Figure 4-3 is the protoflight and F-1 model test sequence taken from the System Test Plan, Revision A, SCN 1, dated 21 July 1980. As the test program evolved, significant differences developed between the plan and the actual test program and between the protoflight test program and the F-1 test program. Details of the test sequences as they were actually conducted for each model are described in 7.2 and 10.2 of this report.

5. TEST CONFIGURATIONS

The test configurations for MSS-D were quite similar to those used in the earlier MSS programs. This was brought about, in part, by the use of the same test fixtures and adapters, as well as by a program office decision to use similar test procedures so that performance data would be comparable to the data taken during previous MSS programs.

5.1 PERFORMANCE TESTING

The basic test configuration for MSS system testing was that used during abbreviated system performance tests (ASPT) and complete system performance tests (CSPT). Since performance parameters were measured during some environmental exposures, the performance test configuration was basic in those tests and was augmented by fixtures or adapters to permit the environmental exposure during performance testing.

In the basic test configuration the scanner and the multiplexer were mounted to the collimator cart thermal plate. The scanner was mounted at the spacecraft mounting interface and oriented so the optical line-of-sight (LOS) pointed into the collimator. The collimator was mounted on legs that straddled the scanner and rested on the collimator cart thermal plate. The collimator was oriented so that the scanner looked directly into the collimator aperture. The scanner and collimator were optically aligned so that each performance test was conducted with the scanner viewing the same portion of the collimator scene. The several targets that were required to demonstrate system performance were located at the collimator focal plane on the MTF reticle wheel; they consisted of a chevron pattern, selected MTF bar patterns, and an open reticle. Also included in the collimator was a background, or flooding lamp, mounted in front of the collimator telescope to provide a variable intensity flat field source.

This test arrangement provided the targets and sources necessary to demonstrate all system performance parameters. Figure 5-1 shows the scanner, multiplexer, collimator, and collimator cart in a typical system performance test configuration. These performance tests were being conducted in conjunction with the electromagnetic interference/electromagnetic compatibility (EMI/EMC) tests.

5.2 ALIGNMENT

The optical alignment of the scanner is specified and referenced to the plane of the mounting interface and to the orientation of the mounting screws. The alignment configuration was therefore designed around a simulated mounting plate where orientation could be precisely measured and located. The scanner was then mounted on this

ORIGINAL PAGE IS
OF POOR QUALITY

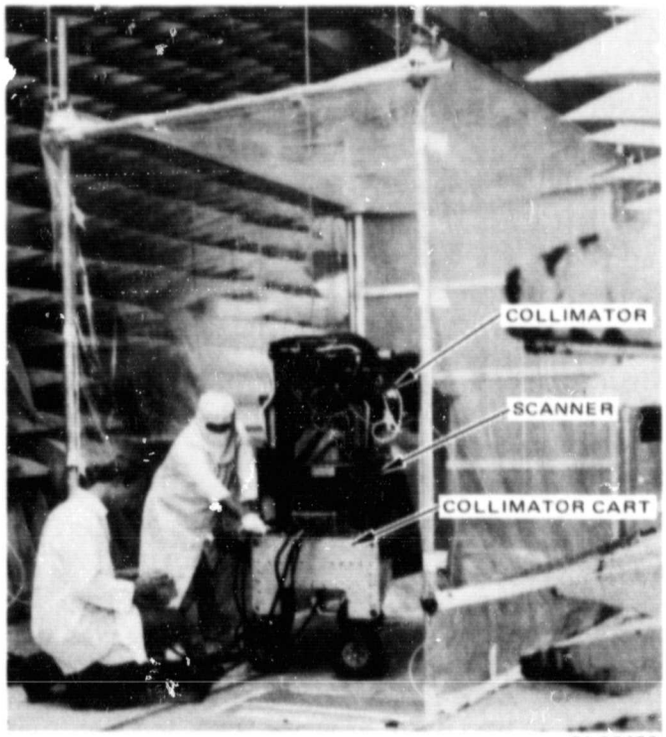

820015-21

81-95488

FIGURE 5-1. MSS-D IN SYSTEM PERFORMANCE TEST CONFIGURATION

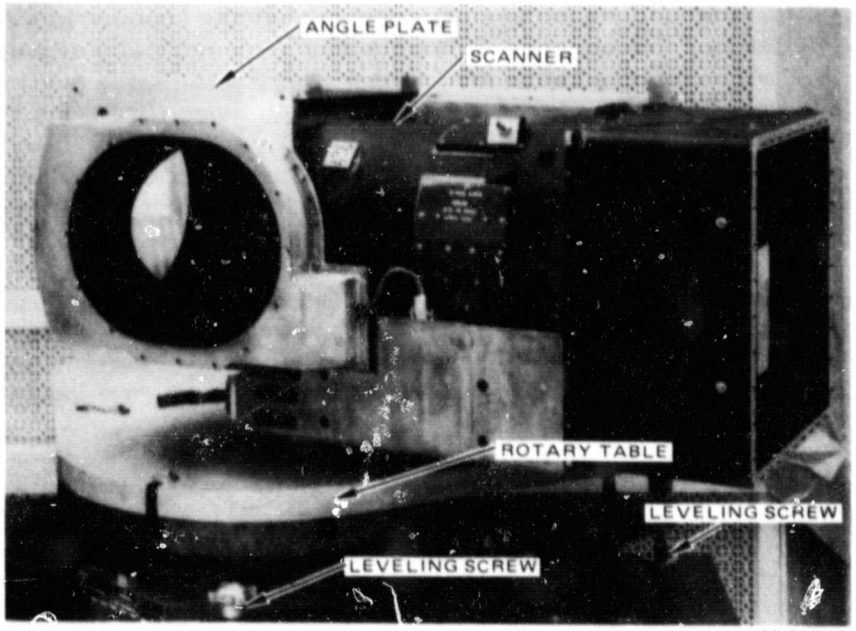

820015-22

4S-22336

FIGURE 5-2. MSS-D ALIGNMENT CONFIGURATION

precision reference interface and the optical axis measured relative to the plane of the interface. Also, the scan mirror axis of rotation was measured relative to a line joining two alignment pins on the mounting plate, which then related the direction of scan to the mounting screws. An alignment cube on the scanner structure was then measured in the same coordinate reference frame so that its orientation could be used in the future to align the MSS on the spacecraft.

Figure 5-2 shows the alignment configuration with the scanner mounted on the angle plate (precision mounting interface), which, in turn, was mounted on a precision rotary table with provision for three axis adjustments. Actual alignment measurements were taken with a theodolite which was used to autocollimate along the line of sight of the scanner to the optical fibers and to autocollimate against the alignment cube. The setup with the theodolite is not shown in Figure 5-2.

5.3 SYSTEM RADIOMETRIC CALIBRATION

The hardware configuration for the system radiometric calibration was similar to the setup for system alignment with the scanner mounted on the angle plate. The integrating sphere, a traceable radiance standard, was positioned about 8 feet from the scanner aperture, with the line of sight of the scanner aligned with the center of the sphere exit port (Figure 5-3). During system radiometric calibration the field of view of the scanner was protected from stray light by shielding with an opaque plastic tunnel and reducing room lighting to a minimum.

5.4 COLLIMATOR TRANSFER CALIBRATION

The hardware configuration for the collimator transfer calibration was the same as that for the system performance tests, with the collimator and scanner mounted on the collimator cart thermal plate and mutually aligned. Figure 5-1 illustrates a configuration suitable for collimator transfer calibration. The normal MSS-D test sequence was to move directly from collimator transfer calibration to either an abbreviated system performance test or a complete system performance test without disturbing the hardware configuration.

5.5 EMI/EMC TESTING

The hardware configuration for EMI/EMC testing was the system performance test configuration modified to adapt to the screen room. Figure 5-1 shows the protoflight system in EMI/EMC test; Figure 5-4 is a slightly different view of the protoflight system in the EMI/EMC tests. During radiated interference tests the collimator was removed from the test setup so that it would not interfere with the test results.

5.6 VIBRATION TESTING

During vibration tests the scanner was in the launch operate mode, i.e., with power applied and all units off except the rotating shutter and full time telemetry. However, no attempt was made to evaluate any performance parameters during the

ORIGINAL PAGE IS
OF POOR QUALITY

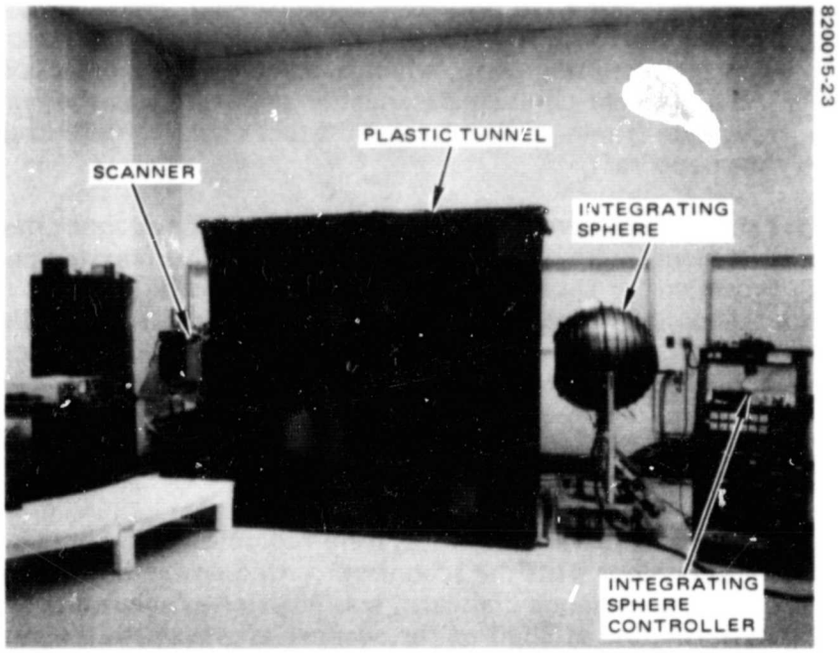

a) TEST SETUP

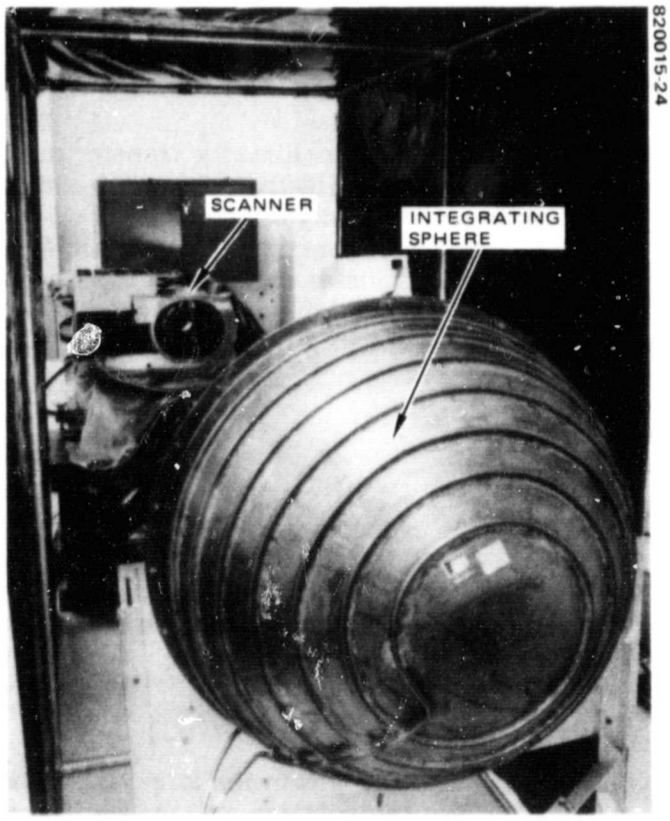

b) TEST CONFIGURATION

FIGURE 5-3. SYSTEM RADIOMETRIC CALIBRATION

vibration exposure. As a result, the scanner was mounted on the vibration fixture attached to the shaker head or the slip-table, with only the power cable attached. Figure 5-5 shows the protoflight scanner mounted on the shaker head being prepared for the Z-axis vibration exposure.

5.7 ACOUSTIC TESTING

During acoustic tests the scanner was in the same operating mode as for vibration and was electrically configured the same. However, the nature of the acoustic exposure required different fixtures and adapters. The scanner was mounted on its shipping container frame and suspended from a scaffold with bungee cords. This assembly was positioned in the reverberant chamber in front of the acoustic horn to obtain the most uniform acoustic field for the exposure. Figure 5-6 shows the engineering model and the protoflight MSS-D configured for the qualification acoustic exposure.

5.8 THERMAL-VACUUM TESTING

For thermal-vacuum tests the MSS was configured as in the system performance tests. To adapt this configuration for operation in the thermal-vacuum chamber, a thermal blanket was added to the scanner and a temperature controller was attached to the collimator cart thermal plate via feedthrough couplings in the penetration plate.

Experience gained during previous MSS thermal vacuum tests indicated that some geometric performance parameters were adversely affected by vibration transmitted through the thermal-vacuum facility into the scanner. An isolation fixture, consisting of a 3500 pound steel plate suspended by springs from a cage structure, was constructed and used during MSS-C thermal-vacuum tests to reduce line length variations and cross-axis motion. This isolation fixture was used as the adapter for the MSS-D thermal-vacuum tests. This test configuration is shown in Figure 5-7.

5.9 SPECIAL SYSTEM TESTS

During the protoflight MSS-D thermal-vacuum test, anomalous characteristics in the corrected signal levels for some channels, and to a lesser extent anomalous gain characteristics at different temperature levels for some channels, indicated a change in the optical performance of these channels; i.e., the spectral sensitivity of some channels changed with baseplate temperatures and did so repeatably. Two tests were devised to investigate these anomalies.

The relative spectral response tests were similar to tests conducted during system integration and utilized the scanner, multiplexer, collimator, and collimator cart in a system performance configuration. The collimator was modified by replacing the visible source and reticle pattern with a monochromator, a device capable of providing radiant energy with a very narrow frequency band. By sweeping through the required spectrum, the spectral response of each detector channel was measured. The setup for this test is shown in Figure 5-8. Further temperature tests required mounting the scanner to the angle plate and aligning to the integrating sphere similar to the system

ORIGINAL PAGE IS
OF POOR QUALITY

820015-25

81-95489

FIGURE 5-4. EMI/EMC TEST CONFIGURATION

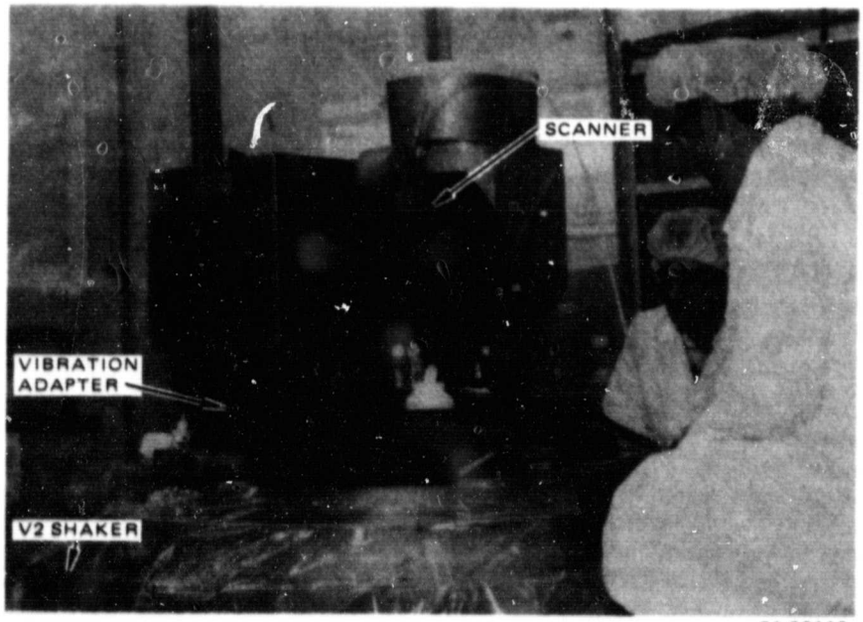

820015-26

81-96116

FIGURE 5-5. VIBRATION TEST CONFIGURATION

ORIGINAL PAGE IS
OF POOR QUALITY

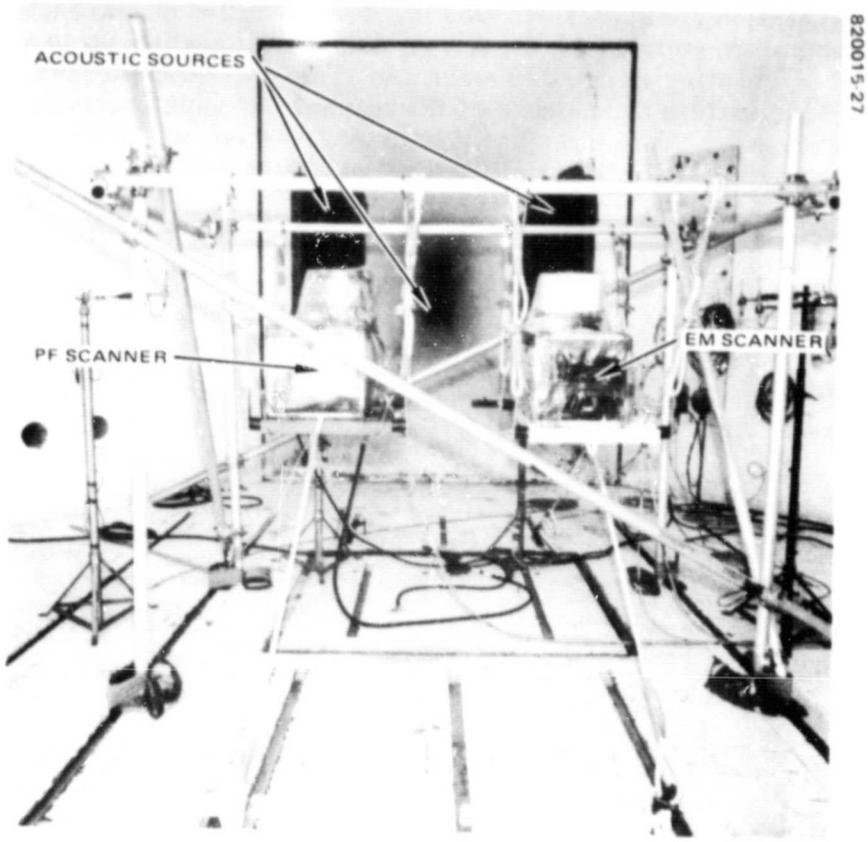

FIGURE 5-6. ACOUSTIC TEST CONFIGURATION

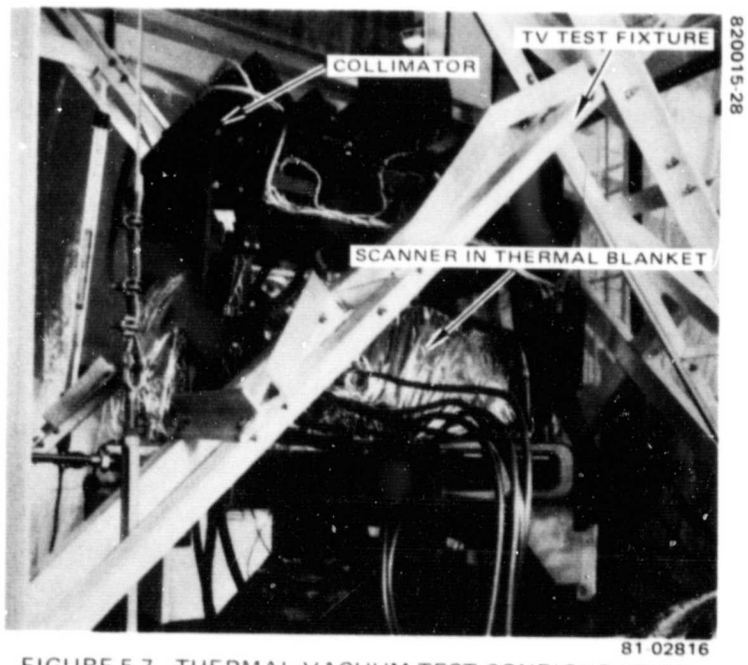

FIGURE 5-7. THERMAL-VACUUM TEST CONFIGURATION

ORIGINAL PAGE IS
OF POOR QUALITY

radiometric calibration configuration. Heaters were installed on the angle plate so the base plate temperature could be varied from ambient temperature up to 40°C. System response to the integrating sphere was measured at several temperatures. These tests confirmed the temperature dependence of the response of some channels. Photographs of the fiber optics array taken through the scanner telescope at various temperatures indicated a temperature dependence of the optical characteristics of these channels. With the exception of the heaters on the angle plate, Figure 5-3 describes the hardware configuration for the second of these tests.

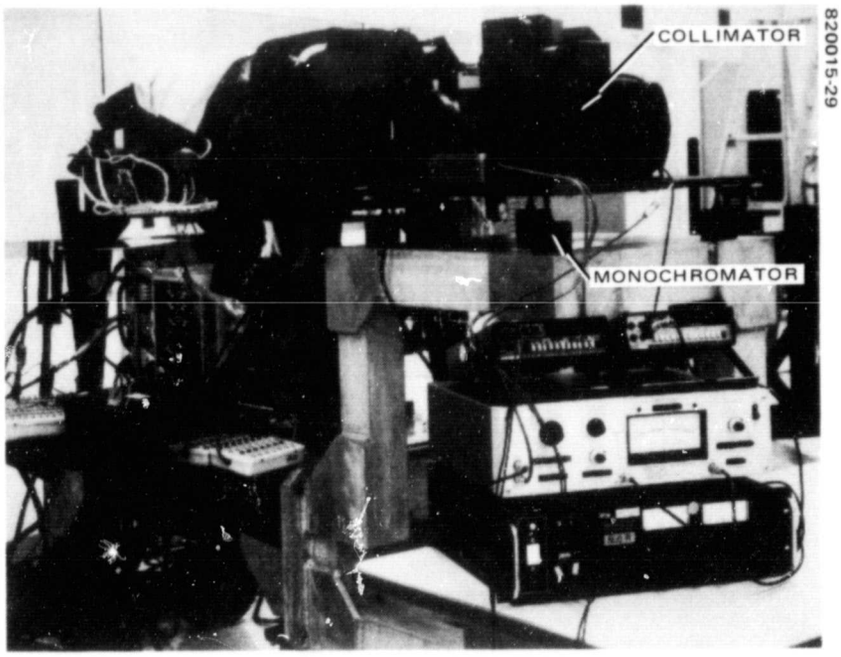

FIGURE 5-8. RELATIVE SPECTRAL RESPONSE TEST CONFIGURATION

ORIGINAL PAGE IS
OF POOR QUALITY

6. DATA REDUCTION SYSTEM

6.1 INTRODUCTION

This section describes the Data Reduction System (DRS), which consists of a Prime 300 test computer, a special purpose digital processor that collected the MSS video data, and a large amount of software for manipulating these data. The section begins with a description of the MSS-C DRS configuration. Some of the problems and limitations of this system are discussed, along with the hardware and software changes which were implemented to overcome these difficulties. The MSS-D hardware configuration is then described in more detail, including the interfaces to the rest of the test equipment. A guide to the associated software is also presented. The algorithms for on-line calibration and measurement of scanner performance are described next. The section concludes with a comparison of the off-line and on-line analyses.

6.2 DRS DEVELOPMENT

6.2.1 MSS-C

6.2.1.1 Configuration

The MSS-C DRS consisted of a Prime 300 computer with associated peripheral equipment and software. The hardware was on the same pallet as the digital bench test equipment. Two different operating systems were used. The primary system was DOS (equivalent to PRIMOS II), which was a single user system. This system was employed for all data collection and data reduction programs. Unfortunately, the operating system had to be changed to DOSVM (a precursor to PRIMOS III) to run the graphics programs. DOSVM was also required if two people wanted to access the system at one time. Changing back and forth between operating systems was a distracting and time-consuming process.

The Prime 300 had four memory boards of 16 kbytes each, for a total of 64 kbytes or 32 kilowords. Mass storage was provided by a 6 Mbyte cartridge disk. Three Mbytes were located on a removable cartridge from which program modules were obtained. The other 3 Mbytes were on a fixed platter and were used for the DOSVM paging area and a data collection area.

Two magnetic tape units maintained a tape history of the data reduction program outputs. Both drives were 9-track with a recording density of 800 bpi and an operating speed of 45 in/sec.

ORIGINAL PAGE IS
OF POOR QUALITY

Three different types of terminals were attached to the system. A Teletype ASR-35 served as a control console, operating at 110 baud and providing a hardcopy of operator requests to the operating system. A Tektronix 4010 was available for use with DOSVM, primarily for generating graphics output. The Tektronix had a hardcopy unit attached. The primary terminal was a Hazeltine 2000 CRT; it could be used either as one of the DOSVM user terminals or as the control console when executing the data collection and data reduction programs under DOS.

Except for the outputs of the Teletype and Tektronix hardcopy devices, all printed and plotted outputs were produced by a Gould 5000 electrostatic printer-plotter.

MSS data from the demux or 28-track tape drive were handled by a special purpose digital processor built by IKON Corporation of Seattle, Washington. This device, which was called the front-end, selected video data and copied it to the data disk under control of a specially modified Prime general purpose interface board.

In addition to this video input, telemetry data were also processed by the DRS. Twelve analog signals and 64 bilevel signals were connected to an analog-to-digital conversion board and a digital input board, both of which were connected to the Prime 300 central processor unit (CPU). A box called the computer interface tester (or "kludge box") was built to simulate these analog and digital inputs.

6.2.1.2 Problems and Limitations

Despite the fact that the configuration described above satisfactorily completed MSS-C testing, improvements were needed in several areas. In addition, telemetry for MSS-D is generated differently, requiring several modifications to the software.

The computational power of the Prime 300 was not being effectively utilized. Since only one user could be active during data collection and data reduction, calibration programs could not be run in a background mode and consequently had to be run on off-line computers. This meant that the DRS portion of radiometric calibration took approximately 3 days, requiring two outside computers and conversions from magnetic tape to punched cards and back. Memory size was so limited that even under the DOSVM operating system, two users had difficulty operating at the same time.

The available disk space was so small that only the executable modules for system test would fit on one cartridge. Any modification to these modules required modifying the source program on one of four system cartridges and rebuilding the test disk. In addition, up to 12 other disks were used for program development. Dish space limitations resulted in severe operational problems and made configuration control nearly impossible.

Apart from the program changes required by the new MSS-D telemetry format, several other programs had to be modified. The utility programs for examining raw data and history tapes produced output which was very hard to read. Errors had been detected in some of the data reduction modules, and it was felt that the modulation transfer function (MTF) algorithms might fail given the higher line length variations expected from the new scan mirror assembly.

ORIGINAL PAGE IS
OF POOR QUALITY

Finally, some of the peripherals were getting old. The Teletype was very slow and had experienced numerous failures on the MSS-C program. The Gould 5000 electrostatic printer/plotter had been repaired several times because of poor print quality. This was felt to be a result of the print load imposed on this device. The Hazeltine 2000 had performed adequately, but no backup for this terminal was available in case of failure during system test.

6.2.1.3 Solutions Considered

In addition to the problems discussed above, the schedules of the protoflight and flight models suggested that an additional DRS would be required for some stages of the testing. Five options were considered, and in May 1978, a feasibility study of these options was completed. One option involved purchasing two PDP 11/70 computers and rewriting all software from scratch or modifing Thematic Mapper (TM) software if appropriate. A second option was to buy only one computer and borrow the other from TM when required. These options had the advantage of compatibility with the TM program and an increased level of hardware redundancy, but also had the highest hardware and software costs and greatest schedule risk. A third option was to spend approximately $65,000 to upgrade the Prime 300 system to relieve some of the problems mentioned above. The conclusion of the feasibility study was that the prime upgrade would be the least costly solution, since program delays without the changes would end up costing nearly five times the cost of the hardware upgrade. This fact quickly eliminated the fourth option, which was to leave the Prime 300 as it was and absorb the extra personnel costs and program risks. The fifth option was to upgrade the existing Prime 300 and purchase an additional Prime 300 system. This option was eventually implemented when the testing schedules showed that two test computers were indeed required.

6.2.2 Modifications for MSS-D

6.2.2.1 Operating System Update

The ability to run background jobs and avoid having to change operating systems to run graphics programs could only be solved with a new operating system. DOS and DOSVM were replaced with PRIMOS III (Revision 15), the most advanced operating system for a Prime 300 then available. Prime modified this operating system to incorporate system calls to the IKON front end. This added a real time data collection ability to what was basically a multiuser programming system. PRIMOS III would not run on the DRS as then configured, but performed very satisfactorily with the additional hardware, described below, purchased at the same time.

6.2.2.2 Hardware Upgrade

To remedy the problems of limited memory and disk space and to allow the installation of PRIMOS III, several hardware updates were made to the DRS. Four 64 kbyte memory boards were purchased, and the original four 16 kbyte memory boards were traded for a new 64 kbyte board. An 80 Mbyte storage module disk and controller were also added to the system. The 6 Mbyte cartridge disk was originally retained, but because of numerous hardware problems it was dropped from the DRS.

Much of the remaining Prime equipment was several revision levels below the current version. To incorporate all of the hardware fixes which had been made since the DRS was decommissioned, and to simplify maintenance procedures, all of these items were brought up to the current revision level. This involved trading in the CPU and backplane for newer versions and replacing the control panel programmable read-only memory (PROMs). In addition, the extra memory boards and controllers required that the power supplies be traded for new units with a higher amperage rating.

A Printronix 300 dot matrix printer/plotter was added to the DRS, attached to the system option controller (SOC) board. The original intention was to use this device for printed output and reserve the Gould for plotted output. Unfortunately, severe problems occurred in incorporating the special software required for the Gould printer/plotter into the customized version of the PRIMOS III operating system. At about the same time, pallet space was becoming critical because of the limited floor space available for test equipment at Santa Barabara Research Center. Since the Printronix also worked as a plotter, the decision was made to eliminate the Gould printer/plotter. Regrettably, the slow speed of Printronix plotting caused time problems once actual testing started.

The Teletype control console was replaced with a higher speed DecWriter. Two ADDS Regent 100 CRT terminals were also purchased. The test conductor display software was modified to operate on the ADDS terminals, and the Hazeltine CRT was retained as a general access terminal.

6.2.2.3 Off-Line Programs

All MSS-C calibration programs were either executed on other computers or had not been automated and were performed by hand. One of the primary goals of the DRS team was to bring the existing programs on-line and finish the development of the other required calibration programs. This would save a great deal of testing time, and was the only way to ensure control of the calibration process.

Of the existing off-line programs, development of the band 5 calibration and band 4/5 alignment programs was halted when the decision to drop band 5 from MSS-D was made. The remaining off-line program, bands 1 to 4 radiometric calibration, was successfully converted to operate on the Prime and resulted in a reduction of procedure run time from 3 days to approximately 3 hours. Finally, the collimator calibration program, designed to assess the health of the collimator/scanner system, was developed and implemented.

6.2.2.4 Data Collection

Two major modifications were made to the data collection portion of the existing software modules. Calls to the IKON front end for data were replaced with calls that accessed the front end through the newly modified operating system. This involved converting sequences of subroutine calls to a new and shorter calling sequence. Instead of writing the acquired data onto the fixed platter of the cartridge disk, these routines were modified to write into a standard PRIMOS data file. This allowed much easier access to the data by utility programs and allowed representative data sets to be saved on disk or tape. The corresponding routines which retrieve data for the data reduction modules were modified to read from these data files.

6.2.2.5 Data Reduction

A few minor errors that had been detected in the data reduction modules after completion of MSS-C testing were corrected. In addition, all algorithms were studied to determine their validity in light of the increased scan angle of the MSS-D mirror. Engineering model tests indicated that the new mirror would have increased line length variations which would invalidate the then current MTF algorithm. A new MTF algorithm was developed which is insensitive to line length variation.

6.2.2.6 Telemetry

Several changes in the method of handling telemetry were implemented. Instead of having telemetry values continuously available through the digital input and analog-to-digital input boards, the new scanner test set encoded telemetry onto three serial telemetry streams. These serial streams were connected to the DRS through the AMLC (asynchronous multiline controller), and the test conductor software was changed to interrogate these lines for telemetry values. Since more telemetry values were available with this new system, the test conductor software and the history tape routines were modified to collect and save more telemetry items.

In addition, several new programs were developed to monitor the telemetry streams. The primary program examined the spacecraft and ground telemetry streams and produced a two-page printout of critical temperatures, voltages, currents, and bilevel conditions.

During the MSS-C programs, telemetry for re-reductions from tape could be simulated with the computer interface tester (kludge box). The test conductor software was modified to perform this function for MSS-D.

6.2.2.7 Utilities

The existing utility programs which collected video data were modified to use the new operating system calls. Additional programs were written to diagnose the condition of the front end and/or the video data. A new family of utilities, with an output format much improved over the comparable routines from MSS-C, was developed to examine the files of video data produced during data collection. A new utility to format and display the contents of a history tape was also developed. Finally, the graphics software was modified to read the new history tape format and produce plotted output on the Printronix.

6.3 MSS-D DRS CONFIGURATION

6.3.1 Hardware

MSS-D had two DRS systems, functionally identical but with slightly different components. In the following discussion, where a difference exists, the systems are identified as DRS 1, which is the upgraded MSS-C test computer, and DRS 2, which is the more recently purchased system. Figure 6-1 shows the configuration of the MSS-D DRS and its relationship to the rest of the test system. The shaded areas show the portions of DRS 1 which were modified to arrive at the current DRS configuration.

ORIGINAL PAGE IS
OF POOR QUALITY

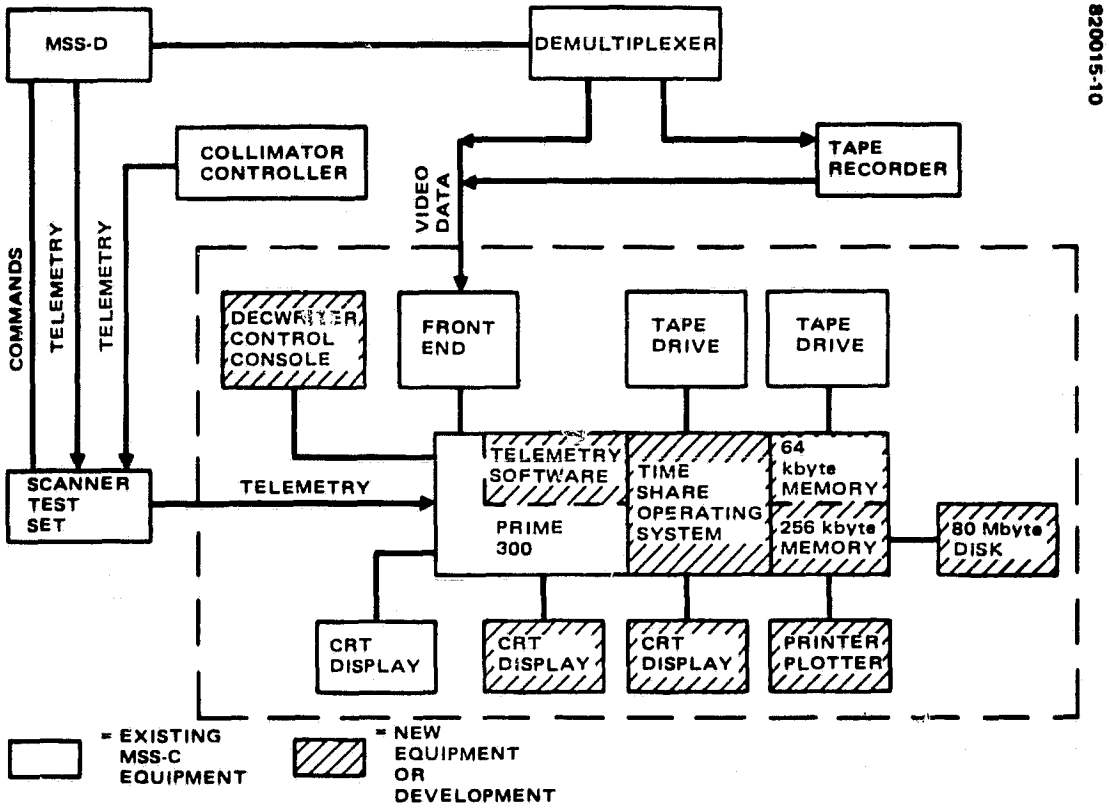

FIGURE 6-1. MSS-D DATA REDUCTION SYSTEM

Each DRS has a Prime 300 CPU with a real time clock and the floating point arithmetic option. High speed memory consists of four 64 kbyte boards of byte parity MOS memory (256 kbytes, or 128 kilowords). Two additional boards are available as spares. Disk storage is provided by an 80 Mbyte storage module moving head disk system which has been partitioned into three logical disks. DRS 1 has two 9-track, 800 bpi, 45 in/sec, tension arm tape drives. DRS 2 has two 9-track, dual density (800/1600 bpi), 75 in/sec, vacuum column tape drives, and an associated data formatter. Each DRS also has the required controllers for the disk and tape drives.

The DRSs are controlled by interchangeable 300 baud hardcopy devices. DRS 1 has a DecWriter LA 36, while DRS 2 has a Prime supplied Terminet 300 control console. The DRS test conductor software is written for ADDS Regent series CRT terminals. DRS 1 has three Regent 40 terminals and DRS 2 has two Regent 100 terminals. The slight differences between these two types of terminals do not affect their interchangeability.

Except for the control consoles, all graphic and printed output is produced on the Printronix 300 dot matrix printer/plotter. The DRS 1 printer is driven serially by the SOC board. DRS 2 has a unit record controller (URC) board which is not present in DRS 1; the DRS 2 printer is driven by a parallel data stream from this URC board.

The IKON front end was essentially unchanged from the MSS-C program. The front end is controlled by a specially modified Prime general purpose interface board (GPIB). Subroutine calls select the source of video data desired, the channels to be examined, and the location and duration within the scan of data to be collected. The GPIB converts these instructions to commands to the front end. The source of the data is either the set of line drivers attached to the demux (25 channels plus clock) or the line drivers attached to the 28-track tape recorder (25 channels plus 25 clocks). Data enter each channel of the front end at a rate of 600 kbits per second. The portions of the scan which have been selected are retained in a buffer and then passed to the Prime's memory through the GPIB. The data are then written from memory to the disk data files.

The IKON is the main interface between the DRS and the rest of the test system, but information also enters the DRS through the three telemetry lines. Spacecraft telemetry, ground telemetry (bus voltage and current and collimator settings), and command telemetry are each connected to an RS-232-C port on the asynchronous multiline controller, the same board that controls the CRT terminals. The telemetry lines appear like terminals continuously sending data to the DRS, but the ports to which they are attached are assigned in such a way that the telemetry programs can access them for telemetry values.

6.3.2 Software

Figure 6-2 depicts in a simplified manner the software component of the DRS. Each rectangular box represents a collection of related software modules. The circles represent inputs or outputs (data streams, disk files, listings, or magnetic tapes). The following paragraphs describe briefly the purpose of each of the software groups, the data they require for input, the files and listings they produce as output, and their location within the DRS file structure. The location is specified by a statement of the User File Directory (UFD) which contains the program module or command file. Section 6.4 describes the algorithms used by the data reduction and calibration programs. Otherwise, no attempt has been made to describe the operation of any of these modules in detail, since this is documented elsewhere.

ORIGINAL PAGE IS
OF POOR QUALITY

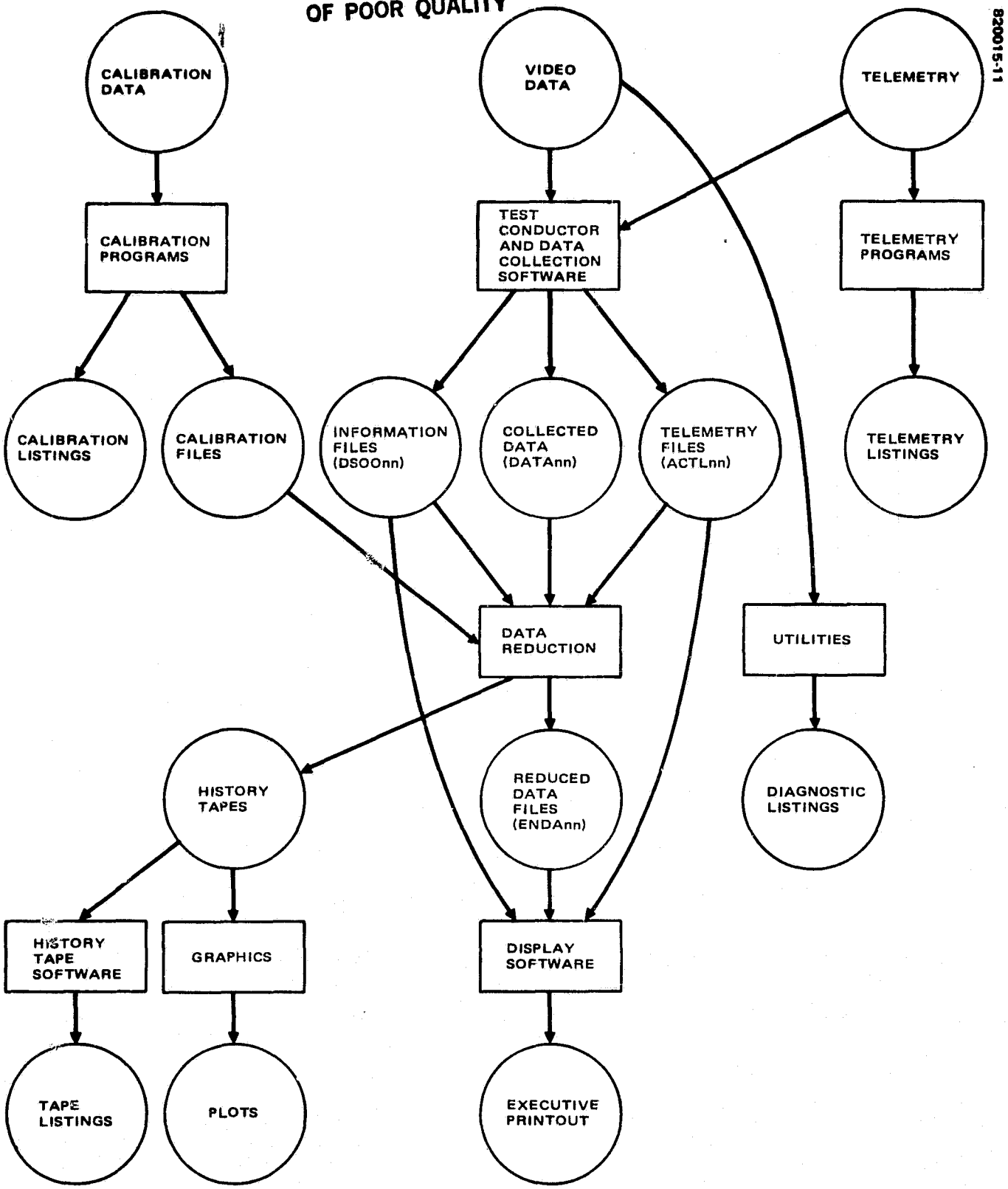

FIGURE 6-2. DATA REDUCTION SYSTEM SOFTWARE

6.3.2.1 Operating System

The operating system does not appear in Figure 6-2, but it specifies the file structures and governs the operation of all of the other modules. The operating system that the DRS employs is basically PRIMOS III (Revision 15), modified to accommodate the unique requirements of the MSS program. The main addition was the inclusion of the front-end data buffers and subroutines within the operating system. A change was also made to allow a user accessing the front end to lock out other users, so that real time data collection was possible in a multiuser environment. To make room for these additions, the facilities for adding several kinds of peripherals to the Prime and the ability to network the Prime were deleted.

The modified operating system resides in the UFDs HPRIME and HPRSRC. The front-end routines are located in the UFD CEA, which also contains instructions for their use.

6.3.2.2 Test Conductor and Data Collection Software

The test conductor software controls the data collection process. For each sequential data set specified by the DRS operator, the test conductor software checks internal tables for the required scanner and collimator configuration. It then reads the spacecraft and ground telemetry streams to determine if this configuration exists. If so, the telemetry is written to a file DATUFD>ACTLnn and certain control information is written to DATUFD>DS00nn (where nn is the sequential data set number). Program control is then passed to the data collection module, along with constants required by the front end.

The data collection module selects the required samples out of the video data stream and writes them to the file COLLECT>DATAnn. Control is then returned to the test conductor software. If no more data sets are to be collected, the data reduction driver is initiated.

Most of the routines and command files required by the test conductor and data collection modules are located in the UFD MSSTC, while the executable modules are found in TEST.

Command File	Executable Module	Function
C_EXEC	*EXEC	Initiates new orbit or restarts orbit
C_TCON	TSTCON	Requests data set number and checks telemetry
C_DC	DACOLL	Collects data

6.3.2.3 Data Reduction

The data reduction driver (DATRED) is initiated by the test conductor software. DATRED sequentially processes each data set by first reading the appropriate information and telemetry files (DATUFD>DSOOnn and DATUFD>ACTLnn). The correct data reduction procedure is determined from the information file and is then initiated.

The data reduction procedure (DROOxx) reads the collected data from the file COLLECT>DATAnn, operates upon it, and writes the reduced results to the file TEST> ENDAnn. The history tape module which writes the results and the telemetry to tape is initiated, after which DATRED is resumed for the next sequential data set. If all data sets have been completed, control is passed to the display software.

Most of the routines which made up the data reduction modules are found in the UFD MSSDR, as are all of the command files required to generate the executable modules. The executable modules are located in the UFD TEST. The command file and the executable module for each procedure (CSLEVL is initiated by DROO01) are listed:

Command File	Executable Module	Function
C_DARD	DATRED	Data reduction driver
C_STN	DROO01	Signal-to-noise
C_INTCL	DROO01	Radiometric calibration
C_MTF	DROO03	Modulation transfer function
C_CX	DROO04	Cross-axis repeatability
C_ESTN	DROO10	Special signal-to-noise
C_SR	DROO16	Scan repeatability and line length
C_COSL	CSLEVL	Corrected signal level

6.3.2.4 Calibration

The calibration algorithms are described in 6.4. This subsection describes the input/output file structure and the location of the calibration programs. In the following discussion, several references to the creation of data files are made. In nearly every case, the corresponding file from the previous calibration is saved and renamed by appending the date to the file name. A history of calibration results is therefore maintained on the DRS for later analysis or re-reductions.

Radiometric Calibration

Radiometric calibration data are collected and reduced in much the same manner as the regular test orbits. The main exception is that these orbits each creates a file in the INTEGRATION-SPHERE UFD named SPHERE.xx, where xx is the standard orbit number. An optimization program then processes these files to produce estimates of internal calibration system (both primary and redundant) radiance output at 20 selected locations, or words, for each channel in both low and high gain modes. These values are copied to the file TEST>XNOMNL where they are used by the corrected signal level data reduction procedure. All of the programs and command files required for radiometric calibration are contained in INTEGRATION-SPHERE.

Collimator Calibration

Once the scanner has been calibrated with the integrating sphere, the calibration is transferred to the collimator. Two orbits are run to produce eight data files named UPDATE>DSNnnx, where nn is the data set number and x is the system (A or B) tested. From these files, collimator characteristics, such as shading factors, are determined and copied into the files UPDATE>FACTRA and UPDATE>FACTRB, which are subsequently used by the corrected signal level algorithms. All of the programs and command files required for this calibration transfer are found in the UFD COLLIMATOR.

Other programs, located in the UFD UPDATE, use FACTRA and FACTRB to compute the new corrected signal level band-to-band deviation reference files (UPDATE>BBREFA and UPDATE>BBREFB) and the new signal-to-noise specifications (UPDATE>STN-SPECS).

Collimator Diagnostic Program

When overall system performance changes, the cause can be either the scanner or the collimator or both. An additional program exists which attempts to determine the most likely cause of the change. This program, which is found in the UFD COLL, uses as input the signal-to-noise history file named UPDATE>DSHIST which is maintained by the corrected signal level data reduction procedure.

6.3.2.5 Telemetry

The telemetry software is divided into two parts. The first group of telemetry routines is found in the UFD MSSTC. These routines, which are incorporated into the test conductor software, read the spacecraft and ground telemetry streams, convert this telemetry into engineering units, and store the results in internal memory. These values are then written to the telemetry files (DATUFD>ACTLnn) by the test conductor software and to the history tapes by the history tape software.

The second group of telemetry programs consists of diagnostic routines, which check the operation and contents of the three telemetry streams, and status routines, which format and display spacecraft and ground telemetry. All of the latter routines reside in the UFD>TDUMP, and their operation is described in the DRS Operator's Guide.

6.3.2.6 Display Software

The display software operates on the files created during data reduction (the files TEST>ENDAnn, where nn is the sequential data set number). The contents of these files are formatted and displayed on the operator's CRT screen or printed out or both. The DSOOnn and ACTLnn files are also read for control information and telemetry.

The executable module is named TEST>DISPLA, and is created from routines in the UFD MSSTC by the command file MSSTC>C_HZ.

6.3.2.7 History Tapes

During data reduction, much of the available telemetry and most of the reduced results are written onto to nine-track history tapes. Several modules are required to do this, one for each of the different types of data sets. These tapes can then be examined at a later time with programs that format and display the contents of the tape, or by use of the graphics software. The programs which display the tapes, along with other programs which position the tapes, are located in the UFD HISTAPE and are documented in the DRS Operator's Guide.

The modules that write the history tapes are also located in HISTAPE. The executable versions reside in the UFD TEST where they are initiated by their respective data reduction module.

Command File	Executable Module	Function
C_SR	TAPSCR	Write scan repeatability
C_CX	TAPCXA	Write cross axis
C_SN	TAPSTN	Write signal-to-noise ratio
C_MT	TAPMTF	Write MTF

6.3.2.8 Graphics

The graphics programs copy the history tapes generated during data reduction into a disk file, and then plot the following items:

Average signal level	Offset
Noise level	MTF
Signal-to-noise ratio	Scan repeatability
Corrected signal level	Line length variation
Gain	Cross-axis repeatability

All of the programs, and command files for their use, are contained in the UFD GRAPHICS.

6.3.2.9 Utilities

Several programs exist which check the integrity and quality of the incoming video data, and allow the examination of the collected data files. The programs which check data integrity are located in the UFD UTIL; they allow the operator to determine whether or not all channels are being collected, if the start-scan code is present, and other such questions. The data quality programs are located in UTIL and JLC. These programs allow a quick check of the position of the video pulse, the presence of data, and the signal-to-noise ratio. A family of programs in UFD SNAP access the collected data files and produce a listing of collected data for any specified channel.

All of the utilities are documented in the DRS Operator's Guide.

6.4 ALGORITHM DESCRIPTIONS

6.4.1 Signal-to-Noise Ratio

Signal-to-noise ratio (STN) is one of three measurements made of system radiometric performance, the other two being square wave response (SWR), or MTF, and corrected signal level (COSL), described in 6.4.2 and 6.4.3, respectively. The system STN performance is measured for four different configurations of the collimator and scanner. In addition to assessing the performance of the instrument the signal-to-noise algorithm performs auxiliary processing of information required by the COSL algorithm. The programs STN and COSL are called sequentially whenever an STN estimate is requested.

Several algorithms were employed during acceptance testing of the two MSS-D instruments. The first, used throughout testing of the protoflight model and up to (but not including) thermal-vacuum testing of the flight model, is identical to that ultimately used on MSS-C: the average signal level is approximated by the sample mean and the system noise by the sample standard deviation. This approach was plagued, from the beginning of testing, by collimator spatial light intensity nonuniformities which are interpreted as scanner noise by this algorithm. This lead to apparent violations of the signal-to-noise specification which, upon subsequent analysis, were found to be unwarranted. Numerous attempts were made to correct this fault in the collimator with only partial success. This collimator defect led to the development of the current algorithm which has the capability of estimating collimator nonuniformity contributions to the estimated system noise level. The collimator contribution is then subtracted before specification compliance is verified. Both approaches are discussed in the following sections.

6.4.1.1 General Test Description

The system test plan calls for STN ratio estimates to be made to verify system performance at each gain setting and muliplexer mode for all channels. The system specification states minimum STN performance for the linear/low and compression/low (multiplexer/scanner gain) mode for maximum and half-maximum input radiance levels. In HS 248-0935, Revision A, this specification is extended to include all other mode combinations; i.e., linear/ high (L/H), compression/low (C/L), and compression/high (C/H) as a continuous function of input radiance. The actual specification values to be used during system test are determined at the time of the initial collimator calibration immediately following a radiometric calibration. At this time the radiance output of the collimator is measured and STN specification values determined for the following configurations:

Neutral Density Filter Position, Percent	Multiplexer Mode	Scanner Gain
50	Linear	Low
25	Linear	Low
10	Linear	High
50	Compression	Low
25	Compression	Low
10	Compression	High

Although specification limits for the above six configurations are available within the STN program, in practice only the four configurations corresponding to the 50 percent and 10 percent neutral density filter (NDF) settings were used for acceptance testing.

6.4.1.2 Data Reduction Description

Upon selection of any one of the data sets described in Table 6-1, the system computer collects 20 consecutive words for the selected channels starting at 1550 words after SMP1 for 100 scans. For each data set (except 1) these will consist of 100 consecutive scans containing a calibration wedge; and for data set 1, every other scan containing a calibration wedge.

Signal-to-Noise Ratio Algorithm

Let the samples collected from the video pulse be denoted by

X_{ij} multiplexer output (QL)

where

$i = 1, 2, \ldots\ldots, 20$ word number in scan j

$j = 1, 2, \ldots\ldots, 100$ scan number

then

$$S = \frac{1}{2000} \sum_{j=1}^{100} \sum_{i=1}^{20} X_{ij} \tag{6-1}$$

ORIGINAL PAGE IS OF POOR QUALITY

$$\sigma^2 = \frac{1}{1999} \sum_{j=1}^{100} \sum_{i=1}^{20} (X_{ij} - S)^2$$

$$ASL = S + 0.5$$

$$ANL = (\sigma^2 - \sigma_c^2)^{1/2}$$

$$STN = ASL/ANL$$

where,

ASL = average signal level estimate

ANL = average scanner noise level

σ_c = collimator spatial nonuniformity induced "noise"

STN = scanner signal-to-noise ratio estimate

ORIGINAL PAGE IS
OF POOR QUALITY

TABLE 6-1. SYSTEM (COLLIMATOR/SCANNER) CONFIGURATION FOR SIGNAL-TO-NOISE RATIO DATA SETS

Data Set No.	NDF, %	MTF	Flooding Lamp	Scanner Gain	Multiplexer Mode	Channel
1	50	Open	Out	Low	Linear	1 to 24
3	50	Open	Out	Low	Compression	1 to 18
22	10	Open	Out	High	Linear	1 to 12
23	10	Open	Out	High	Compression	1 to 12

NDF = neutral density filter
MTF = modulation transfer function

For the protoflight model throughout test and the flight model (up to thermal-vacuum), σ_c was identically zero; i.e., no correction for the collimator was used. From the commencement of thermal-vacuum testing for the flight model, σ_c was approximated by

$$\sigma_c^2 = (5.78\, g)^2 + 0.93\, \delta^2 \tag{6-2}$$

The parameters g and δ are computed from the samples X_{ij} as follows. Let

$$W_i = \frac{1}{100} \sum_{j=1}^{100} X_{ij} \tag{6-3}$$

i.e., W_i is the average over the 100 scans for word i. A linear regression over W_i is performed to obtain the least squares straight line fit to the average response; i.e., solve for g and ϕ that minimizes

$$J = \sum_{i=1}^{20} [W_i - (gi + \phi)]^2 \tag{6-4}$$

where

S = slope (QL/word)

ϕ = intercept (QL)

i = word number

ORIGINAL PAGE IS
OF POOR QUALITY

Then the quasi-random collimator nonuniformity variance, δ^2, is given by

$$\delta^2 = \frac{1}{20} \sum_{i=1}^{20} [W_i - (gi + \phi)]^2 \tag{6-5}$$

and finally,

$$\sigma_c^2 = (5.78\, g)^2 + 0.93\, \delta^2 \tag{6-6}$$

Analysis in support of this technique is presented in Hughes IDC HS248-1484.

6.4.1.3 Auxiliary Data Processing

In addition to the signal-to-noise assessment, auxiliary data processing is conducted in STN to retrieve calibration data obtained during radiometric and collimator calibration orbits. This is done twice in the program via calls to two subroutines, SHADE and RNOM. These two subroutines extract data from the data files FACTRA (for calibration system A) or FACTRB (for system B) and XNOMNL, respectively. Briefly, FACTRA (or FACTRB) contains current estimates of calibration lamp and collimator light levels and shading factors, while XNOMNL contains the reference calibration wedge word values obtained from a radiometric calibration.

6.4.2 COSL, DCC, and DBB

This section is concerned with the establishment, use, and maintenance of the brightness calibration of the internal calibration system. These topics relate to three specific procedures: transfer of calibration from the integrating sphere standard to the internal calibration system, calculation of the scanner gains and offsets based on observations of the internal calibration system, and use of an external reference (i.e., the collimator) to monitor the stability of the internal calibration system through three parameters: corrected signal level (COSL), deviation channel to channel (DCC), and deviation band to band (DBB).

6.4.2.1 Radiometric Calibration

The purpose of the integrating sphere calibration procedure is to transfer the calibration of the integrating sphere to the internal calibration system of the scanner. The integrating sphere is itself previously calibrated by NASA Goddard from data supplied by the National Bureau of Standards. Once the internal calibration system has been calibrated, it can then be used as a reference, assumed stable in time, to determine instantaneous values of the scanner gain and offset, both of which vary in time.

The raw data used to accomplish this transfer of calibration consist of observations of the scanner response to the integrating sphere operating at a known radiance, as well as the near simultaneous response of the scanner to the internal calibration system. These observations are then repeated over a variety of different integrating sphere radiances.

The basic approach of the data reduction procedure which actually accomplishes the transfer of calibration is first to estimate the gain and offset of the scanner response to the integrating sphere. The gain and offset are then used to derive the internal calibration radiances from observations of the internal calibration system. This process is greatly complicated by the realization that the scanner gain and offset are not stable in time, and thus will likely be significantly different from one observation of the integrating sphere to the next. The solution to this problem is an iterative bootstrap procedure which uses the internal calibration radiances as derived above to arrive at a new estimate of scanner gain and offset, then uses this result to recalculate the internal calibration radiances, and so on. This process is discussed in more detail below.

The physical model on which the transfer of calibration from the integrating sphere to the internal calibration system is based is more precisely described as follows. Let the scanner signal level (in units of quanta) observed in response to the integrating sphere be given by the relationship

$$S(d, b, k) = G(d, b, k)\ R(d, b) + O(d, b, k) \tag{6-7}$$

where G(d,b,k) and O(d,b,k) represent the gain and offset of the kth channel of band b when collecting data set d, which corresponds to the particular integrating sphere radiance R(d,b). The scanner signal level observed in response to the internal calibration system is given by an analogous relationship

$$s(d, b, k, w) = G(d, b, k)\ q(b, k, w) + O(d, b, k) \tag{6-8}$$

where q(b,k,w) is the actual radiance seen by the kth channel of band b in response to the wth internal calibration sample radiance during the collection of data set d.

The observed signal levels, S(d,b,k) and s(d,b,k,w), are averages over multiple observations in order to reduce the uncertainty of the resultant calibration. In particular, s(d,b,k,w) is averaged over 100 alternate scans of the internal calibration system, while S(d,b,k) is averaged over 20 words from each of 100 alternate scans of the integrating sphere. The corresponding noise levels, N(d,b,k) and n(d,k,w), are also estimated from the corresponding sample variances.

Under the assumptions of the model described above, the transfer of calibration problem reduces to the determination of the internal calibration radiances, q(b,k,w), when given the observations S(d,b,k) and s(d,b,k,w) and the corresponding integrating sphere radiances, R(d,b). By way of arriving at the values of q(b,k,w), it is also required to determine the relevant scanner gains and offsets, G(d,b,k) and O(d,b,k). The actual algorithm used to determine the transfer of calibration may now be described as follows,

for a given channel, k, and band, b. First, the scanner gain and offset, G(d,b,k) and O(d,b,k), are determined from a least squares analysis based on Equation 6-7, under the assumption that G(d,b,k) and O(d,b,k) are both independent of data set, d. The assumption that the scanner gain and offset are independent of the data set is equivalent to assuming them to be independent of time, and will later be removed. This assumption is required at present since otherwise Equation 6-7 would reduce to one equation in two unknowns for each data set, d. The resulting gain and offset are then substituted into Equation 6-8 to yield estimates of q(b,k,w) for each data set, which are then averaged over all available data sets. The process of averaging removes the direct connection between the estimated q(b,k,w) and the gains and offsets, G(d,b,k) and O(d,b,k), as expressed in Equation 6-8. It is therefore reasonable to expect that a new least squares analysis based on both Equations 6-7 and 6-8 will yield new and improved estimates of the G(d,b,k) and O(d,b,k). These new estimates are no longer constrained to be independent of the data set number, d. The cycle is closed by using Equation 6-8 to derive improved estimates of the internal calibration radiances, q(b,k,w), which are then used as inputs to a new least squares analysis based on both Equations 6-7 and 6-8 and so on.

The iterative search just described is deemed to have converged when each of two separate conditions is satisfied. First, it is required that the sum of the mean square changes (since the last iteration) in the fitted gains, offsets and internal calibration radiances over all data sets must be less than 0.000001. Second, the sum of the mean square differences between the fitted and observed values of the observed signal levels, S(d,b,k) and s(d,b,k,w), must be less than 0.0001.

It should be noted that the above least squares analysis involves a weighted least squares fit. In particular, the scanner signal levels, S(d,b,k) and s(d,b,k,w), are inversely weighted by the squares of the corresponding noise levels, N(d,b,k) and n(d,k,w), when processing bands 1 through 3. In band 4, on the other hand, the signal levels are uniformly weighted. This latter weighting scheme is intended to reflect a physical model wherein the noise in the signal from the photodiode detectors is dominated by dark current, which is independent of signal level.

The procedure just described for the transfer of calibration from the integrating sphere to the internal calibration system of the scanner relates to only a single channel. This is repeated for all 24 scanner channels in the low gain mode, and then again for channels 1 through 12 in the high gain mode. As a result of all this, one has (for each band) a set of roughly 120 internal calibration radiance estimates (20 internal calibration radiances from each of six channels). Actually, there will be somewhat fewer than this number since not all of the internal calibration radiances are usable (i.e., some result in saturated signal levels). At this point, it is assumed that the radiance, q(b,k,w), may be factored according to the relationship

$$q(b,k,w) = r(b,w)\ u(b,k) \tag{6-9}$$

Here r(b,w) is the brightness of the wth internal calibration radiance in band b, and u(b,k) accounts for the "shading" of the kth channel of band b when viewing the internal calibration source. The "shading factors," u(b,k), are defined in such a way that their geometric product over all six channels in a band is unity. The shading model expressed

ORIGINAL PAGE IS
OF POOR QUALITY

by Equation 6-9 may now be used to reduce the number of degrees of freedom from 120 to 25; i.e., 20 internal calibration radiances, r(b,w), and five independent channel shading factors, u(b,k). Again, this is only an estimate insofar as not all the internal calibration radiances are usable. This reduction in the number of degrees of freedom of the set of measured internal calibration radiances is effectively a smoothing operation based on the form of the assumed shading model as formulated in Equation 6-9.

6.4.2.2 Collimator Transfer of Calibration

Since the integrating sphere cannot be used inside the thermal-vacuum chamber, it is necessary to have an alternate standard if the stability of the internal calibration radiances is to be monitored during thermal-vacuum testing. This role is filled by the collimator lamp, together with a set of three neutral density filters (10, 25, and 50 percent) for varying its intensity. The collimator source differs from the integrating sphere in that its radiance is not sufficiently uniform over the field of view that channel shading can be ignored.

The collimator source must be calibrated by a transfer of calibration similar to that described above. In this case, however, the calibration is being transferred from the internal calibration system of the scanner to the collimator. This is done independently for each setting of the neutral density filter. Using the same model as described above, the signal level observed in response to the collimator source is given by

$$S(d, b,k) = G(d, b, k)\ Q(d, b,k) + O(d, b, k) \tag{6-10}$$

where Q(d,b,k) represents the shaded collimator radiance as viewed by the kth channel of band b during the collection of data set d. The data set index, d, corresponds to one of the three possible neutral density filter settings (10, 25, or 50 percent), and is assumed distinct from those relevant to the integrating sphere calibration, as discussed above. As before, one may express the shaded collimator radiance as the product of the true radiance, R(d,b), of the collimator source times a shading factor, U(d,b,k)

$$Q(d, b, k) = R(d, b)\ U(d, b, k) \tag{6-11}$$

The process of transferring calibration from the internal calibration system to the collimator now becomes simply a matter of determining the scanner gain and offset by a least squares analysis based on Equation 6-8. This is a straightforward process, since the shaded radiances, q(b,k,w), are known. The least squares algorithm used for this weights each observed signal level, s(d,b,k,w), by the inverse square of the corresponding noise level, n(d,k,w). In contrast to the approach used above, this same weighting scheme is used for all four bands. The channel gains and offsets so determined are then used to directly calculate the Q(d,b,k) based on Equation 6-10. These may in turn be used to determine the band average collimator radiance, R(d,b), and the collimator shading, U(d,b,k), by application of Equation 6-11, recalling that the shading factors, U(d,b,k), are normalized so that their product over all six channels in a band is unity. Once the Q(d,b,k) have been determined, one has an independent calibrated radiance source in thermal-vacuum which may be cross-checked against the internal

ORIGINAL PAGE IS
OF POOR QUALITY

calibration system at any time. Such a cross-check would effectively involve a redetermination of the Q(d,b,k) and a comparison against the original.

The calibrated radiances of the internal calibration system and the collimator source (transferred from the integrating sphere as described above) are completely contained in the shaded radiances q(b,k,w) and Q(d,b,k). These parameters are saved on disk for later reference in a procedure known as data reduction system (DRS) loading, which is normally accomplished just prior to beginning thermal-vacuum testing. The q(b,k,w) are saved in the file XNOMNL, and the Q(d,b,k) in the files FACTRA and FACTRB.

6.4.2.3 Corrected Signal Level, DCC, and DBB

The determination of the gain and offset of the scanner during data reduction normally consists of a least squares analysis of the internal calibration data based on Equation 6-8 above. This determination is performed in two different ways for two different applications of the results.

The gain and offset used in the offline analysis are determined by means of a least squares fit of Equation 6-8 to the internal calibration data where the observed signal levels, s(d,b,k,w), are weighted by the squares of the corresponding noise levels, n(d,k,w). This procedure is equivalent to that used in the transfer of calibration from the internal calibration system to the collimator. The offline collimator analysis is discussed in detail in 6.5, and therefore is not treated here.

The on-line analysis, on the other hand, uses gains and offsets determined by means of a least squares fit of Equation 6-8 to the internal calibration data with the observed signal levels weighted by the inverse of the observed signal level (bands 1 through 3) or unity (band 4). As mentioned earlier, the difference between these two weighting schemes is intended to reflect specific physical models of the dominant noise processes in the two cases. Bands 1 through 3 have photomultiplier detectors which are taken to have a dominant noise contribution characterized by photoelectron statistics. Band 4, on the other hand, has photodiode detectors whose dominant noise contribution is taken to be from dark current.

The on-line gains and offsets so determined are the ones monitored during acceptance testing. They are also the ones used in the computation of any parameters upon which specification constraints are imposed. Thus, the terms gain and offset as used in the remainder of this section refer exclusively to the on-line gain and offset, respectively.

The stability of the internal calibration system is monitored by means of three parameters: COSL, DCC, and DBB. These effectively serve to measure changes in the apparent collimator brightness, as described above.

The fundamental parameter is COSL, which indicates the response of a particular scanner channel to the collimator, assuming nominal values of the channel gain and offset. In particular, if L(b) is the specified maximum radiance to which band b will respond without saturation, COSL is given by the relationship

ORIGINAL PAGE IS
OF POOR QUALITY

$$COSL(d,k,b) = \frac{64\,R(d,b)}{L(b)} = \frac{64\,[S(d,b,k) - O(d,b,k)]}{L(b)\,G(d,b,k)\,U(d,b,k)} \tag{6-12}$$

where the data set index, d, is understood to refer to a collimator (as opposed to integrating sphere or flooding lamp) data set. Every channel in a given band should in principle yield the same COSL value for a particular data set, and that value should not change in time. However, the measured values of the COSL parameter do vary, due to statistical uncertainties in the measurement process, if for no other reason. There may also be real changes in the collimator or scanner which cause the COSL parameter to vary. Under the assumptions of the model described here, either the shaded collimator radiance, Q(d,b,k), or the shaded internal calibration radiance, q(d,k,w), would have to change to explain a change in corrected signal level.

DCC is the peak-to-peak spread in COSL across all six channels of a particular band. The system specification on DCC requires it to be less than 2 percent of a reference band average at all times.

$$DCC(d,b) = \max_{k\epsilon b} COSL(d,b,k) - \min_{k\epsilon b} COSL(d,b,k) \tag{6-13}$$

$$< 0.02\,\pi_{k\epsilon b}[COSL^{*}(d,b,k)]^{1/6}$$

where * refers to COSL measurements made at the time of a collimator transfer of calibration.

Examination of Equations 6-12 and 6-13 reveals that the constraint on DCC is equivalent to a constraint on channel shading, U(d,b,k). In particular, dividing both sides of Equation 6-13 by the geometric mean of the corrected signal level and observing that the corrected signal level is proportional to the apparent collimator brightness as seen by the scanner (after correction for known collimator shading) reveals that Equation 6-13 is really a constraint on the peak-to-peak spread in the residual shading of the collimator. Ideally, this should be zero. Nonzero values are expected, however, if only because of statistical uncertainties in the measurement process. Nonzero values may also be due to real changes in either the collimator or the scanner itself. In particular, changes in either the shading of the collimator, U(d,b,k), or the internal calibration system, u(b,k), would be implied under the assumptions of the model described in this section.

Finally, DBB is the peak-to-peak spread in the ratio of the (geometric) mean of COSL across all six channels of a band relative to the value of this mean at some canonical time (e.g., transfer of calibration to the collimator) across all four bands. There is a specified constraint on DBB which requires it to be less than 3 percent of the ratio of the (arithmetic) mean of the (geometric) means of COSL in each of the four bands relative to

the value of this quantity at the same canonical time as mentioned previously. Symbolically, this is expressed as

$$DBB\ (d) = \underset{b}{MAX} \frac{t(d,b)}{t^*(d,b)} - \underset{b}{MIN} \frac{t(d,b)}{t^*(d,b)} < 0.03 \qquad (6\text{-}14)$$

where

$$t\ (d,b) = \frac{\prod_{k \epsilon b} [COSL\ (d,b,k)]^{1/6}}{\frac{1}{N} \sum_{b=1}^{N} \left\{ \prod_{k \epsilon b} [COSL\ (d,b,k)]^{1/6} \right\}} \qquad (6\text{-}15)$$

N = number of active of active bands (e.g. N=3 for compress/low)

and $t^*(d,b)$ is the same as t(d,b), except that it is calculated based on data from a reference data set, normally data taken during a collimator transfer of calibration. The DBB parameter effectively measures relative changes in the apparent band average radiance of the collimator over all four bands. As with DCC, it is ideally zero, but nonzero values can be expected, if only because of statistical uncertainties in the measurement process. Of course, nonzero values may also be due to real changes in either the collimator or the scanner itself. Under the assumptions of the model described in this section, these would have to be changes in the value of either R(d,b) or r(d,w) relative to their arithmetic means over all four bands. This is in a sense analogous to the shading constraint on DCC.

6.4.3 Square Wave Response (MTF)

One measure of MSS system performance is provided by square wave response (MTF) measurements performed regularly during acceptance testing of the instrument. This measurement, also referred to as the scanner modulation transfer function, is an indirect estimate of the system frequency response. This assessment is made at three spatial frequencies (i.e., those corresponding to the half-cycle wavelengths of 235', 450', and 650' as measured on the ground) using a square wave pulse train radiance input. The input radiance signal is generated within the collimator by the use of several reticle patterns. These patterns differ from those used on MSS-C in that they are rectilinear rather than radial. Although all three frequencies are tested during acceptance testing, it is only the pattern corresponding to 235' that is subject to specification. The others are measured for diagnostic and information purposes only.

Problems were encountered with the MTF algorithms during MSS-C testing which were characterized by abnormally low MTF estimates. This was subsequently attributed to excessive line length variations, to which the MSS-C algorithms were particularly sensitive. For MSS-D, a new algorithm was developed that is insensitive to these variations. The new algorithm employs a multiple linear regression technique that has proved to be extremely robust in terms of its ability to operate in adverse environments.

ORIGINAL PAGE IS
OF POOR QUALITY

6.4.3.1 General Test Description

In the system specification, the MTF of the instrument at a spatial half-wavelength of 235' (as measured on the ground) is required to be greater than 0.36. The MTF of the system is measured at 235', 450', and 650' bar patterns whenever data sets 4, 5, and 6 respectively, are called for during testing. The system configuration for these data sets is provided in Table 6-2.

The fundamental equation for estimating MTR is given by

$$MTF = \frac{V_{max} - V_{min}}{V_{max} + V_{min}} \tag{6-16}$$

where

V_{max} = maximum value of modulated response to the reticle pattern

V_{min} = minimum value of modulated response to the reticle pattern

If the bar space pattern is symmetrical, i.e., a 50 percent duty cycle, the dc value of the modulated response is V0/2 when

$$V0 = V_{max} + V_{min}$$

and Equation 6-16 can be rewritten in the following ways

$$MTF = \frac{2\,V_{max} - V0}{V0} = \frac{2\,V_{max}}{V0} - 1 \tag{6-17}$$

$$MTF = \frac{V_{max} - V_{min}}{V0} \tag{6-18}$$

TABLE 6-2. SYSTEM CONFIGURATION FOR DATA SETS 4, 5, AND 6

Parameter	Data Set		
	6	5	4
Neutral density filter position	50%	50%	50%
MTF reticle position	650'	450'	235'
Folding mirror position	TBD	TBD	TBD
Flooding lamp position	Out	Out	Out
Scanner gain	Low	Low	Low
Multiplexer mode	Linear	Linear	Linear
Channels collected	1 to 24	1 to 24	1 to 24

ORIGINAL PAGE IS
OF POOR QUALITY

Equation 6-17 is used for 450' and 650' bar pattern MTF estimation since V_{min} can be negative for these patterns, (Note: The multiplexer does not pass negative voltages). For the 235' bar pattern, V_{min} is positive and therefore Equation 6-18 is used.

6.4.3.2 Data Reduction

Upon selection of any one of data sets 4, 5, or 6, the system test computer collects 40 consecutive words in the middle of the bar pattern for 100 consecutive scans. These data are obtained for all 24 channels at the same time and are stored on disk for reduction.

450' and 650' Bar Pattern Data Reduction Algorithms

Let R(i,j) be the output (response) of the system while viewing the j-th word (j=1,2,.....,40) during the i-th scan (i=1,2,.....,100). Let $R_{AVG(j)}$ be the average response (over scans) for the 40 words; i.e.,

$$R_{AVG(j)} = \sum_{i=1}^{100} R(i,j)/100 \qquad (6\text{-}19)$$

Then letting

$$V_{MAX} = \max\left\{V_{MAX(j)}\right\}, \qquad j = 1, 2, \ldots, 40$$

and V_{open}* be, by definition, the average response obtained while viewing the open reticle (measured during a signal-to-noise test), then

$$MTF = \frac{2\,V_{MAX}}{V_{open}} - 1 \qquad (6\text{-}20)$$

This process is repeated until 24 channel estimates of MTF have been computed.

235' Bar Pattern MTF Algorithm

A bar pattern of 235' half-wavelength corresponds to an electrical frequency of approximately 40 kHz. However, after the signal passes through the low-pass Butter-

*V_{open} = VO, in theory.

worth filter, only the dc and fundamental frequencies remain of the original square-wave input; i.e., the multiplexer output resembles a sampled sinusoid of the form

$$R_i = A + B\sin(\omega T_i + \phi) \tag{6-21}$$

ORIGINAL PAGE IS
OF POOR QUALITY

where subscript i=1,2,.....,40 is the word number, ω is the fundamental frequency (approximately 40 kHz), ϕ is the phase, B is the amplitude of the fundamental, and A is the dc offset. since the frequency, ω, is assumed constant during the 100 scans where data are collected, only A, B, and ϕ need be determined. By trigonometric identity, Equation 6-13 can be rewritten as

$$R_i = A + (B\cos\phi)\sin(\omega T_i) + (B\sin\phi)\cos(\omega T_i) \tag{6-22}$$

$$B' \triangleq B\cos\phi$$

$$B'' \triangleq B\sin\phi$$

Equation 6-22 is a linear equation in the unknowns A, B', and B", and therefore can be solved by multiple linear regression to obtain a minimum least-squares estimate of these parameters.

Now,

$$\mathrm{MTF} = \frac{V_{max} - V_{min}}{V_{max} + V_{min}} \tag{6-23}$$

where

$$V_{max} = \max\left\{A + B\sin(\omega T_i + \phi)\right\}$$
$$= A + B$$

and similarly

$$V_{min} = A - B$$

Therefore, for a given scan,

$$\mathrm{MTF} = B/A = \frac{\sqrt{(B')^2 + (B'')^2}}{A} \tag{6-24}$$

ORIGINAL PAGE IS
OF POOR QUALITY

Therefore, the MTF estimation algorithm for the 235' bar pattern can be summarized as follows: Let R(i,j) be the response of the system to the 235' bar pattern for word j (j=1,2,....,40) of scan i (i=1,2,....,100). Using the first scan of data determine the electrical frequency of the pattern. (This is accomplished by finding the frequency at which the sum of the residuals after least-square fitting with respect to A, B', and B" yield a minimum. Analysis has shown this point to correspond to the actual reticle pattern electrical frequency.) Using this frequency, process all 100 scans of data as follows:

For scan i

$$MTF(i) = \frac{\sqrt{B'(i)^2 + B''(i)^2}}{A(i)} \tag{6-25}$$

where

$$\left.\begin{array}{l} B'(i) \\ B''(i) \\ A(i) \end{array}\right\} \text{Estimates of A, B' and B" obtained from multiple linear regression analysis from 40 samples of scan i.}$$

Then, the MTF for the channel is given by

$$MTF = \sum_{i=1}^{100} MTF(i)/100 \tag{6-26}$$

This process is repeated for the remaining 23 channels of data.

6.4.4 Mean Line Length, Line Length Variation, and Scan-to-Scan Repeatability

Three of the four algorithms used in the MSS-D system test DRS to measure the geometric fidelity of the scanner are described in this section: 1) active scan period, or mean line length (MLL), 2) line length variation (VLL), and 3) scan-to-scan repeatability (SRO). The fourth algorithm, used to assess scan-to-scan cross-axis motion, is described in 6.4.5.

6.4.4.1 General Test Description

In the system specification the active scan period (MLL) of the MSS-D scanner is specified to lie in the interval [31.5,34.0] ms. The active scan period (ASP) is, by definition, the time interval required for the scan mirror to traverse the angle between SMP1 (beginning of scan pulse) and SMP3 (end of scan pulse). A measure of this interval is provided by the system demultiplexer, which counts the number of multiplexer words that occur between SMP1 and SMP3. This, together with the basic multiplexer word rate, provides the necessary data to compute MLL.

The scan-to-scan line length variation or, equivalently, active scan period variation, is called out to be less than 42 μrad, rms, over 100 consecutive scans. MLL data, together with the active scan angle (i.e., the angle between SMP1 and SMP3 measured in the image space), provide the necessary data to compute VLL.

The objective of the SRO algorithm is to measure the time variation (scan-to-scan) between SMP1 and the instant of arrival of a stationary target. This measurement is performed for a selected target (i.e., video pulse) position in the scanner field of view. The requirement is specified so that contiguous points on adjacent scans are displaced by no more than approximately ±27.8 feet (rms). Correction for line length variation through the use of the active scan period code is allowed in the verification of the specification. This requirement is equivalent to an rms jitter of 24 μrad (scan-to-scan) in the scan mirror image space.

Each of the algorithms described above is performed whenever a data set 0 is specified during system test operations. The system configuration for this data set is provided in Table 6-3.

6.4.4.2 Data Reduction

Upon selection of a data set 0, the system test computer collects 40 consecutive words from channel 17 starting at a prespecified location (currently 1550 words after SMP1) and the three line length words (word number 3773, 3774, and 3775 after SMP1) for each of 100 consecutive scans and stores these data on disk.

Active Scan Period (MLL) Algorithm

After collection, each of the 100 scans is individually processed as follows. The three computer words containing the line length code are decoded to yield the number of multiplexer words that occurred between SMP1 and SMP3. An example of the procedure required to decode the code is provided in Table 6-4. Given the word count for scan j, W(j), the active scan period, T(j), is given by

$$T(j) = 0.3983\, W(j)\ \mu\text{sec} \tag{6-27}$$

where 0.3983 (μsec/word) is the basic multiplexer word rate.

ORIGINAL PAGE IS
OF POOR QUALITY

TABLE 6-3. SYSTEM CONFIGURATION FOR DATA SET 0

Neutral density filter position	50%
MTF reticle position	Open
Folding mirror position	TBD
Flooding lamp position	Out
Scanner gain	Low
Multiplexer mode	Linear
Channel collected	17

TABLE 6-4. LINE LENGTH DECODING EXAMPLE

- The demultiplexer word count is contained in (computer) array locations ILL(1, j), ILL(2, j), and ILL(3, j) for scan j, j=1, 100.
- To determine the word count, the array elements must be converted to binary, concatenated, bits reversed, and converted back to decimal for each scan as follows:

	ILL(1, j)	ILL(2, j)	ILL(3, j)
Decimal	35	37	50
Binary	100011	100101	110010
Bit reversal	110001	101001	010011
Decimal	49	41	19
	ILL(1, j)	ILL(2, j)	ILL(3, j)

- Denoting (as indicated) the reversed decimal representation of ILL(i, j) by ILL(i, j) the word count can then be written as

$$L(j) = 4096\, ILL(3, j) + 64\, ILL(2, j) + ILL(1, j)$$

For the example shown, the word count is given by

$$L = 4096\,(19) + 64\,(41) + 49$$
$$= 80{,}497 \text{ multiplexer words}$$

ORIGINAL PAGE IS
OF POOR QUALITY

The active scan period specification is considered met if all 100 scans have line lengths that lie in the interval [31.5,34.0] ms.

Line Length Variation Algorithm

The VLL algorithm utilizes the same 100 estimates of T(j) used in determining ASP compliance. The VLL specification is considered met if

$$VLL = \sqrt{\frac{1}{99} \sum_{j=1}^{99} \left(T(j+1) - T(j)\right)^2} \cdot \frac{\theta_{as}}{MLL} \leqslant 42 \ \mu rad \tag{6-28}$$

where

θ_{as} = active scan angle (image space), μradians

MLL = average active scan period, μsec

$$= \frac{1}{100} \sum_{j=1}^{100} T(j)$$

Scan Repeatability Algorithm

In the initial stages of scanner integration, analog measurements are made of scanner response to the leading edge of the collimator video pulse. From these data a model is developed to estimate the "arrival time" of the video pulse given a sample on the leading edge. This step is necessitated by the relative coarseness of the sampling interval. Based upon this model an estimate of the video pulse arrival time, Ta(j), for scan j measured from SMP1 is computed. The SRO specification is assumed met if

$$SRO = \sqrt{\frac{1}{99} \sum_{j=1}^{99} [P(j+1) - P(j)]^2} \cdot \theta_{as} \leqslant 24 \ \mu rad$$

where (6-29)

$$P(j) \triangleq \frac{T_a(j)}{T(j)}$$

ORIGINAL PAGE IS
OF POOR QUALITY

TABLE 6-5. SYSTEM CONFIGURATION FOR DATA SET 7

Neutral density filter position	50%
MTF reticle position	Chevron
Folding mirror position	TBD
Flooding lamp position	Out
Scanner gain	Low
Multiplexer mode	Linear
Channel collected	17

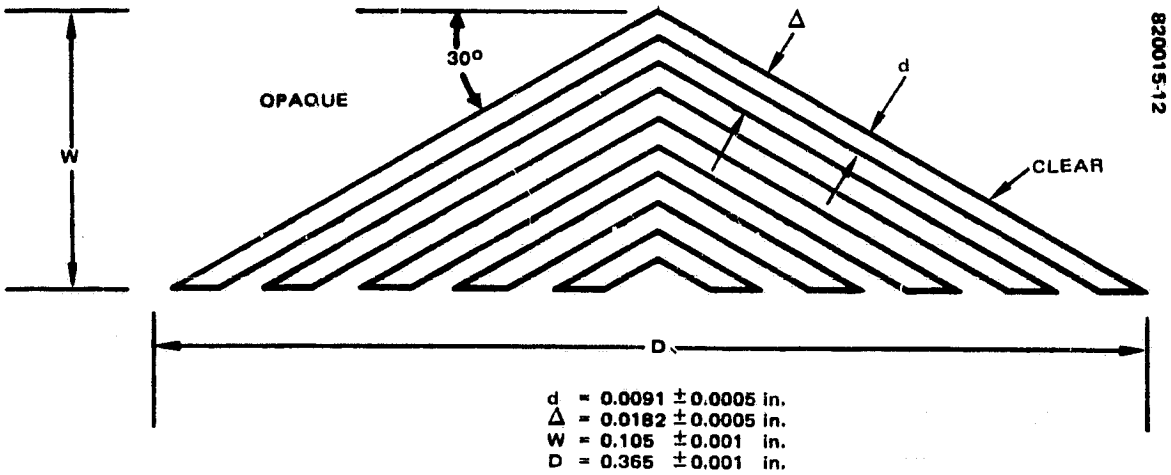

NOTES: 1. ALL CHEVRON BAR EDGES SHALL NOT DEVIATE FROM PARALLEL STRAIGHT LINES BY MORE THEN ±0.00025 in.
2. COLLIMATOR FOCAL LENGTH IS 90 in.

FIGURE 6-3. COLLIMATOR CHEVRON PATTERN RETICLE DIMENSIONS

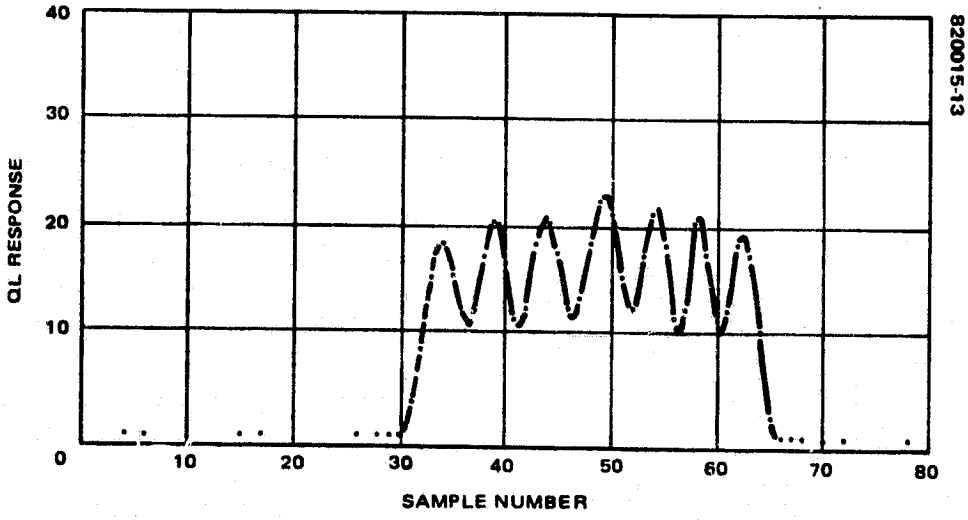

FIGURE 6-4. TYPICAL CHEVRON PATTERN SYSTEM RESPONSE

6.4.5 Cross-Axis Repeatability

Cross-axis motion is defined as mirror movement perpendicular to the desired scan direction. The system specification limits this motion from one scan to the next to be, on the average, less than 33 μrad, rms. The cross-axis repeatability determination is made whenever a data set 7 is specified during system test operations. The system configuration for this data set is provided in Table 6-5.

6.4.5.1 General Test Description

Cross-axis motion is measured by repeated scans across the collimator chevron pattern depicted in Figure 6-3. A single scan across the chevron produces a tone burst signal at the detector output whose duration is proportional to the scan height relative to the base of the pattern. Therefore, from a knowledge of the scan velocity and chevron pattern geometry, the cross-axis amplitude may be inferred. Typical multiplexer response data are shown in Figure 6-4. Unfortunately, due to sampling coarseness a direct measurement of response pulse duration is not possible. Instead, an extrapolation estimation scheme must be employed to compute leading edge arrival and trailing edge departure times and therefore response duration. The available data consist of 80 samples taken from each of the 100 consecutive scan lines. The tone burst duration is approximately 40 samples.

6.4.5.2 Data Reduction

The leading and trailing edges of the scanner response to the chevron pattern are estimated by linear extrapolation from the first and last multiplexer output word greater than a predetermined threshold. The thresholds are determined independently for the leading and trailing edges.

Upon selection of a data set 7 by the test conductor, the system test computer collects 80 consecutive words from channel 17 starting at a prespecified location (currently 1550 words after SMP1). After collection, each of the 100 scans is individually processed as described below. The first step is to find the maximum signal level in the entire 100 scan lines. The integer variable MAX5 is set to 20 percent of this level. Maximum responses on the leading and trailing edges of the j-th scan are then computed using the following levels and indices:

JB(j) = word number of first word >MAX5

JC(j) = word number of last word >MAX5

JD(j) = (JB(j) + JC(j))/2

MAXL(j) = max {CXI(i,j)}, i = JB(j) to JD(j)

MINL(j) = min {CXI(i,j)}, i = JB(j) to JD(j)

MAXT(j) = max {CXI(i,j)}, i = JD(j) to JC(j)

MINT(j) = min {CXI(i,j)}, i = JD(j) to JC(j)

where CXI(i,j) is the scanner response (QL) for word i of scan j, where i runs from 1 to 80 and j from 1 to 100.

$$AVEL(j) = (MINL(j) + MAXL(j))/2$$
$$AVET(j) = (MINT(j) + MAXT(j))/2$$

JF(j) = index of last word in left half >AVEL

JG(j) = index of first word in right half >AVET

$$XMAXL(j) = \max \{CXI(i,j)\}, \quad i = JB(j) \text{ to } JF(j)$$
$$XMAXT(j) = \max \{CXI(i,j)\}, \quad i = JG(j) \text{ to } JC(j)$$

Let AMAXL and AMAXT be the average of XMAXL(j) and XMAXT(j) for 100 scans

$$AMAXL = \sum_{j=1}^{100} XMAXL(j)/100$$
$$AMAXT = \sum_{j=1}^{100} XMAXT(j)/100 \qquad (6\text{-}30)$$

Now that the thresholds are set, the response pulse arrival and departure times for the individual scans can be determined:

$$TL(j) = 9.958\, UT2(j) - 22.0\, \big(CXI(UT2(j), j\big)/AMAXL$$
$$TT(j) = 9.958\, UT3(j) + 22.0\, \big(CXI(UT3(j), j\big)/AMAXL \qquad (6\text{-}31)$$

where 1) UT2(j) is the index of the first multiplexer word in the j-th scan line that is greater than MAXL5, 2) UT3(j) is the index of the last multiplexer word greater than MAXT5, 3) 9.958 μsec/word is the multiplexer channel word rate, and 4) 22 QL/word is the average leading and trailing edge response slope magnitude.

The cross-axis motion amplitude for the j-th scan line is given by

$$PHI(j) = 1.774[TT(j) - TL(j)] \tag{6-32}$$

The rms scan-to-scan cross-axis repeatability for 100 scans is then given by

$$CXAXO = \sqrt{\frac{1}{99} \sum_{j=1}^{99} [PHI(j+1) - PHI(j)]^2} \tag{6-33}$$

and the specification is met if CXAXO $\leq$ 33.0 μrad.

6.5 OFF-LINE ANALYSIS

Three classes of parameters are used in the off-line analysis of internal calibration stability: band average radiances, collimator shading, and shading of the internal calibration system. These are described in the following paragraphs; the discussion focuses on interpretation of the parameters and their relationships to the parameters more commonly used in evaluating calibration stability, i.e., COSL, DCC, and DBB.

The term "radiance" as used in this discussion refers to the radiance of the collimator external calibration source as measured by the scanner, averaged arithmetically over all six channels in a particular spectral band. This parameter is expected to be proportional to the true brightness of the collimator lamp as viewed through the neutral density filter currently in place; in fact, the two are expected to be equal if the scanner is well calibrated. However, the observed radiance will also be inversely proportional to the brightness of the internal calibration source, the exact specification of which will be left undefined except to comment that it incorporates in some way the entire range of the calibration wedge. It should be noted that the band average radiance of the collimator, as just defined, uses an arithmetic average over radiances. This differs from the usual definition (e.g., as used in COSL, DCC, and DBB), which involves a geometric average over radiances measured by each channel in a given band.

The term "internal calibration shading" refers to the radiance of the internal calibration source as viewed by a particular channel relative to the (arithmetic) average of the radiances observed by all channels in the band. As previously mentioned, the "radiance" of the internal calibration source is in some fashion (not precisely defined) averaged over all positions in the calibration wedge. This parameter is deduced from observing the flooding lamp source in the collimator. The apparent shading of the

flooding lamp is defined as its radiance measured using a particular channel relative to the (arithmetic) average of its radiance as viewed by all channels in the band. This is, in principle, proportional to the actual shading of the flooding lamp source, i.e., the physical brightness of the flooding lamp in the field of view of the particular channel of interest relative to its brightness averaged over the fields of view of all channels in the band. It is inversely proportional to the internal calibration shading as defined above. It is assumed that the flooding lamp is flat (i.e., having no actual shading or equally bright in the field of view of each channel of a band), the apparent shading of the flooding lamp reduces to the inverse of the internal calibration shading. This relationship is used in the off-line analysis to monitor the internal calibration shading during thermal-vacuum testing.

Finally, the term "collimator shading" refers to the apparent shading of the collimator (analogous to the apparent shading of the flooding lamp as defined) divided by the corresponding apparent flooding lamp shading (as defined). In contrast to the case of the flooding lamp, the collimator is assumed not to be flat (i.e., it is shaded). The division by the apparent flooding lamp shading serves to replace any dependence on internal calibration shading by a dependence on flooding lamp shading (assumed uniform). As a result, the collimator shading parameter is modelled as proportional to the physical shading of the collimator source and inversely proportional to the physical shading of the flooding lamp source.

These parameters are calculated using data from the collimator data sets (1, 22, and, occasionally, 11) and the flooding lamp data sets (24 and 25). The collimator data sets correspond to neutral density filter settings of 50 percent (data set 1), 25 percent (data set 11), and 10 percent (data set 22). The flooding lamp data sets correspond to data from channels 1 through 12 (data set 24) and channels 13 through 24 (data set 25), and thus may be viewed as effectively comprising a single data set, hereafter, referred to as the flooding lamp data set. Independent estimates of band average collimator radiance are calculated using data from data sets 1, 11 (when available), and 22. The flooding lamp data set is used to estimate internal calibration shading. Finally, separate estimates of collimator shading are derived from each of data sets 1, 11 (when available), and 22 used in conjunction with the flooding lamp data set. This last calculation (of collimator shading) is dependent on the assumption that nothing changes over the time span required to collect an entire orbit of data (i.e., all the data involved in the calculation).

The on-line parameters relating to calibration stability are COSL, DCC, and DBB. The relationship of each of these to the off-line parameters described above is discussed.

COSL essentially measures the apparent brightness of the collimator source as seen by a single channel, corrected for any shading measured at the transfer of calibration to the collimator. COSL is reported in units of "idealized quanta," where radiance 0 is mapped to the bottom of quantum level 0, and the maximum radiance for the band is mapped to the top of quantum level 63. The collimator lamp is used with any one of the three neutral density filters (10, 25, or 50 percent) in place. The flooding lamp is not used in the calculation of COSL, DCC, or DBB. Every channel in a given band should, in principle, yield the same COSL when viewing a particular external source, and this value should be independent of time. However, the measured values of the COSL parameter will vary due to statistical uncertainties in the measurement process, if for no other

reason. There may also be real changes in the collimator and/or scanner. In terms of the parameters used in the present discussion, COSL may be modelled as proportional to the product of the collimator band average radiance and the appropriate collimator shading factor; it is inversely proportional to the corresponding internal calibration shading factor.

The general analysis involves testing the hypothesis of no change in each of the parameters analyzed (i.e., collimator band average radiances, collimator shading factors, and internal calibration shading factors). Statistics are accumulated on the number of times the probability of no change falls below 0.1 percent for each parameter. In doing this, all observations are modelled as independent Gaussian random processes. Figure 6-5 summarizes the results of such an analysis in the MSS flight model during thermal-vacuum testing. Scatter plots are also used in the analysis (on selected subsets of the data) to illuminate correlations with time, temperature, and others of the parameters analyzed. In particular, all of the parameters investigated are plotted against the corresponding band average radiance; correlations between collimator and internal calibration shading are also investigated.

In interpreting the cross plots of collimator and internal calibration shading, it should be recalled that the collimator and internal calibration shading (as described above) are both inversely proportional to the shading of the flooding lamp source, which is assumed uniform. If the assumption of constant flooding lamp shading should fail, then one would expect the data to be distributed along a line of slope 1 in a scatter plot of collimator versus internal calibration shading. Although this is not the only possible explanation of such behavior, it does seem to be the only one where the scanner itself is not implicated. Under more ideal conditions, one would expect the data on such a plot to be clumped about the origin. The shape of the clump would be roughly that of an ellipse, whose axes are aligned with the coordinate axes. The major and minor axes of the ellipse would be determined by the uncertainties in the parameters estimated. Since the original transfer of calibration to the collimator is statistically no better than any of the points plotted, bias errors may be anticipated which would cause the data clump to be offset somewhat from the origin. When this offset is anomalously large, it may lead to an increase in the DCC failure rate. Finally, the contribution of a given channel to DCC (which is computed over an entire band) may be viewed as the distance (along either axis) of a specific data point from a line of slope 1 through the origin on the shading factor cross plot. The DCC specification would then require that the peak-to-peak variation in contribution to DCC across a band not exceed 2 percent. This is qualitatively equivalent to requiring the large majority of data to fall in a band between lines of slope 1 through ±1 percent on the shading cross plot. Note that this latter statement replaces a constraint on an entire band at a fixed time with a constraint on a single channel over an extended time, thus effectively ignoring the other channels in the band. It cannot, therefore, be expected to be true in any more than a statistical sense.

An example of such a cross plot is given in Figure 6-6, which relates to the performance of channel 11 during thermal-vacuum testing of the MSS flight model. As can be seen, there is a correlation exhibited between collimator and internal calibration shading in this case. However, the correlation is not 1 to 1, as would be expected if the flooding lamp shading were changing. Therefore, it must be concluded (under the assumptions of the shading model used) that at least two of the three parameters (collimator shading, internal calibration shading, and/or flooding lamp shading) must be

TEST SYSTEM A		BAND 1						BAND 2						BAND 3						BAND 4						COLLIMATOR RADIANCE			
		CH 1	CH 2	CH 3	CH 4	CH 5	CH 6	CH 7	CH 8	CH 9	CH 10	CH 11	CH 12	CH 13	CH 14	CH15	CH 16	CH 17	CH 18	CH 19	CH 20	CH 21	CH 22	CH 23	CH 24				
SON	TEMP	COLL DS 1 / COLL DS 22 / INT CAL	COLL DS 1 / COLL DS 22 / INT CAL	COLL DS 1 / COLL DS 22 / INT CAL	COLL DS 1 / COLL DS 22 / INT CAL	COLL DS 1 / COLL DS 22 / INT CAL	COLL DS 1 / COLL DS 22 / INT CAL	COLL DS 1 / COLL DS 22 / INT CAL	COLL DS 1 / COLL DS 22 / INT CAL	COLL DS 1 / COLL DS 22 / INT CAL	COLL DS 1 / COLL DS 22 / INT CAL	COLL DS 1 / COLL DS 22 / INT CAL	COLL DS 1 / COLL DS 22 / INT CAL	COLL DS 1 / COLL DS 22 / INT CAL	COLL DS 1 / COLL DS 22 / INT CAL	COLL DS 1 / COLL DS 22 / INT CAL	COLL DS 1 / COLL DS 22 / INT CAL	COLL DS 1 / COLL DS 22 / INT CAL	COLL DS 1 / COLL DS 22 / INT CAL	COLL DS 1 / COLL DS 22 / INT CAL	COLL DS 1 / COLL DS 22 / INT CAL	COLL DS 1 / COLL DS 22 / INT CAL	COLL DS 1 / COLL DS 22 / INT CAL	COLL DS 1 / COLL DS 22 / INT CAL	BAND 1 DS 1 / BAND 1 DS 22	BAND 2 DS 1 / BAND 2 DS 22	BAND 3 DS 1	BAND 4 DS 1
104	21.2																									XX	XX	X	X
106	24.6											X														XX	XX	X	X
108	31.3											X														XX			X
114	31.6											X														XX	X		X
116	29.9											X														XX	X	X	X
118	19.9																									XX	XX	X	X
120	9.3											X								X						XX	XX	X	X
126	4.3	X					X				X	X								X				X		XX	XX	X	X
129	9.5						X					X								X				X		XX	XX	X	X
131	10.0						X					X														XX	XX	X	X
133	19.2																									XX	XX	X	X
135	20.2																									XX	XX	X	X
138	29.3	X										X														XX	XX	X	X
140	30.9											X														XX	XX	X	X
142	30.3	X										X														XX	XX	X	X
148	31.6											X		X												XX	XX	X	X
150	26.9											X														XX	XX	X	X
152	15.9	X					X																			XX	XX	X	X
154	10.1						X					X												X		XX	XX	X	X
160	11.3	X				X	X					X														XX	XX	X	X
162	11.8						X					X												X		XX	XX	X	X
164	24.1																									XX	XX	X	X
629	29.9											X														XX	XX	X	X
166	30.3											X														XX	XX	X	X
172	31.6											X														XX	XX	X	X
174	30.3											X														XX	XX	X	X
180	28.7											X														XX	XX	X	X
182	28.4											X														XX	XX	X	X
631	10.1	X		X			X					X														XX	XX	X	X
186	9.5			X			X					X														XX	XX	X	X
192	10.6						X		X			X												X		XX	X	X	X
194	10.0	X					X					X												X		XX		X	X
200	10.8	X					X					X															XX	X	
633	15.9																									XX	XX		X
635	14.9																									XX	XX		X
204	20.9																									XX	XX	X	X
211	21.2								X																	XX	XX	X	X
212	23.5																									XX	XX	X	X
214	23.5																									XX	XX	X	X

X = Change detected by hypothetical test.

a) SYSTEM A

FIGURE 6-5. F-1 CALIBRATION STABILITY DURING THERMAL-VACUUM TESTING

820015-14

ORIGINAL PAGE IS OF POOR QUALITY

TEST SYSTEM B		BAND 1						BAND 2						BAND 3						BAND 4						COLLIMATOR RADIANCE			
		CH 1	CH 2	CH 3	CH 4	CH 5	CH 6	CH 7	CH 8	CH 9	CH 10	CH 11	CH 12	CH 13	CH 14	CH15	CH 16	CH 17	CH 18	CH 19	CH 20	CH 21	CH 22	CH 23	CH 24				
		COLL DS 1	COLL DS 1	COLL DS 1	COLL DS 1	COLL DS 1	COLL DS 1	COLL DS 1	COLL DS 1	COLL DS 1	COLL DS 1	COLL DS 1	COLL DS 1	COLL DS 1	COLL DS 1	COLL DS 1	COLL DS 1	COLL DS 1	COLL DS 1	COLL DS 1	COLL DS 1	COLL DS 1	COLL DS 1	COLL DS 1	COLL DS 1				
		COLL DS 22	COLL DS 22	COLL DS 22	COLL DS 22	COLL DS 22	COLL DS 22	COLL DS 22	COLL DS 22	COLL DS 22	COLL DS 22	COLL DS 22	COLL DS 22	COLL DS 22	COLL DS 22	COLL DS 22	COLL DS 22	COLL DS 22	COLL DS 22	COLL DS 22	COLL DS 22	COLL DS 22	COLL DS 22	COLL DS 22	COLL DS 22				
		INT CAL	INT CAL	INT CAL	INT CAL	INT CAL	INT CAL	INT CAL	INT CAL	INT CAL	INT CAL	INT CAL	INT CAL	INT CAL	INT CAL	INT CAL	INT CAL	INT CAL	INT CAL	INT CAL	INT CAL	INT CAL	INT CAL	INT CAL	INT CAL				
SON	TEMP																									BAND 1 DS 1	BAND 1 DS 22	BAND 2 DS 1	BAND 2 DS 22	BAND 3 DS 1	BAND 4 DS 1
99	20.9				X	X																							
105	20.4																									X	X	X	X	X	X
107	31.6					X	X					X														X	X				X
109	32.6				X	X	X	X				X																X	X	X	
115	31.6											X														X	X		X	X	X
117	26.6		X									X														X	X	X	X	X	X
119	11.6											X														X	X	X	X	X	X
121	0.5							X	X			X		X				X				X		X		X	X	X	X	X	X
127	3.4							X	X	X		X		X			X	X	X			X		X	X	X	X	X	X	X	X
130	2.5								X			X												X		X	X	X	X	X	X
132	10.6											X								X				X		X	X	X	X	X	X
134	19.9		X	X																						X	X	X	X	X	X
136	20.4																									X	X	X	X	X	X
139	30.6				X	X						X														X	X	X	X	X	X
141	30.6											X														X	X	X	X	X	X
143	31.3					X			X			X														X	X	X	X	X	X
149	30.6		X				X		X																	X	X	X	X	X	X
151	20.9		X		X	X																				X	X	X	X	X	X
153	13.0											X						X								X	X	X	X	X	X
155	10.8		X						X			X						X						X		X	X	X	X	X	X
161	10.1				X	X				X		X						X						X		X	X	X	X	X	X
163	15.4				X																					X	X	X	X	X	X
165	28.7											X														X	X	X	X	X	X
130	30.3											X														X	X	X	X	X	X
167	30.0				X							X														X	X	X	X	X	X
173	24.4			X								X														X	X	X	X	X	X
175	29.3											X														X	X	X	X	X	X
181	29.6			X	X							X														X	X	X	X	X	X
183	26.0																									X	X	X	X	X	X
632	10.4		X					X	X	X		X										X				X	X	X	X	X	X
182	10.4							X				X										X		X		X	X	X	X	X	X
193	10.4		X	X					X	X		X						X						X		X	X		X	X	X
195	10.0			X						X		X												X		X			X	X	X
201	12.0									X		X														X	X	X			X
634	15.9																									X	X	X			
636	15.4																									X	X	X			
205	20.4																									X	X	X	X	X	X
213	23.5																									X	X	X	X	X	X
215	23.5																									X	X	X	X	X	X

X = Change detected by hypothetical test.

b) SYSTEM B

FIGURE 6-5. (CONTINUED). F-1 CALIBRATION STABILITY DURING THERMAL-VACUUM TESTING

820015-15

ORIGINAL PAGE IS OF POOR QUALITY

**ORIGINAL PAGE IS
OF POOR QUALITY**

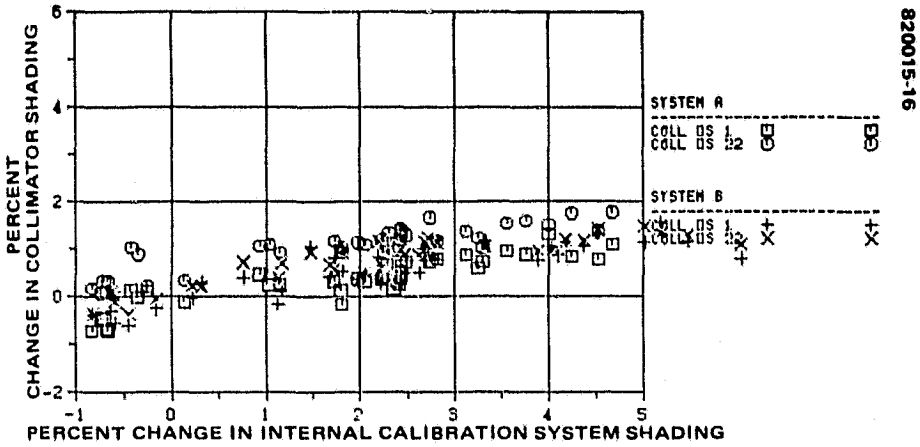

FIGURE 6-6. SHADING CORRELATION – CHANNEL 11

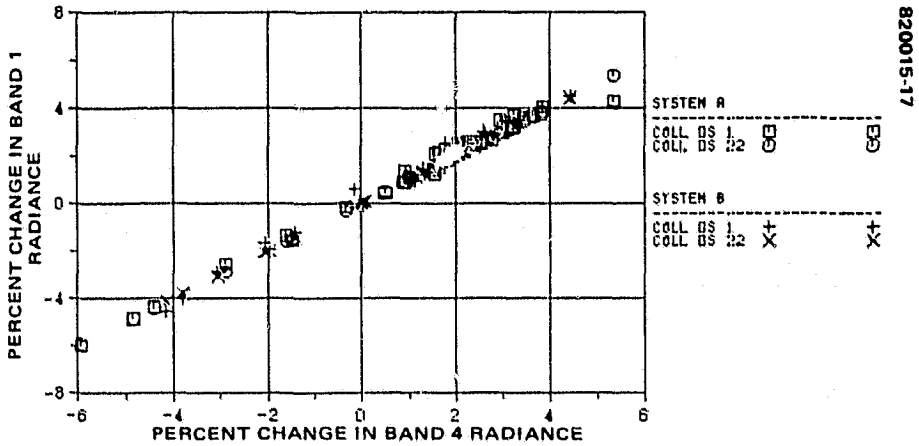

FIGURE 6-7. RADIANCE CORRELATION – BANDS 1 AND 4

simultaneously changing in a correlated fashion. Because the observed correlation is not 1 to 1, there is a strong contribution to DCC from channel 11.

The cross plots of radiances may be interpreted in much the same way, except that now DBB rather than DCC is involved in the interpretation. In particular, there is no contribution to DBB as long as the data are confined to a line of slope 1 through the origin in the radiance cross plots. The DBB specification requires that no point on any such plot lie outside a band defined by lines of slope 1 through ±3 percent.

An example of a cross plot of radiances is given in Figure 6-7, in this case for bands 1 and 4 during thermal-vacuum testing of the MSS flight model. Note that the changes in observed collimator radiance are large and tightly correlated between the two bands. If the 1 to 1 correlation which is observed in this case also appears on all such cross plots (i.e., all possible combinations of the four bands), then there will be no anomalous DBB values as a result of the changes in observed collimator radiance. The fact that the correlation is 1 to 1 suggests that the cause of the problem may well be external to the scanner. However, this would also require that the behavior be replicated in all other such cross plots, and even then the conclusion that the problem is external to the scanner would not be necessary.

Figure 6-8 presents an example of the use of plots of the various parameters as functions of time. This particular case relates to the behavior of the band average collimator radiance observed by band 1 of the MSS flight model during thermal-vacuum testing. The independent variable used is sequential orbit number (SON), rather than time, for convenience. Two phenomena are apparent from this plot. First, there is a systematic long term drift in the observed collimator radiance (in band 1) over the entire period of thermal-vacuum testing, shown in Figure 6-8a. Second, there is a much lower level (inverse) correlation with temperature, as shown by a comparison between Figures 6-8a and b. This latter temperature correlation will not be apparent on plots with temperature (rather than SON) as the independent variable, as it would then be completely masked by the long term drift (which is essentially independent of temperature).

As a final example, Figure 6-9 illustrates the use of plots with temperature as the dependent variable. In this case, the independent variable is the collimator shading of channel 11 during thermal-vacuum testing of the MSS flight model. The strong temperature dependence observed here can, in principle, be corrected since temperature can be measured and the dependence known. This should lead to a vastly improved DCC performance of band 2.

ORIGINAL PAGE IS
OF POOR QUALITY

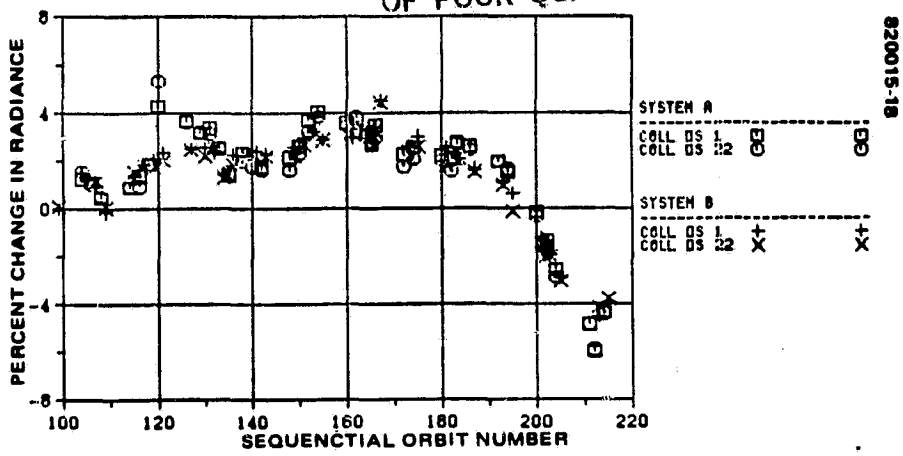

a) RADIANCE HISTORY

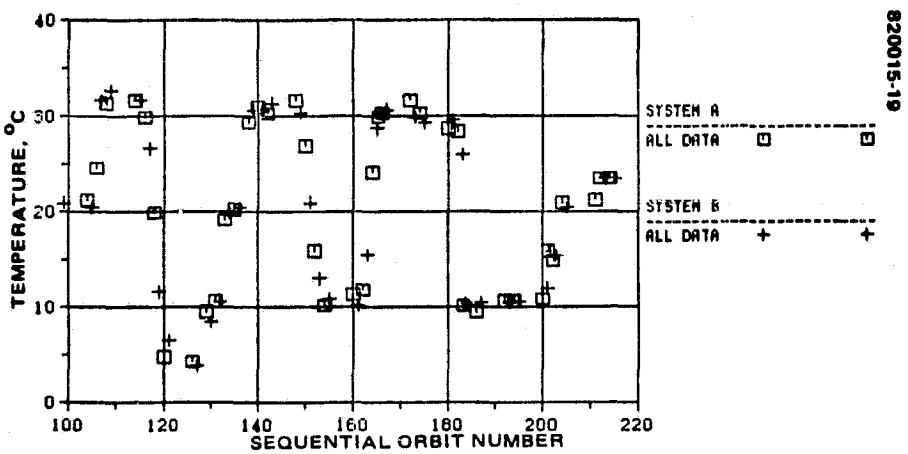

b) THERMAL HISTORY

FIGURE 6-8. BAND 1 AVERAGE COLLIMATOR RADIANCE – F-1 IN THERMAL-VACUUM

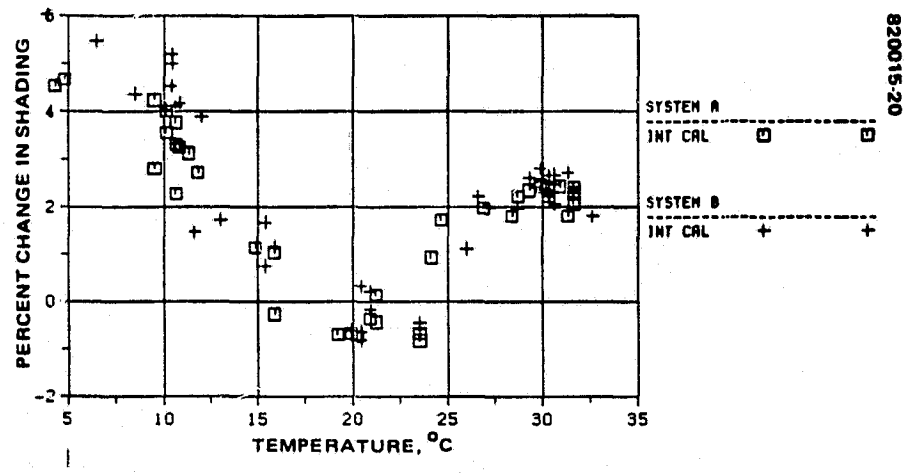

FIGURE 6-9. COLLIMATOR SHADING VERSUS TEMPERATURE – CHANNEL 11

7. PROTOFLIGHT ACCEPTANCE TEST RESULTS

7.1 INTRODUCTION

The MSS-D protoflight (PF) acceptance test history and acceptance test results are presented in this section, which, along with Sections 8 and 9, constitutes the PF acceptance test portion of the Final Report.

This section begins with a detailed, chronological presentation of the PF acceptance test history. The actual PF system test program is presented as it was performed, starting with system integration and ending with system delivery to the spacecraft contractor. Actual test activity is compared with that planned. Changes to the Test Plan (see Section 4) are emphasized and discussed as to cause for deviation from the plan. Configuration changes are highlighted as well. The subsection concludes with an event table which lists each major test activity, the date performed, and the sequential orbit number or special test request (STR) number associated with that activity. In this fashion a (nearly) day-by-day summary of test activity is provided which permits ready correlation of test activity with test performance results.

The remainder of the section is a presentation of the PF acceptance test results for each of the major system-level parameters. Each major parameter is treated in turn for the entire test period, with emphasis on performance as it relates to specification requirement. The discussion does not, however, restrict itself to whether the system met specifications with respect to each performance parameter. An overview of performance is given for each parameter which provides estimates of variability, repeatability, and sensitivity of measured data as a function of test environment and configuration where appropriate. Results are discussed as anomalous when the performance appears to deviate substantially from nominal performance even when the particular parameter is within specification.

To provide a complete overview of the system performance data without having it enlarge to burdensome size, the primary data were recorded on a 9-track computer tape, and plot routines were developed to permit an individual test history for any parameter, for any channel (or band), to be plotted on a single 8-1/2 by 11 plot. This is an approximate 14 to 1 reduction in volume from the on-line plots without substantial loss of information. These plots have the additional advantage of enabling the reader to view easily the major trends and variations in the data and to make comparisons readily of system performance variability and repeatability for recurring test environments and configurations throughout the entire acceptance test program. The graphics actually used for daily review of test performance during system acceptance testing are

presented when the greater resolution provided by those plots is required. A complete set of these on-line graphics has been provided separately.

The program used to provide the single page plot histories gives each data value serially from the first data point that the computer filed to the last and does not identify each orbit (or individual test) by the sequential orbit number used as standard identification for the individual test elsewhere. For easy cross-referencing, Table 7-1 identifies the sequential orbit number, standard orbit number, and major test event description corresponding to each of the serial orbit numbers provided on the plots.

7.2 PROTOFLIGHT TEST HISTORY

The protoflight integration and test plans are discussed in Section 4 of this report; this section describes the actual protoflight system test program as it evolved from system integration through delivery of the system to the spacecraft integration contractor. Figure 7-1 presents the detailed sequence of activities leading to the delivery of the protoflight system. In the figure, the rectangular boxes with solid outlines represent activities which were in the plan prior to the start of system test. The rectangular boxes with broken outlines represent changes to the original plan. The change could be a simple change in the test sequence or it could be a new test added to the program. The truncated ovals indicate a configuration change. This could be repair to a damaged part, replacement of a component to improve performance characteristics, implementation of a new design, or replacement of a complete unit. The number that appears above the boxes is the number of the procedure to which the activity was performed. The numbers below the boxes represent the start (S) and completion (C) dates of the activity within the box.

The first complete system performance test (CSPT) of the MSS-D PF was conducted at Santa Barbara Research Center (SBRC) at the completion of the formal PF system integration. The intent of this test was to establish the first performance baseline for the protoflight system, familiarize the system test team with the flight hardware, and accept the protoflight system from SBRC as ready to proceed into the protoflight qualification phase of the program.

During the CSPT, problems were experienced in scan repeatability (SRO) and signal-to-noise (STN). Four failure reports were generated: FR2443 identified the out-of-specification scan repeatability and FR2444, FR2446, and FR2447 involved STN. FR2443 was determined to be a software problem and was closed out with a software change. During the 2 weeks following the CSPT, special test requests (STRs) 30 through 38 were run to analyze the black/white code dropouts and to investigate video noise. The results of these special tests indicated the multiplexer was the source of the black/white code dropout and tended to indicate the scanner-to-multiplexer (MUX) video cable, W4016, was the most logical area for improvement in the video noise. A special test connector at connector J4, with 50 Ω series resistors in each video channel, improved video noise performance. It was also established that the S/N 1 W4016 cable had significantly better video noise performance than the identical S/N 2 cable. A decision was made to redesign the W4016 cable return lines and shield terminations. This redesigned cable is designated 78622.

ORIGINAL PAGE IS
OF POOR QUALITY

TABLE 7-1. PROTOFLIGHT REFERENCE ORBITS

Serial Orbit	Sequential Orbit	Standard Orbit	Test, Event
1	1	1	First Long Form Performance Test
2	2	2	
3	3	3	
4	4	4	
5	5	5	
6	6	6	
7	7	7	
8	8	8	
9	25	1	Pre-EMI
10	26	2	
11	27	3	
12	28	4	
13	29	5	
14	30	6	
15	31	7	
16	32	8	
17	35	1	
18	36	2	
19	37	7	
20	38	8	
21	52	1	Post-EMI/Previbration
22	53	2	
23	54	7	
24	55	8	
25	73	1	Postvibration
26	74	2	
27	75	7	
28	76	8	
29	83	1	Preacoustic*
30	84	2	
31	85	7	
32	86	8	
33	89	1	Postacoustic
34	90	2	
35	91	7	
36	92	8	
37	99	1	Pre-endbell
38	100	2	
39	101	7	
40	102	8	
41	105	1	Endbell
42	106	2	

*New flex pivots installed

ORIGINAL PAGE IS
OF POOR QUALITY

Table 7-1 (continued)

Serial Orbit	Sequential Orbit	Standard Orbit	Test Event
43	107	7	Endbell (continued)
44	108	8	
45	109	1	GN_2 backfill
46	110	2	
47	111	7	
48	112	8	
49	117	1	20°C
50	118	2	
51	119	3	
52	120	4	
53	121	5	
54	122	6	
55	123	7	
56	124	8	
57	125	1	20 to 40°C
58	126	2	
59	127	1	40°C
60	128	2	
61	130	3	
62	131	4	
63	132	5	
64	133	6	
65	134	7	
66	135	8	
67	136	1	40 to 0°C
68	137	2	
69	138	1	0°C
70	139	2	
71	140	3	
72	141	4	
73	142	5	
74	143	6	
75	144	7	
76	145	4	0 to 10°C
77	146	1	10°C
78	147	2	
79	148	7	
80	149	8	
81	150	6	10 to 20°C
82	151	1	20°C
83	152	2	
84	153	7	
85	154	8	

ORIGINAL PAGE IS
OF POOR QUALITY

Table 7-1 (continued)

Serial Orbit	Sequential Orbit	Standard Orbit	Test Event
86	155	3	20 to 30°C
87	156	1	30°C
88	157	2	
89	158	7	
90	159	8	
91	160	5	30 to 35°C
92	161	1	35°C
93	162	2	
94	163	3	
95	164	4	
96	165	5	
97	166	6	
98	167	7	
99	168	8	
100	169	1	35 to 5°C
101	170	2	
102	171	7	
103	172	8	
104	173	4	
105	174	6	
106	175	1	5°C
107	177	3	
108	178	4	
109	179	5	
110	180	6	
111	181	7	
112	182	8	
113	183	2	
114	184	1	5 to 30°C
115	185	2	
116	186	7	
117	187	8	
118	188	1	30°C
119	189	2	
120	190	3	
121	191	4	
122	192	5	
123	193	6	
124	194	7	
125	195	8	
126	196	2	

ORIGINAL PAGE IS
OF POOR QUALITY

Table 7-1 (continued)

Serial Orbit	Sequential Orbit	Standard Orbit	Test Event
127	197	1	30°C (continued)
128	198	2	
129	199	3	
130	200	4	
131	201	5	
132	202	6	
133	203	7	
134	204	8	
135	205	1	30 to 10°C
136	206	2	
137	207	7	
138	208	8	
139	209	1	10°C
140	210	2	
141	211	3	
142	212	4	
143	213	5	
144	214	6	
145	215	7	
146	216	8	
147	217	1	
148	218	2	
149	219	3	
150	220	4	
151	221	5	
152	222	6	
153	223	7	
154	224	8	
155	225	4	10 to 20°C
156	226	6	
157	227	1	20°C
158	228	2	
159	229	3	
160	230	4	
161	231	5	
162	232	6	
163	233	7	
164	234	8	
165	235	1	Post-thermal-vacuum
166	236	2	
167	237	7	
168	238	8	

ORIGINAL PAGE IS
OF POOR QUALITY

Table 7-1 (continued)

Serial Orbit	Sequential Oribit	Standard Orbit	Test Event
169	246	1	Final Long Form Performance Test
170	247	2	
171	248	3	
172	249	4	
173	250	5	
174	251	6	
175	252	7	
176	253	8	

The PF system and BTE 1 were moved to El Segundo on 9 December 1980. The move was made in accordance with TP32238-100 SCN 1. The first operation at El Segundo, after removing the scanner from the shipping container, was to measure the mounting interface. One of the aft optics cover mounting pads protruded beyond the plane of the interface 0.0055 inch. This is in excess of the specification requirements of ≤ 0.005 inch. A failure report, FR0698, documents this condition. It was concluded that this condition could be tolerated by shimming the interface for test. Then after mass properties tests, if not before, the aft optics cover would be loosened, the mounting interface aligned on a granite flat, and the aft optics cover retaining screws retorqued.

The system alignment conducted on 12 December 1980 was predicated on the assumption that the no-restraint position of the scan mirror corresponded to the zero lock position. This assumption was made, since the zero lock had been removed at SBRC during mass properties (weight) testing of the scanner and had not been replaced. The results of the alignment check indicated the boresight axis was 0.48° ouside the specification requirements of 0.25° of normal to the mounting plane. This test was repeated on 22 December 1980, except the alignment measurements were taken with the scan mirror against the stops at each end of scan. The zero position was calculated from previous measurements and resulted in boresight alignment of 0.072°, well within specification requirements.

Between the first system alignment of 12 December and the system alignment of 22 December, a comprehensive noise investigation was undertaken and completed. As a result of this investigation, video cable feedthroughs in the rear of the video processor were replaced, and the 78622 analog video cable from the scanner to the multiplexer was designed and implemented as standard test hardware.

The MSS-D system was purged, bagged, and packed in shipping containers over the Christmas holidays of 1980 from 23 December through 5 January 1981. During this time, the visible source lamp on the collimator was changed from the lower power, 100 watts, configuration to the new, 150 watt, configuration.

The system radiometric calibration, per procedure HS248 3617000-623, was completed on 8 January. Excessive noise was present in the video data when the collimator transfer calibration was conducted. A series of special tests, STRs 2 through 6, was conducted to evaluate the characteristics of the noise and to further characterize

ORIGINAL PAGE IS
OF POOR QUALITY

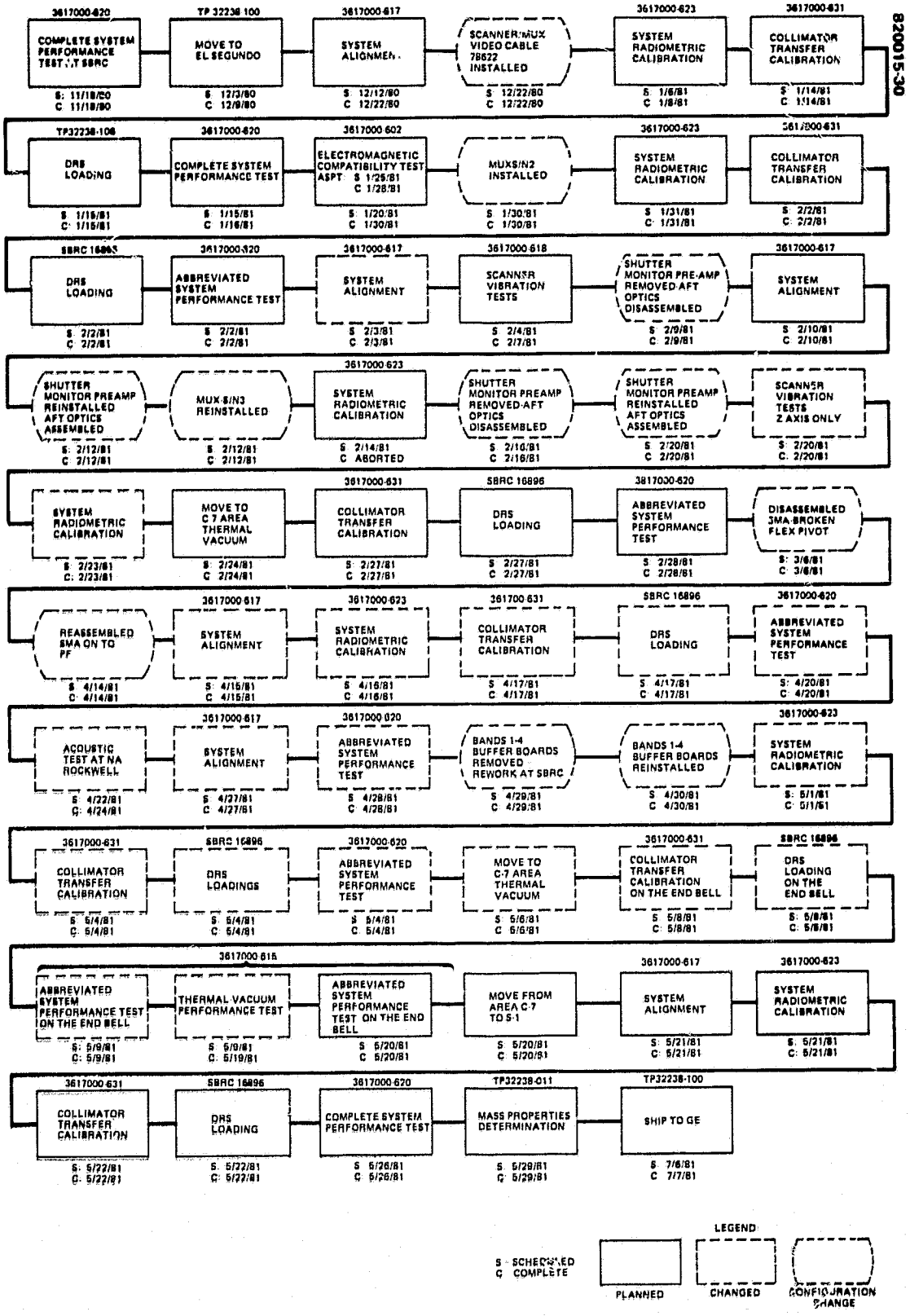

FIGURE 7-1. PROTOFLIGHT TEST SEQUENCE

ORIGINAL PAGE IS
OF POOR QUALITY

the collimator visible source. The new visible source was found to be a principal source of noise and was replaced on 14 January 1981 with the old 100 watt source. A collimator transfer calibration was conducted on 17 January per procedure HS248 3617000-631, after which a data reduction system (DRS) loading was completed per TP32238-106.

The pre-EMI/EMC complete system performance test was conducted per HS248 3617000-620 on 16 January, after which the system, including the bench test equipment (BTE) was moved to the A2 anechoic chamber for the EMI/EMC tests. These tests are described in procedure HS248 3617000-602 and are summarized in Table 7-2. After the move, the system was cabled up through the chamber penetration plate and a BTE functional test TP32238-103 was conducted. The MSS was mounted on the collimator cart in a laminar flow clean tent which had been erected within the A2 anechoic chamber.

The system was configured for the conducted emissions tests. Conducted emissions test, CE01, was performed from 20 Hz to 50 kHz on the 28 volt dc bus and return for modes A and B, narrowband only. Preliminary results of these tests indicated the MSS exceeded narrowband limits on both the 28 volt bus and the return only at the very lowest frequences, i.e., below 45 Hz, and was well within specification limits above 45 Hz. CE03 was similar to CE01 except the frequency requirements were from 50 kHz to 50 MHz. All requirements of CE03 were met. Above 250 kHz MSS conducted emissions were at least 30 dB below specification limits.

Radiated interference tests, RE02, were conducted with MSS in both mode A and mode B for broadband and narrowband measurements from 14 kHz to 18 GHz. MSS-D radiated interference exceeded limits from 14 to 250 kHz and from 1 through 15 MHz at discrete frequencies which were identified as radio station carrier frequencies. At 15 MHz, the approximate multiplexer output bit rate, the radiated interference exceeded limits by about 6 dB. Between 20 and 25 MHz, radiated interference exceeded

TABLE 7 2. EMI/EMC TESTS

Test	Frequency	Limits
Emission		
CE01 Conducted (Power line)	20 Hz to 50 kHz	MIL-STD-461
CE03 Conducted (Power line)	30 kHz to 150 kHz*	MIL-STD-461
RE02 Radiated (E Field)	14 kHz to 18 GHz	**
RE04 Radiated (B Field)	20 Hz to 50 kHz	MIL-STD-461
Susceptibility		
CS01 Conducted (Power line)	30 Hz to 50 kHz	MIL-STD-461
CS02 Conducted (Power line)	50 kHz to 150 kHz	MIL-STD-461
CS06 Conducted (Transient)	60 PPS for 5 min.	56 V Peak
RS03 Radiated (E Field)	150 kHz to 500 MHz	1 V/m
	2.2 GHz to 2.3 GHz	5 V/m
	8.0 GHz to 9.0 GHz	10 V/m
	14.5 GHz to 15.5 GHz	12 V/m

*CE03 was actually run to 50 MHz

**Broadband 14 kHz to 1 GHz

Narrowband 20 kHz to 18 GHz ≤35 dB μV/m, 148 to 150 MHz, 2.0 to 2.2 GHz, 13.4 to 14.3 GHz; ≤60 dB μV/m elsewhere in the range.

specification limits at five sharply defined frequencies by 1 to 4 dB. Above 25 MHz all recorded levels were below the EMI receiver background noise, which exceeded limits only at 13.5 and 14 GHz. Other than the specific frequencies, identified MSS-D radiated interference was generally 10 to 30 dB below specification limits. This performance was achieved by wrapping all command, signal, and power cables with aluminum foil and securely referencing the MSS-D and the command test set chassis to a common ground at the chamber penetration plate.

Radiated magnetic field interference tests, RE04, were conducted from 20 Hz to 50 kHz, narrowband measurements only. Ambient measurements of the facility were run. Narrowband ambient background exceeded limits at 60 and 120 Hz by 30 and 10 dB, respectively. With the MSS "on," narrowband measurements exceeded limits from 20 to 240 Hz. Facility or background noise contributed significantly to these measured violations.

Conducted susceptibility tests, CS01, were performed from 30 Hz to 1.5 kHz at 3.5 volts peak-to-peak, and 1.5 to 50 kHz at 1.5 volts peak-to-peak. In mode A, with the signal injected onto the 28 volt bus, the system failed at 1.43, 7.2, and 16.5 kHz. With signals injected into the power return, the system failed at the same frequencies, 1.43, 7.2, and 16.5 kHz.

A power line noise test was conducted similar to CS01 but at a constant 1.5 volt peak-to-peak signal over the frequency range from 30 Hz to 10 MHz. In this test in mode A MSS passed. With the signal injected into the return, the system failed at 4.3 kHz. This failure was a primary power supply shutdown and seemed to be more associated with major facility transients caused by testing in an adjacent building. During retest this failure could not be duplicated. In mode B MSS failed at 7.2 and 16.5 kHz.

Conducted susceptibility tests, CS02, were performed from 50 kHz to 10 MHz at 1.5 volt peak-to-peak, 1 kHz modulation. MSS passed all requirements of CS02.

Conducted transient susceptibilty tests, CS06, were performed with 28 volt spikes on top of the 28 volt bus with 60 pps repetition rate for 5 or more minutes. After about 3.5 minutes the shutter would lose lock, which it would then reacquire. The shutter would not lose phase lock when the spike transients were reduced to about 10 volts peak-to-peak.

Radiated E-field susceptibility tests, RS03, were conducted from 150 kHz to 500 MHz at 1 V/m, 2.2 to 2.3 GHz at 5 V/m, 8.0 to 9.0 GHz at 10 V/m, and 14.5 to 15.5 GHz at 12 V/m. All requirements of RS03 were met. An overtest was experienced between 14.5 and 15.5 GHz due to the use of uncalibrated semisolid copper shielded coaxial cable from the receiving antenna to the receiver in setting up the field intensity. Subsequent verification of the coaxial cable at 14.5 to 15.5 GHz indicates the tests were actually conducted at about 40 V/m rather than the required 12 V/m.

The criteria for failure during susceptibility tests were any out-of-tolerance performance parameters, loss of shutter phase lock, and primary power supply shutdown. The more sensitive performance parameters were signal-to-noise ratio and line length variations. Marginally out of tolerance signal-to-noise ratios and line length variations were rather severe failure criteria; however, failure in shutter phase lock or primary power supply shutdown were unambiguous and reliable failure criteria.

During the EMI tests STR 9 was performed. This STR required running the PF scanner with the engineering model multiplexer to determine if the design "fix" for the black/white code anomaly incorporated in the EM multiplexer was satisfactory. STR 9 verified that the design change to the multiplexer corrected the black/ white code problem. At the completion of EMI/EMC tests the S/N 3 multiplexer was removed from the PF system to be modified to correct the black/white code problem. S/N 2 was installed in place of S/N 3 during the rework of S/N 3.

During the previbration radiometric calibration, collimator transfer calibration, and abbreviated system performance tests, problems were encountered in deviation signal to noise (DSN), primarily in band 1. These problems were traced to test equipment malfunctions. The performance characteristics of the protoflight system were determined to be within requirements and suitable for proceeding into the vibration phase of the program.

The scanner was moved to area S1 for alignment verification. During this alignment check the boresight axis of the scanner was determined to be within 0.06° of the previous measurements and within 0.07° of being perpendicular to the scanner mounting plate.

In parallel with the scanner alignment, the BTE was moved to the V2 shaker area of the Space Simulation Laboratory (SSL). The BTE was then reassembled and cabled up, and a BTE functional test was run against the self-test unit (STU) and the receiving site equipment (RSE) test set.

The PF scanner, mounted on the vibration fixture and protected with plastic bags and N_2 purge, was brought to the V2 shaker and mounted for the Z-axis vibration test. At this point, it was noted that the clamp for the scan monitor cable to J-17 was not installed. A quick check indicated the cable could not be clamped as designed. An engineering change request/engineering order (ECR/EO) was cut for a new clamp design. With the new clamp installed, the scanner was commanded to the launch mode configuration and decabled. The vibration tests were conducted with only one external cable mated to the scanner. This was the cable to connector J-1 to provide power to maintain shutter motion during the vibration tests.

Table 7-3 defines the PF sinusoidal and random vibration tests. The Z-axis vibration tests consisted of the following sequence:

1) Random burst

2) 1 g sine sweep 5 to 2000 Hz

3) Lateral axis protoflight sine 5 to 100 Hz

4) Random vibration - 6 dB

5) Full level random vibration 12.8 g rms

6) Random burst

The scanner was then cabled up and a functional test was performed.

ORIGINAL PAGE IS
OF POOR QUALITY

TABLE 7-3. MSS-D VIBRATION TEST LEVELS

Sinusoidal Vibration				
Axis	Frequency, Hz	Level, g		Sweep Rate, Oct/Min
		Protoflight	Flight	
Thrust	5 to 50	7.5	5.0	4
	5 to 100	3.0	2.0	
Lateral	5 to 50	5.25	3.5	4
	50 to 100	3.0	2.0	

Random Vibration (Scanner Qualification Levels—Protoflight Model			
Axis	Frequency, Hz	Power Spectral Density	Duration
All	20 to 300	Increasing at a rate of 4 dB/oct + 3 dB to 0.09 g^2/Hz at 300 Hz	1 min/axis. Overall: 12.8 g rms
	300 to 2000	0.09 g^2/Hz width ±3 dB tolerance	±10%

During this post Z-axis functional test, it was noted that the calibration (or cal) wedge moved across the scope, indicating the shutter phase lock was not locked and the shutter control integrator telemetry was out of tolerance, reading 0.47 volt. After about 12 minutes the shutter phase locked, the shutter control integrator telemetry returned to a normal 3.1 volts, and the system appeared to be functioning normally. On the following day the special test (STR 13) was conducted. This time the shutter ran unsynchronized for about 6-1/2 minutes before phase lock was achieved, after which the shutter functioned normally when turned off, then reactivated. Failure report F1699 was generated for the shutter phase locking problems.

The scanner and vibration fixture were then moved to the slip table for the Y- and X-axis vibration tests. After the fixture was secured to the slip table, a functional test was conducted. With the scanner mounted for the Y-axis vibration tests, a final functional test was conducted prior to commanding the scanner to the launch mode and decabling. Telemetry dumps from this functional test indicated the band 4 ±15 volt telemetry regulator was abnormal at 16.76 volts, the shutter control integrator read 4.98 volts, and the scan mirror drive read 3.18 volts. The calibration lamp current was high but not out of tolerance at 109.36 mA.

The Y-axis vibration tests were performed in the same sequence and to the same levels as the Z-axis tests. Some observers indicated they heard an intermediate to high frequency tinkle in the aft optics area of the scanner.

The post Y-axis functional test indicated conditions to be quite similar to the post Z-axis functional. The shutter would not phase lock, the shutter control integrator telemetry indicated 4.98 volts, band 4 ±15 volt regulator telemetry indicated 4.98 volts, and the +15 volt telemetry regulator was high at 16.68 volts. The calibration lamp current read 109.85 mA on side A and went out of tolerance on side B at 110.34 mA.

At this point a meeting was held to consider the feasibility of proceeding with the vibration tests in view of the anomalous indications from the telemetry dumps and oscilloscope observations. It was noted that conditions had not changed significantly during the Y-axis test, and the post Z-axis functional test indicated only a problem with the shutter control integrator and the shutter phase lock. The principal changes in performance occurred during the move from the Z-axis test to the Y-axis test.

A review of the pre- and post-random burst graphs indicated no change in the structural integrity of the scanner. The performance anomalies were thought to be defective solder joints or broken wires. A decision was made to proceed with the X-axis vibration tests.

The X-axis vibration tests consisted of the following sequence:

1) Random burst

2) 1 g sine sweep 5 to 2000 Hz

3) Thrust axis protoflight sine 5 to 100 Hz

4) Random vibration - 6 dB

5) Random vibration - 12.8 g rms

6) Random burst

Difficulty was encountered in running the full qualification level random vibration test. This problem is described in detail in the SBRC internal memorandum HS248-6567. The high frequency tinkle noted during the Y-axis vibration tests was heard throughout the X-axis vibration tests.

A post X-axis functional test was conducted. At this time the shutter would not phase lock and the shutter control integrator telemetry indicated 4.98 volts. Band 4 ±15 volt telemetry regulator was out of tolerance at 16.68 volts. The scan mirror drive was out of tolerance at 3.11 volts, the scan mirror regulator was out of tolerance at 26.41 volts, and the calibration lamp current still indicated 110.34 mA. The band 4 cal wedge as viewed on the scope was low and misshapen. During the Y-axis vibration observers monitored the bus current out of the STS power supply. The bus current dipped as low as 0.48 ampere and was fairly steady but noisy at 0.61 ampere.

Before the X-axis vibration, it had been decided that after post X-axis functional test, the abbreviated system performance test (ASPT) would be deleted and the scanner would be returned to area S1 for visual inspection and disassembly of the aft optics cover. After disassembly it was found that the high frequency tinkle was a loose retaining nut on the synchronizer cable (P5) to the power module. The shutter monitor preamplifier was removed and transported to SBRC for test and rework. There it was found that a lead had broken loose at the E5 terminal of the photodiode. The photodiode was replaced, and the rework of the shutter monitor preamplifier was completed. The shutter monitor preamplifier was returned to El Segundo for reassembly into the PF scanner. While the scanner aft optics cover was removed, several STRs were run to locate, if possible, the problems in the band 4 video (cal wedge), band 4 ±15 volt

regulator, +15 volt telemetry regulator, scan mirror drive telemetry, and the scan mirror regulator telemetry. It was concluded the band 4 ±15 volt regulator malfunction and the band 4 video (cal wedge) distortion were related and were caused by the multiplexer clamping the video signal when dc restore was lost, due to the failure in the shutter monitor preamplifier. Tests and analyses failed to disclose the cause for the anomalous telemetry for the +15 volt telemetry regulator, the scan mirror drive telemetry, the scan mirror regulator, and the calibration lamp current. All these parameters had returned to normal after disassembly while operating with the command test set. These problems were subsequently traced to a Burr-Brown board in the scanner test set (STS) in which all channels on one chip saturated when the band 4 ±15 volt regulator went out of tolerance and saturated the substrate of the chip. This was corrected by installing diode clamps at the input to the chip. The change in bus current was traced to the loose retaining nut on the power supply synchronization cable. STR 15 demonstrated that the bus current drops about 40 mA when the synchronization cable is disconnected from the radiometer power supply.

While the aft optics cover was removed, the scanner was mounted on the angle plate and the postvibration alignment verification was performed. The results of this alignment check indicated the optical axis of the scanner relative to the mounting plate and the alignment cube was within 0.01° of the alignment measurements taken before the vibration tests.

Table 7-4 lists the performance anomalies encountered during and after the vibration tests. Seven failure reports were generated covering these items. During installation of the aft optics cover, the scanner was placed on a granite flat which was used as a tooling jig to hold the mounting pads in plane during torquing of the aft optics cover screws. Postassembly measurements of the interface mounting plane indicated the PF was well within interface specification requirements at 0.004 inch.

After the PF scanner reassembly, the S/N 3 multiplexer was returned and reinstalled in the PF system. A decision was made to proceed into thermal-vacuum test. A system radiometric calibration was initiated; however, the shutter failed to lock up, and the system radiometric calibration was aborted.

TABLE 7-4. ANOMALY LIST FROM VIBRATION TEST

1)	Band 4 ±15 volt regulator out of regulation, saturating at high value.
2)	Band 4 video distorted, cal wedge.
3)	Calibration lamp current out of regulation, as high as 110 mA.
4)	+ 15 volt telemetry regulator out of regulation on high side, as high as + 16.8 volts.
5)	Scan mirror drive telemetry varying from 2.17 to 3.03 volts; specification is 2.5 to 2.9 volts.
6)	Shutter synchronizer signal from shutter preamplifier went dead following Z-axis vibration (shutter integrator telemetry saturated at same time).
7)	Scan mirror regulator telemetry went out of specification as low as -26.28 volts; specification is -27 to -29 volts.
8)	Bus current changed during vibration.
9)	Black paint flakes in aft optics cover.

ORIGINAL PAGE IS
OF POOR QUALITY

The scanner aft optics cover was removed and the shutter monitor preamplifier, which had been repaired after vibration tests, was removed and returned to SBRC for inspection, test, and, if required, rework. It was found the shutter monitor photodiode had been improperly assembled during rework of the shutter monitor preamplifier. The photodiode in the shutter monitor preamplifier was replaced, and the unit was returned to El Segundo and installed in the PF system.

After reassembly of the PF scanner and recheck of the mounting interface, it was decided to conduct a "workmanship" vibration test to verify the quality of the rework and assembly which had been completed after the scanner vibration tests. This penalty vibration test was conducted per STR 27 along the Z-axis only. The Z-axis was the axis of force application when the failures occurred during the scanner vibration test. The penalty vibration test sequence was:

1) Random burst 5 to 125 Hz, 0.22 g rms

2) Random vibration 20 to 2000 Hz, 8.5 g rms

3) Random burst 5 to 125 Hz, 0.22 g rms

The scanner was then returned to Area S1 for the prethermal-vacuum system radiometric calibration. During this system radiometric calibration, noise levels were high, the scan mirror drive and the scan mirror regulator were out of tolerance, and the multiplexer +5V logic telemetry was out of tolerance. The system radiometric calibration was re-run. It was concluded the problems experienced on the previous calibration were largely BTE problems.

The system was moved to the C7 area where the scanner, multiplexer, and collimator were installed on the C7 endbell. After the BTE functional test, a collimator transfer calibration was performed on the endbell. The persistent BTE problems were traced to a Burr Brown board in the STS.

An abbreviated system performance test was conducted on the endbell. At this time the line length variation (VLL) problem surfaced. After many special tests to isolate the VLL problem, the sunshield was removed from the scanner, and it was verified that one of the flex pivots in the scan mirror assembly (SMA) was broken. The SMA was removed and transported to Culver City for rework. The scanner was returned to Area S1 where a series of tests were conducted to resolve recurring telemetry problems.

After rework was complete, the SMA was returned to the system and reinstalled. At this time it was concluded that additional dynamic testing was required to verify the rework; however, grave doubts existed concerning additional random vibration testing. An acoustic test was introduced as an option to random vibration. The system was aligned, calibrated, and given an abbreviated system performance test in preparation for the acoustic test.

The MSS-D acoustic test, introduced into the program as an option to random vibration tests by contract modification 44, dated 14 April, was conducted on 23 April. To accomplish this, in the week between 15 April and 21 April 1981, test fixtures and cables were designed and fabricated, the PF and the engineering model (EM) scanners were instrumented and prepared for tests, and a preliminary contract was negotiated

ORIGINAL PAGE IS
OF POOR QUALITY

with Rockwell International. The PF and EM scanners were transported in their shipping containers to the Rockwell International acoustic facility in El Segundo on 22 April. The scanners were removed from the shipping containers and mounted on the test fixture in the reverberant chamber. A final preacoustic test meeting was convened. It was found that the spectrum to which the chamber had been equalized was not the correct spectrum for MSS-D. The test articles and test fixtures were removed from the chamber; the chamber was re-equalized to the MSS-D spectrum; and the text fixtures and test articles were reinstalled in the chamber.

A functional test was conducted on the PF scanner to verify that the system was in operating condition at the start of the test, and to command and verify that the system was in the launch mode at the start of the acoustic test. In parallel with the functional test, accelerometer channels were connected to the facility recording system and checked.

The acoustic test was to be controlled from the averaged output of four microphones located as shown in Figure 7-2. A fifth microphone was installed to evaluate acoustic attenuation through the plastic wrapping to verify the acoustic exposure of the scanners. During the test no measurable attenuation of sound could be attributed to the plastic wrapping.

The acoustic tests consisted of a sequence of four exposures as indicated below:

1) Run 1 was made at 141 dB overall acoustic sound pressure level (OASPL) (-6 dB) for a period of 30 seconds. The test started at 1:19 p.m. and stopped at 1:20 p.m. The chamber was opened and a visual examination of the test articles was made. No anomalies were observed. The gains on the instrumentation accelerometer

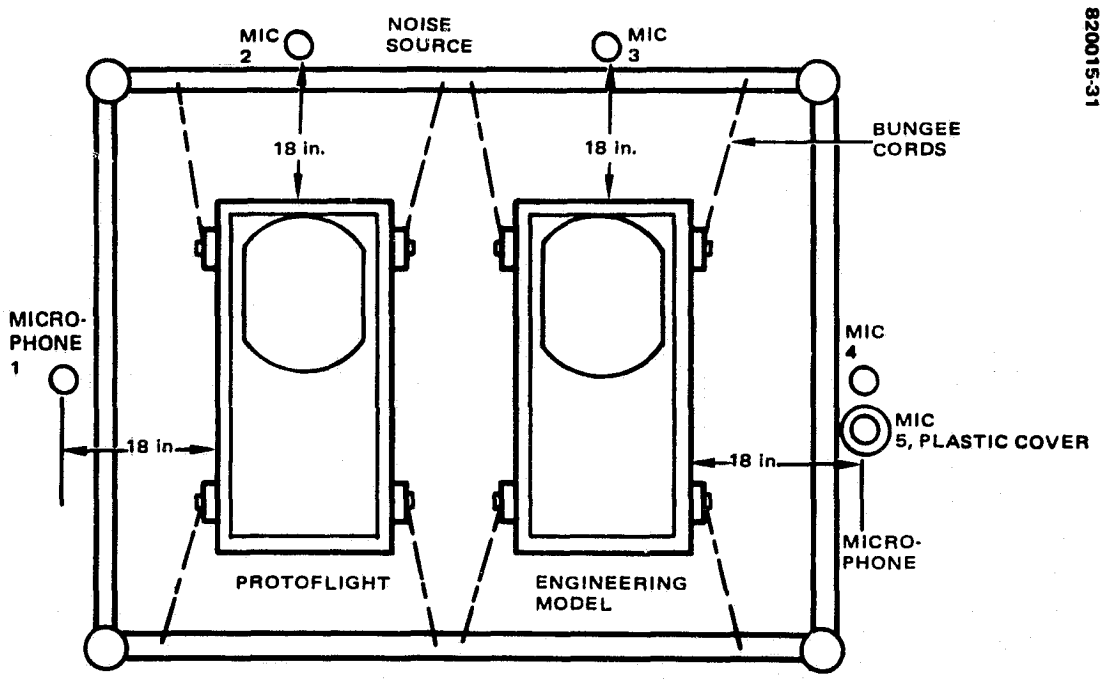

FIGURE 7-2. PROTOFLIGHT ACOUSTIC TEST SETUP

ORIGINAL PAGE IS
OF POOR QUALITY

amplifiers were too high. These were adjusted down. A microphone plot of the average was made and examined, and the decision was made to go into the full level acoustic test.

2) Run 2 was made at 147.5 dB OASPL for a period of 30 seconds. The test started at 2:30 p.m. and stopped at 2:31 p.m. The chamber was opened and a visual inspection of the test articles was made. A microphone plot of the average microphones 1, 2, 3, and 4 was made (see Figure 7-3a).

The instrumentation was changed from the engineering model configuration to the PF configuration. This was done to keep instrumentation channel requirements within the facility capabilities. The new instrumentation configuration was checked out.

3) Run 3 was made at 141 dB OASPL (-6 dB) for a period of 30 seconds. The test was started at 3:01 p.m. and stopped at 3:02 p.m. The chamber was opened and a visual examination of the test articles was conducted. Accelerometer data were checked, and a decision was made to proceed into the final half of the full level test.

4) Run 4 was made at 147.2 dB OASPL for a period of 30 seconds. The test was started at 3:43 p.m. and stopped at 3:44 p.m. The chamber was opened and a visual examination of the test articles was made. A microphone plot of the average of microphones 1, 2, 3, and 4 was made (see Figure 7-3b).

A postacoustic test functional test of the PF scanner was made and indicated the scanner was functionally similar to the preacoustic configuration. The test configuration was disassembled, and the scanners were returned to their shipping containers. The test hardware was returned to Hughes on 24 April 1981.

The PF sunshield was removed to permit inspection of the scan mirror flex pivots. At this time, a mark was observed on one flexure element. Subsequent inspections of the flex pivots have revealed no change in the mark, and there is no compelling evidence to indicate the mark was not present on the flexure element at the time of the flex pivots installation in MSS.

A postacoustic alignment and abbreviated system performance test confirmed that the scanner survived the acoustic test with no measurable performance degradation.

Throughout the PF test program the scanner had evidenced some gain instability and/or drift in selected video channels. The gain of some channels was such that the channels would no longer meet the dynamic range requirements of the system specification. It was decided that prior to going into thermal-vacuum test, the gain select resistors for channels 2, 3, 9, 17, and 19 should be replaced. Bands 1 through 4 buffer boards were removed, the gain select resistors were changed out, and the buffer boards were reinstalled in the scanner prior to beginning the prethermal-vacuum calibration sequence.

After the system radiometric calibration, a decision was made to reinspect the flex pivots to characterize and document the scratch on one of the flexures. The sunshield was reinstalled and the scanner was moved to the collimator cart where the collimator transfer calibration and the abbreviated system performance test were conducted. During this ASPT, signal-to-noise specification violations were noted during each of the four orbits. The primary source of these DSNs was traced to the collimator lamp power

ORIGINAL PAGE IS
OF POOR QUALITY

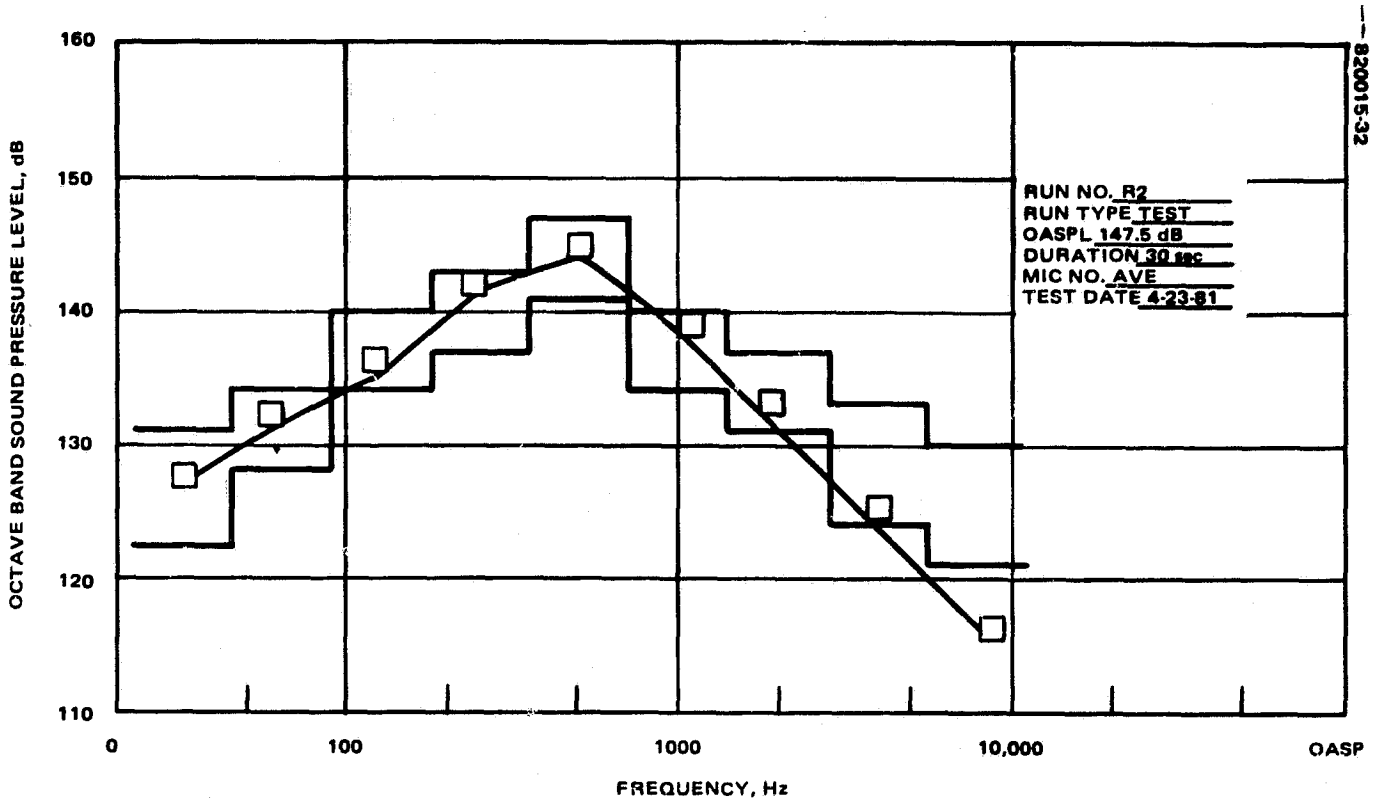

a) TEST R2

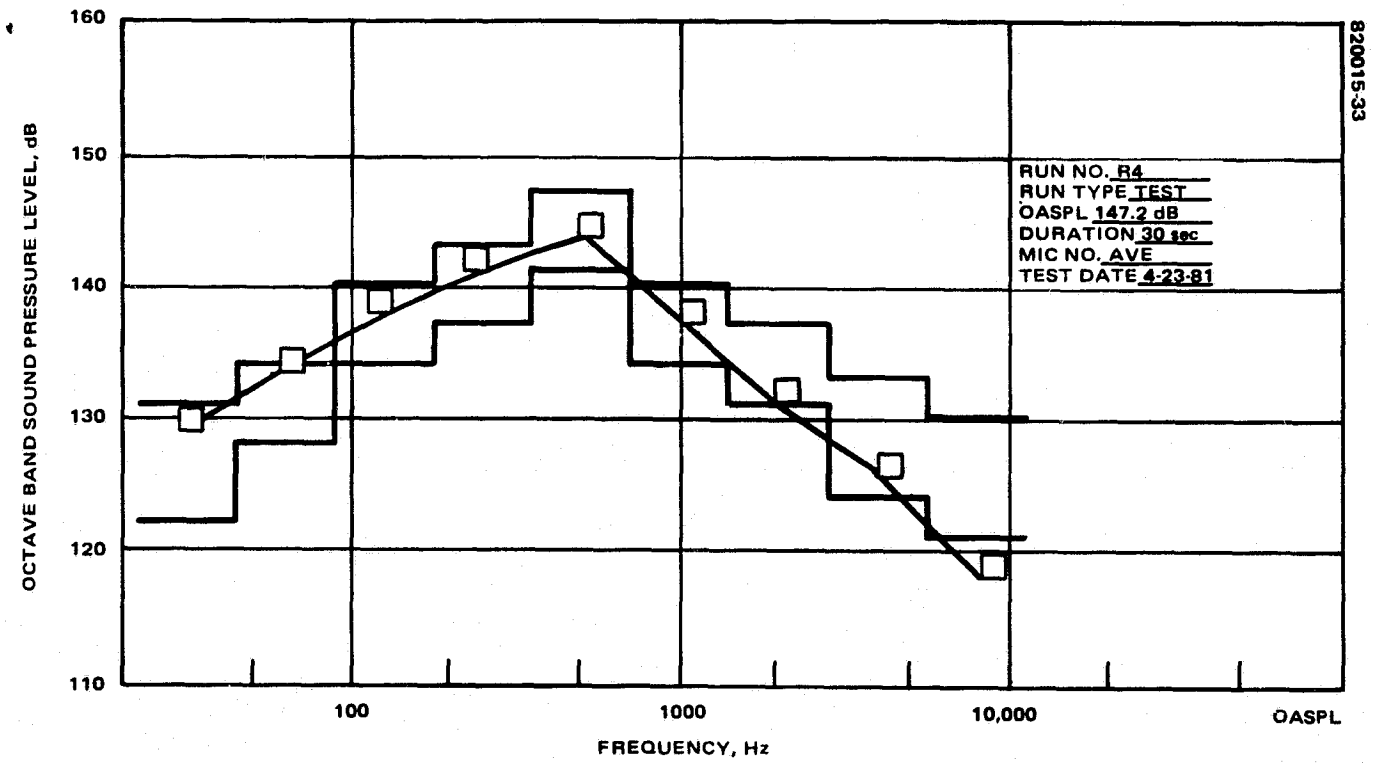

b) TEST R4

FIGURE 7-3. ACOUSTIC SPECTRUM MICROPHONE AVERAGE

ORIGINAL PAGE IS
OF POOR QUALITY

supply. The system was then moved to the C7 area and installed on the endbell. A collimator transfer calibration was first conducted on the endbell after which an ASPT was performed. At this point it was decided the system was ready for thermal-vacuum tests. The chamber endbell was raised, and the thermal-vacuum test was conducted according to the protoflight thermal-vacuum temperature profile, Figure 7-4. The chamber was sealed, pumped down to about 100 Torr, and backfilled with dry gaseous N_2. After the third backfill, chamber pressures were stabilized at 500 Torr and the ambient in-chamber ASPT was conducted. During this test DSNs were noted in the fourth orbit; however, a decision was made to initiate pumpdown.

During the first 45 minutes of pumpdown, the system was in the launch mode, after which the system was turned off and pumpdown continued until chamber pressure stabilized at 10^{-5} Torr. The time at which the chamber pressure reached and held at 10^{-5} Torr is "T-O" on the temperature profile and occurred at 2030, 9 May 1981. The thermal-vacuum test after T-O was strictly time-sequenced, although the planning was sufficiently precise so that of the 120 orbits planned, 119 were conducted.

After reaching T-O the system was permitted to outgas for 12 hours with no power applied. The system was then turned on for the corona and initial vacuum checks. These tests indicated the system was in good condition and ready for the initial vacuum collimator transfer calibration. The balance of the thermal-vacuum test is adequately defined in Figure 7-4 and is described in orbit-by-orbit detail in Table 7-5. The thermal-vacuum test was terminated 240 hours after reaching T-O and chamber ventback was initiated. After reaching room ambient pressure, the endbell was lowered to the retaining pins, and the final in-chamber ASPT was performed.

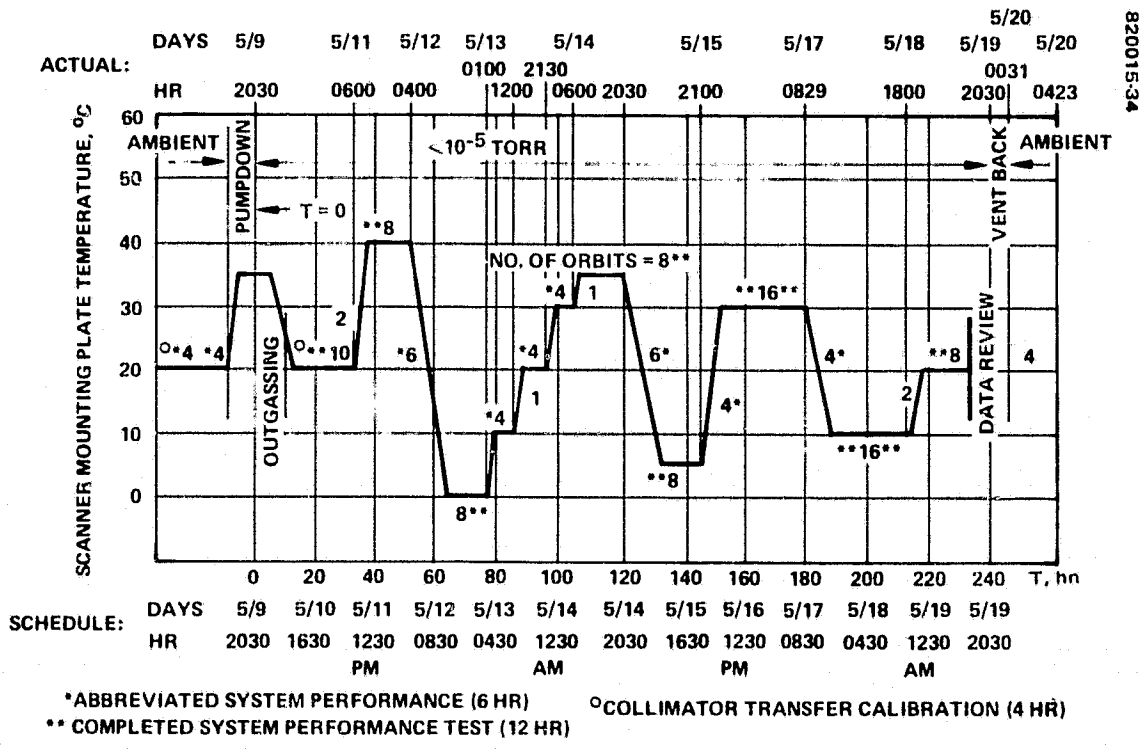

*ABBREVIATED SYSTEM PERFORMANCE (6 HR)
** COMPLETED SYSTEM PERFORMANCE TEST (12 HR)
°COLLIMATOR TRANSFER CALIBRATION (4 HR)

FIGURE 7-4. PROTOFLIGHT THERMAL-VACUUM TEMPERATURE PROFILE

Most of the problems experienced during the thermal-vacuum test involved DSNs and deviation channel to channel (DCCs). On the 40°C orbits the primary power supply B neared its temperature limits. During orbit 131/4 the primary power supply reached 50.6°C, its red lined limit. A failure report, FR 5121, was generated, although it was determined the primary power supplies could stand temperatures to 60.0°C without damage.

After the endbell was lowered to the floor, the PF system was moved from it to Area S1 for the final system alignment and calibration sequence. The collimator transfer calibration was followed by the final complete system performance test, which marked the completion of the formal qualification/acceptance tests. The system was then prepared for the mass properties measurements in which the weight, center of gravity, and moments of inertia about the X- and Z-axis were measured.

Although the formal protoflight tests were completed, three additional flex pivot inspections were conducted from 27 May to 1 July 1981. A relative spectral response test, STR 61, was conducted on the PF scanner. This test required mounting the monochromator to the collimator as the radiance source. The spectral response of each channel was measured to evaluate the apparent change in the characteristics of the focal plane array as viewed through the scanner telescope and/or explain the high incidence of DCC violations when the scanner temperature was driven away from the temperature at which the collimator transfer calibration had been conducted. The results of the relative spectral response test were encouraging. Within the measurement capability of the test setup, the spectral response characteristic of the offending channels had not changed any more than the spectral response characteristics of channels which were behaving quite normally.

Another special test, STR 62, was conducted during this postqualification test period. This test was an analog MTF measurement designed to further characterize the anomalous MTF behavior of channel 14. This test confirmed the high MTF characteristics of channel 14 and further indicated a possible problem in the three-pole Butterworth filter of that channel.

At the completion of the last STR for the protoflight system test, a dye penetration examination of the flex pivots was performed. This examination indicated the flex pivots were acceptable. The protoflight was reassembled (sunshield was installed) and the system was prepared for shipment. The protoflight system was delivered to United Airlines for transportation to Pennsylvania on 6 July 1981.

Table 7-5 presents the detailed protoflight test history, including a day-by-day, orbit-by-orbit chronological listing of all protoflight test activities from the completion of the system integration at SBRC through the delivery of the protoflight system.

ORIGINAL PAGE IS
OF POOR QUALITY

TABLE 7-5. PROTOFLIGHT MSS-D PF TEST CHRONOLOGY

Date	Activity	Problems	Orbit No.
11/18/80	Complete system performance test at SBRC a) Collimator flooding lamp hangup—in b) FR 2443 scan repeatability 25.6 μr (should be 24 μr) c) FR 2444 STNO 52.1 (channel 12), 86.0 (channel 6) d) FR 2447 STNO All channels except 16 and 17 e) FR 2446 STNO All channels except 17		1/1, 2/2, 3/3, 4/4 5/5, 6/6, 7/7, 8/8
11/19/80	STR 30 — Noise investigation STR 31 — Black/white code dropout investigation Reworked DRS front end — noise reduction STR 32 — Noise investigation 50 Ω connector at J4		
11/20/80	STR 33 — Noise investigation — Rerun of STR 32 STR 34 — Investigation of black/white code dropouts		
11/22/80	STR 34 complete — multiplexer identified as source of black/white code dropout — pictures of scan monitor pulses 1, 2 and 3 taken, range +3.8 V to -2.7 V Shutter rundown time measured 11-12 sec		
11/24/80	Black/white code investigation with logic analyzer.		
11/25/80	STR 35 signal-to-noise investigation with different W4016 cables STR 36 black/white code dropout investigation		
11/26/80	STR 35 rerun with various combinations of W4016 cables and resistor connectors		
12/01/80	STR 35 rerun STR 37 noise investigation with wave analyzer		
12/02/80	STR 35 rerun with spectrum analyzer STR 38 noise investigation similar to STR 35 Moved to granite flat for scanner O&M		
12/03/80	Prepared MSS BTE for shipment to El Segundo		
12/09/81	Moved PF MSS-D to El Segundo		
12/11/81	Mounting pad/Landsat interface measurement-out of spec limits 0.0005 inch		
12/12/81	System Alignment — 3617000-617		
12/15/81	STR HS 248-1126-1 video breakup — coaxial cable to demultiplier		
12/16/81	Rerun STR-1 Rerun 3617000-617 system alignment without zero lock Anomalous telemetry dumps, disk read errors		
12/19/81	Replaced video and clock signal feedthroughs on rear patch Panel-demultiplexer input to clear up video breakup		
12/22/81	Completed STR-1 video noise-selected 78622 video cable configuration Completed scanner alignment 3617000-617		
1/6/81	Started system radiometric calibration 3617000-623		9/Cond 10/13, 11/14, 12/15, 12/16
1/7/81	Conducted STR HS 248-1126-2 system noise isolation		14/Cond 15/13, 16/14
1/8/81	Completed system radiometric calibration 3617000-623		17/15, 18/16
1/9/81	Conducted STR HS 248-1126-3 collimator lamp study		19/27, 20/28
1/10/81	Conducted STR HS 248-1126-4 system noise isolation		
1/12/81	Modified shield terminations of 78622 cable Conducted DRS loading TP 32238-106		21/1, 22/2
1/13/81	Conducted STR HS 248-1126-6 signal to noise recheck		
1/14/81	Replaced visible source lamp on collimator Conducted STR HS 248-1126-8 to verify collimator visible source Conducted collimator transfer calibration HS 248-3617000-631		23/27, 24/28

ORIGINAL PAGE IS
OF POOR QUALITY

Table 7-5 (continued)

Date	Activity	Problems	Orbit No.
1/15/81	Conducted DRS loading TP 32238-106		
1/16/81	Completed ACSPT 3617000-620		25/1, 26/2, 27/3 28/4, 29/5, 30/6, 31/7, 32/8
1/17/81	Moved to A2 anechoic chamber for EMI/EMC tests		
1/19/81	Performed BTE functional test TP 32238-103		
1/20/81	Conducted ASPT 3617000-620. Problems with Prime Photographed EMI test setup Repaired Prime Conducted emissions tests CE01 and CE03 3617000-602		33/1, 34/2
1/23/81	Completed radiated emissions tests RE02 and RE04 3617000-602		
1/24/81	Conducted STR HS 248-1126-9 multiplier black/white code anomaly isolation		
1/26/81	ASPT baseline performance for susceptibility tests per 3617000-620		35/1, 36/2, 37/7, 38/8
	Performed STR HS 248-1126-10 scan mirror drive telemetry		
1/28/81	Completed conducted susceptibility test CS01 per 3617000-602		
1/30/81	Completed radiated susceptibility RS03 per 3627000-602 EMI/EMC tests 3617000-602 complete Multiplexer S/N 3 removed for black/white rework. Replaced with S/N 2		
1/31/81	Conducted system radiometric calibration per 3617000-623		46/13, 47/14, 48/15, 49/16
2/2/81	Conducted collimator calibration per 3617000-631		50/27, 51/28
	Completed abbreviated system performance test per 3617000-620		52/1, 53/2, 54/7, 55/8
	Conducted STR HS 248-1126-12 scan monitor pulse measurements		
2/3/81	Completed system alignment per 3617000-617 Moved BTE to SSL		
2/4/81	Conducted BTE functional test per TP 32238-103 Moved scanner to SSL and mounted on shaker		
2/5/81	Conducted Z-axis vibration		56
	During post Z-axis functional noted shutter was very slow to lockup		57
2/6/81	Shutter failed to phase lock-FR 1699 Conducted STR HS 248-1126-13 phase lock loop Completed Y axis vibration Noted problems: — Band 4 ±15V regulator, +15 V telemetry regulator, Shutter control integrator, and Scan mirror regulator		58
2/7/81	Completed X-axis vibration Completed vibration test Moved scanner to Area S1 and removed after optics cover Conducted visual examination		60
2/9/81	Shutter monitor preamplifier investigation — FR 5102 Loose A1P5 sync cable — FR 5101 Returned multiplier SN2 to Digital Labs for rework Returned shutter monitor preamplifier assy to SBRC for rework		
2/10/81	Completed system alignment per HS 248-3617000-617		
2/11/81	Ran STR HS 248-1126-15-bus current with and without A1P5 synchronizer cable connected Ran STR HS 248-1126-16 Band 4 video with no dc restore		

ORIGINAL PAGE IS
OF POOR QUALITY

Table 7-5 (continued)

Date	Activity	Problems	Orbit No.
2/12/81	Reassembled scanner aft optics assembly Conducted STR HS 248-1126-17 post vibration functional test Multiplexer S/N3 returned to PF system		
2/13/81	Ran STR-HS 248-1126-18 flatness check of mounting interface Untorqued and retorqued aft optics cover retaining screws with scanner on granite flat. Interface within 0.004 in.		
2/14/81	Started system radiometric calibration-shutter failed phase lock Generated FR 1699		
2/16/81	Collimator into bakeout in C7 Conducted STR HS 248-1126-20. Shutter phase lock with and without breakout box on connector J-9 Disassembled aft optics assembly, FR 5107-improper assembly of shutter monitor preamplifier photodiode		
2/17/81	Conducted STR HS 248-1126-21 continuity check between pins of redundant connectors. Pin 62 of J-10 to J-11 not continuous		
2/18/81	Conducted STR HS 248-1126-22 continuity check J-2 multiplexer to J-2 scanner Collimator out of C7 bakeout		
2/19/81	Conducted STR HS 248-1126-23 launch mode configuration check Conducted STR HS 248-1126-24 photodiode test Conducted STR HS 248-1126-25 scanner functional test		
2/20/81	Reassembled scanner-measured mounting interface = 0.004 in. Conducted STR HS 248-1126-26 scanner functional test Prepared scanner and moved to V-2 facility for penalty vibration Conducted Z-axis random penalty vibration STR HS 248-1126-27 Moved scanner to angle plate for system radiometric calibration		
2/21/81	Conducted system radiometric calibration per 3617000-623, scan mirror drive low Multiplexer 5 V logic out of tolerance		61/13, 62/14, 63/15, 64/16
2/22/81	Reran and completed system radiometric calibration per 3617000-623		66/ , 66/ , 67/13, 68/14, 69/15, 70/16
2/24/81	Conducted STR HS 248-1126-28-±19 V rectifier output evaluation Moved scanner and collimator to C-7 endbell Moved BTE to C7 area; cabled up started BTE functional test		
2/27/81	Completed BTE functional test per TP 32238-103 Completed collimator transfer calibration HS 248-3617000-631 Completed DRS loading per TP 32238-106 Replaced A13A6 Burr-Brown board in STS telemetry drawer; set gain and offset Ran STRs 29 and 31		71/27, 72/28 73/1, 74/2, 75/7, 76/8
2/28/81	Completed ASPT on endbell HS 248 3617000-615 and 620 Conducted STR HS 248-1126-30 band 4 slew rate check Worked on collimator folding mirror drift		
3/2/81	Conducted STR HS 248-1126-32 SMP measurement Conducted STR HS 248-1126-33 time code test Conducted STR HS 248-1126-34 MSS focus check BTE Problems. Burr-Brown boards, and collimator folding mirror creep Initiated failure reports FR 5111 (out of specification line length variation), FR 5112 (out of specification MTF), STR 34, line length variation investigation		

ORIGINAL PAGE IS
OF POOR QUALITY

Table 7-5 (continued)

Date	Activity	Problems	Orbit No.
3/3/81	Conducted STR HS 248-1126-36 MSS focus check 2 Refocused collimator, added diode clamps to Burr-Brown board		
3/4/81	Conducted STR HS 248-1126-38,VLL investigation Conducted STR HS 248-1126-37,19 V telemetry investigation Burr-Brown board problems		
3/5/81	Continued STR HS 248-1126-38,VLL investigation Installed new Burr-Brown board-new software PROM Removed sun shield to inspect flex pivots Generated FR 5111 VLL		
3/6/81	Verified flex pivot was broken Removed SMA and shipped it to Culver City Prepared system and BTE for move back to Area S-1		
3/9/81	Moved back to area S1 Closed chamber C7 with isolation fixture		
3/10/81	Conducted BTE functional-partial Many problems with collimator, collimator controller		
3/11/81	Repaired pin 7 of P4 of cable W4004		
3/12/81	Removed sunshield and inspected yoke and attachments to the mainframe Completed BTE functional Removed backshell from P4 W4004 for additional rework		
3/19/81	Worked on collimator controller motor driver board		
3/20/81	Assembled EM SMA to PF scanner (deviation request 3/16/81) Conducted STR HS 248-1126-39 telemetry test Removed EM SMA from PF scanner Conducted STR HS 248-1126-40 band 4 frequency response Worked on collimator-returned visible MTF reticle wheel to SBRC		
3/14/81	Instrumented EM SMA for vibration tests		
3/25/81	Inspected all test cables — repaired collimator cables W/4004/P4, W 4003/P3, W 4002A/P2 and scanner test cable W 4013/P12 Installed fix on Phillips motor driver board for collimator folding mirror Modified Burr-Brown 1 and 6 boards - channels 99 and 104 with diode clamps		
3/26/81	Repaired insert in EM/SMA mounting interface Conducted STR HS 248-1126-41 dc restore output check Installed EM/SMA on structural test model (STM) mounted on vibration fixture and moved to SSL		
3/30/81	Changed out flex pivots on EM SMA (3/27-3/30), ready for vibration		
3/31/81	Conducted STR HS 248-1126-43 band 4 ±15 V regulator check		
4/2/81	Continued EM vibration tests (EM SMA and STM)		
4/6/81	Conducted STR HS 248-1126-44 dc restore investigation		
4/8/81	Incorporated EO 2921A (3.9 KΩ resistor on A1A6, band 4 buffer board) Inspected witness mirrors Removed SMA witness mirror and returned to Culver City for cleaning EM SMA removed from STM, flex pivots removed and sent to Culver City		
4/9/81	Completed rough draft acoustics test procedure Started design fabrication of W 40152 cable for acoustics test		
4/10/81	Moved STM from vibrator to shipping container to Bldg S18, Rm 100		

ORIGINAL PAGE IS
OF POOR QUALITY

Table 7-5 (continued)

Date	Activity	Problems	Orbit No.
4/14/81	Conducted STR HS 248-1126-45, dc restore test Assembled PF SMA to PF scanner Refocused collimator Aligned scan monitor		
4/15/81	Assembled sunshield and electronics housing cover Conducted system alignment per HS 248-3617000-617 Removed A1A6 photodiode buffer, band 4, for rework		
4/16/81	Conducted system radiometric calibration per HS 248-3617000-623		77/13, 78/14, 79/15, 80/16
4/17/81	Conducted collimator transfer calibration per HS 248-3617000-631 Performed STR 46 launch mode telemetry		81/27, 82/28
4/20/81	Conducted ASPT per HS 248-3617000-620		83/1, 84/2, 85/7, 86/8
4/21/81	Conducted STR 47, collimator uniformity estimates Conducted STR 48, SMP measurements Inspected PF flex pivots Prepared PF for shipment to Rockwell International for acoustic test		
4/22/81	Moved EM and PF to Rockwell Prepared acoustic chamber and mounted EM and PF Connected and checked out all instrumentation		
4/23/81	Conducted acoustic test per TP 32238-107		87, 88
4/24/81	Returned EM and PF scanners to Area S1		
4/27/81	Inspected flex pivots Conducted system alignment per HS 248-3617000-617		
4/28/81	Conducted ASPT per HS 248-3617000-620 Performed STR 50, collimator check	DSN* DSN*	89/1*, 90/2* 91/7*, 92/8*
4/29/81	Performed STR 49, collimator uniformity Disassembled electronic cover and removed bands 1 through 4 buffer boards Inspected flex pivots		
4/30/81	Reassembled PF sunshield Installed buffer boards 1, 2, 3 and 4		
5/1/81	Conducted system radiometric calibration per HS 248-3617000-623 Removed sunshield and inspected flex pivots Conducted STR 51, noise investigation		93/13, 94/14, 95/15, 96/16
5/4/81	Conducted collimator transfer calibration per HS 248-3617000-631 Conducted ASPT per HS 248-3617000-620	DSN* DSN* DSN*	97/27*, 98/28* 99/1*, 100/2* 101/7*, 102/8*
5/5/81	Performed STR 53, scope photos shutter square wave Performed STA 44, noise spectrum test		
5/6/81	Moved system to C7 thermal-vacuum area Mounted PF on C7 endbell		
5/7/81	Cabled up system and prepared for thermal-vacuum test		
5/8/81	Performed STR 52, collimator uniformity check Conducted collimator transfer calibration per HS 248 3617000-631 Conducted ASPT on endbell per HS 248-3617000-615 Raised endbell and completed purge and backfill		103/27, 104/28 105/1, 106/2, 107/7, 108/8
5/9/81	Conducted ASPT in C7 at 500 Torr per HS 248-3617000-615 Initiated pumpdown in launch mode T-0 at 20:30	DSN*	109/1, 110/2 111/7, 112/8*

ORIGINAL PAGE IS
OF POOR QUALITY

Table 7-5 (continued)

Date	Activity	Problems	Orbit No.
5/10/81	Completed outgassing		
	Conducted corona and initial vacuum checks per HS 248-3617000-615		113/2, 114/1
	Conducted collimator transfer calibration per HS-248-3617000-631		115/27, 116/28
	Conducted CSPT per HS 248-3617000-620		117/1, 118/2
			119/3, 120/4
5/11/81			121/5, 122/6
			123/7, 124/8
	Transition to 40°C		125/1, 126/2
	Conducted CSPT at 40°C per HS 248-3617000-620		127/1, 128/2
		Aborted*	129/3*, 130/3
		FR 5121 (PPS 40°C)*	131/4*, 132/5
			133/6, 134/77
5/12/81			135/8
	Transition to 0°C		136/1, 137/2
	Conducted CSPT at 0°C per HS 248-3617000-620	MTF Channel 21*	138/1, 139/2*
		MTF, DCC, DSN*	140/3, 141/4*
			142/5, 143/6
5/13/81		DRS Problems,	144/7*
	Transition to 10°C	DCA*	145/4
	Conducted ASPT at 10°C per HS 248-3617000-620	FR 5122*, DCC	146/1*, 147*/2*
		FR 5123*, DSN	148/7, 149/8
	Transition to 20°C		150/6
	Conducted ASPT at 20°C per HS 248-3617000-620	DSN*	151/1*, 152/2
	Transition to 30°C	DSN*	153/7*, 154/8
			155/3
5/14/81	Conducted ASPT at 30°C per HS 248-3617000-620		156/1, 157/2, 158/7, 159/8
	Transition to 35°C		160/5
	Conducted CSPT at 35°C per HS 248-3617000-670	DCC, DSN*	161/1*, 162/2, 163/3, 164/4
		DCC*	165/5, 166/6*
		DCC*	167/7*, 168/8
	Transition to 5°C		169/1, 170/2
5/15/81			171/7, 172/8
			173/4, 174/6
	Conducted CSPT at 5°C per HS 248-3617000-620	Aborted*	175/1, 176/2*
			177/3, 178/4, 179/5
			180/6, 181/7, 182/8
	Repeat of aborted orbit 176/2		183/2
5/16/81	Transition to 30°C		184/1, 185/2
			186/7, 187/8
	Conducted CSPT at 30°C per HS 248-3617000-620		188/1, 189/2
			190/3, 194/4
		DSN*	192/5, 193/6*
		FR 5126* DSN* DCC*	194/7*, 195/8*
	Rerun of orbit 189/2		196/2
	Conducted second CSPT at 30°C per HS 248-3617000-620	DSN* DCC*	197/1*, 198/2*
5/17/81			199/3, 200/4
			201/5, 202/6
			203/7, 204/8
	Transition to 10°C		205/1, 206/2
			207/7, 208/8
	Conducted CSPT at 10°C per HS 248-3617-620	DSN* DCC*	209/1*, 210/2*
		DSN* DCC*	211/3*, 212/4*
5/18/81		DSN* DCC*	213/5*, 214/6
			215/7, 216/8
	Conducted second CSPT at 10°C per HS-248-3617000-620		217/1, 218/2
			219/3, 220/4
	Changed command lines, multiplexer line to No. 2, to No. 3, then to No. 4		221/5, 222/6
		DCC*	223/7, 224/8*
	Transition to 20°C		225/4, 226/6

ORIGINAL PAGE IS
OF POOR QUALITY

Table 7-5 (continued)

Date	Activity	Problems	Orbit No.
5/19/81	Conducted CSPT at 20°C, Changed multiplexer line to No. 3 Changed multiplexer line to No. 2, then No. 1 Performed STR 58, low radiance signal-to-noise assessment	DSN* FR 5127* DSN* DSN*	227/1* 228/2* 229/3*, 230/4* 231/5*, 232/6, 233/7, 234/8
5/20/81	Vent back per HS 248-3617000-615 Lowered endbell to retaining pins Conducted ASPT at ambient conditions Lowered endbell to floor, removed system, returned to S-1	DSN* DSN*	235/1*, 236/2* 237/7*, 238/8 239/2
5/21/81	Conducted system alignment per HS 248-3617000-617 Conducted system radiometric calibration per HS 248-3617000-623		240/13, 241/14 242/15, 243/16
5/22/81	Conducted collimator transfer calibration per HS 248-3617000-631		244/27, 245/8
5/26/81	Conducted final CSPT per HS 248-3617000-620 Performed STR 53, scope photos of shutter square wave		246/1, 247/2 248/3, 249/4 250/5, 251/6 252/7, 253/8
5/27/81	Removed sun shield and inspected flex pivots Performed STR 59, thermal test		
5/28/81	Completed STR 59, thermal test Performed STR 60, SMP measurements Prepared for mass properties		
5/29/81	Conducted mass properties tests per TP 32238-011 Returned scanner to area S1 Installed system in shipping containers and prepared for shipment		
6/15/81	Removed scanner from shipping container Removed sun hat and sunshield, prepared for flex pivot inspection		
6/16/81	Inspected flex pivots Reassembled scanner Performed STR 60, SMP measurements		
6/17/81	Set up for STR 61, relative spectral response		
6/18/81	Continued STR 61		
6/19/81	Completed STR 61		
6/22/81	Set up from STR 62, analog MTF, channel 14		
6/23/81	Conducted STR 62 Reassembled scanner and returned it to shipping container		
7/1/81	Removed scanner from shipping container Removed sun hat and sunshield for flex pivot inspection Performed STR 63, flex pivot dye penetrant examination Reassembled scanner and returned it to shipping container		
7/6/81	PF system delivered to United Airlines for transportation to General Electric		

*Out-of-specification condition

ORIGINAL PAGE IS
OF POOR QUALITY

7.3 SIGNAL-TO-NOISE PERFORMANCE EVALUATION

7.3.1 Introduction

This subsection discusses the signal-to-noise performance of the MSS-D protoflight scanner. Two methods of assessing performance are employed. 7.3.2 discusses the noise model used to determine signal-to-noise specifications and the signal-to-noise performance as determined from radiometric results. This is a good method, since the integrating sphere is the most (spatially and temporally) uniform source available for test. Unfortunately, the integrating sphere is not available during thermal-vacuum testing. 7.3.3 summarizes performance with the collimator as the source. Much of the material of this section is concerned with irregularities due to test equipment problems. 7.3.4 discusses the sensitivity of scanner signal-to-noise performance to temperature. 7.3.5 summarizes performance, discussing only those features attributable to the MSS scanner.

Two items must be explained before 7.3.3 and 7.3.5 can be fully understood. First, as mentioned in 7.1, orbit numbers are referred to in two ways: the test schedule sequential orbit number and the plot serial orbit number. These numbers are different since some of the sequential orbits do not appear on the collimator plots (radiometric calibration, etc). For example, if the text refers to orbit 160 (230), this is serial orbit 160 and sequential orbit 230.

Secondly, for reasons of clarity, plots of measured noise are presented instead of plots of signal-to-noise. Since the average input signal level stayed relatively constant throughout system test, these two quantities behave as the reciprocal of each other. Unusually low noise measurements are bounded by zero, but cause very high values of the signal-to-noise measurement. By choosing to plot noise, the range of values is restricted and a more uniform set of scales can be presented to simplify comparisons between plots.

7.3.2 Noise Model Description

An independent, and in some ways more accurate, estimate than one obtained using the collimator of system signal-to-noise performance is provided by the system noise estimation computer program. This off-line program uses data obtained from the radiometric calibration orbits (i.e., standard orbits 13 through 16) to compute estimates of noise power from sources within the scanner. With this information, the system STN performance can be extrapolated to radiance inputs not normally available during the course of acceptance testing, in particular, those resulting in outputs of half-scale and full-scale called out in the system level specifications.

It is felt that STN measurements made using the 30 inch integrating sphere are more accurate (relative to the collimator) for several reasons: 1) the sphere is a superior source in terms of uniformity, both spatially and as a function of time, and 2) its radiant output is a primary standard for the instrument rather than a derived one. Problems in category 1) with the collimator were encountered during acceptance testing and are discussed later in this section.

In the following subsections the basis for the noise estimation algorithm is derived and the accuracy of the technique is discussed. This is followed by program results for the protoflight model.

ORIGINAL PAGE IS
OF POOR QUALITY

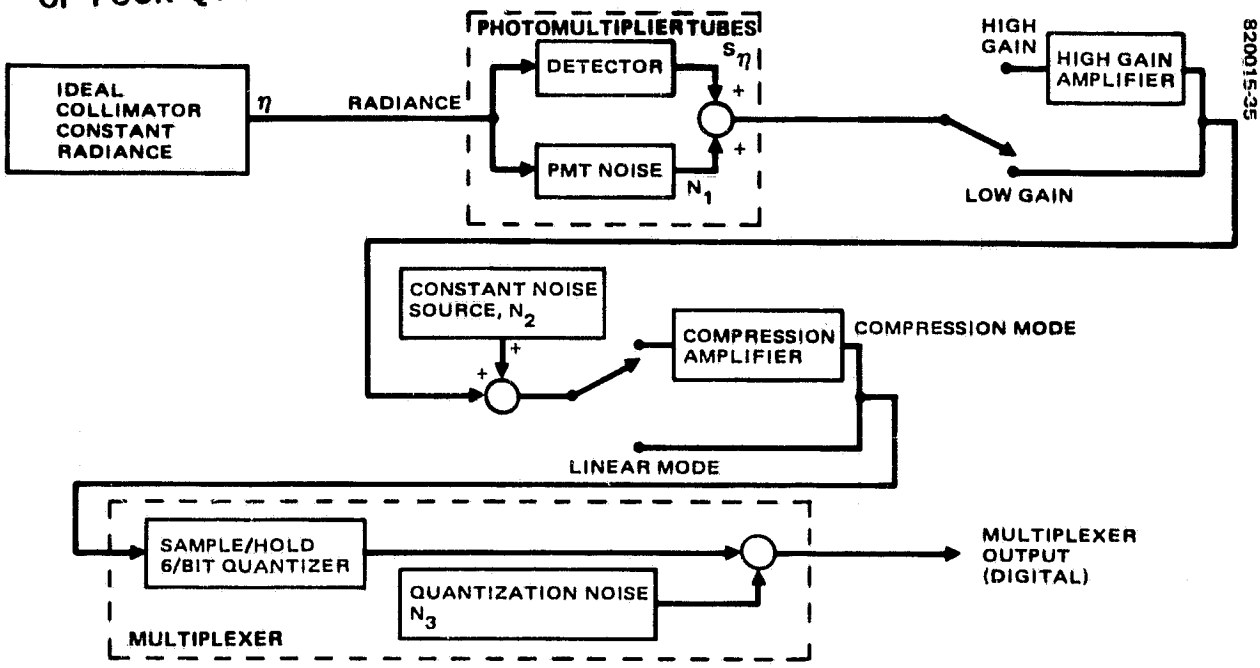

FIGURE 7-5. SIGNAL-TO-NOISE RATIO NOISE MODEL

7.3.2.1 Noise Model Equations

The noise sources N_1 through N_3 (see Figure 7-5) are assumed to have the following properties:

1) They are mutually independent, zero-mean Gaussian, white noise processes

2) The variance of the N_1 (PMT) noise process has a dark current term and a term proportional to input radiance, η; i.e.,

$$\sigma_1^2 = K_1^2 + K_2^2 \eta$$

3) The remaining noise sources are unaffected by input signal level and have variances given by σ_i^2, i = 2, 3.

Under these assumptions the multiplexer output, X, can be written as

$$X = G_{C/L}\left[G_{H/L}(S_\eta + N_1) + N_2\right] + \phi_{C/L} + N_3$$

where

= multiplexer compression gain and offset, respectively

= high/low amplifier gain setting

= signal output of PMT when incoming radiance is

= multiplexer output

ORIGINAL PAGE IS
OF POOR QUALITY

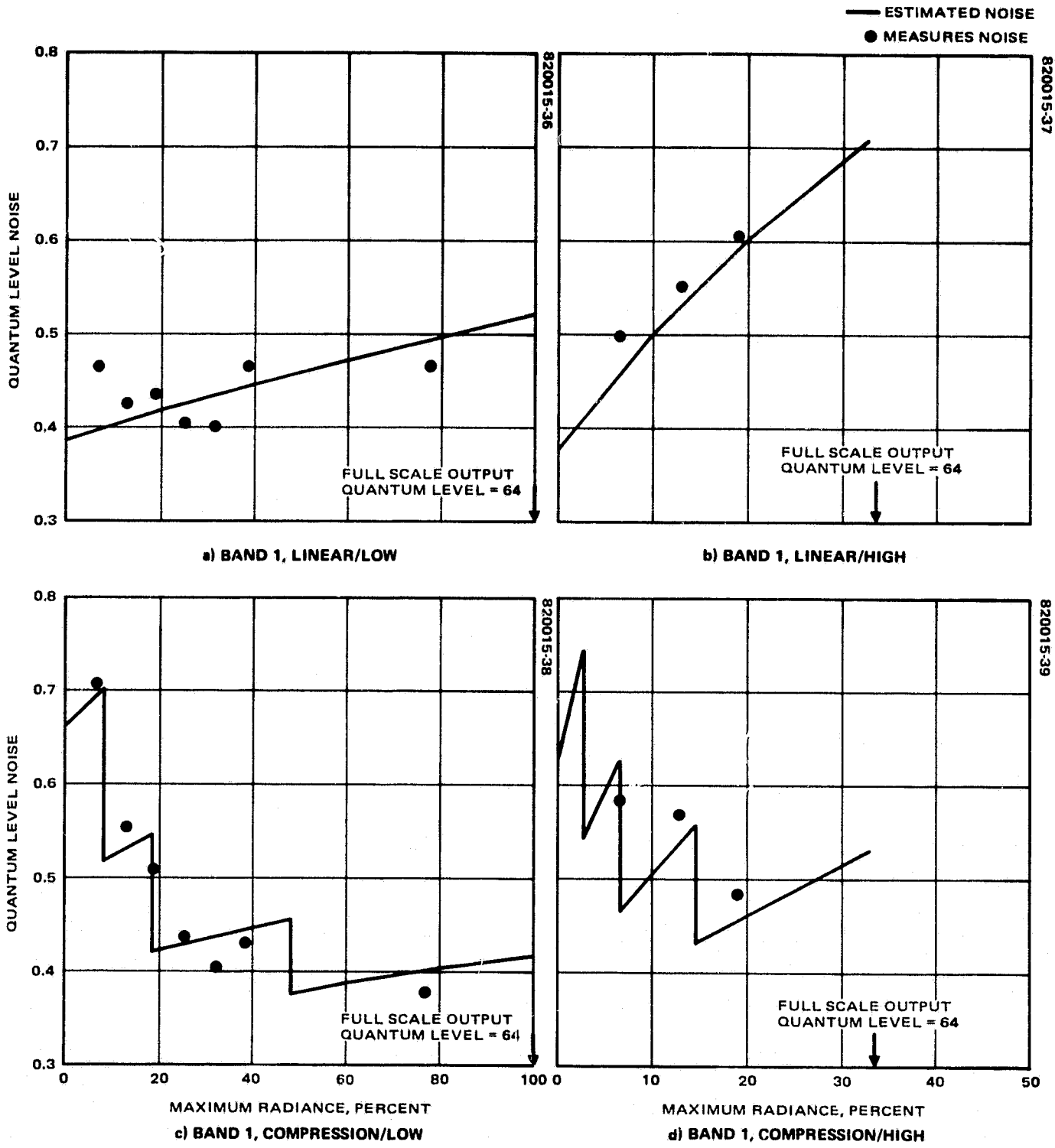

FIGURE 7-6. NOISE MODEL ESTIMATION ACCURACY

ORIGINAL PAGE IS
OF POOR QUALITY

The first and second moments of X are then given by

$$E\{X\} = G_{C/L}\, G_{H/L}\, S_\eta + \phi_{C/L} \tag{7-1}$$

$$E\{X^2\} = G^2_{C/L}\left[G^2_{H/L}(S_\eta{}^2 + K_1{}^2 + K_2{}^2\eta) + \sigma_2{}^2\right] + \phi^2_{C/L} + \sigma_3{}^2 + 2G_{C/L}\, G_{H/L}\, \phi_{C/L}\, \eta \tag{7-2}$$

and the variance by

$$\begin{aligned}\sigma_x{}^2 &= E\{X^2\} - E^2\{X\} \\ &= (G_{C/L}\, G_{H/L})^2\,(K_1{}^2 + K_2{}^2\eta) + G^2_{C/L}\,\sigma_2{}^2 + \sigma_3{}^2\end{aligned} \tag{7-3}$$

σ_x is the system noise as measured at the multiplexer output. Of the parameters in Equation 7-3 σ_x can be estimated by the DRS STN algorithm; $G_{C/L}$, $G_{H/L}$, and are selectable or computable quantities; and

$$K_1{}^2, K_2{}^2, \sigma_2{}^2, \text{and } \sigma_3{}^2$$

are constant but unknown quantities that appear linearly in Equation 7-3. Therefore, a multiple linear regression analysis is applicable provided a sufficient number of samples with different combinations of η, $G_{C/L}$, and $G_{H/L}$ are available to estimate unambiguously the four unknown quantities. A radiometric calibration is an ideal source for these data.

Restrictions and Modifications

The above results apply to bands 1 through 3 only and, in fact, to only bands 1 and 2 without modification, since only the first two bands have data from all scanner gain/multiplexer mode combinations. Band 3 does not have high gain capability, and band 4 has only one mode, linear/low. The lack of high gain in band 3 results in an underdetermined system of equations for the original problem formulation of 7.3.2.1. This is a result of being unable to distinguish contributions from K_1 and σ_2. Therefore, for band 3, the number of unknowns is reduced from four variables to three, the reduction brought about by combining noise source 2 into the K_1 term of noise source 1. Otherwise the procedure is identical.

Accuracy of Estimates

Table 7-6 contains the optimal estimates for the noise coefficients based on data collected from the 7 November 1980 radiometric calibration performed on the proto-flight model. The accuracy of the coefficients in predicting scanner noise performance is quite good, as evidenced by Figure 7-6 in which both predicted and

ORIGINAL PAGE IS
OF POOR QUALITY

TABLE 7-6. NOISE MODEL PARAMETER ESTIMATES

Parameter	Noise Coefficient Estimate		
	Band 1	Band 2	Band 3
K_1^2, mv^2	-4.6	-16.0	586.2*
K_2, $\frac{mv}{(mv/sr\text{-}cm^2)^{1/2}}$	13.8	22.4	6.2
σ_2, mv	16.1	21.3	
σ_3, mv	18.3	14.5	20.5

*This entry is really $K_1^2 + \sigma_2^2$

estimated noise performance is plotted for the four combinations of multiplexer mode and scanner gain: linear/low, linear/high, compression/low, and compression/high.

7.3.2.2 Protoflight Results

The noise estimation program was exercised for each of the radiometric calibrations performed during the course of acceptance testing for the protoflight model. Plots of the noise coefficients as a function of time (i.e., radiometric calibration number) for bands 1 through 3 are provided in Figure 7-7; all units are in millivolts except K_1^2, which is millivolts squared. Full scale signal output of the scanner is 4.0 volts corresponding to quantum level 63 out of the multiplexer. The data corresponding to the 21 May 1981 radiometric calibration is used to extrapolate system STN performance for full (64 quantum level) and half-scale (32 quantum level) output for the protoflight model and is presented in tabular form for both internal calibrations systems A and B in Table 7-7. In each case scanner STN performance is well above lower bounds called out in the system level specification.

TABLE 7-7. PROTOFLIGHT MODEL EXTRAPOLATED SIGNAL-TO-NOISE PERFORMANCE
(Based on Radiometric Calibration of 21 May 1981)

		Specification				Performance							
						System A				System B			
Mode	Gain	Band 1	Band 2	Band 3	Band 4	Band 1	Band 2	Band 3	Band 4	Band 1	Band 2	Band 3	Band 4
Linear													
64 QL	Low	89.1	72.9	49.8	108	127.2	107.5	97.9	150.3	130.1	111.7	98.9	146.8
	High	58.7	45.8	N/A	N/A	84.4	71.5	N/A	N/A	85.8	74.6	N/A	N/A
32 QL	Low	54.3	46.4	33.5	54	79.1	66.1	59.6	75.1	81.2	67.5	60.9	73.4
	High	38.7	31.0	N/A	N/A	57.8	48.1	N/A	N/A	58.8	49.1	N/A	N/A
Compression													
64 QL	Low	110.3	94.8	68.8	N/A	168.9	137.6	125.7	N/A	171.5	139.5	137.7	N/A
	High	79.4	63.8	N/A	N/A	118.1	98.2	N/A	N/A	119.7	101.1	N/A	N/A
32 QL	Low	59.1	51.9	38.9	N/A	86.9	72.2	64.6	N/A	89.4	73.1	66.2	N/A
	High	44.4	36.2	N/A	N/A	68.4	56.2	N/A	N/A	69.6	56.2	N/A	N/A

ORIGINAL PAGE IS
OF POOR QUALITY

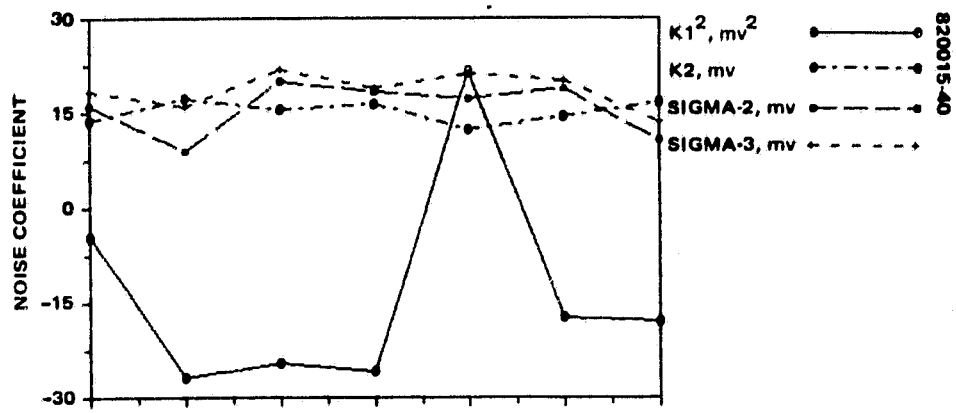

a) BAND 1, SYSTEM A

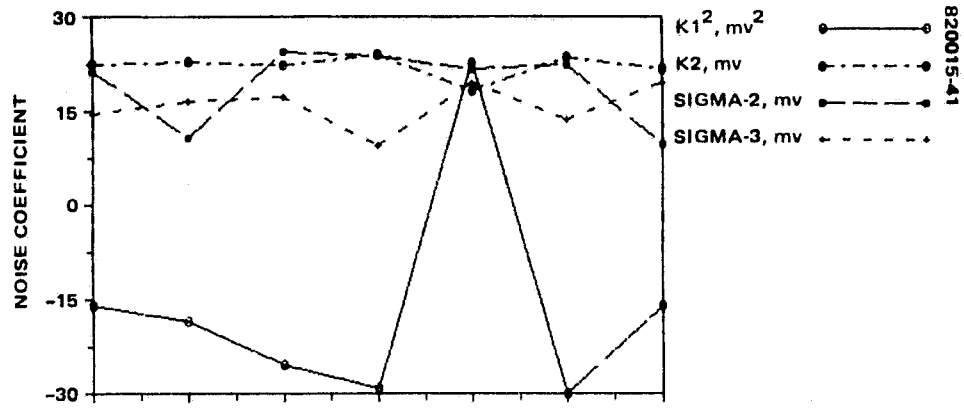

b) BAND 2, SYSTEM A

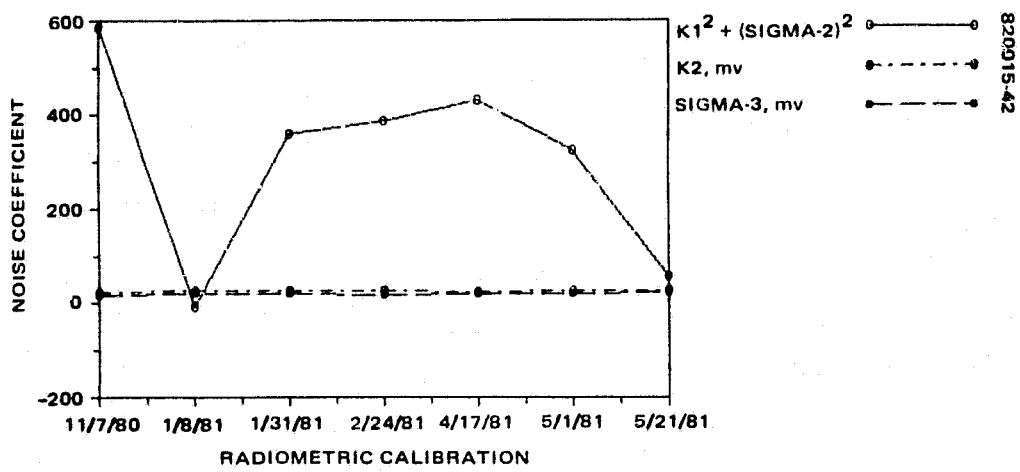

c) BAND 3, SYSTEM A

FIGURE 7-7. PROTOFLIGHT NOISE MODEL COEFFICIENT HISTORY

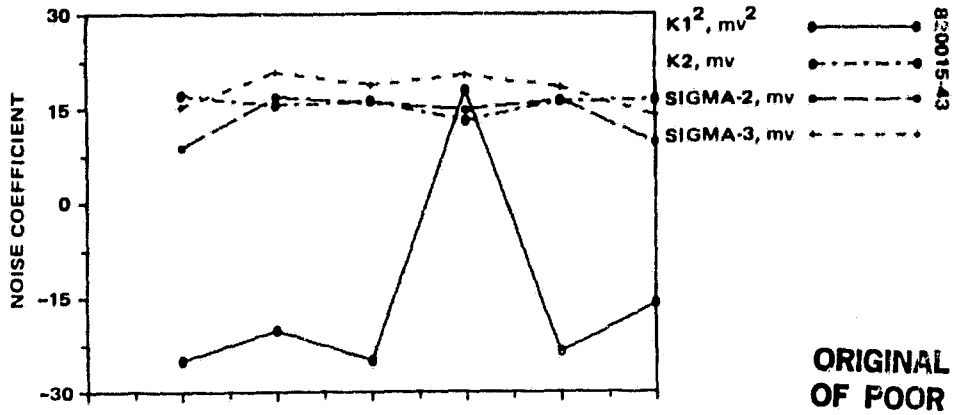

ORIGINAL PAGE IS
OF POOR QUALITY

d) BAND 1, SYSTEM B

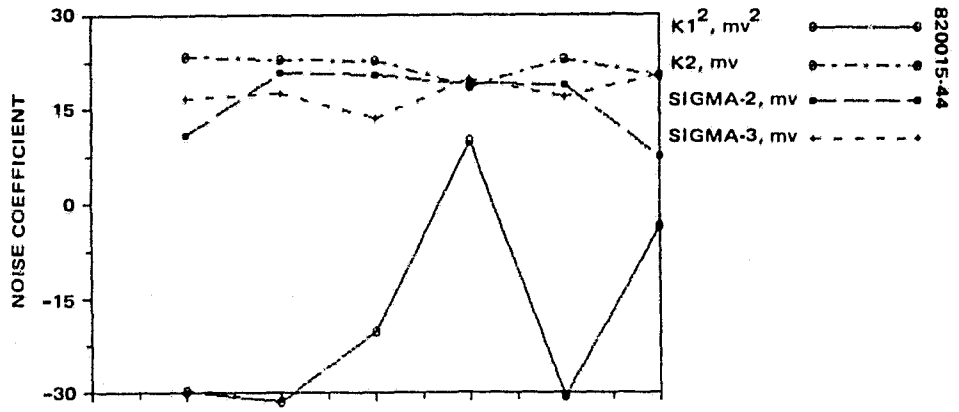

e) BAND 2, SYSTEM B

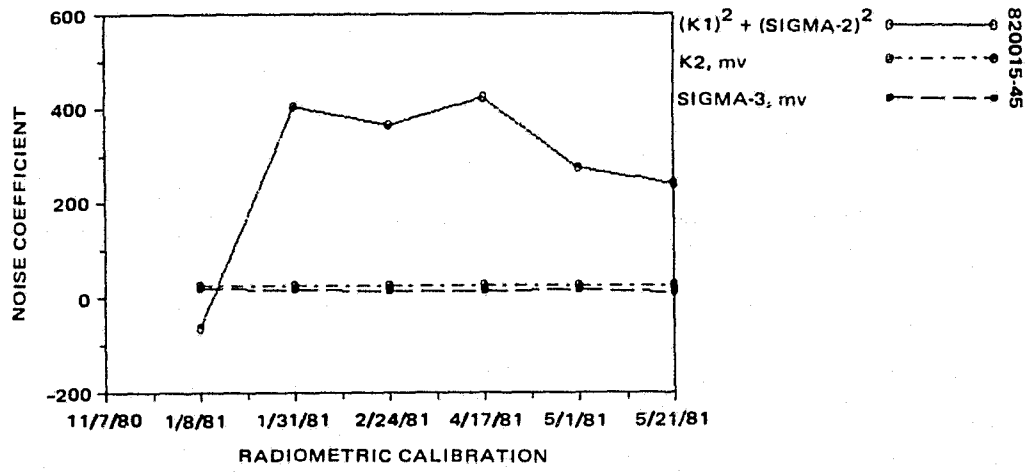

f) BAND 3, SYSTEM B

FIGURE 7-7 (CONTINUED). PROTOFLIGHT NOISE MODEL COEFFICIENT HISTORY

ORIGINAL PAGE IS
OF POOR QUALITY

7.3.3 Performance

Figures 7-8 through 7-11 give the history of the noise measured in all four modes for the entire history of protoflight system test. One feature is apparent in all the plots: the first 40 orbits are much noisier than the remainder. This was traced to a defective cable which was replaced between orbits 40(102) and 41(105). The following discussion focuses on orbits after 40(102), which include all of thermal-vacuum and post-thermal-vacuum tests.

Most plots also indicate higher noise levels for the first one or two channels of each band. This effect is caused by nonuniformities in the collimator video source. When these orbits were reanalyzed to remove collimator noise, the channels were found to be no worse than the other channels in the band. In fact, the scanner noise was much lower than is indicated in these plots. (See 10.3.2 for a discussion of the modifications to the noise model which were made to take the collimator induced noise into account.)

Several anomalies appear on the plots which are the result of test equipment failures or operator errors. These will be indentified, but full documentation is contained in the failure report closures. The following plots represent performance which was generally within specification once these test equipment failures and errors had been factored out. The exceptions are noted in 7.3.5. Table 7-8 lists the approximate maximum allowable noise before a specification was violated. A noise level below this value does not necessarily mean that signal-to-noise is within specification, since a dropping signal level could cause signal-to-noise to deteriorate. This table is a useful guide, however, in determining how much margin each band had in meeting its requirements.

7.3.3.1 Linear/Low

Figure 7-8 plots the linear/low gain mode for bands 1 through 4. The spikes and gaps at orbits 6(6), 7(7), and 23(54) are remnants of a bit slip in the serial data stream at the demultiplexer.

When the collimator-induced noise for the first two channels of each band is removed, the main observation to be made is that although the noise measured for each channel varies from orbit to orbit, the character of the noise changes very little throughout system test. That is, noise was not much affected by changes in temperature during thermal-vacuum testing or by the return to ambient conditions.

A spike appears at orbit 136(206) in band 3. This was probably the first occurrence of the front end bit dropout problem. (See 10.3 for a more complete discussion.)

TABLE 7-8. APPROXIMATE MAXIMUM NOISE PERMISSIBLE WITHOUT VIOLATING SPECIFICATION

Band	Mode			
	Linear/Low	Compression/Low	Linear/High	Compression/High
1	0.53	0.47	0.70	0.72
2	0.65	0.55	0.90	0.71
3	1.10	0.78		
4	0.60			

ORIGINAL PAGE IS
OF POOR QUALITY

7.3.3.2 Compression/Low

Figure 7-9 records the noise measurements of bands 1 through 3 in the compression/low gain mode. The first channel in bands 2 and 3 stands out from the rest because of collimator noise. In this mode, the tightest specification was in band 1. To meet this specification, the noise for each sensor had to be slightly below 0.5. No matter how low the sensor noise was, as the input signal level neared a transition level in the A-D converter, output values tended to be distributed evenly between two adjacent quantum levels. The resulting noise measurement approaches 0.5. This effect is found in many plots, particularly band 1 in compression/low mode where the maximum noise level tends to "clip" at 0.5.

7.3.3.3 Linear/High

Figure 7-10 gives the noise performance for bands 1 and 2 in the linear/high gain mode. Band 1 shows general uniformity with temperature change. Band 2, on the other hand, shows several features associated with the temperature profile. These will be discussed separately below.

7.3.3.4 Compression/High

Figure 7-11 shows the performance of the first two bands in the compression/high gain mode. These are very similar to the set of plots in Figure 7-10 (linear/high) except that some temperature effects are visible in band 1 also. (Note the expanded scale for these two plots.)

7.3.4 Temperature Sensitivity

Although the signal-to-noise performance of the protoflight scanner is relatively insensitive to temperature variations, several exceptions exist in the form of channels which exhibit gain changes with respect to temperature. This effect is discussed in more detail in 7.4.3. Temperature effects are most visible in the plots of band 2, compression/high mode. All four modes are plotted for three individual channels in band 2 (Figures 7-12 through 7-14). These are channels 9 and 11, which were known to be irregular, and channel 12, which is fairly stable. As the temperature increases, the gain in the sensitive channels decreases, resulting in a lower observed signal level. The expectation would be that observed noise would also decrease as gain dropped. This appears to be true in the linear/high mode and is less pronounced in the low gain modes. In the compression/high gain mode, however, the reverse is the case. As temperature rises and gain drops, the noise level also rises. Decreasing observed signal level, particularly with a corresponding rise in noise level, led to several signal-to-noise violations which were not attributable to any test equipment failures or operator errors. These effects are real and a waiver was requested.

7.3.5 Summary Assessment

Proper assessment of the protoflight signal-to-noise performance was hampered by the noise contribution of collimator nonuniformities. In addition, quantization effects cause some of the modes to register higher noise values than expected. When these effects are removed, however, the scanner is shown to be within specification except for those cases of temperature sensitivity discussed above.

ORIGINAL PAGE IS
OF POOR QUALITY

Band 1 is operating very close to the specification value in both the linear/low and the compression/low modes, but has no problem meeting performance requirements in the linear/high and compression/high modes. Band 2 is similar to band 1, but has a larger margin in the low gain modes. It also has a large performance margin in high gain. Band 3 operates with the least stringent requirements. Even collimator nonuniformities and test equipment failiures do not cause this band to indicate out-of-specification operation. Band 4 operates safely within its performance requirements.

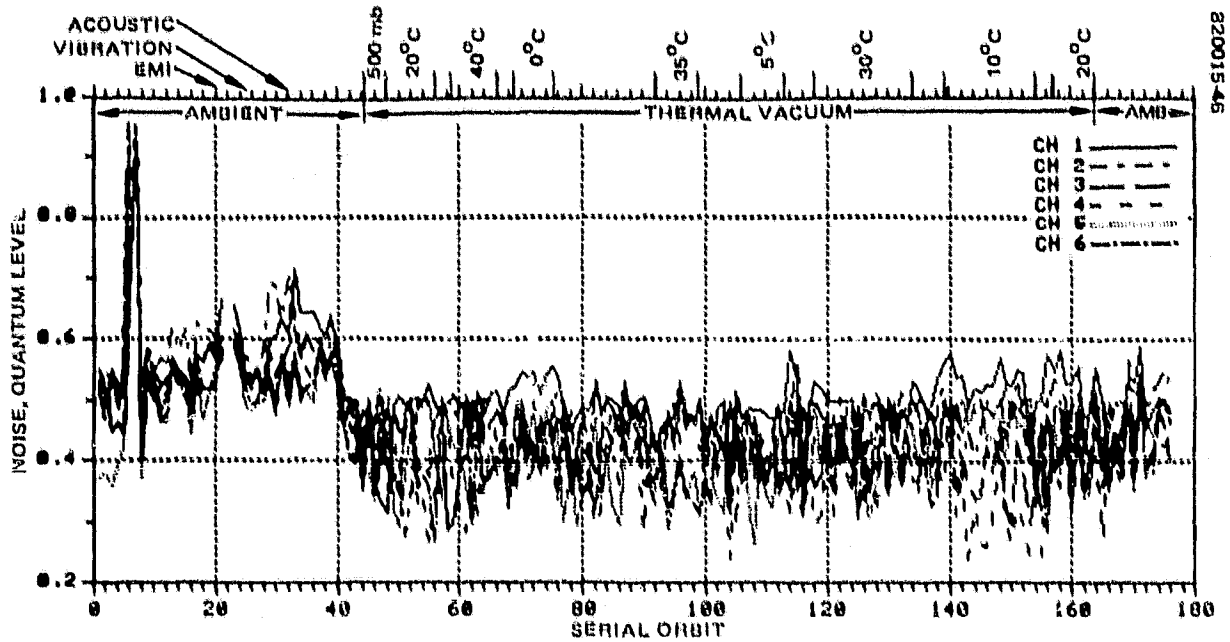

a) BAND 1

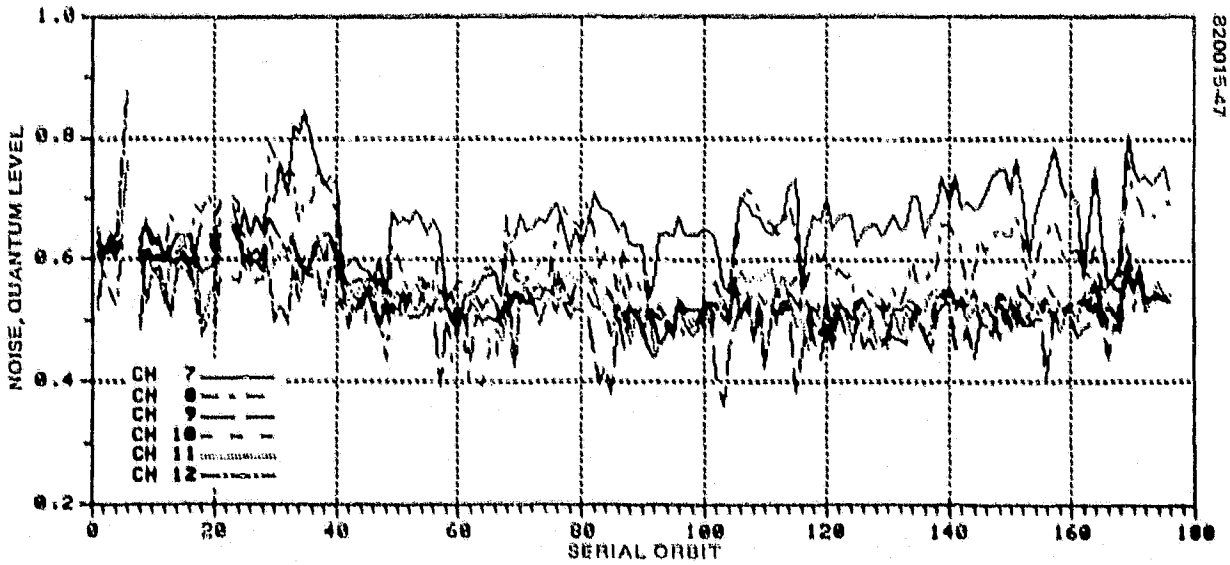

b) BAND 2

FIGURE 7-8. NOISE MEASUREMENTS DURING PROTOFLIGHT SYSTEM TEST – LINEAR/LOW GAIN MODE

ORIGINAL PAGE IS
OF POOR QUALITY

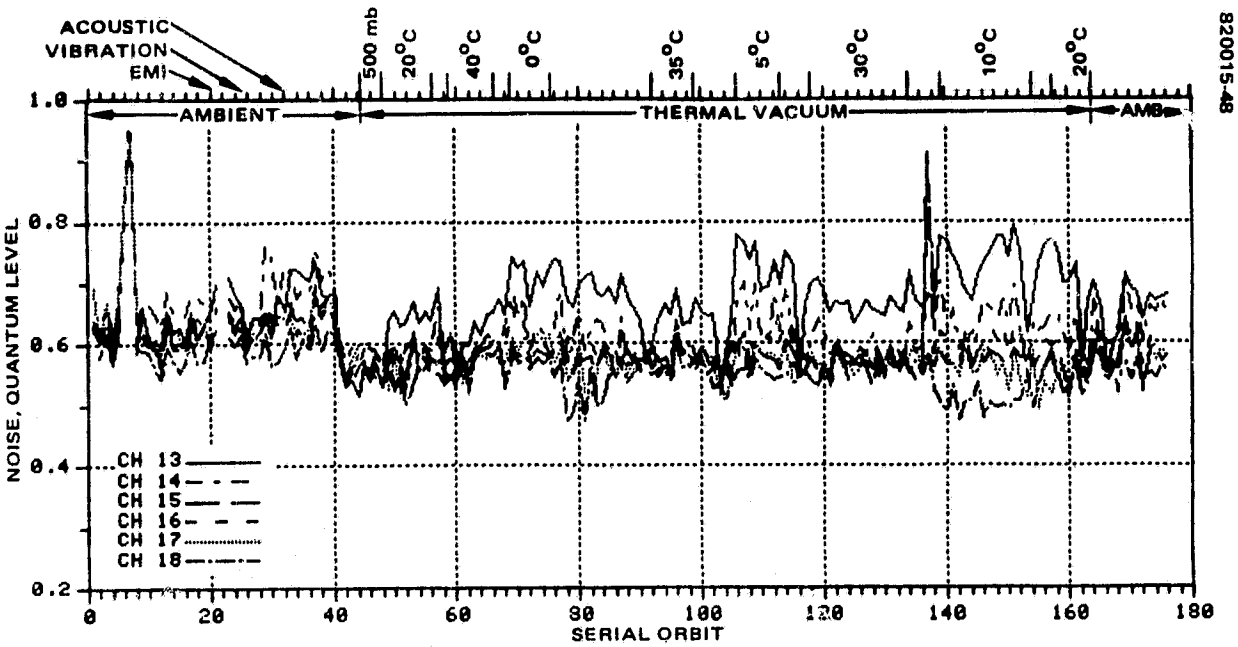

c) BAND 3

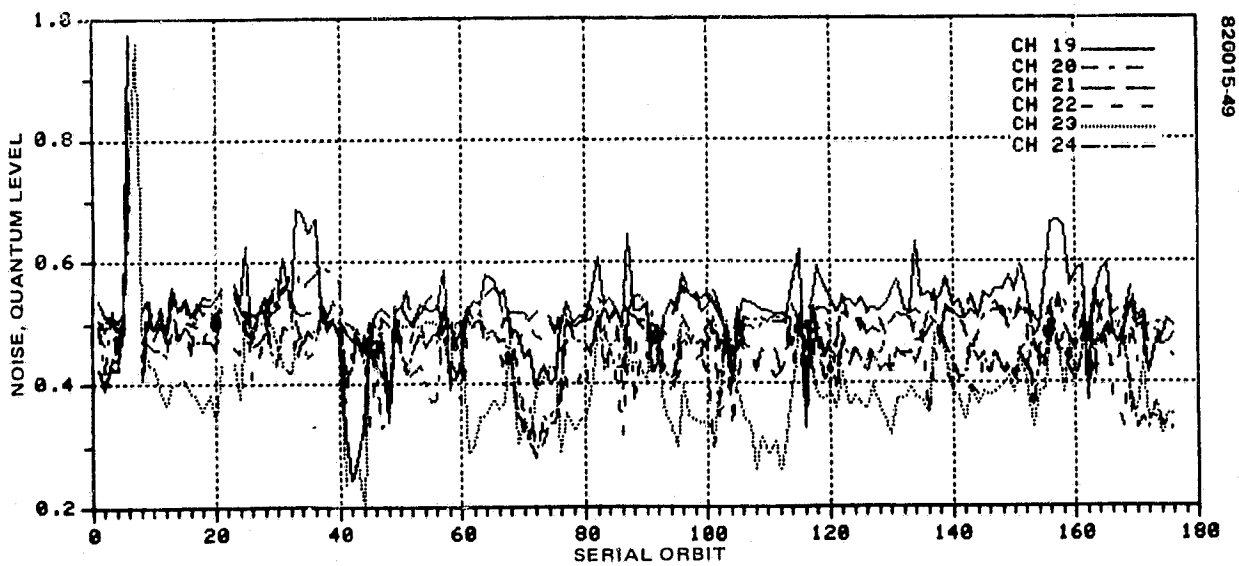

d) BAND 4

FIGURE 7-8 (CONTINUED). NOISE MEASUREMENTS DURING PROTOFLIGHT SYSTEM TEST – LINEAR/LOW GAIN MODE

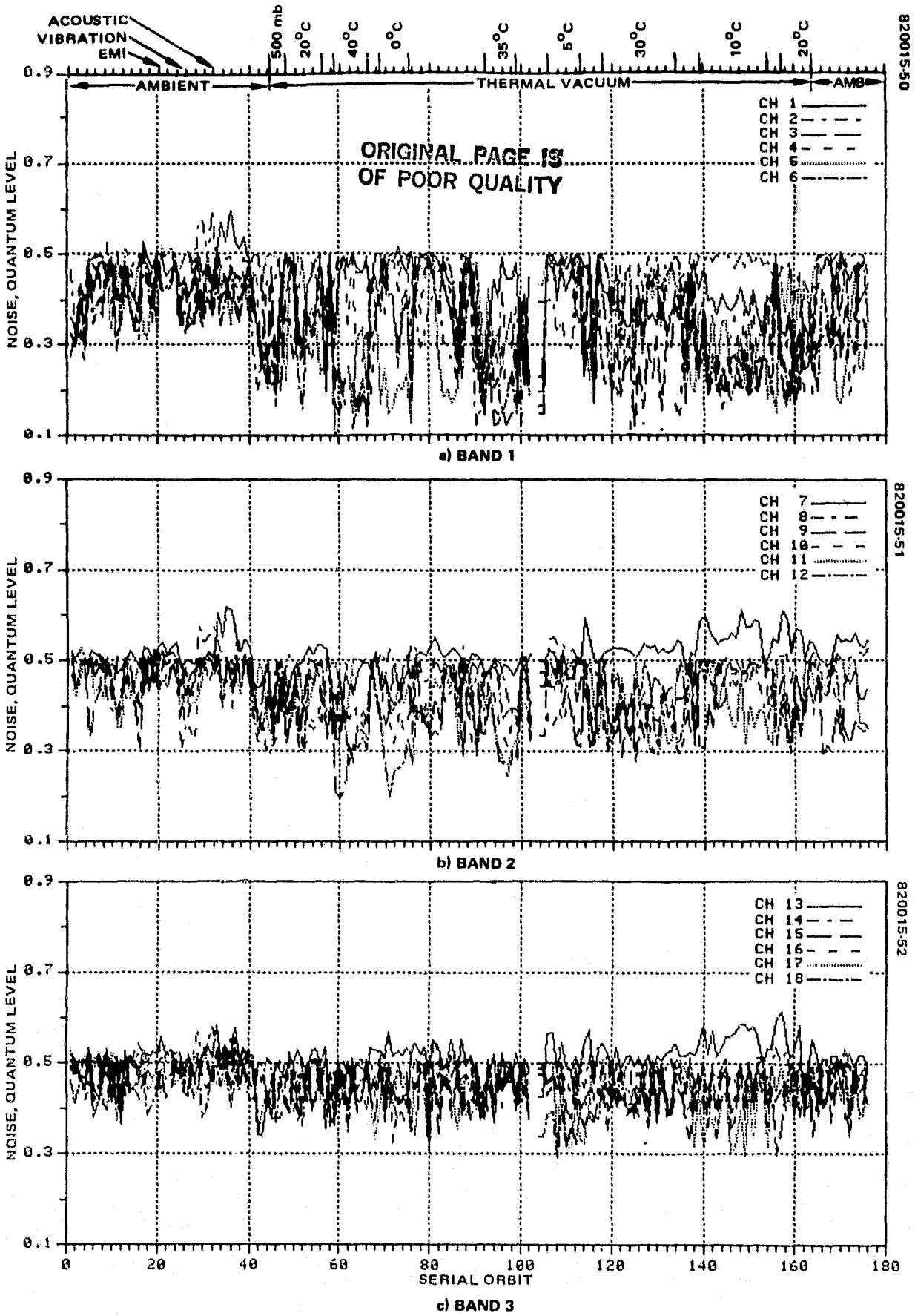

FIGURE 7-9. NOISE MEASUREMENTS DURING PROTOFLIGHT SYSTEM TEST – COMPRESSION/LOW GAIN MODE

ORIGINAL PAGE IS
OF POOR QUALITY

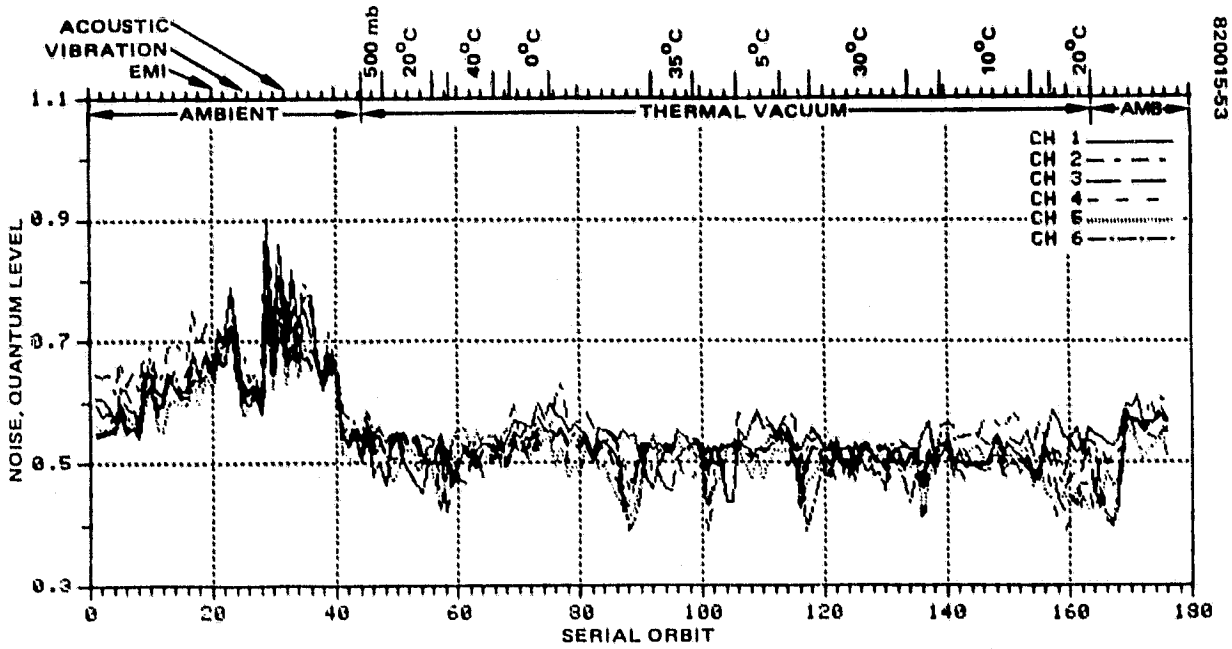

a) BAND 1

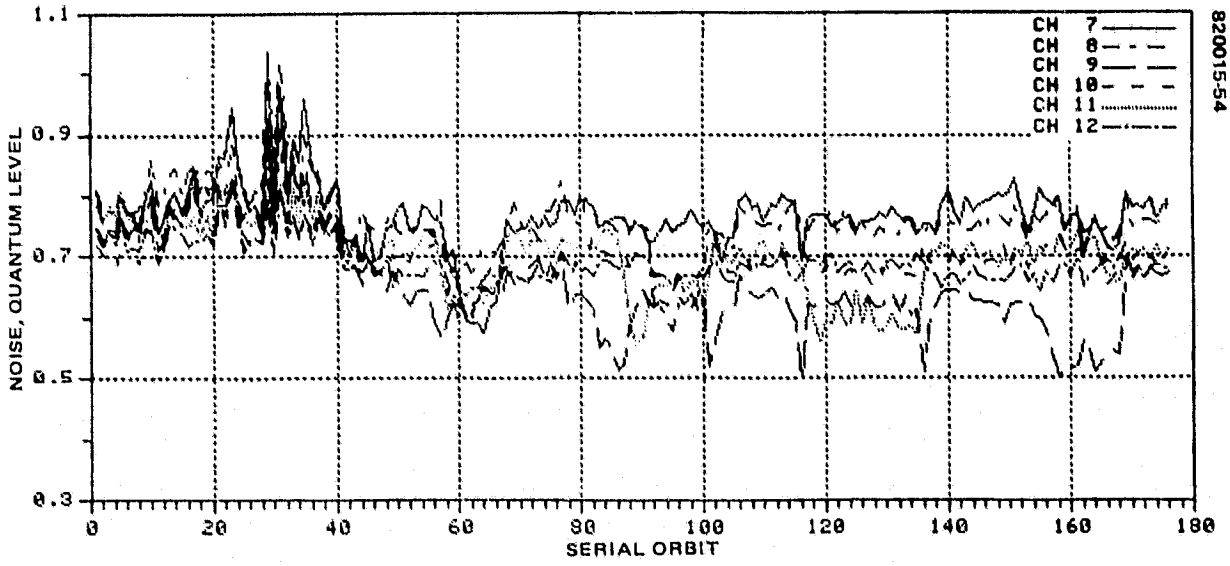

b) BAND 2

FIGURE 7-10. NOISE MEASUREMENTS DURING PROTOFLIGHT SYSTEM TEST – LINEAR/HIGH GAIN MODE

ORIGINAL PAGE IS
OF POOR QUALITY

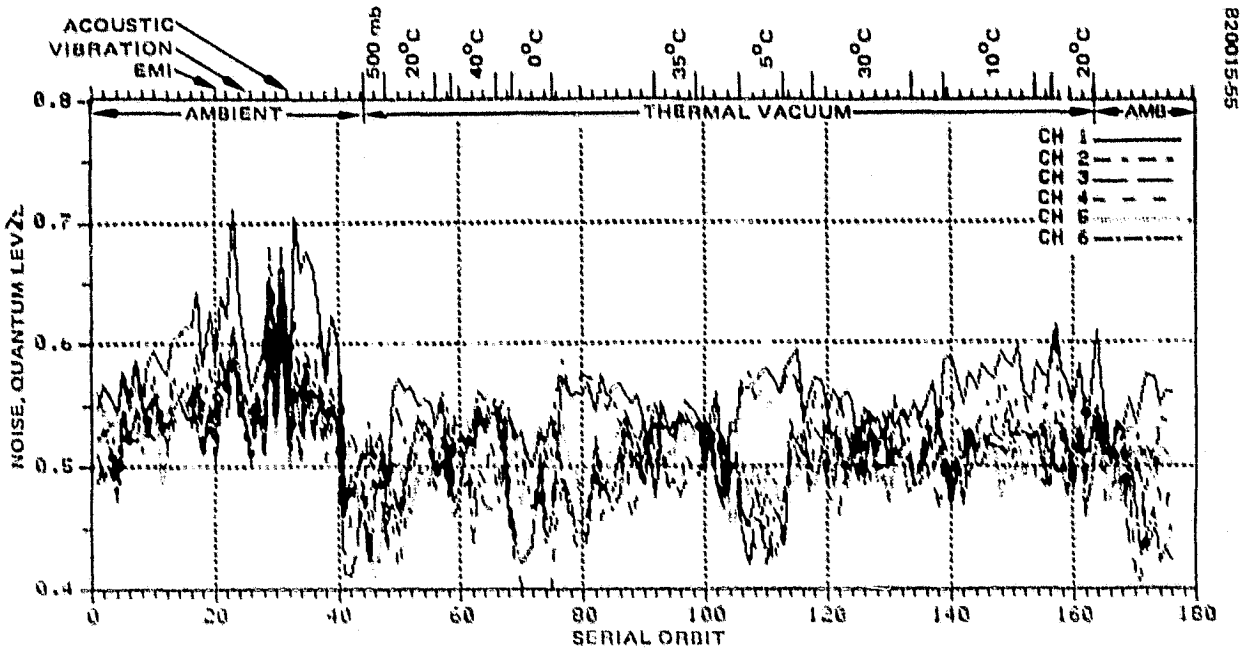

a) BAND 1

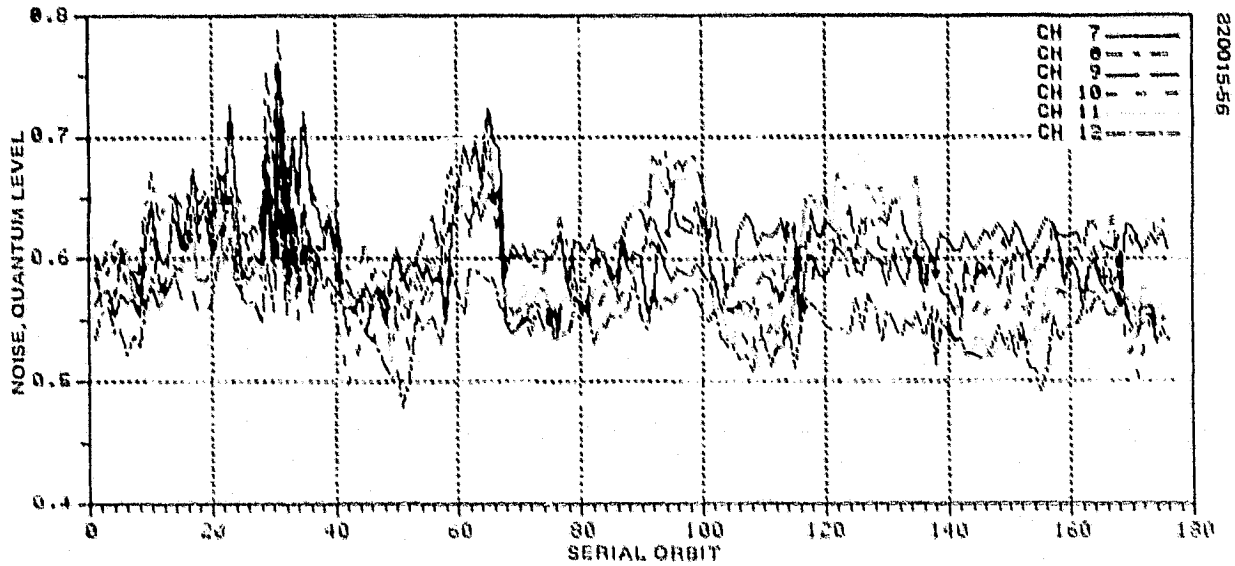

b) BAND 2

FIGURE 7-11. NOISE MEASUREMENTS DURING PROTOFLIGHT SYSTEM TEST — COMPRESSION/HIGH GAIN MODE

ORIGINAL PAGE IS
OF POOR QUALITY

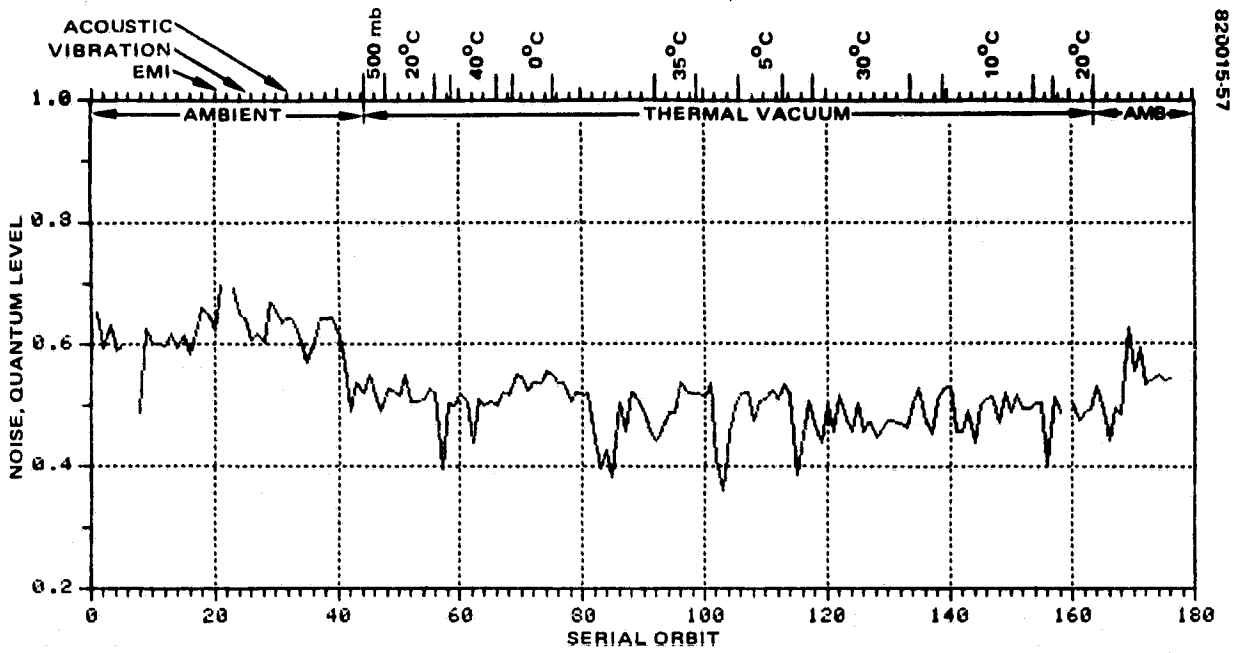

a) LINEAR/LOW GAIN MODE

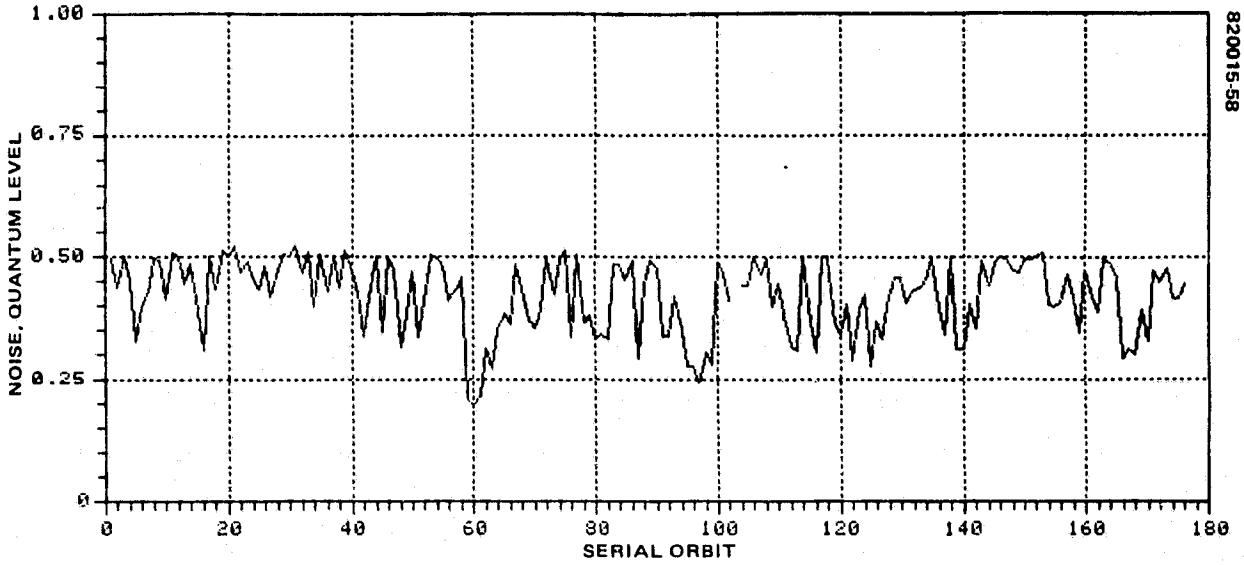

b) COMPRESSION/LOW GAIN MODE

FIGURE 7-12. NOISE TEMPERATURE SENSITIVITY – CHANNEL 9

ORIGINAL PAGE IS
OF POOR QUALITY

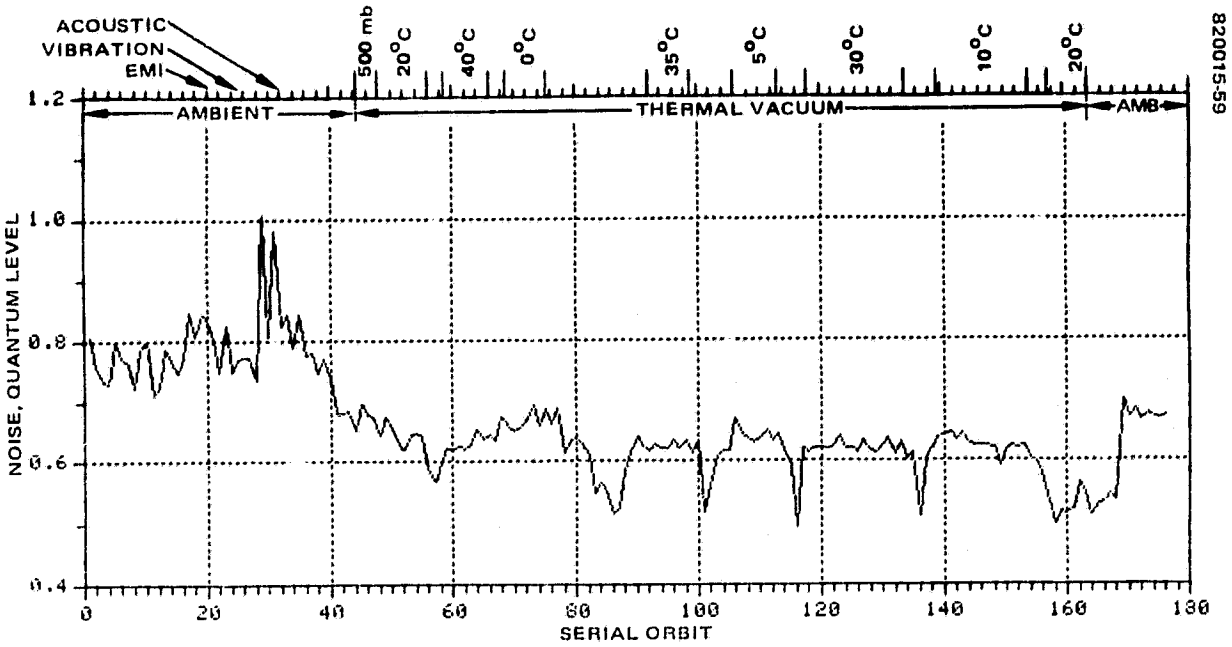

c) LINEAR/HIGH GAIN MODE

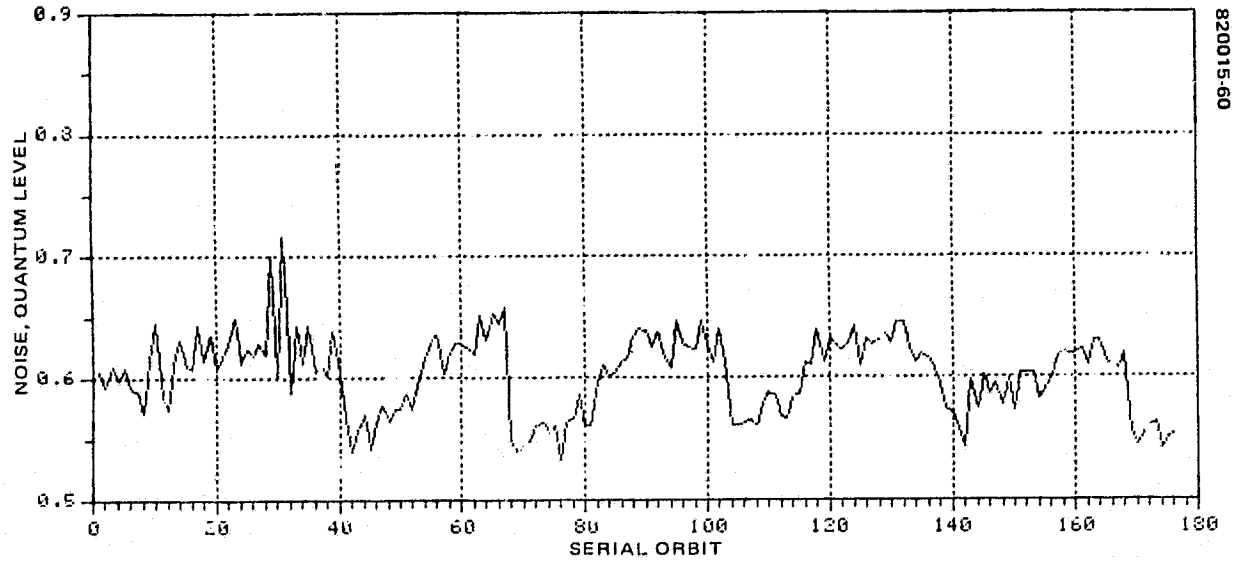

d) COMPRESSION/HIGH GAIN MODE

FIGURE 7-12 (CONTINUED). NOISE TEMPERATURE SENSITIVITY – CHANNEL 9

ORIGINAL PAGE IS
OF POOR QUALITY

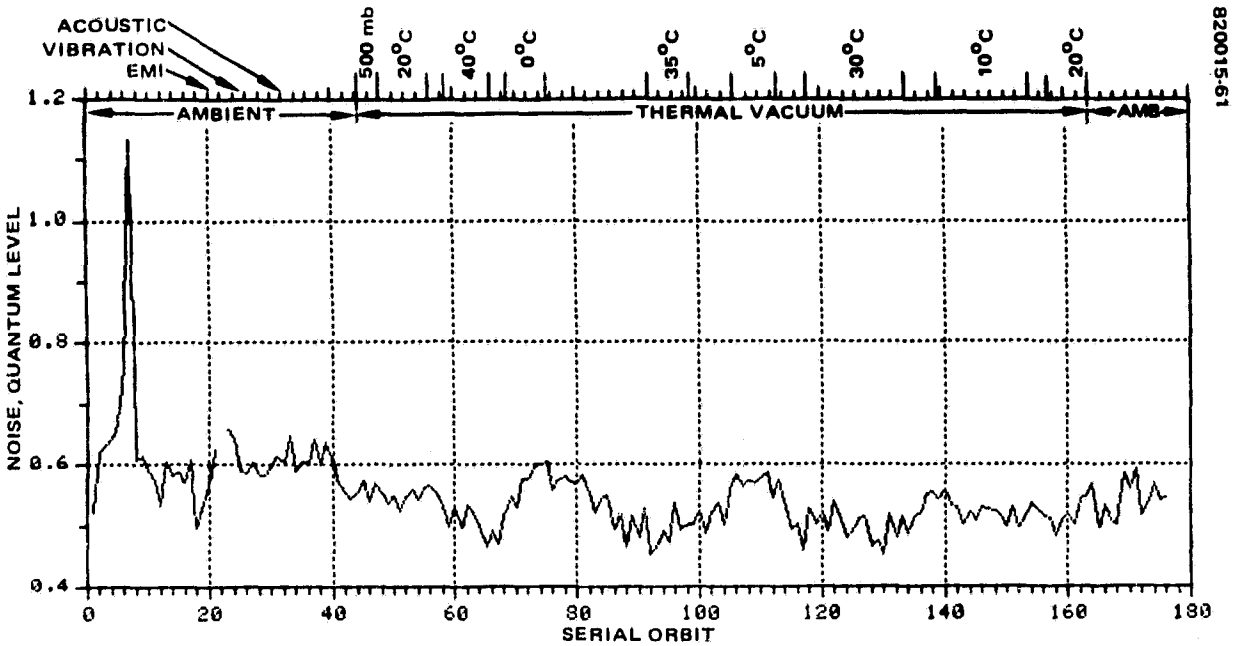

a) LINEAR/LOW GAIN MODE

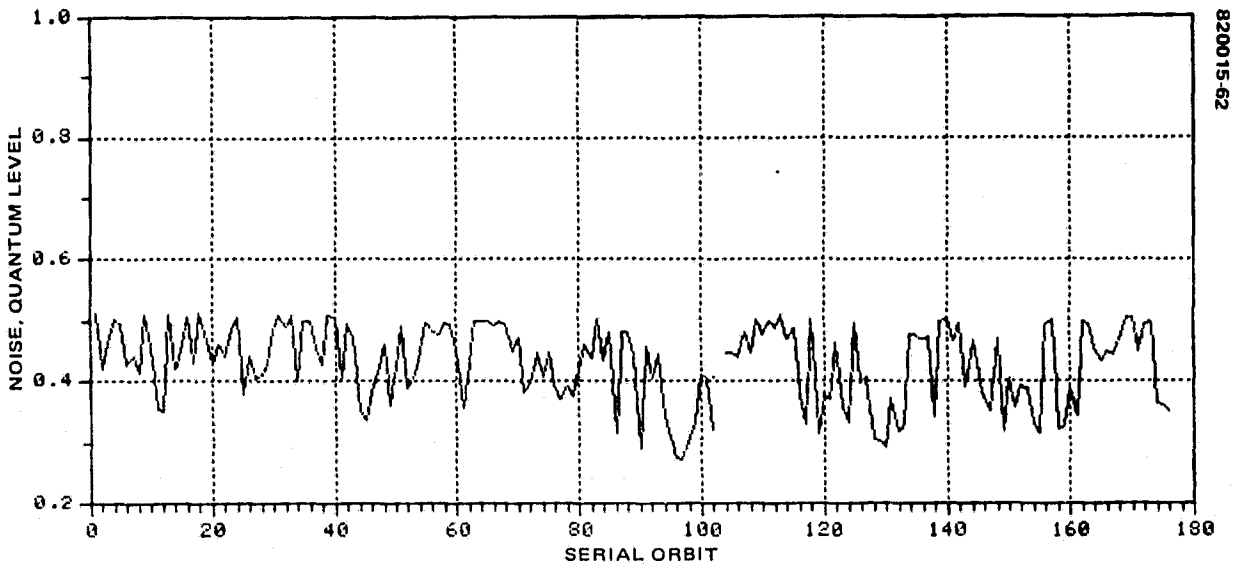

b) COMPRESSION/LOW GAIN MODE

FIGURE 7-13. NOISE TEMPERATURE SENSITIVITY – CHANNEL 11

ORIGINAL PAGE IS
OF POOR QUALITY

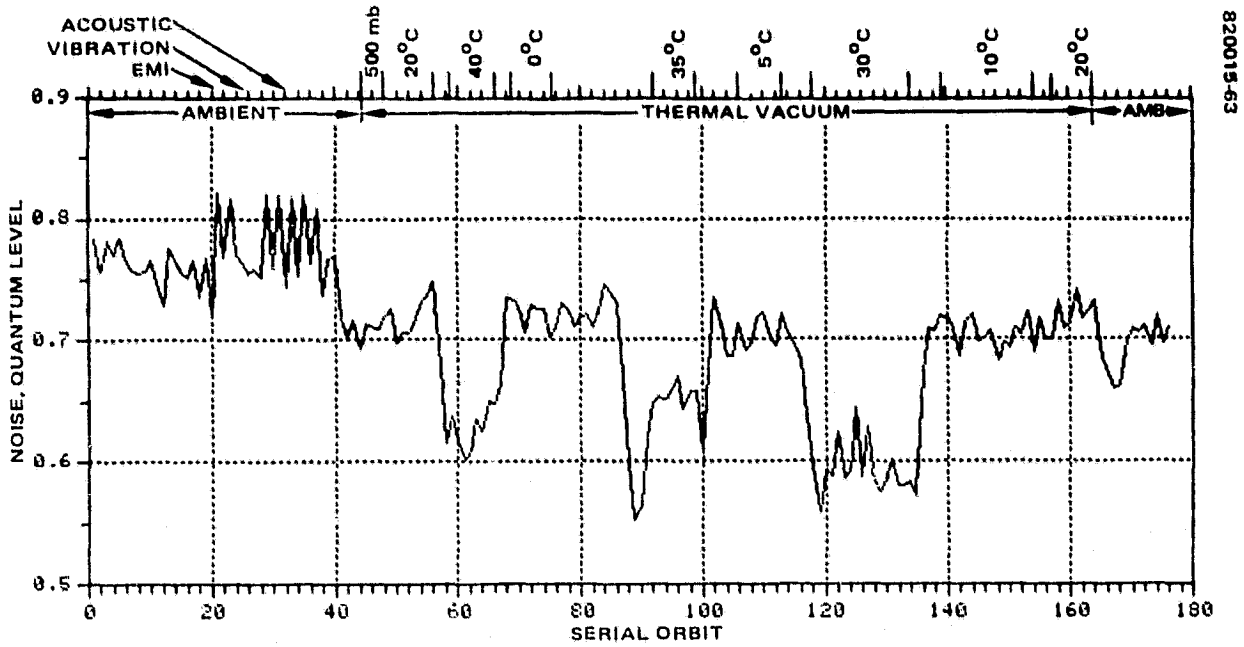

c) LINEAR/HIGH GAIN MODE

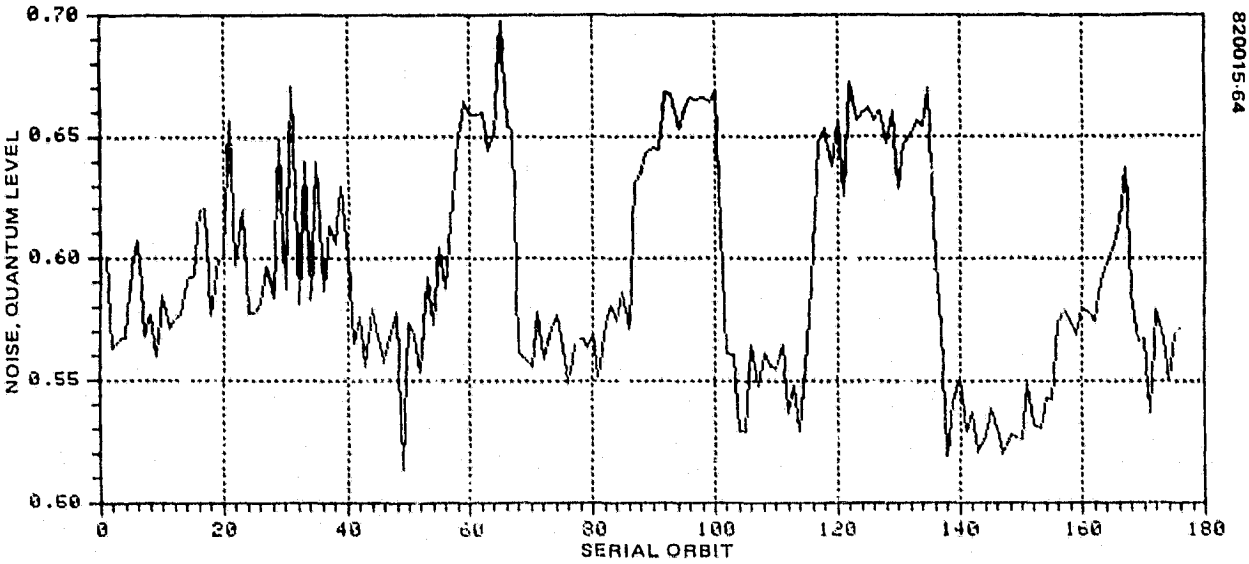

d) COMPRESSION/HIGH GAIN MODE

FIGURE 7-13 (CONTINUED). NOISE TEMPERATURE SENSITIVITY – CHANNEL 11

ORIGINAL PAGE IS
OF POOR QUALITY

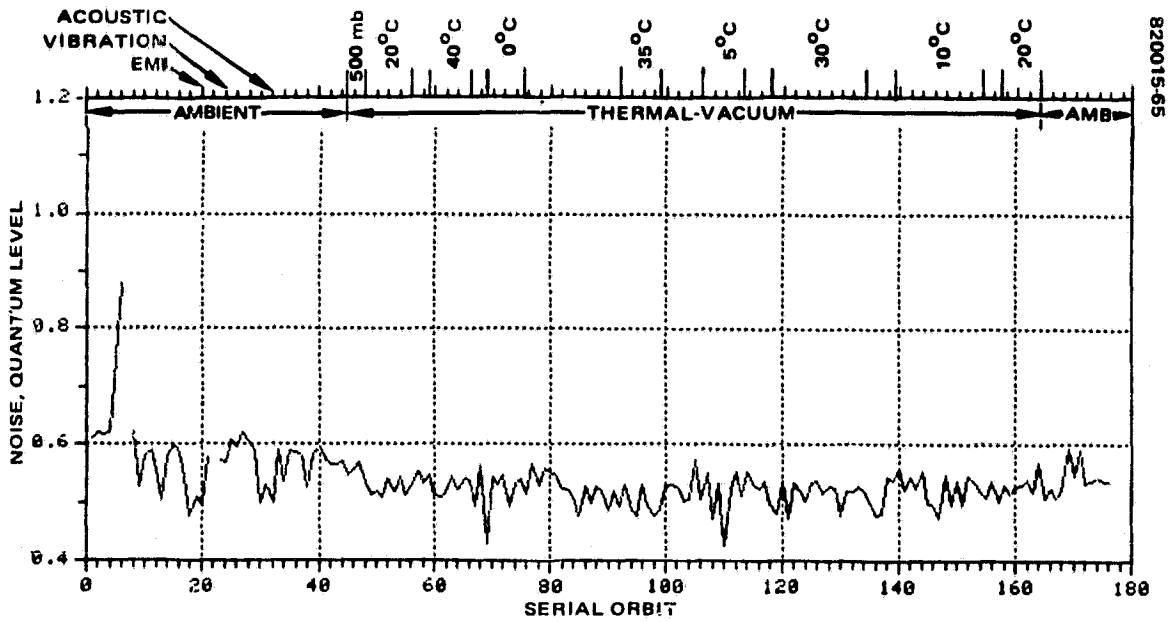

a) LINEAR/LOW GAIN MODE

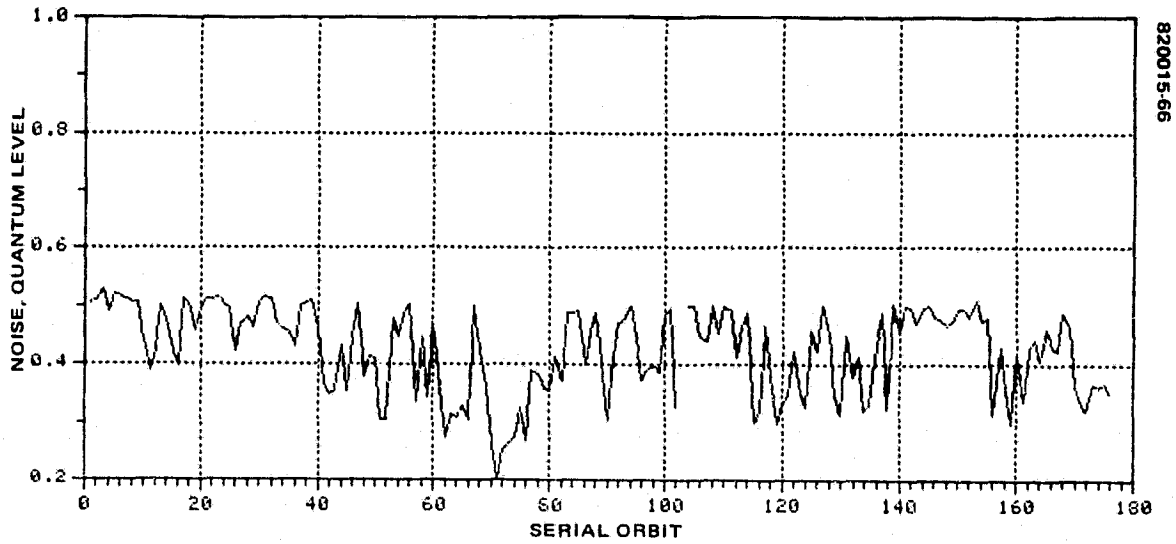

b) COMPRESSION/LOW GAIN MODE

FIGURE 7-14. NOISE TEMPERATURE SENSITIVITY – CHANNEL 12

ORIGINAL PAGE IS
OF POOR QUALITY

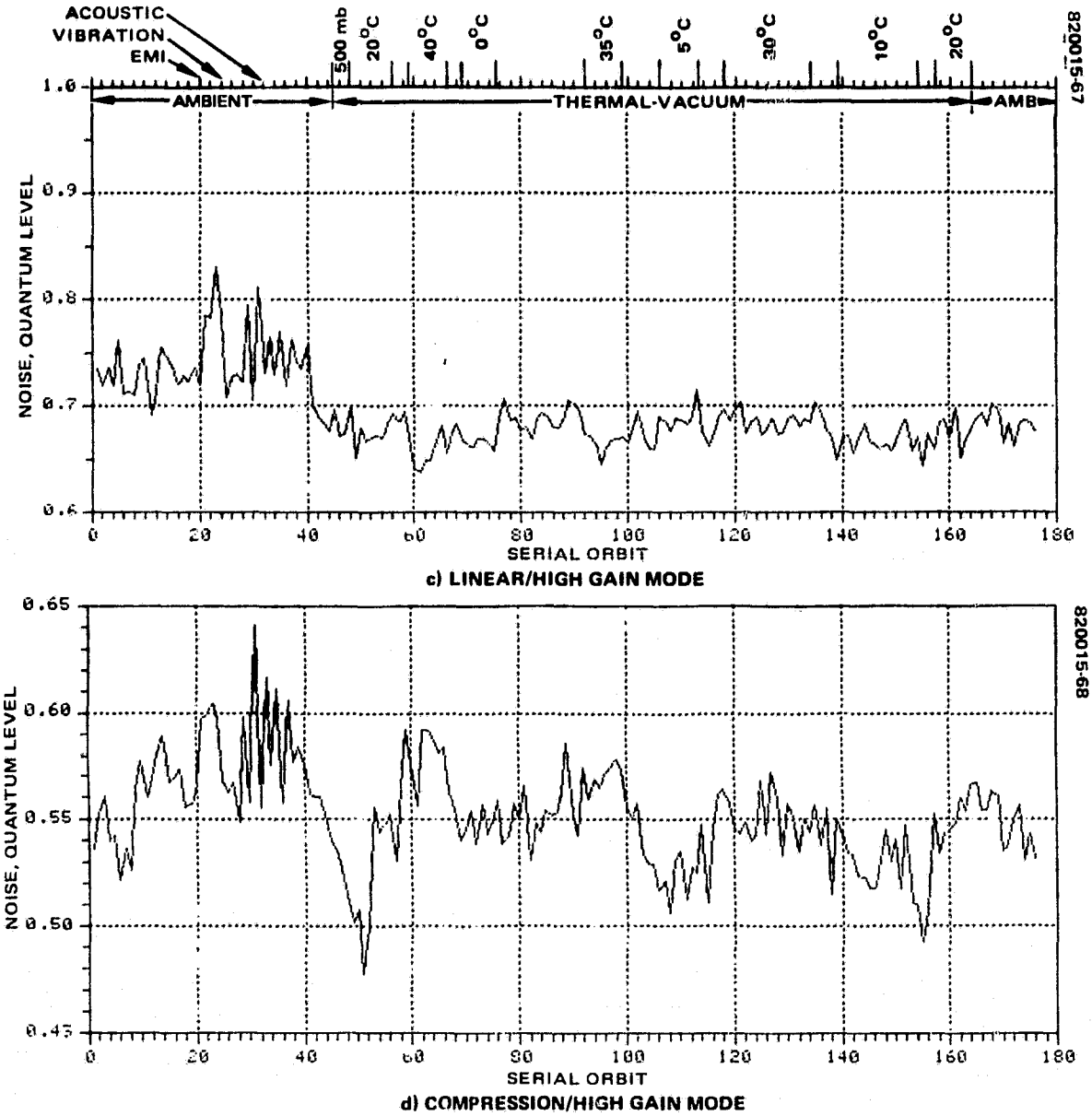

FIGURE 7-14 (CONTINUED). NOISE TEMPERATURE SENSITIVITY – CHANNEL 12

ORIGINAL PAGE IS
OF POOR QUALITY

7.4 CORRECTED SIGNAL LEVEL (COSL)

7.4.1 Introduction

The concept of the corrected signal level was formulated during early testing of MSS-1 and -2 as a means of providing a quantitative estimate of the internal calibration system's capability to provide gain and offset information needed for producing satisfactory ground processing equipment (GPE) pictures. Even with careful design and component selection, individual channels have sufficiently different gain and offset characteristics to result in "uncorrected" pictures which are "striped"; i.e., the intensity variations in the lines of a frame of image data are a replica of channel gain and offset differences.

The corrected signal level is the measured response of the MSS instrument to a radiant input from the collimator, corrected to remove individual channel gain and offset differences. These individual gain and offset estimates are obtained from the electrical signal which results from the radiant input to that channel from the internal calibration lamp. The calibration lamp is assumed to provide a stable but not necessarily uniformly distributed, or "flat," reference source over all the channels in a band.

The calibration lamp radiant intensity is established for each channel during system calibration. System calibration is performed at key test configuration or environment changes utilizing the GSFC 30-inch integrating sphere as the primary calibration standard. The calibration procedure used at these times produces reference calibration wedges, or reference nominal values, of calibration lamp input radiance as a function of angular position along the rotating neutral density (exponential) filter wheel. These calibration wedges are produced on every other back scan of the scanning mirror. Radiance values are presented as a function of time, or word count, from the leading edges of the calibration pulse. The test collimator is calibrated using the scanner calibration system as primary reference. This collimator transfer of calibration procedure is performed following each integrating sphere calibration of the scanner.

Channel gains are expected to vary, especially as a function of temperature and pressure environment. Typically PMT channels (band 1, 2, 3) have gains which decrease with increasing temperature while the photodiode channels (band 4) have gains which increase with increasing temperature. The individual gains also change on entering vacuum from ambient pressure. The magnitude of this vacuum shift in gain is not predictable for any channel but has been evident in this as well as all other MSSs. While not satisfying any strict rule as to behavior, it is typical that the gains in the first two bands (1 and 2) decrease with a decrease in pressure environment, while bands 3 and 4 show an increase in gain with a decrease in pressure. It is typical for MSS that this gain change has a long time constant, more noticeable on returning to ambient pressure conditions than on entering vacuum. Within nominal gain variability, the gains return to the same values after leaving vacuum that were measured before entering vacuum.

Some gain change or variation has been observed to occur with time even in the absence of environmental changes. The degree of this gain wandering in the absence of known environmental changes is normally small and dependent on individual channel characteristics not completely understood and quantified. The effect in some channels is sufficient to be noticeable during extended testing such as that performed on the MSS.

ORIGINAL PAGE IS
OF POOR QUALITY

Ideally, the internal calibration system provides timely gain estimates which permit the elimination of any effect of these changes on scene radiance measurements.

Therefore, in the absence of external (e.g., test equipment) variations, COSL is a measure of internal calibration system stability. Every channel in a given band should, in principle, yield the same COSL value for a particular data set, and that value should not change in time. However, the measured values of the COSL parameter will vary due to statistical uncertainties in the measurement process, if for no other reason. There may also be real changes in the collimator or scanner which cause the COSL parameter to vary. (See 6.4.2 for a detailed explanation of COSL algorithm).

As indicated in 6.4.2, individual channel COSLs are not subject to specification. Primary interest in COSL performance lies in the value of any individual COSL with respect to the COSLs for all of the other channels in a band. The specification states that the absolute value of the difference between the COSLs for any two channels in a band must be less than 2 percent of the band average COSL for all the channels in that band. Since the satisfaction of this requirement for the specific channel pair that possess the maximum and minimum COSL values satisfies, a fortiori, the requirement for any pair of channels, or the specification for channel-to-channel deviation can be symbolically represented by the following:

$$\left| COSL_{MAX} - COSL_{MIN} \right| \leqslant 0.02 \left[\prod_{i=1}^{6} COSL_i \right]^{1/6}$$

The band geometric rather than arithmetic average was used in the earlier development because this formulation was felt to provide a better match to the human eye performance in image evaluation. It is retained in the current algorithms. To evaluate DCC performance, one is interested in following the performance history of the envelope of graphs of all six channels in a band as a function of environment.

The other COSL parameter specified is the band-to-band deviation (DBB). This parameter measures the relative change in the band average radiance of the scene (collimator output). The specification of DBB requires that the peak-to-peak spread, over all bands, in the ratio of band average means of the COSLs for any band relative to the value of this mean for that band at calibration be less than 3 percent of the mean of this ratio over all of the bands. (See Section 6.4.2 for a further clarification of the specification.)

The remainder of the section contains the results of COSL measurements during MSS-D protoflight system acceptance testing. In addition to COSL, DCC, and DBB performance, the behavior of individual channel gains as a function of test environment is presented. In particular, gain-temperature plots are provided which may be of some value for further study of calibration accuracy.

7.4.2 Average Signal Level (ASL) Performance History

The parameters which bear directly on the system signal correction performance are the average signal level (ASL), the corrected signal level (COSL), the gain (G), and

ORIGINAL PAGE IS
OF POOR QUALITY

the offset (ϕ). All these parameters were continuously monitored throughout MSS-D system acceptance testing. Graphics were routinely provided and surveyed to assist in the assessment of system performance and to aid in early identification of potential system problems.

Average signal level (ASL) for the MSS-D protoflight is displayed for all the channels in each band in Figure 7-15 for all of the data taken during regular orbits of acceptance testing. Special test request data and data taken during calibration orbits are not represented. The ASL is a primitive measure of system behavior. It is the average (over 100 scans, 20 words per scan) of the system response to the test collimator input. The units given are in quantum levels, with level 63.5 representing the fully saturated system. The ASL is utilized in the signal-to-noise performance assessment as well as in COSL (DCC, DBB) performance assessment discussed here. These algorithms are discussed in Section 6.

Since the internal calibration system derived gains are not involved in computing the ASL, this parameter provides a very basic view of system performance. For instance, ASL plots may be viewed as providing a separate estimate of relative channel gains and can be used to compare with the internal calibration system estimate of gain described later. The difference between these two types of gain estimates directly impacts on the estimate of the COSL, and the discrepancy between ASL and G changes is responsible for the errors which show up as DCCs and DBBs. Since the scanner does not have a separate, independent calibrated sensor for measuring radiance, considerable difficulty exists in establishing the degree of fault which should be attributed to the scanner versus the test equipment for anomalous COSL performance. The consistency and repeatability of the separate data measure, as well as their correlation with each other and with independent data derived from the flooding lamp and from calibration orbit data, provide a means for developing confidence in calibration system performance estimates.

The treatment given in 6.5 of calibration system stability is highly statistical and utilizes flooding lamp data as an independent data source. The ASL plots given here can provide additional insight into signal correction performance if the following observations are used:

1) Changes in ASL behavior reflect system behavior independent of the internal calibration system. Thus changes in ASL are due either to real gain changes, changes in the collimator output, or both

2) Changes in gain (G) behavior reflect changes in the internal calibration system's estimate of the gain. This may be a real gain change or the result of errors in the gain estimate (G) produced by calibration system changes, or both.

3) Changes in both ASL and G which agree sufficiently to produce good COSL values for all channels in a band, but produce varying or consistently alternating values of the band average for A and B modes, suggest strongly that the results are induced by improperly established calibration wedge nominals during the previous calibration.

4) ASL and G estimates can agree in the direction of change but disagree in amplitude sufficiently to create COSL problems.

ORIGINAL PAGE IS
OF POOR QUALITY

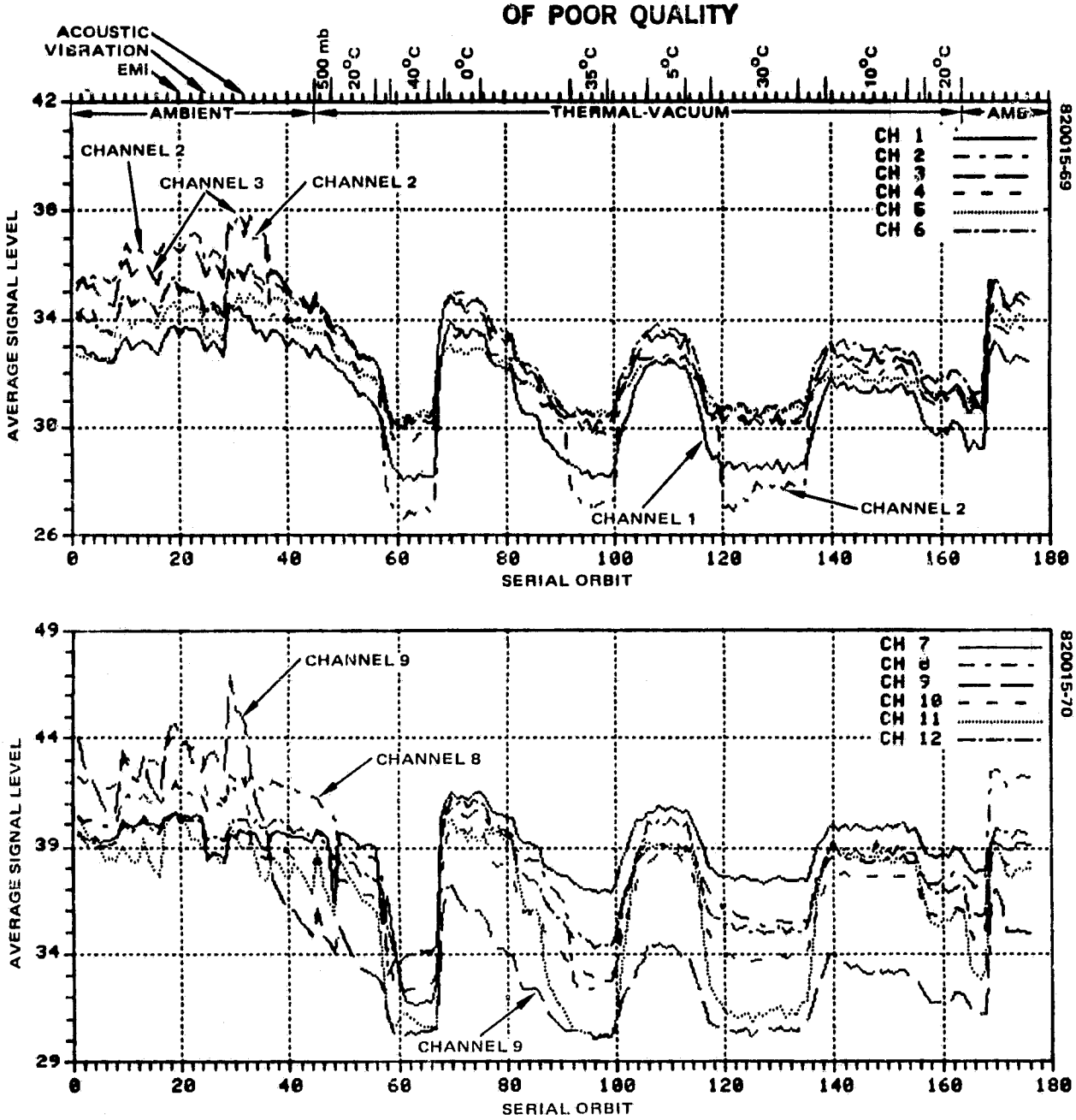

FIGURE 7-15. PROTOFLIGHT AVERAGE SIGNAL LEVEL – LINEAR/LOW GAIN MODE

This last case, which is obtained more often than not when DCC problems occur, is the one most difficult to attribute to a specific cause. The ASL curves presented here should be used as a source of additional information as the description of gain and COSL performance unfolds. A more complete understanding of system performance is obtained if these curves are used as a reference, remembering that the basic relationship among the primary parameters is the following:

$$COSL = K\frac{ASL - \phi}{G}$$

where K contains a factor which relates to shading at time of calibration and a factor which normalizes the estimated collimator output in radiance to quantum levels.

ORIGINAL PAGE IS
OF POOR QUALITY

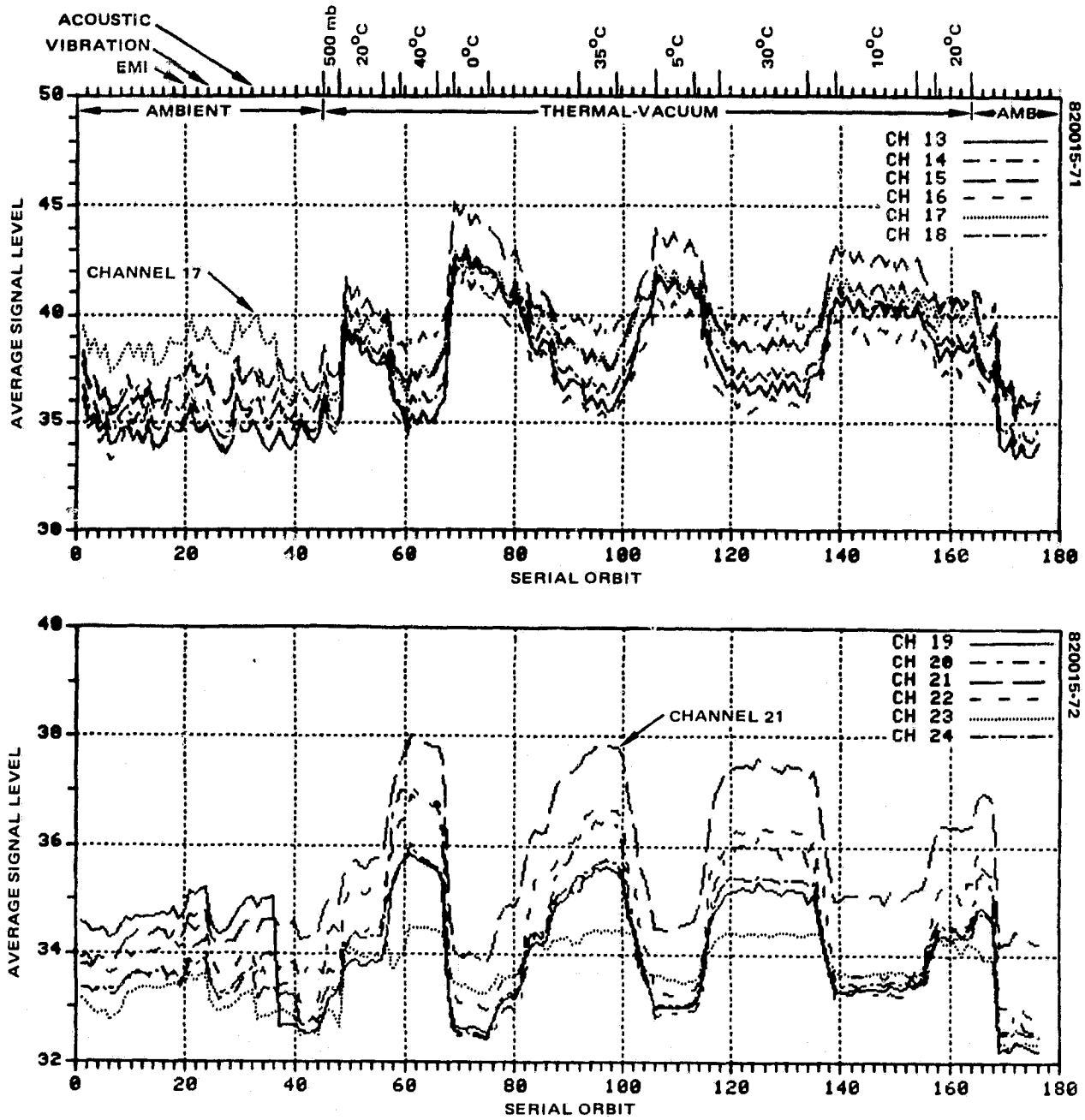

FIGURE 7-15 (CONCLUDED). PROTOFLIGHT AVERAGE SIGNAL LEVEL – LINEAR/LOW GAIN MODE

ORIGINAL PAGE IS
OF POOR QUALITY

7.4.3 System Gain Performance History

The system gain performance is described before the system COSL performance with respect to the specification parameters, DCC and DBB, is discussed. The gain discussed here is the estimate of the channel gain, G, provided by the internal calibration system. The features of this gain estimate which are of interest are the following:

1) The individual channel gain behavior as a function of key environmental changes (temperature, pressure), and test configuration

2) The individual channel gain behavior as compared to the nominal gain behavior for other channels in the band for the same test environment

3) Identification of major test or flight hardware configuration changes that could affect system gain performance estimates

7.4.3.1 Nominal Gain History

The gain history for all channels is presented in Figure 7-16 for the major test events. The nominal performance for each channel, as indicated by these plots, is summarized in Table 7-9. As is evident from the individual plots, each test event may contain from 4 to 16 gain values, depending on the number of orbits run during the test. Table 7-9 provides the basis for the discussion which follows.

During the first long form performance test (LSPT) on through postacoustic, the following observations were made:

1) In band 1, channels 2 and 3 gains are 5 to 9 percent higher than the other band 1 gains.

2) In band 2, channel 9 gain behavior was erratic. In fact, during the preacoustic test event, channel 9 nominal gain was 7 to 17 percent higher than the other band 2 gains. Considerable gain wandering at a newly fixed temperature/pressure environment was evidenced.

3) In band 3, channel 17 nominal gain was 5 to 11 percent higher than the other band 3 gains.

4) In band 4, channel 19 gain was 2 to 8 percent higher than the other band 4 gains.

As a result of the above observations, plus concern over the dynamic range limitations of the instrument that result from higher than nominal gains, the select resistors of channels 2, 3, 9, 17, and 19 were changed 29 April 1981. This change resulted in the

ORIGINAL PAGE IS
OF POOR QUALITY

following nominal gain reductions (which appear in Table 7-9 as the difference between the postacoustic and pre-endbell values):

Channel	Gain Changes, Percent
2	-7.5
3	-5.2
9	-12.0
17	-7.7
19	-7.5

Following these select resistor induced gain changes, the gain characteristics of each channel for the remaining tests are described as follows:

Band 1

All the channels behaved in the same way throughout the tests except for some channels which are more sensitive to certain temperatures during the thermal-vacuum test. Channels 1 and 2 are more sensitive than the average to high temperatures, 40°, 35°, and 30°C. Channel 1 gain was lower than the average gain of the normal channels (3, 4, 6) by 6 percent at 40°C, 5 percent at 35°C, and 4 percent at 30°C. Channel 2 gain was lower than the average gain of the normal channels by 10 percent at 40°C, 8 percent at 35°C, and 7 percent at 30°C. Channel 5 is less sensitive to lower temperatures than the other channels since its gain changed the least during the high temperature to low temperature transitions. Channel 5 gain was lower than the average gain of the normal channels by 6 percent at 0°C and 3 percent at 5°C.

A vacuum shift is observed in all the gains in band 1. The gains went down by 1 to 2 percent during GN_2 backfill, and by 5 to 7 percent going into vacuum. Comparing the gain values during the final LFPT to the post-thermal-vacuum gain values shows a delayed effect of coming out of vacuum into ambient conditions. Eventually the gains returned to the endbell values.

It is important to note that as expected from tests on the earlier MSSs, the band 1 gains tend to decrease due to an increase in temperature. However, some of the gain decrease in subsequent orbits is not due to temperature alone. For example, comparing the first 20°C nominal gains to the last 20°C nominal gains shows that band 1 gains were still in the process of reaching stabilization at the end of thermal-vacuum. This effect is shown in plots given at the end of this section. The following data demonstrate the gain changes as the system went from the first 20°C plateau to the remaining 20°C plateaus using the first 20°C plateau as a baseline:

Channel	Percent Shift, 2nd 20°C Plateau (3 days later)	Percent Shift, 3rd 20°C Plateau (9 days later)
1	-3.1	-4.8
2	-1.7	-3.9
3	-2.8	-5.5
4	-3.2	-5.5
5	-2.2	-3.5
6	-2.5	-3.8

ORIGINAL PAGE IS
OF POOR QUALITY

Band 2

The gain plots indicate that the channels which can be considered having more nearly nominal behavior are channels 10 and 12. Channel 7 gain was not affected as much as the nominal channels by a change in environment (from ambient, to GN_2 backfill, then to vacuum). Channel 7 gain remains essentially the same during the environment changes while the nominal channel gains went down by 1 percent during GN_2 backfill and 4 percent during vacuum. Channel 8 was 6 to 9 percent higher than the nominal channels in ambient conditions. Channel 8 also experienced a vacuum shift, dropping 2 percent during GN_2 backfill and 7 percent going into vacuum. Channel 9 was 7 to 10 percent lower than the nominal channels and also experienced a vacuum shift.

During the thermal-vacuum test, channels 10 and 12 show about the same degree of sensitivity to the various temperatures. Channel 11 showed the highest gain change (drop) during a transition from a low temperature to a higher temperature. Channels 7 and 9 showed the same degree of sensitivity to the different temperatures except at the 40°C plateau where the channel 7 gain dropped relatively greater than the drop in channel 9.

Band 2 gains decrease as the temperature increases. As observed in the band 1 gains, the band 2 gains also showed a drop (decrease) in value as a function of time.

Band 3

Channels 14, 17, and 18 are the nominal channels as indicated by the gain plots. Channel 15 shows a higher degree of sensitivity at both the high and low temperatures. Channels 13 and 16 demonstrate the same degree of changes during the low temperature to high temperature transitions. Channel 15 gain was higher than the nominal channels by 5 percent at 0°C, 4 percent at 5°C, and 3 percent at 10°C. Channels 13 and 16 gains were lower than the nominal channels by 7 percent at 40°C, 5 percent at 35°C, and 5 percent at 30°C.

Band 3 gains increased as the system went through ambient pressure to 500 mbar pressure. A further increase in the band 3 gain showed as the system went from GN_2 backfill to vacuum environment. The following shows how each channel gain reacted to the change in environment:

Channel	Percent Shift into GN_2 Backfill	Percent Shift into Vacuum
13	+1.2	+10.2
14	+1.4	+9.2
15	+1.7	+9.4
16	+1.2	+9.1
17	+0.8	+8.1
18	+1.7	+9.2

ORIGINAL PAGE IS
OF POOR QUALITY

A survey of the gain values at the three 20°C plateau indicates that channel 17 gain stabilized during thermal vacuum but the other band 3 gains did not. A comparison of the gains at post-thermal-vacuum and the last 20°C plateau showed very slight changes. However, the gains went back (down) to the endbell values during the final LFPT. This means that the vacuum shift (going out of vacuum to ambient pressure) occurred a few days later after the actual end of vacuum test.

Band 4

A survey of the gain plots shows that the channels that can be considered having nominal gain behaviors are 19, 20, 22, and 24. Each of the channels reacted differently to change in temperature or pressure; however, to simplify the description of the gain behavior, channel 19, 20, 22, and 24 gains may be considered as behaving as a bundle. Channel 21 gain varied approximately the same as the nominal channels for a certain change in temperature, but it was always 2 to 5 percent higher than any of the nominal channels. Channel 23 was the least sensitive to a 20°C to 40°C transition. The nominal channels changed by as much as 7 percent, while channel 23 changed only by 0.7 percent. Channel 21 changed by 5 percent due to a 20°C increase in temperature.

A vacuum shift is also observed in the band 4 gains. The following data show the shift from ambient to GN_2 backfill and to vacuum.

Channel	Percent Shift into GN_2 Backfill	Percent Shift into Vacuum
19	+0.7	+2.9
20	+1.3	+2.7
21	+1.7	+3.5
22	+0.7	+4.6
23	+0.4	+3.7
24	+1.1	+3.2

All of the band 4 gains seem to remain stable during the thermal-vacuum test. Very slight gain changes occurred between the three 20°C plateaus (see Table 7-9). The effect of going out of vacuum into ambient pressure occurred during the final LFPT where the gains returned to the endbell values.

ORIGINAL PAGE IS
OF POOR QUALITY

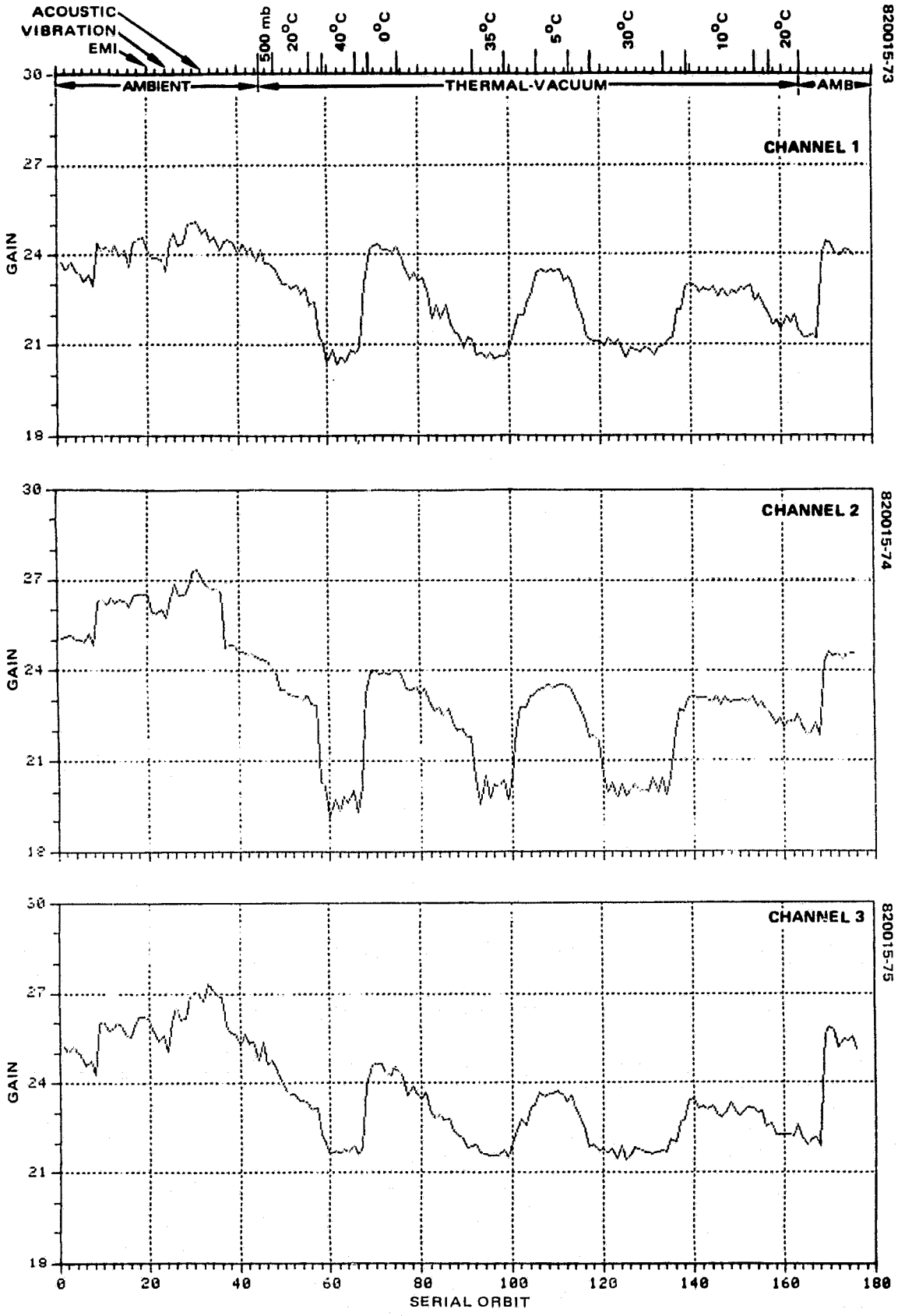

FIGURE 7-16. PROTOFLIGHT GAIN HISTORY – LINEAR/LOW GAIN MODE

ORIGINAL PAGE IS
OF POOR QUALITY

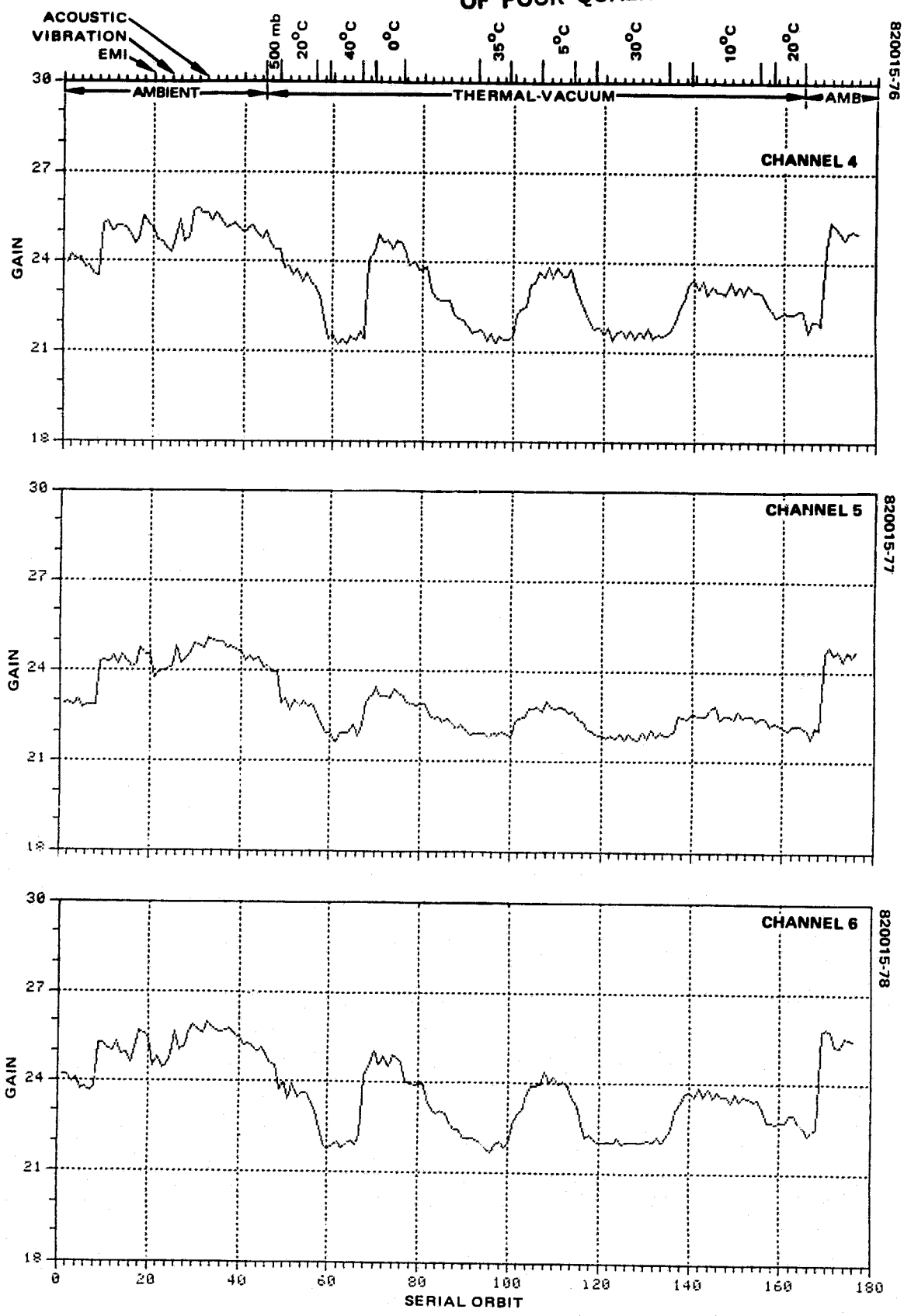

FIGURE 7-16 (CONTINUED). PROTOFLIGHT GAIN HISTORY – LINEAR/LOW GAIN MODE

ORIGINAL PAGE IS
OF POOR QUALITY

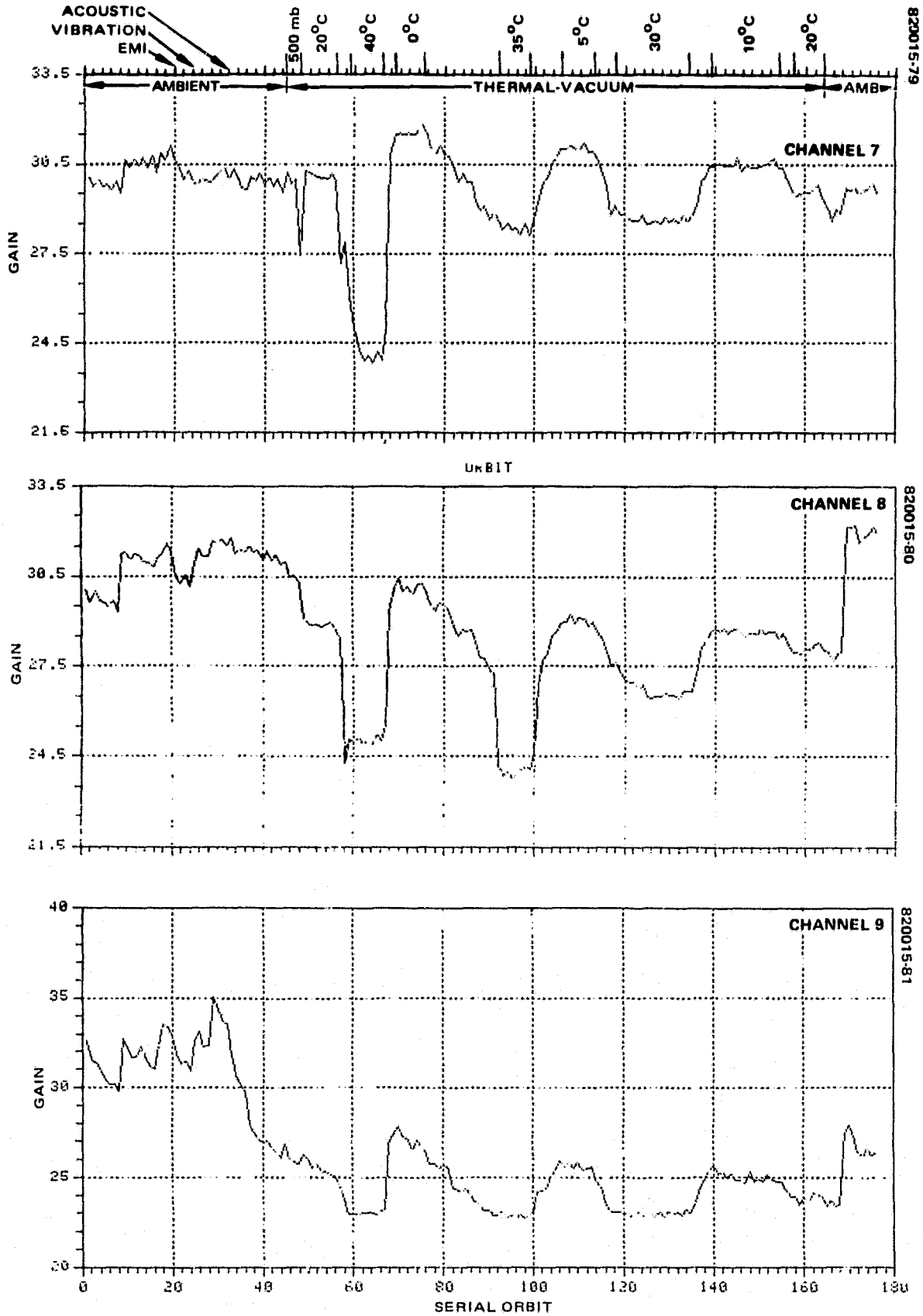

FIGURE 7-16 (CONTINUED). PROTOFLIGHT GAIN HISTORY – LINEAR/LOW GAIN MODE

ORIGINAL PAGE IS
OF POOR QUALITY

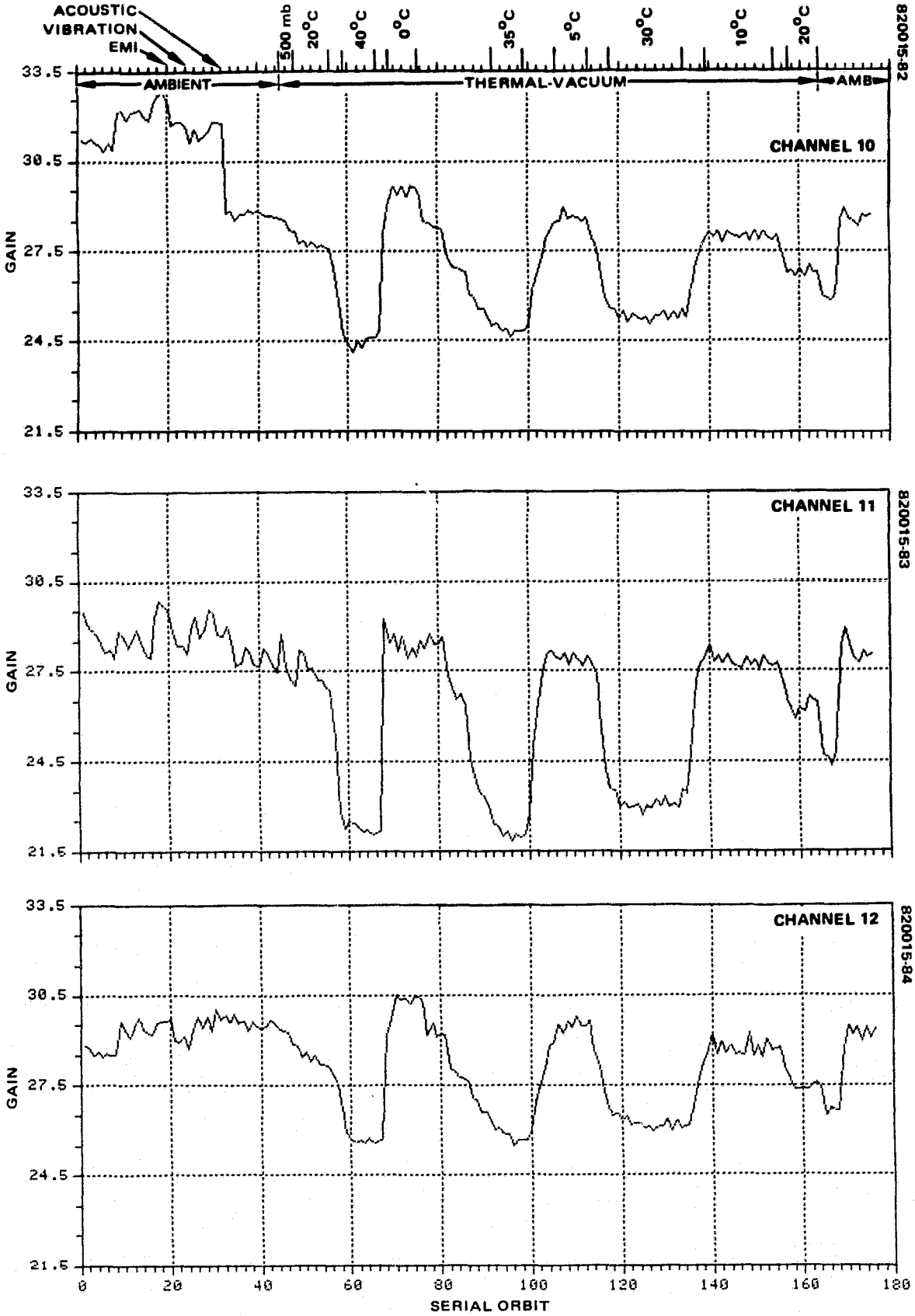

FIGURE 7-16 (CONTINUED). PROTOFLIGHT GAIN HISTORY – LINEAR/LOW GAIN MODE

ORIGINAL PAGE IS
OF POOR QUALITY

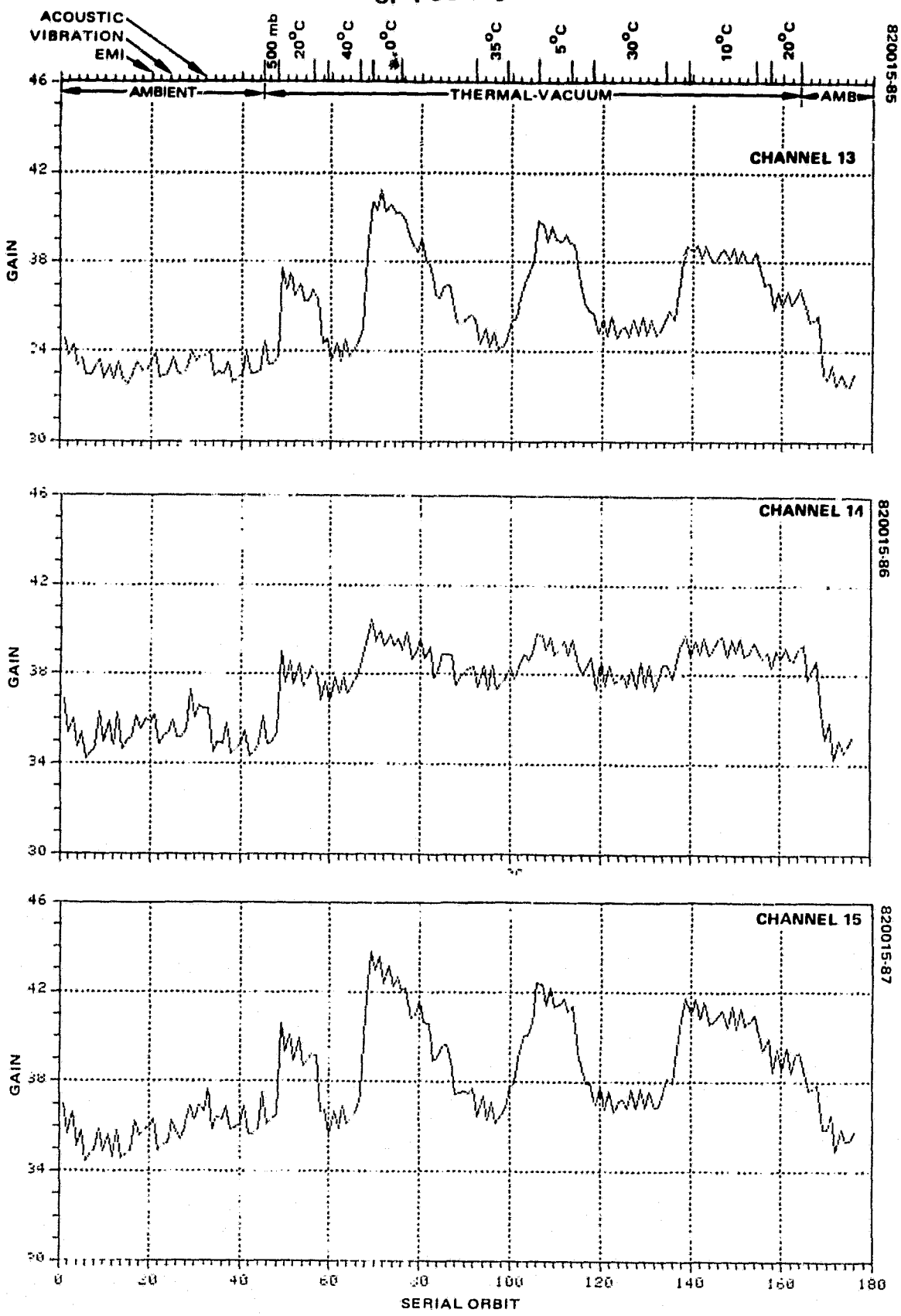

FIGURE 7-16 (CONTINUED). PROTOFLIGHT GAIN HISTORY — LINEAR/LOW GAIN MODE

ORIGINAL PAGE IS
OF POOR QUALITY

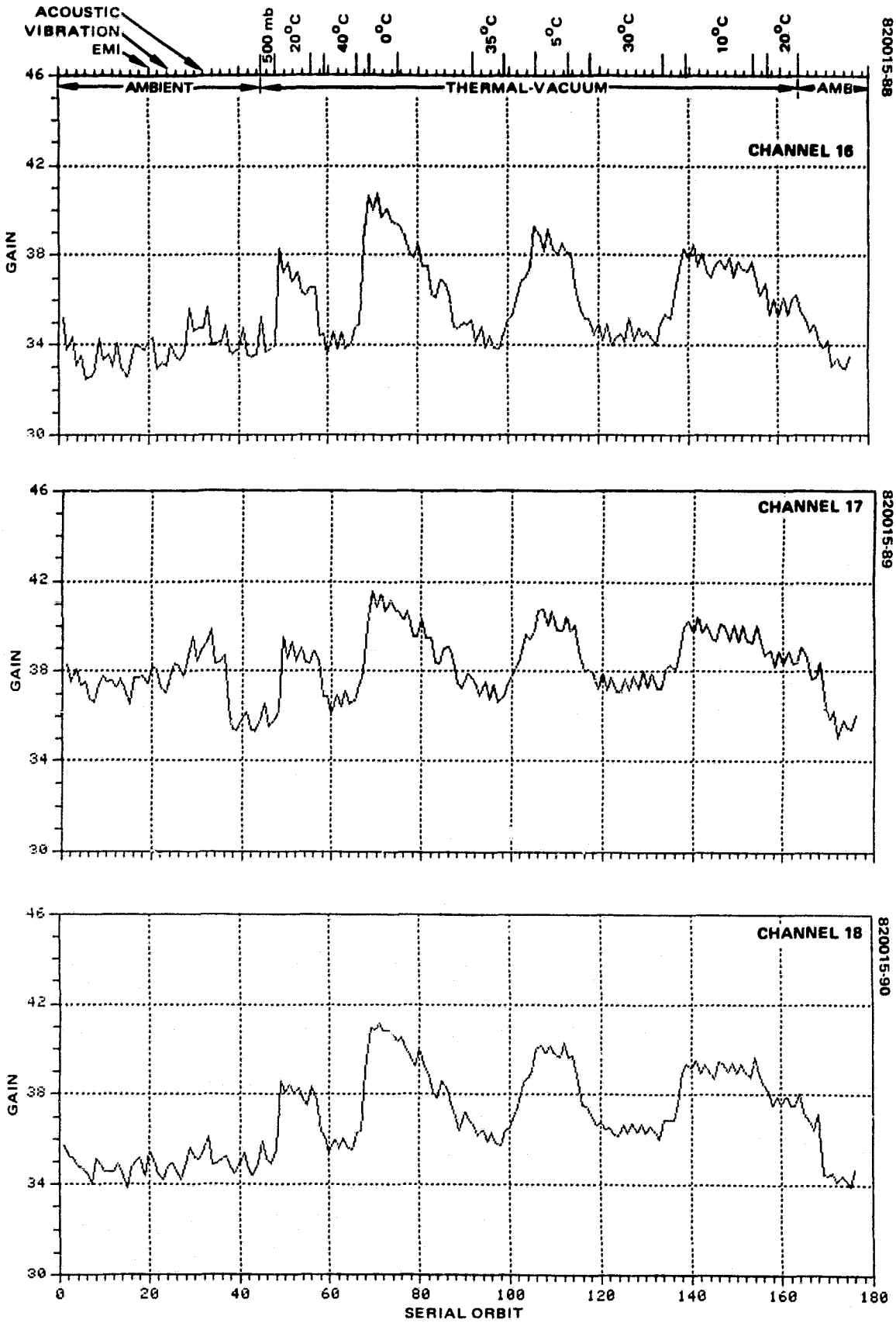

FIGURE 7-16 (CONTINUED). PROTOFLIGHT GAIN HISTORY – LINEAR/LOW GAIN MODE

ORIGINAL PAGE IS
OF POOR QUALITY

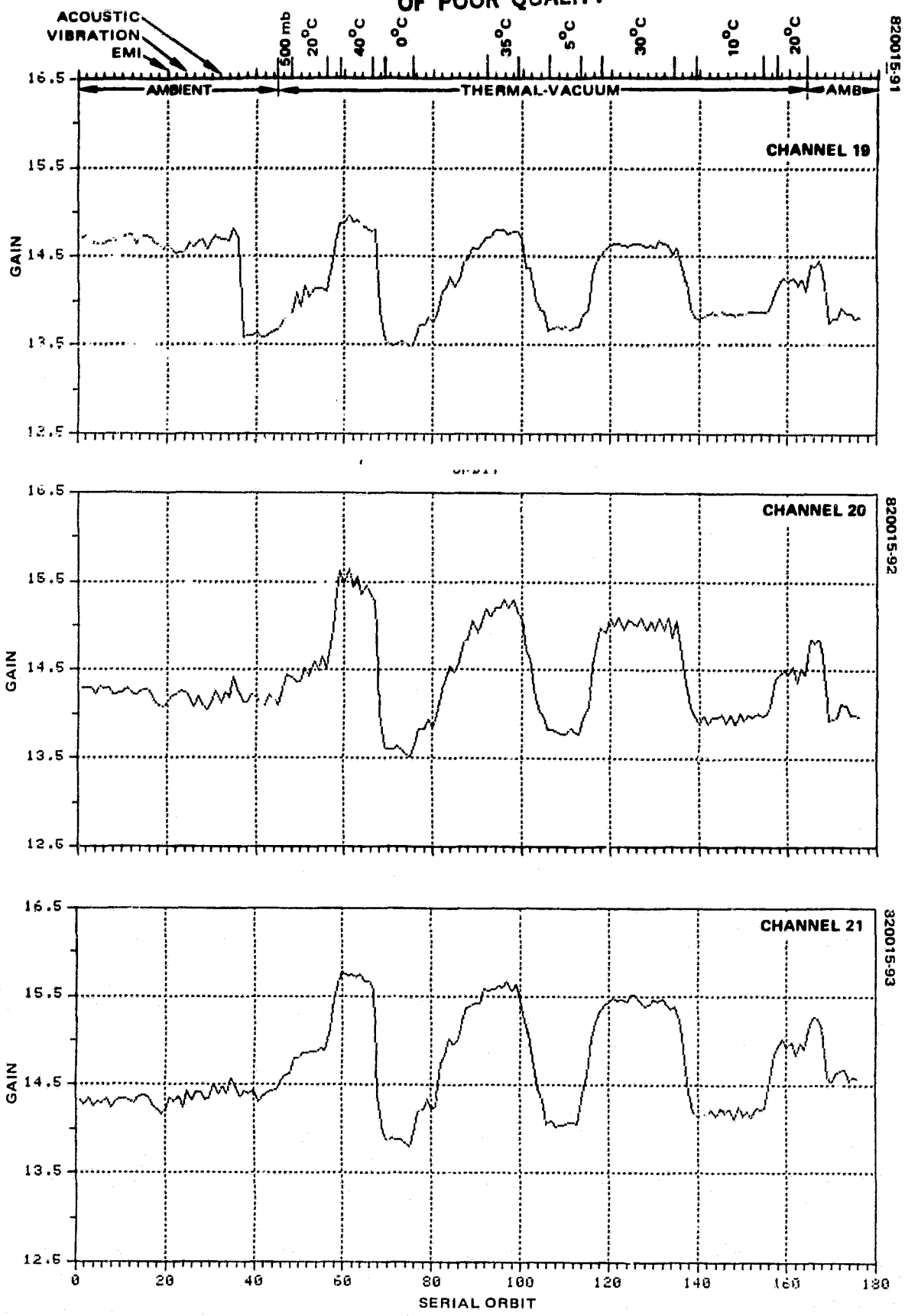

FIGURE 7-16 (CONTINUED). PROTOFLIGHT GAIN HISTORY – LINEAR/LOW GAIN MODE

ORIGINAL PAGE IS
OF POOR QUALITY

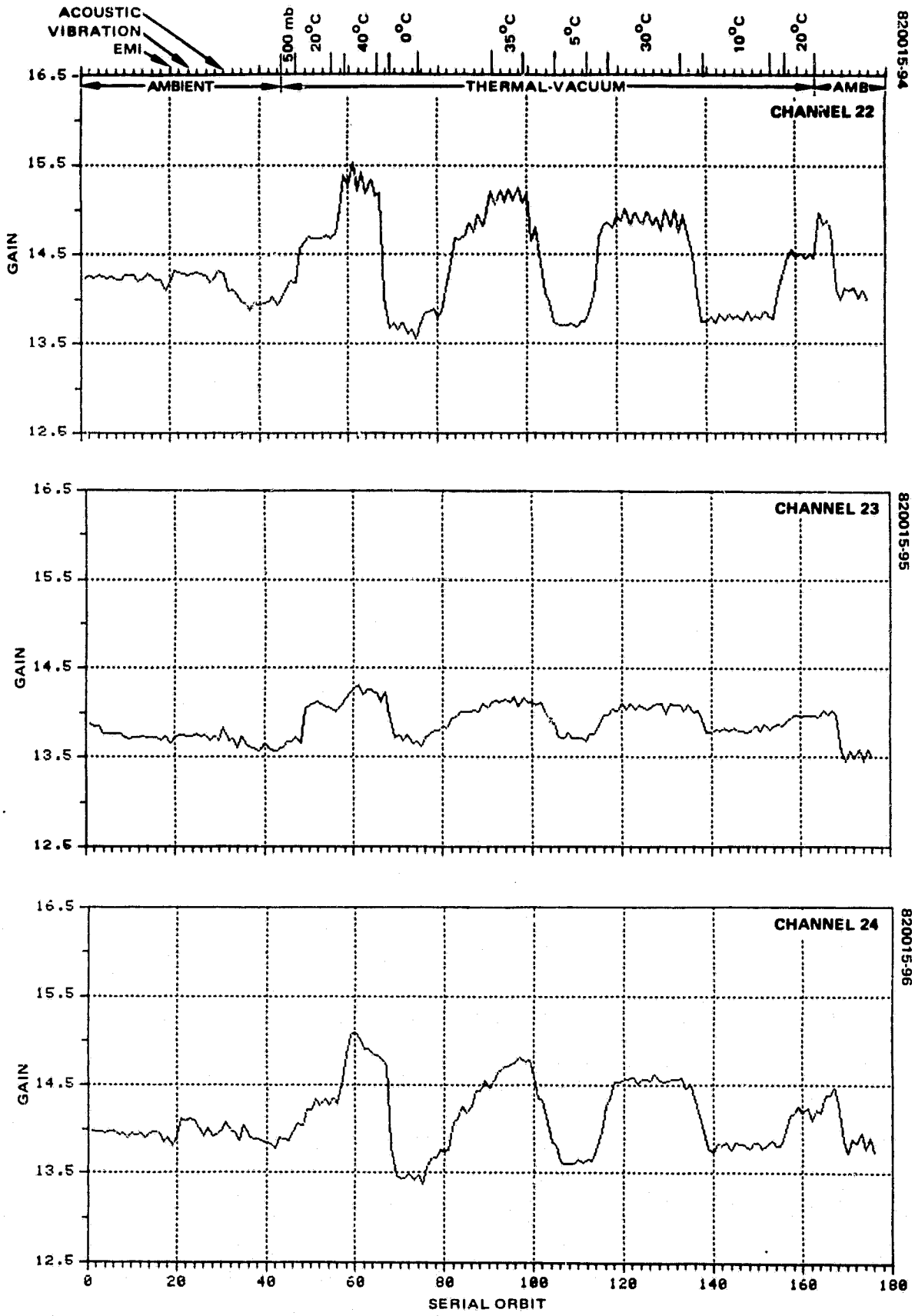

FIGURE 7-16 (CONCLUDED). PROTOFLIGHT GAIN HISTORY – LINEAR/LOW GAIN MODE

ORIGINAL PAGE IS
OF POOR QUALITY

TABLE 7-9. PROTOFLIGHT NOMINAL GAIN PERFORMANCE

Date	Test Event	Channel Nominal Gain					
		Band 1					
		1	2	3	4	5	6
11/18/80	First LEPT (22°C)	23.4	25.0	24.8	23.9	22.9	23.9
1/15 to 1/26/81	Pre-EMI (24°C)	24.0	26.25	25.95	25.0	24.25	25.2
2/02/81	Post-EMI (23°C)	23.8	25.95	25.5	24.5	24.0	24.7
2/28/81	Postvibration (25°C)	24.5	26.7	26.3	25.0	24.5	25.2
4/20/81	Preacoustic (25°C)	25.0	27.2	27.0	25.6	24.7	25.7
4/28/81	Postacoustic (25°C)	24.4	26.70	27.1	25.5	25.0	25.7
5/04/81	Preendbell (25°C)	24.3	24.7	25.7	25.2	24.7	25.6
5/08/81	Endbell (24°C)	24.1	24.5	25.4	25.0	24.5	25.1
5/09/81	GN_2 backfill (25°C)	23.8	24.25	24.8	24.5	24.1	24.7
5/10/81	Thermal-vacuum (20°C)	22.9	23.2	23.5	23.5	22.9	23.6
5/13/81	20°C	22.2	22.8	22.85	22.75	22.4	23.0
5/19/81	20°C	21.8	22.3	22.2	22.2	22.1	22.7
5/20/81	Post-thermal vacuum (26°)	21.4	22.0	22.0	22.0	21.9	22.5
5/26/81	Final LFPT (25°)	24.2	24.6	25.4	25.0	24.6	25.5
		Band 2					
		7	8	9	10	11	12
11/18/80	First LFPT (22°C)	29.8	29.75	31.0	31.1	28.5	28.5
1/15 to 1/26/81	Pre-EMI (24°C)	30.6	31.25	32.0	32.3	28.75	29.5
2/02/81	Post-EMI (23°C)	30.25	30.4	37.5	31.8	28.5	29.0
2/28/81	Postvibration (25°C)	29.8	31.20	32.5	31.4	29.0	29.5

ORIGINAL PAGE IS
OF POOR QUALITY

Table 7-9 (continued)

Date	Test Event	Channel Nominal Gain					
		Band 2					
		7	8	9	10	11	12
4/20/81	Preacoustic (25°C)	30.25	31.6	34.0	31.7	29.1	29.6
4/28/81	Postacoustic (25°C)	29.8	31.4	31.25	28.70	28.4	29.6
5/04/81	Preendball (25°C)	30.0	31.35	27.5	28.70	28.0	29.4
5/08/81	Endbell (24°C)	29.8	31.1	26.5	28.65	27.8	29.5
5/09/81	GN_2 backfill (25°C)	29.8	30.6	26.1	28.4	28.0	29.0
5/10/81	Thermal-vacuum (20°C)	30.1	28.8	25.7	27.6	27.4	28.4
5/13/81	20°C	29.9	28.6	24.2	27.0	26.7	27.9
5/19/81	20°C	29.6	28.1	24.0	26.8	26.5	27.5
5/20/81	Post-thermal vacuum (26°C)	28.9	28.0	23.3	25.9	24.8	26.6
5/26/81	Final LFPT (25°C)	29.5	31.9	26.9	28.5	28.1	29.4
		Band 3					
		13	14	15	16	17	18
11/18/80	First LFPT (22°C)	35.3	33.6	35.6	33.6	37.4	34.7
1/15 to 1/26/81	Pre-EMI (24°C)	35.5	33.1	35.3	33.4	37.3	34.6
2/02/81	Post-EMI (23°C)	35.5	33.4	35.6	33.4	37.75	34.7
2/28/81	Postvibration (25°C)	35.5	33.4	36.0	33.6	38.1	34.6
4/20/81	Preacoustic (25°C)	36.5	33.8	36.7	35.0	39.0	35.4
4/28/81	Postacoustic (25°C)	35.0	33.5	36.6	34.6	39.0	35.3
5/04/81	Preendbell (25°C)	35.0	33.0	36.3	34.1	36.0	35.0
5/08/81	Endbell (24°C)	34.8	33.4	36.0	33.9	35.8	34.9
5/09/81	GN_2 backfill (25°C)	35.3	33.8	36.6	34.3	36.1	35.5

ORIGINAL PAGE IS
OF POOR QUALITY

Table 7-9 (continued)

Date	Test Event	Channel Nominal Gain					
		Band 3					
		13	14	15	16	17	18
5/10/81	Thermal-vacuum (20°C)	38.0	36.8	39.4	37.0	38.7	38.1
5/13/81	20°C	38.4	36.8	39.4	36.6	38.7	38.2
5/19/81	20°C	39.0	36.5	39.0	36.1	38.6	37.8
5/20/81	Post-thermal vacuum (26°C)	38.6	35.7	28.25	35.3	38.4	37.0
5/26/81	Final LFPT (25°C)	35.0	32.8	35.7	33.6	36.0	34.4
		Band 4					
		19	20	21	22	23	24
11/18/80	First LFPT (22°C)	14.7	14.3	14.3	14.25	13.75	13.95
1/15 to 1/26/81	Pre-EMI (24°C)	14.7	14.25	14.3	14.25	13.70	13.95
1/02/81	Post-EMI (23°C)	14.6	14.25	14.3	14.3	13.70	14.1
2/28/81	Postvibration (25°C)	14.65	14.15	14.4	14.3	13.70	14.0
4/20/81	Preacoustic (25°C)	14.7	14.13	14.4	14.23	13.70	14.0
4/28/81	Postacoustic (25°C)	14.75	14.25	14.45	14.10	13.65	14.0
5/04/81	Preendbell (25°C)	13.65	14.2	14.35	13.9	13.60	13.85
5/08/81	Endbell (24°C)	13.7	14.12	14.35	14.0	13.60	13.85
5/09/81	GN_2 backfill (25°C)	13.8	14.3	14.6	14.10	13.65	14.0
5/10/81	Thermal-vacuum 20°C	14.1	14.5	14.85	14.65	14.10	14.30
5/13/81	20°C	14.2	14.45	14.9	14.5	14.0	14.2
5/19/81	20°C	14.2	14.45	14.90	14.5	13.95	14.20
5/20/81	Post-thermal vacuum (26°C)	14.4	14.75	15.2	14.8	13.95	14.35
5/26/81	Final LFPT (25°)	13.8	14.0	14.65	14.05	13.55	13.8

7.4.3.2 Gain Versus Temperature (Thermal-Vacuum Test)

To aid in characterizing the individual channel gain performance, the gain versus temperature plots for each channel given in Figure 7-17 were produced, based on the thermal-vacuum test data. These plots were obtained by first aggregating all gain values at a specific temperature irrespective of when during the test they were obtained. At each specific temperature the mean and standard deviation was computed. These values are plotted in the figures where the standard deviation is represented by a vertical bar about the (plotted) mean value. A linear least squares fit to these mean value points was obtained and is provided on the graph.

As is evident from the plots, the "best fit line" is much better in some channels than in others. The normally greater value of the standard deviation bar at 20°C is due to a time dependent decay of the gain that results from the vacuum shift. The 20°C temperature plateau was used three times during thermal-vacuum and generally the measurements for the first plateau lie to the top of the standard deviation bar, the middle plateau data lie at the center of the bar, and the last plateau data at the bottom of the bar.

The slopes of these plots are given in Table 7-10. The gain versus temperature plots for each channel indicate the following:

1) Band 1 -

   a) The gain decreases as the temperature increases.

   b) Channels 1 and 2 have greater (negative) slopes than other channels in the band.

   c) Channels 3, 4, and 6 have nearly the same slope.

   d) Channel 5 has the smallest (negative) slope.

2) Band 2 -

   a) The gain decreases as the temperature increases.

   b) Channels 7, 8, 10, and 12 have almost the same slopes.

   c) Channel 11 has the largest (negative) slope.

   d) Channel 9 has the smallest (negative) slope.

ORIGINAL PAGE IS
OF POOR QUALITY

TABLE 7-10. GAIN CHANGE/^{o}C

Channel	Slope ($\Delta G/^{o}C$)	Channel	Slope ($\Delta G/^{o}C$)
1	−0.089	13	−0.158
2	−0.114	14	−0.055
3	−0.068	15	−0.169
4	−0.076	16	−0.146
5	−0.032	17	−0.107
6	−0.072	18	−0.126
7	−0.120	19	+0.036
8	−0.134	20	+0.048
9	−0.101	21	+0.052
10	−0.127	22	+0.047
11	−0.189	23	+0.013
12	−0.121	24	+0.037

3) Band 3 -

a) The gain decreases as the temperature increases.

b) Channels 17 and 18 have approximately the same slopes.

c) Channels 13 and 15 have almost the same slopes and are more negative than the slopes of the other three channels.

d) Channel 14 has the smallest (negative) slope.

4) Band 4 -

a) The gain increases as the temperature increases.

b) Channels 20, 21, and 22 have almost the same slopes (0.050 $\Delta G/^{o}C$).

c) Channels 19 and 24 slopes are lower than those of channels 20, 21, and 22.

d) Channel 23 has the least slope.

ORIGINAL PAGE IS
OF POOR QUALITY

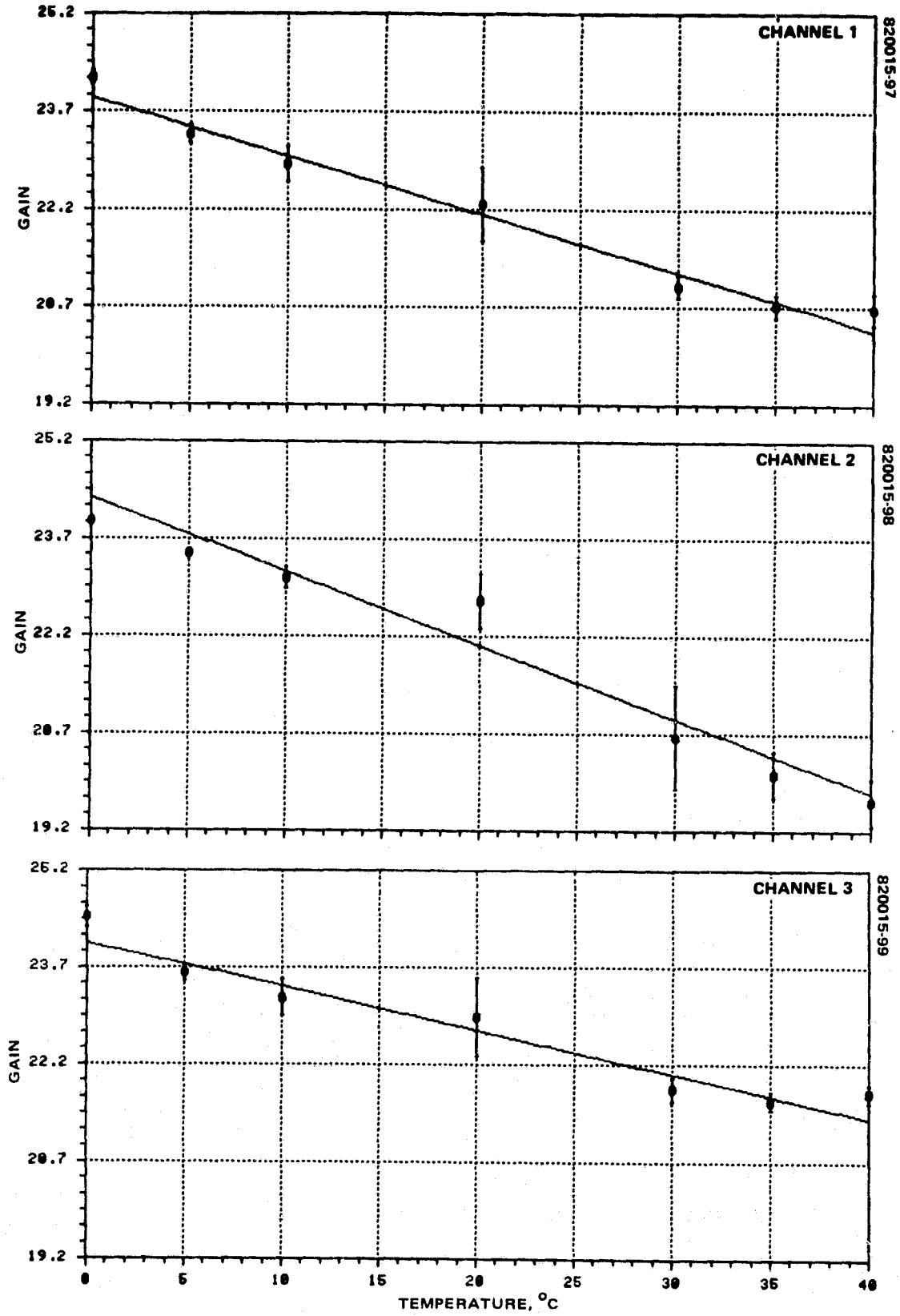

FIGURE 7-17. PROTOFLIGHT AVERAGE GAINS VERSUS TEMPERATURE – LINEAR/LOW GAIN MODE

ORIGINAL PAGE IS
OF POOR QUALITY

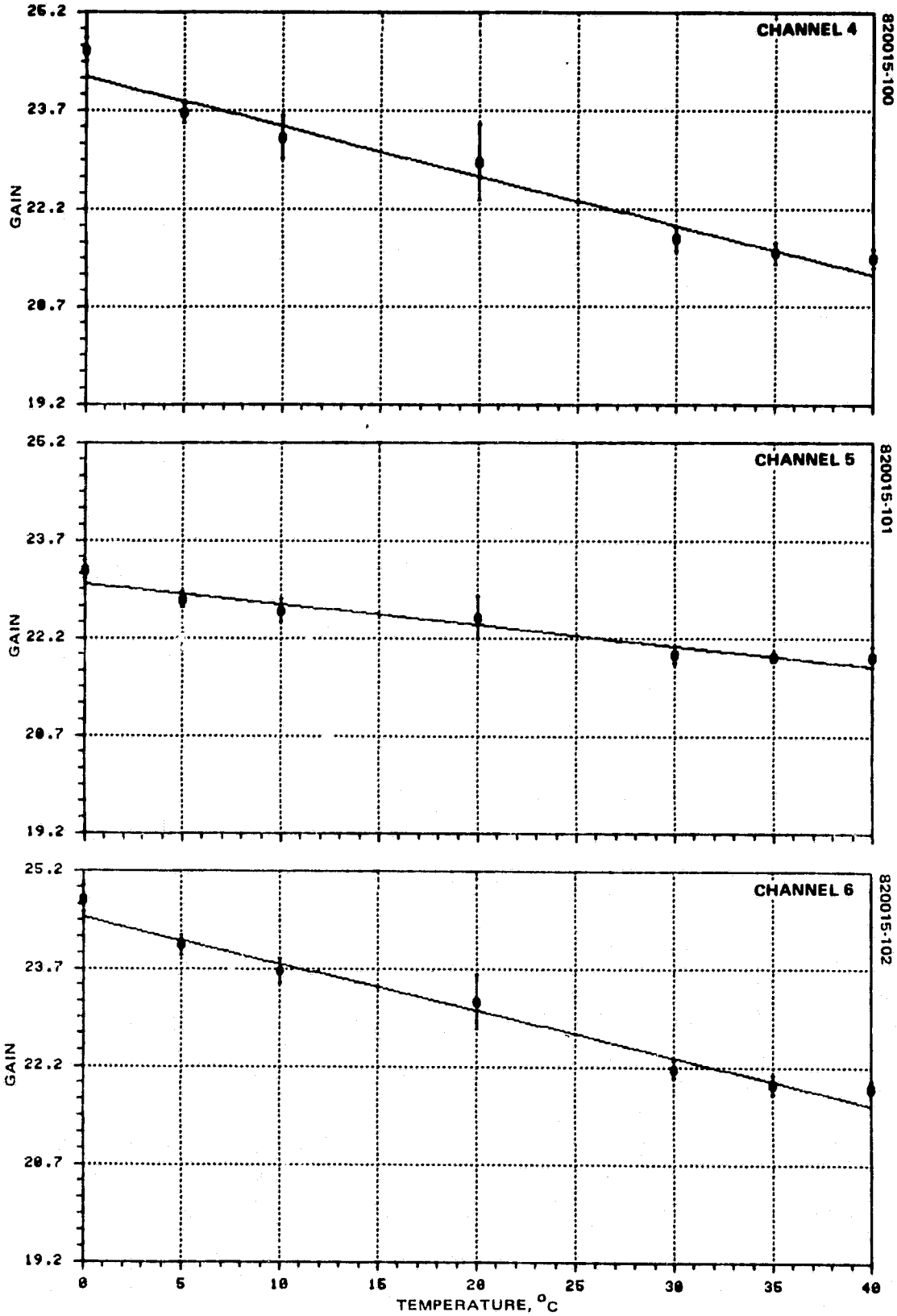

FIGURE 7 17 (CONTINUED). PROTOFLIGHT AVERAGE GAINS VERSUS TEMPERATURE – LINEAR/LOW GAIN MODE

ORIGINAL PAGE IS
OF POOR QUALITY

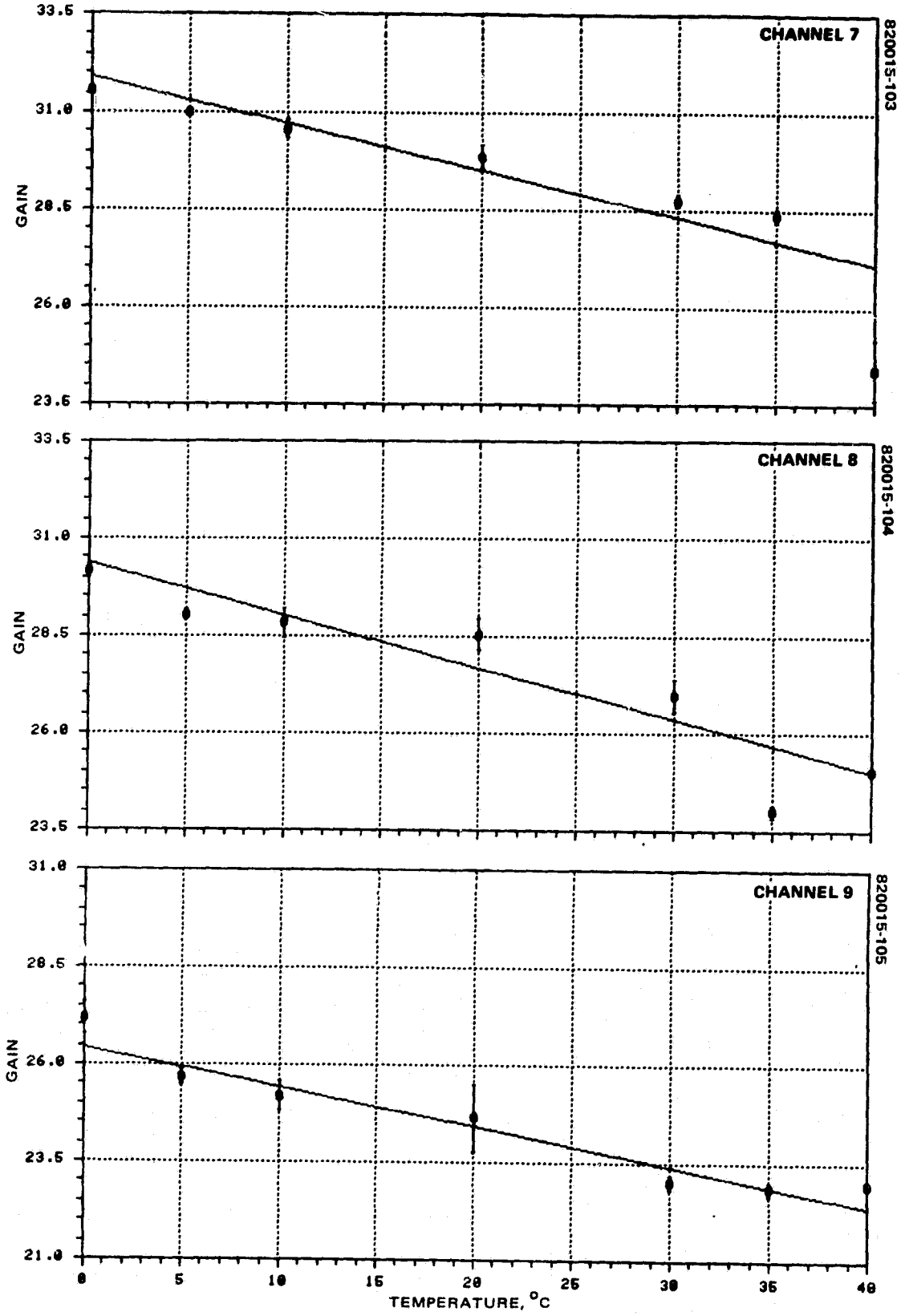

FIGURE 7-17 (CONTINUED). PROTOFLIGHT AVERAGE GAINS VERSUS TEMPERATURE – LINEAR/LOW GAIN MODE

ORIGINAL PAGE IS
OF POOR QUALITY

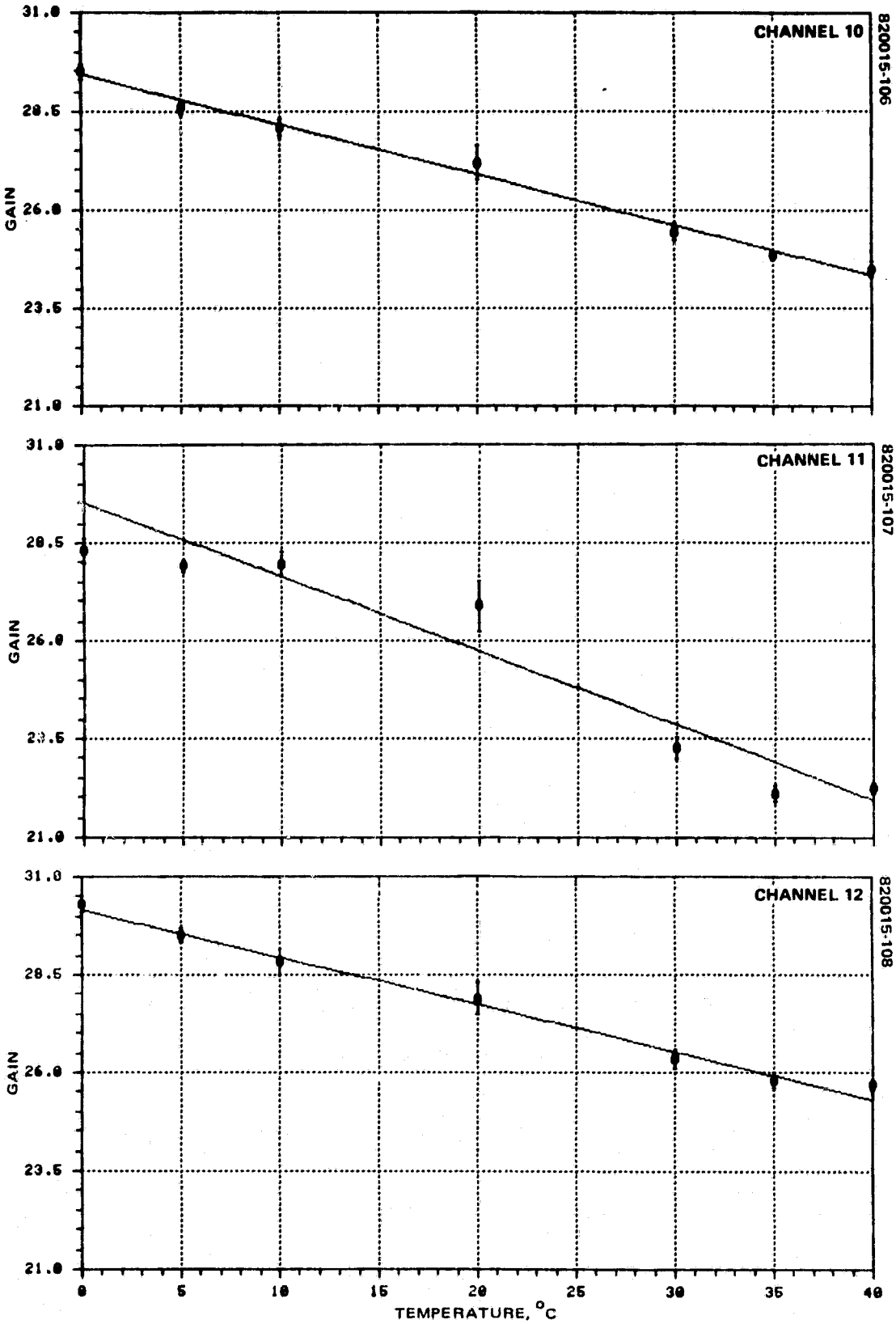

FIGURE 7-17 (CONTINUED). PROTOFLIGHT AVERAGE GAINS VERSUS TEMPERATURE – LINEAR/LOW GAIN MODE

ORIGINAL PAGE IS
OF POOR QUALITY

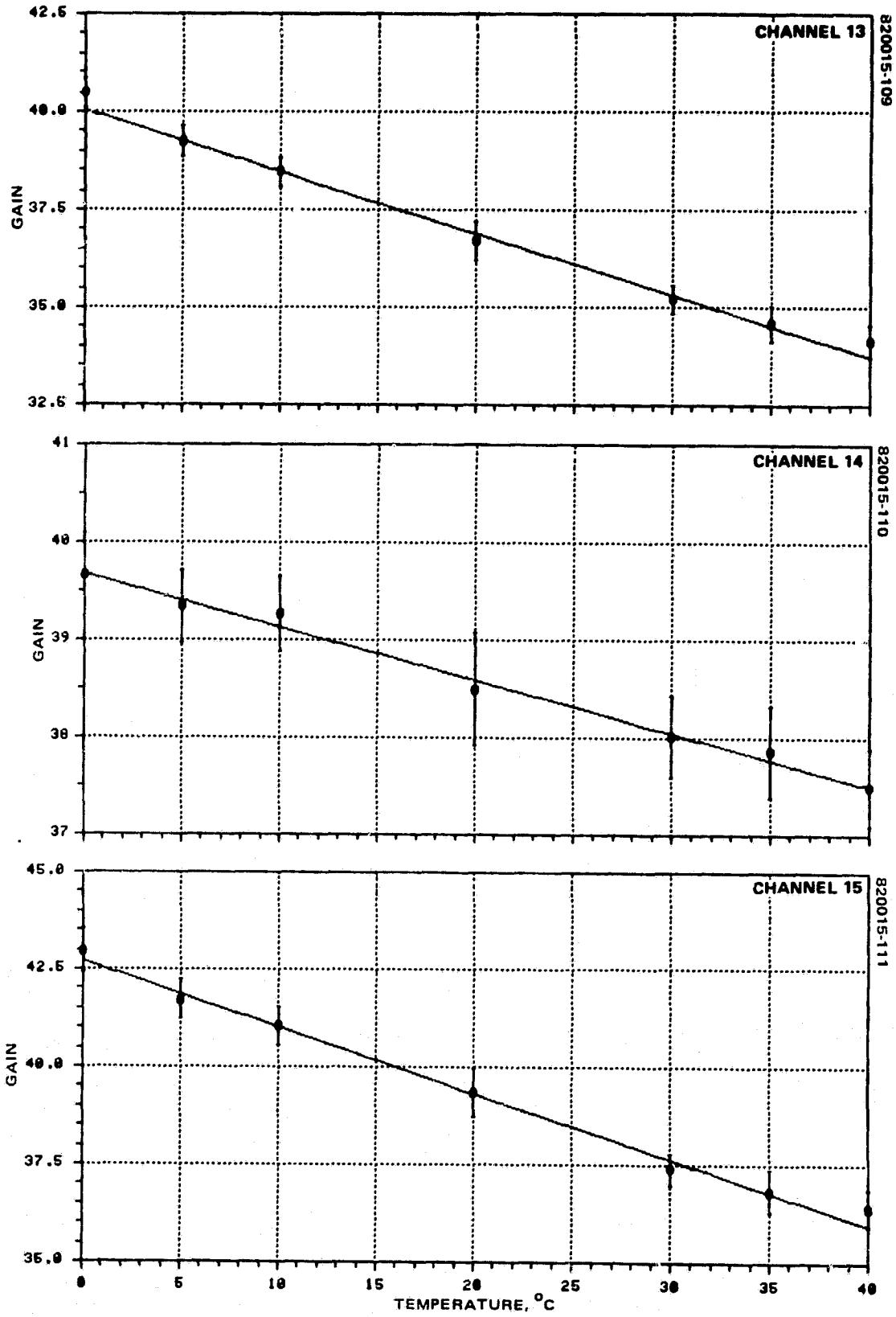

FIGURE 7-17 (CONTINUED). PROTOFLIGHT AVERAGE GAINS VERSUS TEMPERATURE – LINEAR/LOW GAIN MODE

ORIGINAL PAGE IS
OF POOR QUALITY

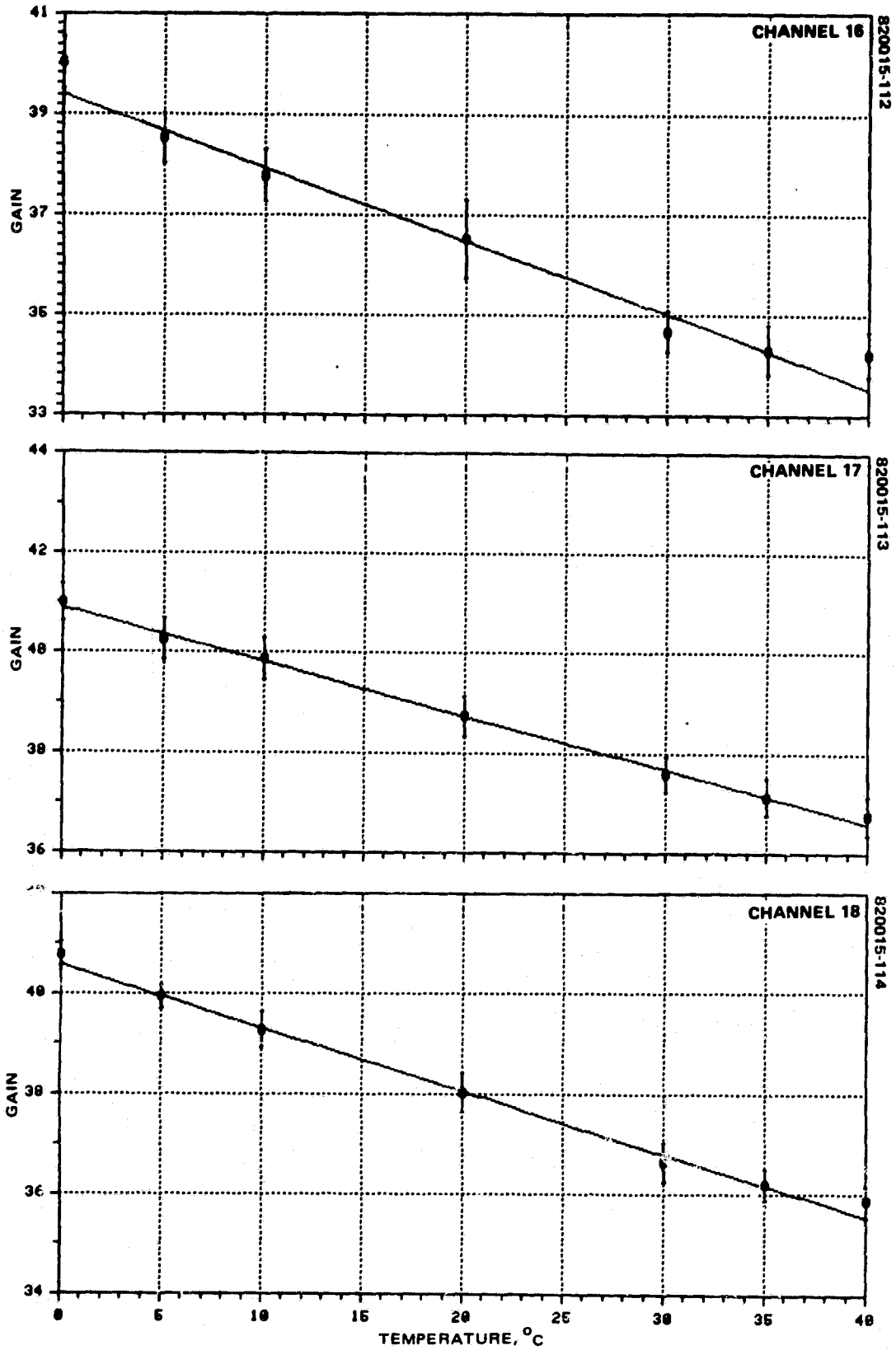

FIGURE 7-17 (CONTINUED). PROTOFLIGHT AVERAGE GAINS VERSUS TEMPERATURE – LINEAR/LOW GAIN MODE

ORIGINAL PAGE IS
OF POOR QUALITY

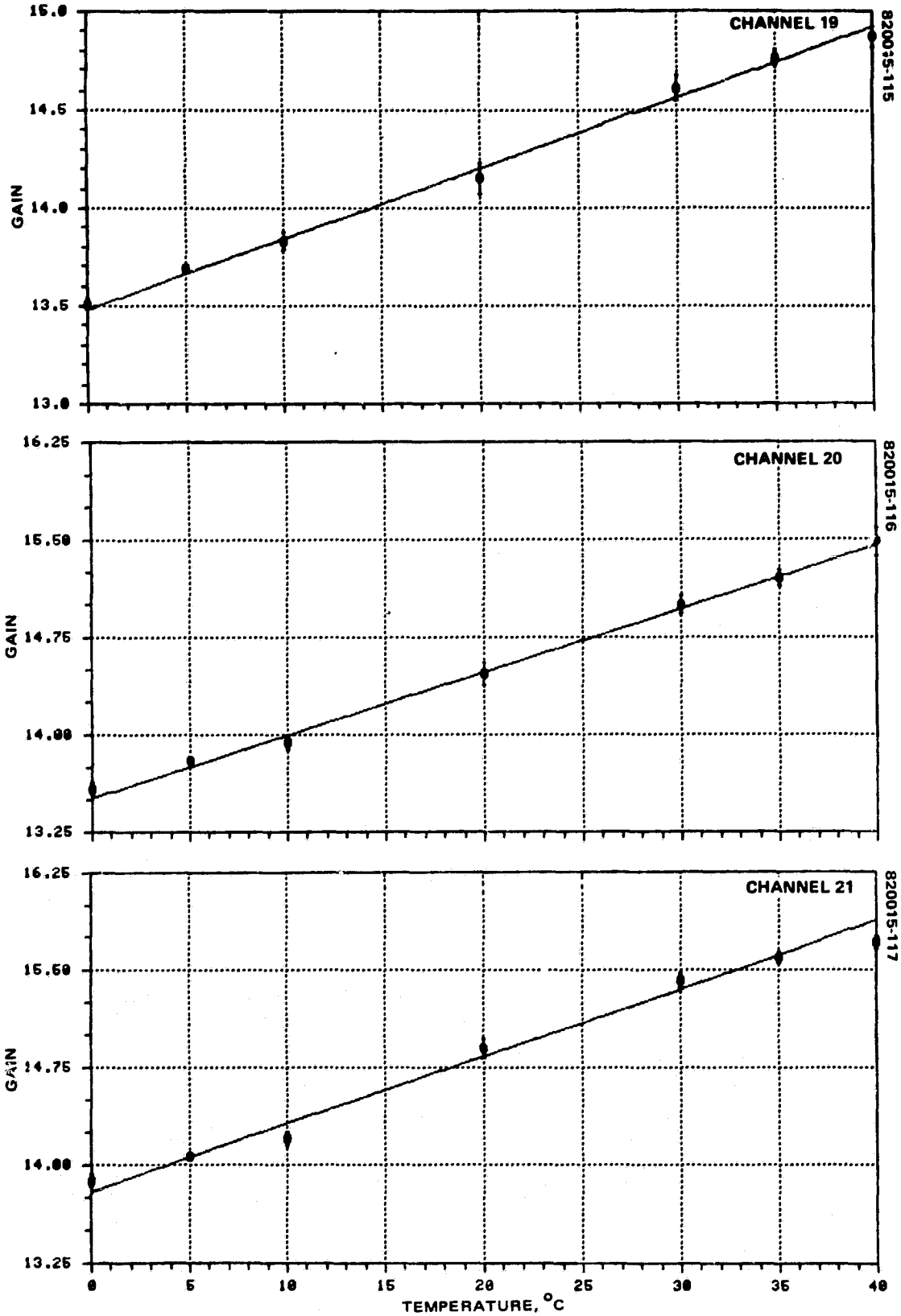

FIGURE 7-17 (CONTINUED). PROTOFLIGHT AVERAGE GAINS VERSUS TEMPERATURE – LINEAR/LOW GAIN MODE

ORIGINAL PAGE IS
OF POOR QUALITY

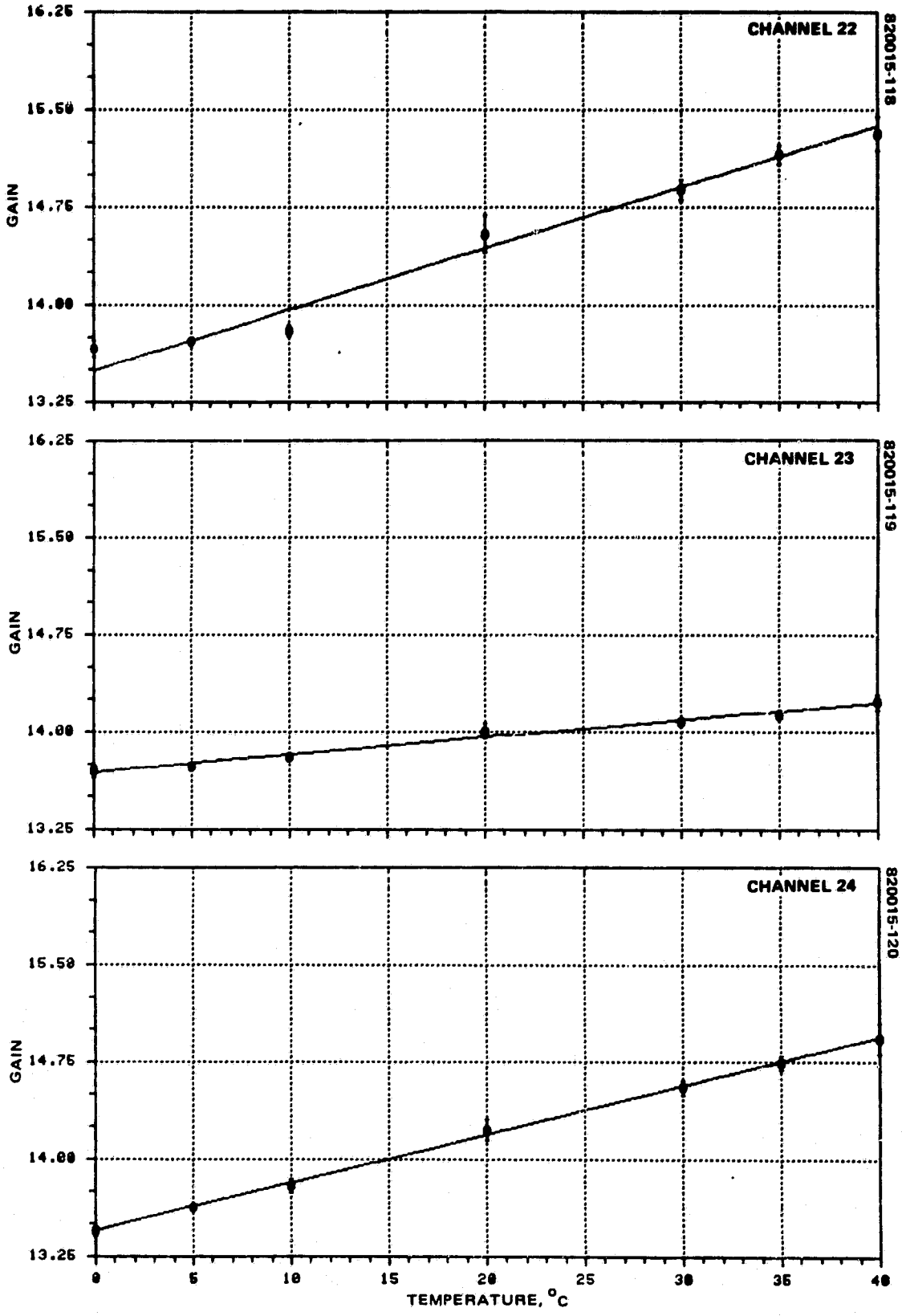

FIGURE 7-17 (CONCLUDED). PROTOFLIGHT AVERAGE GAINS VERSUS TEMPERATURE – LINEAR/LOW GAIN MODE

ORIGINAL PAGE IS
OF POOR QUALITY

7.4.3.3 Vacuum Effect On Gain Performance

As indicated above, a long term change in gain was observed throughout thermal-vacuum testing which is not explained by gain versus temperature behavior. To illustrate this behavior, the channel gain history plots were replotted with the gain-temperature dependence removed. Figure 7-18 illustrates the results of that effort for channels 1 and 3. These cases are sufficiently well behaved to clearly indicate the exponential-like decay of the gain observed over the entire thermal-vacuum period. While these plots differ in value (channel 3 is approximately one-half unit higher than channel 1), the agreement in shape is excellent. This result, as well as similar comparisons for some of the other channels, argues quite strongly for the existence of long time constant gain stabilization component in the data. It indicates that this time constant may be sufficiently large that 9 to 10 days are required before the gains have completely stabilized.

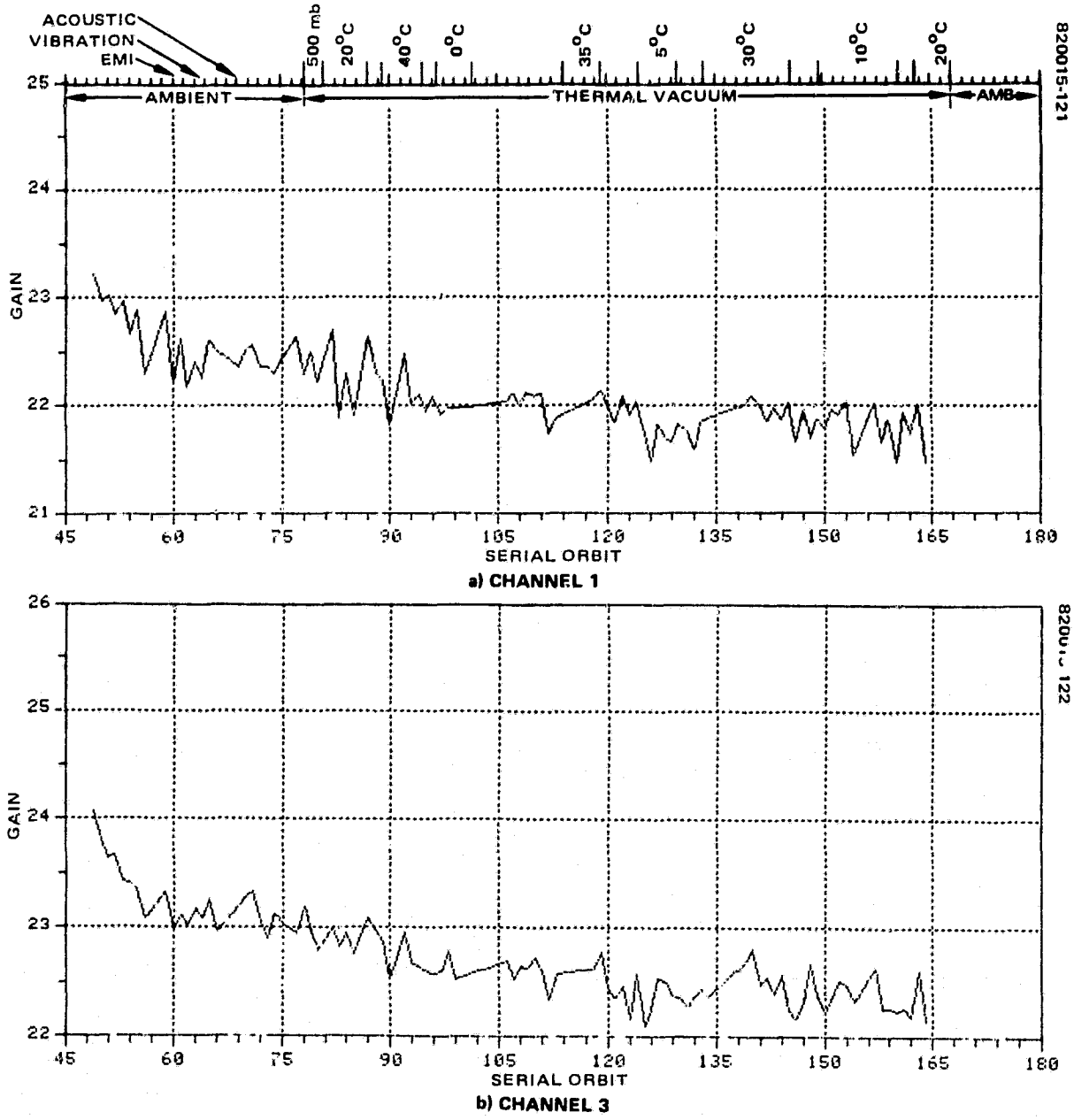

FIGURE 7-18. PROTOFLIGHT CHANNEL GAIN WITH TEMPERATURE DEPENDENCE REMOVED — LINEAR/LOW GAIN MODE

7.4.4 Corrected Signal Level Performance History

The history of corrected signal level performance for the MSS-D PF is presented for all channels in each band in Figure 7-19. In principle, if the calibration system is performing ideally, the initial calibrations have been performed perfectly, and the collimator output is uniform and stable, these plots should be horizontal lines which lie on top of one another; that is, one horizontal line. The plots show the deviation from this ideal behavior.

Realistically, changes will occur in the system which will not be completely corrected by the internal calibration system. Calibrations of the system with the integrating sphere will be subject to errors so that calibration wedge nominals will be approximate at best. Collimator output will be neither constant nor uniform, and collimator shading will not be stable. Similar comments apply to the internal calibration system. Discovery of the causes of anomolous behavior is complicated by the absence of a suitably accurate, independent, calibrated reference source throughout the entire test period, especially during thermal-vacuum testing.

The features of the COSL performance behavior given in Figure 7-19 that are of principal interest are the following:

1) The width of the envelope of the family of COSL for all the channels in a band. This width (called DCC) is the maximum COSL value for all channels in a band at a given environmental condition (serial orbit) minus the minimum COSL value for all channels in that band at the same environmental condition; it is specified to have a value less than or equal to 2 percent of the (geometric) mean value of all of the COSLs in that band during that orbit. It is possible that problems in COSL performance might exist for channels that are masked by more deviant behavior of some other channel in the band. DCC performance is discussed later in this section.

2) The variation of the mean value of the COSL for all channels in a band, while of lesser importance since it is not directly subject to specification, does give some indication of system test performance relative to DCC. Variations in the mean COSL, which is the system estimate of collimator radiance, will vary with collimator lamp output of course. Unfortunately, it will vary also with errors in the gain estimates provided by the internal calibration system. These errors may be due to an initially faulty or not sufficiently accurate initial calibration using the integrating sphere, or they may result from instabilities or environmentally induced changes in the calibration system. The band geometric means are used directly in determining the band-to-band radiometric accuracy (DBB), which is specified to have less than 3 percent deviation relative to its value at the time of integrating sphere calibration (see 6.4.2). This performance parameter is treated at the end of this section.

While the resolution in Figure 7-19 makes it impossible to follow the COSL behavior of individual well behaved channels, those that exhibit anomalous behavior do stand out.

Considering each band in turn and concentrating on the thermal-vacuum orbits (serial orbits 48 to 164), the following behavior is observed:

1) Band 1. The corrected signal levels were normal in thermal-vacuum except during the high temperatures (40°C, 35°C, and 30°C), where some channels deviated significantly from the nominal values. Channel 2 COSL (both systems A and B) spread away

C-3

ORIGINAL PAGE IS
OF POOR QUALITY

from the nominal at temperatures 30°C and above as shown in Figure 7-19a (orbits 57 to 66, orbits 92 to 99, and orbits 118 to 134). Channel 1 COSL showed the same behavior as channel 2 at 30°C (orbits 120 to 126) but to a lesser extent.

2) Band 2. The individual channel COSL with the exception of channel 11 behaved normally at 30°C temperatures. Channel 11 is affected the most by high temperatures (40°C, 35°C, Figure 7-19b, orbits 59 to 66 and orbits 92 to 99) where the channel 11 COSL becomes anomalously higher than the nominal values. Low temperatures (0°C, 5°C and 10°C, Figure 7-19b, orbits 69 to 75, orbits 106 to 113, and orbits 139 to 154, respectively) demonstrate the same effect on channel 11 COSL as the high temperatures. Other channels (channel 7, 8, 10, and 12) showed some deviation from the nominal value at 40°C (Figure 7-19b, orbits 57 to 66) but to a lesser extent than that of

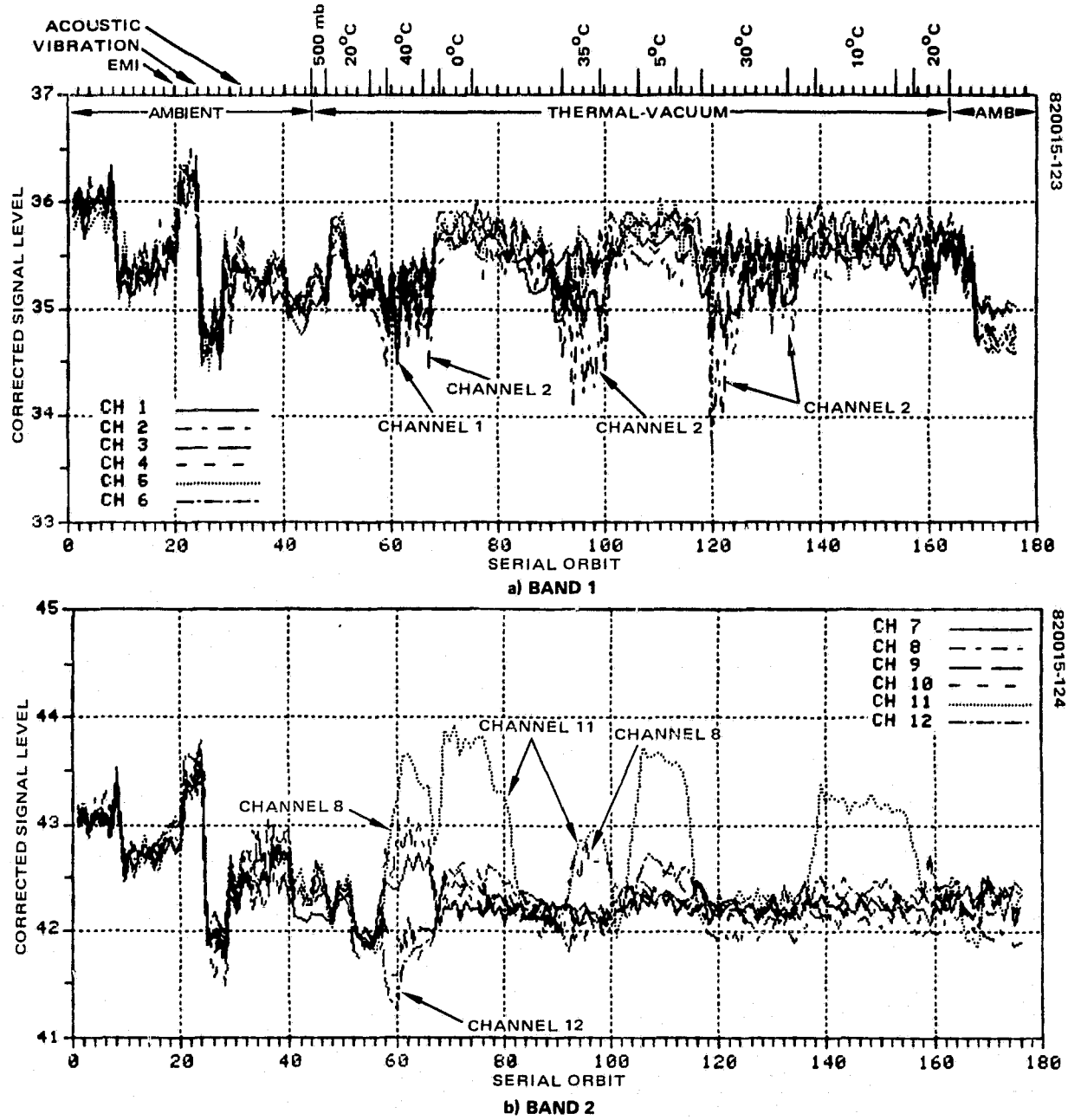

FIGURE 7-19. PROTOFLIGHT COSL PERFORMANCE – LINEAR/LOW GAIN MODE

channel 11. At the 35°C plateau (Figure 7-19b, orbits 92 to 99), channel 8 COSL deviated from the nominal values almost to the same extent as channel 11 COSL.

3) Band 3. COSL behavior throughout thermal-vacuum was normal (Figure 7-19c). No significant deviations from the nominal values occurred as a result of any temperature change. Band 3 has the best COSL performance in thermal-vacuum of all the four bands.

4) Band 4. Channel 21 COSL deviated slightly from the nominal values at low temperatures (0°, 10°C, Figure 7-19d, orbits 69 to 75 and orbits 139 to 159, respectively). Channel 24 exhibited abnormal behavior during the transition to 40°C (orbits 57, 58) but was otherwise normal. The rest of band 4 channels behaved normally throughout vacuum testing.

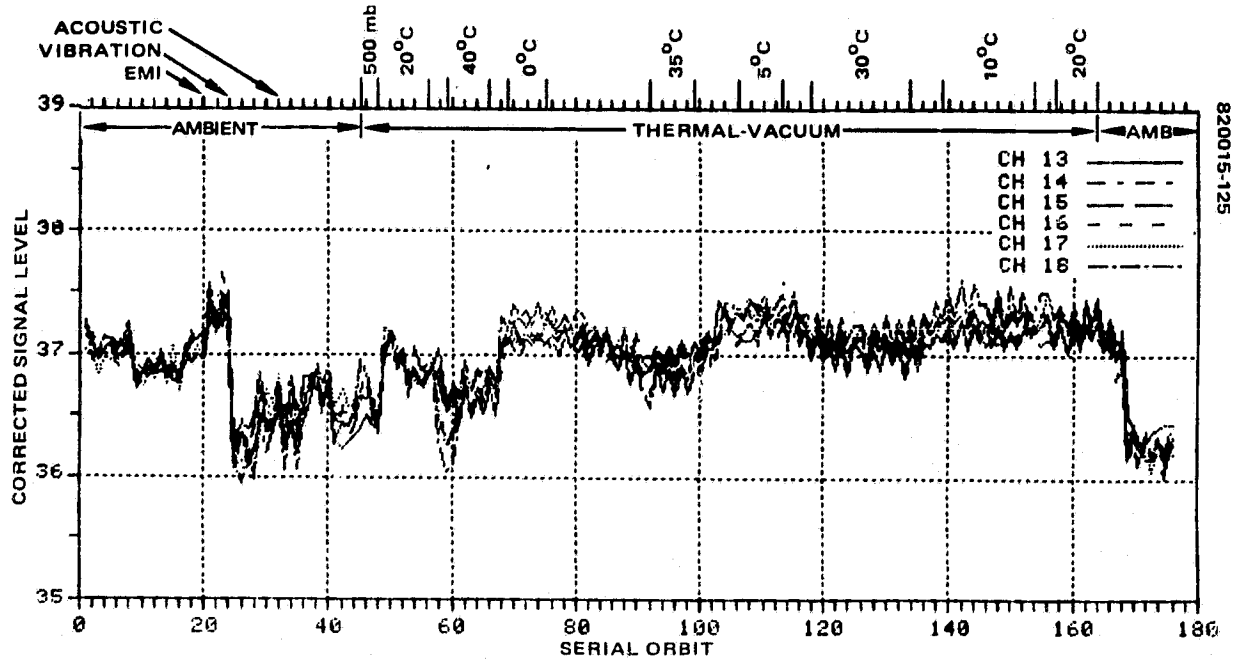

c) BAND 3

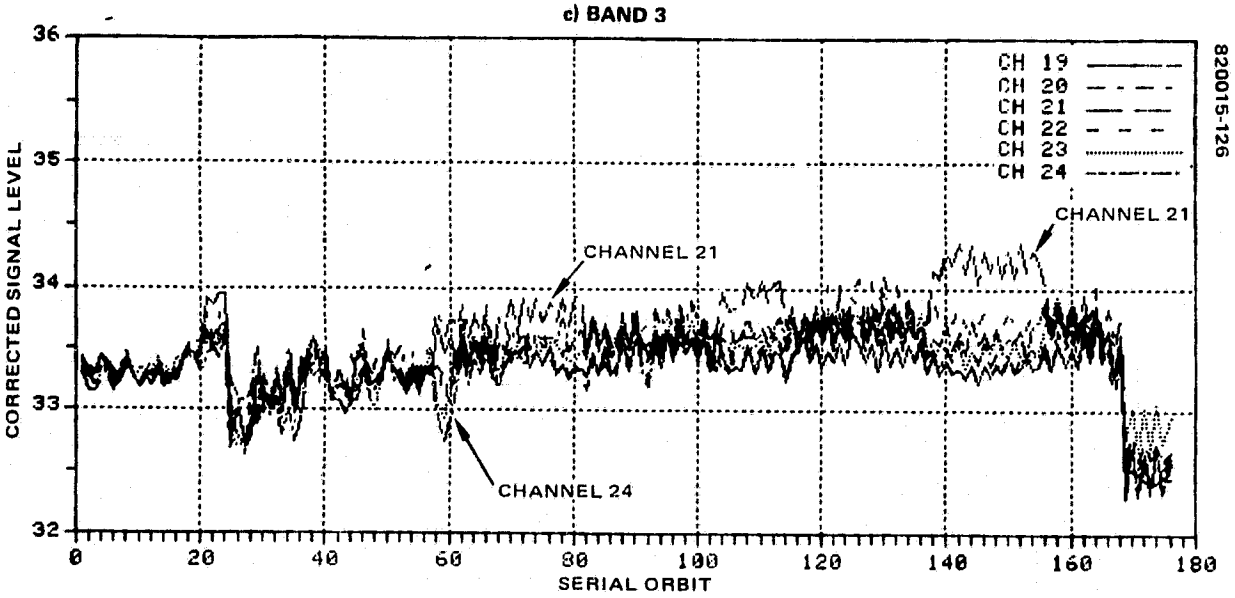

d) BAND 4

FIGURE 7-19 (CONTINUED). PROTOFLIGHT COSL PERFORMANCE – LINEAR/LOW GAIN MODE

7.4.4.1 Band Average COSL Performance

The history of the band average of the COSLs for all channels in each band is plotted in Figure 7-20. Each band is represented by two plots, one each for data taken when the scanner was in mode A or B, respectively. (See Section 5 for a description of the various scanner modes.)

Plotted above and below the band average COSL are the maximum and minimum COSL, respectively, for all the channels in the band. As is evident in these plots, the envelope width exceeds 2 percent of the band average at a number of test orbits. These DCC specification violations will be discussed later from more illuminating plots where the errant channels are identified. Here band average COSL is emphasized, and the envelope behavior provides some insight into the effect of individual channel deviations on the overall average. That is, some "pulling" of the average results from large deviant behavior of individual channels.

Large changes in band average COSL in prethermal-vacuum orbits (prior to serial orbit 48) for the most part are due to variations in integrating sphere calibrations. These changes have been compared with the data resulting from calibration orbits and were found to correspond to variations in integrating sphere calibration which resulted from a lack of adequate current control in the integrating sphere power supply (see MSS-D PF Calibration and Alignment Handbook, July 1981). The calibration history shown in the referenced handbook exhibits behavior which is compatible with the results shown here. Following the institution of tight current control procedures, the stability and repeatability of subsequent calibrations were much improved. The integrating sphere calibration of the scanner prior to entering thermal-vacuum was performed under this discipline.

Since the primary interest for signal correction is the effect on thermal-vacuum performance, the emphasis here was placed on those orbits. For the thermal-vacuum orbits (serial orbits 48 to 164), the following features are indicated in the plots.

The range of variation of band average COSL values over the thermal-vacuum orbits is approximately 2 percent for bands 1 and 2, 2.5 percent for band 3, and 1.5 percent for band 4. As was observed for their respective gain estimates, the band average COSLs for the first three bands are negatively correlated with temperature. A long term upward trend in the data values for all bands tends to mask this correlation with temperature. The correlation of band average COSL with temperature for band 4 appears (locally) positive, but this correlation is much weaker and must take into account the long term upward trend in band average COSL which is evident in this band as well.

This upward trend in band average COSL is suggestive of the "vacuum shift" effect notice on gain performance, but is not compatible with the band 3 and band 4 performance discussed earlier.

ORIGINAL PAGE IS
OF POOR QUALITY

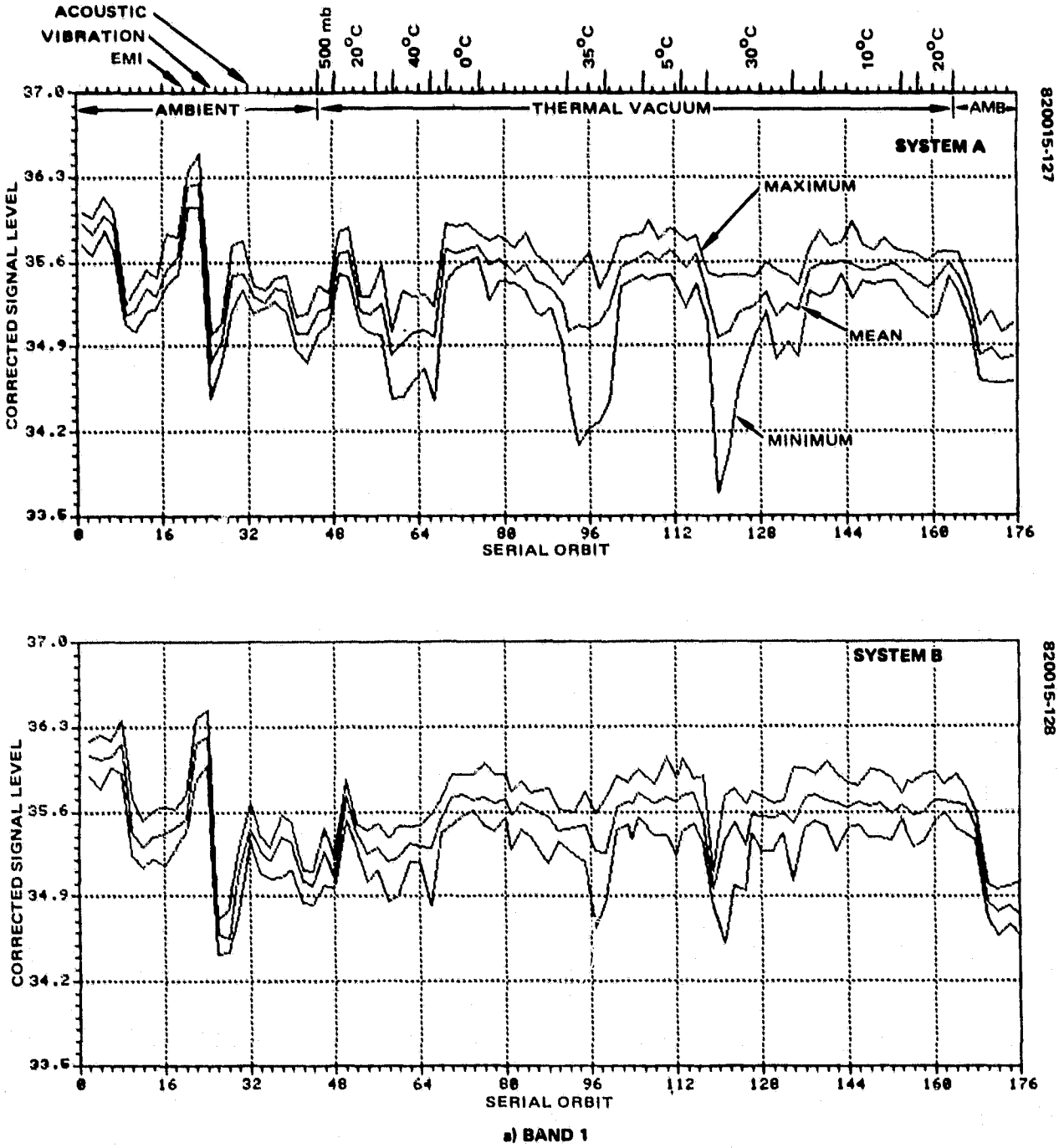

a) BAND 1

FIGURE 7-20. PROTOFLIGHT BAND AVERAGE COSL PERFORMANCE – LINEAR/LOW GAIN MODE

ORIGINAL PAGE IS
OF POOR QUALITY

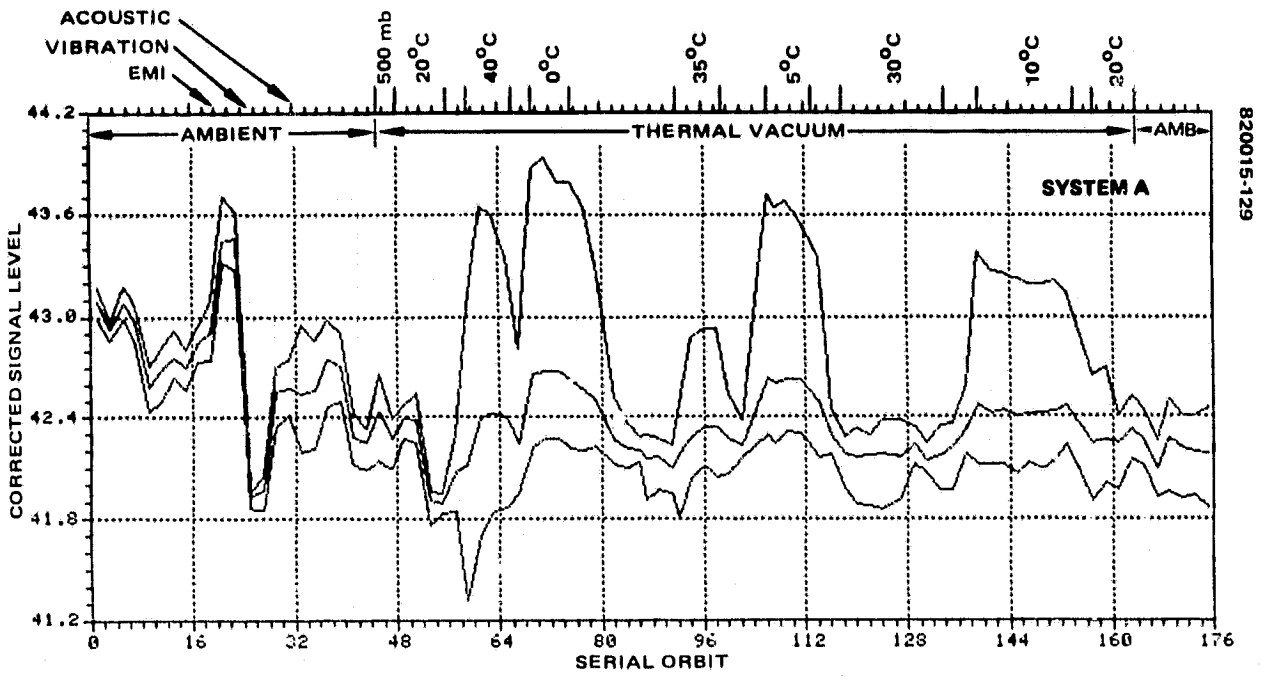

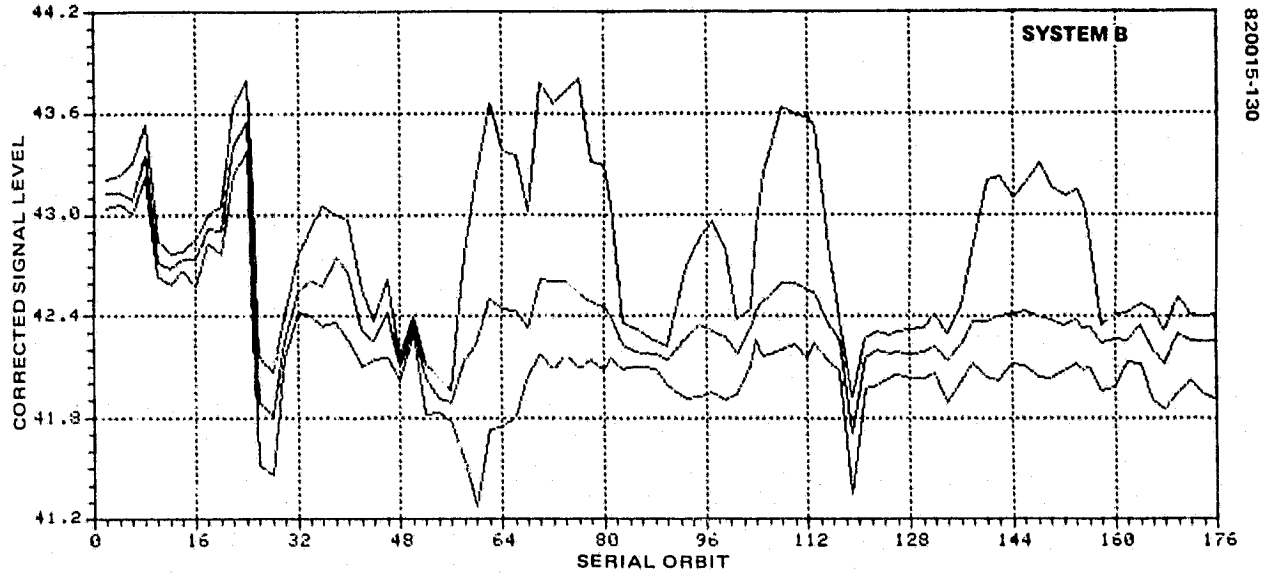

b) BAND 2

FIGURE 7-20 (CONTINUED). PROTOFLIGHT BAND AVERAGE COSL PERFORMANCE – LINEAR/LOW GAIN MODE

ORIGINAL PAGE IS
OF POOR QUALITY

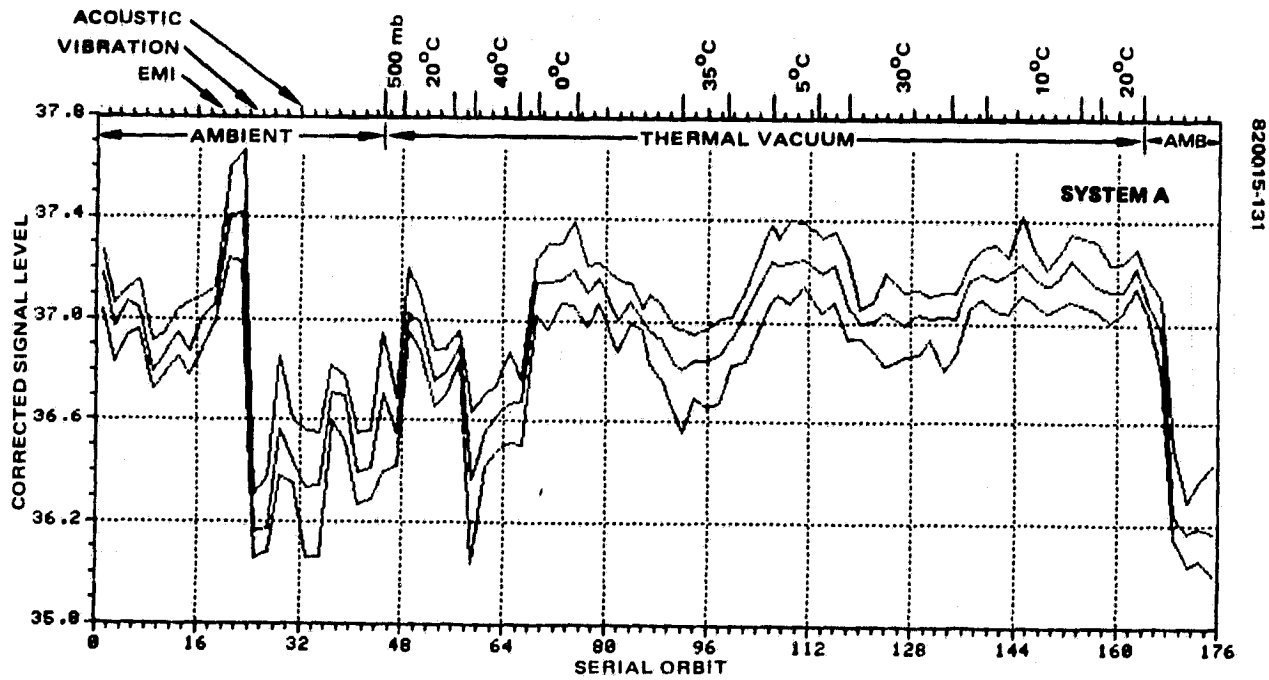

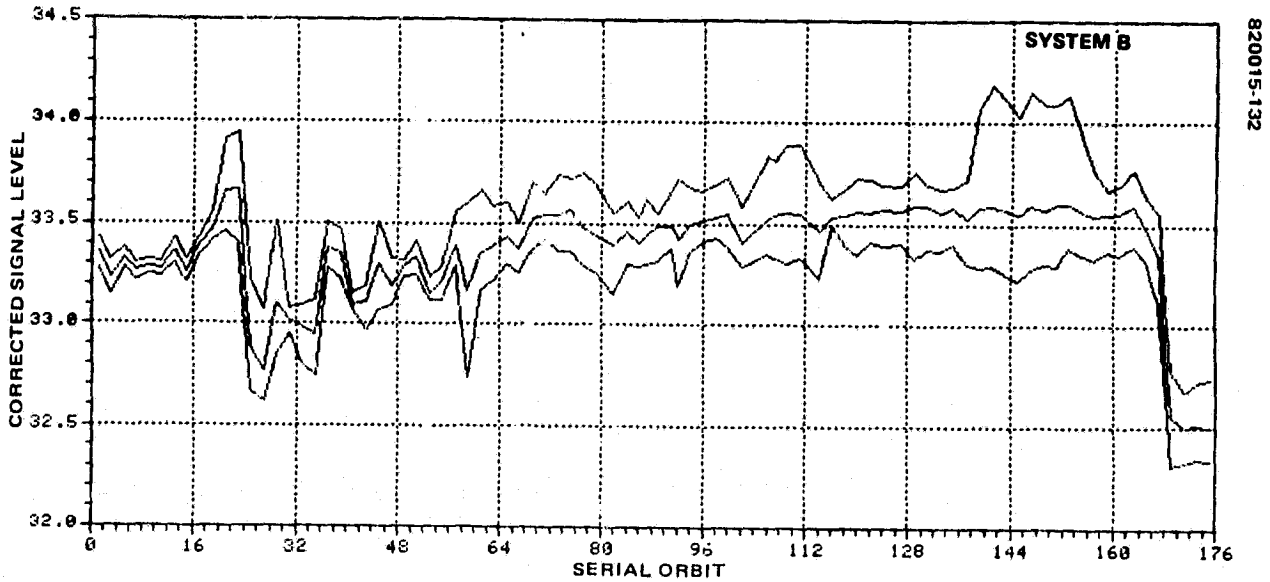

c) BAND 3

FIGURE 7-20 (CONTINUED). PROTOFLIGHT BAND AVERAGE COSL PERFORMANCE – LINEAR/LOW GAIN MODE

ORIGINAL PAGE IS
OF POOR QUALITY

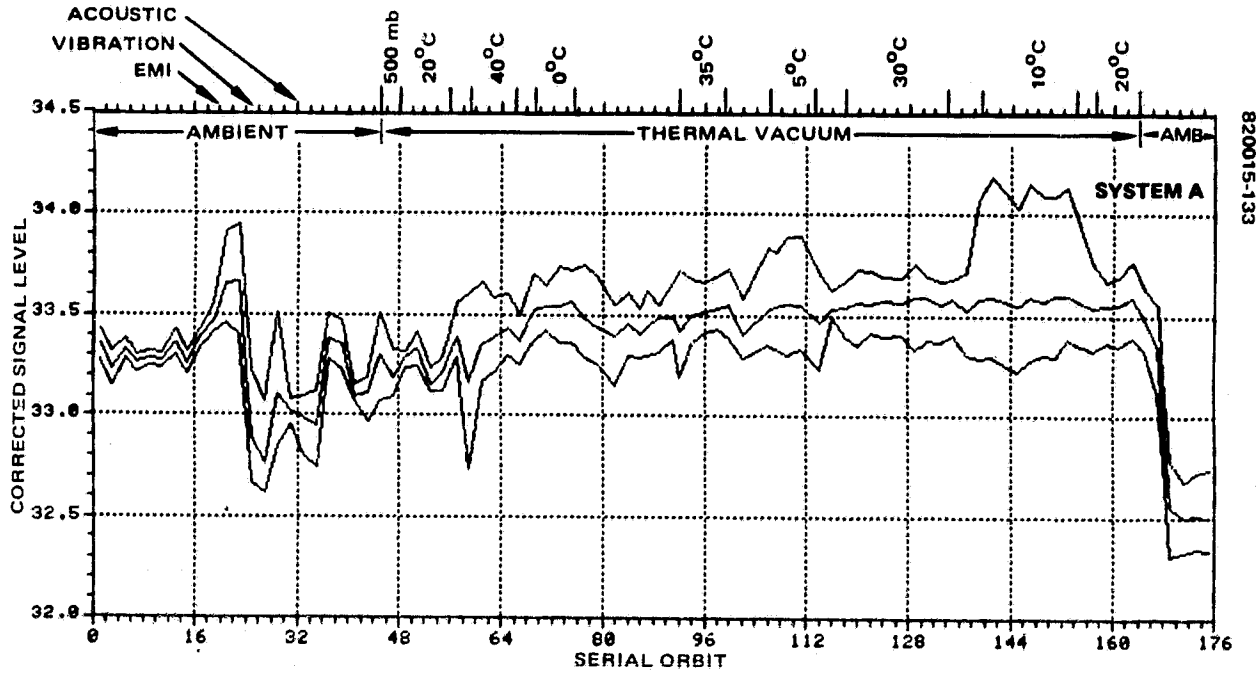

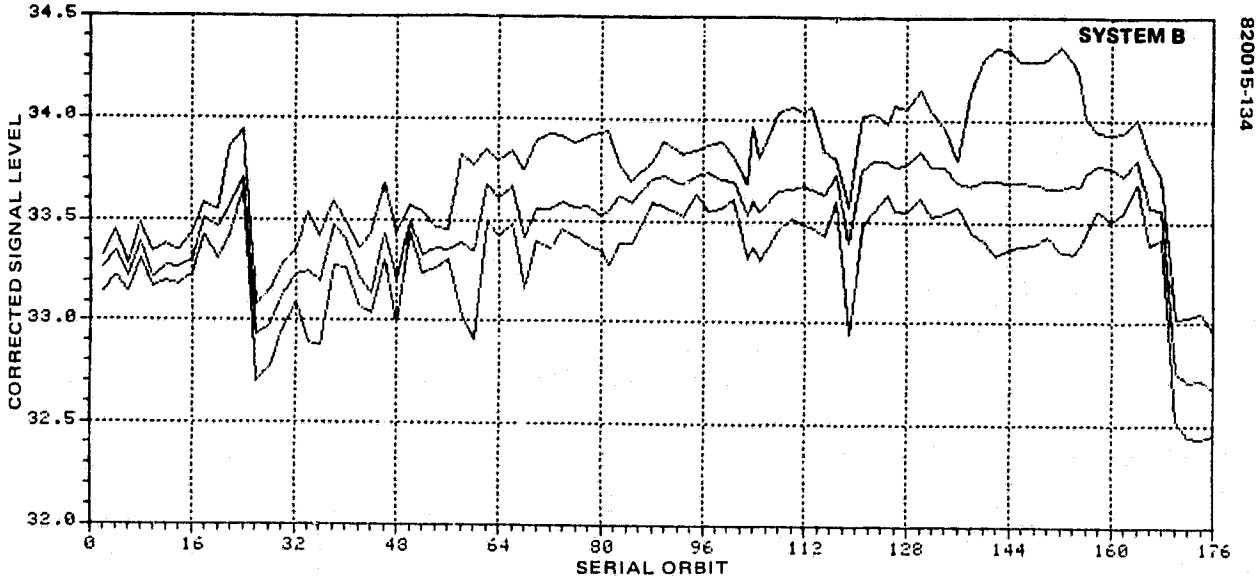

d) BAND 4

FIGURE 7-20 (CONTINUED). PROTOFLIGHT BAND AVERAGE COSL PERFORMANCE – LINEAR/LOW GAIN MODE

7.4.4.2 DCC Performance

DCC is a measure of the internal calibration system stability on a channel-to-channel basis for an individual band in the instrument. DCC is, by definition, the difference between the maximum and minimum calculated COSL in a given band. The specification limits this value to be less than 2 percent of the average COSL over the six channels in the band. (See 6.4.2 for a detailed account of the DCC algorithm.)

The COSL performance history for the MSS-D protoflight is presented in Figure 7-21 in a form very convenient for assessing system DCC performance versus the specificiation. The plots were generated by dividing the individual COSLs for each channel in a band by the band average COSL for that band. These normalized COSLs are plotted for all of the regular (non-STR) orbits run during MSS-D protoflight acceptance testing. To compare the DCC performance of the system using its redundant calibration sources, system configurations modes A and B are plotted separately.

Plotted in this manner, the data exhibit readily recognizable regions of test environment during which DCC specification violations occur. The responsible channels can be identified as well. The 2 percent of band average specification requirement with respect to the family of COSLs in a band are converted to a 2 percent envelope width for the normalized COSLs. One need envision then the mean at unity and the limits of the specifications to be located at 1.01 and 0.99 for the maximum and minimum, respectively. More precisely, the specification is not that the value of the normalized COSL should be between ±1 percent but rather that the peak-to-peak difference over all the channels in a band must be less than 2 percent.

Figure 7-21 indicates that a number of violations of the DCC specification occurred during MSS-D protoflight system acceptance testing. A summary review of each band in turn indicates the following:

1) Band 1. The DCC specification violations are due largely to channel 2 with occasional participation from channels 1, 3, 5, and 6. Channel 2 deviations are not only more frequent, but of greater magnitude.

2) Band 2. Channel 11 is clearly the most frequent offender, with a much larger magnitude of deviation. DCC violations occur as a result of channel 11 behavior at both temperature extremes. Channel 8 is a sometime violator, but other potential violations are masked by channel 11 behavior. Channel 12 exceeds the specification at the transition from 20° to 40°C, and during early 40°C orbits but is otherwise within specification.

3) Band 3. No specification violations are evident in band 3 (system A). Band 3 (system B) has some problems with channels 13 and 18 during the 40°C transition and early 40°C orbits, but this behavior does not repeat for the remainder of the testing.

4) Band 4. Channels 20 and 24 exhibit DCC problems at the same 40°C transition. As with channel 13 and 18 in band 3, the behavior does not repeat. Channel 20 exhibits some problems early in testing (orbits 24 to 28) but is otherwise within specification. Channel 21 is the channel which exhibits the most consistently anomalous behavior, but causes significant DCC specification violation only during the final 10°C orbits.

A detailed summary of the thermal-vacuum DCC violations is reproduced in Table 7-11. Briefly, 183 violations occurred at the four temperature plateaus as

follows: 1) 96 violations during two orbital sequences at 10°C (SONs 146 to 149 and 208 to 224), 2) 32 violations at 5°C (SONs 175 to 183), 3) 25 violations at 30°C (SONs 190 to 205), and 4) 30 violations at 35°C (SONs 161 to 168).

As confirmation of the repeatability of the instrument at temperature, the orbits for the four temperature plateaus at which DCC violations were noted were re-reduced using the first two orbits at each temperature plateau to recalibrate the system. This procedure is similar to that employed for the MSS-2 instrument. The re-reduced orbital data are a measure of internal calibration system stability at the given temprature plateaus. The number of DCC violations was reduced from the original 183 to 38 violations, divided as follows (see Table 7-12): 1) none at 5°C, 2) two minor violations (DCC = 2.14 and 2.08 percent relative to the specification value of 2.00) at 10°C, 3) 28 violations at 30° and 35°C occurred in band 1. Plots of COSL for the two temperature plateaus confirm the increased sensitivity of channel 2 and 5 and indicate that channel 2 in particular is the principal source of the DCC violations, (note that the variations of channel 11 COSL, very apparent in the original data reduction, appear stable when recalibrated at temperature.

Analysis of the thermal-vacuum orbits using the collimator calibration diagnostic program (see 6.5), designed to assess the health of the internal calibration system and collimator flooding and albedo lamp sources, indicated the following anomalies:

1) The apparent light output of the calibration system on a channel by channel basis appears to be temperature dependent but repeatable.

2) The apparent light output of the calibration system in channel 2 for both systems A and B diverges heavily at high temperatures (>30°C) from nominal values, (see Figures 7-22a).

3) The apparent calibration system light output of channel 11 decreases at temperatures greater than and less than 20°C (see Figure 7-22b). This effect is also shown by channel 5 although to a lesser extent than channel 2 and 11 (see Figure 7-22c).

The assumptions upon which the design of the collimator calibration diagnostic (CCD) program is based do not allow changes to be attributed to sources other than the collimator or scanner internal calibration system. Evidence indicates that the changes attributed to the internal calibration by the CCD program are in actuality changes in the transmission characteristics of the individual channel fibers brought about by separation of the fiber ends from their bonding surfaces (see Section 9). It must be emphasized that this hypothesis is not inconsistent with the results of the CCD program.

7.4.4.3 Deviation Band-to-Band (DBB) Performance

The DBB parameter effectively measures relative changes from time of calibration in the apparent band average radiance of the collimator over all four bands. As with DCC, it is ideally zero, but nonzero values can be expected, if only because of statistical uncertainties in the measurement process. Of course, nonzero values may also be due to real changes in either the collimator or the scanner itself (see 6.4.2 for a detailed explanation of the DBB algorithm).

No DBB violations occurred during the entire system testing period. All the DBB measurements were within the 3 percent maximum specification.

ORIGINAL PAGE IS
OF POOR QUALITY

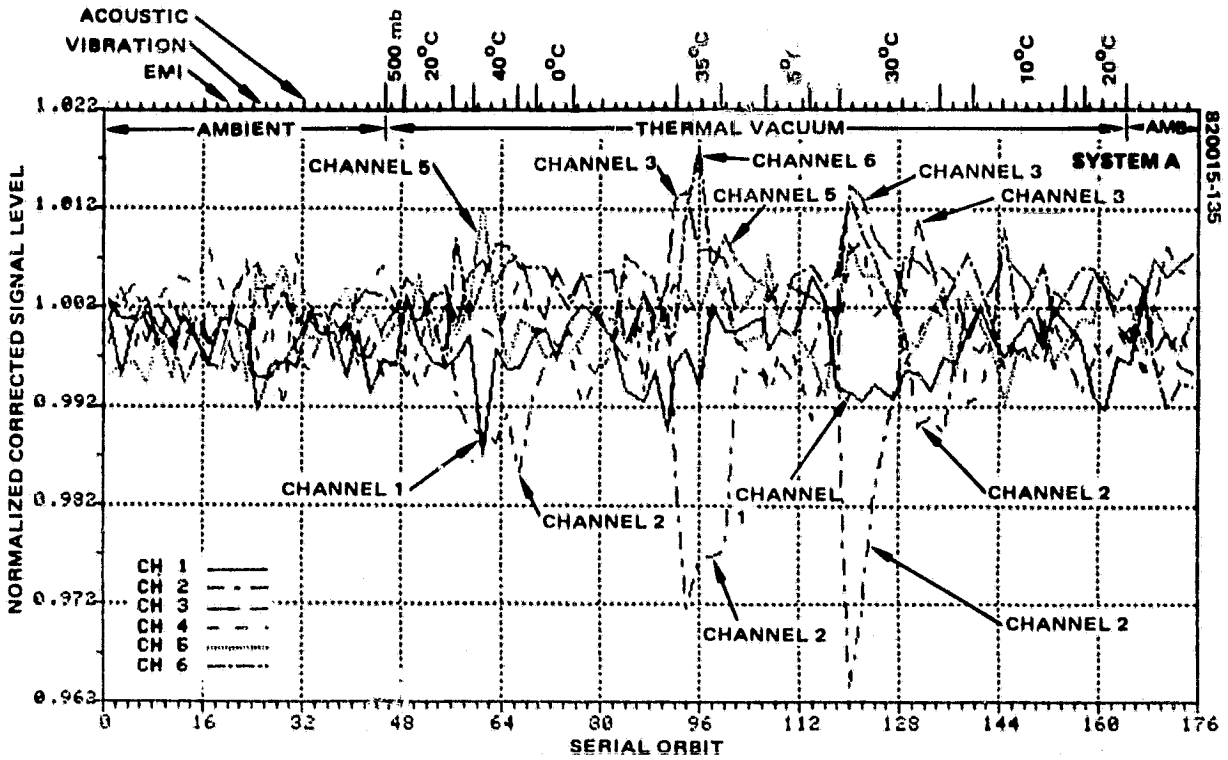

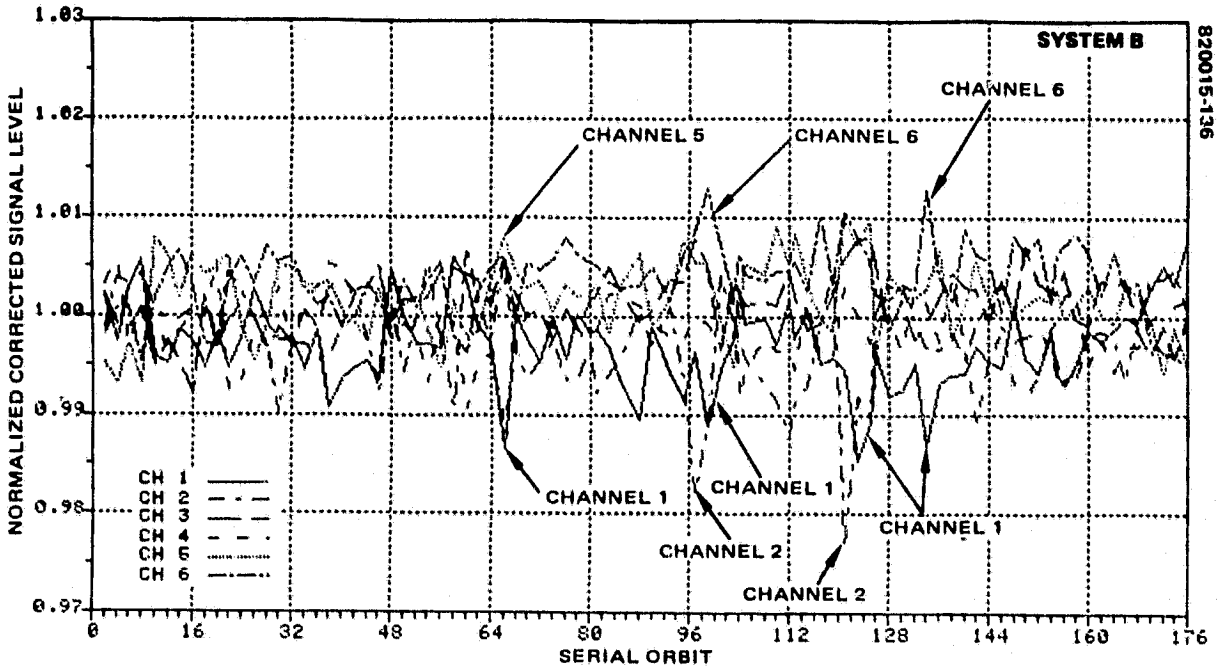

a) BAND 1

FIGURE 7-21. PROTOFLIGHT MEAN-NORMALIZED COSL PERFORMANCE — LINEAR/LOW GAIN MODE

ORIGINAL PAGE IS
OF POOR QUALITY

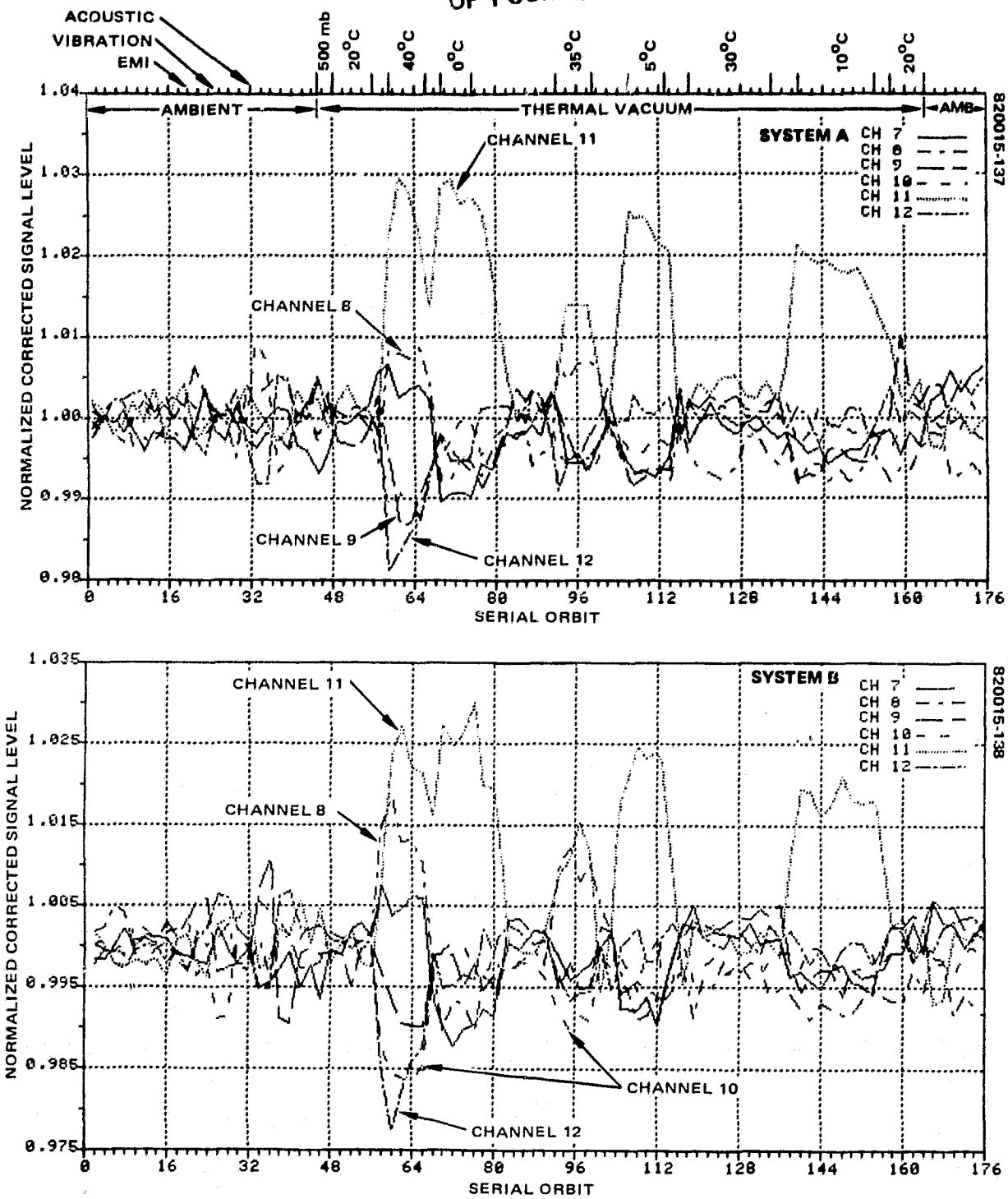

b) BAND 2

FIGURE 7-21 (CONTINUED). PROTOFLIGHT MEAN-NORMALIZED COSL PERFORMANCE — LINEAR/LOW GAIN MODE

ORIGINAL PAGE IS
OF POOR QUALITY

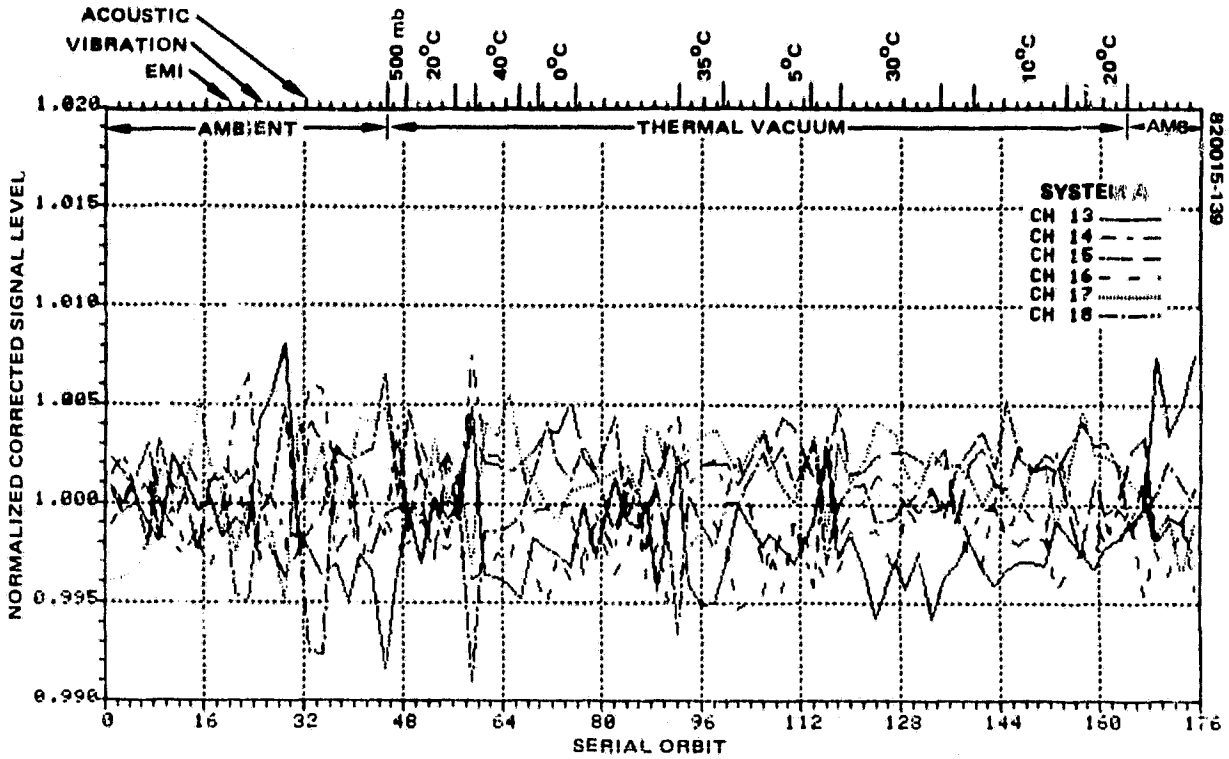

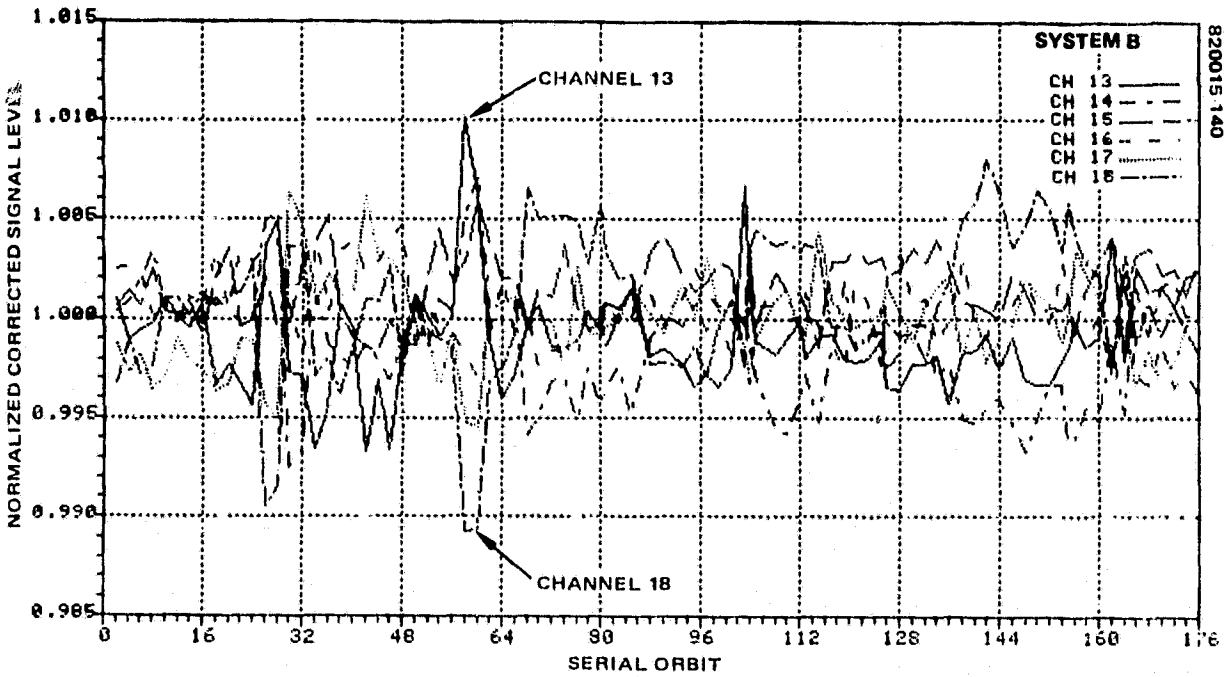

c) BAND 3

FIGURE 7-21 (CONTINUED). PROTOFLIGHT MEAN-NORMALIZED COSL PERFORMANCE — LINEAR/LOW GAIN MODE

ORIGINAL PAGE IS
OF POOR QUALITY

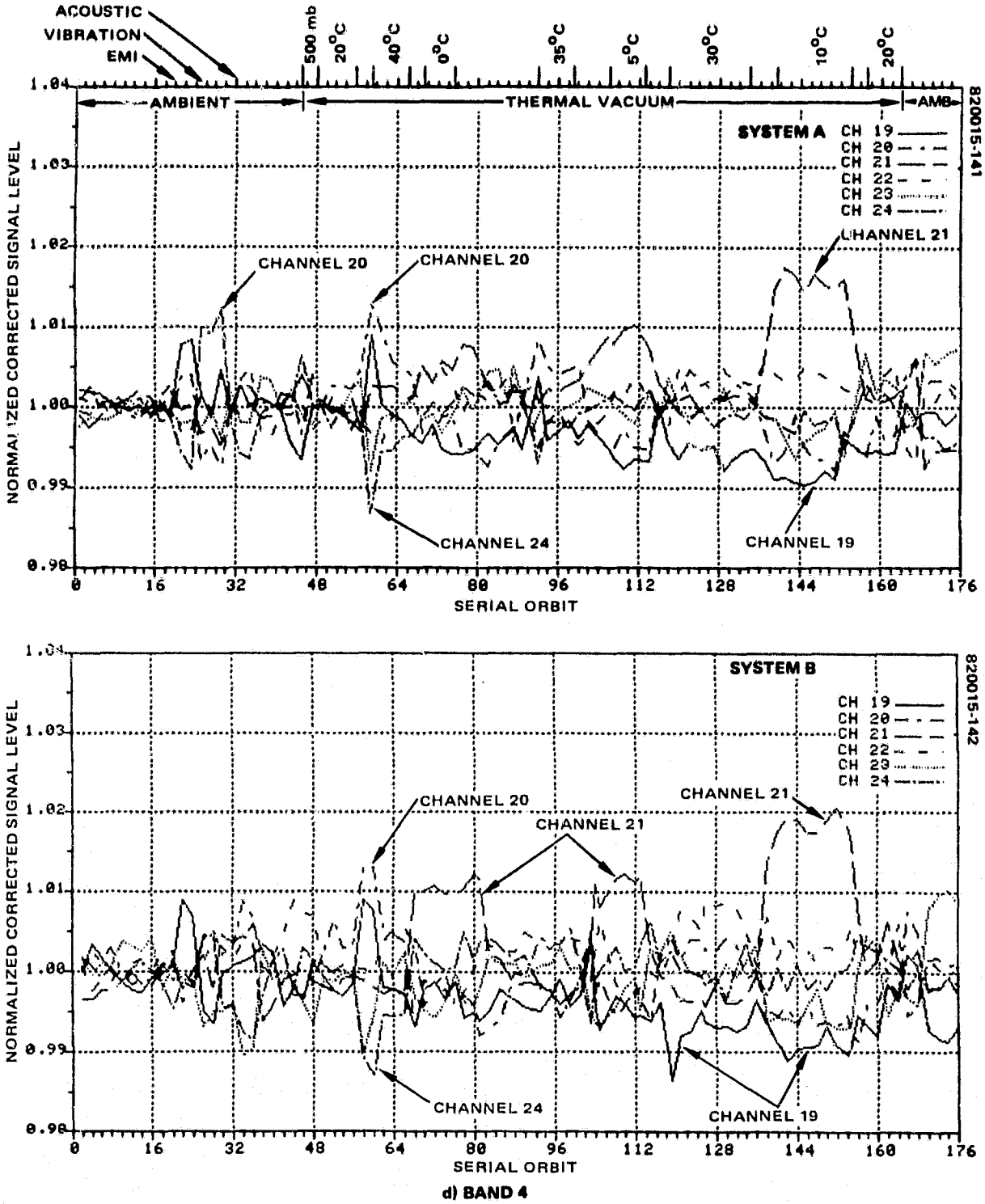

d) BAND 4

FIGURE 7-21 (CONCLUDED). PROTOFLIGHT MEAN-NORMALIZED COSL PERFORMANCE — LINEAR/LOW GAIN MODE

ORIGINAL PAGE IS
OF POOR QUALITY

TABLE 7-11. DCC SPECIFICATION VIOLATIONS BEFORE RECALIBRATION

Temperature Plateau, °C	Temperature, °C	Sequential Orbit	Number of Violations			
			Band 1	Band 2	Band 3	Band 4
10	10.0	146		4		
	10.0	147		4		
	10.0	148		4		
	10.0	149		3		
	10.0	150		2		
35	32.9	161	1	2		
	33.9	162		1		
	34.2	163	1	2		
	35.3	164		4		
	34.6	165	1	3		
	35.3	166	1	4		
	34.6	167	2	4		
	34.2	168	1	3		
5	6.7	175		4		
	6.7	177		4		
	6.1	178		4		
	6.5	179		4		
	6.3	180		4		
	7.2	181		4		
	7.6	182		4		
	7.4	183		4		
30	30.0	190	2			
	30.6	191	1			
	30.7	192	1			
	30.7	193	1			
	30.3	194	1			
	31.3	195	1			
	30.9	196	2			
	30.6	197	2			
	30.2	198	2			
	29.9	199	2			
	29.9	200	2			
	30.3	201	3			
	30.3	202	1			
	30.3	203	2			
	29.0	204	2			
10	10.4	209		4		1
	10.1	210		4		1
	10.8	211		4		1
	11.1	212		3		1
	11.1	213		4		1
	10.8	214		4		1
	11.3	215		4		1
	11.3	216		4		1
	11.1	217		4		1
	11.0	218		4		1
	11.6	219		4		1
	10.8	220		4		1
	10.8	221		3		2
	10.8	222		4		1
	11.6	223		4		1
	11.6	224		4		1

ORIGINAL PAGE IS
OF POOR QUALITY

TABLE 7-12. DCC SPECIFICATION VIOLATIONS AFTER RECALIBRATION

Temperature Plateau, °C	Temperature °C	Sequential Orbit	Number of Violations			
			Band 1	Band 2	Band 3	Band 4
10	10.0	146				
	10.0	147				
	10.0	148				
	10.0	149				
	10.0	150				
35	32.9	161	1			
	33.9	162				
	34.2	163	2			
	35.3	164				
	34.6	165	2			
	35.3	166	1			
	34.6	167	1			
	34.2	168	1			
5	6.7	175				
	6.7	177				
	6.1	178				
	6.5	179				
	6.3	180				
	7.2	181				
	7.6	182				
	7.4	183				
30	30.0	190	2			
	30.6	191	2			
	30.7	192	2			
	30.7	193				
	30.3	194	1			
	31.3	195	1			
	30.9	196	1			
	30.6	197	3			
	30.2	198	2			
	29.9	199	3			
	29.9	200	3			
	30.3	201	3			
	30.3	202	1			
	30.3	203	3			
	29.0	204	1			
10	10.4	209				
	10.1	210				
	10.8	211				
	11.1	212				
	11.1	213				
	10.8	214		1		
	11.3	215				
	11.3	216				
	11.1	217				
	11.0	218				
	11.6	219				
	10.8	220				
	10.8	221				
	10.8	222				
	11.6	223				
	11.6	224				

ORIGINAL PAGE IS
OF POOR QUALITY

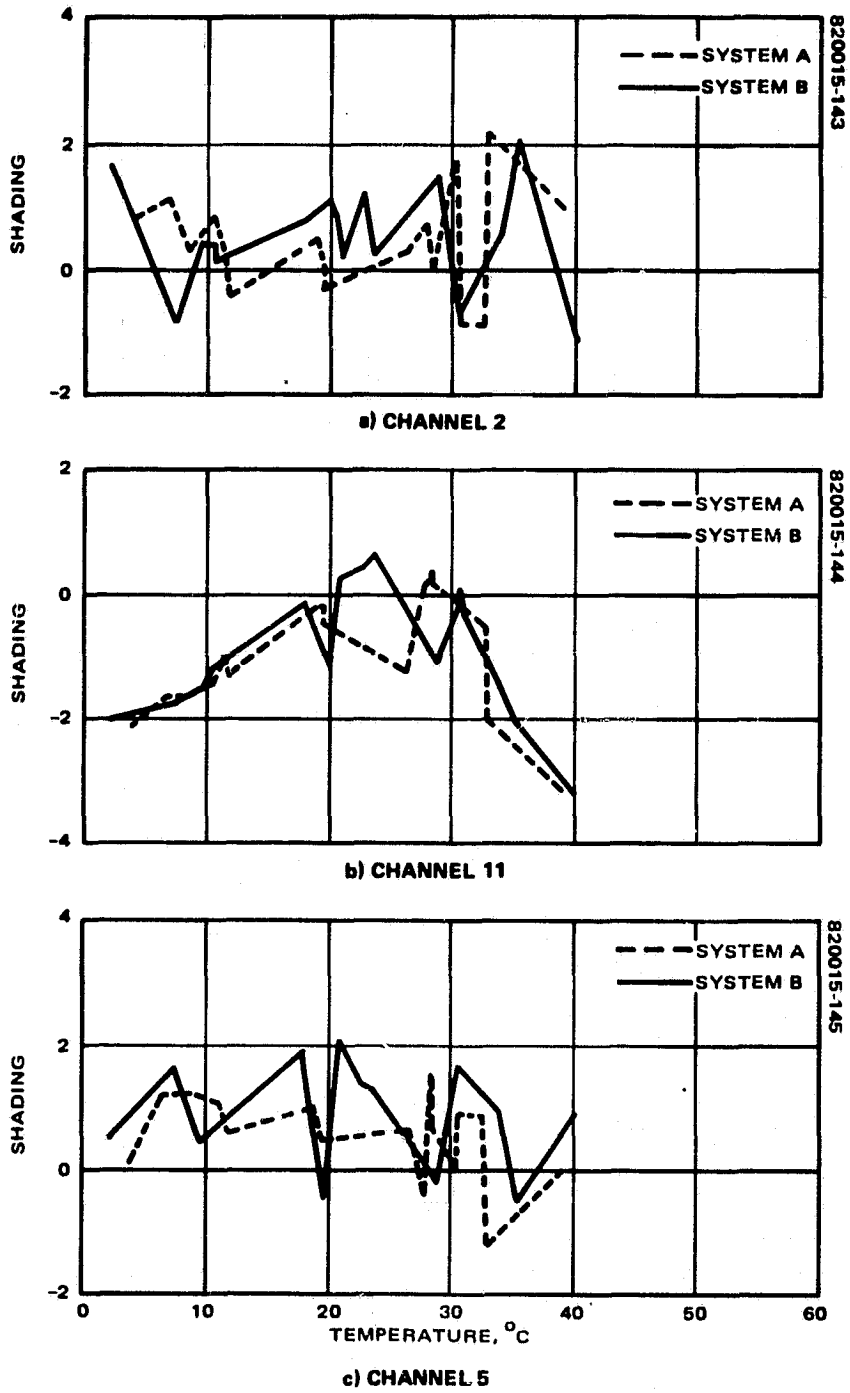

FIGURE 7-22. INTERNAL CALIBRATION SYSTEM — APPARENT RADIANCE VERSUS TEMPERATURE

ORIGINAL PAGE IS
OF POOR QUALITY

7.5 MODULATION TRANSFER FUNCTION (MTF)

7.5.1 Introduction

The modulation transfer function provides an estimate of the spatial frequency response of the MSS system. The function used here is more precisely the square wave response (SWR) of the system since it is the system response to a square wave input. The square wave radiant input to the scanner results from the use of several rectilinear reticle patterns in the collimator. The reticle pattern spacings correspond to half-cycle (spatial) wavelengths of 236', 450', and 650' as measured at the earth's surface. Only the pattern corresponding to 236' is subject to the system specification, which states that the square wave response (here MTF) of the instrument at a spatial half-wavelength of 236' must be greater than 0.36, for temperatures between 10° and 30°C. The responses may be degraded by 20 percent at temperatures extremes of 5° and 35°C. The algorithm developed for making estimates of this parameter is given in 6.4.3. For historical reason, we shall continue to refer to this parameter as the MTF.

This subsection presents the results of the MTF measurements made on the MSS-D protoflight scanner throughout acceptance testing.

7.5.2 MTF Model Description

As stated above and emphasized here, this parameter which is called modulation transfer function and which was specified and measured during MSS-D system acceptance testing is, more precisely, the system square wave response. The following paragraphs describe the relationship between the more conventional MTF and the SWR and provide some insight into the anticipated behavior of MTF as a function of the effect of the test environment (particularly temperature) on various components of the system.

The modulation transfer function is defined conventionally as the system response to a sine wave input. It is a mathematical construction which depends on the applicability of linear systems theory to optical systems. It is of particular importance in the evaluation of the image reconstruction capability of complex optical systems. The image space distribution of a sine wave object space pattern is sinusoidal, independent of the shape of the pupil function for optical systems which are "suitably linear."

This feature, combined with the existence of methods for performing Fourier decomposition of more complex image patterns (e.g., a square wave pattern), provides a powerful tool for optical system image reconstruction evaluation of these more complex patterns.

Before turning to a discussion of the direct application of modulation transfer function anlysis to MSS-D, it is necessary to clarify specifically the relationship that exists between the square wave response (which we call MTF) and the more conventional modulation transfer function, $M(\nu)$.

If a square wave object space distribution is decomposed into its Fourier sine components of spatical frequency $k(\nu)$, and each component passed through the linear filter representing the optical system to form the corresponding sinusoidal image space distribution, the modulation transfer function $M(k\nu)$ for each of these inputs can be

determined. It is not difficult to show from Fourier analysis theory that the system square wave response is given by

$$SWR(\nu) \triangleq MTF(\nu) = \frac{4}{\pi}\left[M(\nu) - \frac{M(3\nu)}{3} + \frac{M(5\nu)}{5} - \frac{M(7\nu)}{7} + \ldots\right]$$

In the remainder of this subsection this more conventional modulation transfer function $M(\nu)$ to avoid any further confusion with the square wave response which labelled MTF. The modulation transfer function $M(\nu)$, plotted as a function of the spatial frequency of the input (object) space pattern, can be used to describe and evaluate complicated optical systems with regard to their preservation of image quality, especially contrast.

7.5.2.1 System Modulation Transfer Function, $M_S(\nu)$

When defined as above the modulation transfer function $M(\nu)$ has the advantage that the $M(\nu)$ for two or more components of a system can be easily combined by multiplication to give the $M_S(\nu)$ of the combined system. Reasonable care must be exercised to assure that the individual components are suitably linear and disconnected. (The relevant theorems require that the object be a sinusoidal, incoherent image over an aplanatic patch, etc). The remainder of this discussion assumes that these theorems apply.

The MSS modulation transfer function, $M_S(\nu)$ can be modeled by cascading the modulation transfer functions of the optical telescope, $M_T(\nu)$, the scan aperture (detectors), $M_D(\nu)$, and presample filter (electronics), $M_F(\nu)$. $M_S(\nu)$ can then be estimated in the following manner:

$$M_S(\nu) = M_T(\nu) \cdot M_D(\nu) \cdot M_F(\nu)$$

7.5.2.2 Telescope Modulation Transfer Function, $M_T(\nu)$

The transfer function for an optical system is the convolution of the aperture function with its complex conjugate or, as conventionally expressed, the transfer function is the autocorrelation function of the pupil function. In the absence of aberrations, the convolution of the aperture function with its complex conjugate is equivalent to the geometric process of computing the area common to overlapping representations of the aperture as viewed in the focal plane displaced with respect to one another. The theoretical MTF for the MSS may be derived by convolution of the annular aperture with an obscuration ratio of $e = 0.411$. (The MSS has a clear aperture of 9 inches with a secondary obscuration of 3.7 inches and a focal length of 32.5 inches.) The modulation transfer function thus obtained is presented in Table 7-13 and represents the aberration-free MTF for the telescope.

However, the telescope $M_T(\nu)$ degrades with baseplate temperature due to an induced change in focus. Defocus due to a change in baseplate temperature was calculated (estimated) for the first MSS's designs and application of worst case

ORIGINAL PAGE IS
OF POOR QUALITY

TABLE 7-13. MSS TELESCOPE MODULATION TRANSFER FUNCTION, $M_T(\nu)$

ν/ν_o	MTF $\epsilon = 0.4$	ν $\lambda = 0.55\ \mu m$	ν $\lambda = 0.90\ \mu m$	Corrected MTF $\lambda = 0.55\ \mu$ $\Delta T = 10^oC$	Corrected MTF $\lambda = 0.55\ \mu$ $\Delta T = 15^oC$	Corrected MTF $\lambda = 0.90\ \mu$ $\Delta T = 10^oC$	Corrected MTF $\lambda = 0.90\ \mu$ $\Delta T = 15^oC$
0	1.00	0	0				
0.05	0.8961	2.08×10^4	1.27×10^4			0.82	
0.10	0.7917	4.16×10^4	3.81×10^4	0.57	0.46	0.65	0.59
0.15	0.6882	6.23×10^4	2.54×10^4				
0.20	0.5880	8.31×10^4	5.08×10^4	0.26	0.12	0.35	0.27
0.25	0.4898	1.039×10^5	7.62×10^4				
0.30	0.3987	1.25×10^5	7.62×10^4				
0.35	0.3404	1.45×10^5	8.89×10^4				
0.40	0.3159	1.66×10^5	1.016×10^5				
0.45	0.3053	1.87×10^5	1.14×10^5				
0.50	0.2968	2.08×10^5	1.27×10^5				
0.55	0.2890						
0.60	0.2780						
0.65	0.2588						
0.70	0.2225						
0.75	0.1443						
0.80	0.1041						
0.85	0.0682						
0.90	0.0374						
0.95	0.0133						
1.00	0.	4.156×10^5	2.54×10^5				

$$\nu_o = \frac{D}{\lambda} = \frac{0.2286}{0.55 \times 10^{-6}} = 4.156 \times 10^5 \text{ cycles/rad}$$

$\lambda = 0.55\ \mu m$

$$\nu_o = \frac{0.2286}{0.9 \times 10^{-6}} = 2.54 \times 10^5 \text{ cycles/rad}$$

$\lambda = 0.9\ \mu m$

ORIGINAL PAGE IS
OF POOR QUALITY

temperature distribution correction appeared to give excellent correlation with thermal-vacuum test data for MSS-3. The calculated defocus ΔZ for that case was shown to be

$$\Delta Z = 1.11 \times 10^{-4}\ \Delta T \text{ inches}$$

where ΔT is the temperature difference from the focus alignment temperature in ^{o}C.

Born and Wolf in Principles of Optics (Figure 9.13, p. 485) show the relative change in modulation transfer function $M_T(\nu)$ for a clear aperture as a function of a parameter "m" which is related to the defocus ΔZ as follows:

$$m = \frac{\pi}{8\lambda}\left(\frac{1}{f\#}\right)^2 \Delta Z$$

where λ is the optical wavelength and f# is the relative aperture, or F-number; ΔZ is the distance between the plane of observation and the Gaussian focal plane. ΔZ is positive when taken in the direction of the focal plane. However, the resultant modulation transfer function ($M_T(\nu)$, as a function of ΔZ (and hence ΔT) is symmetric about the focal point since it is obtained from the autocorrelation function of a pupil function which is a complex exponential, linear in m. The resultant $M_T(\nu)$ is, therefore, a function of m^2. For MSS-D m is given by the following:

$$m = \frac{\pi}{8 \times \begin{Bmatrix} 0.55 \times 10^{-6} \\ 0.90 \times 10^{-6} \end{Bmatrix}} \left(\frac{1}{3.53}\right)^2 \begin{Bmatrix} 28 \times 10^{-6}, \Delta T = 10^{o}C \\ 42.4 \times 10^{-6}, \Delta T = 15^{o}C \end{Bmatrix}$$

m =

$\lambda = 0.55\ \mu m$	$\lambda = 0.9\ \mu m$	
1.6	1.0	$\Delta T = 10^{o}C$
2.4	1.5	$\Delta T = 15^{o}C$

Using Born and Wolf, Figure 9.13, the correction factor for MTF as a function of ΔT is

$\frac{\nu}{\nu_o}$	$\lambda = 0.55\ \mu m$		$\lambda = 0.90\ \mu m$	
	$\Delta T = 10^{o}C$	$= 15^{o}C$	$\Delta T = 10^{o}C$	$= 15^{o}C$
0.05			0.91	
0.10	0.72	0.58	0.82	0.74
0.20	0.44	0.20	0.60	0.46
0.25			0.52	

ORIGINAL PAGE IS
OF POOR QUALITY

The telescope MTF $M_T(\nu)$ for baseplate temperature 10° and 15^oC different from the nominal calibration temperature (nominally assumed to be 20^oC) are listed in Table 7-13.

7.5.2.3 Scanning Aperture Modulation Transfer Function, $M_D(\nu)$

The MTF of a rectangular scanning aperture of dimension "a" and corresponding spatial frequency ν_o = is given by

$$MTF_D = \frac{\sin \frac{\pi \nu}{\nu_o}}{\frac{\pi \nu}{\nu_o}}$$

Where is the spatial frequency of the input pattern and a = $1/\nu_o$ is the scanning aperture instantaneous geometric field-of-view (IGFOV) in radians in the scanning direction. The MSS scanner utilizes square clad glass fiber terminations in the fiber plate as scanning apertures. The internal dimensions of these fibers, which determine the dimension a, correspond to an IGFOV of 111 μrad. (The corresponding value for MSS 1, 2, and 3 was 80 μrad). The fundamental limiting of spatial frequency associated with this dimension is ν_o = 9009 cycles/radian.

The scan aperture MTF_D for MSS is given in Table 7-14.

7.5.2.4 Pre-sample Filter Modulation Transfer Function, $M_F(\nu)$

The presample filter MTF $M_F(\nu)$ is determined by the scan mirror angular velocity and the presample filter frequency response. The MSS presample filter is a third order Butterworth with a 3 dB frequency of 42.3 kHz. The response of a third order Butterworth is

$$\frac{\epsilon o}{\epsilon i} = \frac{1}{1 + \left(\frac{\omega}{\omega_c}\right)^{2m}} = \frac{1}{1 + \left(\frac{\omega}{\omega_c}\right)^{6}}$$

where ω_c is the 3 dB frequency.

The center scan mirror object space scan rate for MSS-C was 6.405 rad/sec. The nominal design center scan mirror angular rate for MSS-D is 8.050 rad/sec. The equivalent spatial frequency for the 3 dB filter frequency is then:

$$\text{MSS-C} \quad \frac{42300}{6.405} = 6604 \text{ cycles/rad}$$

$$\text{MSS-D} \quad \frac{42300}{8.050} = 5255 \text{ cycles/rad}$$

The presample filter MTF's $M_F(\nu)$ for MSS-C and MSS-D are given in Table 7-15.

TABLE 7-14. MSS SCAN APERTURE MODULATION TRANSFER FUNCTION, $M_D(\nu)$

ν/ν_o	$\nu_{MSS\text{-}D}$	$\nu_{MSS\text{-}1}$	MTF $\sin \pi\nu/\nu_o/\pi\nu/\nu_o$
1	9009	12500	0
7/8	7882	10938	0.139
3/4	6757	9375	0.30
5/8	5631	7813	0.47
1/2	4505	6250	0.64
3/8	3378	4688	0.78
1/4	2252	3125	0.90
1/8	1126	1563	0.973
0	0	0	1.

TABLE 7-15. MSS PRESAMPLE FILTER MTF, $M_F(\nu)$

ω/ω_c	$\omega_{MSS\text{-}D}$	$\omega_{MSS\text{-}C}$	MTF $\frac{1}{1+(\omega/\omega_c)^6}$
0.5	2628	3702	0.992
0.6	3135	3962	0.977
0.7	3679	4623	0.946
0.8	4204	5283	0.890
0.9	4730	5944	0.808
1.0	5255	6604	0.707
1.1	5781	7264	0.601
1.25	6569	8255	0.460
1.5	7883	9906	0.284
1.7	8934	11227	0.199
2.0	10510	13208	0.12

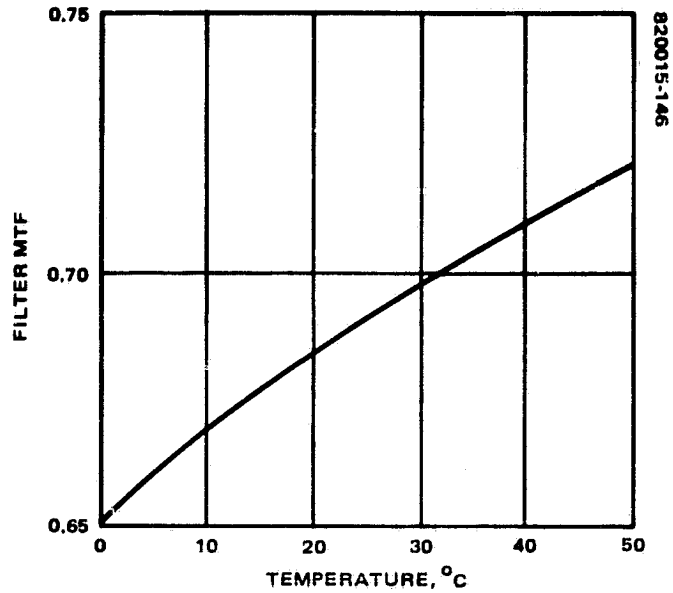

a) MSS C FILTER MTF VERSUS TEMPERATURE

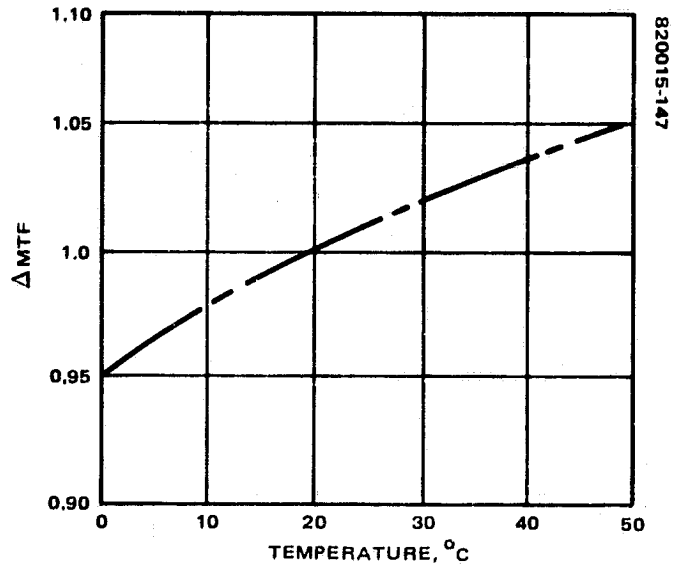

b) MTF CHANGE FROM NOMINAL AT 20°C AS A FUNCTION OF FILTER TEMPERATURE

FIGURE 7-23. FILTER RESPONSE AS A FUNCTION OF TEMPERATURE

The presample filter is also temperature sensitive. Duringthe environmental testing of MSS-3, a single frequency temperature sensitivity test was run as shown in Figure 7-23. We assume a similar effect occurs for MSS-D.

7.5.2.5 Resultant System Modulation Transfer Function, $M_S(\nu)$

The modulation transfer function for the MSS-D, $M_S(\nu)$, is obtained by multiplying the resultant modulation transfer functions $M_T(\nu)$, $M_F(\nu)$, and $M_D(\nu)$. The result is plotted in Figure 7-24 using the calculated telescope, presample filter, and scan aperture modulation transfer functions.

ORIGINAL PAGE IS
OF POOR QUALITY

ORIGINAL PAGE IS
OF POOR QUALITY

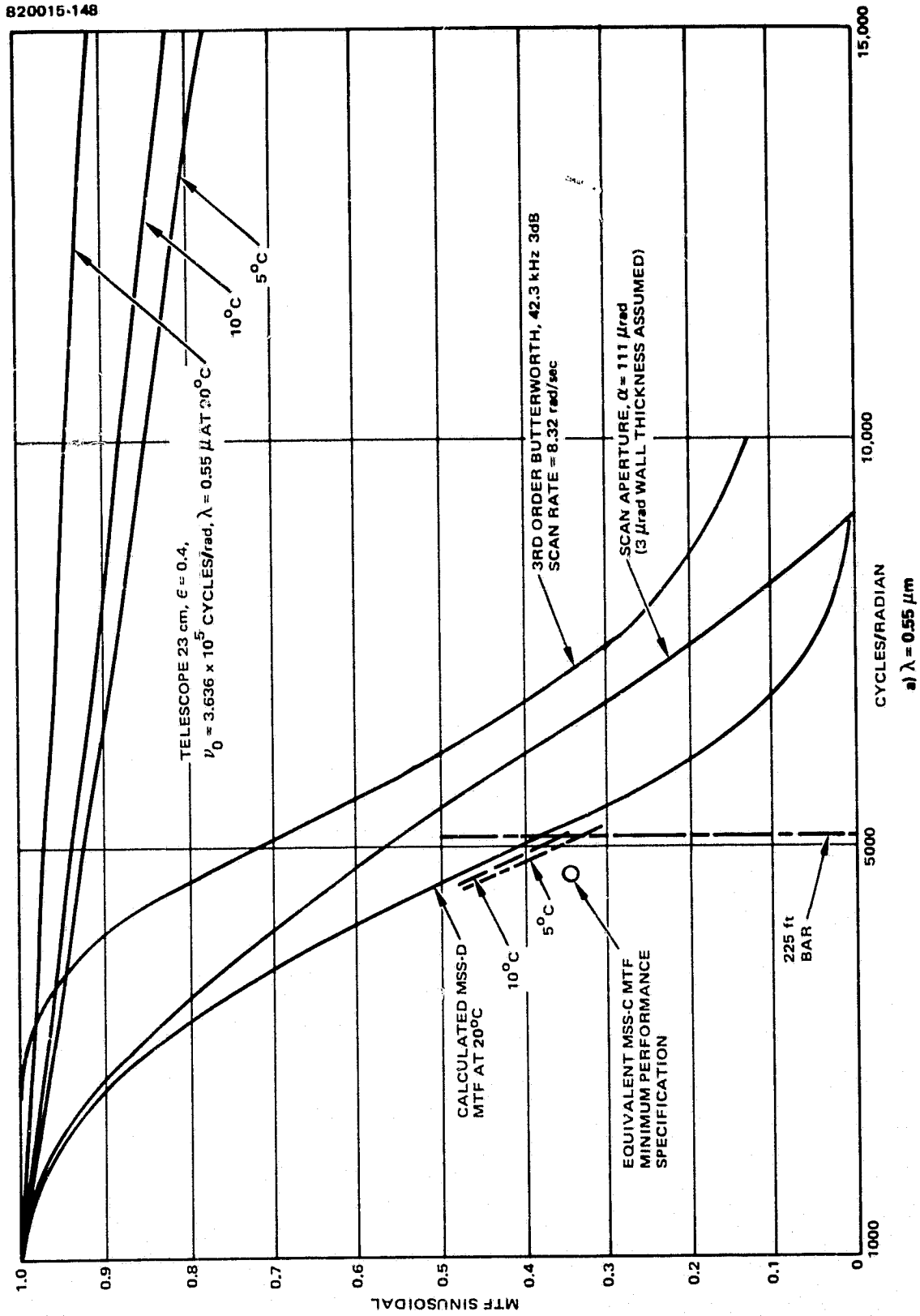

FIGURE 7-24. ESTIMATED MSS-D MTF

ORIGINAL PAGE IS
OF POOR QUALITY

820015-149

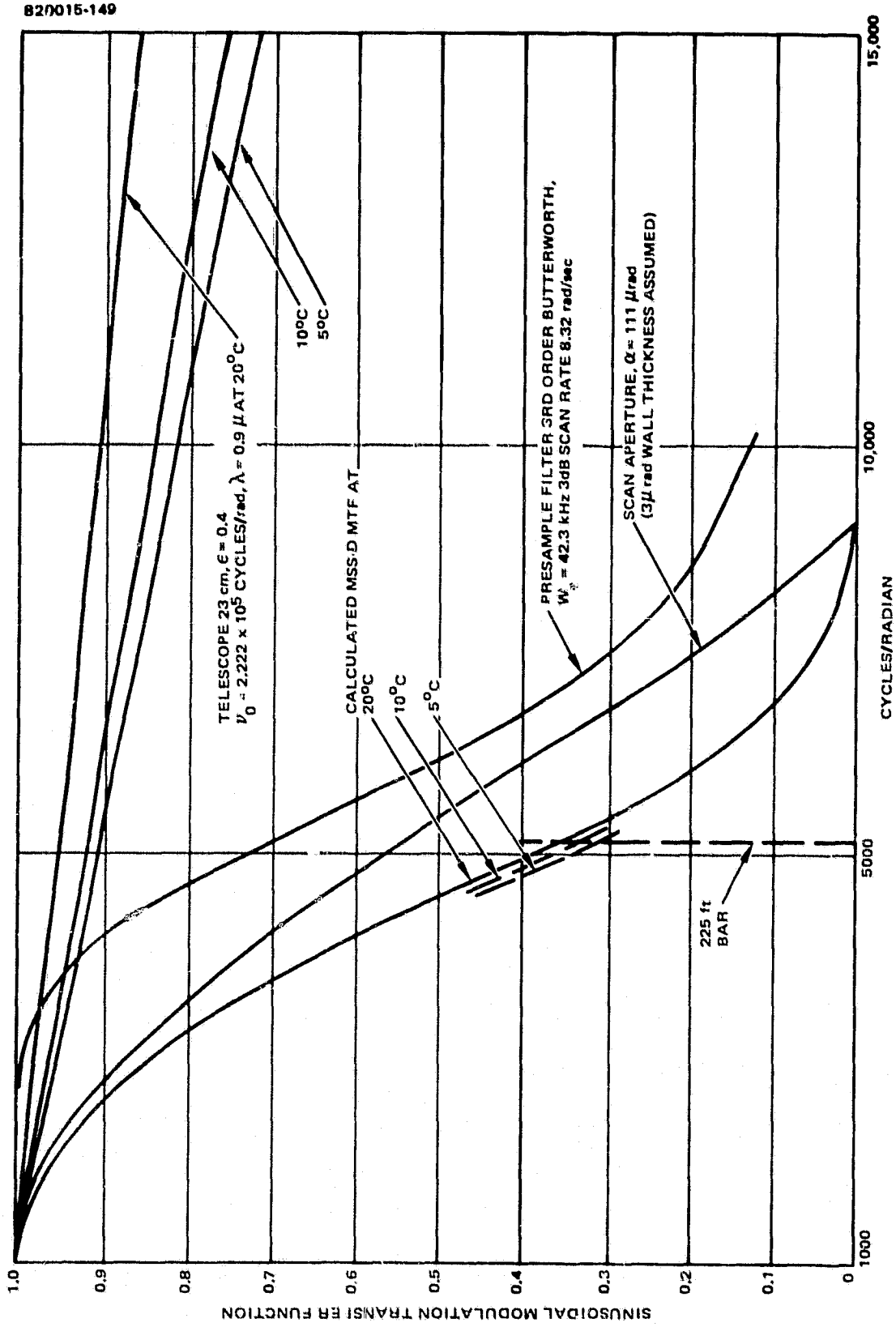

FIGURE 7-24 (CONTINUED). ESTIMATED MSS-D MTF

ORIGINAL PAGE IS
OF POOR QUALITY

820015-150

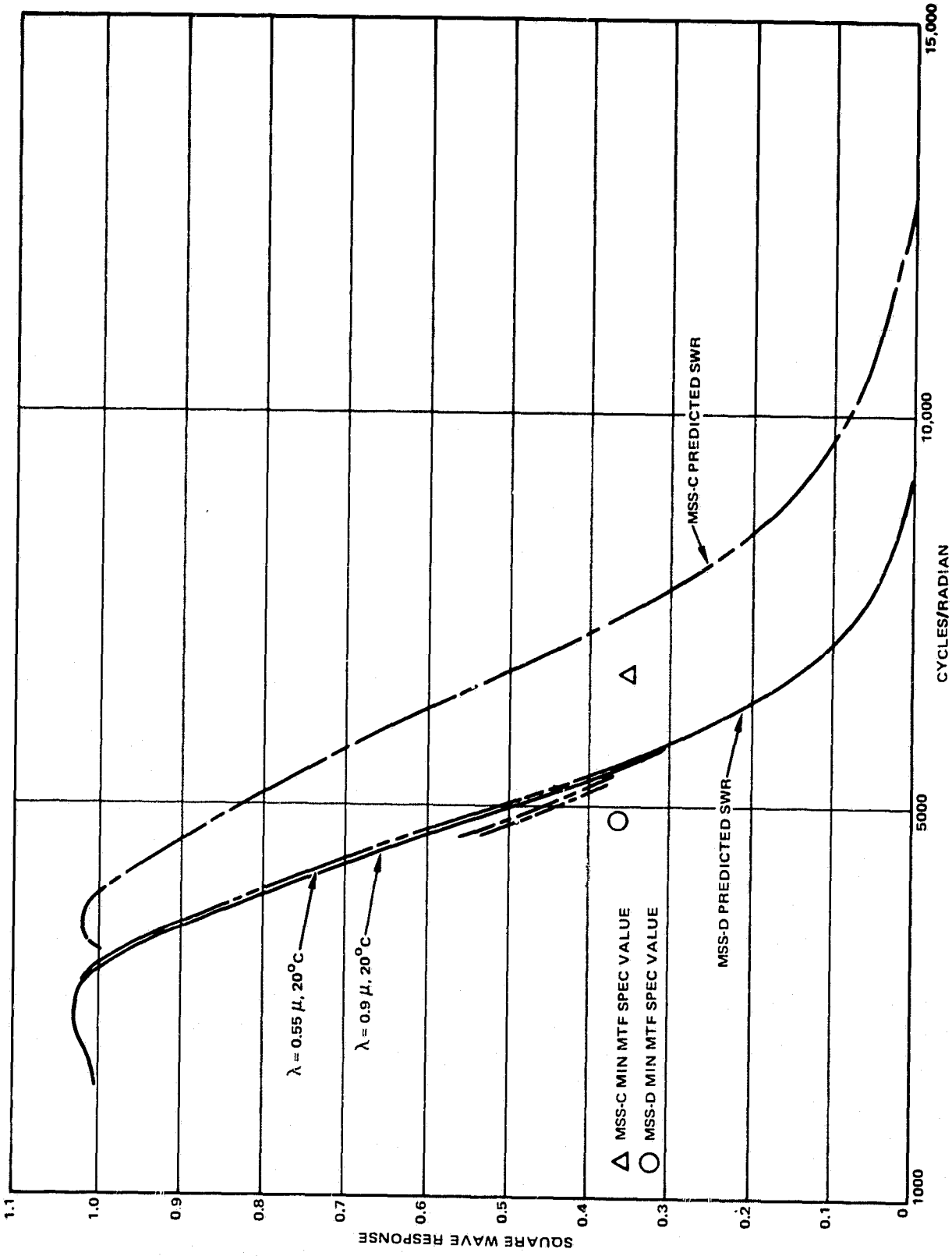

FIGURE 7-25. MSS-C AND MSS-D SQUARE WAVE RESPONSE

ORIGINAL PAGE IS
OF POOR QUALITY

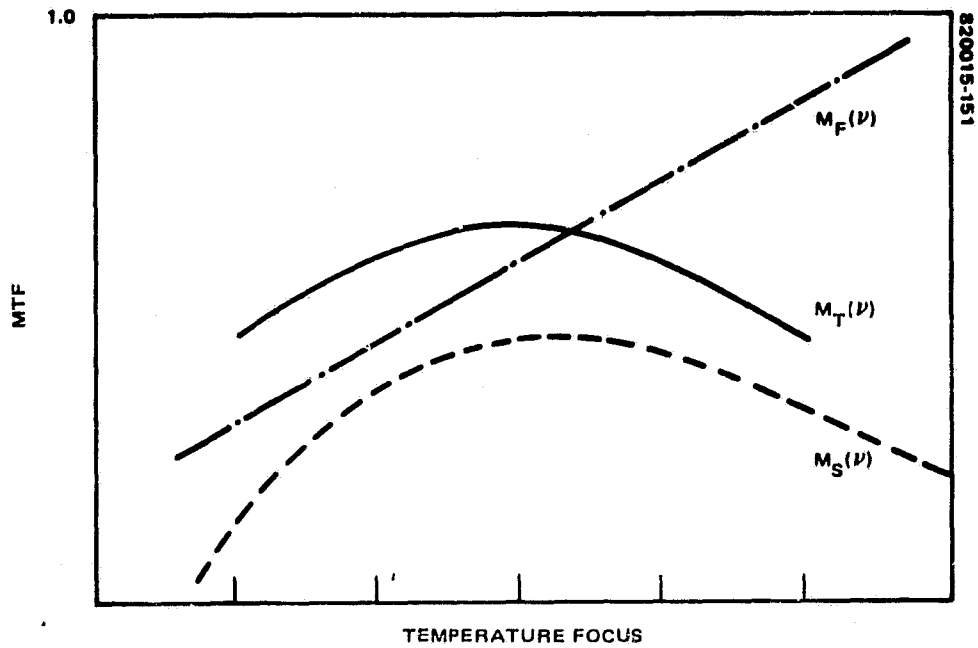

FIGURE 7-26. TEMPERATURE EFFECTS ON MTF

The square wave response, MTF, of the MSS-D is calculated assuming a linear system and by decomposing the input square bar pattern into its Fourier components. The resultant system MTF is shown in Figure 7-25.

7.5.2.6 Temperature Effect on MTF

The anticipated effect of temperature changes on the measured MTF is illustrated in Figure 7-26. The MTF for the telescope is symmetric in ΔT and, therefore, is shown symmetric about some temperature at which the system is in focus. The effect of temperature changes on the filter MTF, shown typically linear and increasing with temperature, is to cause the resulta t MTF to be asymmetric, with a more rapid falloff in MTF toward lower temperture, and an extension of higher MTF values for higher temperatures. The curves, used for illustration, are exaggerated to emphasize the effect.

While the above treatment does not give quantitative estimates as to the effect of temperture changes on the telescope $M_T(\nu)$, it does provide some insight into what can be anticipated as a result of thermal-vacuum testing. In particular, the system square wave response, MTF, should behave in the following manner:

1) The contribution of the telescope transfer characteristics as a function of temperature should tend to provide symmetric values about the temperature of best focus.

2) The contribution of the presample filter (electronics) tends to bias MTF values to higher temperature.

The resultant curves should appear as shown in Figure 7-26 where the MTF peaks close to the temperature of best focus and falls off more rapidly at lower temperture than it does at higher temperatures as a result of the mutual contribution of the optics and electronics transfer characteristics.

ORIGINAL PAGE IS
OF POOR QUALITY

7.5.3 Protoflight MTF Performance

The results of MTF measurements made on the MSS-D protoflight are presented in Figure 7-27, which provides the history of MTF per performance for all channels of each of the four bands. These plots present all of the MTF data taken during regular acceptance testing. Data taken during special test requests are not shown.

A review of Figure 7-27 reveals the following features:

1) All of the channels in any given band exhibit the same relative MTF behavior as a function of environment (as a function of serial orbit number). The significant difference between channels in a band is their spread in measured values. In some cases an individual channel in a band is significantly higher or lower than the nominal for that band. The range of MTF spread for each band and for each major environmental condition, as well as the nominal values for each band, is given in Table 7-16.

2) A major change (drop) in MTFs for all bands took place after vibration testing (serial orbits 25 through 28) and MTFs for all bands vary (generally increase) throughout the prethermal-vacuum period for no apparent reason; i.e., same temperature, ambient pressure environment.

3) Once the system is in thermal-vacuum testing, the MTF performance is relatively stable and repeatable at the temperature plateaus.

4) Some change in MTF for all channels in a band occurs going into, and coming out of, vacuum. This shift affects the bands differently and in a fashion different from the effect of pressure environment change on gains (vacuum shift) (see 7.4.3).

The following paragraphs provide a step-by-step explanation of the important features of these data. Data representing behavior of the system which is typical of a group of data values (e.g., the MTFs for all the channels, or a subset of all of the channels, of a given band at a specific test environment) are referred to as the "nominal" performance of that group for that condition. Anomalous behavior, or behavior not characteristic of the nominal behavior, is discussed separately.

The nominal performance is discussed initially, followed by a discussion of anomalous behavior. Overall performance history is summarized at the end of the discussion (Table 7-16).

7.5.3.1 Nominal MTF Performance

During early acceptance testing at ambient temperature and pressure, the nominal MTF's in all bands were well above specification and tended to increase from the initial long form performance test at SBRC to the post-EMI/previbration test period (serial orbits 1 through 24).

These data were collected over a period of time during which the collimator was repeatedly aligned and focused between test sequences and test configuration changes. Much of the variability exhibited here is believed to be due to increased "learning" in the collimator alignment/focusing procedures. This belief is somewhat substantiated by the

ORIGINAL PAGE IS
OF POOR QUALITY

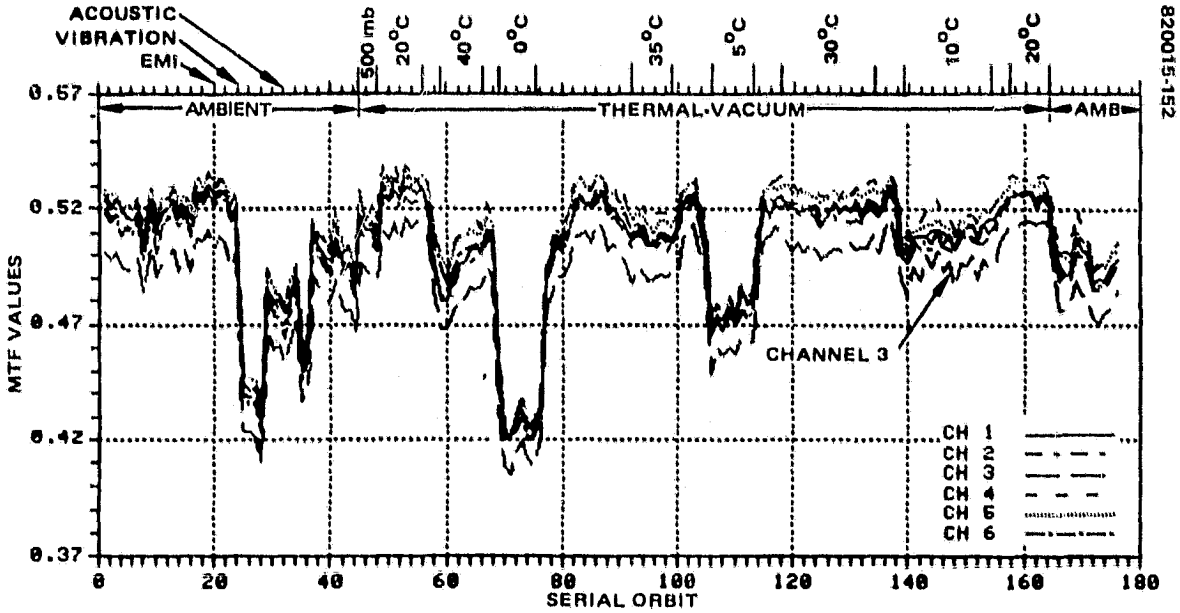

a) BAND 1

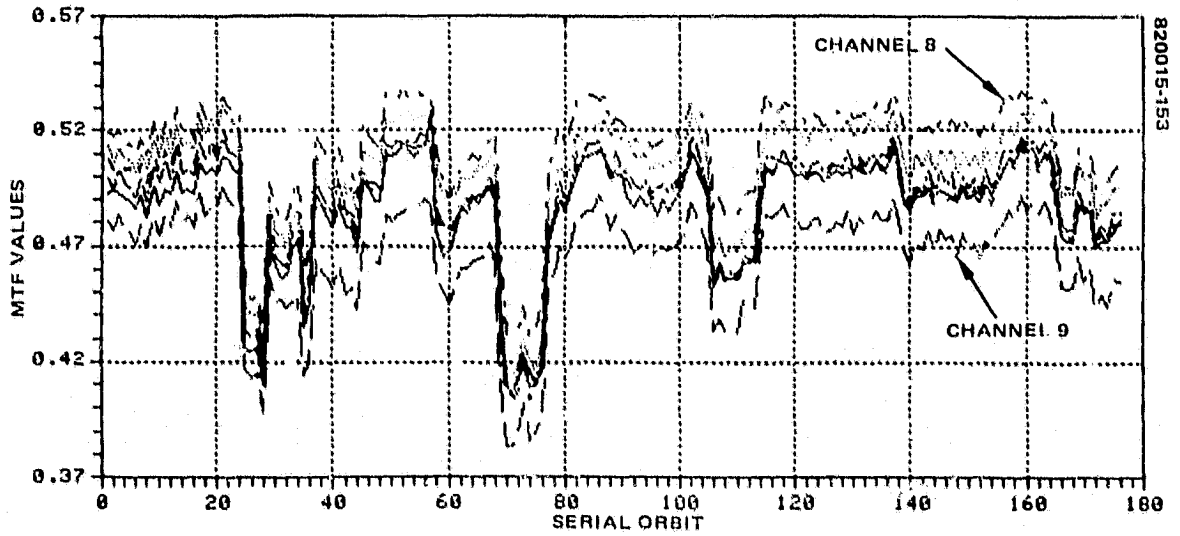

b) BAND 2

FIGURE 7-27. PROTOFLIGHT MTF PERFORMANCE

ORIGINAL PAGE IS
OF POOR QUALITY

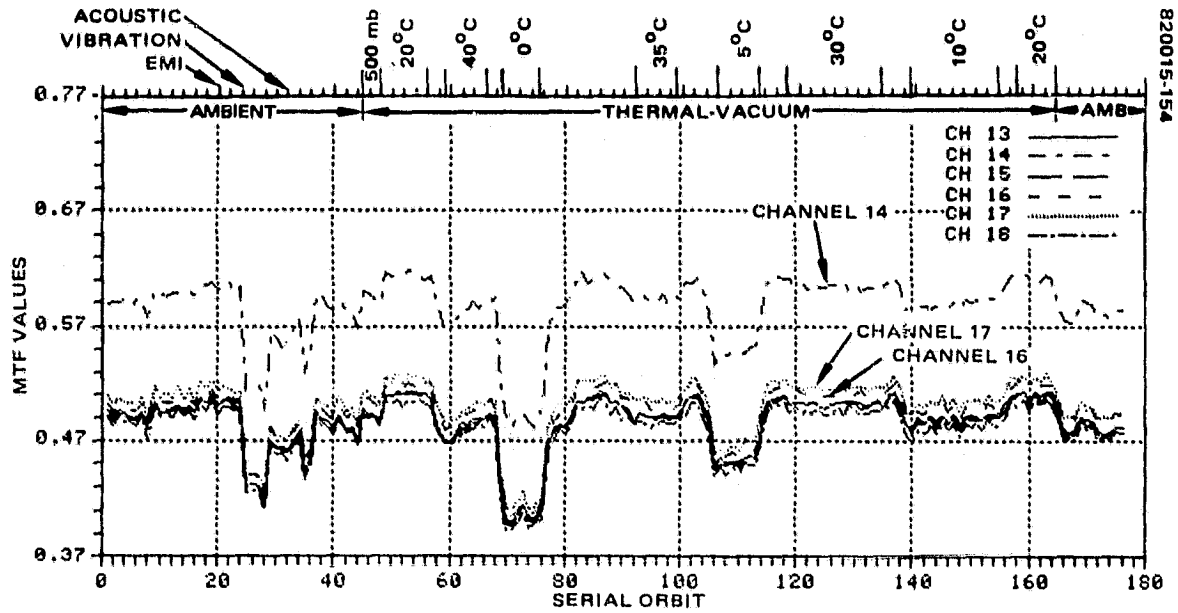

c) BAND 3

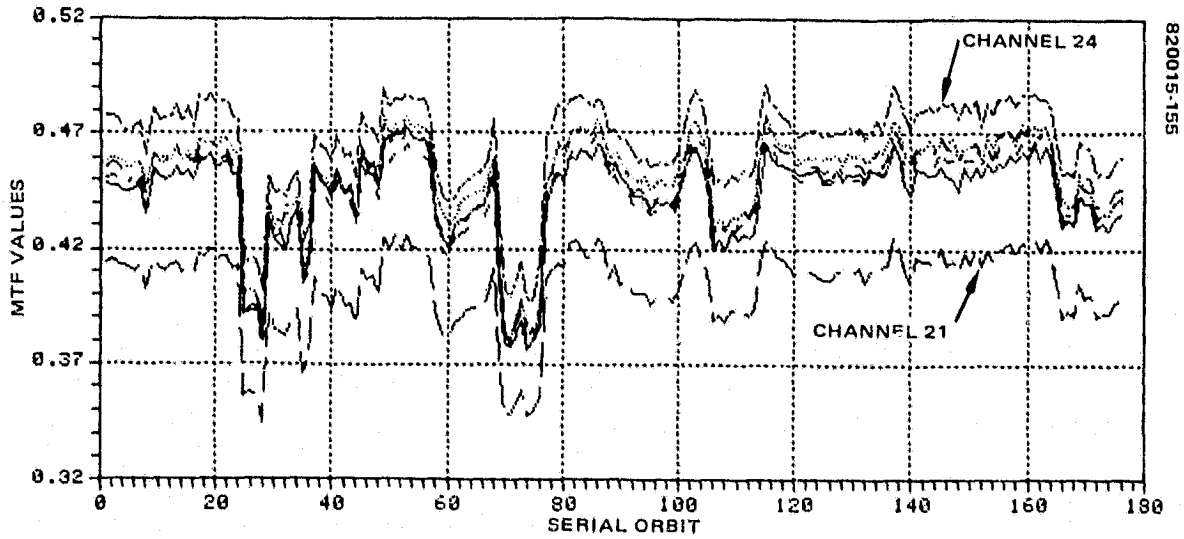

d) BAND 4

FIGURE 7-27 (CONTINUED). PROTOFLIGHT MTF PERFORMANCE

ORIGINAL PAGE IS
OF POOR QUALITY

recognition that MTF changes affecting all of the bands were correlated to the occurrence of this procedure and seemed to be absent from data taken during thermal-vacuum testing, during which the collimator focus is not adjusted. It is supported as well by the events which occurred following vibration testing and prior to thermal-vacuum testing (serial orbits 25 through 44).

The MTFs measured immediately following vibration testing (serial orbits 25 through 28) were performed on the C7 endbell and were 15 percent to 18 percent lower in all bands from those measured earlier. In spite of this drop in MTF, only channel 21, which is anomalously low in band 4, dropped below the specified value of 0.36 (see Figure 7-27d). It was during this endbell test that the line-length variation went well out of specification and subsequent STRs and engineering investigations revealed that the flex pivot was broken (see 7.6.2).

Following flex pivot replacement, preacoustic and postacoustic ASPTs were run, each preceded by collimator alignment and focussing. The MTFs for these orbits (serial orbits 29 through 36) had increased from the post vibration values but were still significantly lower than those measured in early testing. A series of STRs was run to examine collimator focus and alignment. It was discovered that the collimator was badly misaligned and defocussed. In the process of being moved from the vibration test area to the C7 vacuum chamber (for thermal-vacuum endbell test during which the broken flex pivot was discovered), the collimator had been tipped over one of its legs and bumped sufficiently hard to severely disturb the prior focus and alignment. Subsequent investigations revealed that one of the clamps holding the MTF reticle had been bent as well. The reticle assembly was repaired and installed. The MTF improved in the following pre-endbell/endbell tests to values which are within 2 percent to 4 percent of those measured during post EMI. These values are used here as a baseline for comparison of subsequent system MTF behavior.

Comparison of endbell (ambient pressure, 25°C) MTF values to thermal vacuum 20°C values seems to indicate that the system MTF is pressure (vacuum) sensitive. The MTF for these cases show an increase of 3 percent to 7 percent which cannot be attributed to the temperature difference. Using the MTF versus temperature plot (Figure 7-28) developed from thermal-vacuum data, the 5°C drop in temperature should result in an MTF decrease of about 1 percent. Removing the temperature dependence leaves a 4 percent to 8 percent increase in MTF as a result of pressure change. Vacuum shift of MTF was observed in earlier scanners, e.g. MSS-3. A corresponding decrease in MTF is evidenced in returning to ambient pressure.

The MTF behavior during thermal-vacuum testing is characterized in Figure 7-28. These plots indicate that the system is focussed near 20°C. As indicated, the nominal band performance is given for all channels in the band with the exception of band 3, where channel 14 is excluded from the nominal group and in band 4, where channel 21 is excluded. The MTFs for these channels are plotted separately. Channel 9, which did appear to be anomalously lower from its band numbers, is balanced by channel 8 (see Figure 7-27b) and is included in the nominal for band 2. The individual MTFs for channels 8 and 9 are plotted in the figure to show that their values fall within the overall system MTFs.

ORIGINAL PAGE IS
OF POOR QUALITY

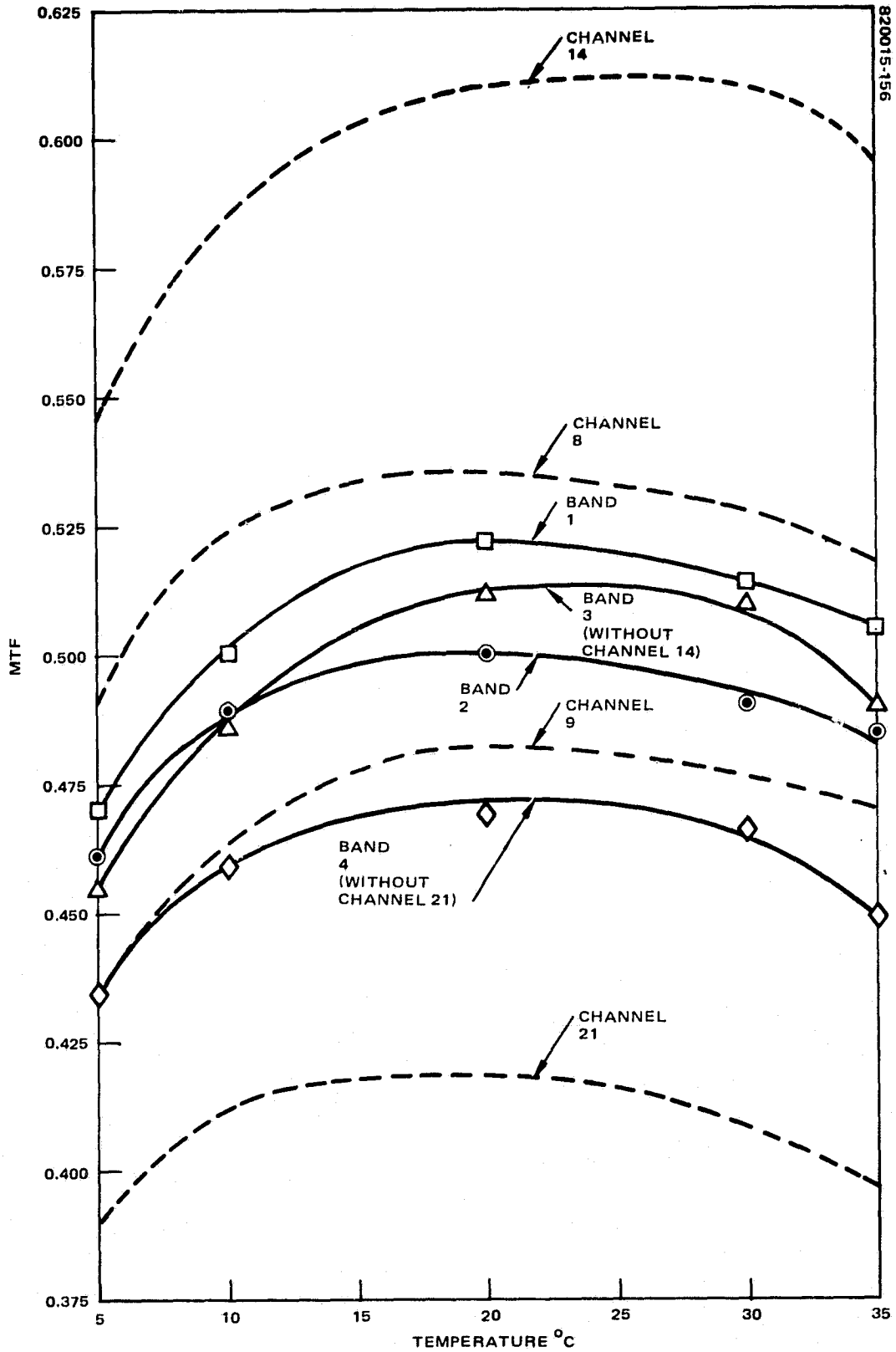

FIGURE 7-28. PROTOFLIGHT NOMINAL MTF VERSUS TEMPERATURE

ORIGINAL PAGE IS
OF POOR QUALITY

A comparison of prethermal-vacuum (baseline) MTF values with post-thermal-vacuum values indicates a rather stable MTF, as does the data taken at the various temperature plateaus while the system was in thermal-vacuum testing. Thus there was no adverse effect on the system MTFs resulting from thermal-vacuum exposure.

7.5.3.2 Anomalous Behavior

The individual channel history plots for bands 3 and 4 (Figures 7-27c and d) indicate that channels 14 and 21 have MTFs which are significantly different in value from other channels in their respective bands. Moreover, the MTF versus temperature plot (Figure 7-28) shows clearly that channel 14 has an MTF much higher than all other channels, and that channel 21 has an MTF much lower than all other channels. Compared to the nominal channels in band 3, channel 14 has an MTF approximately 18 percent higher. Channel 21 has an MTF approximately 10 percent lower than the nominal channels in band 4. The behavior of the MTFs for these channels as a function of test environment is otherwise quite normal compared to the other channels in their respective bands.

The MTFs for these channels could have been changed to bring them more in line with the values of the other channels by careful selection of values of the trim capacitor in the buffer board which controls the location of one pole of the Butterworth filter. This change was subsequently made at General Electric for channel 14, and the installed trim capacitor was found to be open. The substitution brought the channel 14 MTF in line with the MTF of the other channels in band 3.

7.5.3.3 Summary

Table 7-16 gives a chronology of MTF performances of MSS-D protoflight. Each band is listed in terms of the nominal performance of the channels in that band. Anomalous channels 14 and 21 are listed separately. As indicated, the overall system MTF performance meets specification and is acceptable.

7.6 SCAN PRECISION PARAMETERS

7.6.1 Introduction

The parameters used to evaluate the MSS-D scan precision performance are mean line length, line length variation, scan repeatability, and cross-axis repeatability. A discussion of the meaning of these parameters and a description of the algorithms used to compute their values measured during testing are given in 6.4.4 and 6.4.5.

In this section the scan precision performance of the MSS-D protoflight throughout system testing is presented. Each parameter is treated in terms of the effect on the MSS-D protoflight system of the test environment. A summary description is given of nominal performance, deviation from nominal behavior, data variability, and estimated effects of the test environment. Anomalous behavior is highlighted and, where possible, its probable cause discussed.

TABLE 7-16. PROTOFLIGHT MTF MEASUREMENT HISTORY

Date	Test Event (Remarks)	Nominal MTF				Errant Channels MTF Range		MTF Range			
		Band 1	Band 2	Band 3 Without Channel 14	Band 4 Without Channel 21	Channel 14	Channel 21	Band 1	Band 2	Band 3 Without Channel 14	Band 4 Without Channel 21
11/18/81	First LFPT at SBRC, orbits 1 to 8, nominal temperature 22°C	0.515	0.500	0.491	0.460	0.580 to 0.590	0.404 to 0.415	0.485 to 0.527	0.470 to 0.520	0.470 to 0.510	0.432 to 0.460
1/15/81; 1/16/81; 1/24/81; 1/26/81	Pre-EMI tests Orbits 25 to 38, nominal temperatue 24°C	0.515	0.503	0.508	0.465	0.594 to 0.610	0.410 to 0.420	0.490 to 0.540	0.475 to 0.535	0.490 to 0.520	0.450 to 0.488
2/02/81	Post-EMI (previbration); orbits 52 to 55, nominal temperature 23°C	0.515	0.510	0.508	0.460	0.597 to 0.610	0.412 to 0.415	0.492 to 0.531	0.485 to 0.536	0.493 to 0.515	0.451 to 0.485
2/16/81	While collimator was being moved to the C-7 chamber, it tipped over on one leg, which disturbed the prior alignment and focus.										
2/18/81	Attempted to realign and refocus collimator										
2/28/81	Postvibration; orbits 73 to 76, nominal temperature 25°C	0.427	0.425	0.415	0.390	0.499 to 0.515	0.346 to 0.358	0.412 to 0.450	0.400 to 0.450	0.411 to 0.440	0.376 to 0.415
3/2/81	STE 34 was performed to improve MTF										
3/06/81	Flex pivot broken										
3/20/81	Visible MTF reticle wheel assembly sent to SBRC for repair. Reticle clamp bent.										
4/15/81	Optical alignment done after reassembly of scanner post flex pivot changeout										
4/20/81	Preacoustic orbits 83 to 86, nominal temperature 25°C	0.475	0.470	0.470	0.436	0.550 to 0.565	0.385 to 0.390	0.453 to 0.490	0.441 to 0.434	0.451 to 0.485	0.416 to 0.450
4/27/81	Scanner alignment done										
4/28/81	Postacoustic orbits 89 and 90, 25°C	0.480	0.480	0.475	0.440	0.562 to 0.576	0.386 to 0.391	0.463 to 0.491	0.448 to 0.499	0.472 to 0.486	0.435 to 0.451
	Postacoustics orbits 91 and 92, 26°C	0.450	0.440	0.450	0.415	0.530 to 0.549	0.365 to 0.373	0.436 to 0.462	0.413 to 0.470	0.436 to 0.460	0.404 to 0.430
4/28/81	Realigned reticle with optical axis and refocussed on plane mirror.										

ORIGINAL PAGE IS OF POOR QUALITY

Table 7-16 (continued)

Date	Test Event (Remarks)	Nominal MTF				Errant Channels MTF Range		MTF Range			
		Band 1	Band 2	Band 3 Without Channel 14	Band 4 Without Channel 21	Channel 14	Channel 21	Band 1	Band 2	Band 3 Without Channel 14	Band 4 Without Channel 21
5/04/81	Pre-Endbell (baseline) orbits 99 to 102, 25°C	0.500	0.490	0.486	0.450	0.585 to 0.598	0.395 to 0.409	0.476 to 0.515	0.476 to 0.520	0.475 to 0.508	0.439 to 0.470
5/08/81	Endbell (on floor) orbits 105 to 108; nominal temperature 24°C	0.490	0.487	0.485	0.440	0.570 to 0.590	0.389 to 0.402	0.465 to 0.515	0.467 to 0.514	0.466 to 0.510	0.427 to 0.471
5/09/81	GN_2 backfill orbits 109 to 112 nominal temperature 25°C	0.510	0.485	0.500	0.460	0.590 to 0.600	0.400 to 0.410	0.488 to 0.526	0.461 to 0.525	0.485 to 0.515	0.440 to 0.476
5/10/81	Thermal vacuum; 20°C	0.522	0.500	0.512	0.470	0.610 to 0.610	0.417 to 0.426	0.510 to 0.535	0.432 to 0.537	0.500 to 0.520	0.460 to 0.483
5/14/81	35°C	0.510	0.485	0.490	0.449	0.586 to 0.596	0.397 to 0.401	0.490 to 0.515	0.470 to 0.515	0.485 to 0.508	0.440 to 0.460
5/15/81	5°C	0.470	0.460	0.455	0.435	0.536 to 0.545	0.390 to 0.395	0.460 to 0.475	0.435 to 0.485	0.440 to 0.460	0.417 to 0.450
5/16/81	30°C	0.514	0.490	0.510	0.467	0.601 to 0.610	0.411 to 0.415				
5/17/81	10°C	0.500	0.488	0.488	0.460	0.585 to 0.590	0.415 to 0.417	0.485 to 0.513	0.465 to 0.520	0.473 to 0.495	0.445 to 0.477
5/19/81	20°C	0.522	0.500	0.512	0.470	0.610 to 0.610	0.420 to 0.425	0.510 to 0.535	0.482 to 0.537	0.500 to 0.520	0.460 to 0.483
5/20/81	Post-television orbits 235 to 238 nominal temperature 26°C	0.490	0.485	0.485	0.440	0.574 to 0.586	0.390 to 0.408	0.476 to 0.520	0.451 to 0.512	0.470 to 0.508	0.430 to 0.465
5/26/81	Final LFPT orbits 246 to 253 nominal temperature 25°C	0.490	0.490	0.486	0.440	0.576 to 0.591	0.390 to 0.402	0.473 to 0.524	0.474 to 0.512	0.470 to 0.501	0.426 to 0.465

ORIGINAL PAGE IS OF POOR QUALITY

ORIGINAL PAGE IS OF POOR QUALITY

7.6.2 Mean Line Length (MLL)

The MLL or, more accurately, the mean active scan period is not directly the subject of a system specification. It is indirectly specified, however, by the requirement that the active scan period for each of the individual scans of the 100 scans used in constructing this average (mean) value lies within the interval from 31.5 to 34.0 ms. To ensure that the performance of the scanner is monitored to determine that the scanner has met this specification, the maximum scan period, LL_{MAX}, and the minimum scan period, LL_{MIN}, were displayed in the computer printouts and checked to determine if they fell within the specified limits. The specification is met if 31.5 ms $\leq LL_{MIN}$ and $LL_{MAX} \leq$ 34 ms. The mean line length falls between LL_{MAX} and LL_{MIN}. It is necessary, but clearly not sufficient, for meeting the specification that the MLL fall within the specified interval.

The plot in Figure 7-29 provides the values of MLL obtained during the testing of the MSS-D protoflight. The specification values of LL_{MAX} and LL_{MIN} lie outside the range of values represented on the graph. Since during testing the line length values differed at most in the second decimal place, it is clear from Figure 7-29 that the maximum and minimum values did not exceed the specification values.

The entire range of variation of the MLL is only slightly greater than 1 percent. Its variation at any given environment is less than 0.2 percent. From the plot it is apparent that the MLL behavior is negatively correlated with temperature, having its largest values at 0°C and smallest at 40°C. This fact can be seen not only at the stable temperature plateaus but also in the calibration steps from 0° to 35°C (serial orbits 72

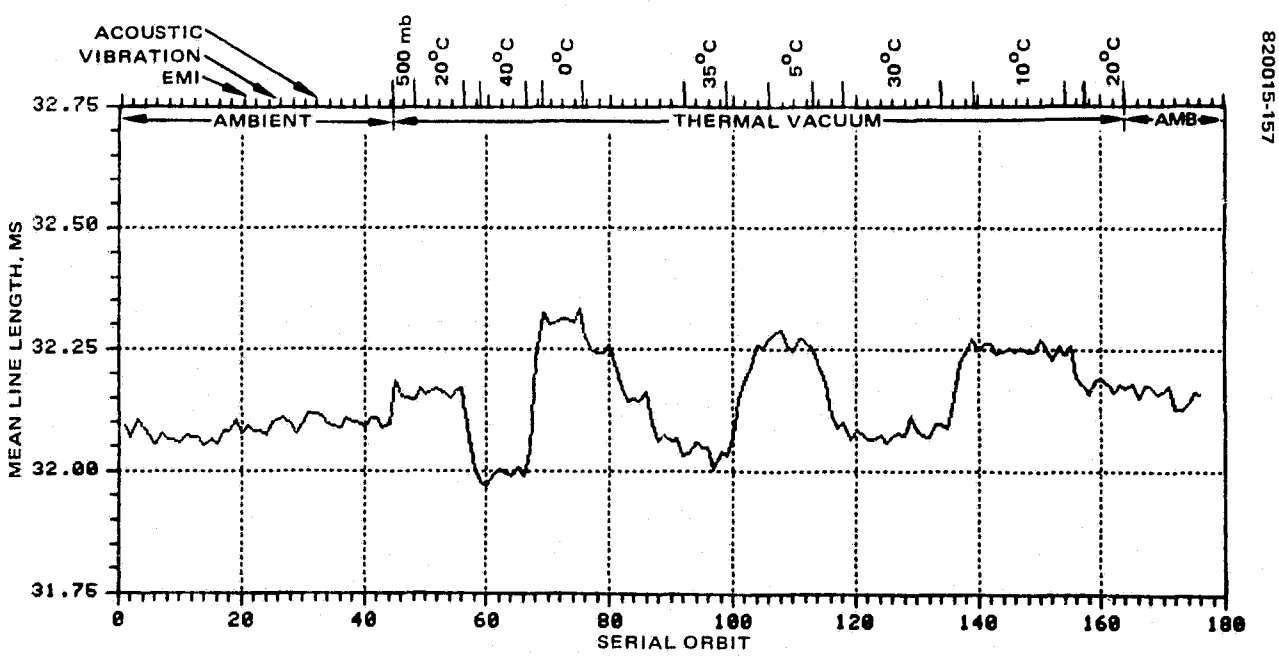

FIGURE 7-29. PROTOFLIGHT MEAN LINE LENGTH

ORIGINAL PAGE IS
OF POOR QUALITY

through 92). The value of MLL goes from 31.95 at 40° to 32.32 at 0°C. Repeatability on return to temperature is within normal data variability.

The temperature correlation of the MLL is consistent with an effect of temperature on bumper coefficient-of-restitution and its concomitant overall effect on scanner "spring constant." That is, as the temperature lowers, the bumper turnaround becomes quicker. Then, since the total round trip of the scan mirror is held constant by the loop dynamics, the active scan titution and its concomitant overall effect on scanner "spring constant." That is, as the temperature lowers, the bumper becomes quicker. Then, since the total round trip of the scan mirror is held constant by the loop dynamics, the active scan period is diminished to account for the quicker (short time spent) turn-around times.

In summary, the MLL performance of the MSS-D protoflight was predictable and well within specification.

7.6.3 Line Length Variation (VLL)

The line length (or, more accurately, active scan period) variation is a measure of the rms scan-to-scan variation in the active scan period. The algorithm used to describe this parameter is given in 6.4.4. Since in the definition VLL is normalized by the mean line length and since VLL is a function defined on the same parameter values as the MLL, the values of these parameters are related. Since the MLL varies only slightly, as was shown in the previous section, the effect on VLL of MLL changes was minimal for the MSS-D protoflight.

The history of MS-D protoflight VLL performance is shown in Figure 7-30. The plot gives VLL performance for the standard orbits shown throughout system testing. The large spike that occurs at serial orbits 25 through 28 (sequential orbits 73 through 76) represents measurements made during the postvibration short form performance tests on the endbell when the system was being prepared to enter thermal-vacuum testing. The

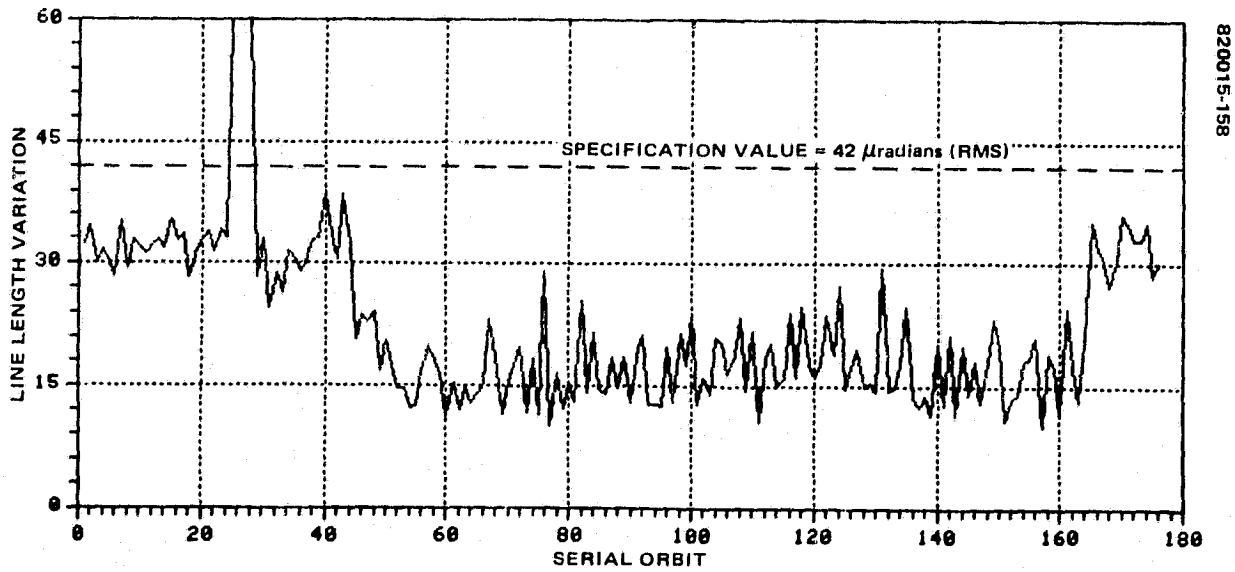

FIGURE 7-30. PROTOFLIGHT VLL PERFORMANCE

ORIGINAL PAGE IS
OF POOR QUALITY

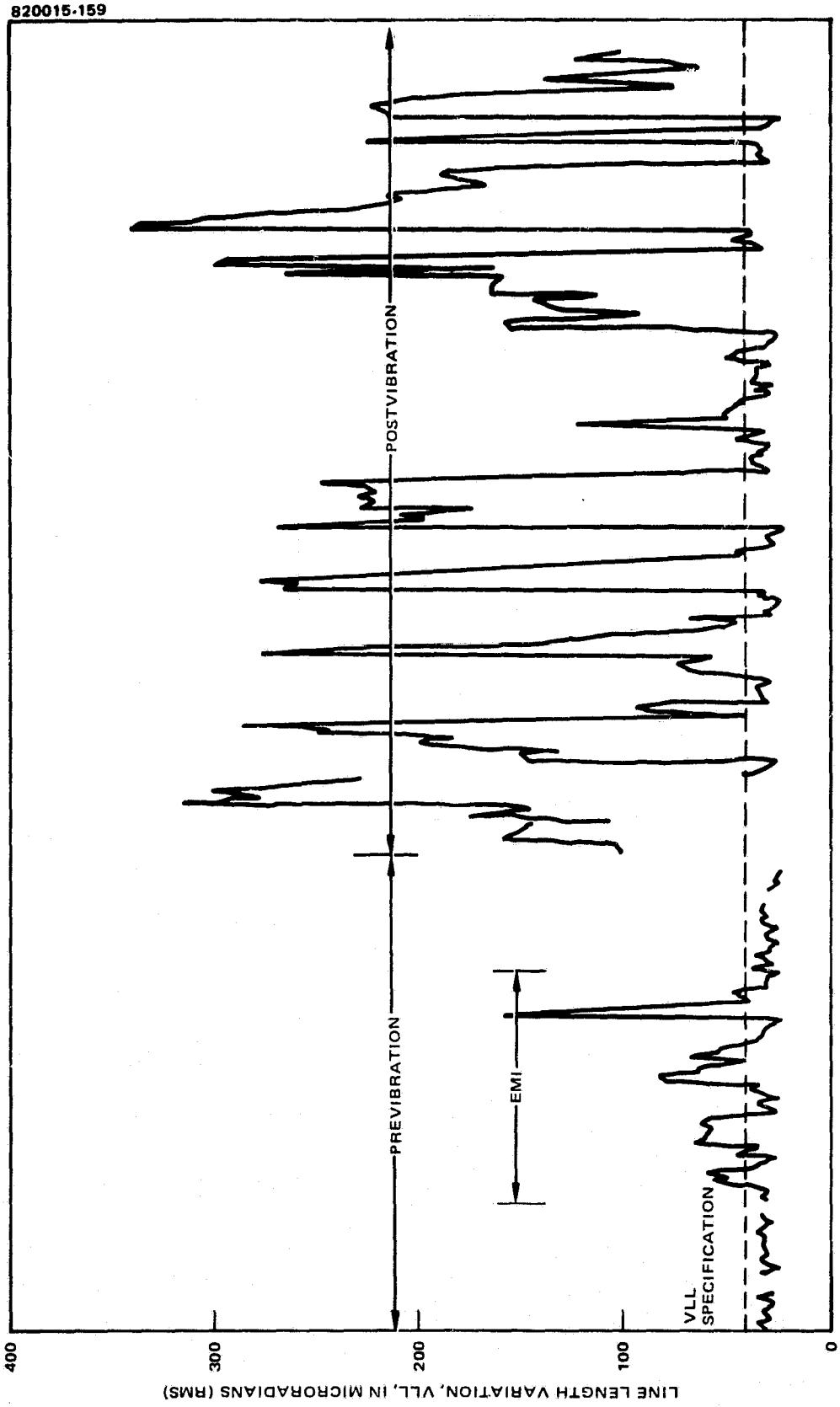

FIGURE 7-31. PROTOFLIGHT VLL PERFORMANCE (PRE/POST VIBRATION)

excessive values obtained, their persistence over a few orbits, and the failure to immediately identify any processing, or test equipment or procedure related causes resulted in a series of investigations and special tests to determine the source of the problem.

Some initial STRs were implemented to determine if the cause was related to test configuration and/or test vibration environment. In parallel with this effort the VLL test history was carefully reviewed.

The history of line length variation was obtained from the history tape for the period covering the system ambient performance tests (SAPT) conducted at SBRC on 18 November 1980 to the final postvibration STR's performance at El Segundo on 5 March 1981.

This period spans the sequential orbits 1 through 76. These data along with the STR data are plotted in Figure 7-31 in historical sequence. The specification value for the line length variation (VLL = 42 rad) is plotted for comparison. As is evident from the Figure 7-31, the VLL remained well within the specified value for all orbits and STRs except those performed during EMI testing (prior to vibration) and during postvibration. With the exception of the two data points (which result in the large spikes near the end of EMI) and a few other exceptions, the value of VLL remained below 75. More than 56 percent of the data points taken during EMI were within specification.

In comparison, only 29.6 percent of the measurements plotted in Figure 7-31 remained within the specified range in the postvibration period. Moreover, the amplitude of the plot exceeds the value of 200 many times and even met or exceeded a value of 300 on several occasions.

This plot strongly suggested that something rather drastic had happened during vibration. This is evident especially when it is observed that the specification violations of VLL which occurred during EMI were induced by system EMI susceptibility. (The sensitivity of line length variation measurements to electromagnetic noise inputs was used as a secondary measure of system susceptibility.) Thus, there had been no serious concern over VLL performance until the abbreviated system performance test (orbits 73 through 76) was conducted on the thermal-vacuum chamber endbell.

This was the first sequence of tests run following vibration, and the values obtained indicated a problem with either the MSS-D system or the test configuration. A series of special test runs were made to determine whether external vibration noise was entering the test setup. The vibration isolation cage ("shark cage") was clamped and unclamped, and various other attempts were made to determine whether the system was susceptible to various levels of isolation. No correlation was found between these test configuration changes and measured VLL performance.

Over the following 2 days several special tests were performed to determine if the problem was in the electronics. VLL data were collected throughout the period as well. When these tests eliminated the possibility of an electronic problem, it was decided to make a "hands-on" inspection of the mechanical condition of the scan mirror assembly. This inspection revealed a broken flex pivot.

It is remarkable that the system continued to return to "in-spec" operation from time to time even after a flex pivot was broken in several places. This behavior indicates that VLL performance cannot be used (exclusively) to assure flex pivot health or

condition. It is quite possible that a cracked flex pivot might successfully pass all VLL measurement tests, and that a broken flex pivot might escape detection through VLL measurement if these data are taken no more frequently than that provided by an orbital duty cycle.

Following the replacement of the broken flex pivots, the MSS-D protoflight scanner was subjected to an acoustic test and limited sinusoidal vibration testing. The remainder of performance with these flex pivots is shown in Figure 7-30. As indicated in the figure, the VLL is sensitive to changes in the ambient pressure environment. On the floor prior to endbell installation, the VLL value was approximately 30 μrad with local deviations of ±3 μrad. Once installed on the endbell and prior to initial GN_2 backfill, the VLL value increased to 35 ±4 μrad. This was probably due to a change in the test configuration vibration environment. On backfill with gaseous nitrogen (GN_2) to a pressure of 0.5 atmosphere the VLL dropped to approximately 22.5 ±1.5 μrad. On further decrease in presssure during pumpdown to 10^{-5} Torr, the VLL dropped to approximately 18 μrad. The change of VLL as a result of pressure environment is attributed to the effects of turbulent wind loading on the scanning mirror, and the absence of this effect in vacuum. It should be noted that on venting to ambient pressure following the completion of thermal-vacuum testing, the VLL returned to the value measured prior to thermal-vacuum testing.

During thermal-vacuum testing the VLL was consistently within specification and varied from 10 to 25μrad, with occasional values as high as 29 μrad.

7.6.4 Scan Repeatability (SRO)

Scan repeatability is a parameter used to measure the ability of the scanner to repeatably (line-to-line) map the along-scan position of a target in the scanner field of view. The time variation (scan-to-scan), after scaling out line length variation, in the measured value of the time from scan start, SMP 1, to a target (collimator generated video pulse) in the scanner field of view is used to make this estimate. The measurement is specified to be less than or equal to 24μrad. The algorithm used to compute SRO during MSS-D protoflight testing is discussed in 6.4.4.

The SRO performance of the MSS-D protoflight Scanners is shown in Figure 7-32. Even during endbell short form performance testing following the flex pivot failure, the SRO remained within specification. The only time the SRO exhibited any anomalous behavior was during the STRs performed immediately following the VLL specification violations (discussed in 7.6-3). During these tests, the SRO only rarely exhibited out-of-specification behavior.

The measured values of SRO for MSS-D protoflight were well within specification, nominally 3 to 9 μrad with occasional values from 9 to 13 μrad.

7.6.5 Cross-Axis Repeatability (CXAXO)

The cross-axis repeatability algorithm and method of measuring the cross-axis position using the chevron pattern are discussed in 6.4.5. Cross-axis repeatability is specified to be less than or equal to 33 μrad.

ORIGINAL PAGE IS
OF POOR QUALITY

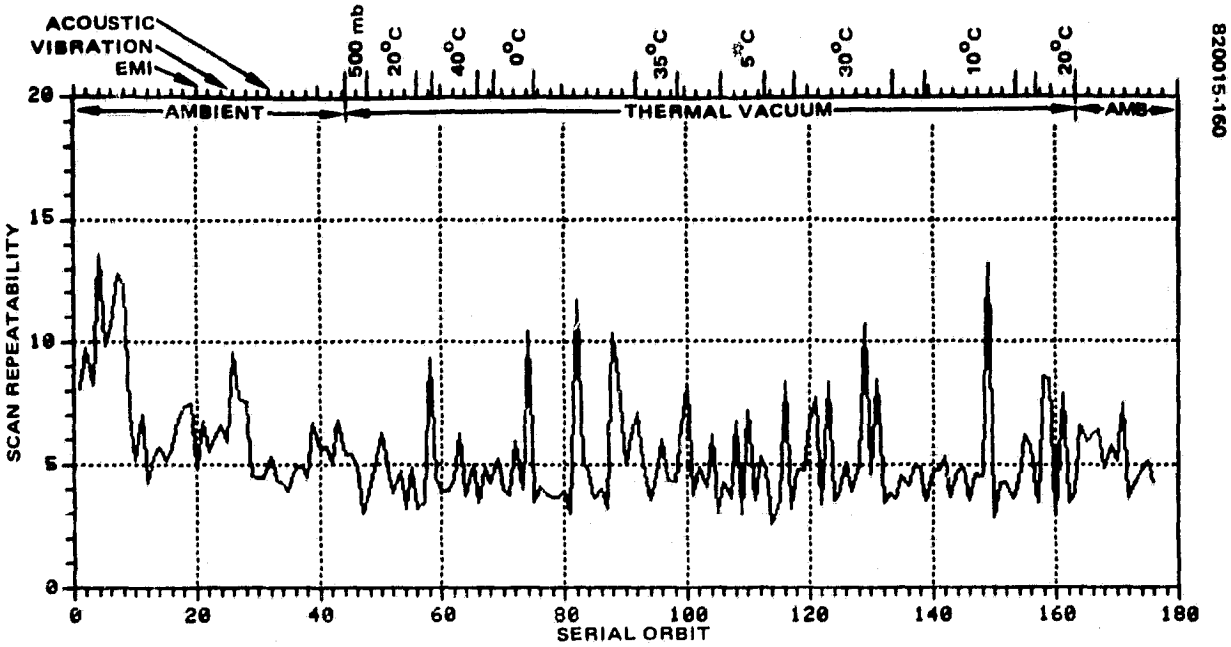

FIGURE 7-32. PROTOFLIGHT SCAN REPEATABILITY PERFORMANCE

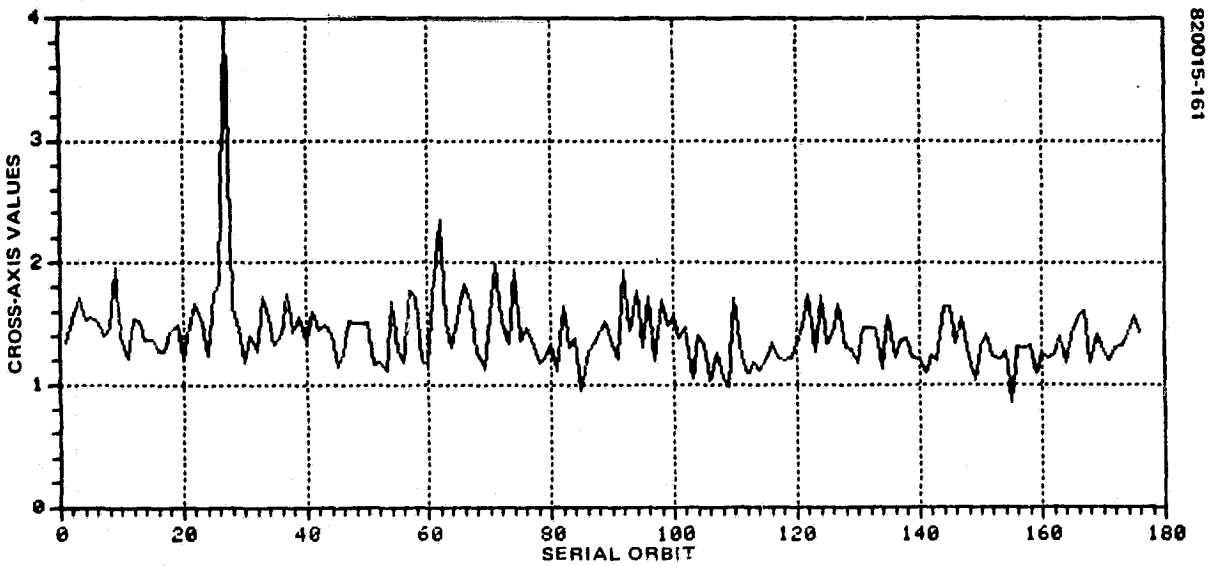

FIGURE 7-33. PROTOFLIGHT CROSS-AXIS REPEATABILITY PERFORMANCE

During MSS-D protoflight testing the cross-axis performance was always well within specification. As shown in Figure 7-33 this parameter was consistently less than 2 μrad. The single exception to this performance was observed during the ASPT on the endbell following vibration testing, i.e., following flex pivot failure. No out-of-specification values were observed in CXAXO throughout MSS-D protoflight testing.

8. PROTOFLIGHT PICTURE ANALYSIS

End-to-end evaluation of the MSS flight subsystem and ground equipment was performed by photographic reproduction of images viewed by the flight equipment. Two types of images were produced during the test program for evaluation purposes, the video processor image recorder (VPIR) pictures and the ground processing equipment (GPE) pictures.

The VPIR pictures, made with the video processor (VP) working in conjunction with the image recorder (IR), were reproduced in near real time for quick look qualitative assessment of general system performance. Since the VPIR does not reproduce the data in an operational band-by-band format, its use was diagnostic, and the flight subsystem performance assessment was confined to the GPE pictures.

The VPIR pictures were very useful in surfacing system problems in a timely manner and in troubleshooting these problems. In particular, microphonics, intensity variations, and channel-to-channel gain variations were enhanced by the VPIR picture presentations. Anomalies associated with scan monitor pulses and line synchronization problems were also diagnosed using VPIR pictures.

The ground processing equipment produces images in a manner similar to that of the operational system. These pictures were the primary tool for assessing overall system performance. The pictures were made under conditions chosen to enhance undesirable interference characteristics which may detract from the scene information. High gain, compression mode, and low light level conditions were thus chosen to overemphasize interference. In addition, the images were produced from the flooding lamp and the collimator simultaneously to provide in-focus detail as well as broad areas of near uniform gray scenes.

8.1 GROUND PROCESSING EQUIPMENT

The GPE reads and processes multispectral scanner data that have been stored on magnetic tape. These data are converted into photographic images for analysis of MSS performance. The simplified block diagram, Figure 8-1, shows how the various units

ORIGINAL PAGE IS
OF POOR QUALITY

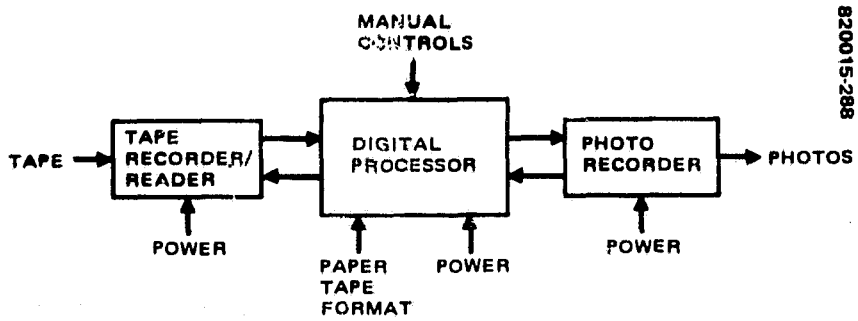

FIGURE 8-1. GROUND PROCESSING EQUIPMENT BLOCK DIAGRAM

of the GPE are functionally related to each other. The GPE units are illustrated in Figure 8-2 and briefly described below:

1) Tape Recorder/Reader

The tape recorder reads 25 channels (tracks) of prerecorded multispectral digital data into the digital processor. The tape recorder receives a tape speed sync signal (servo reference) from the digital processor.

2) Digital Processor

The digital processor converts the output of the tape recorder to a video signal for recording by the photo recorder and provides all necessary timing signals. It also supplies alphanumeric character generators for annotation and a reference grey scale for calibration.

3) Photo Recorder

The photo recorder is a Litton Datalog Pressfac 501-1H, consisting of a console and a rack mounted remote control panel. The photo recorder converts the analog video output of the digital processor into photo transparencies (positive or negative) containing spectral images of each of four MSS spectral bands. The photo transparencies also contain annotation data.

8.1.1 Qualification Test Picture Content

Figure 8-3 shows picture content and the corresponding time-amplitude plot of typical video output from any one of six channels comprising the picture video. The figure represents the general pattern used throughout the qualification test program. Typically, the video level formed by the background lamp was approximately 0.6 volt out of 4.0 volt full scale near the left of the picture scene (beginning of scan), and after midscan sloped down to produce a dark area near the end of scan.

820015-289

ORIGINAL PAGE IS
OF POOR QUALITY

TAPE RECORDER

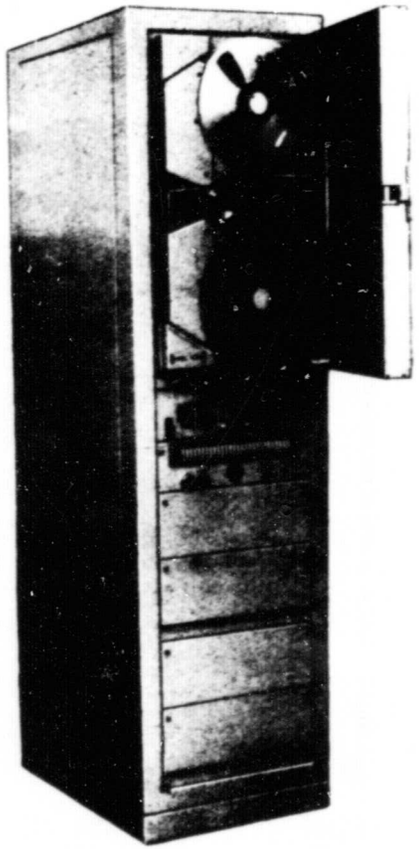

DIGITAL PROCESSOR

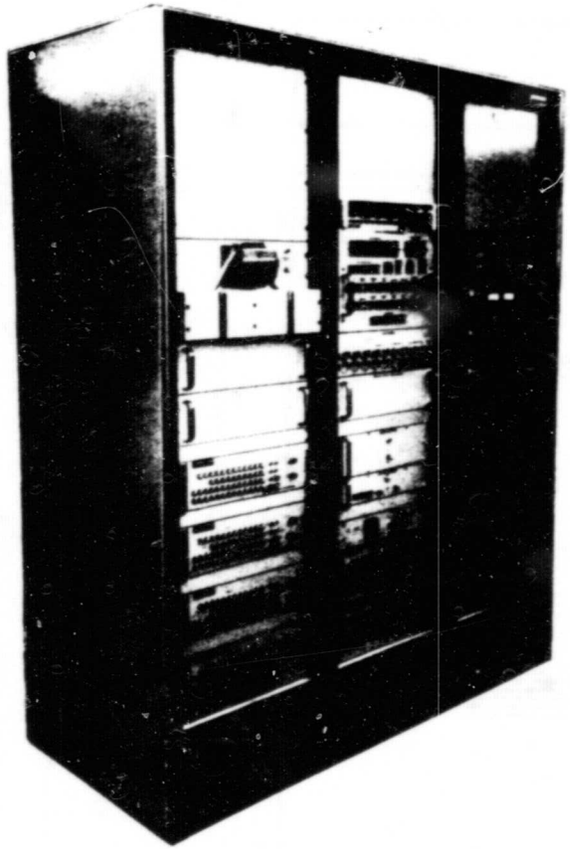

PHOTO RECORDER

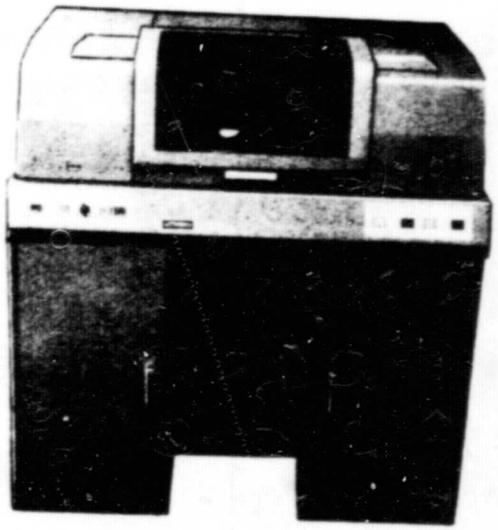

FIGURE 8-2. GROUND PROCESSING EQUIPMENT

ORIGINAL PAGE IS
OF POOR QUALITY

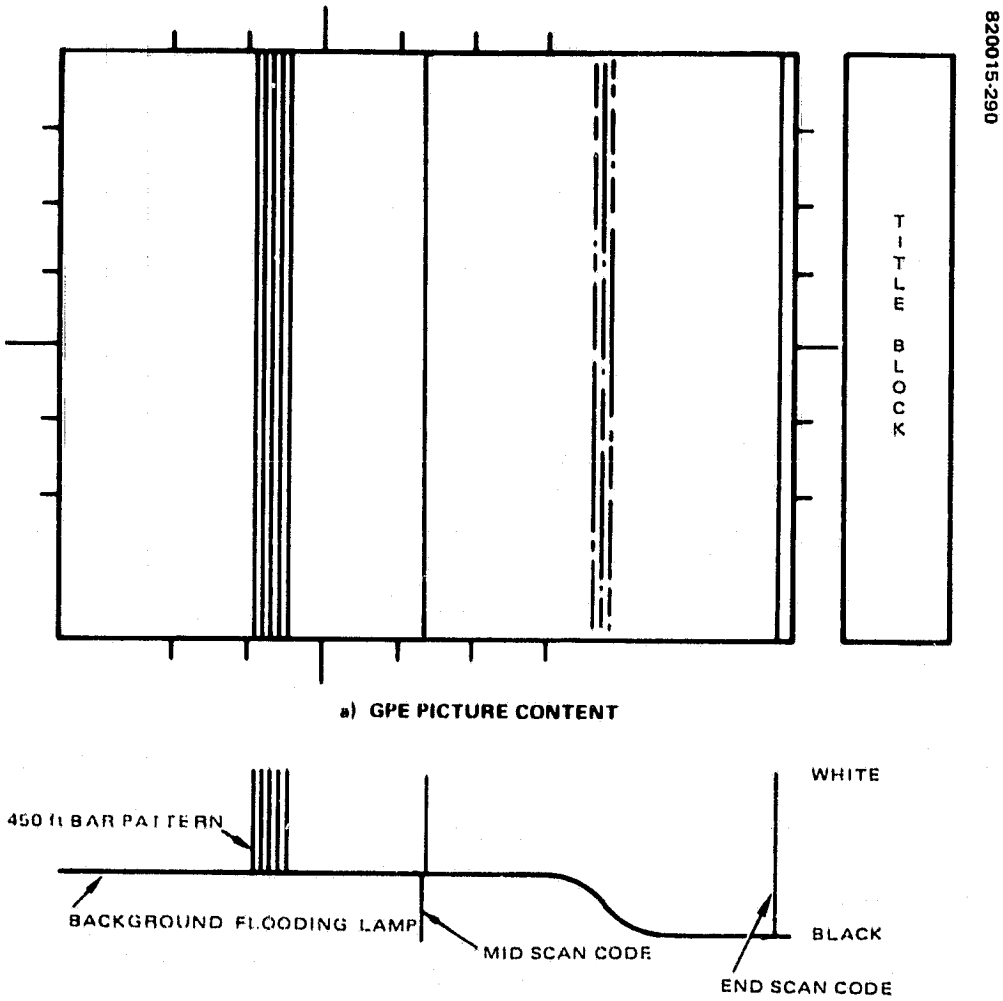

FIGURE 8-3. GPE PICTURE CONTENT FROM QUALIFICATION TEST PATTERNS

ORIGINAL PAGE IS
OF POOR QUALITY

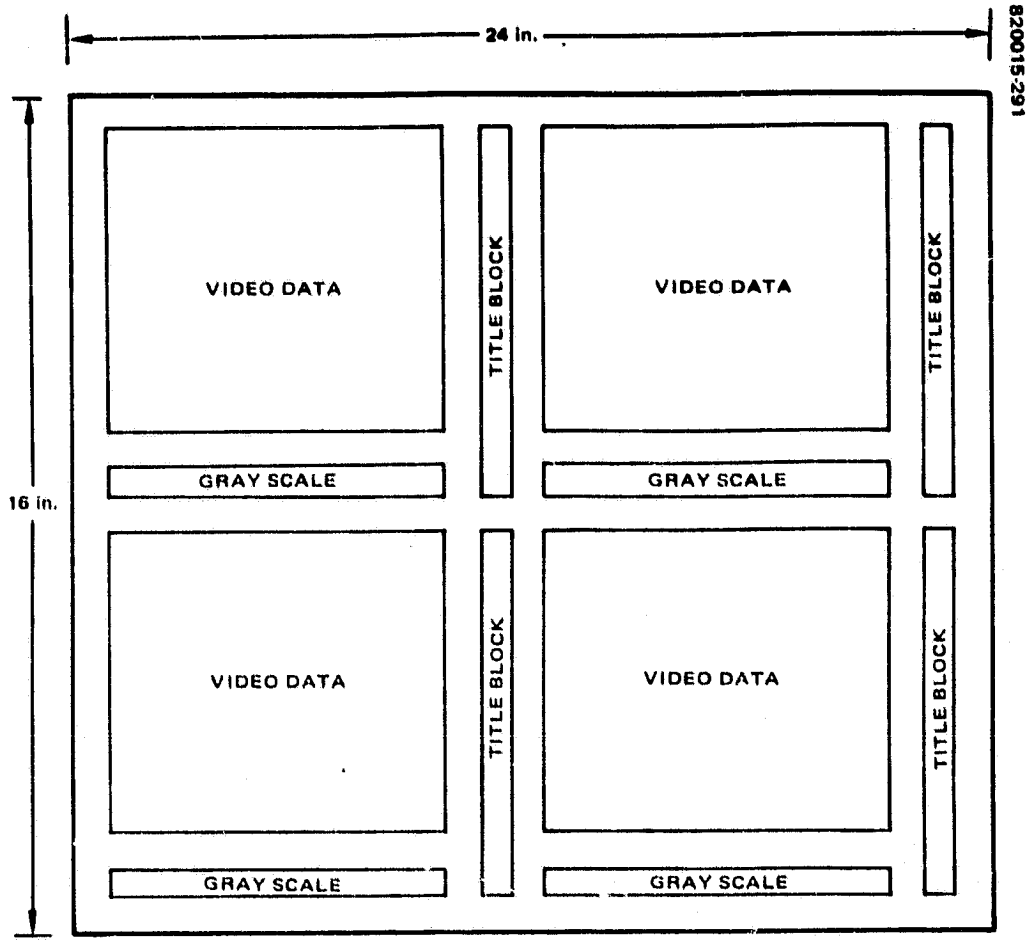

FIGURE 8-4. GROUND PROCESSOR PRINT FORMAT

The GPE picture format is shown in Figure 8-4, exhibiting four separate spectral band reproductions of the same scene. Format of a spectral band reproduction is shown in Figure 8-5. The picture quality is assessed in terms of the following phenomena:

1) Microphonics - Banding at right angles to the scan lines, occurring at regular intervals

2) Coherent noise - Noise observable under low power magnification, occurring at regular intervals

3) Woodgrain - A wave pattern caused by coherent noise, observable as a gross overall pattern covering large portions of a frame, and having the appearance of woodgrain

4) Random noise - Noise observable under low power magnification having no set frequency or pattern

ORIGINAL PAGE IS
OF POOR QUALITY

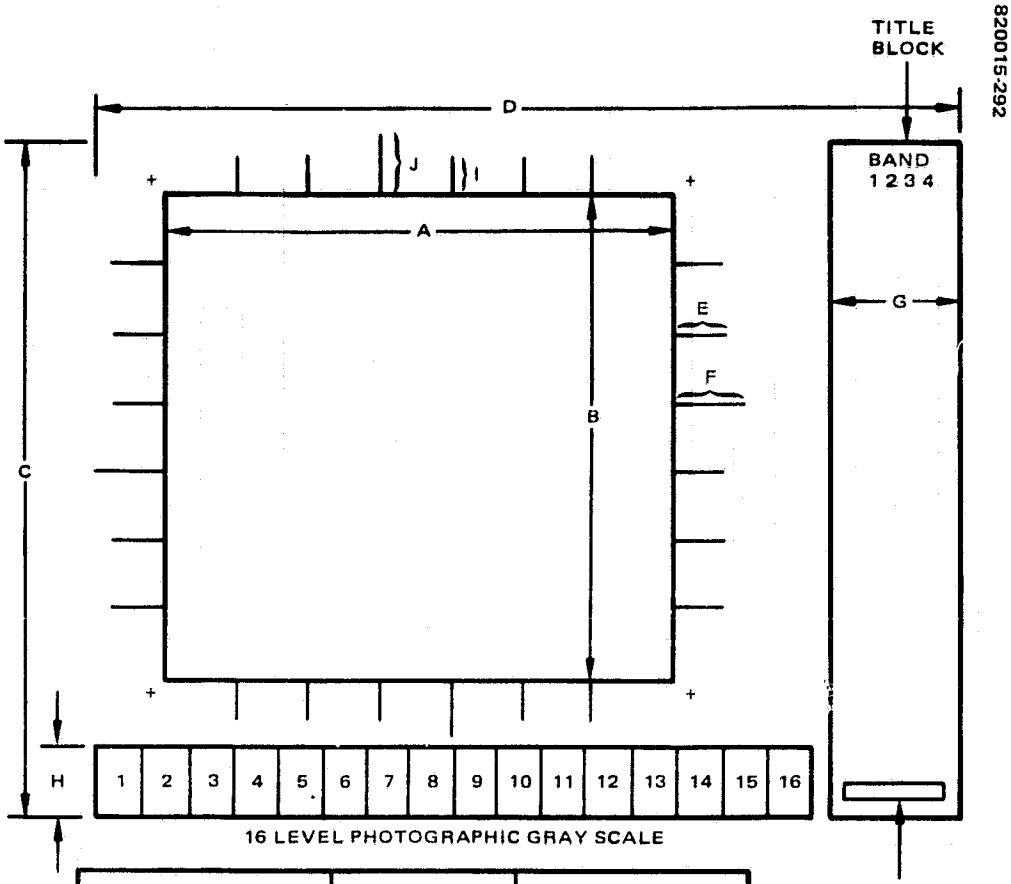

DIMENSIONS, in.	NUMBER OF LINES	NUMBER OF CYCLES
A = 7.393		2651
B = 7.291	2343	
C = 7.999	2574	
D = 9.000		3376
E = 0.089		32
F = 0.178		64
G = 1.017	365	
H = 0.336	105	
I = 0.087	28	
J = 0.186	60	

FIGURE 8-5. GPE INDIVIDUAL BAND PICTURE FORMAT

ORIGINAL PAGE IS
OF POOR QUALITY

5) Horizontal image jitter - Relative image displacement occuring parallel to direction of scan, resulting in breaks in image continuity

6) Stray light - Banding on each side of collimator target image caused by multiple reflections in test collimator

7) Collimator bar target washout - Occurs in band 2; caused by saturation of image highlights in compression high mode

8) Scan dropouts - Dropout of information within an individual scan line, usually occurs randomly within a frame

9) Scan line nonuniformity - Photographic density nonuniformity of scan lines caused by variations in sensor outputs; dependent on degree of video correction imposed to compensate for variations in sensor outputs

10) Time code error - Errors in time code pattern on the leading edge of each frame

11) Corona noise - Spike noise visible under low power magnification

8.1.2 Picture Quality Rating

An evaluation was performed on all GPE and VPIR pictures to detect any interference or anomaly which might detract from the information content of in-orbit scenes. Since large areas of the images were essentially void of any detail, even low level interference was readily detectable. The collimator image in the pictures allowed evaluation of the resolution and scanning stability of the MSS subsystem.

Evaluation of picture image quality is largely a subjective matter. A rating scale was developed for each of the interfering phenomena. Table 8-1 gives the meaning of levels 0 through 2 for each form of interference.

TABLE 8-1. GPE/VPIR PICTURE RATING SCALE

(Degree of interference caused by microphonics, random, woodgrain, and coherent noise)

Scale	Degree of Interference	Comments
0	Not discernible	No interference to very low level interference
1	Barely discernible	Low level interference considered acceptable
3	Easily discernible	Marginally acceptable to unacceptable

TABLE 8-2. PROTOFLIGHT GPE EVALUATION SUMMARY*

Ambient									
Problem	SBRC CSPT	Pre-EMI	EMI	Pre-Vibration	Post-Vibration	Pre-Acoustic	Post-Acoustic	Post-Gain Select	Pre-Endbell
Microphonics	0	0	0	0	0	0	0	0	0
Coherent noise	1 Bands 1,2,3	1 Bands 1,2,3	See Table 8-3	1 Bands 1,2,3	1 Bands 1,2,3	1 Bands 1,2,3	1 Bands 1,2,3	1 Bands 1,2,3	0
Random noise	0	0	0	0	0	0	0	0	0
Corona noise	0	0	0	0	0	0	0	0	0
SMP dropout	3	3	3,4	3	No dropout	No dropout	No dropout	No dropout	No dropout
Time code error	5 Band 4 only	5 Band 4 only	6	6	5 Band 4 only	7	7	No time code error	7

Thermal-Vacuum															
Thermal Vacuum Performance Test (10-5 Torr or less)															
Problem	Pre-Thermal Vacuum	Corona and Arcing	No. 1 20°C	40°C	0°C	No. 1 10°C	No. 2 20°C	No. 1 30°C	35°C	5°C	No. 2 30°C	No. 2 10°C	No. 2 20°C	Post Thermal Vac	Pre-Mass Properties CSPT
Microphonics	0	0	0	0	0	0	0	0	0	0	0	0	0	0	0
Coherent noise	0	0	0	0	0	0	0	0	0	0	0	0	0	1 Bands 1,3	0
Random noise	0	0	0	0	0	0	0	0	0	0	0	0	0	0	0
Corona Noise	0	0	0	0	0	0	0	0	0	0	0	0	0	0	0
SMP dropout	← No dropout →														
Time code error	7	7	7	7	7	7	No time code error	7	7	7	No time code error	7	7	No time code error	7

*See Table 8-1 and GPE code discription.

ORIGINAL PAGE IS OF POOR QUALITY

ORIGINAL PAGE IS
OF POOR QUALITY

Aside from the noise rating, the pictures were also evaluated as to the presence of extra pulses, horizontal image jitter, stray light, MTF bar washout, time code errors, and all other interfering phenomena. To simplify the summary performance tabulations in Table 8-2, code numbers were assigned for the various problems observed:

	Code	Comments
Scan monitor pulse (SMP) dropout		
Midscan code dropout	3	At least one midscan code missing
End of line code dropout	4	At least one code of line code missing
Time code error		
Time code in error	5	Error in same channel
No time code	6	Time code missing in all bands; test equipment problem
At least one black or white code missing	7	Time code glitch

8.1.3 EMI Noise Evaluation

The GPE pictures taken during the EMI test (CS01) were evaluated and the results are shown in Table 8-3. The table specifies the degree of interference due to the injection on the power input line of signals at different frequencies into the system.

8.1.4 Performance History During Acceptance Test

A general review of Table 8-2 indicates that overall picture quality is excellent. Microphonics, random, and corona noise are totally nonexistent in the GPE pictures. There were traces of coherent noise in both systems A and B with frequencies ranging from 1.8 to 7.2 kHz. The degree of coherent noise is barely discernible to not

TABLE 8-3. GPE CONDUCTED SUSCEPTIBILITY TEST (CS01) RESULTS

Frequency	Result
1430 Hz at 3.5 V p-p	Coherent noise excessive in all bands
1450 Hz at 3.5 V p-p	Coherent noise excessive in all bands
7200 Hz at 1.0 V p-p	Coherent noise barely discernible in band 2
4320 Hz at 1.5 V p-p	No noise apparent

ORIGINAL PAGE IS
OF POOR QUALITY

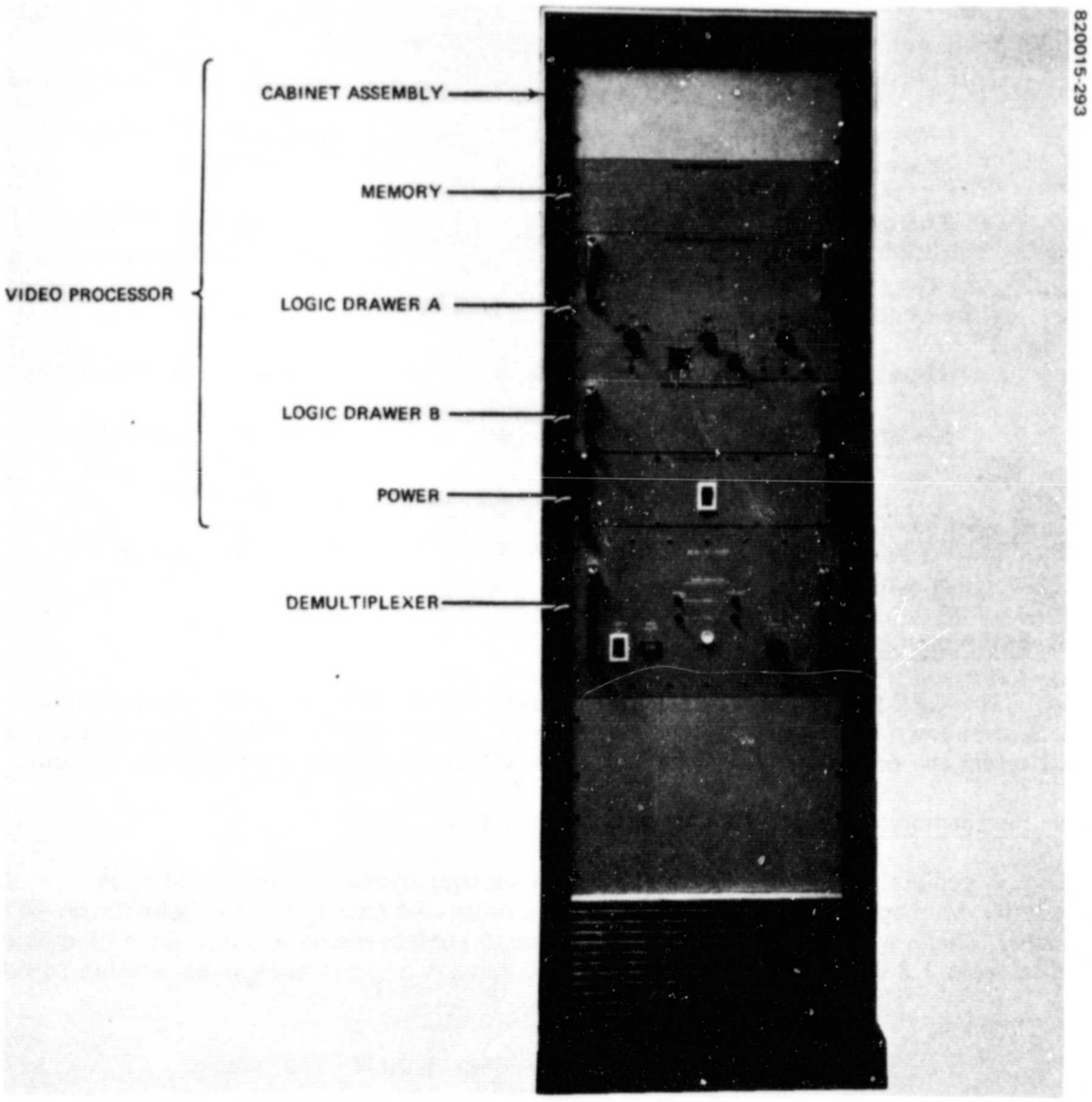

FIGURE 8-6. VIDEO PROCESSOR AND DEMULTIPLEXER

discernible during ambient conditions and a very slight trace of noise was seen in band 3 during thermal-vacuum test at 20°C.

A problem in the multiplexer caused end of line code and midscan code dropouts during the early ambient performance tests. After the multiplexer was fixed, no scan monitor pulse dropouts were observed in the GPE pictures. Another observation made was the presence of an extra white word in the end of line and midscan codes. The extra white word was a documented result of the redesign of the multiplexer for MSS-D.

Time code errors were also observed throughout the performance tests. All of the errors were due to test equipment or operator error. One particular error, where the black time code is grey or missing and two or three words of data are missing, was traced to poor recording of data.

8.1.5 GPE Anomalies

The following anomalies observed during MSS tests were attributed to GPE performance.

8.1.5.1 Scan Dropouts

Random scan line dropouts are caused by tape recorder malfunction and usually are traced to dirty recording heads. These are revealed as a white scan line on a positive picture. The lines caused by dropout can be continuous or broken into segments.

8.1.5.2 Overlap or Underlap of Scan Lines

This anomaly varies with the accuracy of crater lamp image focus on the photographic image recorder. An out-of-focus image creates wider lines that overlap. A sharply focused crater lamp image produces narrower scan line traces that underlap and have spaces between them. Ideally, the scan lines should just touch with no space between adjacent lines. Decentered crater lamp optics result in scan lines that exhibit nonuniform density transversely across the line. Scan line width also varies with line density, and lines tend to become wider with increasing density due to spreading of line image on film. This is a property of the photographic film.

8.2 VIDEO PROCESSOR AND IMAGE RECORDER PICTURE EVALUATION

The VPIR pictures are made with the video processor working in conjunction with the image recorder. These pictures are produced in near real time and used for quick look assessment of the system health. The video processor (Figure 8-6) takes the digital data from the demultiplexer, reformats it, adds annotation information; and digital-to-analog converts it to a form suitable for reproduction on the image recorder (Figure 8-7). The picture format is discussed below.

8.2.1 VPIR Picture Format

Although various modes and annotation options are available from the video processor in producing a VPIR picture, the only one discussed here is the one used

ORIGINAL PAGE IS
OF POOR QUALITY

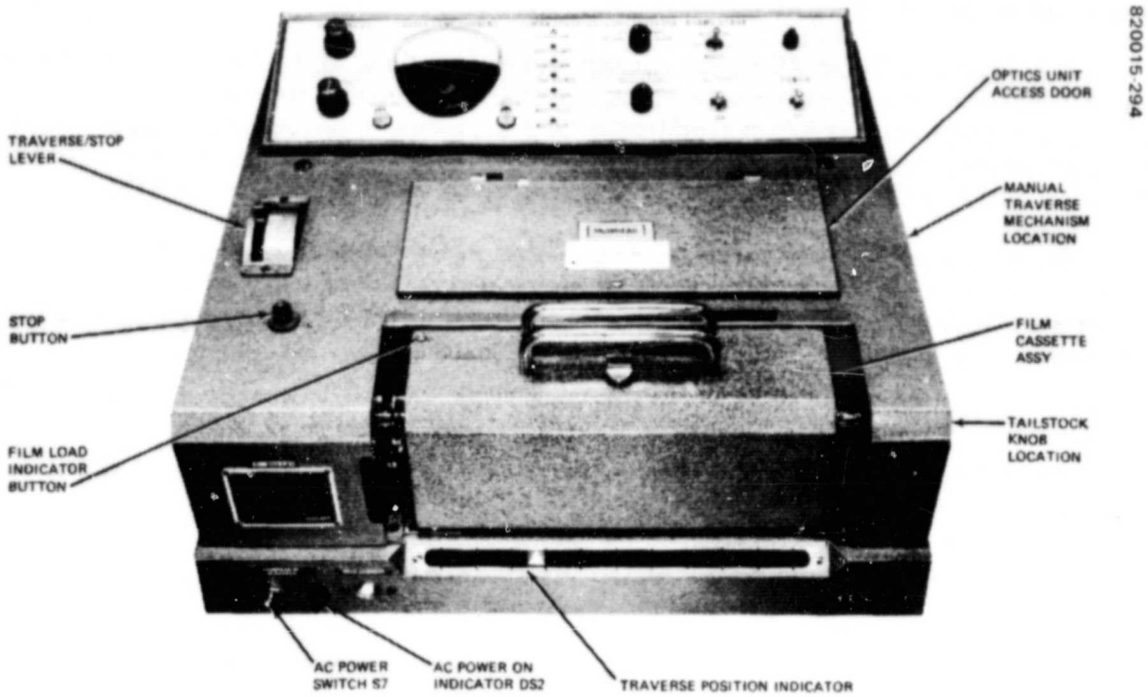

FIGURE 8-7. IMAGE RECORDER, FRONT VIEW

routinely in the MSS-D test program. For a discussion of the other possibilities, the interested reader is referred to the MSS Operation and Maintenance manuals.

The overall format for the VPIR pictures is shown in Figure 8-8, the scan lines are laid down from left to right in the figure. A grey scale is provided for calibration reference. An end of channel index is provided as a tick mark to indicate the transition from one channel of video data to the next. Three equally spaced vertical cursor lines are provided to assess the proper operation of the test equipment. The cursor lines are straight as long as the test equipment is functioning properly.

The format of the video data from MSS is shown in Figure 8-9. There are 72 lines of video printed for each video channel in sequence, starting with channel 1 at the top of the picture. The index marks are generated at the end of each 72 lines by the video processor to separate the video channels. At the end of the picture, channel 1 and 52 lines of channel 2 data are repeated. Channels 25 and 26 do not contain video data in the MSS-D pictures.

8.2.2 VPIR Picture Quality Rating

In the VPIR noise evaluation, the same rating scale is used as for the GPE shown in Table 8-1. A summary of the protoflight performance throughout the tests is

ORIGINAL PAGE IS
OF POOR QUALITY

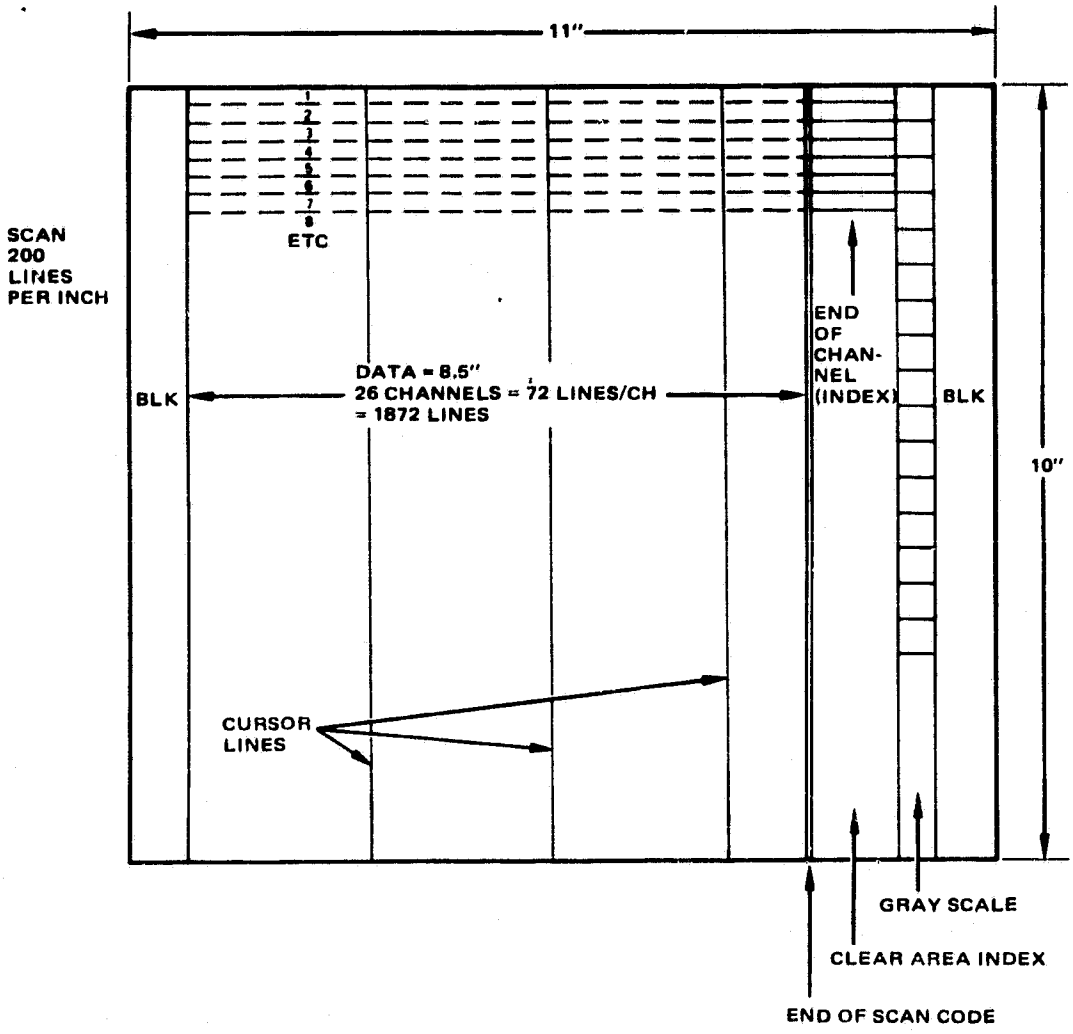

820915-295

FIGURE 8-8. TYPICAL TEST PHOTO FORMAT (MODE 2)

ORIGINAL PAGE IS
OF POOR QUALITY

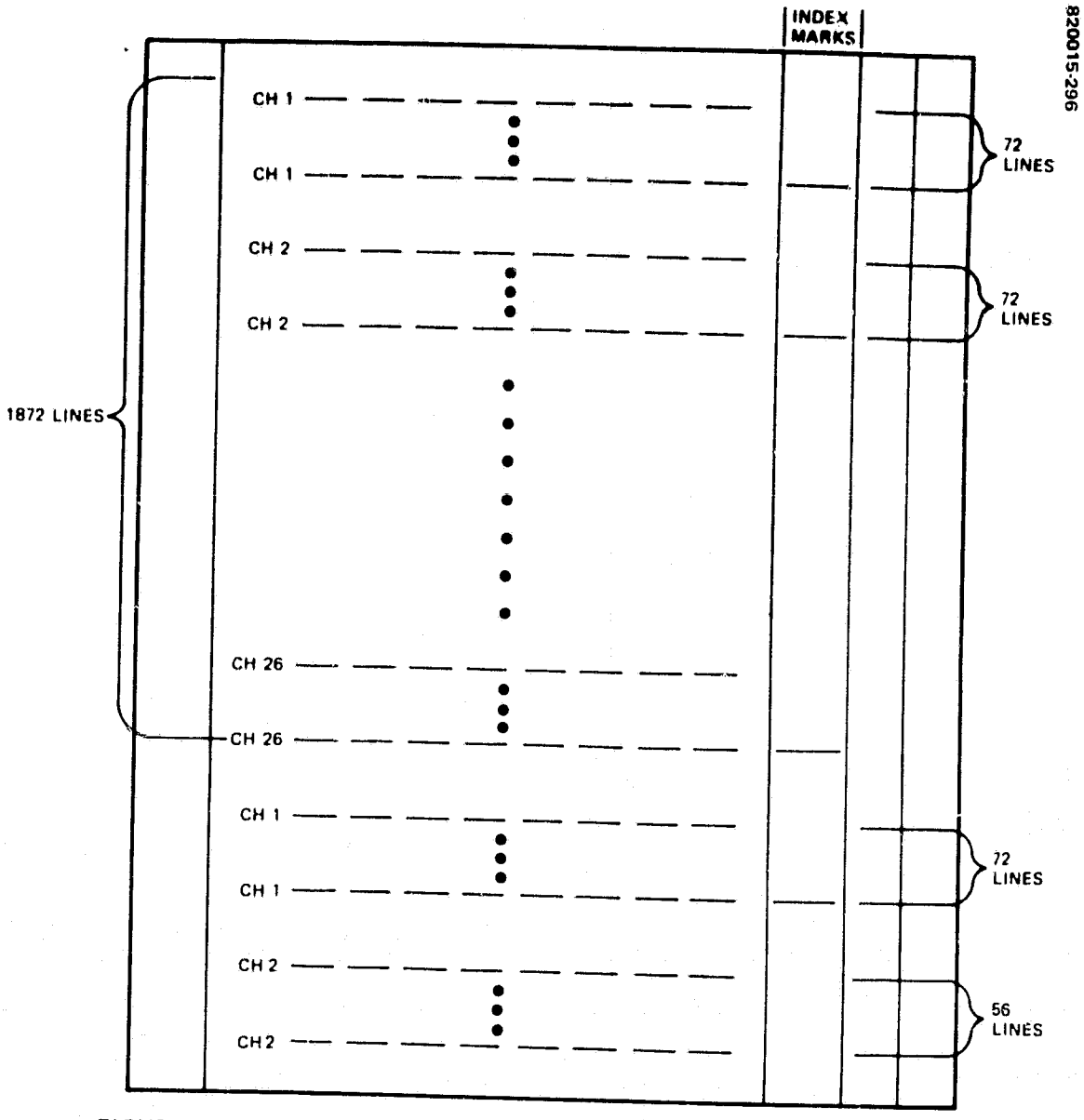

FIGURE 8-9. CHANNEL SCANNING SEQUENCE MODE 2, PICTURE FORMAT

TABLE 8-4. PROTOFLIGHT VPIR EVALUATION SUMMARY*

Ambient									
Problem	SBRC CSPT	Pre-EMI	EMI	Previbration	Postvibration	Preacoustic	Postacoustic	Postgain Select	Pre-endbell
Microphonics	0	0	See Table 8-5	0	0	0	0	0	0
Woodgrain	2 Bands 1, 2, 3	2 Bands 1, 2, 3	See Table 8-5	2 Bands 1, 2, 3	2 Bands 1, 2, 3	2 Bands 1, 2, 3	2 Bands 1, 2, 3	2 Bands 1, 2, 3	2 Bands 1, 2, 3
Random noise	2 Bands 4, 5	1 to 2 Band 4	See Table 8-5	1 Band 4	2 Band 4	1 Band 4	1 Band 4	1 Band 4	1 Band 4
Corona noise	0	0	0	0	0	0	0	0	0
SMP dropout	3, 4	3, 4	3, 4	3, 4	No dropout	No dropout	No dropout	No dropout	No dropout

Thermal Vacuum															
		Thermal Vacuum Performance Test 10^{-5} Torr or Less													
Problem	Prethermal vacuum	Corona and Arcing	No. 1 20°C	40°C	0°C	No. 1 10°C	No. 2 20°C	No. 1 30°C	35°C	5°C	No. 2 30°C	No. 2 10°C	No. 3 20°C	Post-thermal-vacuum	Premass Properties CSPT
Microphonics	0	2 Bands 1, 2 Channels 1, 3, 4, 5, 6, 7, 9, 10, 12	0	2 Bands 1, 2 Channels 1, 4, 6, 10, 11	1 to 2 Band 1 Channels 1, 3, 4, 5	1 Band 1 Channels 2, 4	0	1 Band 2 Channel 10	2 Bands 1, 2 Channels 1, 7, 10	1 Band 1 Channels 1, 4	1 Band 2 Channel 10	2 Band 1	1 Bands 1, 2 Channels 1, 12	1 to 2 Bands 1, 2 Channels 1, 10	2 Band 2 Channel 10
Woodgrain	2 Bands 1, 2, 3	2 Bands 1, 2, 3	2 Bands 1, 2, 3	2 Bands 1, 2, 3	2 Bands 1, 2, 3	2 Bands 1, 2, 3	2 Bands 1, 2, 3	2 Bands 1, 2, 3	2 Bands 1, 2, 3	2 Bands 1, 2, 3	2 Bands 1, 2, 3	2 Bands 1, 2, 3	2 Bands 1, 2, 3	2 Bands 1, 2, 3	2 Bands 1, 2, 3
Random noise	1 Band 4	1 Band 4	1 Band 4	1 to 2 Band 4	1 Band 4	1 Band 4	1 Band 4	1 Band 4	2 Band 4	1 to 2 Band 4	1 to 2 Band 4	2 Band 4	1 to 2 Band 4	2 Band 4	2 Band 4
Corona noise	0	0	0	0	0	0	0	0	0	0	0	0	0	0	0
SMP dropout	← No dropout →				3 Band 5	← No dropout →									

*See Table 8-1 and VPIR code description.

ORIGINAL PAGE IS OF POOR QUALITY

ORIGINAL PAGE IS
OF POOR QUALITY

presented in Table 8-4. The following codes are used in the table in addition to the noise rating scale:

	Code	Comments
SMP dropout		
Midscan code dropout	3	At least one midscan code missing
End of line code dropout	4	At least one end-of-line code missing

8.2.3 EMI Noise Evaluation

VPIR pictures taken during the EMI test were analyzed, and the results are listed in Table 8-5. The table shows which frequencies caused excessive interference in the system outputs.

8.2.4 Performance History During Acceptance Test

The VPIR picture analysis tabulations (Table 8-4) show that the system performance throughout the tests is generally acceptable.

TABLE 8-5. VPIR CONDUCTED SUSCEPTIBILITY TESTS RESULTS

Test	Frequency	System Mode	Results
CS01	300 Hz AT 3.5 V p-p	A	Woodgrain noise easily discernible in bands 1, 2, 3; random noise barely discernible in band 4; microphonics easily discernible in channel 10
	1430 Hz AT 3.5 V p-p	A/B	Band 2 – coherent noise excessive; bands 1, 3 – woodgrain noise easily discernible; band 4 – random noise barely discernible
	1000 Hz AT 2.8 V p-p	A	Bands 1, 2, 3 – woodgrain noise easily discernible; band 4 – random noise barely discernible; microphonics in channel 10 easily discernible
	7200 Hz AT 2.0 V p-p	B	Bands 1, 2, 3 – coherent noise excessive; band 4 – random noise barely discernible; band 3 – woodgrain noise easily discernible
CS02	114 kHz AT 0.37 V p-p	B	Bands 1, 2, 3 – woodgrain noise easily discernible; band 4 – random noise barely discernible
CS06	60 pps AT +56 V p-p	A	Bands 1, 2, 3 – woodgrain noise easily discernible; band 4 – random noise easily discernible
	60 pps AT -56 V p-p	A	Bands 1, 2, 3 – woodgrain noise easily discernible; band 4 – random noise easily discernible

Microphonics interference was not discernible during the prethermal-vacuum ambient tests except during EMI. Easily discernible microphonics appeared in channel 10 at 300 Hz (3.5 volts peak-to-peak) and 100 Hz (2.8 volts peak-to-peak). The degree of microphonics interference was higher in the thermal-vacuum environment which fluctuated from barely discernible to easily discernible. Woodgrain noise was easily discernible throughout the tests, but the level was generally acceptable. Random noise fluctuated from barely to easily discernible in band 4 throughout the tests; the degree of interference was also acceptable. Some midscan and end of line code dropouts occurred due to a problem in the multiplexer. After the multiplexer was fixed, no dropouts were seen except for one which occurred in band 5, at $0^{\circ}C$ vacuum environment. Extra white words in the midscan and end-of-line codes also appear in the VPIR pictures. As mentioned previously, these occurrences are inherent in the multiplexer design.

ORIGINAL PAGE IS
OF POOR QUALITY

9. PROTOFLIGHT SPECIAL PROBLEMS

This section focuses on the special problems encountered during the qualification test program of the protoflight system. As of the time this final report was written all of the problems discussed were well understood, and corrective action was implemented for all but the gain drift problem of channel 9 (9.5). In the case of the channel 9 gain drift, it is thought to be caused by a slightly anomalous dynode string in the photomultiplier tube. The gain changes were limited to ±10 percent over the period of acceptance testing, and the channel showed no anomalous behavior when subjected to a controlled duty cycle operation in thermal-vacuum testing. None of the problems is expected to be a source of difficulty for future in-orbit performance of the MSS-D protoflight system.

9.1 FLEX PIVOT FAILURE

9.1.1 Summary

During qualification level vibration on the MSS-D protoflight model, a flex pivot failure was experienced. Evidence indicated that the failure occurred during the X-axis qualification random vibration. Subsequent detailed analysis of the broken flex pivot revealed no serious defects in the pivot itself which were responsible for the failure. Minor workmanship defects were found in the failed pivot, i.e., burred edges, braze splatter, but nothing that could be directly related to the failure.

The flex pivot failure during qualification vibration was surprising in that basically the same design passed qualification tests in 1971 at the same random vibration levels. The failure analysis found no design change, test configuration difference, or component defect which provided a clear explanation of the failure. Subsequent analysis indicated the tests were more likely a random success in 1971 and a random failure in 1981.

Tests were conducted with the structural test model and engineering model scan mirror assembly to establish response levels at various critical locations around the flex pivots. These tests were conducted up to -6 dB below qualification random vibration levels. In parallel a Nastran finite element model was put together to model the stress levels in the flex pivot structure as a function of applied load. In estimating the fatigue life of the flex pivots from extrapolated data on the structural test model and the Nastran finite element model, it was concluded that a significant fraction of the fatigue life probably was used up during the qualification level random vibration tests. Within the modelling uncertainties and the statistical nature of the actual stress levels achieved during random vibration, a given set of flex pivots could either pass or fail the

ORIGINAL PAGE IS OF POOR QUALITY

TABLE 9-1. RANDOM VIBRATION LEVELS, ALL AXES
(Scanner Qualification Levels)

Frequency Range (Hz)	Power Spectral Density
20 to 300	Increasing at a rate of 4 dB/octave +3 dB to 0.09 g^2/Hz at 300 Hz
300 to 2000	0.09 g^2/Hz with a tolerance of ±3 dB
Test duration: 4 minutes each axis	Overall: 12.8 g rms ±10 percent

TABLE 9-2. SCANNER ACOUSTIC NOISE LEVELS
(Sound Pressure Level, dB*)

Center Frequency, Hz		Acceptance		Protoflight		
One-Third Octave	Octave	One-Third Octave	Octave	One-Third Octave	Octave	Test Tolerance, dB
25	32	119	125	122	128	+3, −6
32		120		123		
40		121		124		
50	63	123	128	126	131	+3, −3
63		124		127		
80		124		127		
100	125	127	134	130	137	+3, −3
125		129		132		
160		131		134		
200	250	130	137	133	140	+3, −3
250		132		134		
315		134		137		
400	500	134	141	137	144	+3, −3
500		139		142		
730		134		136		
800	1,000	131	134	134	137	+3, −3
1,000		129		132		
1,250		129		130		
1,600	2,000	127	131	130	134	+3, −3
2,000		126		129		
2,500		124		127		
3,150	4,000	124	127	127	130	+3, −6
4,000		122		125		
5,000		122		125		
6,300	8,000	120	124	123	127	+3, −6
8,000		118		121		
10,000		118		121		
Overall		144		147		+3, −1

*Reference level: 0 dB = 20 $\mu N/m^2$.
Test duration: 1 minute.

ORIGINAL PAGE IS
OF POOR QUALITY

qualification level random vibration test. In any case, the stress levels seen and consequent fatigue life used up during the test were greater than desirable in flight hardware.

As a result of the analyses and tests and after replacing the flex pivots, GSFC and Hughes decided to proceed with a retest of the protoflight consisting of an acoustic test to replace the severe random vibration test. The acoustic levels selected were based on measured levels by the spacecraft contractor. The original random vibration levels are given in Table 9-1, and acoustic levels used to replace the random vibration test are shown in Table 9-2.

The failed flex pivots were changed out in the protoflight scan mirror assembly (SMA), and a penalty test program, culminating in a qualification acoustic test, was conducted on the protoflight system. The system passed the acoustic test with no damage to the flex pivots, which was not surprising in view of the analysis and testing results described in the following sections.

9.1.2 Analysis and Test Program

To determine why the MSS protoflight flex pivots failed during qualification random vibration and to evaluate the severity of an alternate acoustic test, a program of analysis and testing was conducted. The analysis involved a Nastran finite element model of the MSS flex pivots. This model had 118 elements representing the pivot flexures. Two different sets of boundary conditions were imposed on the model to estimate maximum and minimum stress levels.

Vibration testing involved instrumenting the MSS engineering model unit with accelerometers located as shown in Figure 9-1. The random vibration test was then repeated at -6 dB from qualification level, and rms accelerations on the scan mirror were measured. The estimated g levels seen by the flex pivots on protoflight at failure were obtained by multiplying the -6 dB accelerations by two. Accelerations were also measured during qualification level acoustic tests.

Combining the results of the Nastran model, which calculates stress per unit acceleration, with acceleration data from vibration and acoustic testing, the rms stress level in the flex pivot was estimated. Based on this rms stress level and the assumption that the scan mirror response to the random vibration input is narrowband, the fatigue life of the flex pivots during qualification testing was calculated.

9.1.2.1 MSS Flex Pivot History

In the early part of the MSS program (circa 1971), flex pivot failures during qualification random vibration were also experienced. At that time it was felt that excessive compliance of the SMA interface surface resulted in crosstalk between the axis of vibration input and the two orthogonal axes. The resultant g load on the flex pivot due to this crosstalk was then high enough to cause failure. To correct this problem, an interface stiffener was designed to reduce crosstalk. Called the "horsecollar," this stiffener apparently did its job, and qualification vibration tests were successfully passed.

The MSS-D program, predicated on the success of MSS-A and -B, had the same design and test requirements. Specifically, the horsecollar stiffener was used and the

ORIGINAL PAGE IS
OF POOR QUALITY

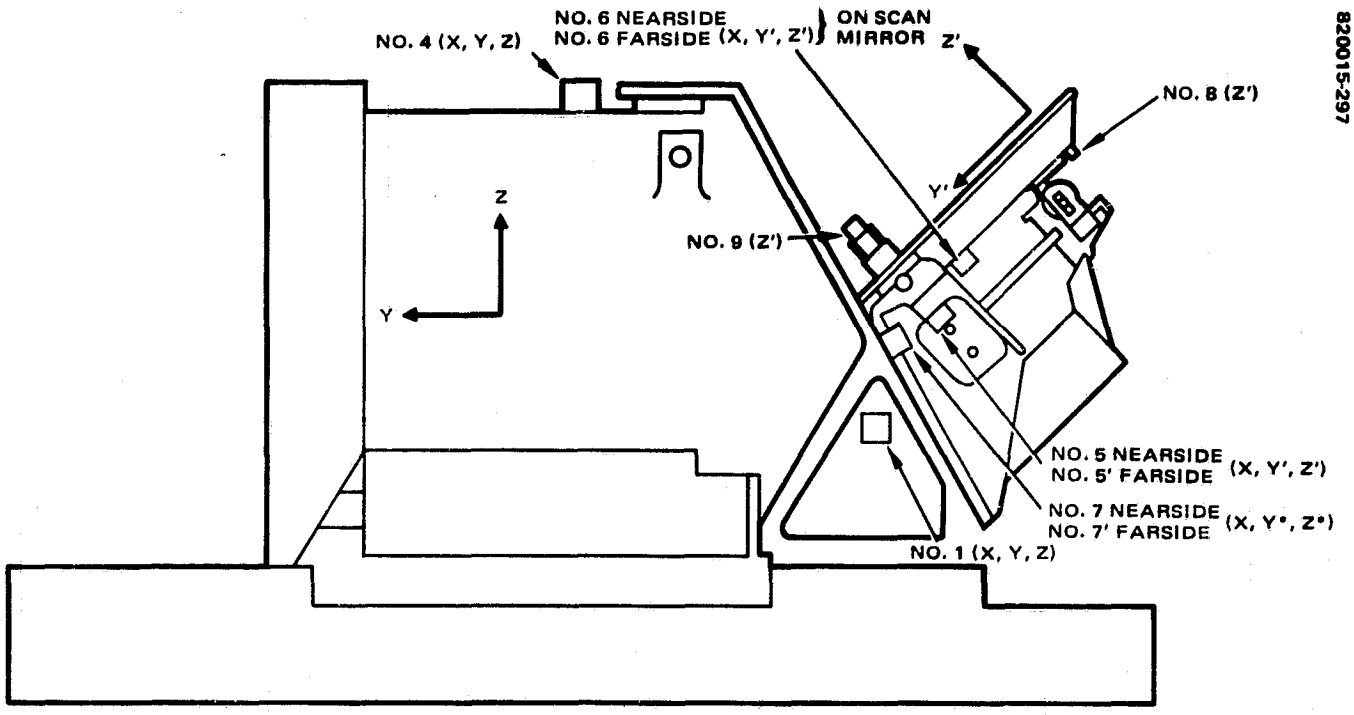

820015-297

FIGURE 9-1. ENGINEERING MODEL SCAN MIRROR ASSEMBLY ACCELEROMETER LOCATIONS

random vibration qualification test was the same (12.8 g rms input level, 20 to 2000 Hz). After the MSS-D protoflight unit failed, a study was initiated to determine if there were major differences between the behavior of MSS-D and MSS-A and -B. The vibration signatures revealed no obvious differences between MSS-D and previous units which had successfully passed the qualification level random vibration. Minor differences (such as mirror weight, component relocations on the casting, and different flex pivot lots) could be sufficient to conclude that passing or failing the random vibration qualification test was a unit-to-unit variable, subject to several relatively minor factors. The analysis and testing which followed the protoflight failure supported this conclusion.

It is generally agreed that the 12.8 g rms qualification level test is excessively severe, and as a result of the protoflight failure, a test specification change was initiated. NASA proposed an acoustic qualification test to replace the random vibration test as more representative of the launch environment. The acoustic qualification test (OASPL = 147 dB) was successfully passed by the protoflight unit. Test results show that the peak acoustic qualification test acceleration is more than 12 dB below the random vibration level, as measured by accelerometers on the scan mirror. Since the flex pivots successfully withstood both the -6 dB vibration and the acoustic qualification testing, the failure of the flex pivot in protoflight vibration (i.e., at 0 dB) should not be construed as an inability to survive the launch environment.

9.1.2.2 Nastran Model

Computer analysis of stress levels in the flex pivot webs was accomplished with the Nastran finite element program. Figure 9-2a shows a cutaway view of a cantilever type flex pivot; and Figure 9-2b the finite element model of the flex pivot interior used in this analysis. The three flexures are divided into 118 elements.

ORIGINAL PAGE IS
OF POOR QUALITY

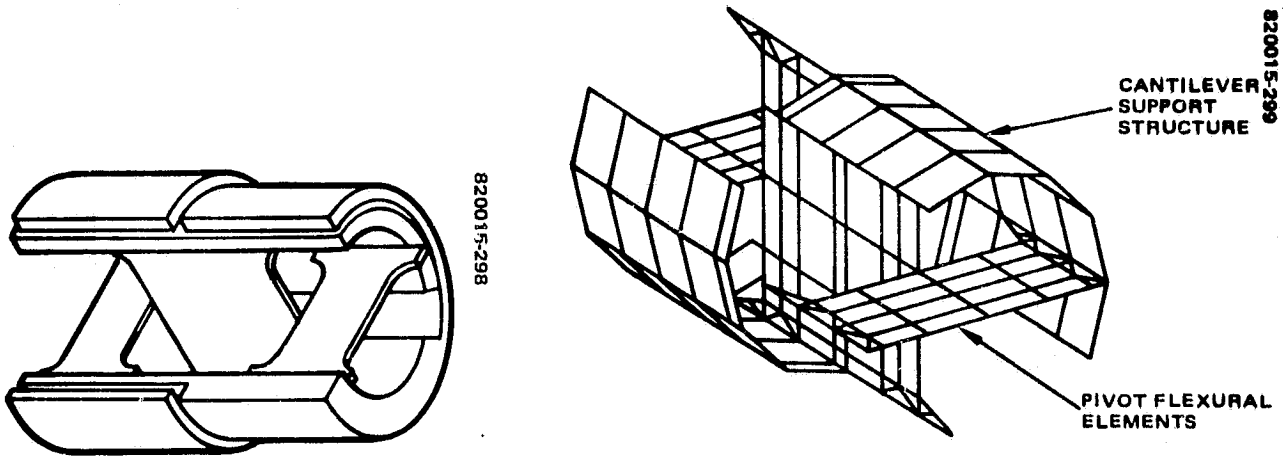

a) CANTILEVER FLEX PIVOT CUTAWAY VIEW

b) FLEX PIVOT INTERIOR FINITE ELEMENT MODEL

FIGURE 9-2. FLEX PIVOT

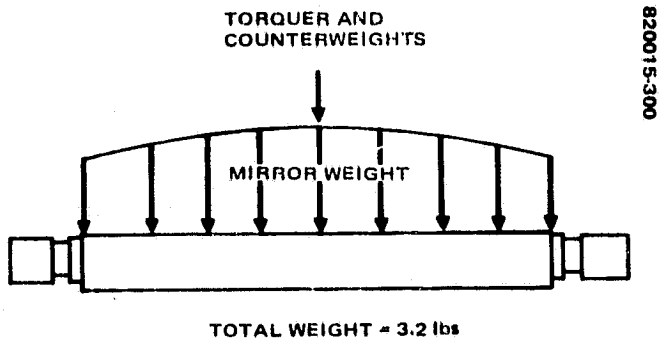

FIGURE 9-3. LOAD DISTRIBUTION ON MSS SCAN MIRROR

In the MSS application two flex pivots are used to support the scan mirror. Figure 9-3 shows a load diagram. The flex pivots are shown with free boundary conditions on the frame side. The fixed ends of the pivots are coupled together by the mirror.

Stresses in the flex pivot webs were computed for two sets of boundary conditions. One boundary condition, called fixed-fixed, assumes infinite mirror and frame stiffness. Each flex pivot then carries one-half the mirror weight by deflecting in a pure shear direction only. The second boundary condition, called fixed-free, assumes zero frame (or mirror) flexural stiffness. Each flex pivot then supports one-half the mirror weight by deflecting in both shear and angular directions. The load vectors and two boundary conditions used as input for the Nastran model are shown in Figure 9-4. Stress levels in the flex pivot webs due to the radial force vector F_R were calculated for four different angular positions of F_R around the pivot circumference. Stress due to an axial load F_A, and a unit moment M_X, were also calculated. Defining $\theta = 0^o$ as being in the plane of the center flexural element, the stress level was determined for $\theta = 0^o, 45^o, 90^o, 135^o$. These positions, along with the numbering system used to define the finite elements, are shown in Figure 9-5.

ORIGINAL PAGE IS
OF POOR QUALITY

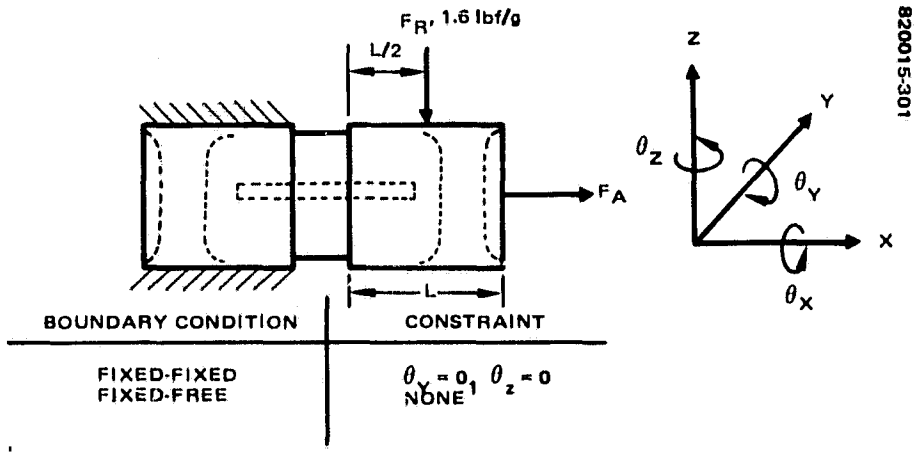

FIGURE 9-4. LOADING CONDITIONS FOR NASTRAM MODEL

Because of the linear analysis limitations of the Nastran program, angles greater than 135° would result only in a sign change from the stress calculated 180° before. It should be pointed out that this is a limitation of the model, as real flex pivots do vary somewhat for loads applied in equal and opposite directions. Bendix measurements of flex pivot stiffness show this direction sensitivity can vary ±13 percent for MSS pivots.

The principal nonlinearity of a flex pivot results from applying loads that put the flexures in compression. For loads near the stability limit where buckling can occur, flex pivot behavior is nonlinear. Since the MSS protoflight unit failure was not associated with buckling, the linear Nastran model was considered acceptable for analysis purposes.

Maximum stress levels for the four radial loads, axial load, and unit moment are given in Table 9-3 for both the fixed-fixed and fixed-free boundary conditions. Combined stress levels may also be determined by providing the Nastran program with the X, Y, and Z rms accelerations experienced during vibration or acoustic tests. Not surprisingly, the stress levels were higher for the less constrained fixed-free condition. Since actual flex pivot boundary conditions were somewhere between fixed-fixed and fixed-free, these values were used to bound the analysis.

Stress Distribution

The design of the flex pivot housing causes the inner cantilever support structure to deflect when loads are applied; this deflection, in turn, causes the stress in the flexure to vary along the pivot axial direction. Stress distribution is plotted in Figure 9-6 for a 1 pound load in the plane of the outer flexural elements ($\theta = 90^\circ$) of an MSS flex pivot (5/8 inch diameter series 600). Note the symmetry of the stress distributions in the figure for the pure shear (fixed-fixed) loading. Peak stresses occur at elements 657 and 687 where the peak stress concentration factor is $\sigma/\sigma_{nom} = 3.7$. For cantilever loads applied to the flex pivot (fixed-free), it is seen that stress distribution symmetry does not exist at opposite ends of the pivot. Stress gradients occur exclusively in the outer flexure directly under the applied load (element 3 in Figure 9-6). The peak stress concentration factor for cantilever loading is $\sigma/\sigma_{nom} = 6$ which occurred at element 687.

ORIGINAL PAGE IS
OF POOR QUALITY

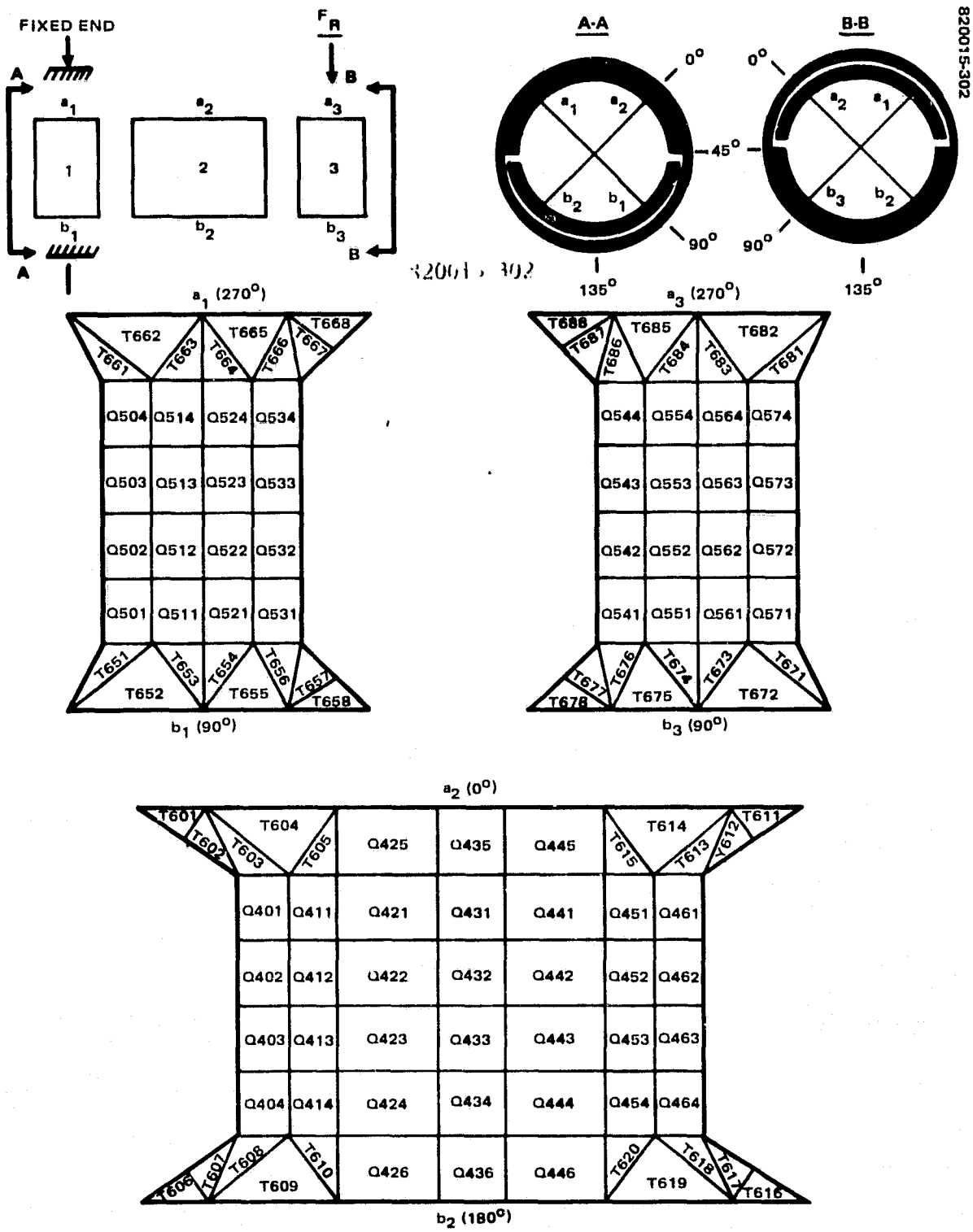

FIGURE 9-5. IDENTIFICATION OF FINITE ELEMENTS ON FLEX PIVOT WEBS

ORIGINAL PAGE IS
OF POOR QUALITY

820015-303

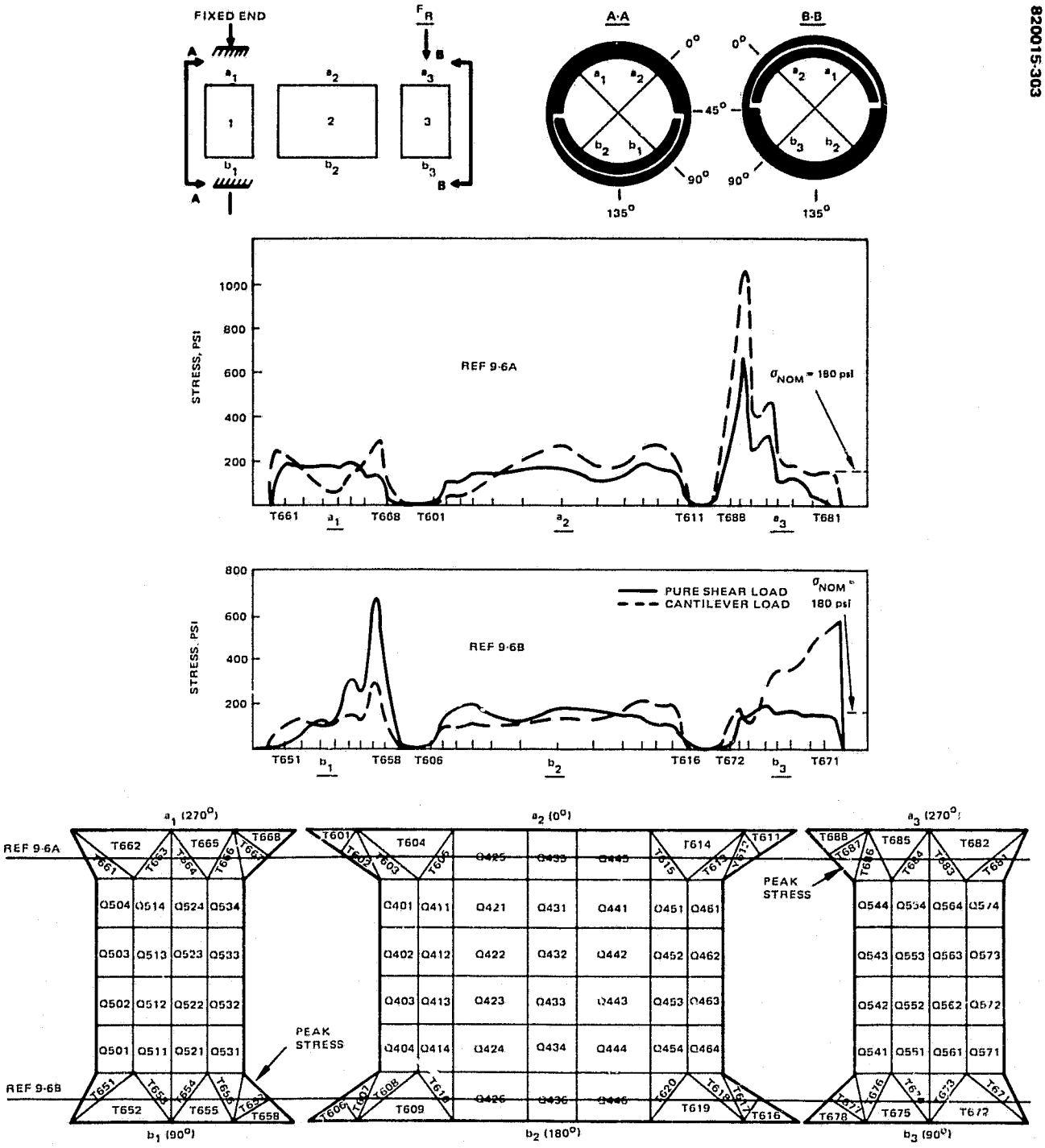

FIGURE 9-6. FLEX PIVOT WEBS STRESS DISTRIBUTION (1 LBF LOAD APPLIED AT $\theta = 90^{\circ}$)

ORIGINAL PAGE IS
OF POOR QUALITY

TABLE 9-3. MSS MAXIMUM STRESS FROM 1 G LOAD, 1.6 LBF

Load Direction	Fixed-Fixed		Fixed-Free	
	Stress, psi	Location (Node)	Stress, psi	Location (Node)
$\theta = 0^o$	410	436	1,770	464
45°	890	657	1,500	464
90°	1,090	657	1,710	687
135°	660	687	1,170	464
Axial	580	464	580	401
Unit moment*, in-lbf	43,300	404	43,700	401

*For MSS 1 in-lbf = 4.3^o rotation.

It was determined that the highest stress point almost always occurs at the inner radius of the outer flexural elements at the end of the flexure attached to the cantilever support structure.

The stress concentration results of Figure 9-6 are in excellent agreement with the findings noted in Hughes IDC 704212/100, 1 December 1977, which demonstrated that stress concentation factors are inversely related to flex pivot diameter, the reason being that larger flex pivots have sturdier support structures.

9.1.2.3 Vibration Test Results

MSS Accelerations

To estimate the rms acceleration level experienced by the MSS protoflight scan mirror, the engineering model SMA and casting were vibrated at -6 dB down from qualification level. Accelerometers, located on the scan mirror adjacent to the flex pivots, provided spectral information on the scan mirror response to the random vibration input. Acceleration transfer functions from scan mirror to SMA frame helped separate the bounce frequency of the scan mirror from resonant frame modes. RMS accelerations measured by accelerometers 6 and 6' (X, Y', Z'), located on the scan mirror during -6 dB testing are given in Table 9-4 after being doubled to represent qualification level (0 dB) accelerations. Also included are the accelerations measured during the new acoustic qualification test. Note the difference in response accelerations for the acoustic versus vibration qualification tests.

MSS Stresses

Using the acceleration values from Table 9-4, the combined stress level at all 118 finite elements was determined. Both fixed-fixed and fixed-free cases were

ORIGINAL PAGE IS
OF POOR QUALITY

TABLE 9-4. MSS VIBRATION AND ACOUSTIC RMS ACCELERATIONS COMPARISON
(Frequency of Peak Response is in Parentheses)

Acceleration	Location	Excitation, grms			
		Vibration X-axis	Vibration Y-axis	Vibration Z-axis	Acoustic Test (147 dB)
6X	Axial direction	43.6* (480)	11.8 (480)	18.4 (480)	6.3 (500)
6'X		43.2 (470)	11.6	16.8 (480)	6.6 (500)
6Y'	In plane of mirror	27.2 (470, 590)	32 (470)	30 (470)	9.9 (500)
6'Y'		28.2 (600)	28.6	29.4 (460)	10.7 (530)
6Z'	Normal to mirror	28.2 (590)	22.8 (550)	30.2 (630)	5.4 (500)
6'Z'		30.6 (470)	23.0	–	6.1 (510)

*Underlined values used to compute stress.

considered. The flex pivot orientation relative to accelerometer response axes was as follows:

X direction - pivot axial direction

Y' direction - 90° radial direction (in plane of mirror)

Z' direction - 0° radial direction (normal to mirror)

Since no phase correlation exists between response accelerations in X, Y', and Z', all possible combinations of loading conditions were modeled. From these loading conditions and the fixed-fixed, fixed-free boundary conditions, the stress level in the flex pivot was bounded. Table 9-5 summarizes the maximum, minimum, and expected mean values of stress for the qualification level vibration and acoustic tests. Expected mean stress was determined using worst case loading conditions and fixed-fixed boundary conditions.

TABLE 9-5. MSS FLEX PIVOTS MAXIMUM, MINIMUM, AND BEST ESTIMATE OF STRESS LEVELS

Test	Maximum Stress, rms	Minimum Stress, rms	Expected Value of Stress, rms	Locations of Worst Stress (Node)
Vibration qualification*	83,800 psi	29,800 psi	50,000 psi	657, 687
Vibration acceptance* (–3 dB from qualification level)	59,300 psi	21,100 psi	35,400 psi	657, 687
Acoustic qualification	24,000 psi	11,700 psi	15,000 psi	657, 687

*Based on X-axis input response.

ORIGINAL PAGE IS
OF POOR QUALITY

9.1.2.4 Fatigue

The estimation of fatigue damage to a structure subjected to random vibration was an exceedingly difficult problem. The random nature of the test only served to compound the uncertainties inherent in any fatigue analysis. If information on the endurance, or S-N, curve for cyclical loading is available, then an equivalence relationship between random and cyclical loading can be derived. Also, if certain additional conditions are met, an expected mean time to failure can be calculated for random loading.

Derivation of Mean Time to Failure

The equivalence relationship between random and cyclical loading is established by following the derivation from Curtis.*

1) The S-N curve for cyclical loading is known and can be described by the equation

$$N\sigma^b = C \tag{9-1}$$

where

N = No. cycles to failure

σ = Stress Level, lb/in^2

2) Cyclical failure is predicted for a Miner's rule damage coefficient of $D_c = 1$

$$D_c = \sum_i \frac{n_i}{N_i} \tag{9-2}$$

3) Random failure is predicted for a Miner's rule damage coefficient of $D_r = 1/2$

$$D_r = \sum_i \frac{n_i}{N_i} \tag{9-3}$$

4) Fatigue damage is the result of narrowband resonant response of the scan mirror.

*A. Curtis, et al., "Selection and Performance of Vibration Tests," The Shock and Vibration Monograph Series, Vol 8, 1971, p. 85.

ORIGINAL PAGE IS
OF POOR QUALITY

Solving Equation 9-1 for the number of cycles to failure for a peak amplitude of σ_p yields

$$N = \frac{c}{(\sigma_p)^b}$$

The damage coefficient from the accumulation of stress cycles at random amplitudes σ_p is found by substituting the above value of N in Equation 9-3.

$$D_r = \sum_i \frac{(\sigma_{pi})^b n_i}{c} \tag{9-4}$$

Defining an equivalent stress, S_e, as a constant amplitude stress which produced equal damage (this does not imply that $D_r = D_c$!!) after the same number of total cycles we get from Equation 9-2 yields

$$D_c = \sum_i \frac{(S_e)^b n_i}{c} \tag{9-5}$$

Equation 9-2 shows that cyclical fatigue failure occurs when $D_c = 1$; therefore, Equations 9-4 and 9-5 yield

$$\frac{(S_e)^b}{c} \sum_i n_i = \frac{1}{D_r c} \Sigma_i (\sigma_{pi})^b n_i = 1$$

or

$$S_e = \left(\frac{1}{D_r}\right)^{1/b} \left(\frac{\Sigma_i (\sigma_{pi})^b n_i}{\Sigma_i n_i}\right)^{1/b} \tag{9-6}$$

Equation 9-6 is the equivalent constant amplitude, cyclical stress to cause failure in the same total number of cycles as the random vibration.

ORIGINAL PAGE IS
OF POOR QUALITY

Knowing that the probability of realizing a peak stress of σ_p is Rayleigh distributed, Equation 9-6 can be reduced to the following integration problem

$$S_e = \left(\frac{1}{D_r}\right)^{1/b}\left[\int_{\sigma}^{\infty}(\sigma_p)^b p(\sigma)\,d\sigma \Big/ \int_{\sigma}^{\infty} p(\sigma)\,d\sigma\right]^{1/b} \tag{9-7}$$

which when solved yields

$$S_e = \left(\frac{1}{D_r}\right)^{1/b}(\pi b)^{1/2b}\left(\frac{b}{e}\right)^{1/2}\sigma_{RMS} \tag{9-8}$$

where σ_{rms} is the root mean square of the narrowband response (assumption 4).

To elaborate on assumption 4, it is required that the stress wave oscillates with completely reversed loading at the resonant frequency f_N. The random vibration problem, therefore, reduces to a random amplitude modulation of a stress wave with frequency f_N.

Continuing with Equation 9-8, the equivalent stress S_e can be substituted into Equation 9-1 to find the expected cycles to failure

$$N = c(S_e)^{-b} = c\,D_r\left[\frac{1}{(\pi b)^{1/2}}\,\frac{e}{b}^{\,b/2}\,\frac{1}{(\sigma_{RMS})^b}\right] \tag{9-9}$$

Finally, to obtain the fatigue life of the flex pivot in terms of allowable exposure time to the random vibration test, Equation 9-9 is divided by f_N

$$T_R = \frac{c\,D_r}{(\pi b)^{1/2}(b/e)^{b/2}(\sigma_{RMS})^b f_N} \tag{9-10}$$

Using the S-N curve of Figure 9-7, the coefficients b and c are found to be

$b = 6.5$

$c = 4.4 \times 10^{37}$

ORIGINAL PAGE IS
OF POOR QUALITY

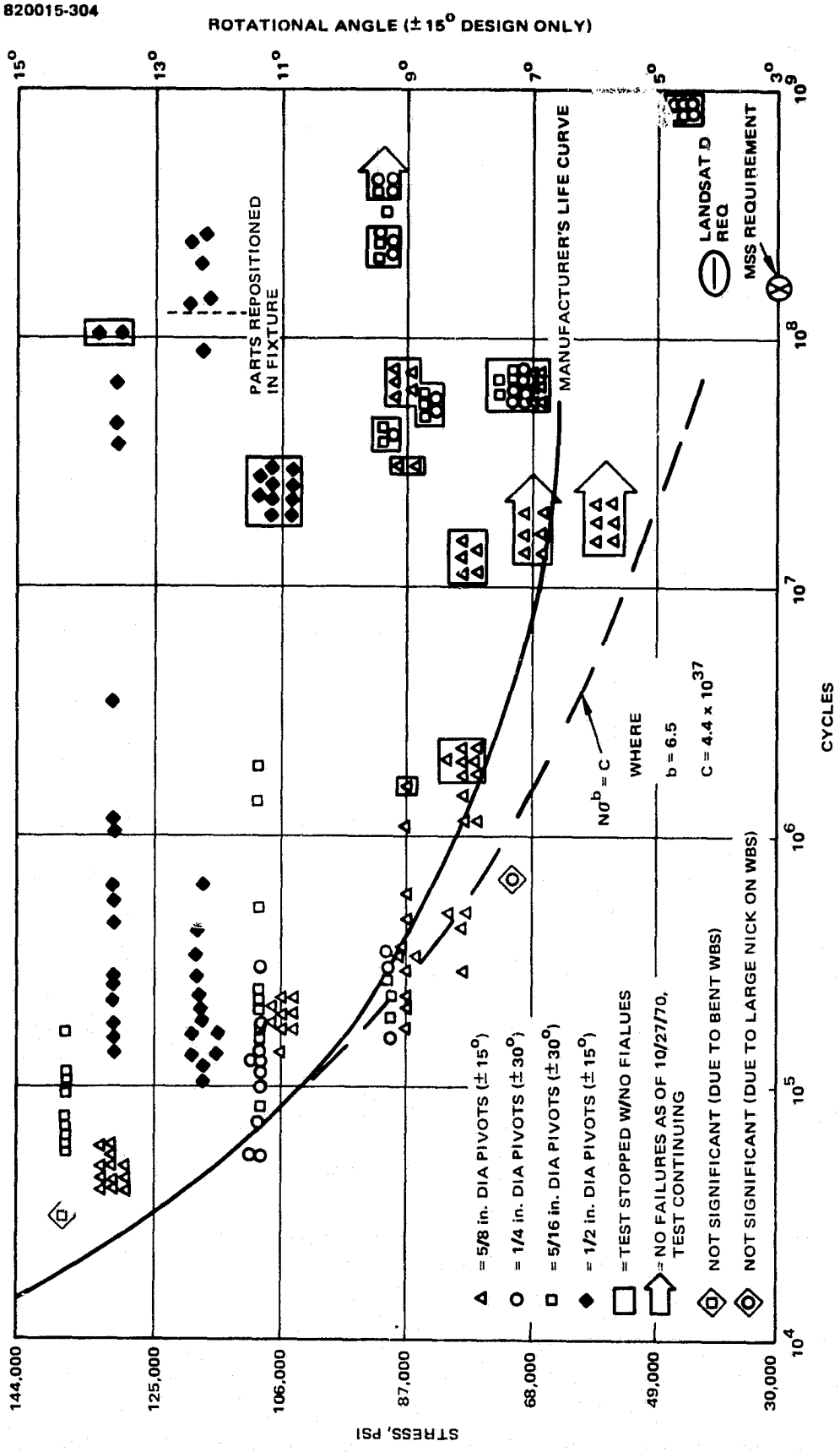

FIGURE 9-7. FATIGUE CYCLING TEST RESULTS

ORIGINAL PAGE IS
OF POOR QUALITY

D_r can vary from 1/5 to 2/3 and as stated in assumption 3, a value of

D_r = 1/2 will be used

Substituting these constants into Equation 9-10 results in the simplified formula applicable for MSS flex pivots.

$$T_R = \frac{2.86 \times 10^{35}}{f_N (\sigma_{RMS})^{6.5}} \text{ sec} \qquad \begin{array}{l} \sigma_{RMS} \text{ is in psi} \\ f_N \text{ is in Hz} \end{array} \tag{9-11}$$

MSS Flex Pivot Fatigue Life

The rms stress levels from Table 9-5 are used in Equation 9-11 to estimate the fatigue life of the MSS flex pivots. A natural frequency of f_N = 500 Hz is used in the equation. Figure 9-8 shows the average spectral distribution (ASD) curves for the engineering model unit during acoustic testing at qualification level. These curves show that the narrowband assumption is reasonable since most of the energy is concentrated near 500 Hz.

For the vibration qualification test, the estimated time to failure is

$$6 \text{ sec} < T_{fail} < 61 \text{ minutes}$$

with an expected mean time of

$$T_{fail} = 135 \text{ seconds}$$

For the vibration acceptance test the estimated time to failure is

$$54 \text{ sec} < T_{fail} < \infty$$

with an expected mean time of

$$T_{fail} = 26 \text{ minutes}$$

ORIGINAL PAGE IS
OF POOR QUALITY

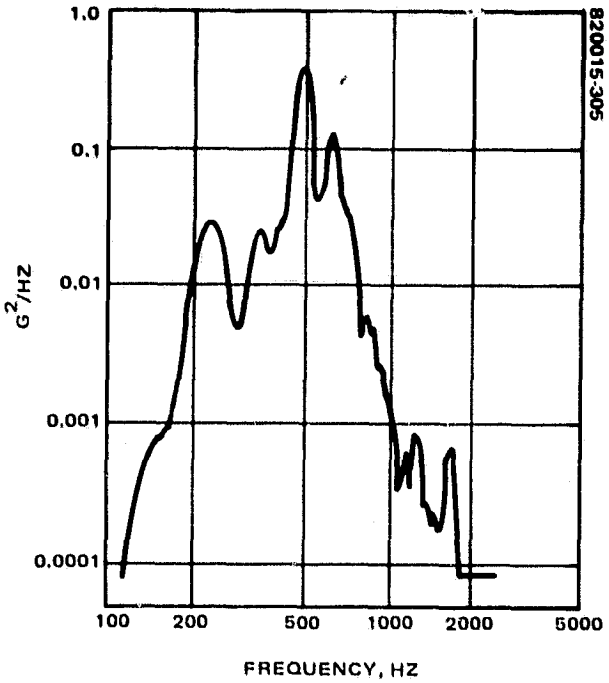

a) X-AXIS RESPONSE

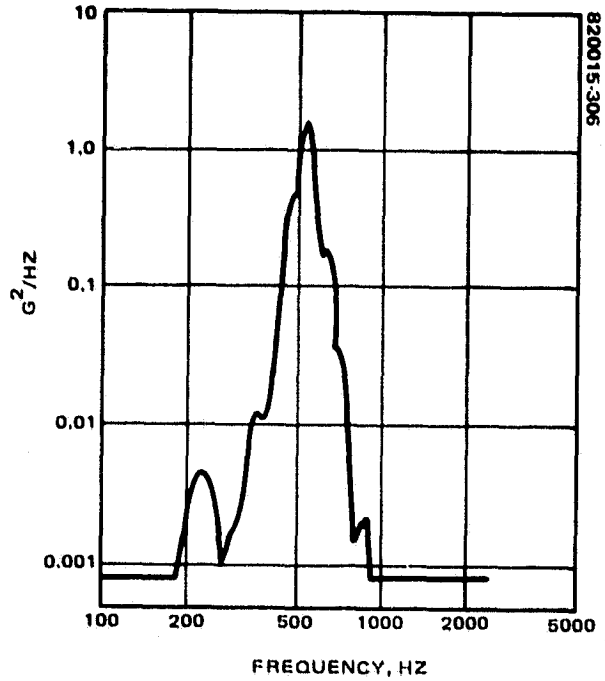

b) Y'-AXIS RESPONSE

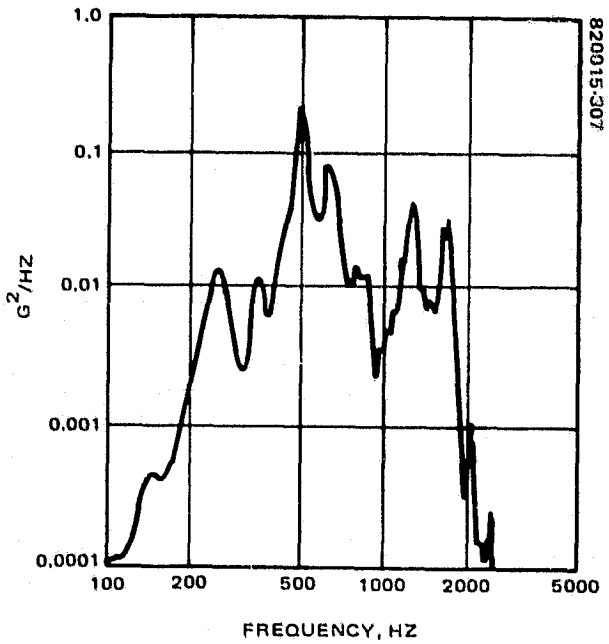

c) Z'-AXIS RESPONSE

FIGURE 9-8. ASD CURVES OF SCAN MIRROR RESPONSE DURING QUALIFICATION ACOUSTIC TEST (147 dB)

ORIGINAL PAGE IS
OF POOR QUALITY

For the MSS acoustic qualification test of 147 dB the estimated time to failure is

$$4.4 \text{ hours} < T_{fail} < 400 \text{ hours } (\rightarrow \infty)$$

with an expected mean time of

$$T_{fail} = 91 \text{ hours} \rightarrow \infty \text{ since the } 3\sigma \text{ stress level is below the endurance limit}$$

9.1.2.5 Conclusions

Data from the MSS random vibration qualification test and the acoustic qualification test were used as input to the Nastran finite element model of the flex pivot. An rms stress level was determined. Based on the assumption that the scan mirror response ASD was narrowband, an estimate of the time to fatigue failure was also made.

For each of the three vibration tests, a worst case, best case, and expected time to failure were determined. These values are summarized in Table 9-6. The worst case estimate is a result of assuming worst case loading conditions (i.e., all three accelerations, X, Y', and Z', remain in phase and peak simultaneously throughout the test) imposed on a flex pivot with no support against angular deflections. Conversely, the best case estimate is based on the minimum practical load (the maximum load in one axis only, crosscoupling effects ignored) applied to a flex pivot that takes the load in pure shear only.

The conclusion is that the Multispectral Scanner is in no danger from acoustic qualification testing. While the above results do not predict certain failure for MSS in random vibration qualification testing, they do indicate a real possibility of failure. When MSS is vibrated at qualification level, an occasional flex pivot failure should be anticipated.

TABLE 9-6. ESTIMATED TIME TO FATIGUE FAILURE* SUMMARY

Test	Worst Case	Best Case	Expected Value
MSS qualification vibration test (12.8 g rms input)	6 sec	61 min	135 sec
MSS acceptance vibration test (−3 dB from qualification)	54 sec	∞	26 min
MSS acoustic qualification test (147 dB OASPL)	4.4 hr	∞	∞

*In Equation 9-11 the fatigue time depends on $\sigma^{6.5}$. If stress level increases by 1.42 (3 dB) factor, the fatigue time is reduced by 10. Therefore, without very accurate knowledge of stress levels, it is difficult to closely bound the expected time to failure.

ORIGINAL PAGE IS
OF POOR QUALITY

9.2 SHUTTER SYNCHRONIZER ANOMALY

After the Z-axis vibration, the calibration shutter failed to phase lock for a period of 12 minutes, and the shutter control integrator telemetry was at 0.47 volt. After the initial period of delay, operation of the phase locked loop seemed to be normal. Failure report F1699 was written. Vibration testing was continued in the Y- and X-axes. Following the Y-axis vibration the shutter phase lock loop was completely inoperative. In fact, there was an indication of a complete loss of the shutter preamplifier outputs: Band 4 calibration wedge appeared abnormal, indicating a loss of dc restore pulses, which are controlled by the shutter preamplifier outputs.

Subsequent to the protoflight vibration tests, the scanner was partially disassembled to remove the shutter monitor preamplifier. The light emitting diodes (LEDs) for modulation of the shutter were observed to be putting out a strong signal. Supply voltages to the preamplifier were normal, and there was every indication that the preamplifier had an internal defect.

The protoflight shutter monitor preamplifier was returned to Santa Barbara Research Center (SBRC) for disassembly, test, and evaluation. It was determined that a solder was broken where the receiving photodiode was connected to a bifurcated terminal at the preamplifier input (see Figure 9-9). The solder joint was judged to have been broken by vibration because the photodiode had insufficient strain relief. Such lengths of wire (approximately 1 inch) are typically stranded rather than single conductor. This design, however, precludes the use of stranded wire except by an illegal splice. After the photodiode was replaced, the wire was secured by encapsulation of the terminal in epoxy bonding material. The protoflight scanner was tested electrically and then reassembled.

After reassembly, the shutter would phase lock only when the buffer wear adapter box was connected to the J9 test point connector. This behavior was confirmed by a special test with the shutter synchronization pulse as shown in Figure 9-10.

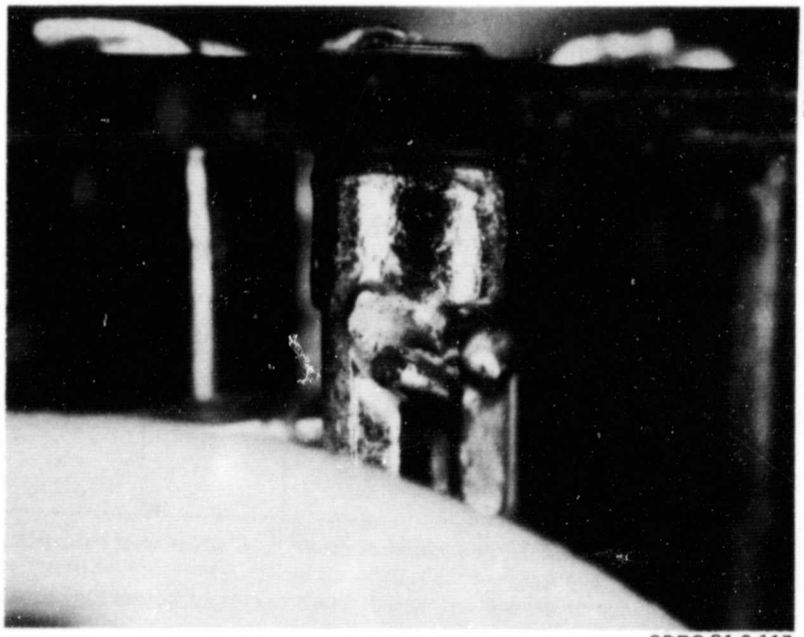

SBRC 81-2-117

FIGURE 9-9. BROKEN PHOTODIODE LEAD IN SHUTTER PREAMPLIFIER

ORIGINAL PAGE IS
OF POOR QUALITY

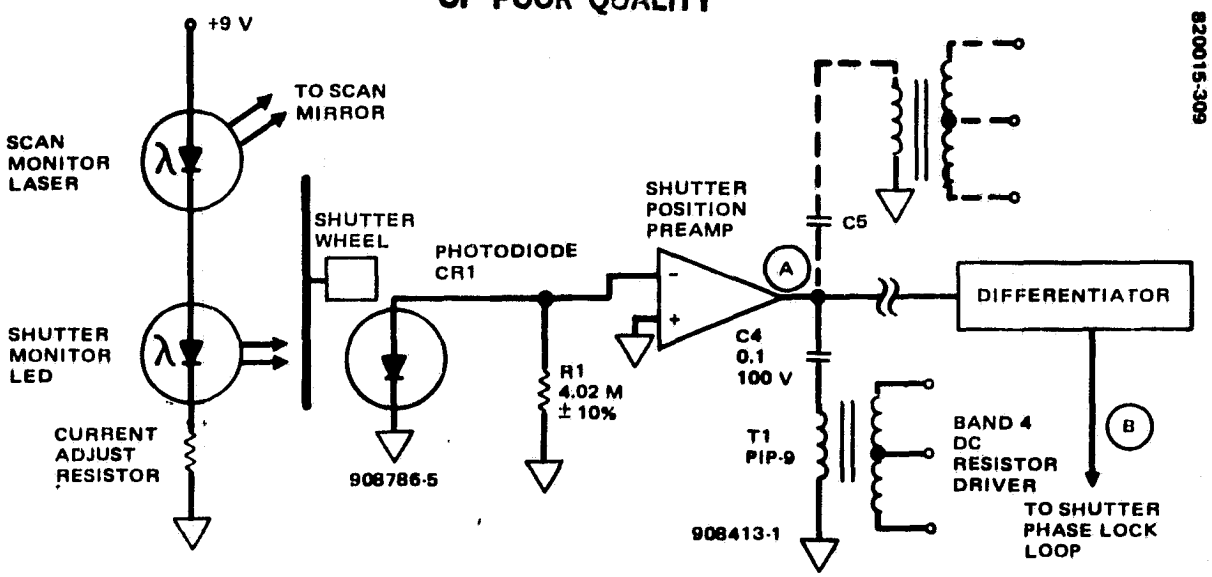

NOTE: BASIC ELEMENTS ONLY ARE SHOWN (C5 HAS BEEN CUT OUT)

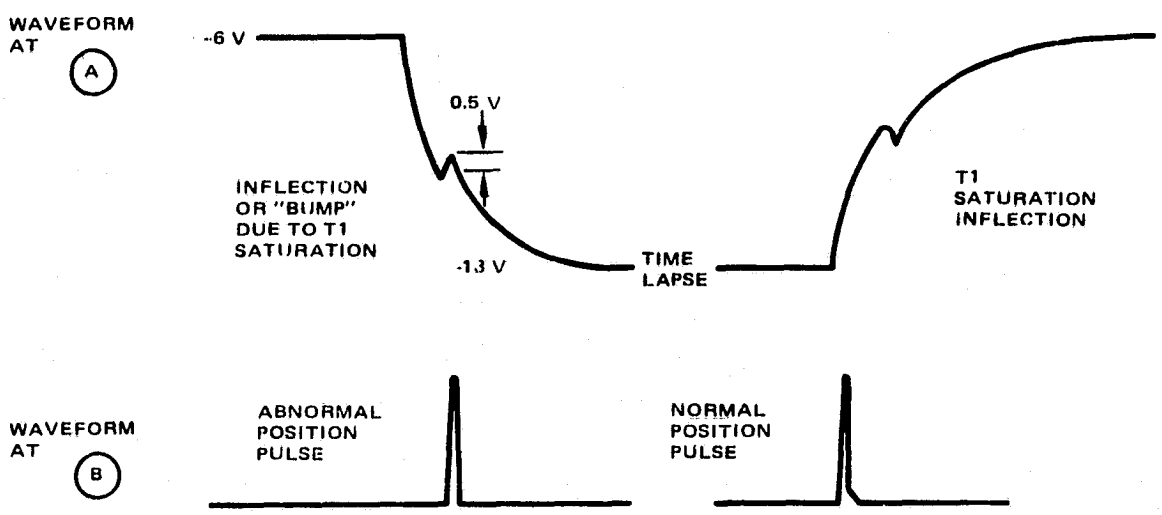

FIGURE 9-10. MSS-D SHUTTER POSITION SENSING METHOD

ORIGINAL PAGE IS
OF POOR QUALITY

820015-310

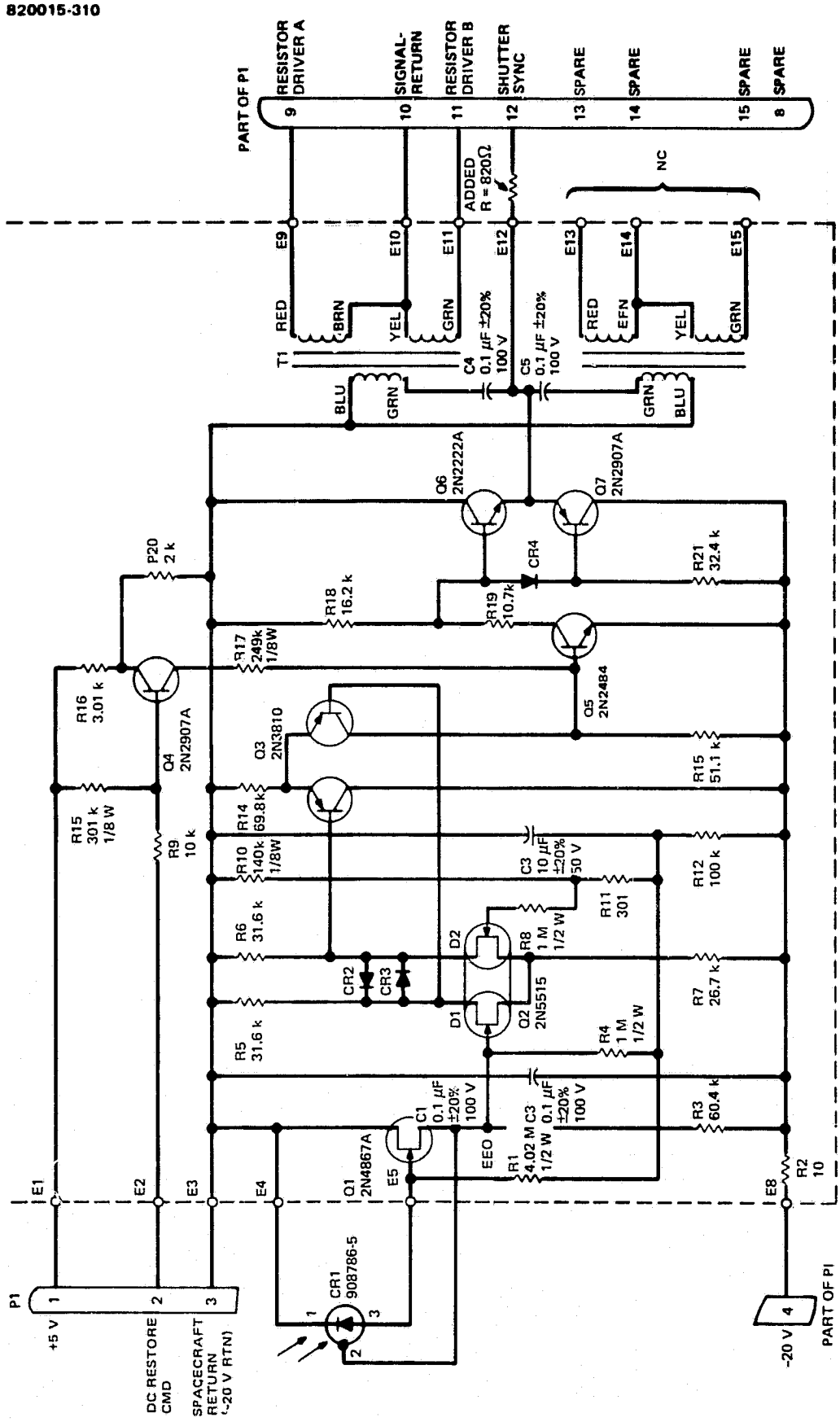

FIGURE 9-11. SHUTTER MONITOR PREAMPLIFIER SCHEMATIC

ORIGINAL PAGE IS
OF POOR QUALITY

A similar problem had occurred previously in the F-1 scanner, which would not phase lock. It was determined that a small amount of capacitive loading on the shutter preamplifier output would allow phase lock to occur. The preamplifier was removed from the F-1 scanner and tested in a unit tester on the bench. A waveshape similar to that shown in Figure 9-10 was observed with a rising inflection on the descending slope of the square wave. The inflection was of sufficient amplitude to trigger a circuit designed to sense only the positive going voltages on the trailing edge of the square wave. An empirical determination was made that the position and amplitude of the inflection on the square wave were controllable by the amount of light into the preamplifier photodiode. Corrective action to the F-1 scanner was to remove C4 (Figure 9-11) to partially unload the output transistors and to change the amount of current in the shutter LED from 13 mA to 25 mA. With these changes, the F-1 scanner phase locked successfully. A retrofit of the protoflight shutter monitor preamplifier was not done at the time since there were no functional problems with it. After the solder joint failure in the protoflight occurred in vibration, C4 was removed from the preamplifier when the photodiode was replaced. The protoflight LED current was already set at 25 mA.

The protoflight preamplifier was returned to SBRC. It was speculated that the failure occurred because the second photodiode was not positioned far enough forward in its mounting sleeve, and insufficient light was reaching the photodiode from the shutter LED for proper circuit operation. A third photodiode was installed, mounted further forward, but the phase lock problem remained. To more thoroughly investigate the shutter synchronizer circuit performance, the engineering model shutter position preamplifier was connected to the laboratory test fixture and a breadboard differentiator was constructed to load the preamplifier. It was determined that the lack of phase lock was caused by false triggering of the synchronizer circuitry on the preamplifier output inflection shown in Figure 9-10.

The shutter position pulse differentiator is normally activated by the rising (trailing) edge of preamplifier output when the photodiode light is obscured by the shutter. The normal preamplifier output waveform falls from approximately -6 to -13 volts for a swing of 7 volts peak-to-peak. The small inflection on the falling edge that causes a false position pulse was only about 0.5 volt peak-to-peak, but of sufficient amplitude to trigger the differentiator circuitry and prevent phase lock.

The inflection is initiated by the progressively heavier loading on the preamplifier output as current increases in the T1 primary (Figure 9-11). The loading transient that results causes the inflection by the ringing that results due to the T1 primary leakage inductance and circuit capacitance responding to the increase in output impedance as the preamplifier runs out of current gain.

Although it is not understood why the first photodiode worked before vibration and the second or third did not, it was decided that, in any case, the operation of the circuit was marginal, and that a change was required to reduce sensitivity of the differentiator to false triggering. Two general methods were considered to solve the problem: elimination of the inflection and the reduction of susceptibility of the differentiator to inflection. Because of easier implementation the second approach was used.

The method chosen was to reduce the effect of the inflection by adding an 820 ohm resistor in series with the preamplifier output to the shutter position reference differentiator (Figure 9-11) and, thereby, increasing the differentiator noise immunity.

ORIGINAL PAGE IS
OF POOR QUALITY

820015-312

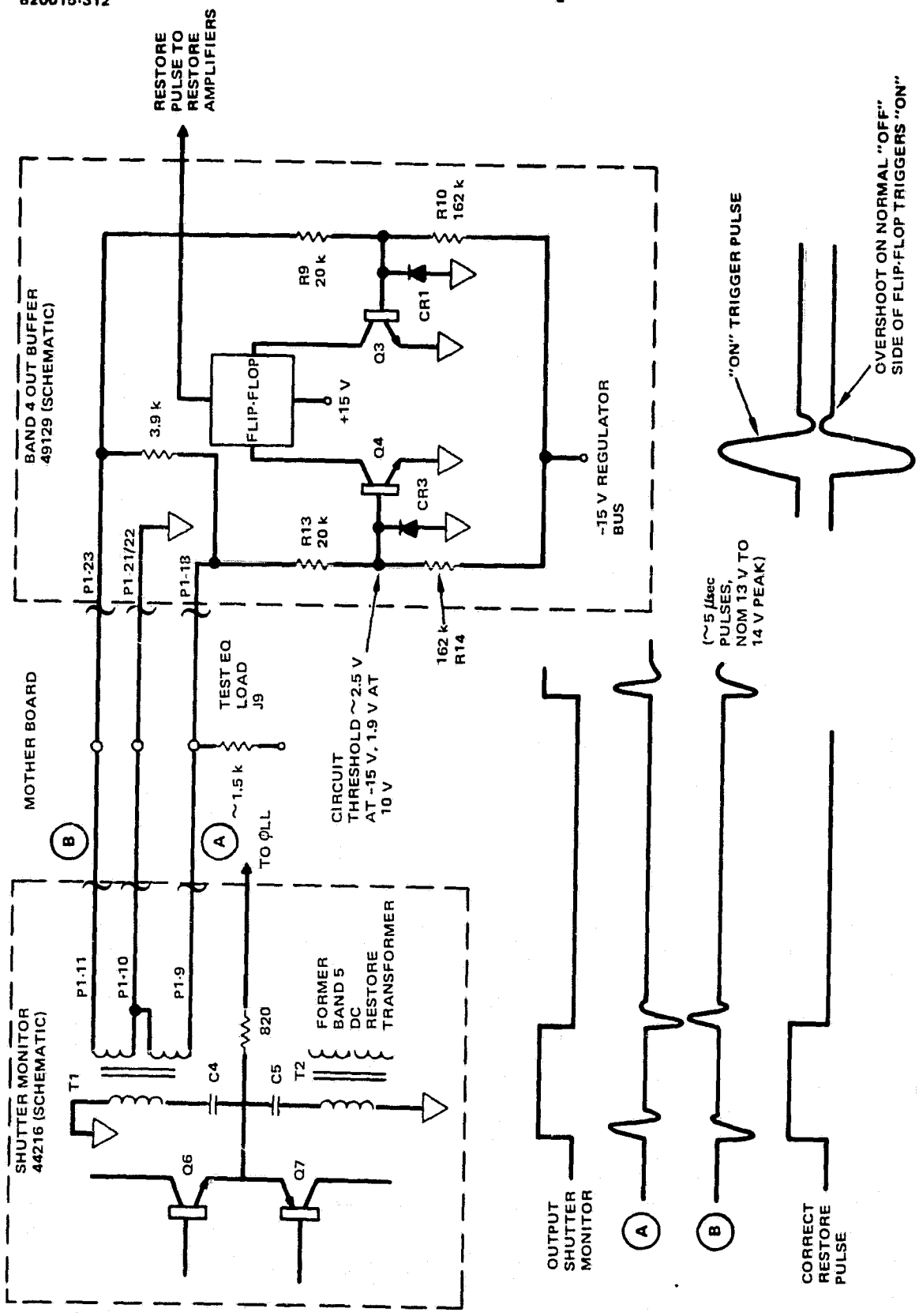

FIGURE 9-12. DC RESTORE PROBLEM

ORIGINAL PAGE IS
OF POOR QUALITY

This method works by taking advantage of the low initial (small signal) input impedance of the differentiator to highly attenuate small signal excursions without significant large signal attenuation. It greatly increases the noise immunity of the differentiator so it will not respond to the 0.5 volt (peak-to-peak) inflections.

As part of the evaluation of the anomaly a design review committee met to discuss all known circumstances surrounding the failure. After careful consideration of all known related events and facts concerning the engineering model, protoflight, and flight model scanners, the reason for proper functioning of the protoflight and flight model instruments prior to the 820 ohm resistor addition could not be explained. The only recommendation was a test of the engineering model shutter motor control board to see whether it could lock up in any mode with a false position pulse present. This test showed the loop could not possibly have been locking up in any way with a false position pulse present.

The margin of safety with the 820 ohm resistor in series with the preamplifier output is also high because the protoflight shutter preamplifier did not fail to produce a correct position pulse until the resisitor value was increased approximately four times the nominal value. The false pulse did not occur until the resistor was reduced to approximately one-fourth its nominal value. The 820 ohm resistor also has been added to the F-1 and the engineering model units. No phase lock problems have been experienced since the fix was installed.

9.3 DC RESTORE PROBLEM

The F-1 scanner was configured for a radiometric calibration according to procedure 16894 on 14 March 1981. This procedure requires the output of the demultiplexer to be monitored on an oscilloscope. On this occasion the calibration wedge signal in band 4 looked abnormal. The abnormality was determined to be caused by a lack of dc restoration. Further troubleshooting revealed that when the J9 buffer wear adapter was connected at the test point connector, band 4 had normal dc restoration. Specifically, loading of J9 pin 4 (band 4 dc restore command) caused normal operation of the dc restore circuitry. This test point is designated Ⓐ on the Figure 9-12 schematic. Additional testing showed that the dc restore pulses were 13 volts in amplitude with approximately 2.5 volts of overshoot. This amount of overshoot was of sufficient amplitude to trigger the downstream circuit on the band 4 buffer card.

The block diagram for the band 4 signal processing circuits is shown in Figure 9-13. The normal operation of the dc restore circuitry is as follows: Scene radiance is sensed by a photodiode in each band 4 channel. The amplified photodiode signal is ac coupled through long time constant circuits and is converted to a dc level controlled signal by means of the dc restore amplifier. This amplifier removes long term dc offset drifts. When there is no light input to the detectors during the time the shutter is closed, the drift corrections are made by setting the dc level of the output signal of each band 4 channel to zero volt potential. The repetition rate of the dc restore function is every second scan line or approximately 7 times a second.

Figure 9-12 shows the circuit configuration of interest to the problem. The shutter monitor preamplifier has a dual output. The first output is a square wave used to control the phase locked loop for shutter speed and phase control. The second output is

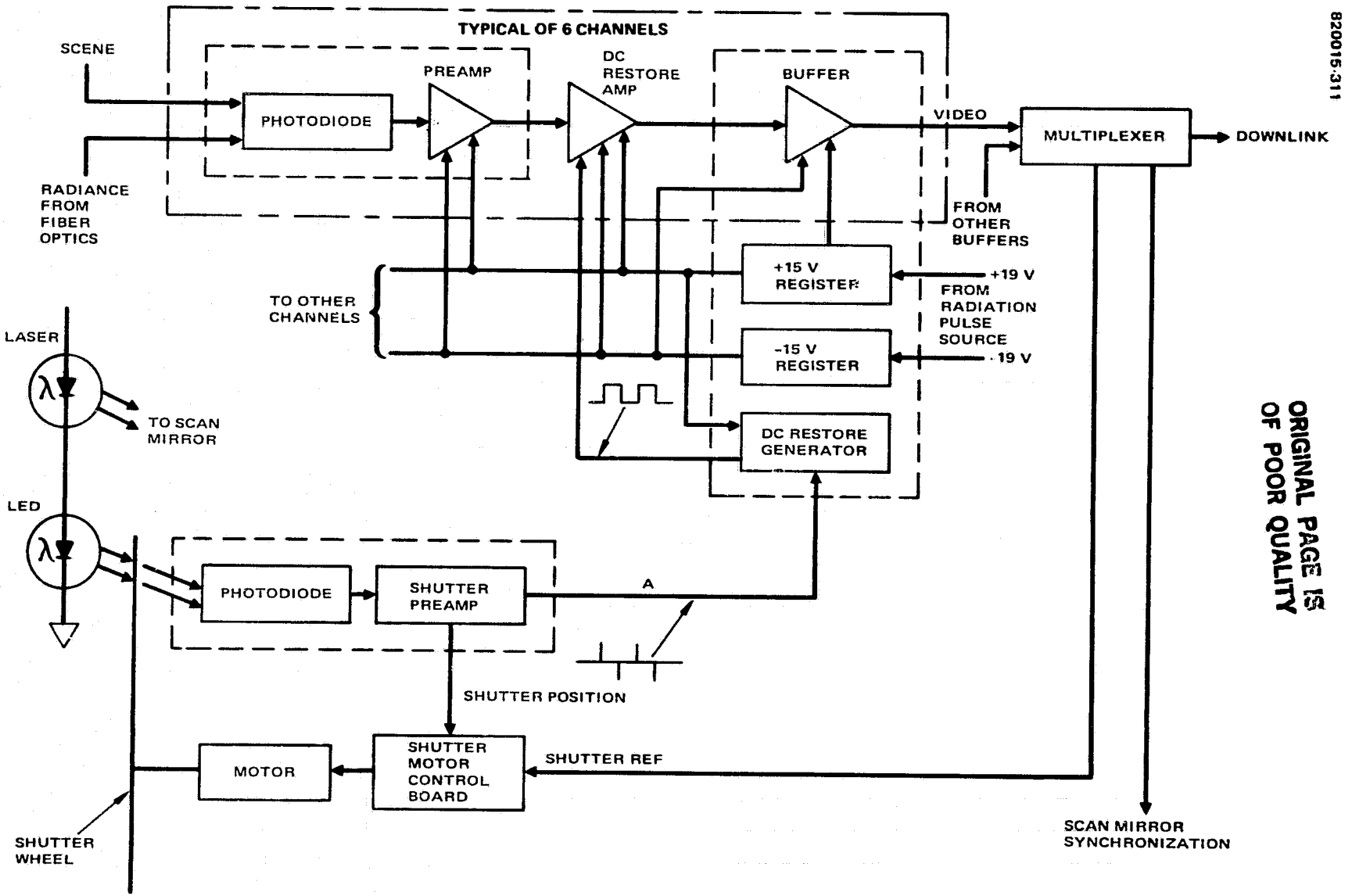

FIGURE 9-13. MSS-D BAND 4 PHOTODIODE SIGNAL PROCESSING BLOCK DIAGRAM

ORIGINAL PAGE IS OF POOR QUALITY

ORIGINAL PAGE IS
OF POOR QUALITY

from a transformer which provides ground isolation of the servo and signal processing circuits. The shutter position pulse is differentiated on both edges by the pulse transformer T1 and its coupling capacitor C4. The outputs of T1 are isolated electrically from spacecraft ground. Figure 9-12 shows how the T1 pulses are used to trigger a flip-flop via inverting switches Q3 and Q4. If the -15 volt regulator output is not in current limit, the nominal triggering threshold for Q4 reflected to the output of T1 is the sum of V_{BE} in Q4 and the V across the 20K resistor R13, where

$$V_{BE}\,(20^{o}C) = 0.6\ V$$

$$V_t = 0.6\ V + \frac{15.6\ V}{162\ K}\,(20\ K) = 2.53\ V$$

With a 2.5 volt overshoot on the transformer output, the flip flop circuitry had no margin against false triggering.

Up until now the discussion has considered only the condition that existed after the -15 volt regulator on the photodiode buffer board (schematic 49129) risen to its full output voltage after power turnon. However, the regulator had a 4.7 ohm current limit resistor (R6). The value of R6 was chosen to produce current limiting at only a small incremental current above normal operating load current. As a result, each time the power was turned on, the large positive going signal from the band 4 preamplifiers drove the dc restore amplifiers (schematic 44314) positive at their outputs, which in turn saturated the buffer outputs in a negative sense. In series with the buffer outputs is a 200 ohm resistor (R34-X) and inside the multiplexer is a 151 ohm resistor and a negative clamp diode to prevent the multiplexer inputs from swinging below -0.6 volt. When the buffer outputs saturated and the multiplexer clamp diodes conducted, each buffer output had a load of 351 ohms to ground. The high currents that flowed in these load resistances also flowed from the -15 volt regulator, causing it to current limit and its voltage output to rise to -10 volts. This is the same -15 volt source used to bias the fip-flop circuits for the dc restore function (Figure 9-12).

The only way that the -15 volt regulator could get out of current limiting was for the dc restore amplifiers to reduce the positive initial bias from its output to a level where the buffer outputs could rise and unload the -15 volt regulator. However, the dc restore amplifiers could not function properly until the -15 volt regulator had come out of current limiting. The design was caught in a Catch-22 situation.

The inverting switches Q3 and Q4 on the buffer board are normally held off by R10 and R14 returned to the -15 volt bus. When the -15 volt bus magnitude was low during turnon, the Q3 and Q4 triggering thresholds were lowered, and the overshoots from the shutter preamplifier caused false triggering. This false triggering resulted in a dc restore waveform which prevented the dc restore amplifiers from recovering from their turnon transient.

This latchup phenomenon had not been observed previously in any of the MSS scanners. Subsequent measurements on the protoflight scanner showed it also to be falsely triggering during power turnon when the -15 volt bus was pulled down, but the protoflight was not latching as Flight-1 had because of the following phenomenon.

ORIGINAL PAGE IS
OF POOR QUALITY

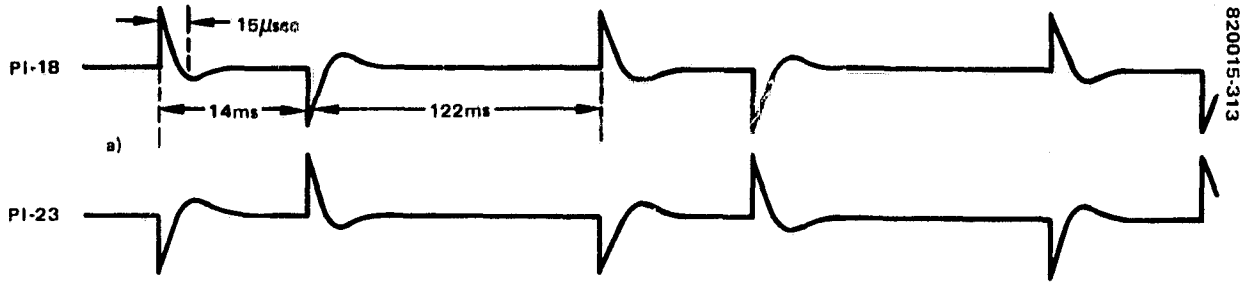

a) PREAMPLIFIER OUTPUTS (FIGURE 9-12)

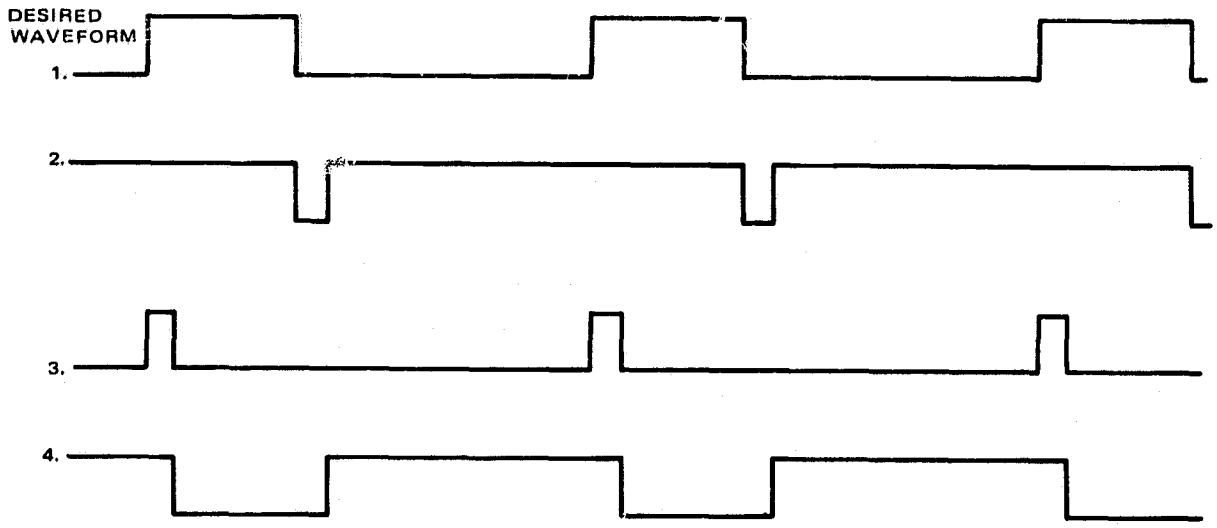

CONDITIONS:

1) NEITHER OVERSHOOT TRIGGERS
2) PI-18 OVERSHOOT TRIGGERS
3) PI-23 OVERSHOOT TRIGGERS
4) BOTH OVERSHOOTS TRIGGER

b) POSSIBLE RESTORE PULSE OUTPUTS. FLIP FLOP OUTPUTS (FIGURE 9-12)

FIGURE 9-14. DC RESTORE PULSES AND RESULTING DC RESTORE WAVEFORMS

ORIGINAL PAGE IS
OF POOR QUALITY

Figure 9-14 is a timing diagram showing time-magnified dc restore pulses from the shutter preamplifier T1 and possible restore pulse waveforms. The actual preamplifier output pulses can be seen in Figure 9-15. If the overshoots are large enough or the -15 volt magnitude small enough, the positive going overshoots, as well as the normal positive going part of the dc restore pulse, can trigger the flip-flop that generates the actual dc restore waveform. The timing diagram shows four possible combinations:

1) Neither overshoot triggers (normal)

2) Only the overshoots on P1-18 of the buffer board trigger (abnormal)

3) Only the overshoots on P1-23 of the buffer board trigger (abnormal)

4) Both overshoots trigger (abnormal)

The overshoots are not equal in amplitude because of differences in T1 secondary windings and capacitive loading of only restore driver A by the J9 breakout box during test. At the threshold of triggering, only one overshoot may trigger. In case 1), the dc restoring action occurs for 14 ms each period, the intended time. Cases 2) and 4) allow longer dc restoring each cycle, which is fine as long as the overshoots stop triggering as the -15 volt power comes up and re-establishes case 1). Case 3) dc restores for only approximately 15 μs each cycle, an insufficient time to recover the dc restore amplifiers in a reasonable time. Based on the 10 second stabilization time observed on the PF scanner and allowing oversimplification of zero memory mode drift, the band 4 stabilization time would be:

$$t_s = \frac{14\ \text{ms}}{15\ \mu\text{s}} \frac{10\ \text{s}}{3600\ \text{s/hr}} = 2.59\ \text{hr}$$

Capacitor leakage in the downstream might be large enough to prevent it from recovering at all. Case 3) is apparently the situation which occurred on the F-1 instrument when band 4 did not stabilize after turnon. A test was run on the protoflight to determine its turnon dc restore characteristics. The results were that the dc restore circuits were initially triggering on both overshoots, case 4, Figure 9-14, and transitioning to a normal output, case 1, as the -15 volt regulator came out of current limiting. To reduce the amplitude of the overshoots a 3.9K resistor was connected across the secondary windings of T1. The value of this resistor was chosen experimentally to make the dc restore pulses out of T1 be the same amplitude as they had been before C5 was clipped to remove T2, the band 5 dc restore coupling transformer.

The transformer T1 and associated circuitry is shown as:

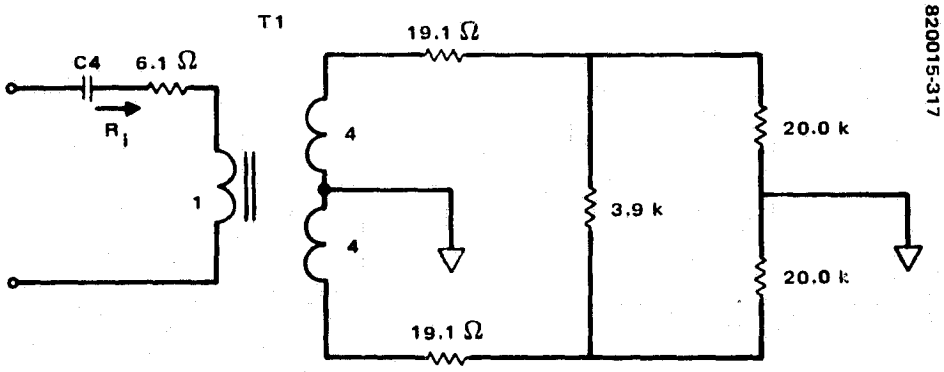

ORIGINAL PAGE IS
OF POOR QUALITY

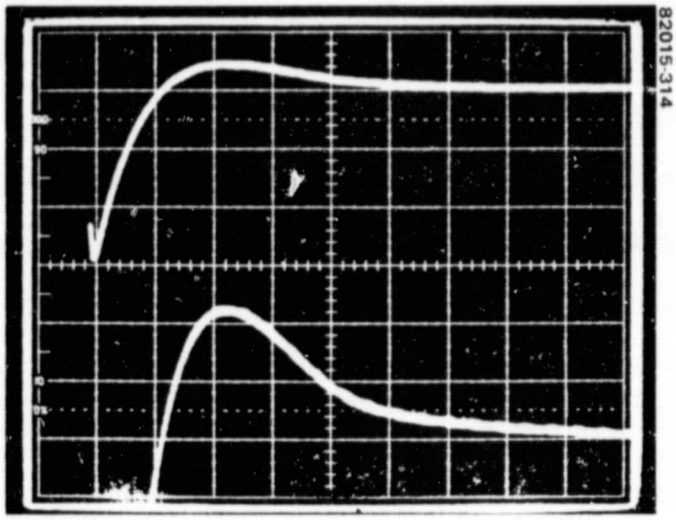

a) BEFORE ADDING
3.9 K RESISTOR

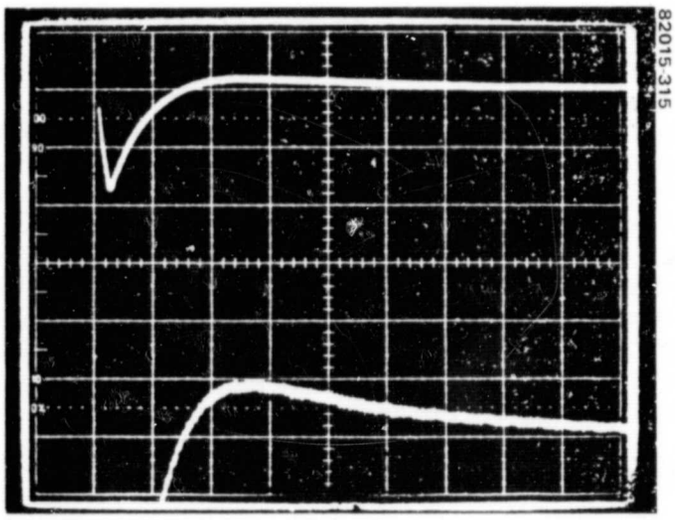

b) AFTER ADDING
3.9 K RESISTOR

FIGURE 9-15. PROTOFLIGHT PREAMPLIFIER OUTPUT PULSES

ORIGINAL PAGE IS
OF POOR QUALITY

The 6.1 and 19.1 ohm resistors are winding resistances. The base-emitter junctions and the 162K base return resistors to -15 volt in the inverting switches ahead of the dc restore flip-flop on the photodiode buffer board are omitted because their effects are negligible. The whole secondary load is:

$$R_L = \frac{3.9\text{ K }(40\text{ K})}{43.9\text{ K}} + 2(19.1) = 3.55\text{ K} + 0.038\text{ K} = 3.59\text{ K} \tag{9-12}$$

The primary input resistance is:

$$Ri = 6.1 + \frac{3590}{8^2} = 6.1 + 56.1 = 62.2\text{ ohm}$$

The primary equivalent circuit is approximately as follows, ignoring small core losses:

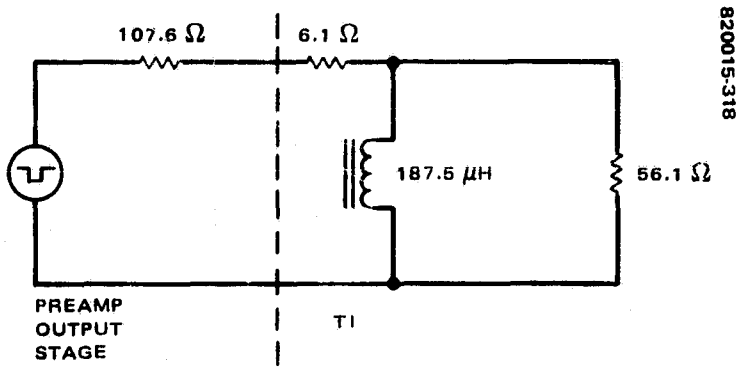

$$T_P = \frac{L_p}{R_p} = (187.5)\frac{113.7 + 56.1}{113.7\,(56.1)} = 4.99\ \mu S$$

When the preamplifier output falls or rises, the voltage applied to the primary of T1 during the fast edge is determined by the output impedance of Q6 and Q7 and how much current it can supply to the primary. With h_{FE} = 100 and an open circuit negative swing at the preamplifier output of 6.2 volts (calculated from schematic), the peak T1 primary voltage would be ideally:

$$V_p = 6.2\text{ V}\,\frac{56.1}{107.6 + 56.1 + 6.1} = 2.048\text{ V} \tag{9-13}$$

This applies to the pulses of both polarities if the h_{FE} of Q6 and Q7 are equal. With a turn ratio of 1:4 the secondary voltage with respect to ground will be:

$$V_s = (2.048)\,(4)\,\frac{3550}{3588} = 8.1\text{ V} \tag{9-14}$$

Figure 9-15 shows the actual V_s on the protoflight to be approximately 8.0 volts for the negative going trigger pulse, after adding the 3.9K resistor.

ORIGINAL PAGE IS
OF POOR QUALITY

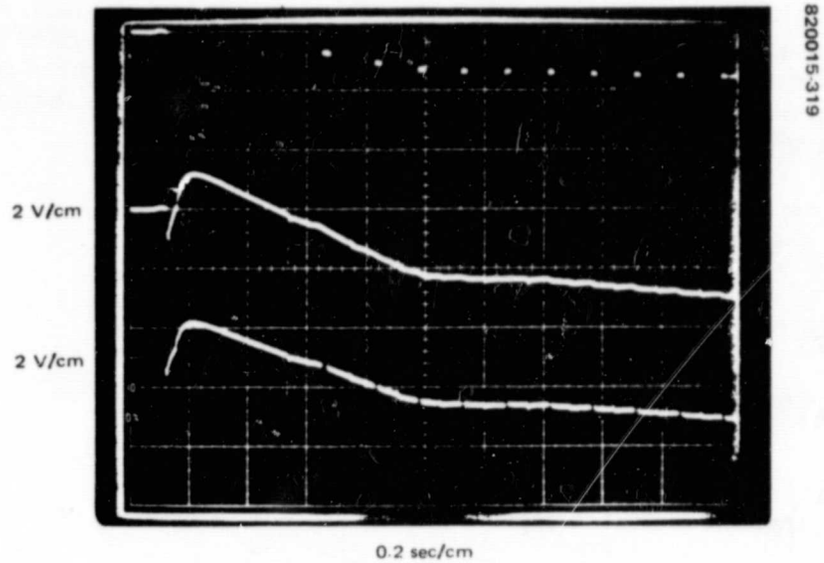

FIGURE 9-16. PROTOFLIGHT DC RESTORE WAVEFORMS WITH 3.9K RESISTOR

Figure 9-16 shows what happens when the 3.9K resistor is added to the protoflight. The early upper trace is the -15 volt at 2 volt/cm and 0.2 sec/cm, with zero at the top. It swings negative to -7.0 volt, then rises to -4.9 volt before ramping down toward -15.0 volt. The early lower trace is the dc restore waveform. It starts at 0.0 volt at 3 cm down from the top and swings negative at 2 volt/cm. Then its baseline proportionally tracks the -15 volt with the correct dc restore pulse polarity starting at 0.65 second Recovery is normal in this photograph.

During the turnon sequence with the 3.9K resistor, the protoflight scanner's -15 volt output reaches a minimum amplitude of -4.9 volt (F-1 may be more or less). This means that the false triggering threshold at the interface between the shutter preamplifier and the photodiode buffer is

$$V_t = 0.6\ V + \frac{4.9\ V + 0.6\ V}{162\ k}(20\ k) = 1.28\ V \tag{9-15}$$

Figure 9-15 shows overshoots of 0.90 volt after addition of the 3.9K resistor. This means that a safety margin against triggering by overshoots then existed of

$$Ms = \frac{1.28\ V - 0.90\ V}{1.28\ V} = 29.7\%\ \text{(lab temperature)} \tag{9-16}$$

As stated earlier, the -15 volt current limiting played a role in the amount of overshoot that would cause false triggering by holding the voltage to less than -15 volt at system turnon. The current limiting resistor was then changed from 4.7 to 2.7 ohms after it was determined that the pass transistor could handle the extra load. The net effect of the change in current limiting is that the -15 volt is only pulled down to -9.0 volt at system turnon rather than the -4.9 volt shown in Figure 9-16.

ORIGINAL PAGE IS
OF POOR QUALITY

TABLE 9-7. SUMMARY OF DC RESTORE TRIGGER MARGINS

Condition	Pulse Amplitude	Overshoot Amplitude	Trigger Turnon	Threshold Steady State
Original	14	2.2	1.28	2.5
Added 3.9 K	8	0.9	1.28	2.5
Changed current limit to 2.7 Ω	8	0.9	1.78	2.5

Table 9-7 summarizes the effects of adding the 3.9K resistor to the transformer load and the subsequent change in current limiting of the -15 volt regulator. There is no doubt that an adequate margin of safety exists after the changes for proper operation of the band 4 dc restore circuitry.

9.4 VIDEO CABLE NOISE

As the protoflight system was being integrated and evaluated in August 1980, the system noise levels became a concern. VPIR pictures and data reduced on the system test computer indicated a larger than expected level of noise in the signal channels. Excessive noise had been encountered in earlier MSS scanners and had been reduced to acceptable levels by modifications in the system grounding and filtering of the power supply switching transients. These techniques for noise reduction were carried forward to MSS-D. However, further improvements were needed for the larger switching currents associated with the new primary power supply and more stringent signal-to-noise requirements of MSS-D.

Special tests for evaluation of the signal to noise ratio were conducted on 4 9, and 10 September 1980. These tests indicated an undesirable level of video noise. On 12 September another special test was conducted to determine the effects of coherent noise. Oscilloscope photographs were taken at the interface between the scanner and the multiplexer. Subsequent to these tests, a signal-to-chassis ground short was located and corrected. Retesting on 15 September indicated no improvement of signal-to-noise. After some coaxial cable problems were resolved on 20 September, the demultiplexer output was found to have a coherent noise of sufficient amplitude to be synchronized on the oscilloscope. This coherent noise pattern changed character as a function of spacecraft bus line voltage, strongly suggesting that the noise was associated with the power supply switching currents. It was thought that the observed effect was caused by an oscillation in the control loop of the primary power supply.

Extensive "hands off" testing was conducted 22 and 23 September 1980. Empirical results indicated that an improvement might be made by grounding the shields of the signal channels to chassis rather than to the analog video returns. This possibility was the result of an observation that the noise level on the analog video outputs evident within the electronics housing collapsed when the load (to the multiplexer) on J4 was removed.

At the time, the cable configuration was thought to be as shown in Figure 9-17; it was then intended to revise to the configuration of Figure 9-18. Instead, a review of

ORIGINAL PAGE IS
OF POOR QUALITY

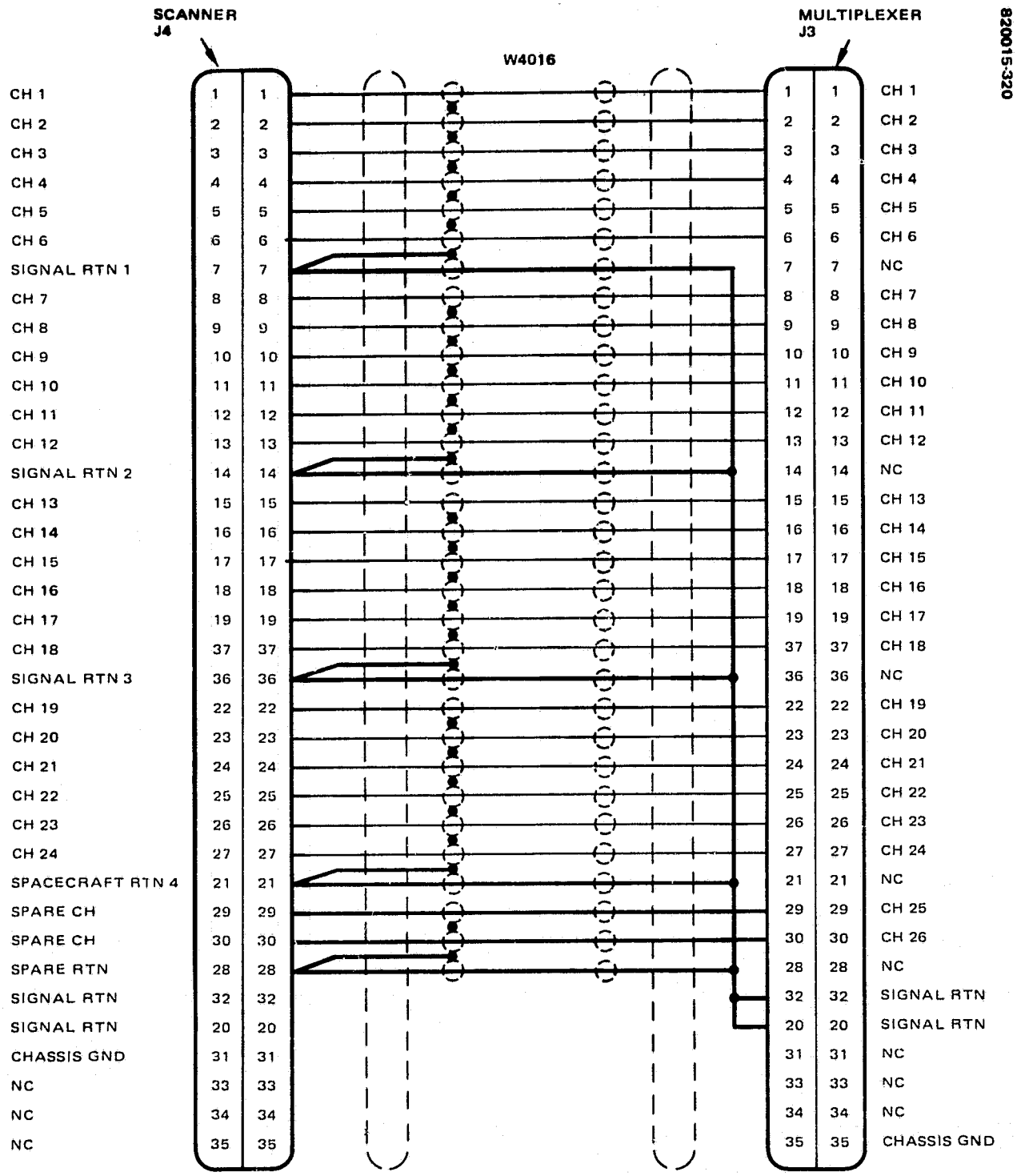

FIGURE 9-17. VIDEO CABLE, INTERFACE SPECIFICATION CONFIGURATION (EO1724A)

ORIGINAL PAGE IS
OF POOR QUALITY

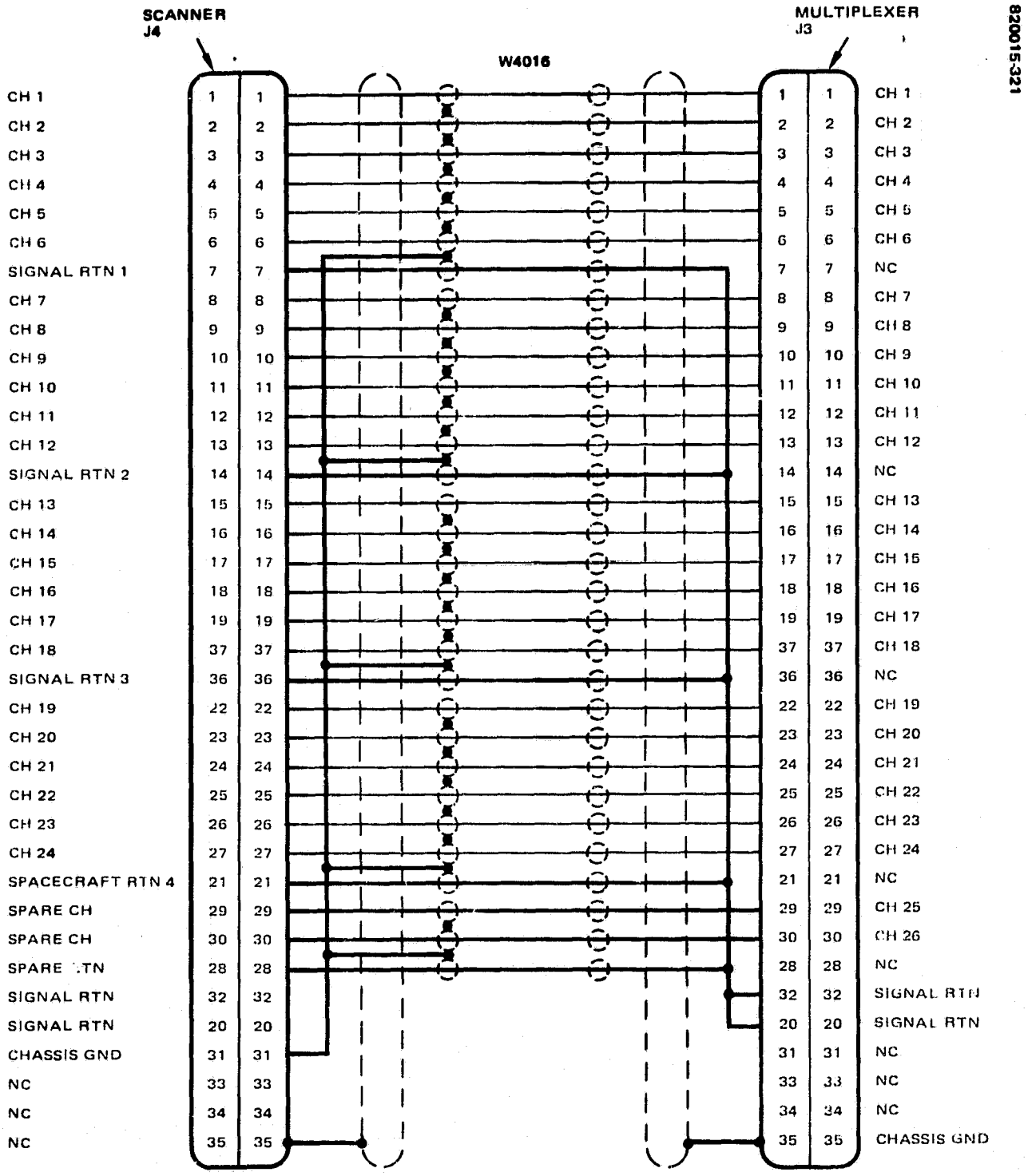

FIGURE 9-18. VIDEO CABLE, EO2061A CONFIGURATION

ORIGINAL PAGE IS
OF POOR QUALITY

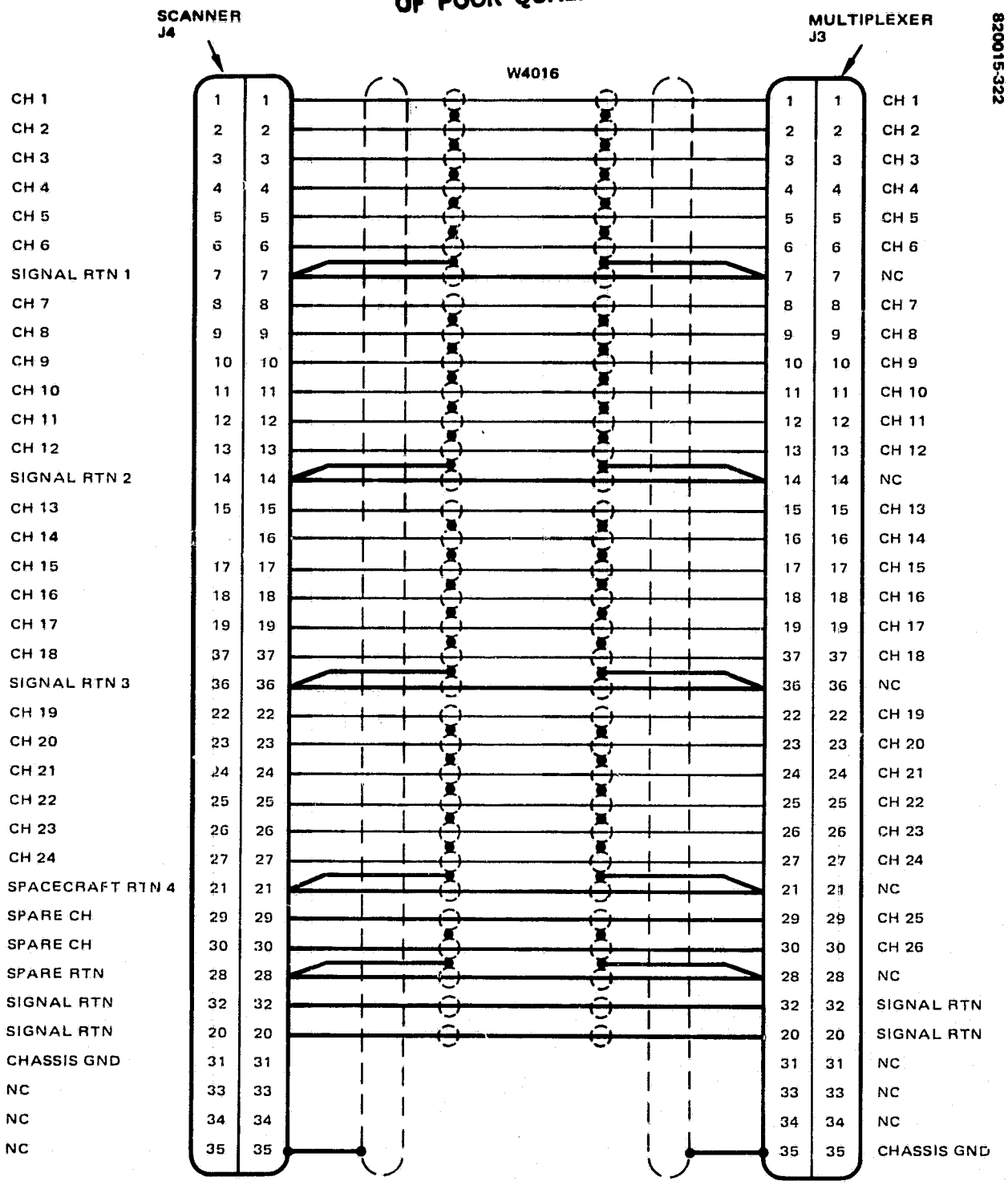

FIGURE 9-19. VIDEO CABLE INITIAL CONFIGURATION

the drawings showed that the cable was configured according to Figure 9-19. (Note, in Figure 9-19, that the signal returns for each of the four bands is a no connection termination at the multiplexer.) The cable was then revised to Figure 9-17 configuration. The signal-to-noise data sets using data out of the multiplexer were improved after the change; however, the noise amplitudes observed on the analog video within the electronics housing showed little or no change.

The engineering model multiplexer was then tested in conjunction with the protoflight scanner. A significant improvement in the signal-to-noise ratio was observed. A separate result was a notable reduction in line length variations. The F-1 multiplexer became available and was integrated with the protoflight scanner. The reason for the change of multiplexers was not signal to noise ratio, but rather to evaluate the cause of anomalous line length variation. However, the signal to noise ratios measured using the F-1 multiplexer in the system were determined to be between those measured using the protoflight and the engineering model multiplexers.

On 1 October 1980, testing of the W4016 (analog video) cable proceeded in the Figure 9-18 configuration. There seemed to be a performance improvement with the individual channel shields connected to chassis ground instead of to the signal returns for each band. The signal-to-noise ratios were still below anticipated levels. Noted at this time was the fact that connection of the J box no longer attenuated noise levels but aggravated them. The J box provides a T function which connects a cable from the scanner test set to the connections of the analog signal from the scanner to the multiplexer. The cable to the scanner test set was in the Figure 9-19 configuration and the cable between the scanner and multiplexer was the Figure 9-18 configuration.

The next change in cable configuration was to that of Figure 9-20, with the returns for each band lifted and the signal return from the scanner connecting directly to the signal return input to the multiplexer. The results in this configuration were not as good as for the previous configuration.

IDC HS248-6407, written 9 October 1980, stated the difference in system performance with different multiplexers, indicating performance to be marginal with the F-1 multiplexer and improvement still required in the protoflight multiplexer.

System integration proceeded near the beginning of November using the protoflight scanner, the F-1 multiplexer, and the W4016 analog video cable in the Figure 9-18 configuration. The first complete system performance test was conducted on 18 November, following the completion of system integration. Several signal-to-noise failure reports were initiated against the results of this complete system performance test.

At this point it was decided to run tests with the multiplexers alone to try to understand the differences in system level noise performance as a function of which multiplexer was used. The protoflight and enginering model multiplexers were chosen for the test becuase they had the extremes of noise performance. The PF and EM multiplexers were tested for input switch turnon transients in the laboratory. All of the analog input channels of both multiplexers were investigated, with analog voltage inputs varied between 0 and 4 volts and driven from 100 ohm source impedance. Voltage transients were consistently formed when the selected channel switch was turned on. The peak values of these transients for the two units are shown in Tables 9-8 and 9-9.

ORIGINAL PAGE IS
OF POOR QUALITY

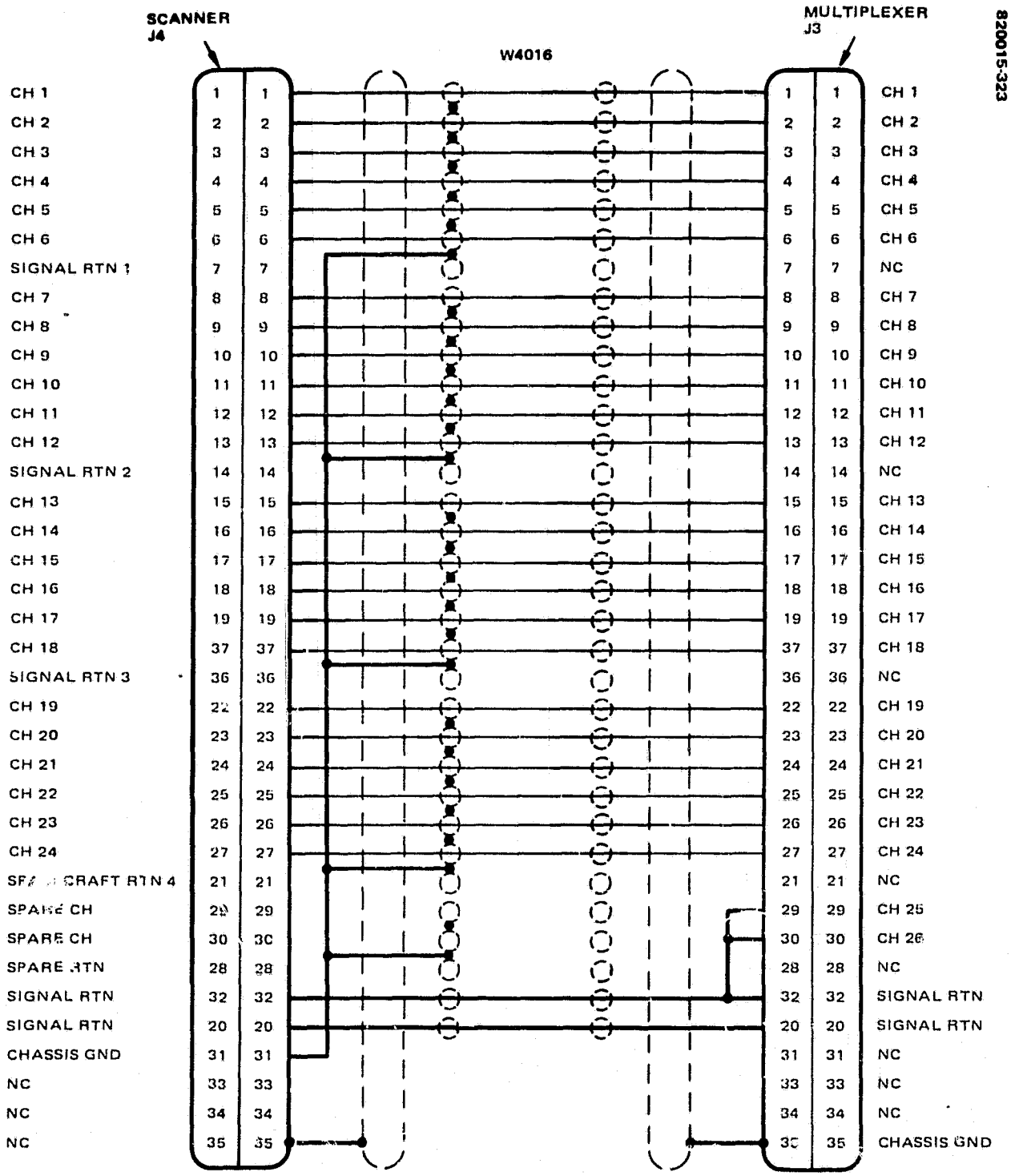

FIGURE 9-20. VIDEO CABLE E01747A CONFIGURATION

ORIGINAL PAGE IS
OF POOR QUALITY

TABLE 9-8. MSS-D ENGINEERING MODEL MULTIPLEXER TEST DATA

Channel	Peak Voltage Coupling to Source By Input Multiplexer Switches Turnon, V			
	0 Volt Input	1.3 Volt Input	2.6 Volt Input	3.8 Volt Input
1	0.17	0.12	0.10	0.06
2	0.13	0.10	0.08	0.02
3	0.16	0.10	0.06	0.03
4	0.16	0.15	0.11	0.06
5	0.15	0.14	0.10	0.07
6	0.18	0.15	0.10	0.07
7	0.19	0.14	0.10	0.06
8	0.17	0.13	0.08	0.05
9	0.12	0.10	0.05	0.02
10	0.14	0.11	0.06	0.03
11	0.17	0.14	0.10	0.06
12	0.20	0.13	0.10	0.05
13	0.15	0.12	0.08	0.04
14	0.18	0.14	0.11	0.07
15	0.22	0.15	0.13	0.08
16	0.20	0.13	0.10	0.07
17	0.15	0.12	0.09	0.06
18	0.22	0.13	0.10	0.07
19	0.18	0.12	0.08	0.06
20	0.17	0.10	0.06	0.04
21	0.15	0.10	0.06	0.04
22	0.15	0.10	0.06	0.04
23	0.21	0.14	0.11	0.06
24	0.23	0.14	0.12	0.07
Average	0.173	0.125	0.089	0.054

ORIGINAL PAGE IS
OF POOR QUALITY

TABLE 9-9. MSS-D PROTOFLIGHT MULTIPLEXER TEST DATA

Channel	Peak Voltage Coupling to Source by Input Multiplexer Switches Turnon, V			
	0 Volt Input	1.3 Volt Input	2.6 Volt Input	3.8 Volt Input
1	0.22	0.10	0.03	0.02
2	0.27	0.11	0.03	0.02
3	0.35	0.20	0.15	0.08
4	0.20	0.12	0.07	0.05
5	0.17	0.09	0.02	0.02
6	0.30	0.20	0.18	0.08
7	0.32	0.20	0.16	0.09
8	0.28	0.11	0.05	0.04
9	0.24	0.10	0.05	0.04
10	0.33	0.20	0.17	0.13
11	0.35	0.22	0.17	0.11
12	0.27	0.10	0.04	0.02
13	0.31	0.18	0.10	0.06
14	0.35	0.27	0.19	0.11
15	0.30	0.10	0.05	0.03
16	0.35	0.20	0.12	0.07
17	0.30	0.21	0.16	0.10
18	0.24	0.11	0.05	0.04
19	0.27	0.10	0.05	0.03
20	0.29	0.12	0.06	0.05
21	0.22	0.11	0.06	0.05
22	0.33	0.25	0.18	0.10
23	0.36	0.26	0.19	0.11
24	0.35	0.24	0.15	0.09
Average	0.290	0.162	0.103	0.061
PF/EM Ratio	1.68	1.30	1.16	1.13

ORIGINAL PAGE IS
OF POOR QUALITY

General wave shapes of the transients were very consistent for all channels of a particular multiplexer but were different for the two units. Figures 9-21 and 9-22 are representative pictures of transients of the two units. The protoflight unit transient has a very fast rise time and decays with a 120 ns time constant. The engineering model multiplexer transient also has a fast rise time but decays with a 220 ns time constant. In addition, the EM input transient does not rise to a sharp spike and then decay, as does the PF input transient, but rises and holds that level for 100 to 200 ns before decaying.

The results of a comparison of the PF and EM multiplexers depend on the criterion set. If peak voltage only is considered, the PF unit exhibits an average of 68 percent higher input transients with zero volt analog inputs than does the EM. This difference gets progressively smaller as the analog input voltage is increased until it is only an average 13 percent higher at 3.8 volts input.

If the input transients of the two units are compared using the area under the voltage versus time curve as the criterion, the protoflight unit exhibits less input transient coupling than does the EM. When the worst channel in each of the two units (PF channel 14 and EM channel 15) are compared in this way, the EM unit has 34 percent more coupling at the zero volt analog input than does the PF. Input transients measured at SBRC on the PF multiplexer do not resemble what is seen here with either the PF or EM unit. A picture of the PF multiplexer input (see Figure 9-23) when connected to the scanner electronics shows a transient of about the same amplitude that is observed in the laboratory but indicates a rapid decay which undershoots the baseline and appears to ring for an undetermined time. This behavior suggests that the impedance of the scanner is reactive and is not dissipating the turnon transient energy as is the resistive termination of the laboratory tester.

A scanner amplifier was breadboarded and used to drive the selected analog input channels to the multiplexer, replacing the normal tester circuitry. Series inductance was added in the line between the amplifier and the multiplexer channel input until a wave shape approaching that seen at SBRC was observed at the multiplexer input. The value of this inductance is 1.6 μhenries. Methods of reducing the induced noise level were then attempted.

Part of the noise observed during system integration resulted from ringing in the line between the scanner and the multiplexer. The scanner's output amplifier provides a low impedance drive to the multiplexer. The multiplexer places a high frequency energy impulse on to its input lines each time the associated channel is selected, and if the impedance of the line between the units is sufficiently large and reactive, the line will ring at its natural frequency with little resistance to absorb the energy.

A series resistor placed at the amplifier end of the cable will absorb the voltage transient received from the multiplexer so that the ringing damps out quickly. With impedance used in the test setup, 51 ohms damps out the transient with almost no ringing. A 17 ohm resistor also damps out the ringing but not as quickly as the larger value. Figure 9-24 shows the multiplexer input wave shapes with series resistors is place.

ORIGINAL PAGE IS
OF POOR QUALITY

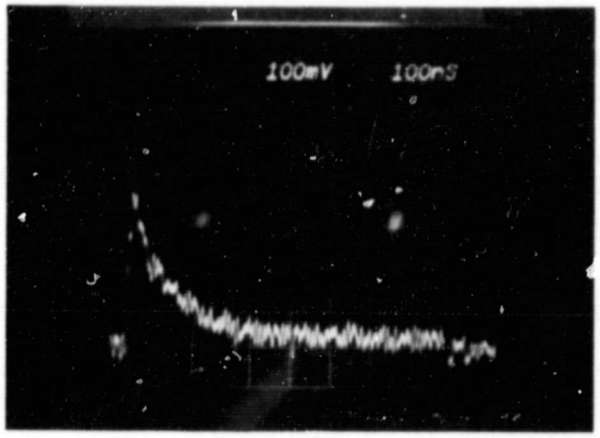

820015-324

FIGURE 9-21. PROTOFLIGHT CHANNEL ANALOG SWITCH TRANSIENT CONNECTED TO LABORATORY TESTER

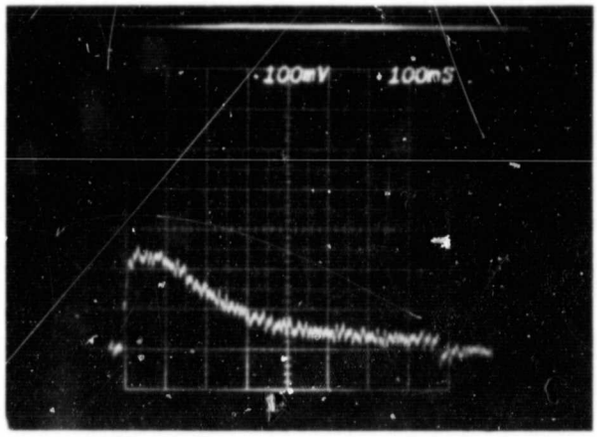

820015-325

FIGURE 9-22. ENGINEERING MODEL CHANNEL 15 ANALOG SWITCH TRANSIENT CONNECTED TO LABORATORY TESTER

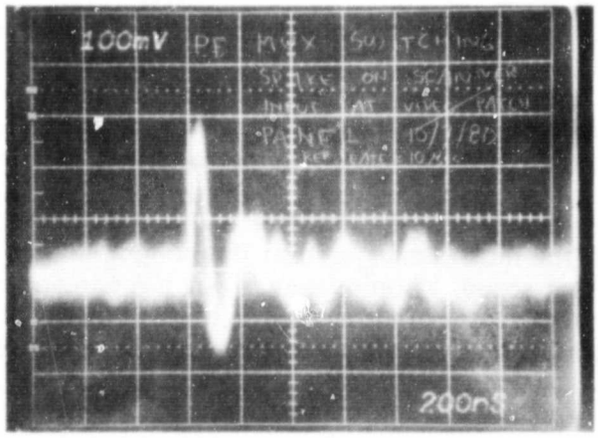

820015-326

FIGURE 9-23. PROTOFLIGHT ANALOG SWITCH TRANSIENT CONNECTED TO SCANNER AT SBRC

C-4

ORIGINAL PAGE IS
OF POOR QUALITY

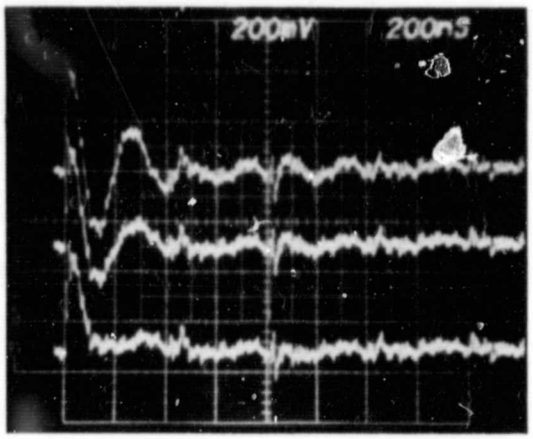

820015-327

FIGURE 9-24. MULTIPLEXER INPUT WAVE SHAPES WITH SERIES RESISTORS IN PLACE

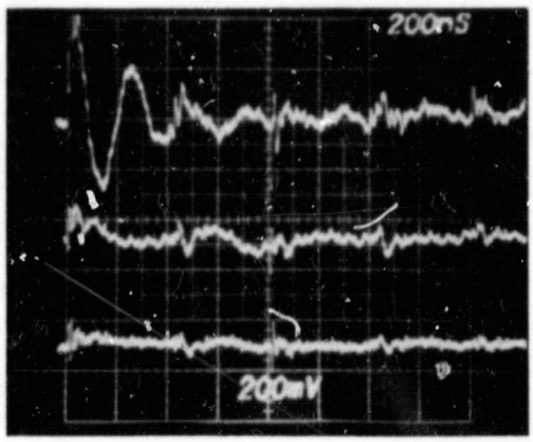

820015-328

FIGURE 9-25. MULTIPLEXER INPUT WAVE SHAPES WITH SHUNT CAPACITOR ADDED

A capacitor connected from the multiplexer end of the input cable to ground also reduced the transient to a low level with no ringing indicated. For the test setup impedance, a 0.01 μf capacitor worked well. This value is large enough to shunt the transient to ground but still small enough not to affect the frequency response of the analog inputs appreciably. Figure 9-25 shows the multiplexer input wave shapes with the shunt capacitor added.

The ringing might also be reduced by a change in the cable between the scanner and the multiplexer. The laboratory test cable normally used for analog inputs to the multiplexer is made up of twisted, shielded pairs, 4 feet long. The grounds are connected together for all 24 channels and connect to analog ground of the multiplexer and tester. The shield connects the chassis ground. The multiplexer input noise coupling, with no series inductance added, is observed on this cable to be a sharp transient which lasts for less than 200 ns. The cable was lengthened to 8 feet with a corresponding increase in delay time which was still acceptable. Figure 9-26 shows the scanner amplifier output and multiplexer input wave shapes with this cable.

An 8 foot RG 173, 50 ohm coaxial cable was subsituted for one channel input in the laboratory test setup. The input transient then also decayed in less than 200 ns. Figure 9-27 shows the scanner amplifier output and multiplexer input wave shapes with this cable.

Laboratory tests indicated that there were various options available to reduce the noise coupling of the multiplexer analog switches to acceptable levels; all of these could be implemented in the cable between the units and did not require modification of either the multiplexer or scanner:

1) Series resistance - A resistor placed in series with each analog channel on the scanner end of the scanner/multiplexer interface cable will absorb the energy of the noise coupling and prevent ringing.

ORIGINAL PAGE IS
OF POOR QUALITY

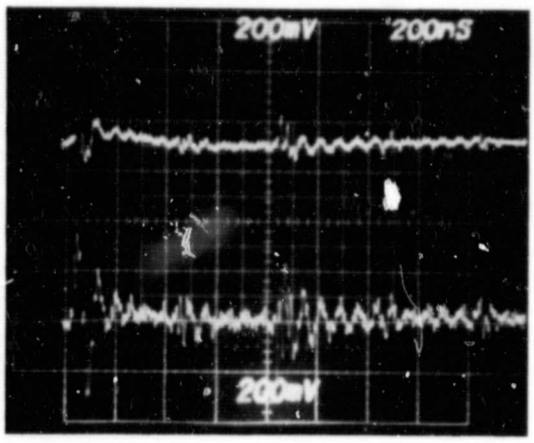

820015-329

FIGURE 9-26. SCANNER AMPLIFIER OUTPUT AND MULTIPLEXER INPUT WAVE SHAPES WITH CABLE

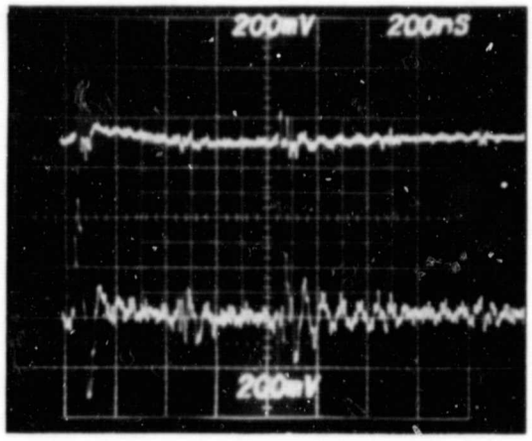

820015-330

FIGURE 9-27. SCANNER AMPLIFIER OUTPUT AND MULTIPLEXER INPUT WAVE SHAPES WITH RG 173, COAXIAL CABLE

2) Shunt capacitor - A capacitor connected from each analog channel to ground at the multiplexer end of the scanner/multiplexer interface cable will reduce the transients to acceptable levels.

3) Cables - A scanner/multiplexer interface cable consisting of either twisted, shielded pairs of wires or of 50 ohm coaxial cables reduces the decay time of the transients to acceptable levels.

After the initial complete system performance test had been compieted, an attempt was made to evaluate the options at the system level. A device was assembled that placed 51 ohm series resistances in every analog channel. This test connector was placed in series with the W4016 cable at J4 of the scanner. On 19 November 1980, the system was tested with and without the test connector. The computer printouts of the noise levels with no signal input showed improvement. However, the signal-to-noise data sets did not show the same amount of improvement. On 20 November the testing was repeated at lower light values. At the lower light levels, bands 1 and 2 showed a significant improvement by use of the test connector with the series resistors, but bands 3 and 4 showed little change.

The W4016 cables, 001 and 002, were reworked to the Figure 9-18 configuration and tested on 25 November to evaluate performance for similarity. The cables acted differently in the system until the test connector with the 51 ohm resistors was added at J4 of the scanner. Then, the cables were about equivalent. On 2 December the W4016 cables were used with the 51 ohm resistor test connector to establish a signal-to-noise baseline for the protoflight system before departure from the SBRC facility. At the time, there were plans for trying test connectors with other resistance values and new cables.

After transfer of the system to the EL Segundo facility, there was additional testing of noise to evaluate each possible improvement for optimum performance. Test connectors with various values of resistance were tested along with the W4016 cables and a new cable with a P/N 78622.

ORIGINAL PAGE IS
OF POOR QUALITY

The 78622 cable configuration is shown in Figure 9-28. It was assembled from the same shielded wire as the W4016 cables, but the shielded wire was terminated to make it look like coaxial cable. Further noise tests were conducted in late December 1980. Scope photographs and power spectra were taken of the analog video signal between the scanner and the multiplexer, and system signal-to-noise performance was calculated by the data reduction system from the quantized multiplexer output. The conclusions of these test were as follows:

1) With the W4016 configuration cable Figure 9-17 resistive or capacitive terminations on multiplexer end of the scanner to multiplexer, video cable improved the system signal to noise performance by reducing the ringing in the cable caused by closing the input sampling switches in the multiplexer.

2) With the lower impedance 78622 cable configuration, the resistive and capacitive terminations changed the character of transients in the cable due to multiplexer switching, but did not improve the system signal-to-noise ratios over the values obtained with the 78622 cable alone.

3) The 78622 configuration cable performed significently better than the W4016 configuration. In fact, its performance was good enough to allow the system to meet the signal-to-noise requirements.

4) Using the 78622 cable configuration the dominant remaining noise source injected into the system at the scanner to multiplexer interface is a 220 to 230 kHz modulation originating from the power system switching currents.

Figure 9-29 shows a typical spectrum of the signal at the input to the multiplexer using the 78622 video cable without any special terminations. The small peaks occurring at ≈100 kHz, and integral multiples come from the multiplexer sampling frequency. These peaks were reduced in amplitude by changing from the W4016 to the 78622 configuration cable. The large peak at 224 kHz is the second harmonic of the power system switching frequency. Its amplitude was little affected by the cable configuration change. From different measurements it was determined that the 224 kHz modulation shown in the figure is mostly a potential difference appearing across the signal return lead between the scanner and multiplexer. As a result of the tests, it was decided to change the baseline cable configuration to the 78622 configuration.

When the system was set up early in January 1981, new signal-to-noise problems appeared. Troubleshooting determined that the outer shield of the cable was inadequately secured to the cable clamp on the connector backshell. The cable clamp could not provide a sufficiently low resistance contact. As a result, EO 2355A was released against the cable drawing. This engineering order specified terminating the outer shield of the cable through the connector pins to chassis ground connections already provided by the scanner and multiplexer.

On 1 May 1981, additional testing was performed for evaluation of an apparent deterioration of the 78622 cable. An RC filter at the multiplexer end of the analog video cable improved the signal-to-noise ratio. On 5 May, the testing was repeated, using an assortment of values for the RC filter. The F-1 78622 cable was substituted and showed marked signal-to-noise improvement. It was used for the remainder of protoflight testing. The two cables differed in the way the outer shield was grounded. The cable

ORIGINAL PAGE IS
OF POOR QUALITY

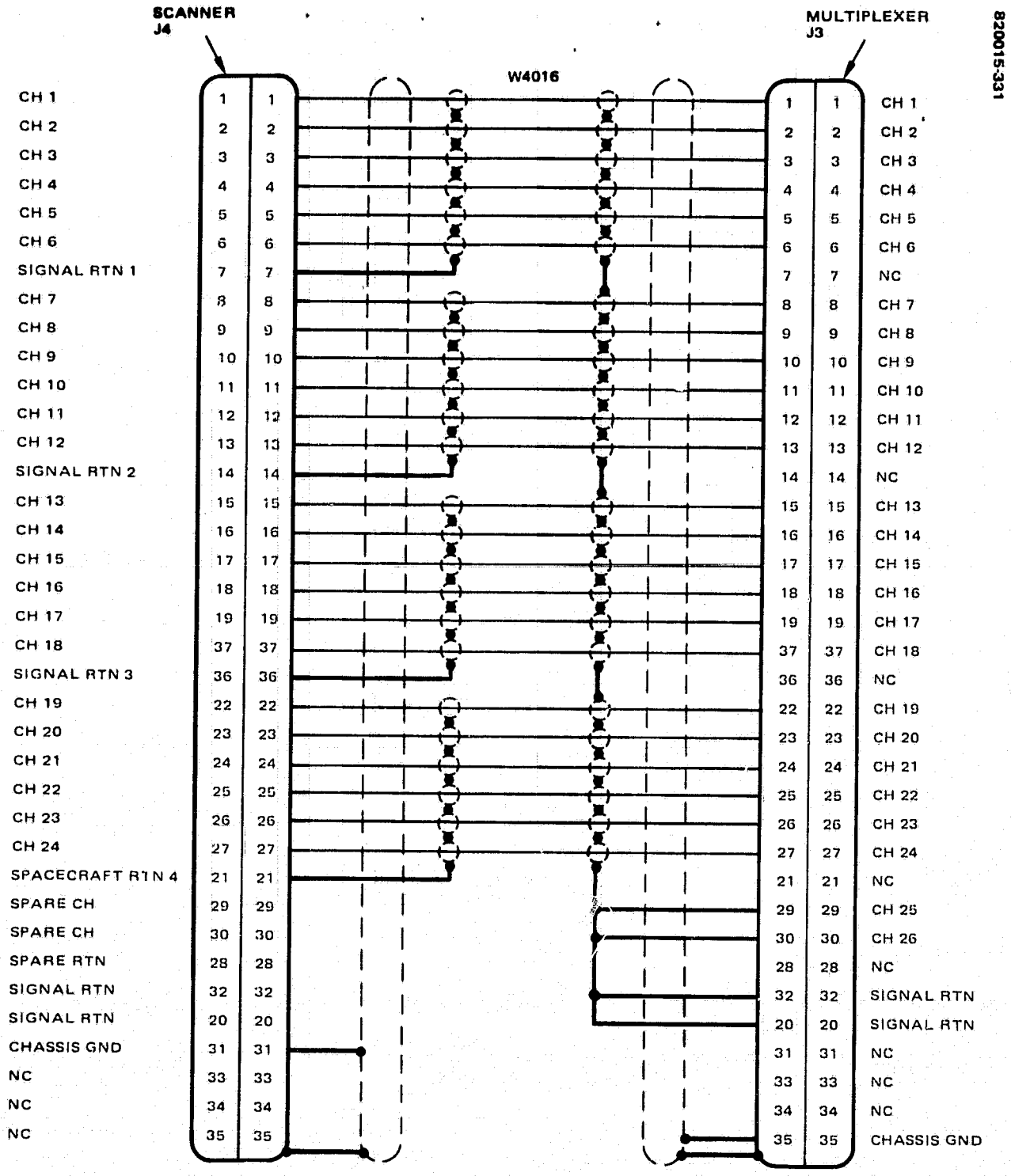

FIGURE 9-28. P/N 78622 CONFIGURATION

ORIGINAL PAGE IS
OF POOR QUALITY

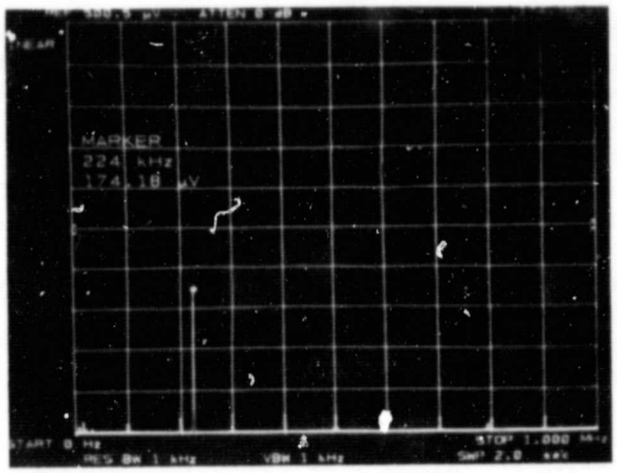

820015-332

FIGURE 9-29. SPECTRUM OF ANALOG VIDEO NOISE WITH 78622 CABLE

that had been used for testing the protoflight had the outer shield grounded through the connector pins as required by the engineering order to the drawing. The cable borrowed from the F-1 system not only had the shield routed through the connector pins, but also the outer shield at the multiplexer end of the cable was secured firmly by the connector backshell cable clamp. The S/N 003 cable, which was the replacement F-1 cable, was specified to have the connector backshells securing the outer braid of the cable in a firm and complete manner. On 16 June, the three 78622 cables were tested in conjunction with the F-1 system. There was no doubt that the extra care in grounding of the outer braid caused a significant improvement in performance. System signal-to-noise performance on both instruments has been within specification since the last of the cable changes.

9.5 CHANNEL 9 GAIN VARIATIONS

From the beginning of the protoflight system test program, the gain variation of channel 9, the third video channel in band 2, was a concern. Gain, as used here, is defined as the system transfer function of quantum level out of the multiplexer divided by radiance into the MSS aperture. Its nominal value for band 2 is 31.5 QL/mW/cm^2-Sr as set up at ambient temperatures and pressures. Figure 9-30 shows a history plot of the gains of channels 9, 10, 12 and instrument temperature throughout the system test program. The data shown are only from the orbits taken in conjunction with the collimator and excludes the integrating sphere data. The worrisome character of channel 9 gain is demonstrated by the gain slope in orbits 1 through 8, the high gain value around orbit 83, and the subsequent rapid decrease in gain out to orbit 92. Between orbits 76 and 81 an integrating sphere calibration was run where the gain of channel 9 was around 35 QL/mW/cm^2-Sr. Failure Report 5109 was generated as a result of this high gain and the erratic gain behavior of channel 9 up to that time. Between 28 April and 4 May 1980, a gain select resistor change was made which decreased the gain of channel 9 by 10.5 percent to assure that the channel 9 gain would not get so high that the multiplexer output would saturate at a light level inputs near the top of the specified radiance range.

ORIGINAL PAGE IS
OF POOR QUALITY

Subsequent to the change of the gain select resistor, the system was taken through the thermal-vacuum test, orbits 109 through 234. During this test, channel 9's behavior was in all respects normal. Its gain was lower than channels 10 and 12 by roughly the 10 percent gain select change mentioned previously. The temperature dependence of the channel 9 gain looked very similar to channels 10 and 12. During the thermal-vacuum test phase, the protoflight was run at a constant duty cycle of roughly 1/3: 35 minutes on, 65 minutes off sequences.

Following thermal-vacuum, the gains of all three channels recovered from their low levels in vacuum, the so-called "vacuum to ambient shift." In the two remaining orbital series of tests, orbits 246 through 253 at Hughes and orbits 302 through 311 at General Electric, channel 9 was once again displaying its anomalous gain behavior. Through each set of orbits, the gain started at a high value and fell off over the course of the test. Factoring out the 10.5 percent gain change put into channel 9 before thermal-vacuum, there was no discernible change in gain from the first series of tests on 18 November 1980 to the last set of tests on 17 July 1981.

Several mechanisms might be responsible for the anomalous gain variation:

1) Temperature driven gain instability - Photomultiplier tube gain is known to be temperature dependent. This phenomenon is readily apparent in Figure 9-30 in looking at the gain temperature dependence of all three channels over the temperature swings in thermal-vacuum. However, channel 9's temperature dependence during thermal-vacuum was similar to the other channels plotted. Furthermore, during the times that channel 9 gain was misbehaving, the system was in an ambient environment with temperatures running nearly constant around 25°C. Evidently unusual temperature dependence of channel 9 will not explain the anomaly.

2) Fiber optics plate - Channels other than channel 9 had unusual gain changes due to a bonding problem in the fiber optics plate assembly. The characteristics of this problem were: a) the gain changes would occur as the system temperature was driven up and down, and b) when the gains of these channels would change, the calibration system would not correct adequately for the changes, causing the corrected signal for the affected channels not to be matched to the other channels in the band. As mentioned previously, channel 9 has demonstrated no unusual temperature dependence. At the times when its gain was varying quickly, there was no failure of the calibration system to correct out of the gain change.

3) High voltage - Photomultiplier gain is a sensitive function of the high voltage applied to the dynode string. MSS PMT channels change gain by roughly 4.5 percent for every 1 percent change in high voltage. MSS high voltage power supplies are built in such a way that one power supply provides high voltage to every channel in a particular spectral band. If the high voltage were changing in one of these supplies, one would expect to see the gains of all channels in a band vary together. As can be seen from Figure 9-30, such behavior is evident with the temperature variations during thermal-vacuum, but not evident when channel 9 gain is varying anomalously at ambient temperature and pressure. When the band 2 high voltage telemetry was looked at against channel 9 gain, it was not found to vary directly with high voltage applied to band 2.

4) Buffer amplifier - An instability in the electronics chain downstream of the PMT is a possible cause of the channel 9 gain instability. No direct evidence is available

ORIGINAL PAGE IS
OF POOR QUALITY

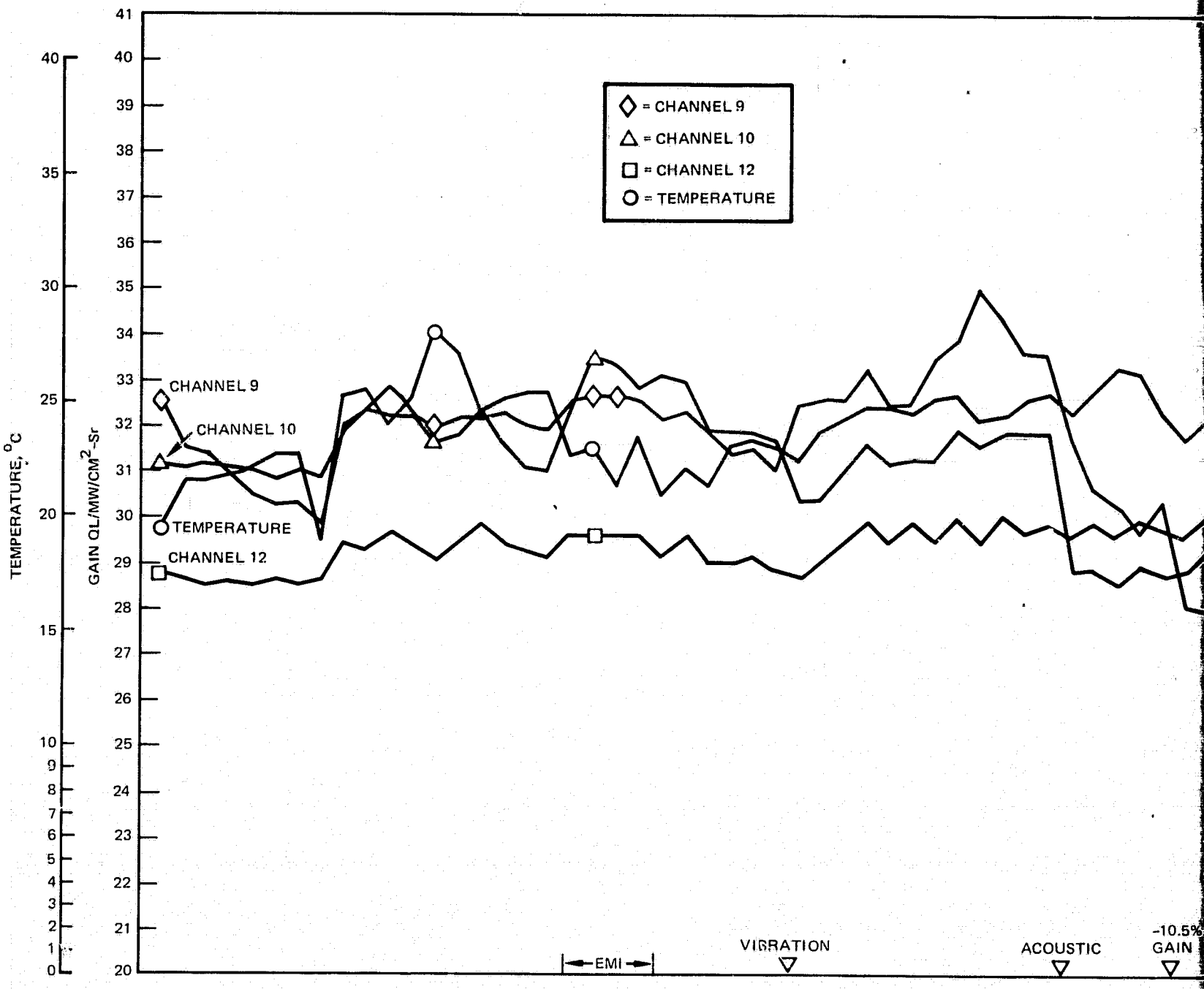

FIGURE 9-30. BAND 2 GAIN HISTORY

FOLDOUT FRAME

ORIGINAL PAGE IS
OF POOR QUALITY

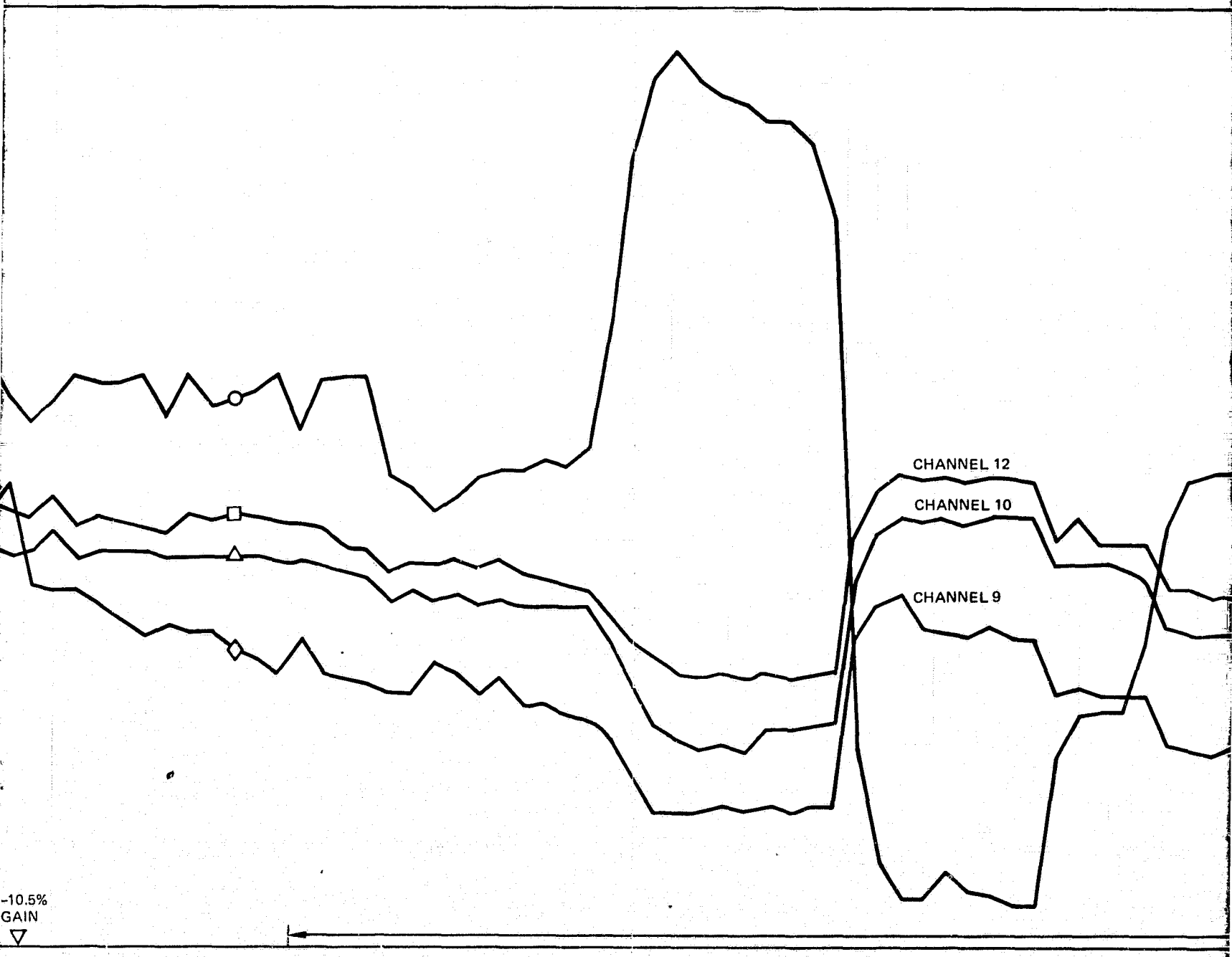

FOLDOUT FRAME 2

ORIGINAL PAGE IS
OF POOR QUALITY

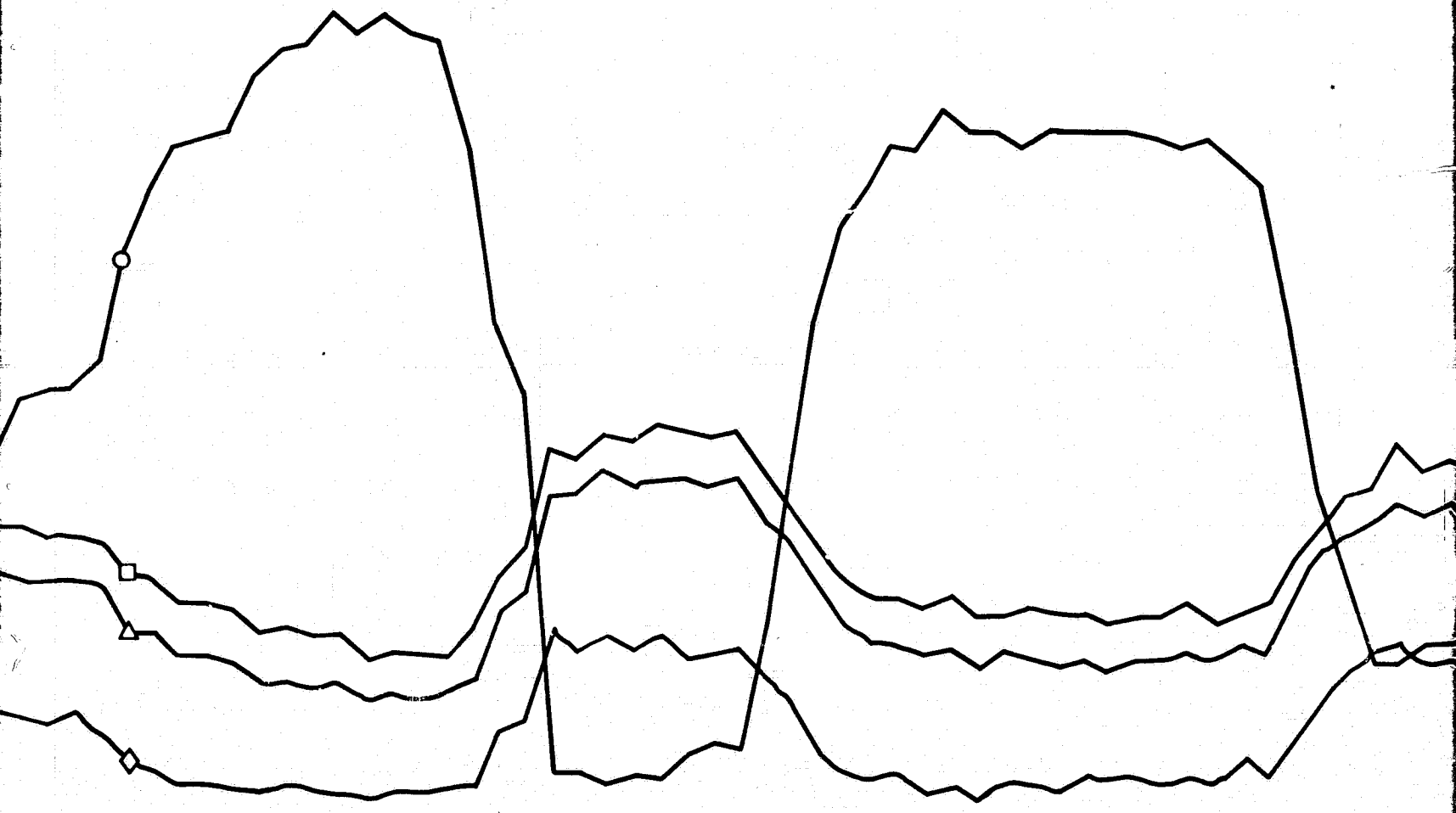

THERMAL VACUUM

3 FOLDOUT FRAME

ORIGINAL PAGE IS
OF POOR QUALITY

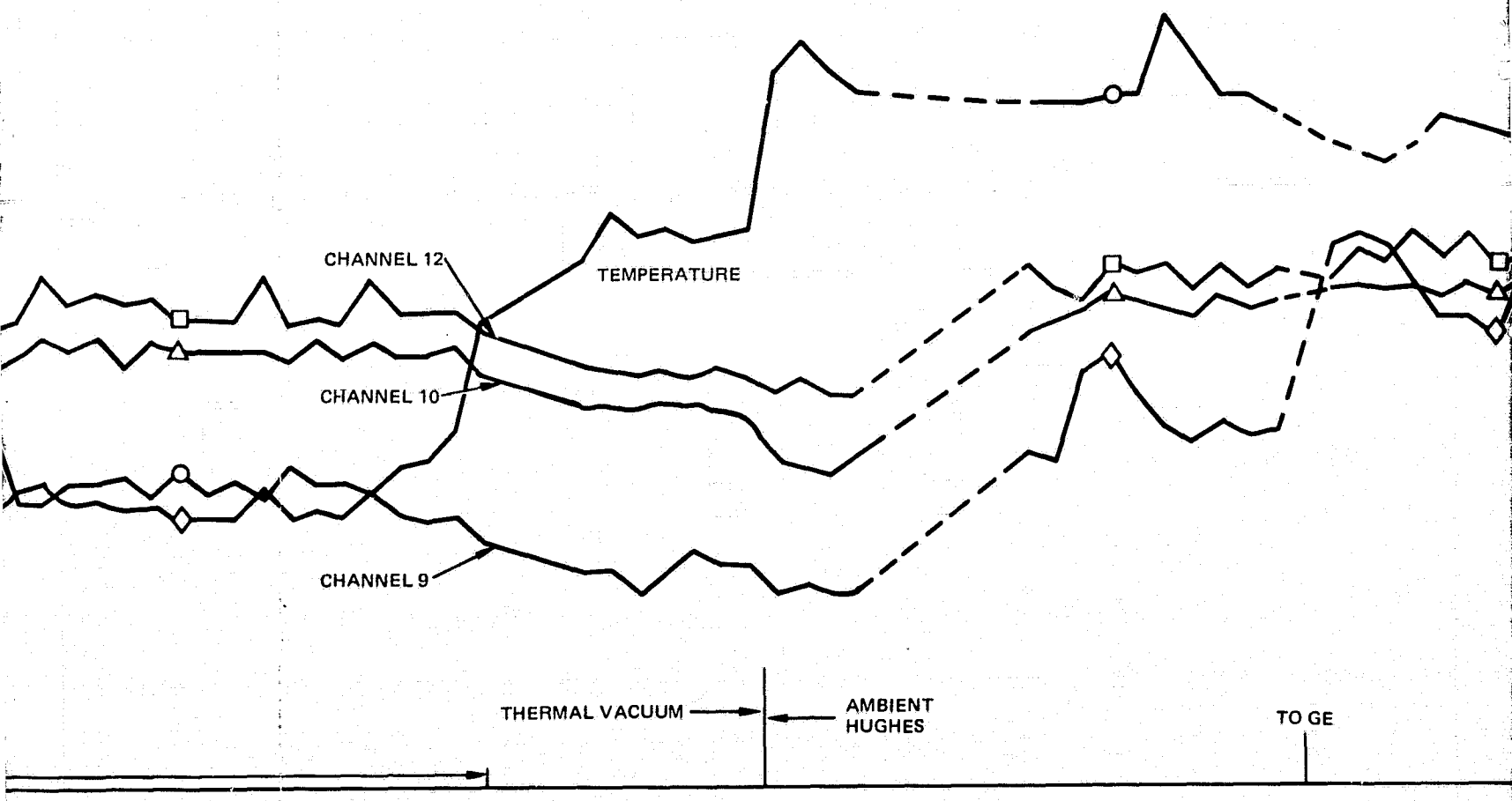

4 FOLDOUT FRAME

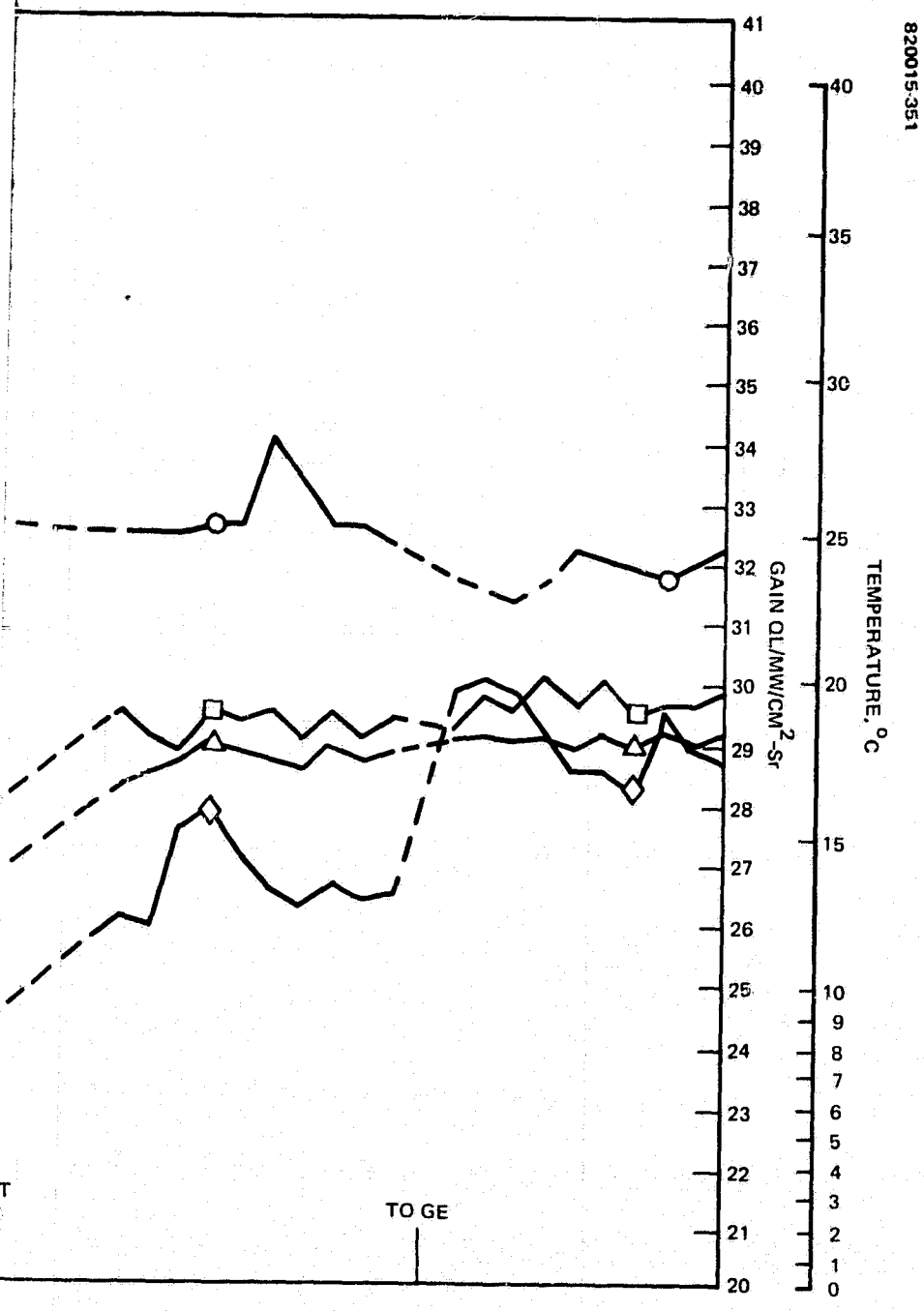

ORIGINAL PAGE IS
OF POOR QUALITY

FOLDOUT FRAME 5

to either prove or disprove this possibility. The circumstantial evidence argues against this mechanism. The gain of channel 9 was well behaved during the major environmental exposure, thermal-vacuum. During vibration and acoustic testing there were only minor changes. The anomalous gain behavior occurred mostly after extended periods of very little test activity and consequently little system operating time. The general pattern is that the channel 9 gain was anomalously high after periods of little test activity followed by a decline in gain with a period of more intense testing. If the source of the instability were in the video electronics, one would expect to see changes associated with the system environmental exposures, and little change associated with periods of inactivity.

5) Enhancement prism delamination - On the MSS-C instrument a problem with the enhancement prism bond onto the PMT faceplate manifested itself by a large gain increase, ≈ 30 percent, in going from an ambient pressure to vacuum environment. A partially failed bond on the enhancement prism would open and close as the PMT faceplate "oil-canned" as a result of a one atmosphere pressure change. The change in optical transmission characteristics of the bond as it opened and closed modulated the light intensity reaching the photocathode, causing the channel gain to vary. The PMT procurement specification was revised to more carefully control the bond line thickness and in vacuum to ambient cycling tests to check the bond integrity on the MSS-D phototubes. No problems of this type have been experienced with the MSS-D photomultiplier tubes. Channel 9 experienced no abrupt gain changes going into or coming out of a vacuum environment; it is therefore highly unlikely that the channel 9 gain anomaly is related to enhancement prism bonding problems.

6) Dynode gain - Long term gain changes, gain changes as a function of light exposure, and gain changes as a function of operating time are known phenomena associated with changing characteristics of the electron multiplication efficiency of the dynode chain in photomultiplier tubes. Figure 9-31 shows an example of these types of phenomena observed on the band 2 protoflight photomultipler channels. Plotted on the ordinate is the gain of the system and on the abscissa the light intensity to which the instrument was exposed in terms of number of lamps on in the integrating sphere. The data for five and four lamps were taken at the end of one orbit, ≈ 30 minutes on time, followed by an hour of off time, followed by collecting of the data for three, two, and one lamps. Notice there is a break in the curves, indicating an increase in gain of each of the tubes with system off time between orbits. Also note that there is an increase in gain with light level exposure of the tubes to the integrating sphere source. Both of these gain change effects are associated with the characteristics of the dynode multiplier stages. Note also that out of the channels in band 2, channel 9 is more susceptible by about a factor of 2 to the gain variation with light exposure than are the other channels in the band. The channel 9 gain instability seems to be associated with gain instability in its dynode chain. The circumstantial evidence is in agreement with this phenomenon. Channel 9 is inherently sensitive to this problem as evidence by the data in Figure 9-31. The dynode surface structure should be insensitive to environmental exposures of vibration, vacuum, and temperature. The dynode gain characteristics are sensitive to the long periods of nonoperation, and would tend to stabilize during periods of constant duty cycle operation such as thermal-vacuum operation.

In a visit to the PMT vendor, ITT, Fort Wayne, Indiana, ITT personnel also felt the gain instability associated with channel 9 was likely caused by dynode string gain variation. As a means of further isolating the problem, they suggested a careful examination of the system noise data. Their idea was simple and elegant. If the changes in

PRECEDING PAGE BLANK NOT FILMED

ORIGINAL PAGE IS
OF POOR QUALITY

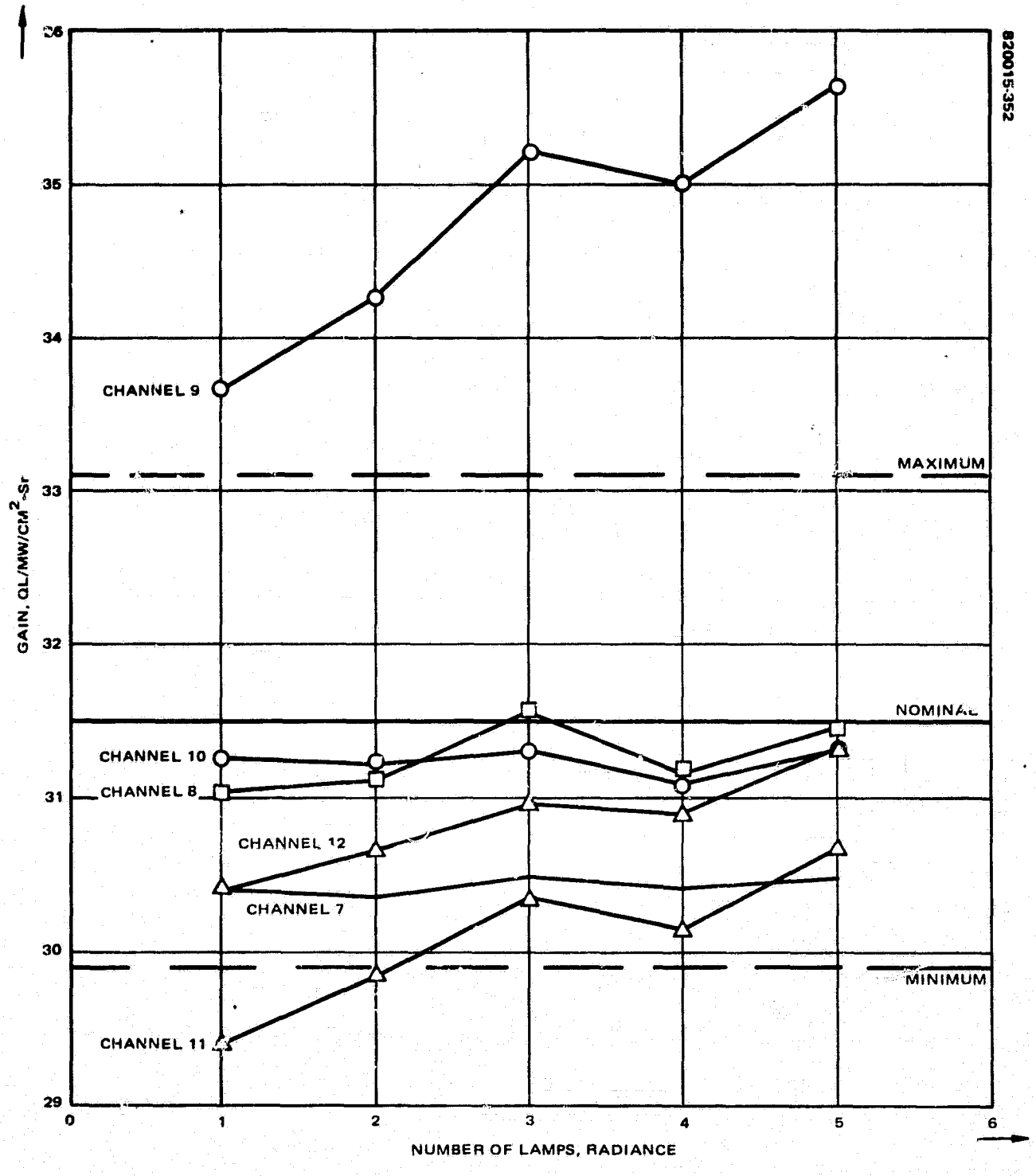

FIGURE 9-31. BAND 2, SYSTEM B, INTEGRATING SPHERE CALIBRATION

ORIGINAL PAGE IS
OF POOR QUALITY

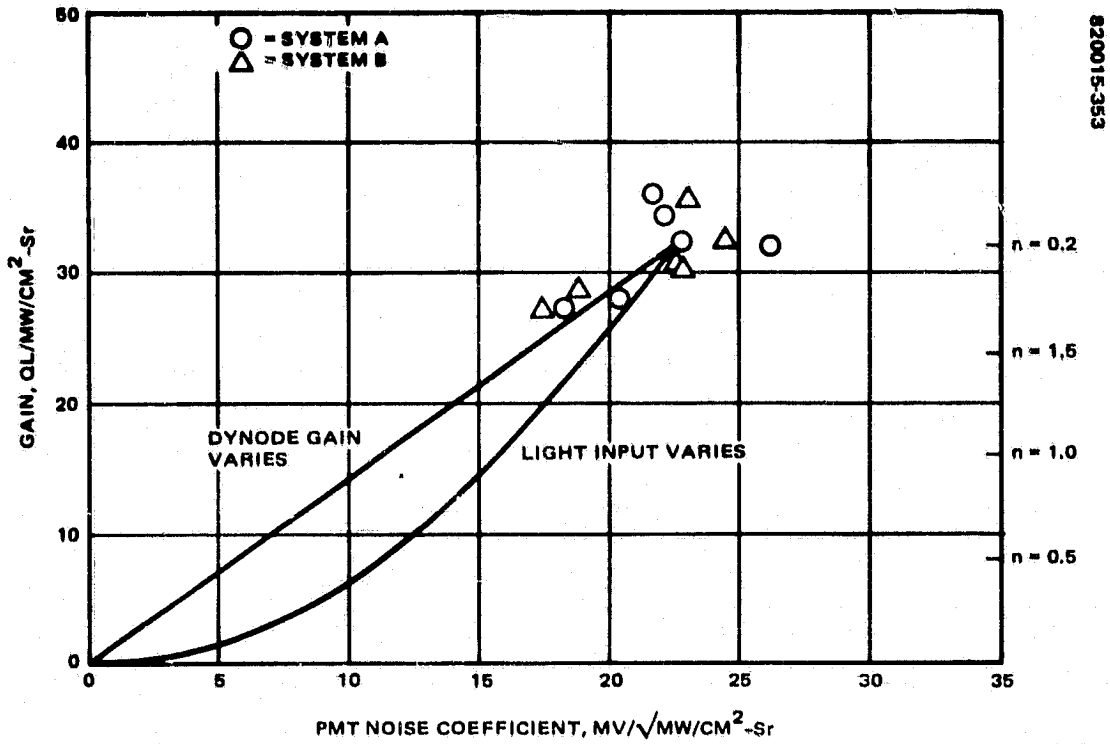

FIGURE 9-32. CHANNEL 9 GAIN VERSUS PMT NOISE

gain were due to loss of light into the PMT or to changes in the photocathode sensitivity, the noise characteristics would be affected in one way, and if the gain changes were due to a change in the dynode gain or in any of the following electronics, noise would be affected in a different way. The MSS photomultiplier tubes are shot noise limited devices so that with a constant electronic gain including dynode gain the noise out of the PMT preamplifier will be proportional to the square root of the light level being detected by the PMT. Any gain change due to photocathode detection efficiency or loss of light into the tube would result in a noise change following a square root relation to gain. On the other hand, a gain change due to a dynode characteristic change will result in a noise change which is linearly proportional to dynode gain. The system noise model developed by Miyagi was used to extract the noise contribution at the output of the PMT from all calibration runs with the integrating sphere to see what the character of the noise versus gain was. Figure 9-32 gives the results of that analysis. The two solid lines shown are the noise trends to be expected for the two gain change mechanisms. It is impossible to tell from the data which, if either, trend line is being followed as the gain varies. The suspected reason for the poor fit lies in the several system configuration changes made in other areas of the system over the course of the half a year that the data shown in Figure 9-32 were collected. The model does a best fit to four noise coefficients for noise arising from different points in the system. One of the PMT noise coefficients is plotted in Figure 9-32. As the configuration is changed, e.g., changing scanner to multiplexer video cable configurations, all the noise coefficients are allowed to change to get a best fit to the next set of calibration data. Unfortunately, these other changes have apparently masked the functional form of the noise change due to channel 9 gain variations above.

ORIGINAL PAGE IS
OF POOR QUALITY

If it is assumed that the source of the channel 9 gain instability is the dynode string, what is the likely long term effect of this problem? In discussions with ITT personnel, several observations were made. The manufacturing community has never completely solved the problem of dynode gain stability because of an incomplete understanding of the physics of the electron emission properties of the dynode surfaces. All photomultiplier tubes suffer from a degree of dynode instability, the magnitude of which varies from tube to tube. The only failure (no output) mechanism discussed associated with dynodes was carbon poisoning. ITT was confident that its tubes did not suffer from this problem because of its manufacturing process. Furthermore, this failure mechanism leads to a monotonic decrease in gain with time and not an oscillation of gain. As to the long term stability of channel 9, the ITT people were noncommittal. They said that the gain could possibly vary as much as a factor of two to three from its initial value, but it would likely become more stable with operating time. As the data in Figure 9-31 show, up to the present there has been no permanent gain change in channel 9 from the beginning to the end of the test program once the 10.5 percent gain reduction made in the buffer amplifier is factored out. It should be noted that the PMT acceptance program would not detect the instabilities we have experienced. The gain stability requirement on the vendor is that the PMT gain be stable to within ±5 percent for any 24 hour period after operation for at least 96 hours at room ambient conditions. Most of the data shown in Figure 9-30 were taken within 30 minutes of turnon of the PMTs.

Other failure mechanisms mentioned by ITT were associated with the destruction of the photocathode either by contamination from a leak or by diffusion of helium through the glass envelope of the tube. In either case, the effect on gain would be a steady decrease, not a long term up and down behavior as evidenced by channel 9.

In summary, the gain variations seen in channel 9 of the protoflight over its history in system test are very probably due to slow time constant changes in the electron multiplication efficiency of the dynode stages of the photomultiplier tube in that channel. This effect is present but more pronounced in channel 9 than in other tubes in the instrument. Although there could be long term permanent gain changes associated with this problem, the test history gives no evidence of permanent changes. There is little if any chance of a complete failure (gain goes to 0) due to this phenomenon.

9.6 MISING BLACK-WHITE CODE

During testing of the MSS-D protoflight unit, it was found that the multiplexer occasionally did not generate the black and white pattern normally put out in response to scan monitor pulse inputs (SMP-2 and SMP-3). Specific tests were then performed to establish if the fault was due to the scanner not generating the multiplexer input pulses or if the multiplexer did not respond properly. Counters were placed in the scanner-to-multiplexer SMP line while a logic analyzer checked for missing black and white pulses in the multiplexer output. The counters confirmed that there were no missing SMPs from the scanner, but the logic analyzer showed missed black and white (B/W) output pulses from the multiplexer, proving that the multiplexer occasionally did fail to respond to the scan monitor pulses. A digital memory oscilloscope confirmed that the SMPs from the scanner were normal in waveform and amplitude at the time the missing black and white code was detected.

A detailed examination of the multiplexer circuits involved in the black and white code generation and insertion into the data stream was then started, and measurements were made on the engineering model multiplexer. A timing race condition was identified, caused by the one-word delay change made to fix an MSS-C problem. Details of the tests and the analysis are given in IDCs HS248-1127 dated December 1980 and HS248-1209 dated March 1981.

As a result of the investigation, a change was made in the internal timing of the engineering model to eliminate the problem. The fix was proven on the engineering multiplexer and was subsequently incorporated in S/N 003 (protoflight) and S/N 002 (F-1) multiplexers. Penalty tests were performed on both multiplexers to prove the effectiveness of the change and to ensure that the units remained flightworthy.

10. FLIGHT MODEL (F-1) ACCEPTANCE TEST RESULTS

10.1 INTRODUCTION

The MSS-D F-1 acceptance test history and acceptance test results are presented in this section. Section 10, along with Section 11, and Section 12, constitute the F-1 acceptance test portion of the Final Report.

This section begins with a detailed, chronological presentation of the F-1 Acceptance test history. The actual F-1 system test program is presented as it was performed, starting with system integration and ending with system delivery to the spacecraft contractor. Actual test activity is compared with that planned. Changes to the Test Plan (see Section 4) are emphasized and discussed as to cause for deviation from the plan. Configuration changes are highlighted as well. The subsection concludes with an event table which lists each major test activity, the date performed, and the sequential orbit number or special test request (STR) number associated with that activity. In this fashion a (nearly) day-by-day summary of test activity is provided which permits ready correlation of test activity with test performance results.

The remainder of the section is a presentation of the F-1 acceptance test results for each of the major system level parameters. Each major parameter is treated in turn for the entire test period, with emphasis on performance as it relates to specification requirement. The discussion does not, however, restrict itself to whether the system met specifications with respect to each performance parameter. An overview of performance is given for each parameter which provides estimates of variability, repeatability, and sensitivity of measured data as a function of test environment and configuration where appropriate. Results are discussed as anomalous when the performance appears to deviate substantially from nominal performance even when the particular parameter is within specification.

To provide a complete overview of the system performance data without having it enlarge to a burdensome size, the primary data were recorded onto the disk of a computer and plot routines were developed to permit an individual test history for any parameter, any channel (or band), to be plotted on a single 8-1/2 by 11 plot. This is an approximate 14 to 1 reduction in volume without substantial loss of information. These plots have the additional advantage of enabling the reader to view easily the major trends and variations in the data and to make comparisons readily of system performance variability and repeatability for recurring test environments and configurations throughout the entire acceptance test program. The graphics actually used for daily review of test performance during system acceptance testing are presented when the greater

ORIGINAL PAGE IS
OF POOR QUALITY

820015-162

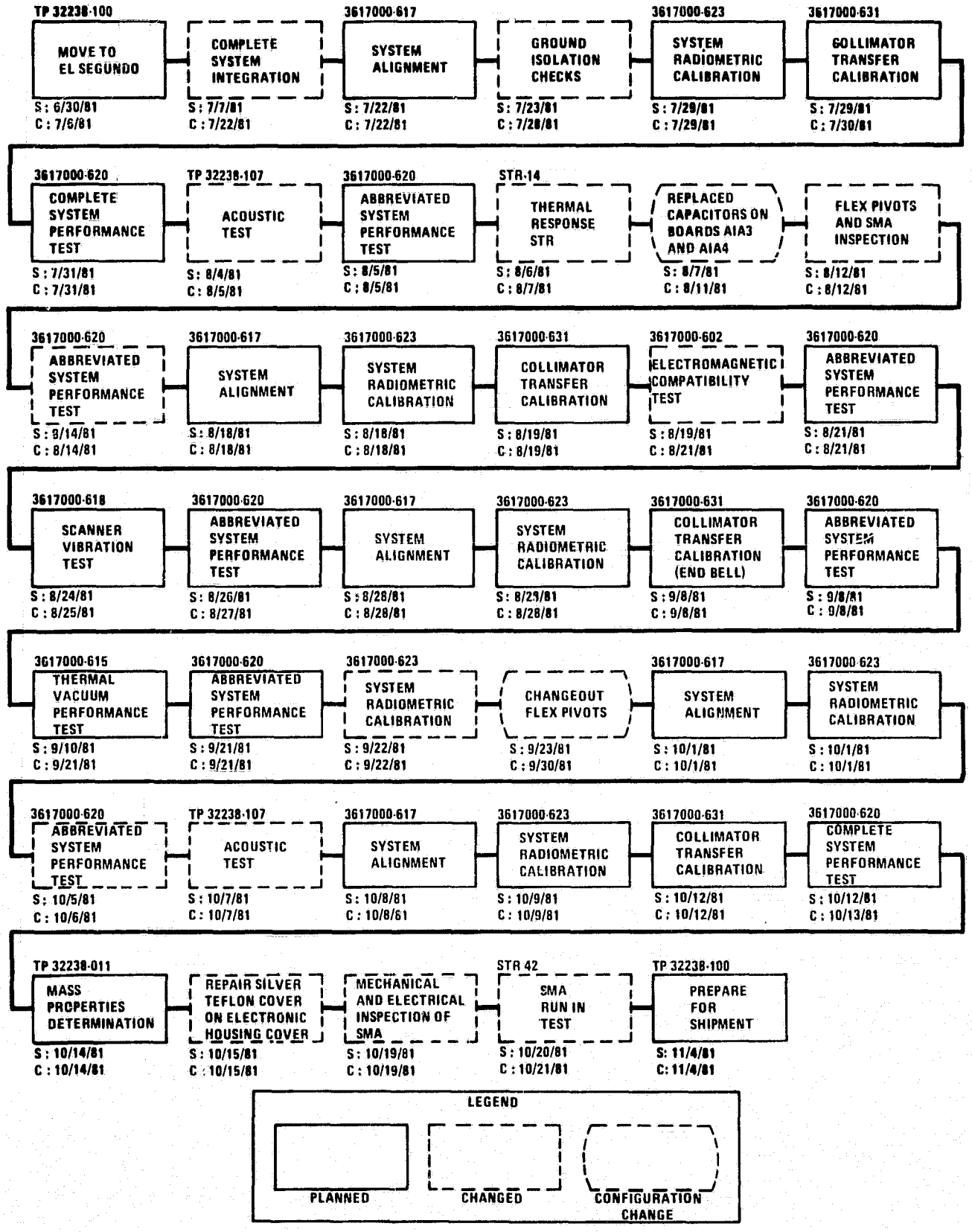

FIGURE 10-1. F-1 TEST SEQUENCE

resolution provided by those plots are required. A complete set of these on-line graphics has been provided separately.

The program used to provide the single page plot histories gives each data value serially from the first data point that the computer filed to the last, and does not identify each orbit (or individual test) by the sequential orbit number used as standard identification for the individual test elswhere. For easy cross-referencing, Table 10-1 identifies the sequential orbit number, standard orbit number, and major test event description corresponding to each of the serial orbit numbers provided on the plots.

10.2 F-1 TEST HISTORY

The F-1 integration and test plans are discussed in Section 4 of this report; this section describes the actual F-1 system test program as it evolved from system integration through delivery of the system to the spacecraft integration contractor. Figure 10-1 presents the detailed sequence of activities leading to the delivery of the F-1 system. In the figure, the rectangular boxes with solid outlines represent activities that were in the plan prior to the start of system test. The rectangular boxes with broken outlines represent changes to the original plan. The change could be a simple change in the test sequence or a new test added to the program. The truncated ovals indicate a configuration change. This could be repair of a damaged part, replacement of a component to improve performance characteristics, implementation of a new design, or replacement of a complete unit. The numbers above the boxes are the numbers of the procedures to which the activity was performed. The numbers below the boxes represent the start (S) and completion (C) dates of the activity within the box.

The original planning for the F-1 system required completion of system integration at SBRC, followed by a complete system performance test (CSPT) performed by the program office system test team at SBRC prior to shipment to the system to El Segundo for the system environmental tests. The CSPT at SBRC was intended to serve as a performance baseline for the F-1 system and to accept the system from SBRC as ready to proceed into the F-1 flight acceptance test program. As the schedule actually developed, the protoflight system and bench test equipment (BTE) 2 were shipped during the first week of July 1981. In order to suppport F-1 integration testing it was necessary either to ship BTE 1 to SBRC or F-1 to El Segundo to complete integration. A request to deviate from the plan and move F-1 to El Segundo to complete integration was granted. This system was delivered into area S1 on 6 July 1981. System integration required an additional 2 weeks and was completed at El Segundo on 22 July.

Formal system acceptance tests started 22 July with the system alignment; however, these tests were interrupted and a week was spent performing STR's to measure isolation of the signal and power returns and chassis ground, and to verify polarity of the command diodes. During these special tests, noise problems were investigated and traced to the scanner to multiplexer cable 78622. Both the PF and F-1 proved to be very sensitive to this test cable configuration. The cable was returned to SBRC for rework.

The system was then radiometrically calibrated using the "new" 30 inch integrating sphere set up with Kepco dc power supplies rather than the EG&G ac power supplies used for calibration of previous MSS systems. Problems were experienced in setting up the Kepco power supplies to prevent long term drift. The solution was to operate the dc

ORIGINAL PAGE IS
OF POOR QUALITY

TABLE 10-1. FLIGHT REFERENCE ORBITS

Serial Orbit	Sequential Orbit	Standard Orbit	Test Event
1	35	1	First long form performance test
2	36	2	First long form performance test
3	37	3	First long form performance test
4	38	4	First long form performance test
5	39	5	First long form performance test
6	40	6	First long form performance test
7	41	7	First long form performance test
8	42	8	First long form performance test
9	45	1	Postacoustic
10	46	2	Postacoustic
11	47	7	Postacoustic
12	48	8	Postacoustic
			Capacitor change
13	49	1	Pre-EMI
14	50	2	Pre-EMI
15	51	7	Pre-EMI
16	52	8	Pre-EMI
17	69	1	Post-EMI, Previbration
18	70	2	Post-EMI, Previbration
19	71	7	Post-EMI, Previbration
20	72	8	Post-EMI, Previbration
21	76	1	Postvibration
22	77	2	Postvibration
23	78	7	Postvibration
24	79	8	Postvibration
			Collimator lamp change
25	86	1	Endbell
26	87	2	Endbell
27	88	7	Endbell
28	89	8	Endbell
29	628	1	Special test request (STR)
30	90	1	GN_2 backfill
31	91	2	GN_2 backfill
32	92	7	GN_2 backfill
33	93	8	GN_2 backfill
34	98	1	20^oC
35	99	2	20^oC
36	100	3	20^oC
37	101	4	20^oC
38	102	5	20^oC
39	103	6	20^oC
40	104	7	20^oC
41	105	8	20^oC

ORIGINAL PAGE IS
OF POOR QUALITY

Table 10-1 (continued)

Serial Orbit	Sequential Orbit	Standard Orbit	Test Event
42	106	1	20° to 32°C
43	107	2	20° to 32°C
44	108	1	32°C
45	109	2	32°C
46	110	3	32°C
47	111	4	32°C
48	112	5	32°C
49	113	6	32°C
50	114	7	32°C
51	115	8	32°C
52	116	1	32° to 5°C
53	117	2	32° to 5°C
54	118	7	32° to 5°C
55	119	8	32° to 5°C
56	120	1	5°C
57	121	2	5°C
58	122	3	5°C
59	123	4	5°C
60	124	5	5°C
61	125	6	5°C
62	126	7	5°C
63	127	8	5°C
64	128	4	5° to 10°C
65	129	1	10°C
66	130	2	10°C
67	131	7	10°C
68	132	8	10°C
69	133	1	20°C
70	134	2	20°C
71	135	7	20°C
72	136	8	20°C
73	137	3	20° to 30°C
74	138	1	30°C
75	139	2	30°C
76	140	7	30°C
77	141	8	30°C
78	142	1	30°C
79	143	2	30°C
80	144	3	30°C
81	145	4	30°C
82	146	5	30°C

ORIGINAL PAGE IS
OF POOR QUALITY

Table 10-1 (continued)

Serial Orbit	Sequential Orbit	Standard Orbit	Test Event
83	147	6	30°C
84	148	7	30°C
85	149	8	30°C
86	150	1	30° to 10°C
87	151	2	30° to 10°C
88	152	7	30° to 10°C
89	153	8	30° to 10°C
90	154	1	10°C
91	155	2	10°C
92	156	3	10°C
93	157	4	10°C
94	158	5	10°C
95	159	6	10°C
96	160	7	10°C
97	161	8	10°C
98	162	1	10° to 30°C
99	163	2	10° to 30°C
100	164	7	10° to 30°C
101	165	8	10° to 30°C
102	166	1	30°C
103	167	2	30°C
104	168	3	30°C
105	169	4	30°C
106	170	5	30°C
107	171	6	30°C
108	172	7	30°C
109	173	8	30°C
110	174	1	30°C
111	175	2	30°C
112	176	3	30°C
113	177	4	30°C
114	178	5	30°C
115	179	6	30°C
116	180	7	30°C
117	181	8	30°C
118	182	1	30° to 10°C
119	183	2	30° to 10°C
120	186	1	10°C
121	187	2	10°C
122	188	3	10°C
123	189	4	10°C

ORIGINAL PAGE IS
OF POOR QUALITY

Table 10-1 (continued)

Serial Orbit	Sequential Orbit	Standard Orbit	Test Event
124	190	5	10°C
125	191	6	10°C
126	192	7	10°C
127	193	8	10°C
128	194	1	10°C
129	195	2	10°C
130	196	3	10°C
131	197	4	10°C
132	198	5	10°C
133	199	6	10°C
134	200	7	10°C
135	201	8	10°C
136	202	4	10° to 15°C
137	633	1	15°C
138	634	2	15°C
139	635	7	15°C
140	636	8	15°C
141	203	6	15° to 20°C
142	204	1	20°C
143	205	2	20°C
144	206	3	20°C
145	207	4	20°C
146	208	5	20°C
147	209	6	20°C
148	210	7	20°C
149	211	8	20°C
150	212	1	Post thermal-vacuum
151	213	2	Post thermal-vacuum
152	214	7	Post thermal-vacuum
153	215	8	Post thermal-vacuum
			New flex pivots
154	231	1	Final LFPT
155	232	2	Final LFPT
156	233	3	Final LFPT
157	234	4	Final LFPT
158	235	5	Final LFPT
159	236	6	Final LFPT
160	237	7	Final LFPT
161	238	8	Final LFPT

ORIGINAL PAGE IS
OF POOR QUALITY

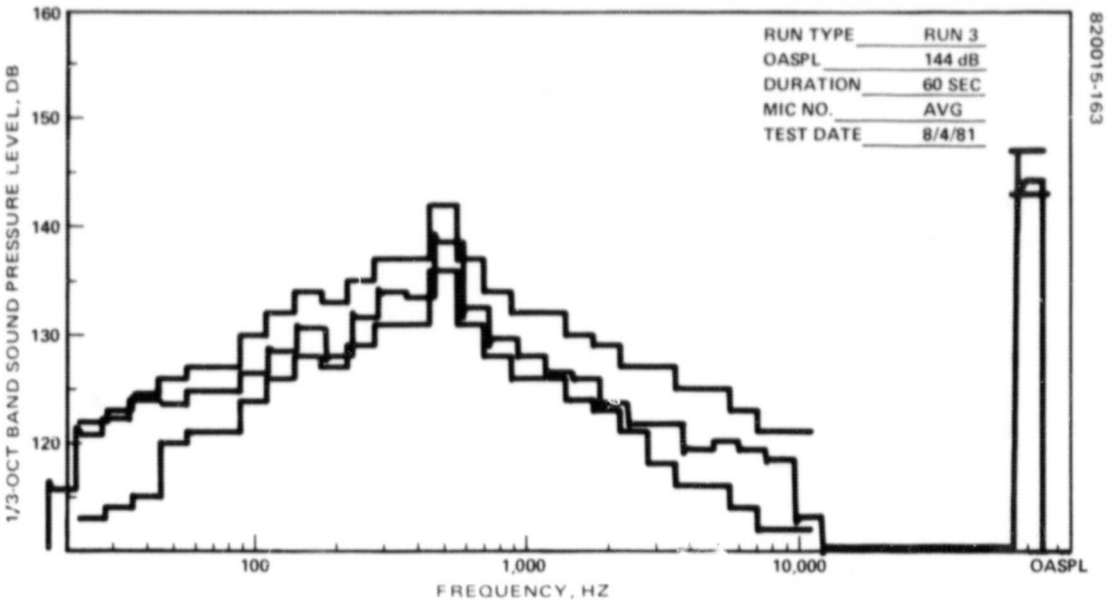

FIGURE 10-2. F-1 ACOUSTIC TEST SPECTRUM

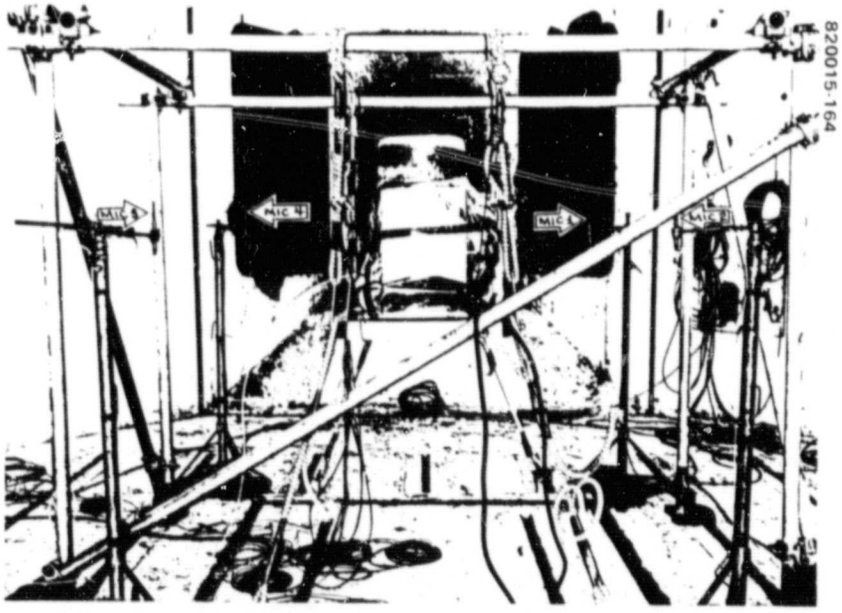

FIGURE 10-3. ACOUSTIC TEST SETUP

supplies in a voltage regulation mode rather that current regulation and to reference the voltage regulator to a precision series resistor. This effectively regulated lamp current but permitted the power supply to operates in its most stable and sensitive mode.

The calibration sequence was completed with the collimator transfer calibration on 30 July. During the calibration sequence, calibration coefficients are derived from the system radiometric calibration and the collimator transfer calibration. These coefficients are loaded into the DRS after each of these calibration runs. These steps, DRS loading, are not included in the F-1 Test Sequence, Figure 10-1; however, they were routinely conducted after all system radiometric and collimator transfer calibrations.

The complete system performance test conducted on 30 July 1981 served as both the ambient CSPT that was deleted from the test sequence at SBRC and CSPT that was planned to be performed upon delivery of the system to El Segundo. The CSPT is conducted to establish a performance baseline against which other performance tests can be compared to evaluate long term drifts and also to establish performance degradation as a result of environmental tests. During this CSPT violations in specification performance requirements were observed in deviation channel to channel (DCC) and deviation signal to noise (DSN). One failure report, FR 5123, was generated for this test. It was generally concluded that most of the problems were BTE (collimator) related and that the system was sound and ready to proceed into the environmental tests.

It was originally planned to conduct the EMI/EMC tests as the first of the environmental exposures of the F-1 acceptance test; however, schedule conflicts developed in both the availability of the Hughes anechoic chamber and the planned acoustic test facility at Rockwell International. At Rockwell a space shuttle wing was being brought to the acoustic facility and would be installed on 7 August 1981. Our window for acoustic testing at Rockwell would therefore close on 7 August and would not reopen for the balance the F-1 acceptance test program. It was necessary to move to Rockwell as soon as possible or to renegotiate a new acoustic test contract with another facility. Also, the thematic mapper was in the Hughes screen room so the EMI/EMC tests were not possible. A request for deviation from the planned test sequence, D028, was submitted and approved. The acoustic test of F-1 was completed 4 August 1981.

The acceptance acoustic test consisted of three runs: a 20 second run at -138 dB, a 20 second run at -141 dB, and a 60 second run at 144 dB OASPL. The spectrum for the F-1 acoustic test is shown in Figure 10-2, which shows the average of the four facility microphones which was the signal from which the test was controlled. The outer bands indicate the specification requirements for the test, and the center trace is the averaged signal from the four microphones. All requirements for the acoustic test were met with no waivers for tolerance violations required.

The acoustic test setup, Figure 10-3, was similar to the one for the protoflight scanner except that the instrumented engineering model (EM) scanner was not present. The F-1 scanner was instrumented with five triaxial accelerometers which coincided with previous scanner instrumentation for vibration and acoustic tests.

At the completion of the acoustic exposure, the F-1 system was returned to Area S1 for the postacoustic abbreviated system performance test (ASPT) to evaluate the condition of the system. The test indicated the characteristics of the F-1 scanner had not changed measurably from the preacoustic CSPT. One failure report, FR 5735, was generated for specification performance violations in deviation signal to noise.

The acceptance test program was interrupted at this time to conduct STR 14, a test to photograph the focal plane array and measure channel gains at various temperatures between ambient and 32°C. While the system was down, it was decided to inspect and, if required, change out the filter capacitors on band 2 and 3 buffer boards, A1A3 and A1A4.

During the F-1 integration activities at SBRC, and while problems were being experienced with the protoflight flex pivots, the F-1 flex pivots were inspected and found to have a trace of red residue on the surface - possibly rust. While the system was down for filter capacitor changeout, it was decided to remove the sunshield, reinspect the flex pivots, and map the areas of corrosion for future reference. After these activities were completed and the scanner reassembled, it was decided another ASPT should be conducted to verify the integrity of the system prior to proceeding on with the acceptance test. During this test DSN violations were noted. It was also decided that the collimator albedo source lamp was on borrowed time and would be a considerable risk during the thermal-vacuum tests. The collimator source lamp was changed out, replacing the old 100 watt lamp with a new 150 watt lamp; however, the collimator uniformity was unacceptable, and the old 100 watt source was reinstalled. An effort was initiated to flatten the 150 watt source to make it suitable for use during thermal-vacuum tests.

A system alignment and calibration sequence was conducted prior to the EMI/EMC tests. The requirements for the F-1 EMI/EMC tests were defined in deviation request D028 which mandated only conducted susceptibility tests CS01, CS02, and CS06. Adequate EMI safety margins had been demonstrated during the protoflight EMI/EMC test so that conducted and radiated emissions tests and radiated susceptibility tests were not required for F-1. This reduction in the scope of the EMI tests also eliminated the need for a shielded screen room. Deviation request D029 was submitted to conduct the F-1 EMI tests in Area S1, rather than the anechoic chamber A2, eliminating conflicting facility requirements with the thematic mapper and permitting a more expeditious completion of the F-1 EMI tests.

During the F-1 EMI test CS01 problems were encountered over a fairly broad frequency range. It was also noted the BTF indicator lamps were flashing randomly, and the simulated spacecraft power supply was varying from about 20 to 25 volts. It was concluded the problem was in the remote sensing for the power supply voltage regulator. The supply was changed to local sensing and most of the problems went away. Susceptibility was found only at 30 and 300 Hz at 1.5 volts peak-to-peak. The criterion for susceptibility used on F-1 was out-of-tolerance performance in line length variation (VLL) and DSN. This was an unusually severe criterion as DSNs were being experienced in ambient performance tests. No problems were encountered in CS02 which was conducted at 1.5 volts peak-to-peak from 50 to 150 KHz. CS06 was conducted at 56 volts peak at a pulse repetition rate of 60 pps for 5 minutes. No problems were encountered.

It was concluded by test personnel that the problems residual in CS01 were more associated with the test setup rather than flight hardware. The EMI tests are summarized in Table 10-2.

ORIGINAL PAGE IS
OF POOR QUALITY

Since the EMI tests required only 3 days to complete, the pre-EMI alignment and calibrations were deemed adequate for previbration alignment and calibration. As a result, only the ASPT was conducted between EMI/EMC tests and vibration. During this test DCC and DSN violations were noted.

On 24 August the F-1 scanner was moved onto the V2 vibration facility for the acceptance vibration tests. The F-1 vibration tests are summarized in Table 10-3. The actual vibration test sequence for acceptance tests was defined by change notice 7, which permitted a test sequence of a low level random burst, 5 to 2 kHz for structural signature, a sinusoidal vibration exposure at flight levels and durations, followed by another low level random burst. This sequence was carried out for each axis. Prior to each axis of vibration a system functional test was conducted to verify the system was operating and to place the system in the proper operating mode, launch mode, for the vibration exposure. The postvibration ASPT indicated the scanner survived the vibration exposure with no performance change; DCC and DSN performance violations were noted. In an attempt to reduce DCCs, STR 23, a nonplanned collimator transfer calibration, was conducted after vibration and prior to the ASPT.

The system at this point was being prepared for thermal-vacuum tests. Special emphasis was placed upon changeout of the collimator albedo source. The 150 watt lamp which had been reworked at SBRC was placed into the collimator. While uniformity characteristics had improved, the new albedo source was only marginally acceptable for performance testing.

TABLE 10-2. EMI/EMC TESTS

Susceptibility Test	Frequency	Limits
CS01 conducted (powerline and return)	30 Hz to 50 kHz	MIL-STD-461
CS02 conducted (powerline and return)	50 kHz to 150 kHz	MIL-STD-461
CS06 conducted (transient)	60 pps for 5 min	56 V peak

TABLE 10-3. F-1 VIBRATION TEST
SINUSOIDAL VIBRATION LEVEL

Axis	Frequency, Hz	Flight Level, g	Sweep Rate, oct/min
Thrust (X)	5 to 50 50 to 100	5.0* 2.0	4
Lateral (Y and Z)	5 to 50 50 to 100	3.5* 2.0	4

*Exposure limited to 0.50 in. double amplitude (12.7 mm)

A prethermal-vacuum test alignment and system radiometric calibration were completed and the system was moved to the C7 endbell for the collimator transfer calibration and the ASPT on the endbell. After the move, a series of STRs, designated STR 27 but repeated over several days, was conducted to improve the collimator field uniformity. The end result was a satisfactory collimator with the new 150 watt lamp. Installation on the endbell was completed; the collimator transfer calibration was conducted; and the subsequent ASPT confirmed previous suspicions that the DSNs and DCCs were at least in part associated with the collimator. During this period of time an algorithm change was made in the data reduction software which partially corrected for collimator nonuniformity in computing signal-to-noise ratios.

The C7 endbell was raised on 9 September 1981 and followed by the required pumpdown to 100 Torr and backfill with GN_2 repeated three times. The system was then brought to 500 Torr, essentially ambient, for the first in-chamber ASPT. The test was satisfactory, and pumpdown to hard vacuum was initiated. During the first 45 minutes of pumpdown, F-1 was in the launch mode. After 45 minutes the system was turned off and pumpdown continued until chamber pressure reached 10^{-5} Torr. The time at which the chamber pressure reached and held at 10^{-5} Torr is "T-O" on the F-1 thermal-vacuum temperature profile, Figure 10-4, and occurred at 1730 on 10 September 1981. The thermal-vacuum test after T-O was strictly time sequenced, with testing planned to occupy most of the 240 hours in hard vacuum. After reaching T-O the system was permitted to outgas for 12 hours with no power applied; the system was then turned on for the corona and initial vacuum checks. These tests indicated the system was in satisfactory condition to proceed with the initial vacuum collimator transfer calibration.

Performance testing in vacuum was accomplished in accordance with the thermal-vacuum profile, Figure 10-4. Deviations from the planned profile were the addition of two collimator transfer calibrations, one at 30°C and one at 10°C, and ASPT at 15°C just prior to the final CSPT at 20°C.

The thermal-vacuum test is summarized in Figure 10-4 and is discussed in orbit-by-orbit detail in Table 10-4 at the end of this subsection. The thermal-vacuum test was terminated 240 hours after reaching T-O, and chamber ventback initiated. After reaching room ambient pressure, the endbell was lowered to its retaining pins and a final in-chamber ASPT was performed. Most of the problems experienced during the thermal-vacuum test involved DSNs and DCCs. Most DSNs were related to a noisy power supply for the collimator albedo source. The system was removed from the C7 endbell and returned to Area S1 where a post-thermal-vacuum collimator transfer calibration was performed. STR 32 was conducted to measure the unsaturated scan monitor pulse amplitude.

During the thermal-vacuum tests it was concluded the F-1 flex pivots would be changed out for a new lot of flex pivots which were being processed through receiving inspection. These were commercial grade flex pivots which were given special run-in and hysteresis tests during acceptance. The flex pivots changeout was to be at the completion of thermal-vacuum testing or when the new lot was through receiving tests and available for assembly into the scan mirror assembly (SMA), whichever occurred last. These events were almost simultaneous, and at the completion of the post thermal-vacuum system radiometric calibration the SMA was removed from the scanner and sent to Culver City for the changeout and retest.

ORIGINAL PAGE IS
OF POOR QUALITY

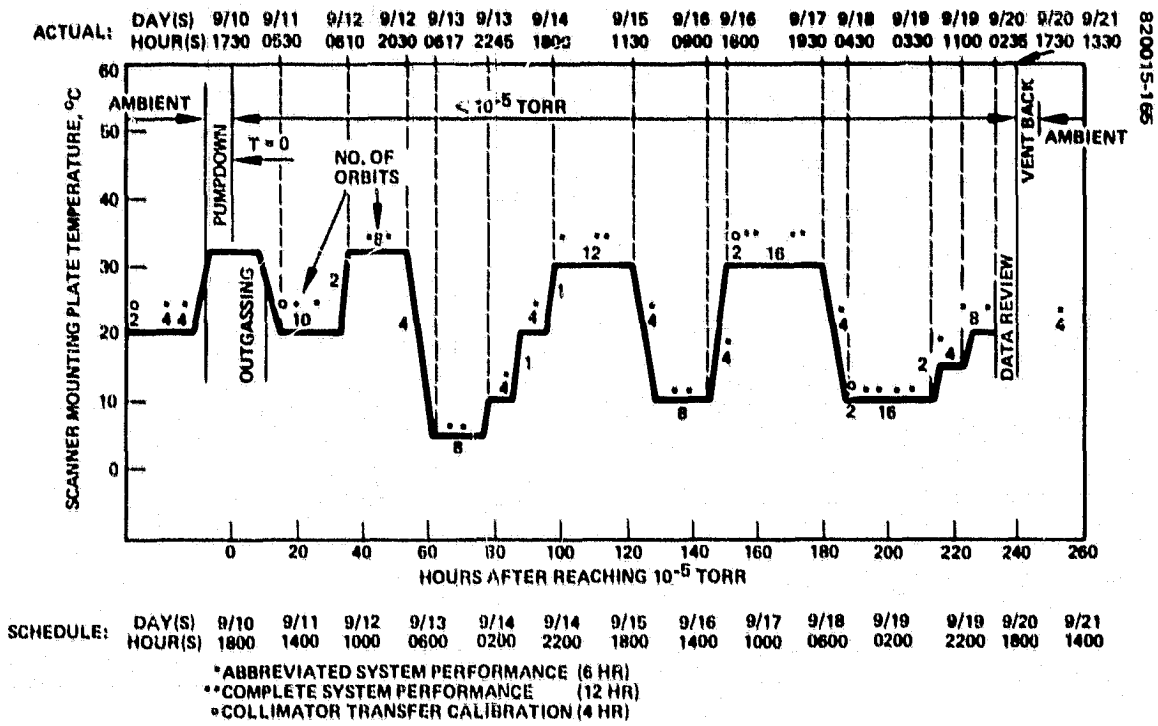

FIGURE 10-4. F-1 THERMAL-VACUUM TEMPERATURE PROFILE

Seven days later, on 30 September, the SMA was returned to system test for assembly into the scanner. The scanner was reassembled, aligned, and calibrated. A postrework STR was conducted to remeasure the unsaturated scan monitor pulse amplitude and to prepare the scanner for the penalty acoustic test. The system alignment indicated the flex pivot changeout changed scanner alignment less than 0.025°.

The penalty acoustic test was conducted as a proof-of-workmanship test after the reassembly of the F-1 scanner. The test was planned as an acceptance level test, duplicating the previous acceptance acoustic test. However, the shuttle wing was still in the Rockwell 9000 ft^3 reverberant chamber previously used. As a result, the penalty acoustic test was conducted in the Rockwell 500 ft^3 reverberant chamber. It was recognized at the time that no energy below 50 Hz was developed in the small chamber. The setup for the penalty acoustic test is shown in Figure 10-5, and the spectrum for it in Figure 10-6 which indicates a sharp dropoff below 45 Hz, but well within acceptance limits above 45 Hz. The F-1 scanner was returned to Area S1 for the final alignment and calibration sequence and the final CSPT. The CSPT indicated specification performance violations in VLL, and cross-axis repeatability CXAXO, and resulted in failure reports FR 5146 and FR 5147.

The scanner was bagged and mounted on the mass properties fixture in preparation for the mass properties measurements. The scanner was moved to the mass properties area on 14 October 1981, and the weight, center of gravity, and moments of inertia about the X- and Z-axes were measured.

ORIGINAL PAGE IS
OF POOR QUALITY

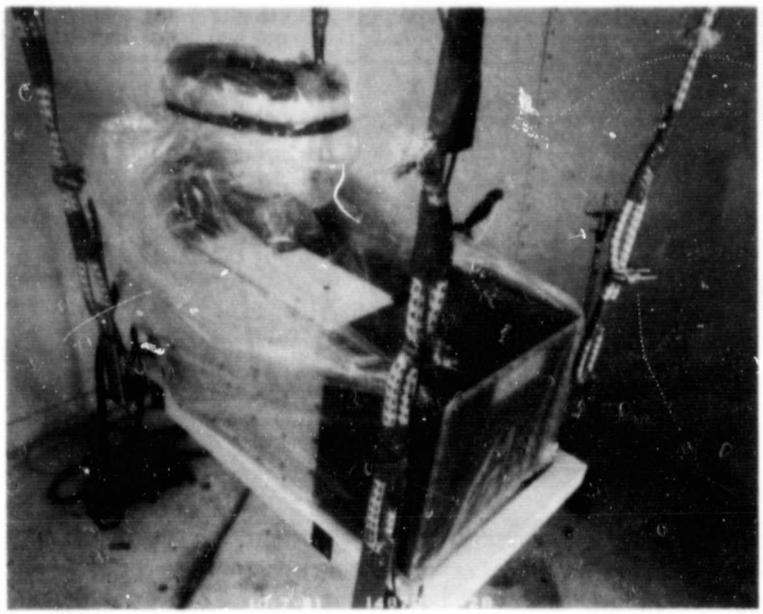

FIGURE 10-5. F-1 ACOUSTIC TEST SETUP

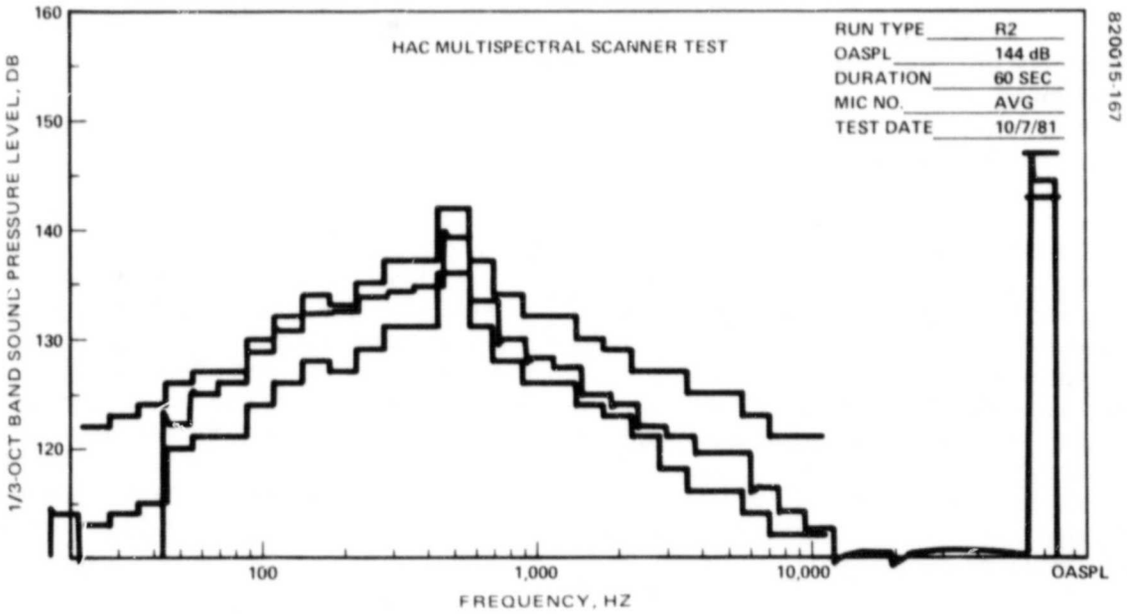

FIGURE 10-6. PENALTY ACOUSTIC TEST SPECTRUM

A discussion with the SMA engineers revealed the excessive VLLs encountered during the CSPT were possibly due to insufficient run-in time on the flex pivots. STR 42, which involved running the SMA for about 48 hours with periodic check of the VLL, was conducted. With the additional run-in time, the SMA settled down and VLLs dropped to the range of 35 to 40 μrad. These values of VLL are satisfactory for a system which is tested in air under laboratory ambient conditions.

The F-1 system was prepared for shipment and moved to United Airlines for transportation to General Electric on 4 November 1981.

Table 10-4 presents the detailed F-1 history, giving a day-by-day, orbit-by-orbit chronological listing of all F-1 test activities from the shipment from SBRC to El Segundo to the delivery of the F-1 system.

10.3 SIGNAL-TO-NOISE PERFORMANCE EVALUATION

10.3.1 Introduction

This subsection discusses the signal-to-noise (STN) performance of the MSS-D flight model scanner. The F-1 signal-to-noise performance as measured on the integrating sphere as part of the off-line system noise estimation is given in 10.3.2; the noise model itself is described in 7.3.2. Subsection 10.3.3 evaluates signal-to-noise performance as measured with the collimator as the source. Subsection 10.3.4 summarizes performance, discussing only those features attributable to the scanner.

As with the protoflight (7.3), noise plots are presented instead of signal-to-noise. Orbit numbers are also given in two ways: orbit (205)143 would represent serial orbit 143, which is sequential orbit 205 (see Table 10-1).

10.3.2 F-1 Noise Estimation Results

The noise estimation program was exercised for each of the radiometric calibrations performed during the course of acceptance testing for the flight model. Plots of the noise coefficients as a function of time (i.e., radiometric calibration number) for bands 1 through 3 are provided in Figure 10-7. The data corresponding to the 9 October 1981 radiometric calibration is used to extrapolate system STN performance for full (64 quantum level) and half-scale (32 quantum level) output for the flight model and is presented in tabular form for both internal calibrations systems A and B in Table 10-5. In each case scanner STN performance is well above lower bounds called out in the system level specification.

10.3.3 Performance

Figures 10-8 through 10-11 give the history of the noise measured during the entire history of flight model testing. Some comments apply to all eleven plots.

Two changes were made at orbit 23(86) when the scanner was placed in thermal-vacuum. Because of the number of hours on the old collimator albedo lamp, it was replaced just before the start of thermal-vacuum testing. The new lamp had a higher output, which also raised the level of noise measured. Also at this time, the collimator

ORIGINAL PAGE IS
OF POOR QUALITY

TABLE 10-4. MSS-D F-1 TEST CHRONOLOGY

Date	Activity	Problems	Orbit
7/6/81	Received F-1 Scanner and multiplexer from SBRC. Moved F-1 to the S1 test area.		
7/7/81	Removed scanner from shipping container and mounted it on the angle plate. Installed buffer boards A2, A3, A4, and A5		
7/8/81	Set up scanner and integrating sphere Performed STR HS 248-1370-1		701/13, 14
7/9/81	Performed STR 2 SMP retrace and preamplifier pulses Problem – Short in cable 4012B, returned to SBRC		
7/10/81	Performed STR 2 with 191Ω J17 adapter Performed STR 3 spacecraft time code check Performed STR 4 shutter sync and dc restore scope photos		
7/13/81	Conducted system radiometric calibration per SBRC 16894		20/13, 21/14 22/15, 23/16
7/14/81	Conducted collimator transfer calibration per SBRC 16895		24/27, 25/28
7/15/81	Performed STR 7 standby and launch mode power profile. Performed multiplexer integration performance, SBRC 16794 Performed STR 6 collimator flooding lamp uniformity check.		26/02
7/16/81	Moved scanner to granite flat; performed O&M Moved scanner to angle plate.		
7/17/81	Performed STR 5 thermal test		
7/22/81	Conducted scanner alignment per HS 248-3617000-617		
7/23/81	Performed STR 10 command diode test Performed STR 9 ground isolation check	FR 5133	
7/24/81	Performed STR 8 scan monitor margin. Troubleshooting short (2500-2) power ground to signal return. Returned cable 78622 to SBRC for rework		
7/27/81	Troubleshooting short power return to SMA power return		
7/28/81	Reassembled scanner		
7/29/81	Conducted system radiometric calibration – HS 248-3617000-623		27/13, 28/14 29/15, 30/16
7/30/81	Conducted collimator transfer calibration – HS 248-3617000-631 Many DSNs both orbits Conducted STR 11 scan mirror drive test Conducted STR 12 collimator uniformity test Conducted collimator transfer calibration – HS 248-3617000-631		31/27, 32/28 712/01 33/27, 34/28
7/31/81	Conducted CSPT HS 248-3617000-620	FR 5134*, DCC High voltage* Band 1 DCC*, DSN* DSN*, DCC*	35/1, 36/2* 37/3, 38/4* 39/5*, 40/6* 41/7*, 42/8
8/3/81	Performed STR 13 high voltage telemetry Prepared scanner for acoustic test		

ORIGINAL PAGE IS
OF POOR QUALITY

Table 10-4 (continued)

Date	Activity	Problems	Orbit
8/4/81	Moved scanner from Rockwell to area S1 Conducted ASPT per HS 248-3617000-620	DSN*, FR 5135	45/1, 46/2, 47/7*, 48/8
8/6/81	Rerun STR 13 high voltage telemetry investigation Performed STR 14 thermal test.		
8/7/81	Replaced select capacitors on boards A1A3 and A1A4 Reran ambient orbit of STR 14 thermal test		
8/10/81	Ran STR 15 VLL investigation		
8/11/81	Completed A1A3 and A1A4 buffer board rework Inspected, photographed, and cleaned flex pivots		
8/12/81	Performed STR 17 scan monitor buffer test Continued STR 15 VLL investigation Reassembled housing cover and sunshield on scanner		
8/13/81	Conducted STR 19 internal calibration stability		619-3
8/14/81	Conducted ASPT per HS 248-3617000-620	DSN*	49/1, 50/2, 51/7*, 52/8
8/15/81	Collimator visible source changed to 150 W lamp Performed STR 20 collimator uniformity estimate Original 100 W lamp replaced in collimator		
8/17/81	Performed STR 21 bit error investigation		
8/18/81	Conducted system alignment per HS 248-3617000-617 Conducted system radiometric calibration per HS 248-3617000-623		53/13, 54/14, 55/15, 56/16
8/19/81	Conducted collimator transfer calibration per HS 248-3617000-631 Started EMI test per HS 248-3617000-602		57/27, 58/28 59/18
8/20/81	Continued EMI tests CS01 Verified four lamp data set of STR 19 was A calibration lamp rather than B		60 66
8/21/81	Completed EMI tests CS02, CS06 Disassembled electrical housing cover, removed A1A9, scan monitor buffer Performed STR 22 scan monitor turnon/off test Conducted ASPT per HS 2483617000-620	 DSN* DCC*	67, 68 69/1*, 70/2 71/7, 72/8*
8/24/81	Prepared F-1 for vibration; moved to V-2 in SSL		
8/25/81	Conducted vibration test per HS 248-3617000-618 (sine only)		
8/26/81	Moved system to area S1 Performed STR 23 collimator transfer calibration Conducted ASPT HS 248-3617000-620	 DCC* DCC* and DSN	 74/27, 75/28 76/1*, 77/2 78/7*
8/27/81	Completed ASPT per HS 248-3617000-620 Replaced collimator visible source with 150 W lamp Performed STR 24 collimator uniformity estimates	DSN*	79/8*
8/28/81	Conducted system alignment per HS 248-3617000-617 Conducted system radiometric calibration per HS 248-3617000-623		80/13, 81/14, 82/15, 83/16
8/29/81	Performed STR 25 collimator uniformity estimate Performed STR 26 launch mode telemetry test		

ORIGINAL PAGE IS
OF POOR QUALITY

Table 10-4 (continued)

Date	Activity	Problems	Orbit
8/31/81	Prepared system for move to C7 in SSL		
9/02/81	Moved system to C-7 and prepared for thermal-vacuum		
9/03/81	Continued preparation for thermal-vacuum Performed STR 27 collimator uniformity estimates		
9/04/81	Continued STR 27 and preparations for thermal-vacuum		
9/05/81	Continued STR 27 and preparations for thermal-vacuum		
9/08/81	Conducted collimator transfer calibration per HS 248-3617000-631 Conducted ASPT per HS 248-3617000-620		84/27, 85/28 86/01, 87/02 88/7, 89/8
9/09/81	Raised endbell, GN_2 backfill and purge Performed STR 28, pre thermal vacuum system check (time code)		
9/10/81	Conducted ASPT per HS 248-3617000-616		90/1, 91/2, 92/7, 93/8
	Initiated pumpdown per HS 248-3617000-615 (launch mode) T-0 (10^{-5} Torr) reached at 17:30, 9/10/81		
9/11/81	Corona and arcing tests Conducted collimator transfer calibration Conducted CSPT at 20°C		94/1, 95/2 96/27, 97/28 98/1, 99/2 100/3, 101/4 102/5, 103/6 104/7, 105/8
9/12/81	Transition to 32°C	DSN* and DCC DCC*	106/1*, 107/2* 108/1*, 109/2 110/3, 111/4 112/5, 113/6 114/7, 115/8
	Transition to 5°C; conducted ASPT		116/1, 117/2
9/13/81	Completed transition to 5°C and ASPT Conducted CSPT at 5°C	DCC* DCC*, DSN	118/7*, 119/8 120/1*, 121/2 122/3, 123/4 124/5, 125/6 126/7, 127/8
	Transition to 10°C		128/4
9/14/81	Conducted ASPT at 10°C	DCC* DCC*	129/1*, 130/2* 131/7*, 132/8*
	Transition to 20°C		133/1
	Conducted ASPT at 20°C		134/1, 135/2, 136/7
	Transition to 30°C		137/3
	Conducted ASPT at 30°C		138/1, 139/2 140/7, 141/8
9/15/81	Conducted CSPT at 30°C	DCC* DCC* and DSN	142/1*, 143/2 144/3*, 145/4* 146/5, 147/6 148/7, 149/8
	Transition to 10°C; conducted ASPT		150/1, 151/2 152/7, 153/8
	Conducted CSPT at 10°C		154/1, 155/2

ORIGINAL PAGE IS
OF POOR QUALITY

Table 10-4 (continued)

Date	Activity	Problems	Orbit
9/16/81		DCC*	156/3*, 157/4
		Coll* Lamp I, DCC	158/5*, 159/6
		DCC*	160/7, 161/8*
	Transition to 30°C; conducted ASPT	DCC*	162/1*, 163/2
		DCC*	164/7, 165/8*
	Performed STR 29 collimator radiometric calibration at 30°C		629/27, 630/28
	Conducted first CSPT at 30°C	Coll* Lamp I, DSN	166/1*, 167/2*
		Coll* Lamp I, DSN	168/3*
9/17/81	Change out collimator albedo source power supply	DSN*, Commands FR 5144	169/4*, 170/5*
		DSN*	171/6*, 172/7, 173/8
	Conducted second CSPT at 30°C	DSN*	174/1*, 175/2
			176/3, 177/4
		DSN*	178/5, 179/6*
		DSN*	180/7*, 181/8
	Transition to 10°C		182/1, 183/2
	Computer crash-disk restored	Aborted*	184/7*
9/18/81	Performed STR 30 collimator transfer calibration		631/27, 632/28
			186/1, 187/2
			188/3, 189/4
		No VPIR Pictures	190/5, 191/6
		No VPIR Pictures	192/7, 193/8
	Conduct second CSPT at 10°C	DSN*	194/1*, 195/2
			196/3, 197/4
9/19/81	Changed to multiplexer line 1, changed to multiplexer line 2, changed to multiplexer line 3, changed to multiplexer line 4	No VPIR	198/5, 199/6
		DCC*, No VPIR	200/7, 201/8*
	Transition to 15°C	DCC*, No VPIR	202/4*
	Perform STR 3, ASPT at 15°C	DCC*, No VPIR	633/1*, 634/2*
		DCC*, No VPIR	635/7*, 636/8
	Transition to 20°C		203/6
	Conduct CSPT at 20°C; changed to multiplexer Line 3, changed to multiplexer line 2, changed to multiplexer line 1	DCC*	204/1*, 205/2
		DCC*	206/3*, 207/4
		DCC*	208/5*, 209/6*
		DCC	210/7*, 211/8
9/20/81	Initiated ventback		
9/21/81	Conduct ASPT on endbell-ambient pressure	DCC*	212/1, 213/2*
		DCC*	214/7, 215/8*
9/22/81	Move F-1 from C7 to area S1		
	Conducted system radiometric calibration per HS 2483617000-623		216/13, 217/14
			218/15, 219/16
	Performed STR 32 scan monitor pulse test		

ORIGINAL PAGE IS
OF POOR QUALITY

Table 10-4 (continued)

Date	Activity	Problems	Orbit
9/23/81	Removed SMA for flex pivot changeout Removed access cover and witness mirrors Sent SMA to Culver City for rework Sent witness mirrors to Culver City Incorporated EO 2842A-aft cover washers		
9/30/81	Reassembled F-1 scanner Conduct system alignment per HS 248-3617000-617		
10/1/81	Conduct system radiometric calibration per HS 248-3617000-623	Aborted 223/16*	220/13, 221/14 222/15
10/2/81	Performed STR 33 scan monitor pulse amplitude test Performed STR 34 band 3 bit drop investigation		
10/5/81	Moved scanner from plate to collimator cart		
10/6/81	Performed STR 35 special performance test Performed STR 36 calibration diagnostic test		
10/7/81	Prepared F-1 for post flex pivot acoustic test Moved scanner to Rockwell Conducted acoustic test per STR HS 248-1370-37 Returned system to area S1		
10/8/81	Conducted system alignment per HS 248-3617000-617		
10/9/81	Conducted system radiometric calibration per HS 248-3617000-623		225/13, 226/14 227/15, 228/16
10/12/81	Conducted collimator transfer calibration per HS 248-3617000-631 Conducted CSPT per HS 248-3617000-620		229/27, 230/28, 231/1, 232/2, 233/3
10/13/81		VLL* FR 5146 VLL*, CXAXO FR 5147 VLL*	234/4* 235/5, 236/6* 237/7*, 238/8*
	Assembled scanner for mass properties test		
10/14/81	Moved scanner to mass properties area Conducted mass properties test per TP 32238-011 Moved scanner back to area S1		
10/15/81	Performed STR 39 scan monitor check Repaired silver teflon coat on electronic cover per NCMR 337710		
10/16/81	Conducted STR 38 VLL study		
10/19/81	Conducted STR 40 shutter sync pulse test Conducted STR 41 VLL investigation — sunshield removed		
10/20/81	Conducted STR 42 SMA run-in test		
10/21/81	Continued STR 42		
10/22/81	Completed STR 42 Performed SMP (saturated) turnaround check Bag, seal, purge scanner Placed scanner in shipping container		
11/4/81	F-1 system moved to United Air Lines for shipment to General Electric		

*Out-of-specification.

ORIGINAL PAGE IS
OF POOR QUALITY

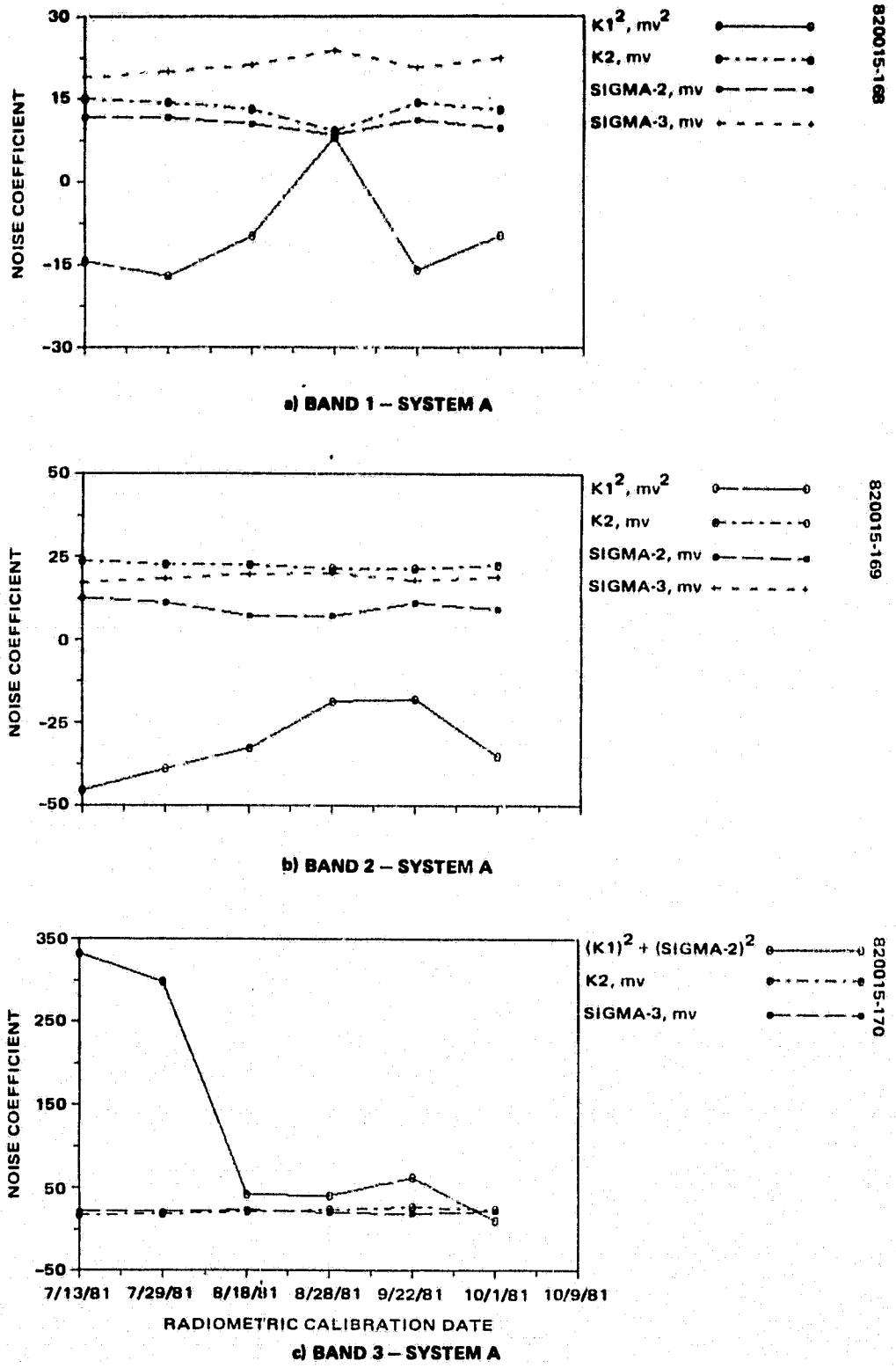

FIGURE 10-7. NOISE MODEL COEFFICIENT HISTORY

ORIGINAL PAGE IS
OF POOR QUALITY

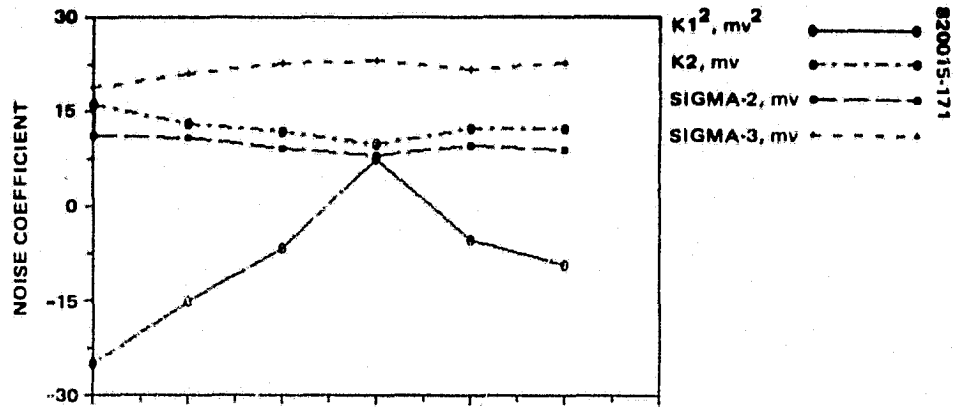

d) BAND 1 – SYSTEM B

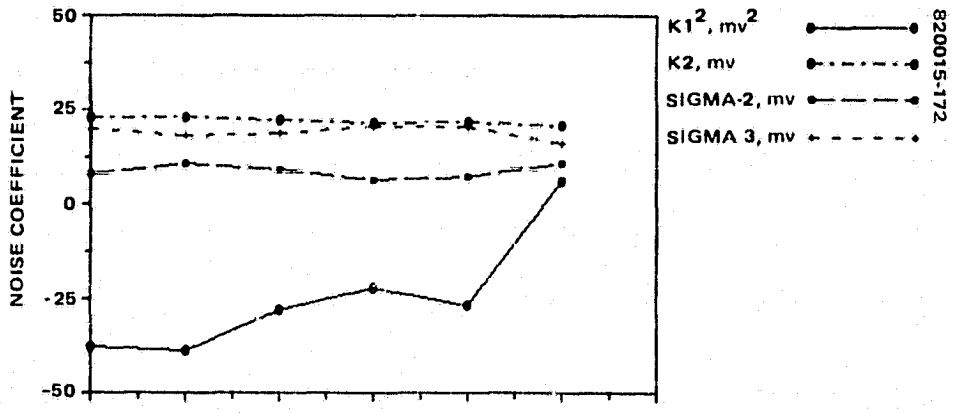

e) BAND 2 – SYSTEM B

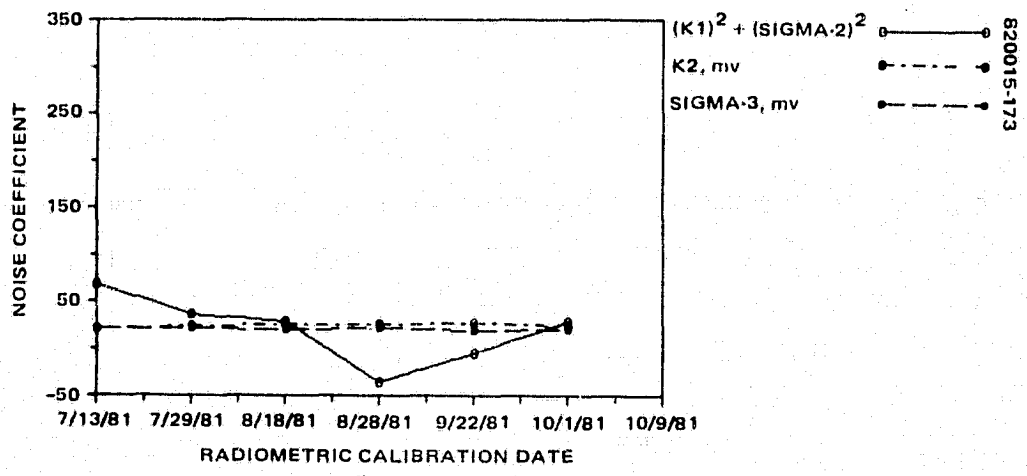

f) BAND 3 – SYSTEM B

FIGURE 10-7 (CONTINUED). NOISE MODEL COEFFICIENT HISTORY

ORIGINAL PAGE IS
OF POOR QUALITY

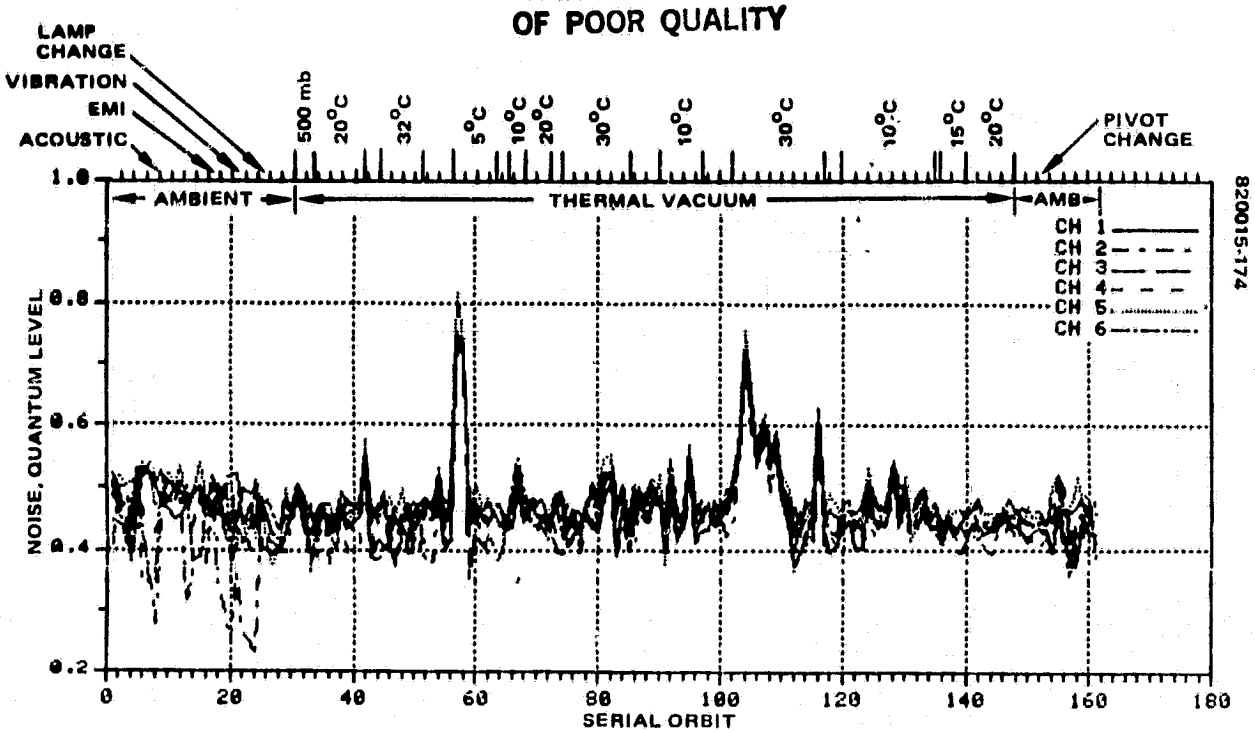

a) BAND 1

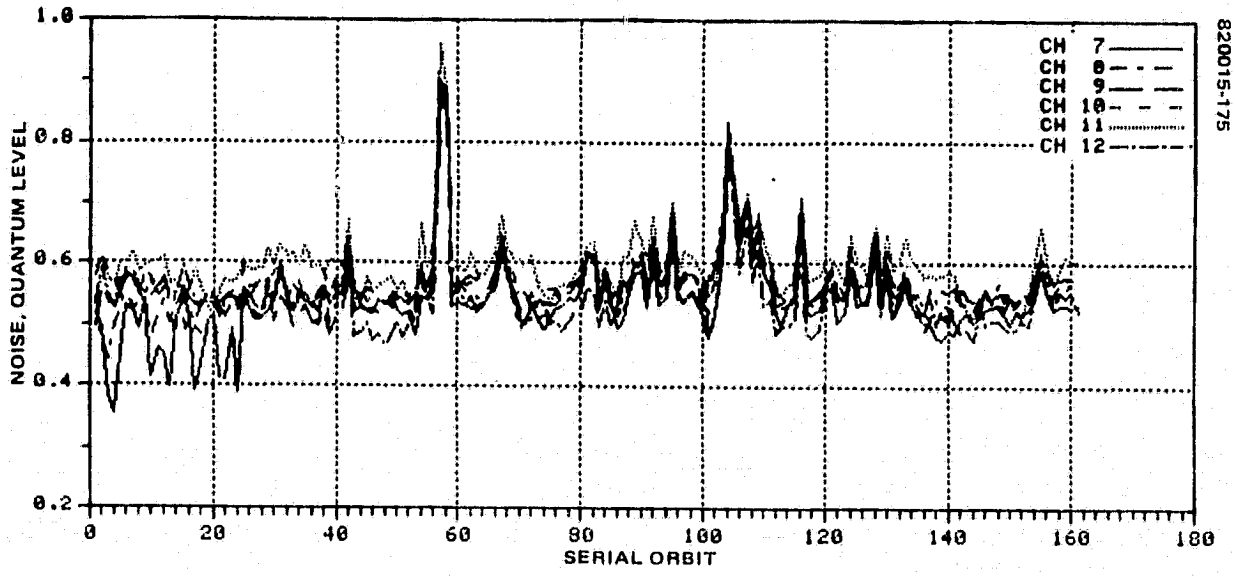

b) BAND 2

FIGURE 10-8. NOISE MEASUREMENTS DURING F-1 SYSTEM TEST – LINEAR/LOW GAIN MODE

ORIGINAL PAGE IS
OF POOR QUALITY

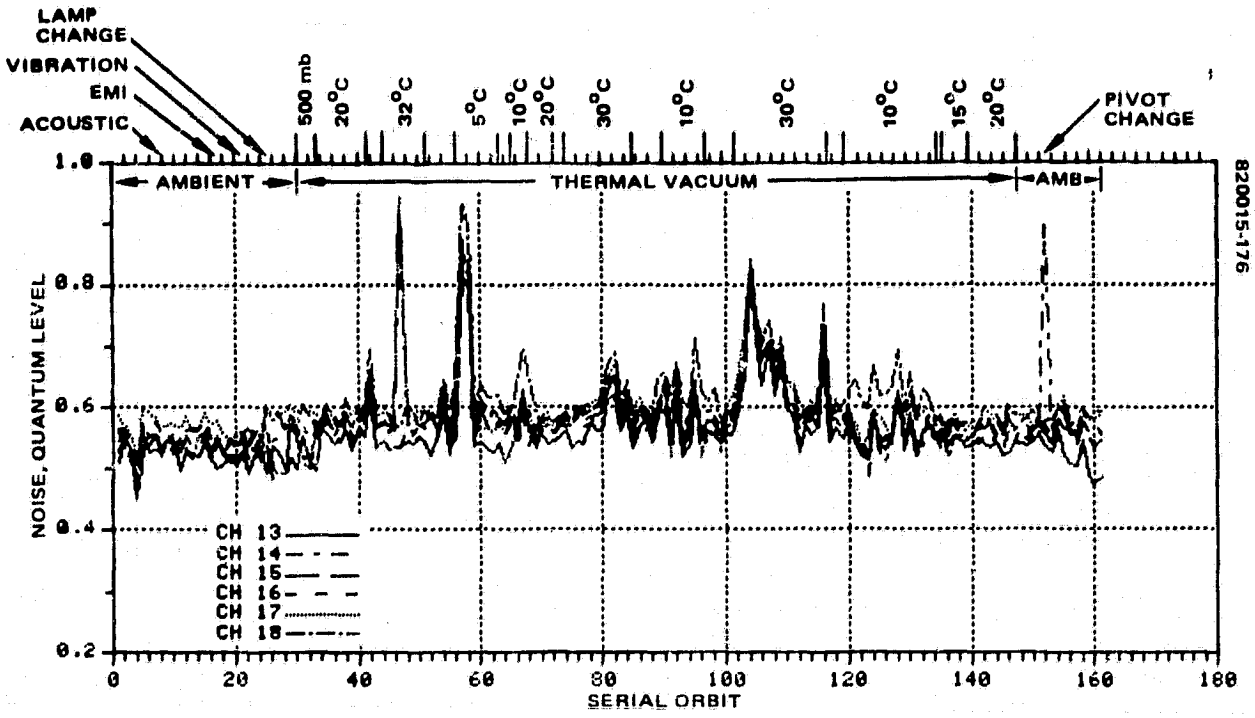

c) BAND 3

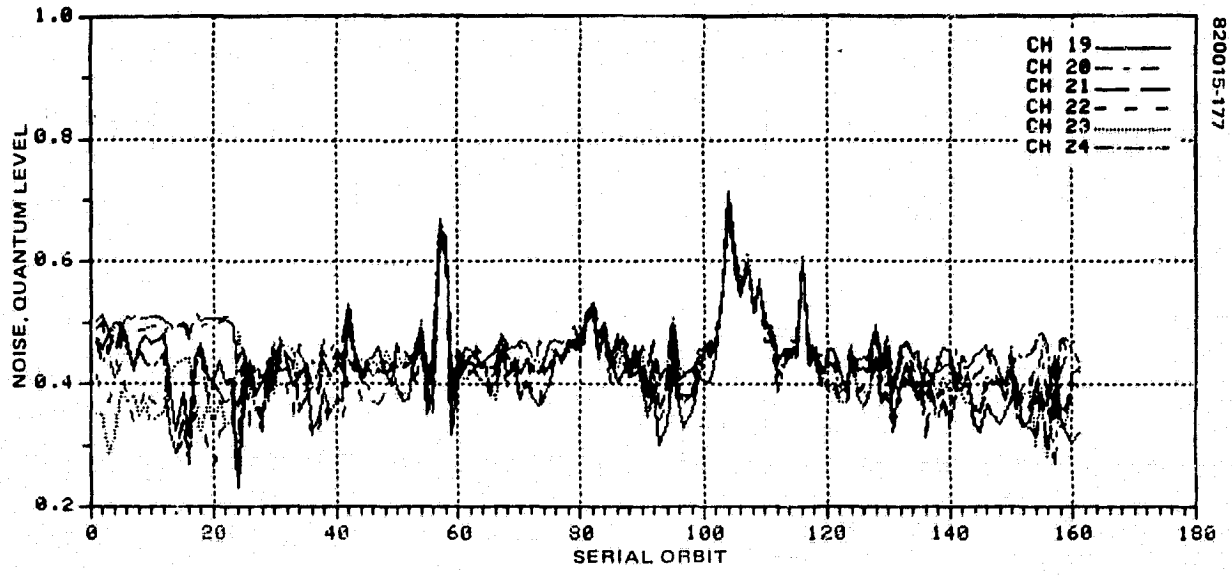

d) BAND 4

FIGURE 10-8 (CONTINUED). NOISE MEASUREMENTS DURING F-1 SYSTEM TEST – LINEAR/LOW GAIN MODE

ORIGINAL PAGE IS
OF POOR QUALITY

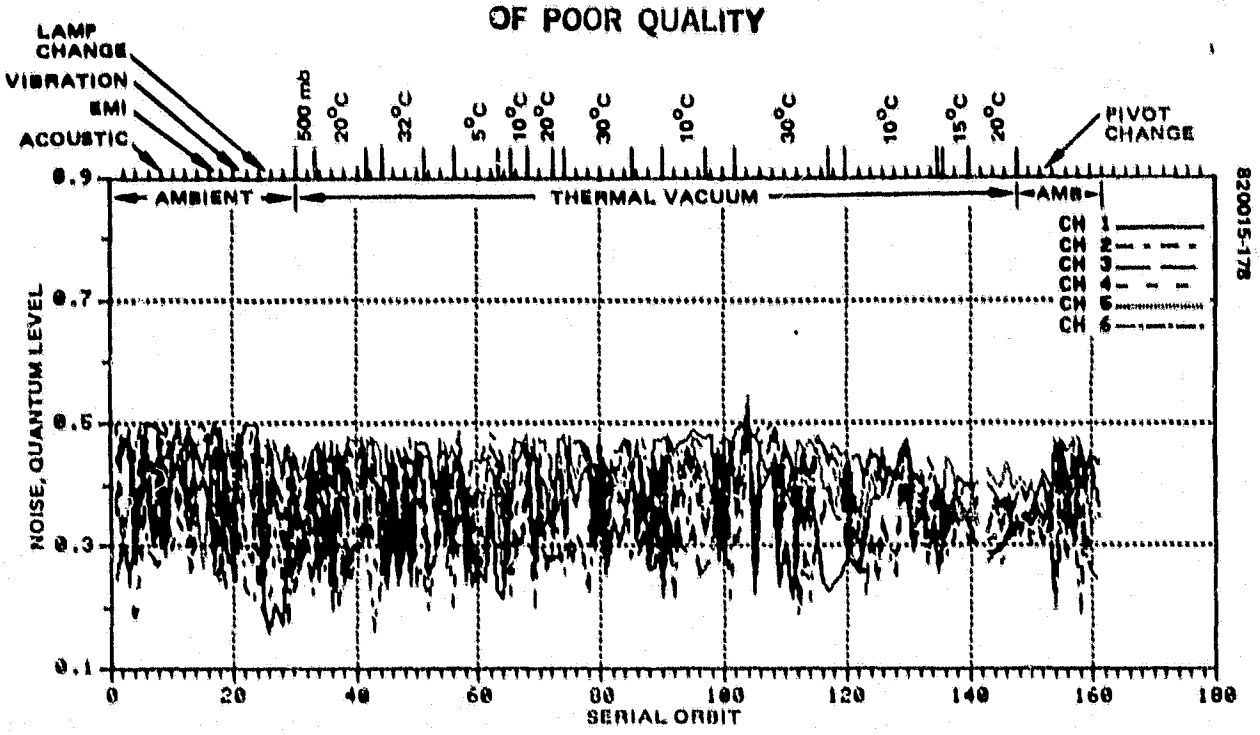

a) BAND 1

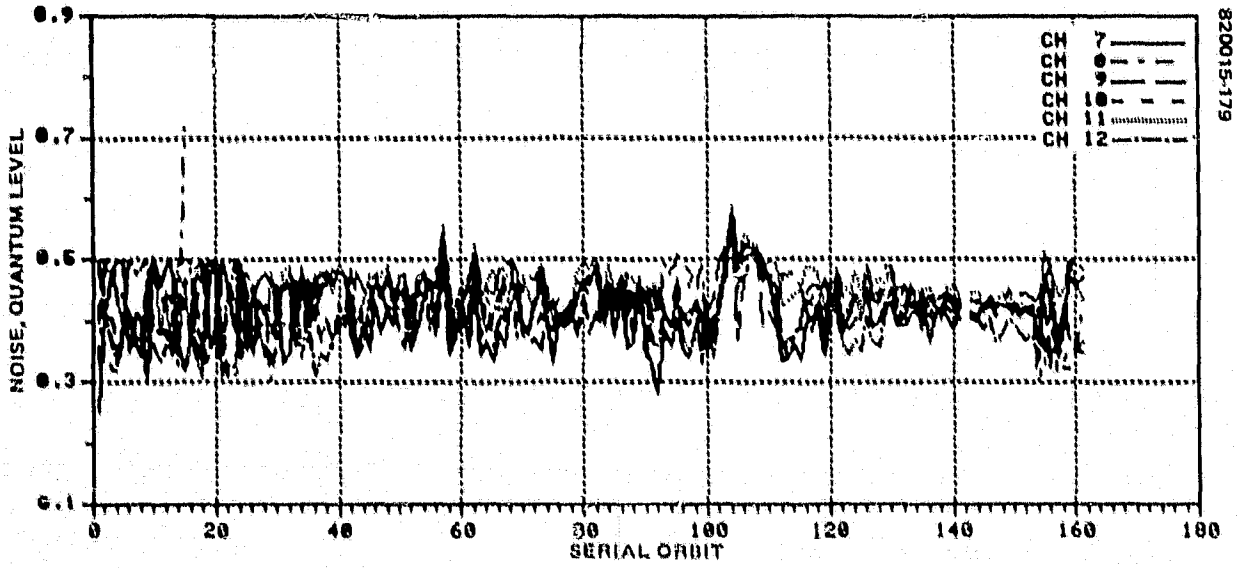

b) BAND 2

FIGURE 10-9. NOISE MEASUREMENTS DURING F-1 SYSTEM TEST – COMPRESSION/LOW GAIN MODE

ORIGINAL PAGE IS
OF POOR QUALITY

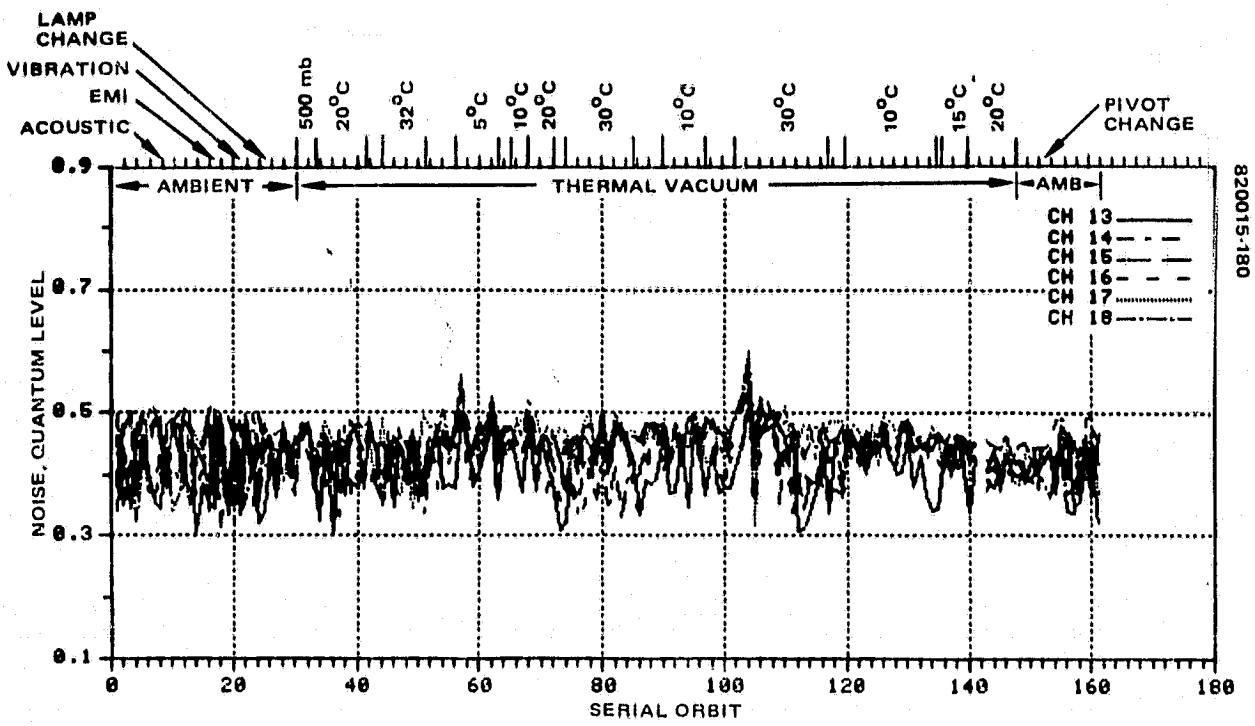

c) BAND 3

FIGURE 10-9 (CONTINUED). NOISE MEASUREMENTS DURING F-1 SYSTEM TEST – COMPRESSION/ LOW GAIN MODE

ORIGINAL PAGE IS
OF POOR QUALITY

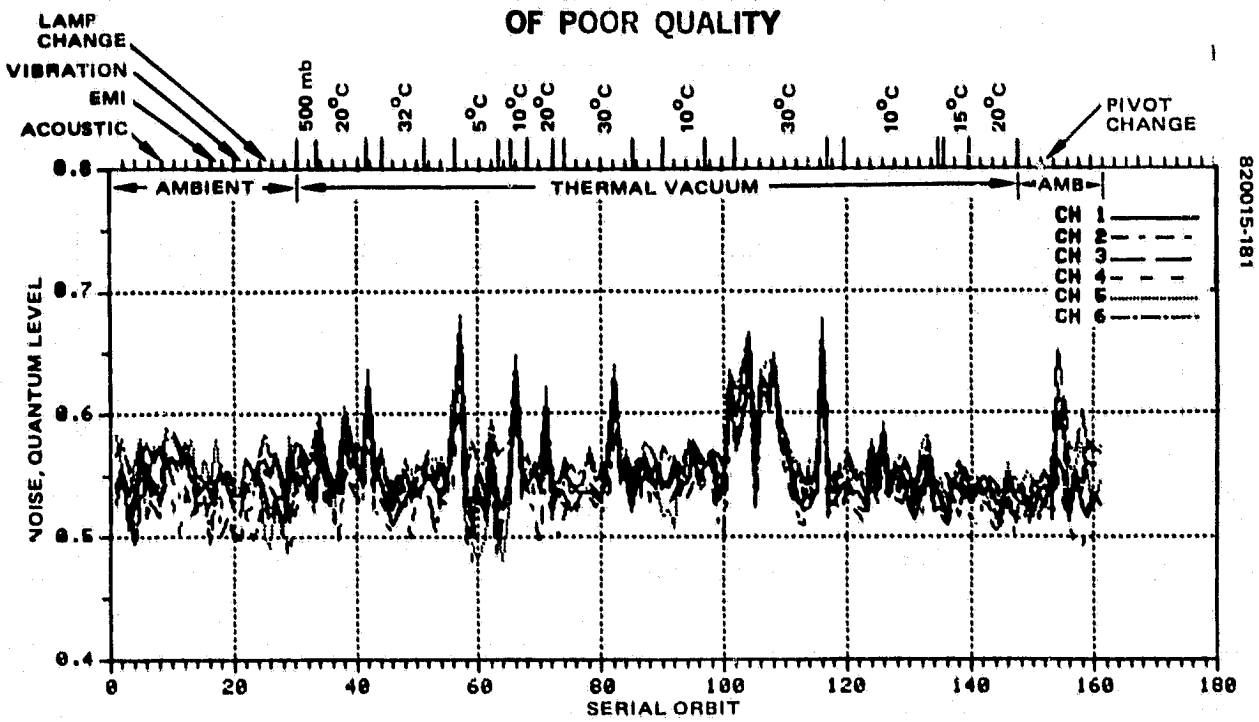

a) BAND 1

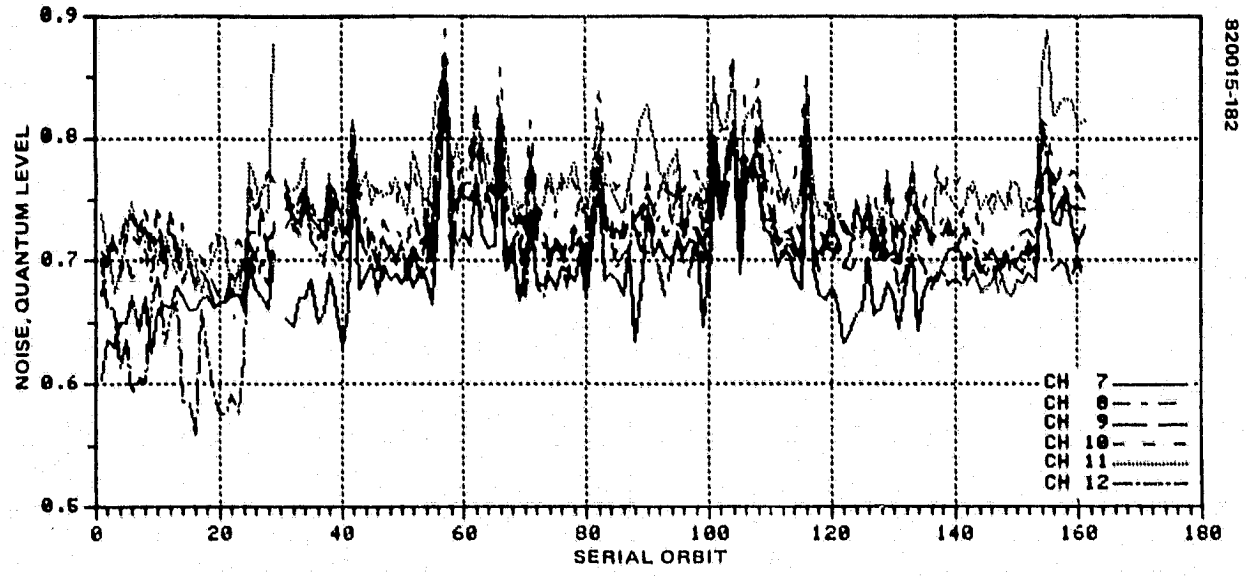

b) BAND 2

FIGURE 10-10. NOISE MEASUREMENTS DURING F-1 SYSTEM TEST – LINEAR/HIGH GAIN MODE

ORIGINAL PAGE IS
OF POOR QUALITY

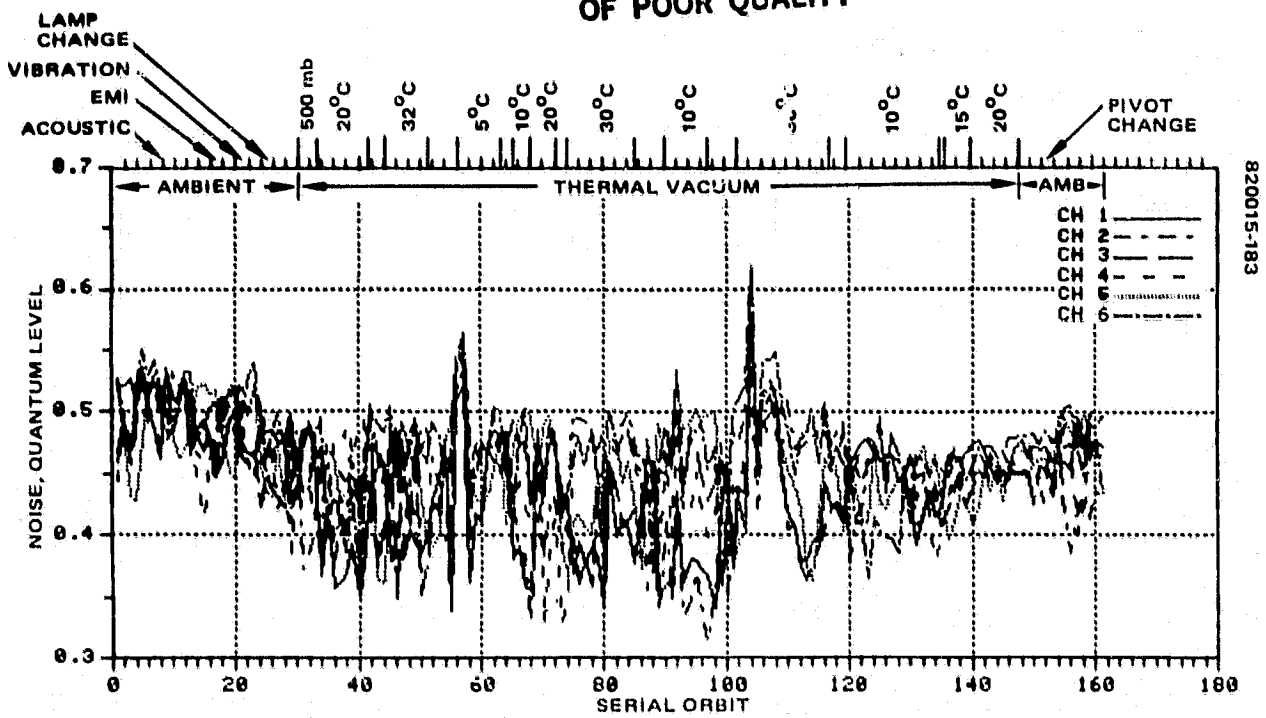

a) BAND 1

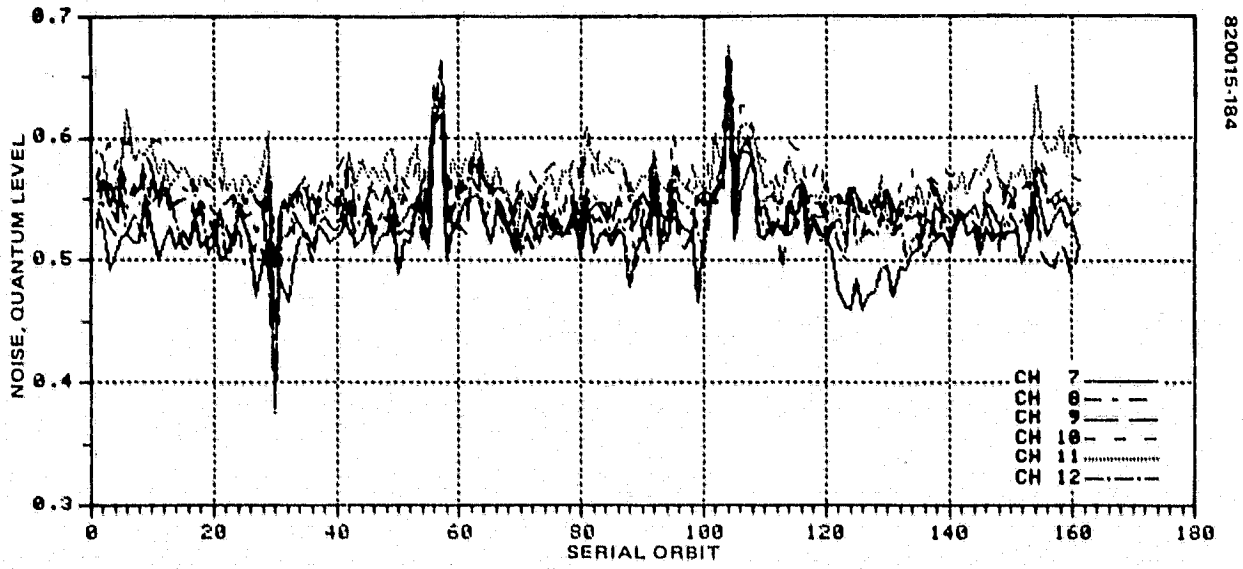

b) BAND 2

FIGURE 10-11. NOISE MEASUREMENTS DURING F-1 SYSTEM TEST – COMPRESSION/HIGH GAIN MODE

noise algorithm was implemented which reduced the upward excursions of the noise plots. The result of these two changes can be seen on the plots as a compression in the range of the noise after orbit 24(79).

A serious problem with the collimator was experienced during thermal-vacuum test. An unstable power supply caused fluctuations in the collimator lamp output, which resulted in higher indicated noise measurements. This effect is most noticeable in orbits 42(106), 52(116), 104(168) to 109(173) and 116(180) in the linear/low mode. Other orbits can be seen to be affected as well. Table 10-6 shows the approximate noise value that can be reached before a signal-to-noise specification violation occurs. This table can be used as a guide to the margin available to each band in meeting its performance requirements.

10.3.3.1 Linear/Low

Once the irregularities due to collimator fluctuations have been discounted, the noise plots for the linear/low gain mode (Figure 10-8) show a very uniform response throughout thermal-vacuum test. Two additional spikes appear in the plots for band 3 at orbits 47(111) and 152(214). These have been traced to a hardware problem in the front end (the device which selects the video data from the demultiplexer). At certain signal levels, the circuits for some of the channels in band 3 occasionally miss one bit (read the bit in error). This could change the observed level of a sample by up to 32 quantum levels, acounting for the sharply increased noise measurement.

10.3.3.2 Compression/Low

The plots for compression/low gain (Figure 10-9) indicate a similarly uniform response. The gap at orbit 142(204) represents an orbit when the collimator pattern for this mode was changed before data collection had been completed (operator error). The anomalous spike for channel 8 at orbits 15(51) and 16(52) has been traced to a bad cable which was used only for these two orbits. The effects of the collimator fluctuations are reduced in compression mode but are still apparent.

The quantization effects which drive the noise to 0.5 at certain signal levels can still be seen, although the noise algorithm which removes the collimator nonuniformity contribution usually keeps the maximum slightly below this value.

10.3.3.3 Linear/High

The linear/high plots (Figure 10-10) are very flat except for the collimator fluctuations (note the expanded scale). The gap at orbit 30(90) in the band 2 plot was caused by an operator error (band 2 was not put in high gain mode).

10.3.3.4 Compression/High

The results in compression/high mode (Figure 10-11) are similar, basically a very uniform response with respect to temperature. The dip in band 2 at orbit 30(90) was caused by the same error mentioned above (band 2 was not in high gain). Some temperature effects may be present, but they are certainly much smaller than those encountered on the protoflight scanner. In any event, the collimator fluctuations make an examination for subtle details impossible.

ORIGINAL PAGE IS
OF POOR QUALITY

TABLE 10-5. FLIGHT MODEL EXTRAPOLATED STN PERFORMANCE
(BASED ON RADIOMETRIC CALIBRATION OF 9 NOVEMBER 1981)

Mode	Gain	Specification				Performance							
						System A				System B			
		Band 1	Band 2	Band 3	Band 4	Band 1	Band 2	Band 3	Band 4	Band 1	Band 2	Band 3	Band 4
Linear													
64 QL	Low	89.1	72.9	49.8	108	125.1	108.4	101.4	162.4	131.2	106 6	88.0	170.7
	High	58.7	45.8	N/A	N/A	92.3	72.1	N/A	N/A	99.0	71.7	N/A	N/A
32 QL	Low	54.3	46.4	33.5	54	71.8	66.9	64.4	81.2	73.4	65.7	53.0	85.3
	High	38.7	31.0	N/A	N/A	59.2	48.8	N/A	N/A	61.1	48.9	N/A	N/A
Compression													
64 QL	Low	110.3	94.8	68.8	N/A	150.9	140.9	134.1	N/A	152.8	134.6	118.0	N/A
	High	79.4	63.8	N/A	N/A	120.5	99.7	N/A	N/A	125.7	97.6	N/A	N/A
32 QL	Low	59.1	51.9	38.9	N/A	75.5	73.1	71.9	N/A	76.3	71.9	57.0	N/A
	High	44.4	36.2	N/A	N/A	66.7	57.1	N/A	N/A	66.9	57.7	N/A	N/A

TABLE 10-6. APPROXIMATE MAXIMUM NOISE PERMISSIBLE
WITHOUT VIOLATING SPECIFICATION

Band	Mode			
	Linear/Low	Compression/Low	Linear/High	Compression/High
1	0.52	0.45	0.70	0.60
2	0.70	0.56	1.00	0.78
3	1.20	0.85		
4	0.60			

10.3.4 Summary Assessment

With the anomalies due to test equipment failures and operator errors removed, the flight model scanner can be seen to have performed very well in the area of signal-to-noise performance. The scanner has a very low sensitivity to temperature changes.

Band 1 is the band operating closest to the specified limit. In linear/low mode it operates close to the specification. Although the signal-to-noise was frequently measured just out-of-specification in the compression/low mode, this was a result of the quantization effect discussed above. With this effect removed, performance in this mode is very good. Band 1 had no problem meeting specification in linear/high or compression/high modes. Band 2 easily met all requirements, being driven out of specification only with the worst collimator fluctuations. Band 3 clearly had the most performance margin. Even collimator problems and digital dropouts did not cause a specification violation. Band 4 was well within the performance limits. As with band 2, band 4 was driven out-of-specification only by test equipment problems.

10.4 CORRECTED SIGNAL LEVEL (COSL)

10.4.1 Introduction

The COSL is the measured response of the MSS instrument to a radiant input from the collimator, corrected to remove individual channel gain and offset differences. The contributors to, and derivation of, COSL is described in 7.4; this subsection contains the results of COSL measurements during MSS-D F-1 system acceptance testing.

10.4.2 Average Signal Level (ASL) Performance History

The parameters which bear directly on the system signal correction performance are the ASL, the COSL, the gain (G), and the offset (O). All of these parameters were continuously monitored throughout MSS-D system acceptance testing. Graphics were routinely provided and surveyed to assist in the assessment of system performance and to aid in early identification of potential system problems.

The average signal level plots for F-1 are displayed in Figure 10-12 for all the data taken during regular orbits of acceptance testing. Special test request (STR) data and data taken during calibration orbits are not represented. The ASL is a primitive measurement of system performance. It is the average (over 100 scans, 20 words per scan) of the system response to the test collimator input. The units given are in quantum levels, with level 64 representing a saturated output. The ASL is utilized in the signal-to-noise (STN) performance assessment as well as in COSL (DCC, DBB) performance assessment discussed here. These algorithms are discussed in Section 6.

Since the internal-calibration-system-derived gains are not involved in computing the ASL, this parameter provides another, and very basic, view of system performance. For instance, these plots may be viewed as providing a separate estimate of relative gains and can be used to compare with the internal calibration system estimate of gain described later. The difference between these two types of gain estimates directly impacts on the estimate of the COSL and the discrepancy between

ORIGINAL PAGE IS
OF POOR QUALITY

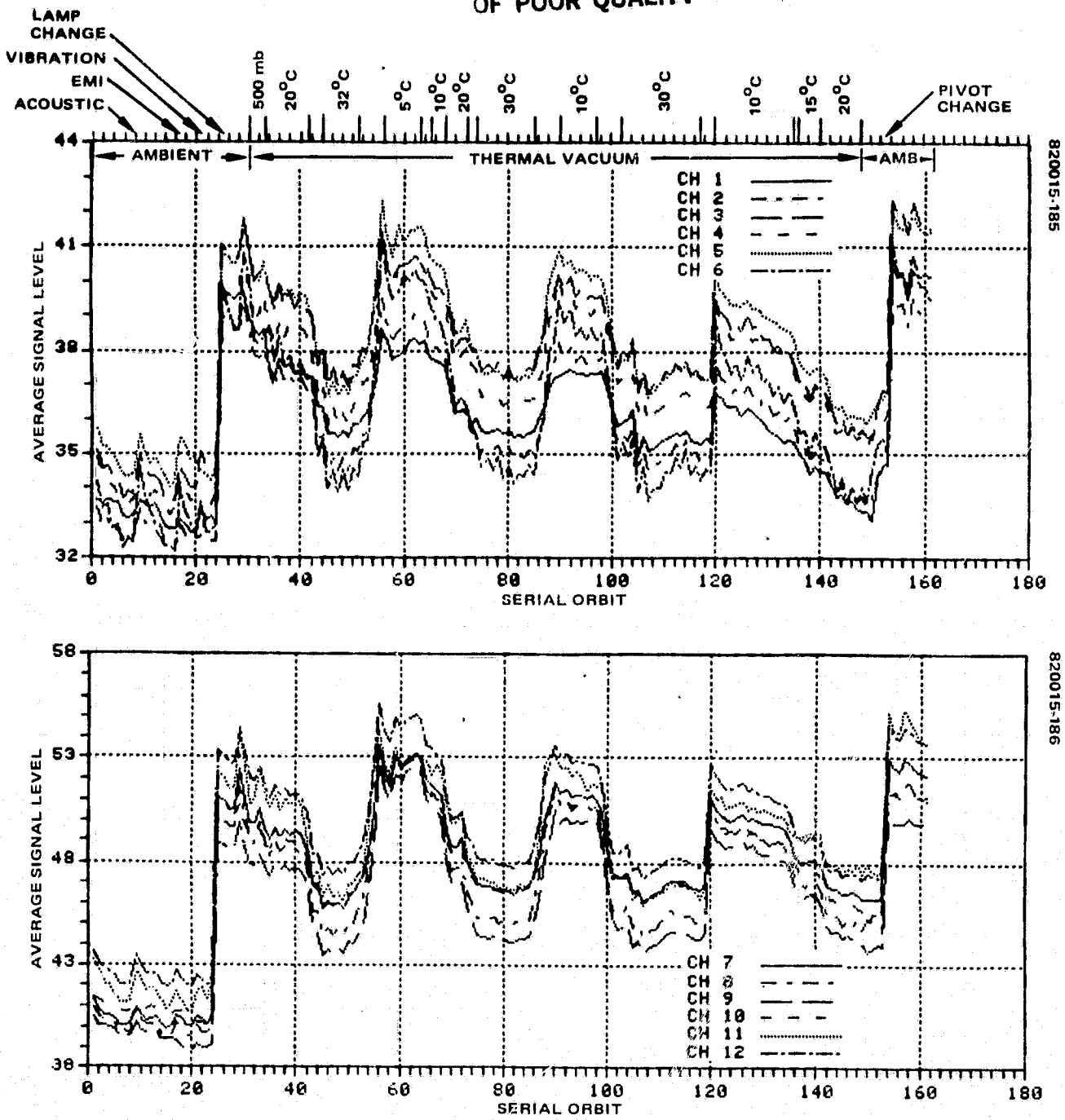

FIGURE 10-12. AVERAGE SIGNAL LEVEL – LINEAR/LOW GAIN MODE

ORIGINAL PAGE IS
OF POOR QUALITY

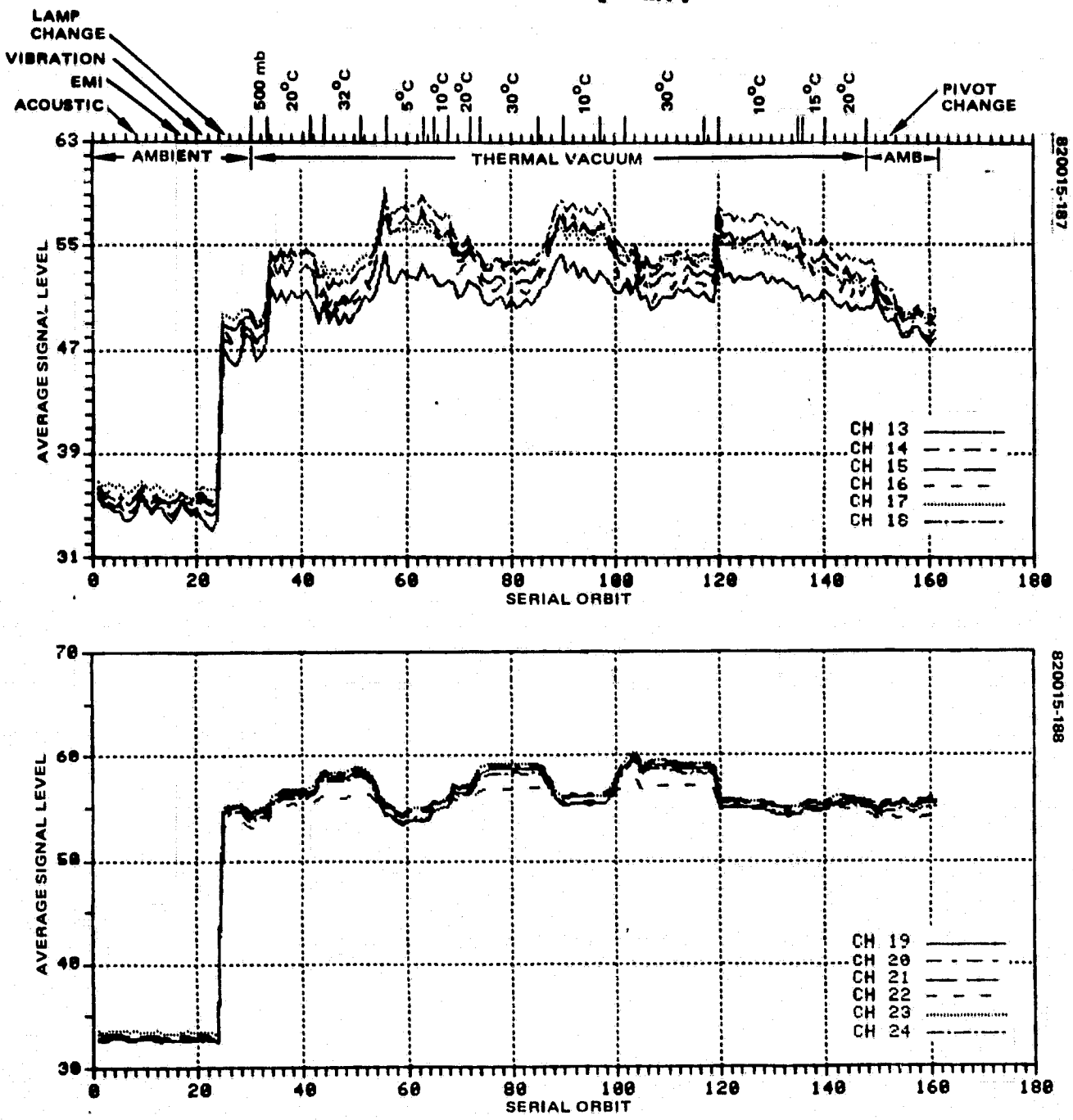

FIGURE 10-12 (CONTINUED). AVERAGE SIGNAL LEVEL – LINEAR/LOW GAIN MODE

ORIGINAL PAGE IS
OF POOR QUALITY

ASL changes and G changes is responsible for the errors which show up as DCCs and DBB. Since the scanner does not have a separate, independent calibrated sensor for measuring radiance, considerable difficulty exists in establishing the degree of fault which should be attributed to the scanner versus the test equipment for anomalous COSL performance. The consistency and repeatability of the separate data measures, as well as their correlation with each other and with independent data derived from the flooding lamp and from calibration orbit data, provide a means (albeit limited) for developing confidence in establishing calibration system performance estimates (see 6.5).

The treatment given in 6.5 is highly statistical and utilizes flooding lamp as an independent data source. The ASL plots given here can provide some additional insight into signal correction performance if the following observations are used:

1) Changes in ASL behavior reflect system behavior independent of the internal calibration system. Thus, changes in ASL are due either to real gain changes, changes in the collimator output, or both.

2) Changes in gain (G) behavior reflect changes in the internal calibration system's estimate of gain. This change may be a real gain change, the result of errors in the gain estimate (G) produced by calibration system changes, or both.

3) Changes in both ASL and G which agree sufficiently to produce good COSL values and which are in sufficient agreement for all channels in a band but produce varying or consistently alternating values of the band average for A and B modes suggest strongly that the results are induced by improperly established calibration wedge nominals during the previous calibration.

4) ASL and G estimates can agree in the direction of change but disagree in amplitude sufficiently to create COSL poblems. This last case, which is obtained more often than not when DCC problems occur, is the one most difficult to attribute to a specific cause. The ASL curves presented here should be used as a source of additional information as the description of gain and COSL performance unfolds. A more complete understanding of system performance is obtained if these curves are used as a reference, remembering that the basic relationship among the primary parameters is the following:

$$\mathrm{COSL} = K\frac{\mathrm{ASL} - \phi}{G}$$

where K contains a factor which relates to "shading" at time of calibration and a factor which normalizes the estimated collimator output in radiance to quantum levels.

10.4.3 System Gain Performance History

Before the system COSL performance is treated, and the system performance with respect to the specification parameters, DCC and DBB, is discussed, and system gain performance is described. It must be emphasized that the gain discussed here is the

ORIGINAL PAGE IS
OF POOR QUALITY

estimate of the channel gain, G, provided by the internal calibration system. The features of this gain estimate which are of interest are the following:

1) The individual channel gain behavior as a function of key environmental changes (temperature, pressure) and test configurations

2) The individual channel gain behavior as compared to the nominal gain behavior for other channels in the band for the same test environment

3) Identification of major test or flight hardware configuration changes that could affect system gain performance estimates

10.4.3.1 Nominal Gain History

The gain history for all channels is presented in Figure 10-13. The nominal performance for each channel, as indicated by these plots, is summarized chronologically for the major test events in Table 10-7. As is evident from the individual plots, each test event may contain from 4 to 16 gain values, depending upon the number of orbits run during the test. The sawtooth pattern in the plots results from a difference in the gain estimate when the system is in mode A from that measured when the system is in mode B. Since it occurs in band 4, as well as the first three bands, it is not due to a difference in high voltage power supply output. It is most likely due to actual differences in the A, B calibration systems or to apparent differences due to integrating sphere calibration inaccuracies. Table 10-7 provides the basis for the discussion of gain performance history which follows. Each band is tested in turn for the entire system acceptance test period.

Band 1

Throughout the test events the channel 5 gain was 4 to 6 percent higher than the other channel gains. Also, channel 5 gain goes down slightly as a function of time (LFPT to endbell) as does channels 1 and 2. Channels 3, 4, and 6 gains tend to be more stable up to the GN_2 backfill test event. Using the endbell values as the ambient baseline and comparing these values to the GN_2 backfill and vacuum values show the following vacuum effect:

Channel	Percent Shift into 500 mbar	Percent Shift into Vacuum
1	-1.5	-6.8
2	-0.9	-5.0
3	-0.4	-5.4
4	0	-7.4
5	-0.2	-5.7
6	0	-4.7

All the band 1 gains seem to be affected by the different temperature changes in the same amount except for channels 1 and 6. Channel 1 gain goes up 10 percent while the other channels go up 5 percent during the 32° to 5°C transition. Channel 6 gain goes down 7 percent while the other channels decrease 5 percent during the 20° to 32°C transition. Generally, all the band 1 gains decrease as the temperature increases.

ORIGINAL PAGE IS
OF POOR QUALITY

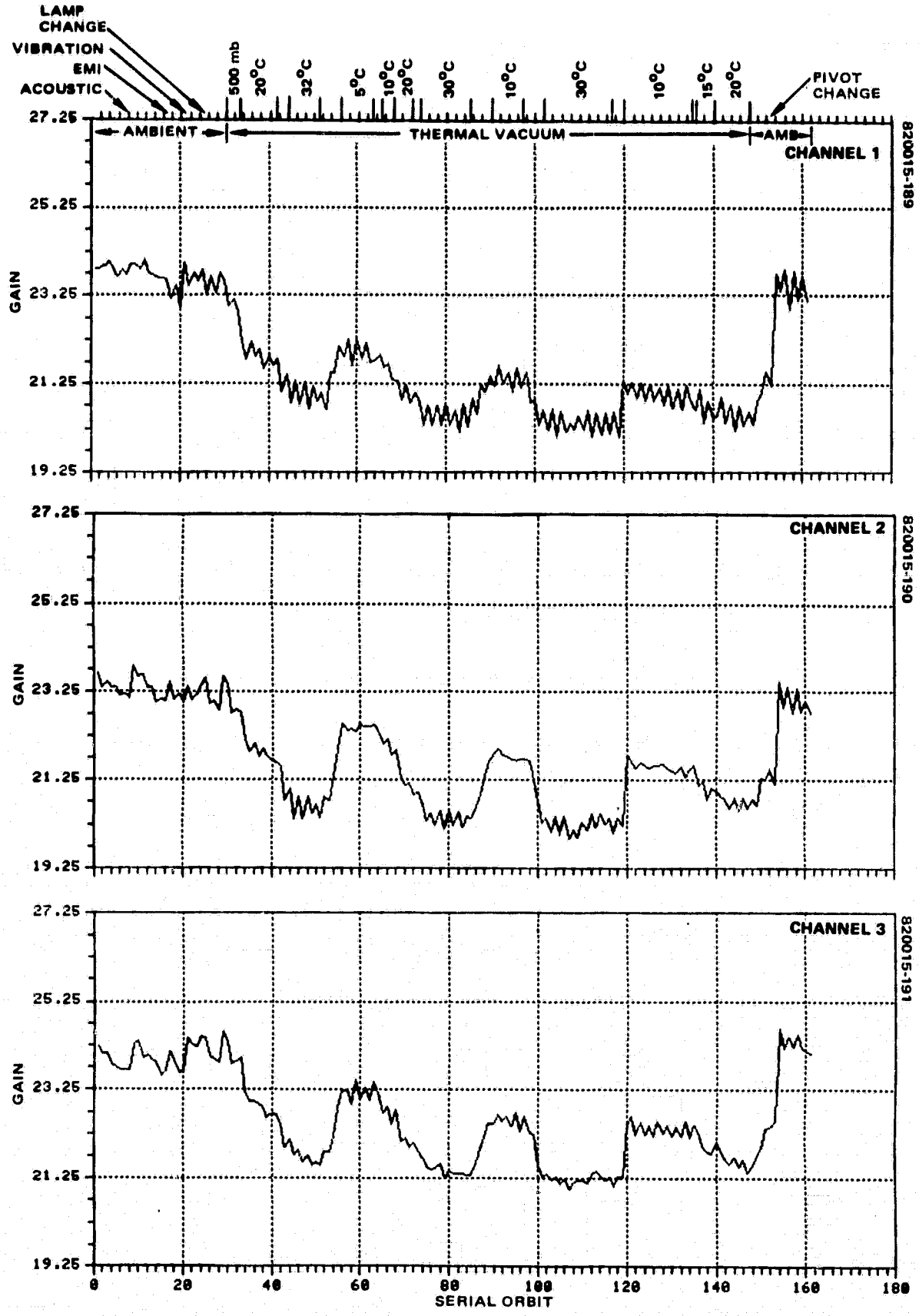

FIGURE 10-13. F-1 GAIN HISTORY – LINEAR/LOW GAIN MODE

ORIGINAL PAGE IS
OF POOR QUALITY

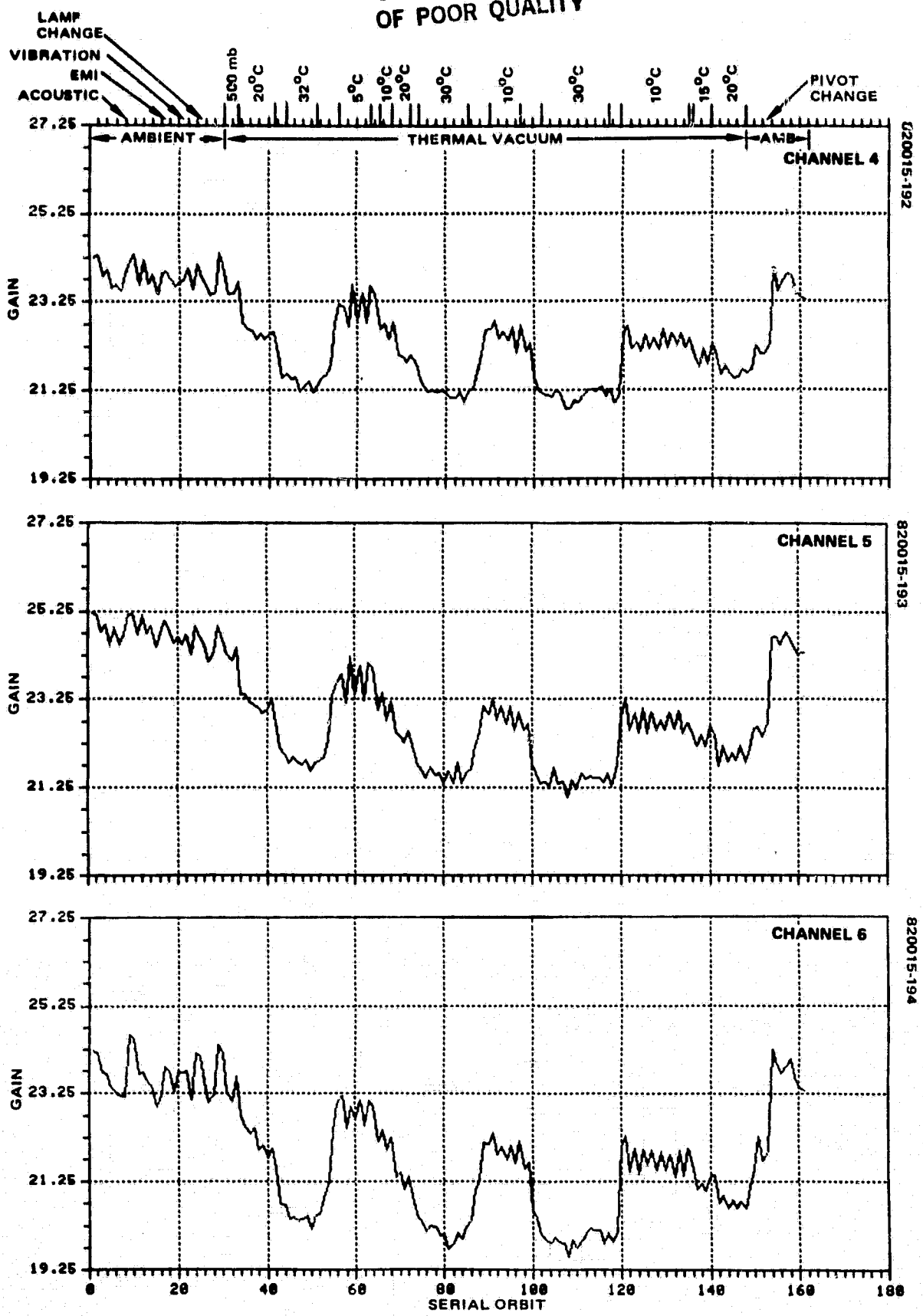

FIGURE 10-13 (CONTINUED). F-1 GAIN HISTORY – LINEAR/LOW GAIN MODE

ORIGINAL PAGE IS
OF POOR QUALITY

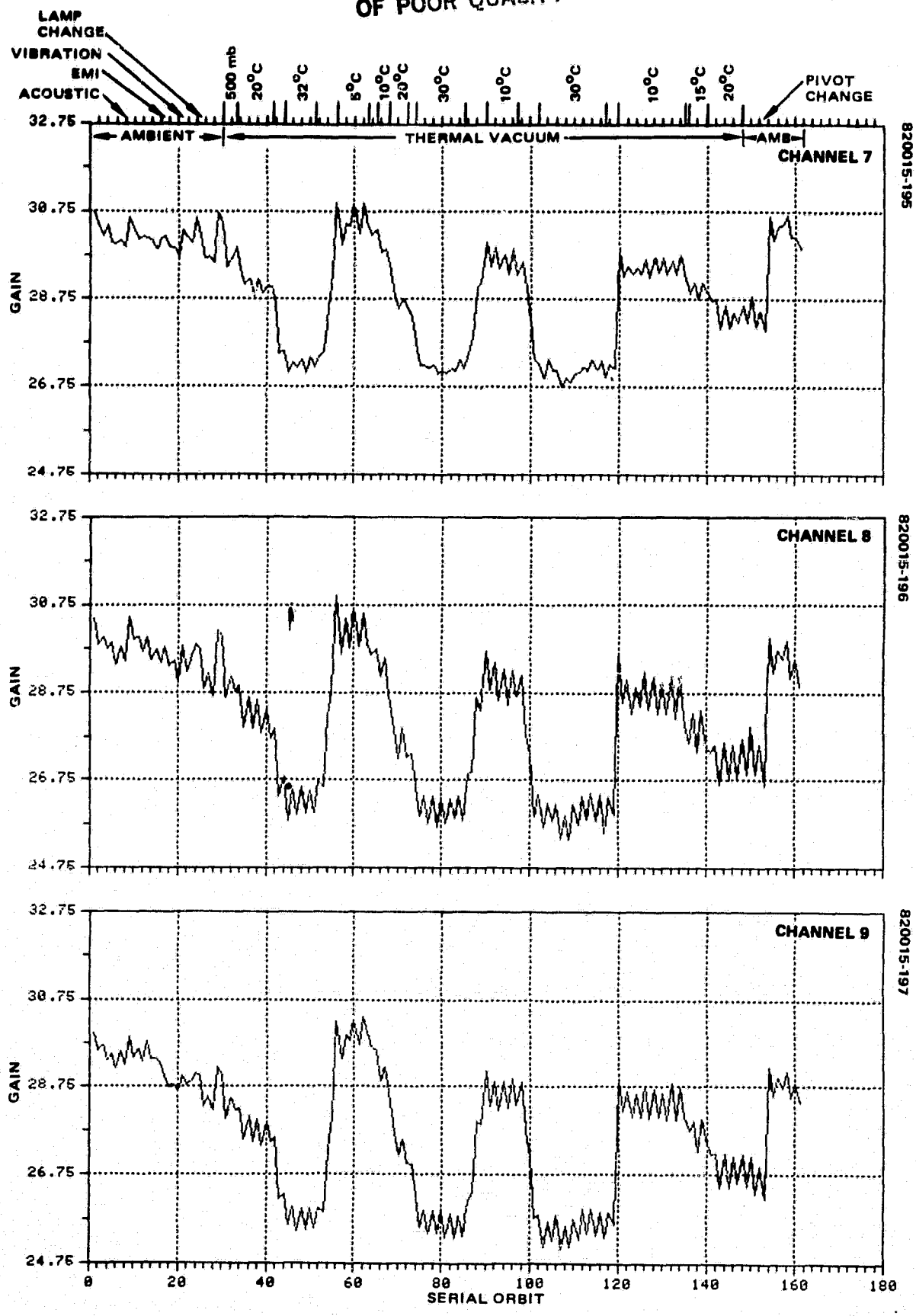

FIGURE 10-13 (CONTINUED). F-1 GAIN HISTORY – LINEAR/LOW GAIN MODE

ORIGINAL PAGE IS
OF POOR QUALITY

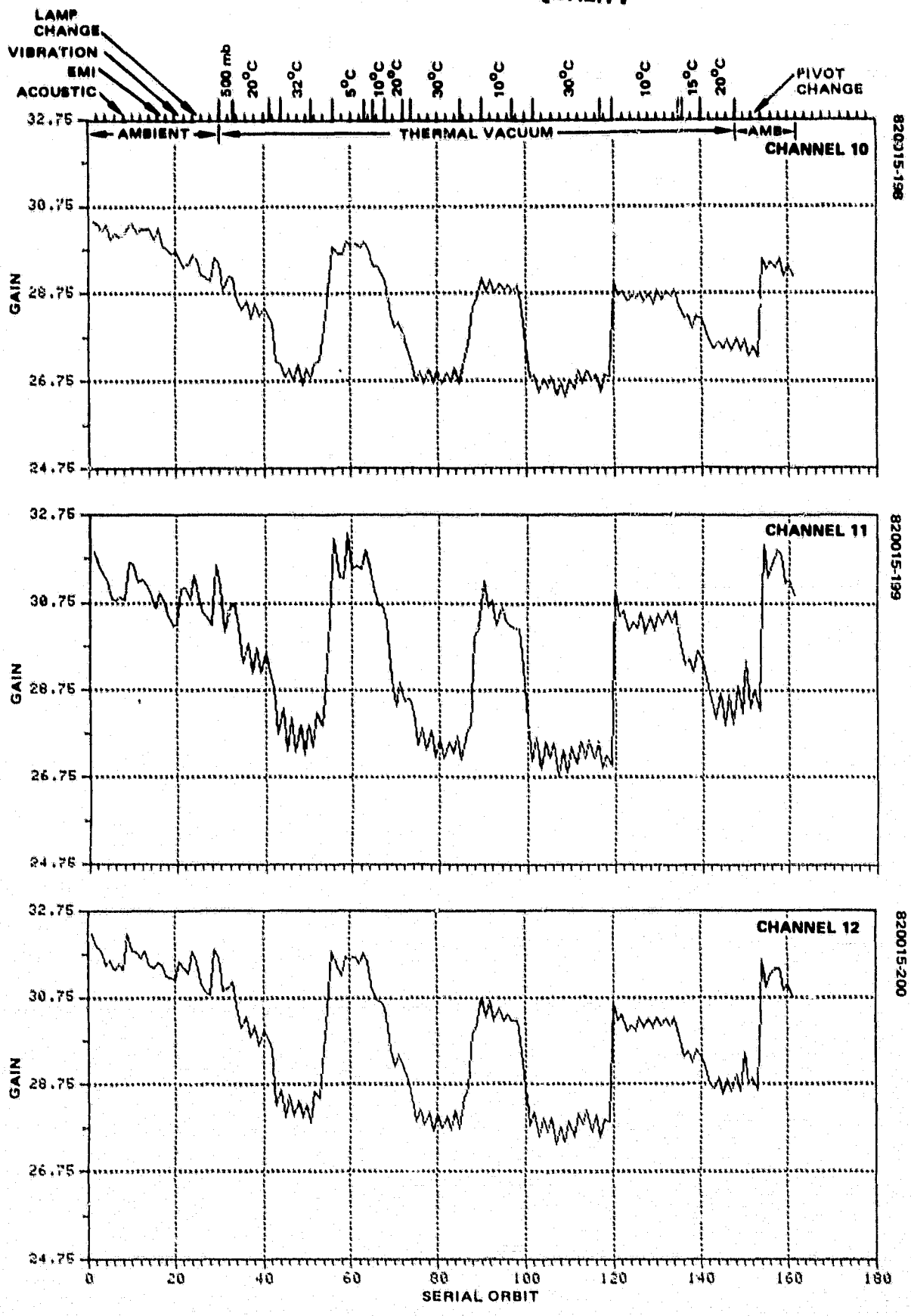

FIGURE 10-13 (CONTINUED). F-1 GAIN HISTORY – LINEAR/LOW GAIN MODE

ORIGINAL PAGE IS
OF POOR QUALITY

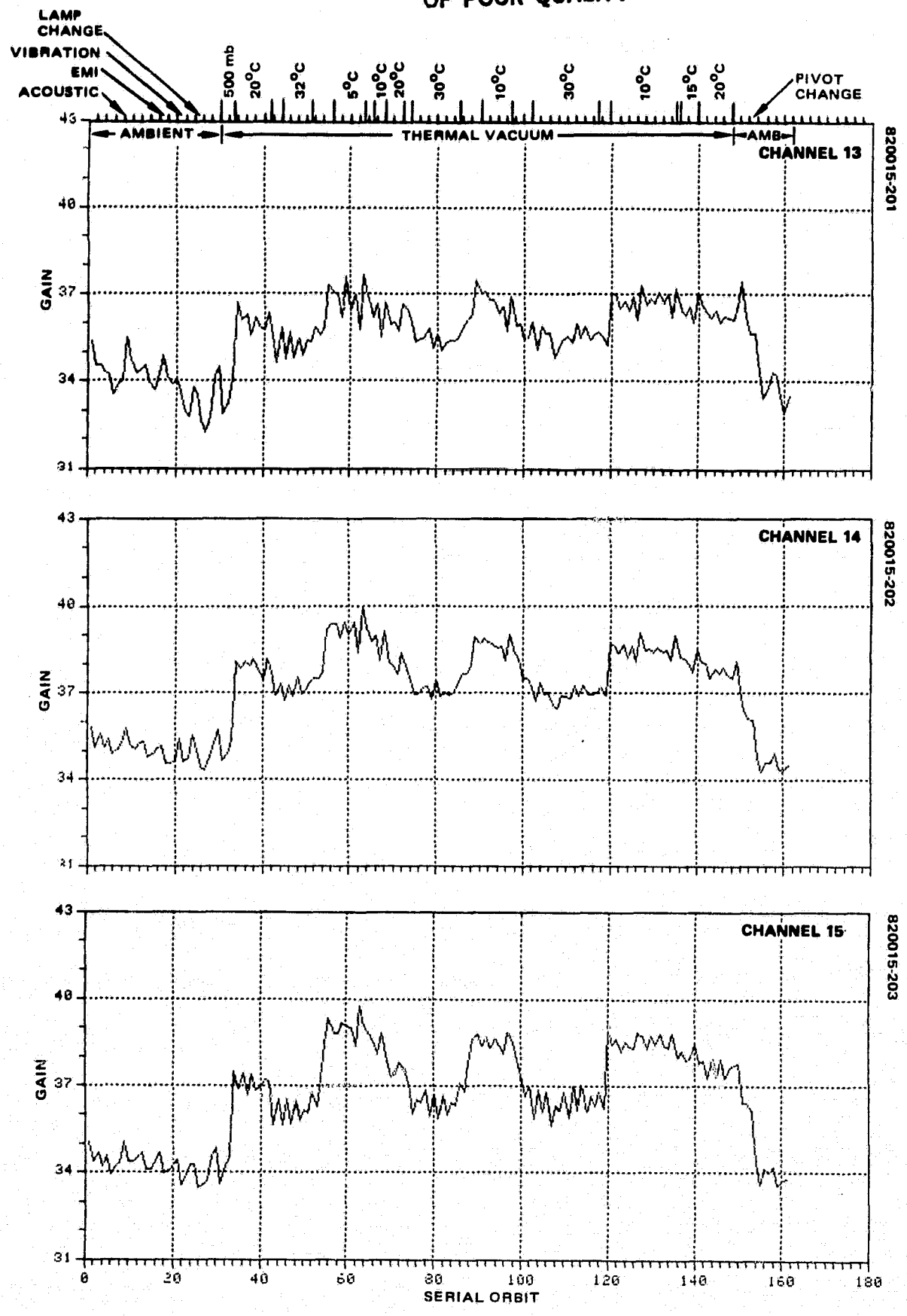

FIGURE 10-13 (CONTINUED). F-1 GAIN HISTORY – LINEAR/LOW GAIN MODE

ORIGINAL PAGE IS
OF POOR QUALITY

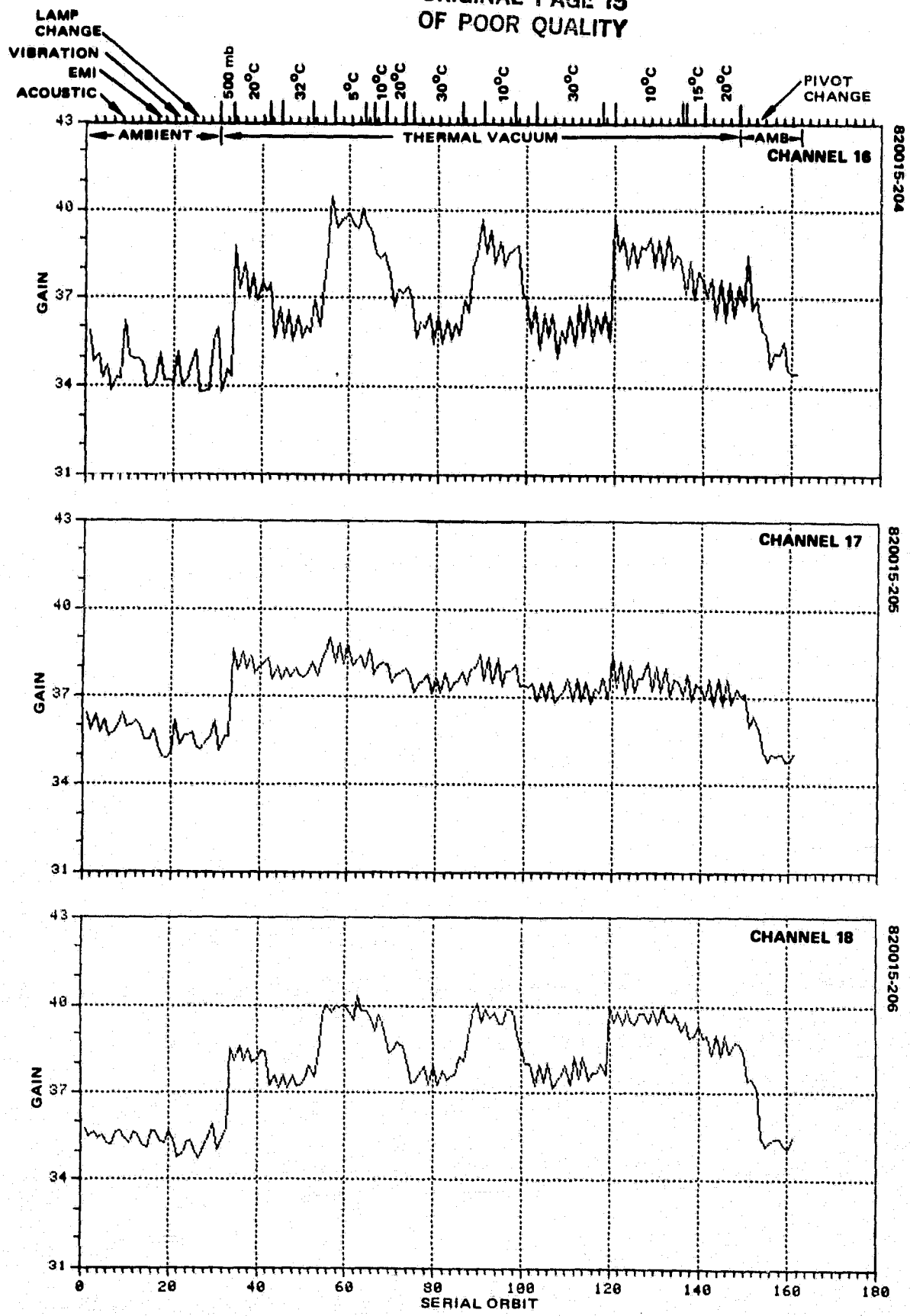

FIGURE 10-13 (CONTINUED). F-1 GAIN HISTORY – LINEAR/LOW GAIN MODE

ORIGINAL PAGE IS
OF POOR QUALITY

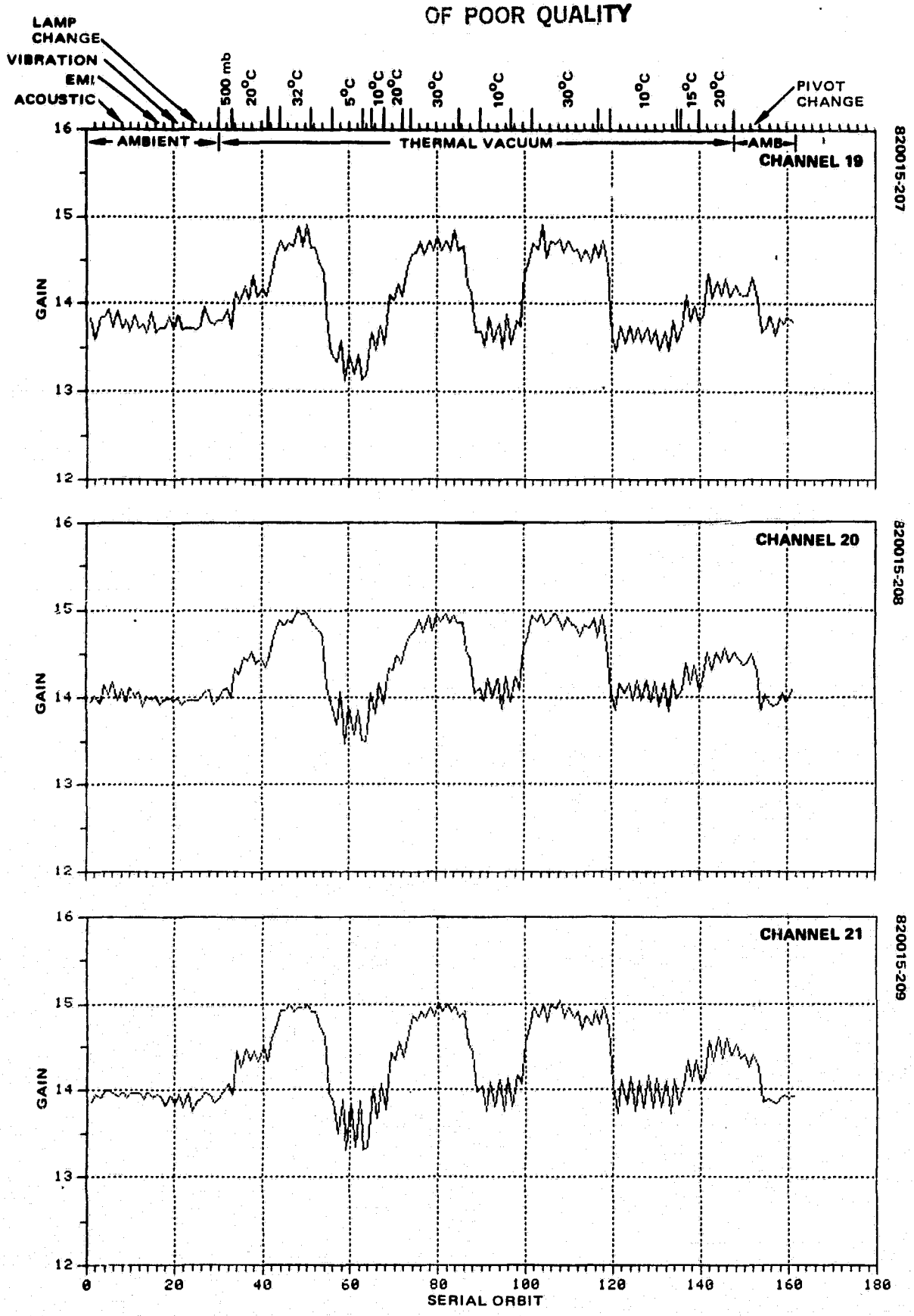

FIGURE 10-13 (CONTINUED). F-1 GAIN HISTORY – LINEAR/LOW GAIN MODE

ORIGINAL PAGE IS
OF POOR QUALITY

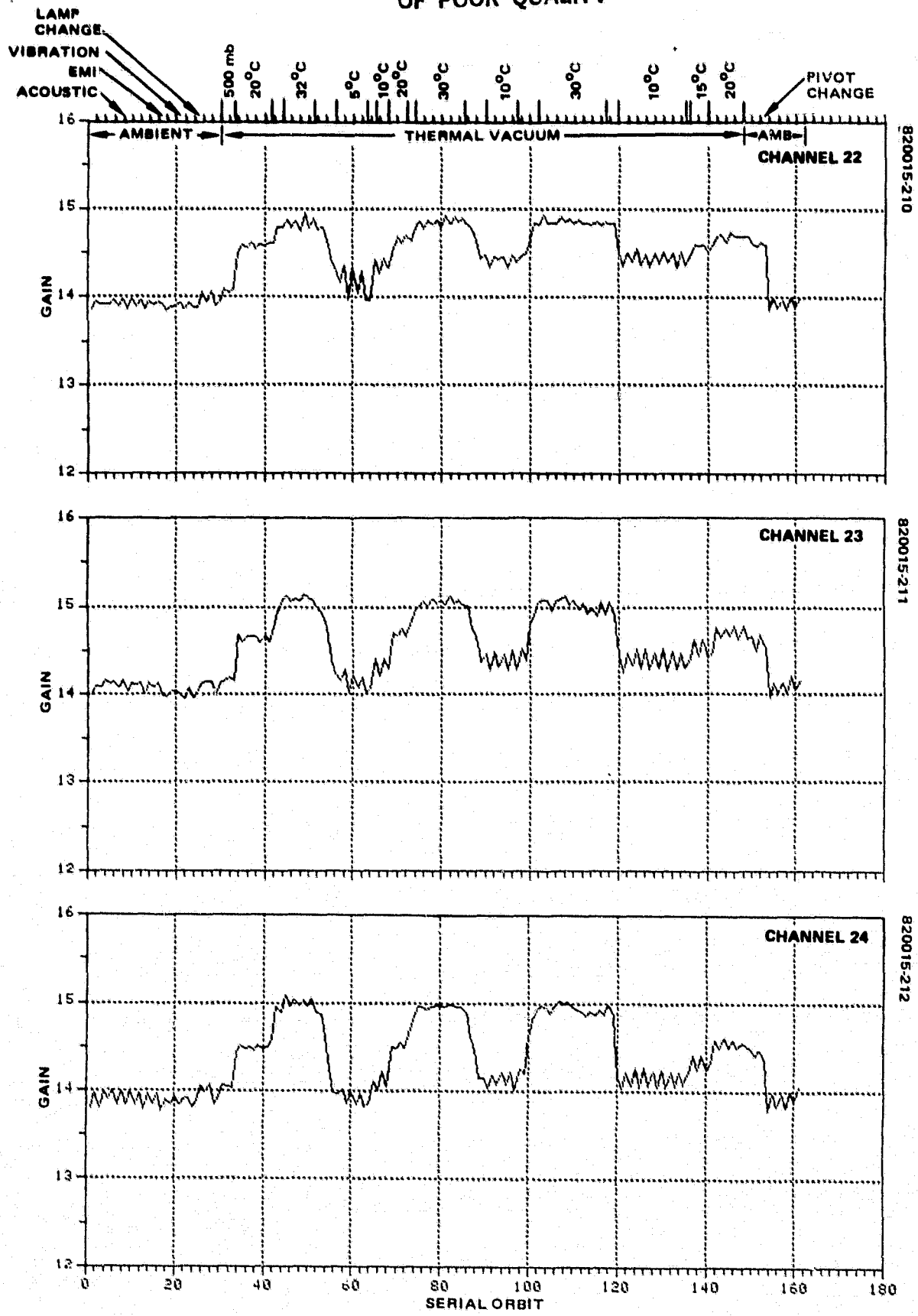

FIGURE 10-13 (CONCLUDED). F-1 GAIN HISTORY – LINEAR/LOW GAIN MODE

ORIGINAL PAGE IS
OF POOR QUALITY

TABLE 10-7. F-1 NOMINAL GAIN PERFORMANCE

Date	Test Event	Channel Nominal Gain					
		Band 1					
		1	2	3	4	5	6
7/31/81	LFPT (24°C)	23.85	23.35	23.90	23.90	24.85	23.60
8/05/81	Postacoustic (24°)	23.90	23.55	24.15	24.00	24.95	24.15
8/14/81	Pre-EMI (24°C)	23.75	23.05	23.85	24.30	24.75	23.35
8/21/81	Post-EMI (24°C)	23.35	23.15	23.85	24.30	24.75	23.60
8/26/81	Postvibration (24°C)	23.65	23.05	24.35	24.30	24.50	23.50
8/27/81	Old visible source replaced with new 150 W source						
9/8/81	Endbell (25°C)	23.50	23.05	24.15	24.30	24.45	23.50
9/10/81	GN_2 backfill (25°C)	23.15	22.85	24.05	24.30	24.40	23.50
9/11/81	Thermal-vacuum 20°C	21.90	21.90	22.85	22.50	23.05	22.40
9/14/81	20°C	20.95	21.05	22.00	21.95	22.45	21.30
9/19/81	20°C	20.55	20.65	21.55	21.65	21.90	20.75
9/21/81	Post thermal-vacuum (22°C)	20.95	21.25	22.05	22.00	22.50	21.95
10/12/81	Final LFPT	23.50	23.05	24.25	23.75	24.50	23.85
10/13/81	(24°C)						
		Band 2					
		7	8	9	10	11	12
7/31/81	LFPT (24°C)	30.25	29.75	29.50	30.15	31.15	31.70
8/05/81	Postacoustic (24°C)	30.30	29.95	29.55	30.25	31.25	31.90
8/14/81	Pre-EMI (24°C)	30.00	29.75	29.50	30.15	30.95	31.55
8/21/81	Post-EMI (24°C)	29.95	29.45	28.85	29.85	30.50	31 25
8/26/81	Postvibration (24°C)	30.25	29.55	28.85	29.5	30.95	31.55

ORIGINAL PAGE IS
OF POOR QUALITY

Table 10-7 (continued)

Date	Test Event	Channel Nominal Gain					
		Band 2					
		7	8	9	10	11	12
8/27/81	Old visible source replaced with new 150 W source						
9/8/81	Endbell (25°C)	29.85	29.15	28.50	29.05	30.75	31.15
9/10/81	GN_2 backfill (25°C)	29.85	29.10	28.50	29.05	30.75	31.15
9/11/81	Thermal vacuum 20°C	29.0	28.25	27.75	28.35	29.40	30.0
9/14/81	20°C	28.55	27.55	27.30	28.05	28.65	29.25
9/19/81	20°C	28.25	27.15	26.85	27.50	28.30	28.75
9/21/81	Post-thermal vacuum (22°C)	28.28	27.30	26.65	27.40	28.70	29.0
10/12/81 10/13/81	Final LFPT (24°C)	30.30	29.50	28.75	29.25	31.55	31.55
		Band 3					
		13	14	15	16	17	18
7/31/81	LFPT (24°C)	34.4	35.2	34.5	34.7	36.0	35.5
8/05/81	Postacoustic (24°C)	34.75	35.3	34.75	35.2	36.15	35.55
8/14/81	Pre-EMI (24°C)	34.2	35.0	34.30	34.35	35.65	35.40
8/21/81	Post-EMI (24°C)	34.4	34.75	34.25	34.25	35.1	35.5
8/26/81	Postvibration (24°C)	33.25	35.0	34.0	34.6	35.6	35.1
8/27/81	Old visible source replaced with new 150 W source						
9/8/81	Endbell (25°C)	32.9	34.6	33.8	33.95	35.4	35.0
9/10/81	GN_2 bacfill (25°C)	33.55	35.1	34.2	34.6	35.5	35.4
9/11/81	Thermal-vacuum 20°C	36.0	37.9	37.1	37.5	38.0	38.2
9/14/81	20°C	35.9	37.8	37.5	37.15	37.6	38.5
9/19/81	20°C	36.0	37.7	37.5	37.0	37.2	38.6
9/21/81	Post-thermal vacuum (22°C)	36.0	36.5	36.6	37.2	36.2	37.6
10/12/81 10/13/81	Final LFPT (24°C)	33.8	34.5	33.8	35.5	35.0	35.5

ORIGINAL PAGE IS
OF POOR QUALITY

Table 10-7 (continued)

Date	Test Event	Channel Nominal Gain					
		Band 4					
		19	20	21	22	23	24
7/31/81	LFPT (24°C)	13.75	14.05	23.93	13.90	14.1	13.9
8/05/81	Postacoustic (24°C)	13.75	14.05	13.93	13.90	14.1	13.9
8/14/81	Pre-EMI (24°C)	13.75	13.95	13.93	13.90	14.1	13.9
8/21/81	Post-EMI (24°C)	13.74	13.94	13.88	13.87	14.0	13.85
8/26/81	Postvibration (24°C)	13.74	13.94	13.88	13.87	14.0	13.85
8/27/81	Old visible source replaced with new] 50 W source						
9/8/81	Endbell (25°C)	13.76	14.02	13.90	13.96	14.12	14.0
9/10/81	GN_2 backfill (25°C)	13.76	14.02	13.95	14.06	14.12	14.0
9/11/81	Thermal-vacuum 20°C	14.1	14.40	14.35	14.60	14.65	14.50
9/14/81	20°C	14.1	14.35	14.40	14.65	14.70	14.51
9/19/81	20°C	14.1	14.41	14.41	14.70	14.70	14.5
9/21/81	Post-thermal vacuum (22°C)	14.1	14.40	14.3	14.60	14.60	14.45
10/12/81 10/13/81	Final LFPT (24°C)	13.75	13.95	13.91	13.90	14.10	13.88

Table 10-7 shows the band 1 nominal gains at the three 20°C plateaus. Comparing the values indicates the following results:

Channel	Percent Shift into Second 20°C	Percent Shift into Third 20°C
1	-4.3	-6.2
2	-3.9	-5.7
3	-3.7	-5.7
4	-2.4	-3.8
5	-2.6	-5.0
6	-4.9	-7.4

This means the band 1 gains have not reached stabilization during the entire vacuum testing period. However, the rate of change (decrease) in the gain as a function of time is diminishing.

A delayed vacuum effect caused the post-thermal-vacuum gains to be lower than the initial ambient gains. The gains increased to their initial values during the final LFPT.

Band 2

The gain plots show that band 2 has more well behaved gain characteristics than the other bands. All band 2 gains were affected by change in environment and temperature to about the same degree. The vacuum effect seen in band 1 is also evident in band 2. The following data describes the vacuum shift:

Channel	Percent Shift into 500 Mbar	Percent Shift into Vacuum
7	0	-2.8
8	-0.2	-3.1
9	0	-2.6
10	0	-2.4
11	0	-4.4
12	0	-3.7

A comparison of the gain values at the three 20°C plateaus shows that band 2 gains were leveling toward stabilization at the end of the thermal-vacuum test.

The effect of going out of vacuum into ambient pressure was evident in the band 2 gains several days after the actual end of thermal-vacuum test. The gains went back up to the ambient gain values before the final LFPT.

Band 3

Channels 15, 16, and 18 had similar gain behaviors throughout the tests and will be considered the normal channels. The rest of band 3 channels deviate from the normal gain behavior, especially during thermal-vacuum testing. As the system went from

ambient pressure to vacuum, the band 3 gains increased, which is opposite to the vacuum effect in band 1 and 2. The following data describe the vacuum shift (endbell = baseline):

Channel	Percent Shift into 500 Mbar	Percent Shift into Vacuum
13	+1.98	+9.4
14	+1.44	+9.5
15	+1.18	+9.8
16	+1.9	+10.5
17	+0.3	+7.3
18	+1.14	+9.1

In thermal-vacuum, channel 13 gain went up 4 percent and channel 17 went up less than 1 percent during a 27°C change (32° to 5°C). All the other channel gains increased about 8 percent.

Comparing the three 20°C plateaus indicates that most of the channels stabilized during thermal-vacuum testing. Channels 16 and 17 did not reach stabilization as shown below:

Channel	Percent Shift into Second 20°C	Percent Shift into Third 20°C
13	-0.3	0
14	-0.3	-0.5
15	+1.1	+1.1
16	-0.9	-1.3
17	-1.1	-2.1
18	+0.8	+1.1

At the end of vacuum testing, the band 3 gains did not recover from the vacuum effect since the gain values at post-thermal-vacuum remain the same as the last 20°C plateau. The gains went back (decreased) to the initial ambient gain values before the final LFPT.

Band 4

During ambient testing, the band 4 gain behavior is nominal except for channel 19 which is 1 to 3 percent lower than the other channel gains. The band 4 gains remain stable during the ambient and the variability in the gain values in each test event was considerably less than in the other bands.

A vacuum shift also occurred in band 4 where the gains increased as the system went from ambient to vacuum. The amount of vacuum shift in each channel is shown below (endbell values = baseline):

Channel	Percent Shift into 500 Mbar	Percent Shift into Vacuum
19	0	+2.5
20	0	+2.7
21	+0.4	+3.2
22	+0.7	+4.6
23	0	+3.8
24	0	+3.6

All band 4 gains except channel 22 stabilized to the initial 20°C values during thermal-vacuum test. Comparison of the initial 20°C values to the subsequent 20°C plateaus show the following:

Channel	Percent Shift into Second 20°C (5 days later)	Percent Shift into Third 20°C (10 days later)
19	0	0
20	-0.4	+0.1
21	+0.4	+0.42
22	+0.3	+0.7
23	+0.3	+0.3
24	+0.1	0

The low temperatures, 5°C and 10°C, seem to have the greatest effect on channels 19, 20, and 21 gains. They tend to spread away from the nominal channels (22, 23) at those temperatures. A 27°C change (32° to 5°C) caused channels 19, 20, and 21 gains to decrease 7 to 10 percent compared to a 4 percent decrease in the nominal channels. At the other temperatures, all the band 4 gains appeared to be stable relative to each other.

The post-thermal-vacuum gain values remained higher than the initial ambient values since it takes several days for the vacuum effect to diminish. Before the final LFPT, the gains returned to their initial ambient values.

10.4.3.2 Gain Versus Temperature (Thermal-Vacuum Test)

To characterize the individual channel gain behavior during thermal-vacuum, gain/temperature plots for each channel were produced; these are given for each channel in Figure 10-14. A linear least square error best fit was performed using the average gains at each temperature plateau. The average gains were taken by collecting all the gain values at a certain temperature and computing the arithmetic mean. The standard deviations from the mean were also computed and are indicated on the plots by a vertical bar through the mean value. These vertical lines represent the spread of the data for all measurements taken during thermal-vacuum testing at that temperature.

ORIGINAL PAGE IS
OF POOR QUALITY

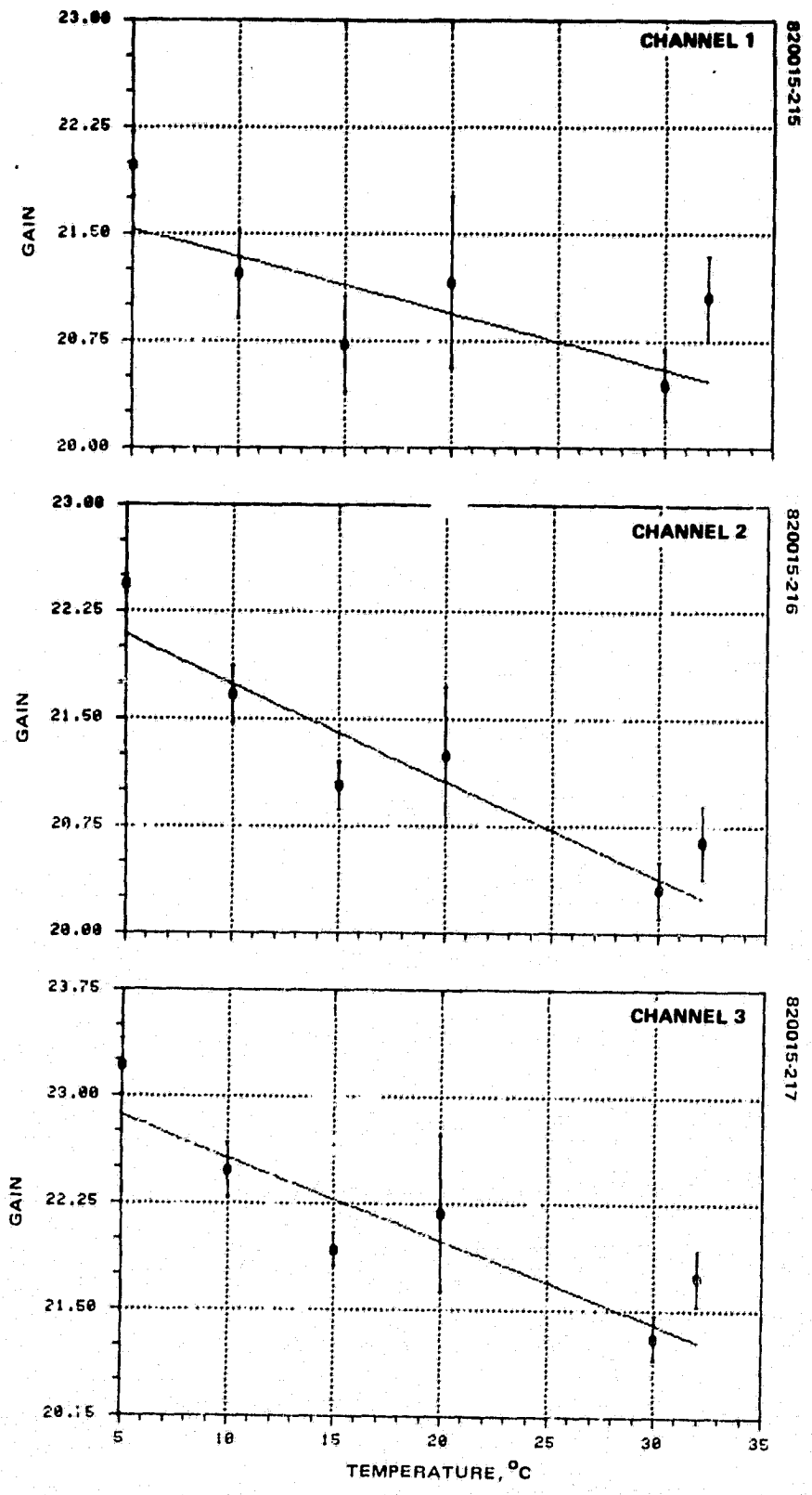

FIGURE 10-14. F-1 AVERAGE GAINS VERSUS TEMPERATURE – LINEAR/LOW GAIN MODE

ORIGINAL PAGE IS
OF POOR QUALITY

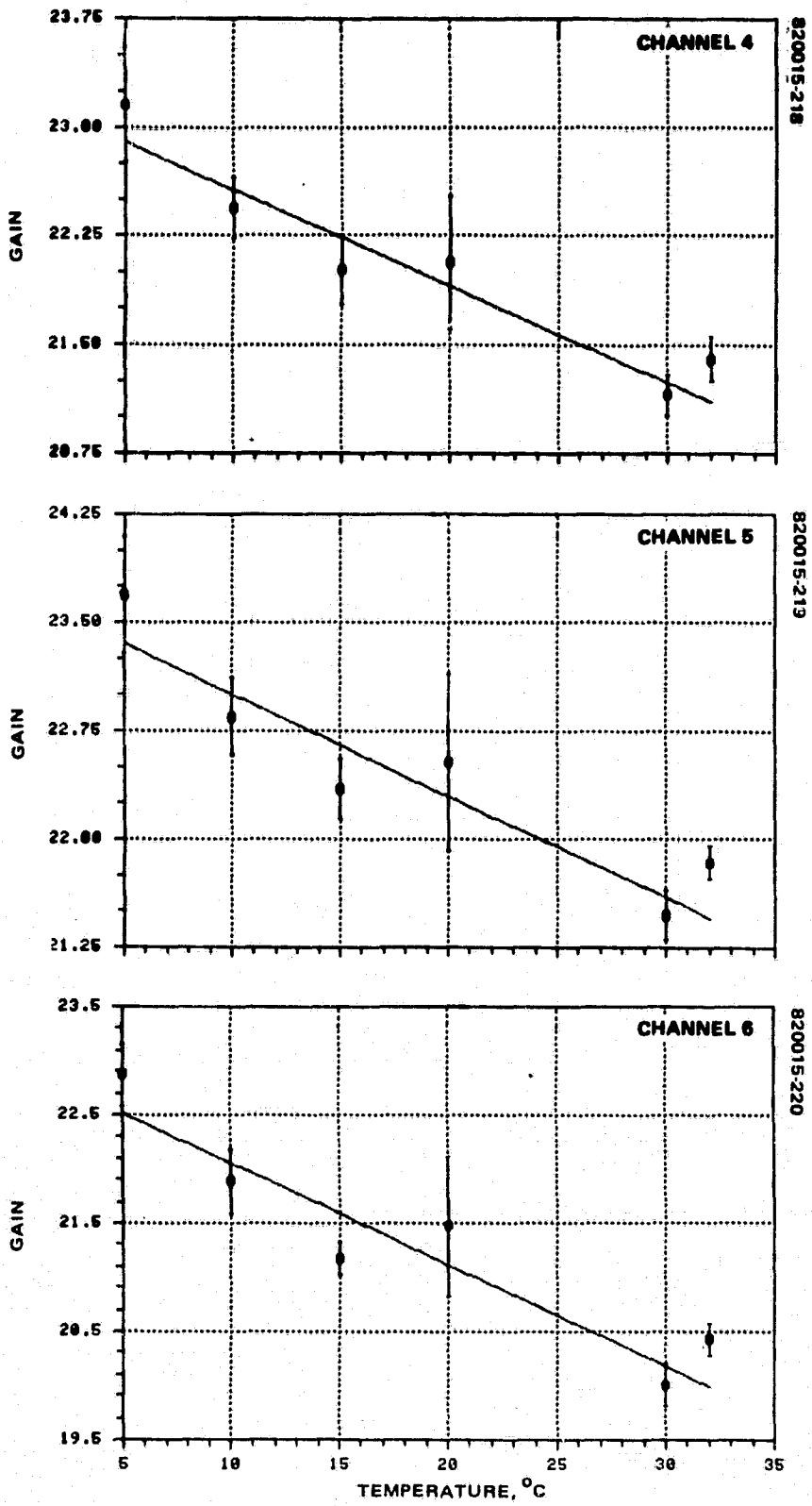

FIGURE 10-14 (CONTINUED). F-1 AVERAGE GAINS VERSUS TEMPERATURE – LINEAR/LOW GAIN MODE

ORIGINAL PAGE IS
OF POOR QUALITY

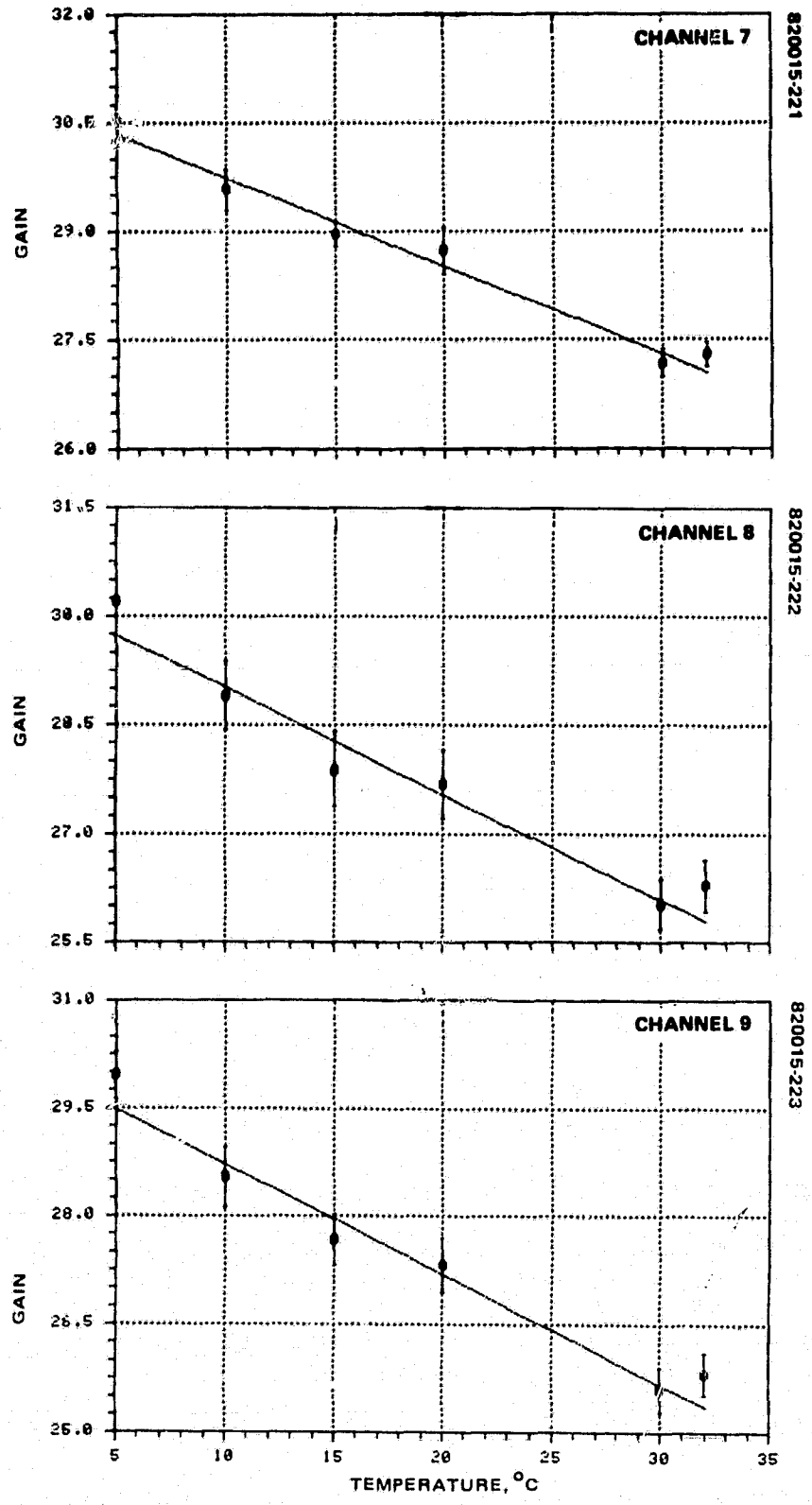

FIGURE 10-14 (CONTINUED). F-1 AVERAGE GAINS VERSUS TEMPERATURE – LINEAR/LOW GAIN MODE

ORIGINAL PAGE IS
OF POOR QUALITY

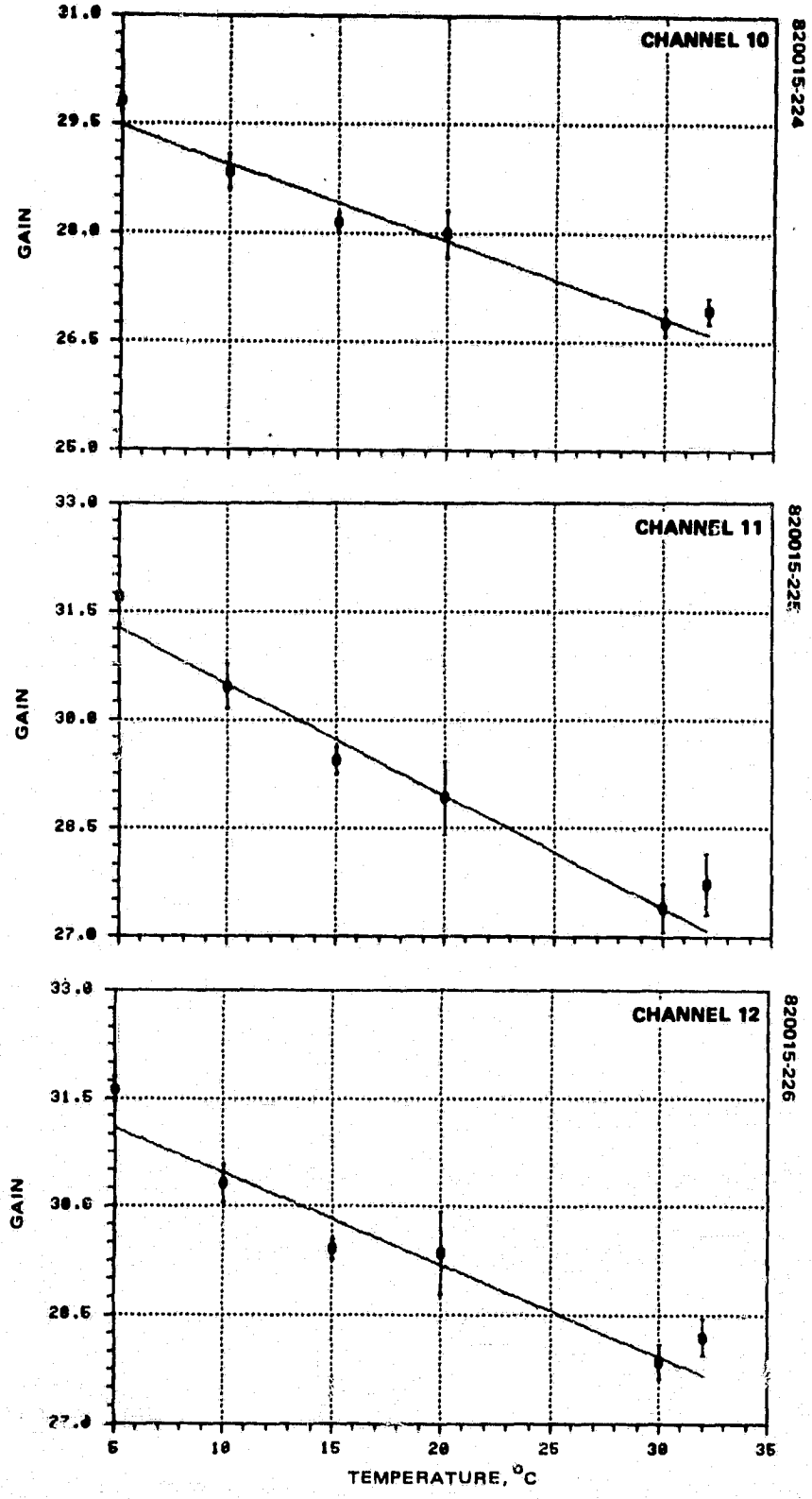

FIGURE 10-14 (CONTINUED). F-1 AVERAGE GAINS VERSUS TEMPERATURE – LINEAR/LOW GAIN MODE

ORIGINAL PAGE IS
OF POOR QUALITY

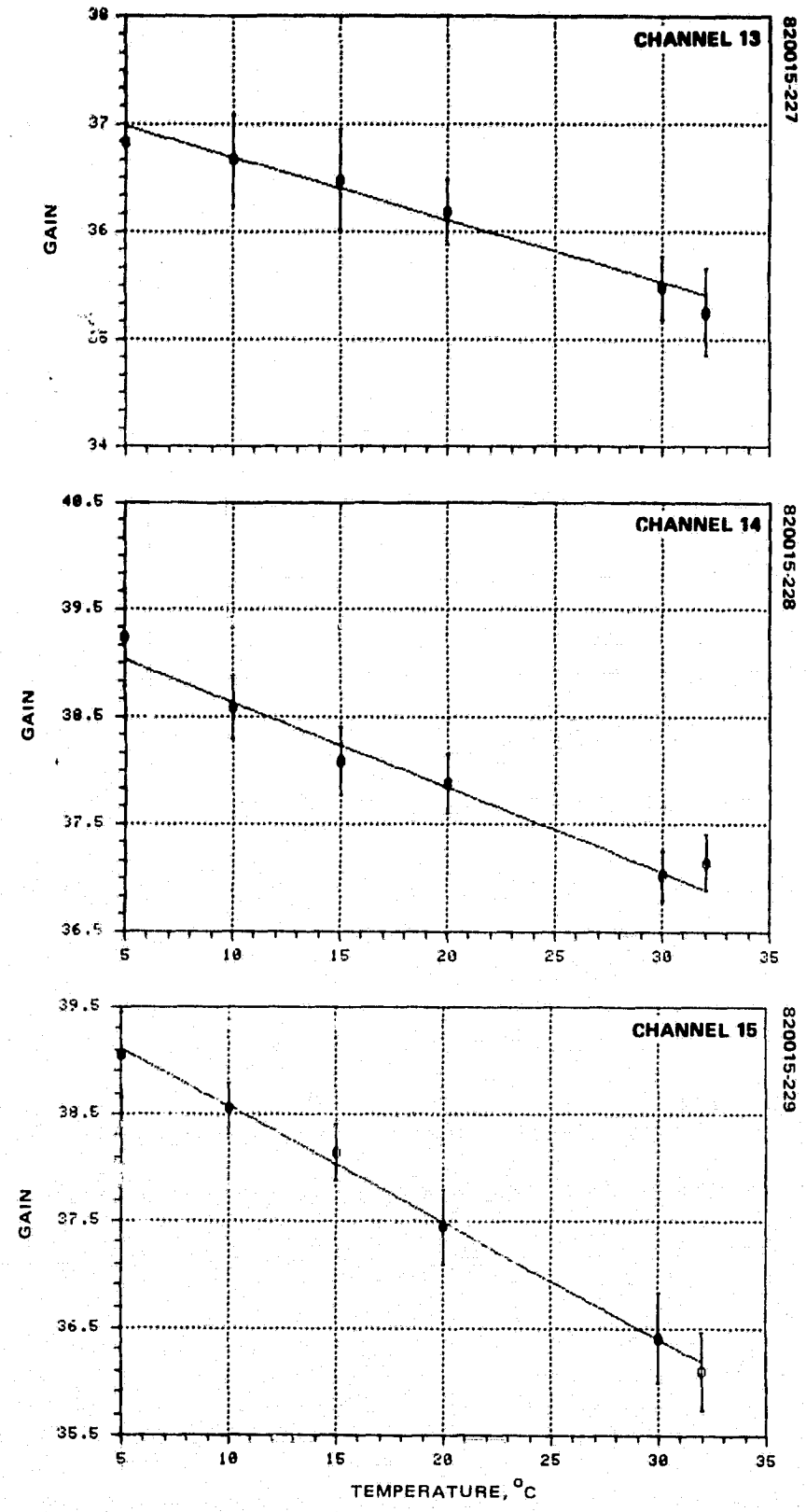

FIGURE 10-14 (CONTINUED). F-1 AVERAGE GAINS VERSUS TEMPERATURE – LINEAR/LOW GAIN MODE

ORIGINAL PAGE IS
OF POOR QUALITY

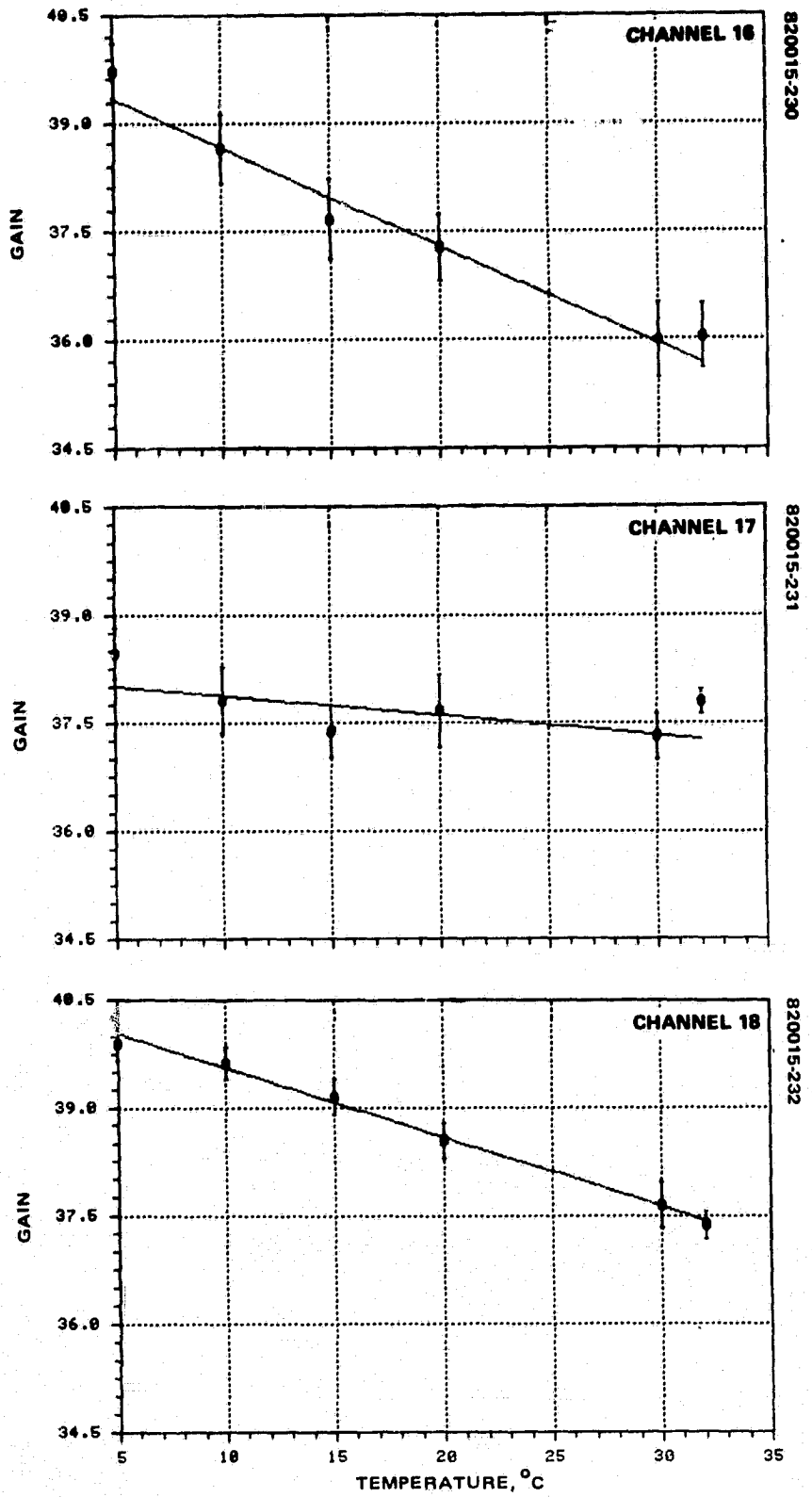

FIGURE 10-14 (CONTINUED). F-1 AVERAGE GAINS VERSUS TEMPERATURE – LINEAR/LOW GAIN MODE

ORIGINAL PAGE IS
OF POOR QUALITY

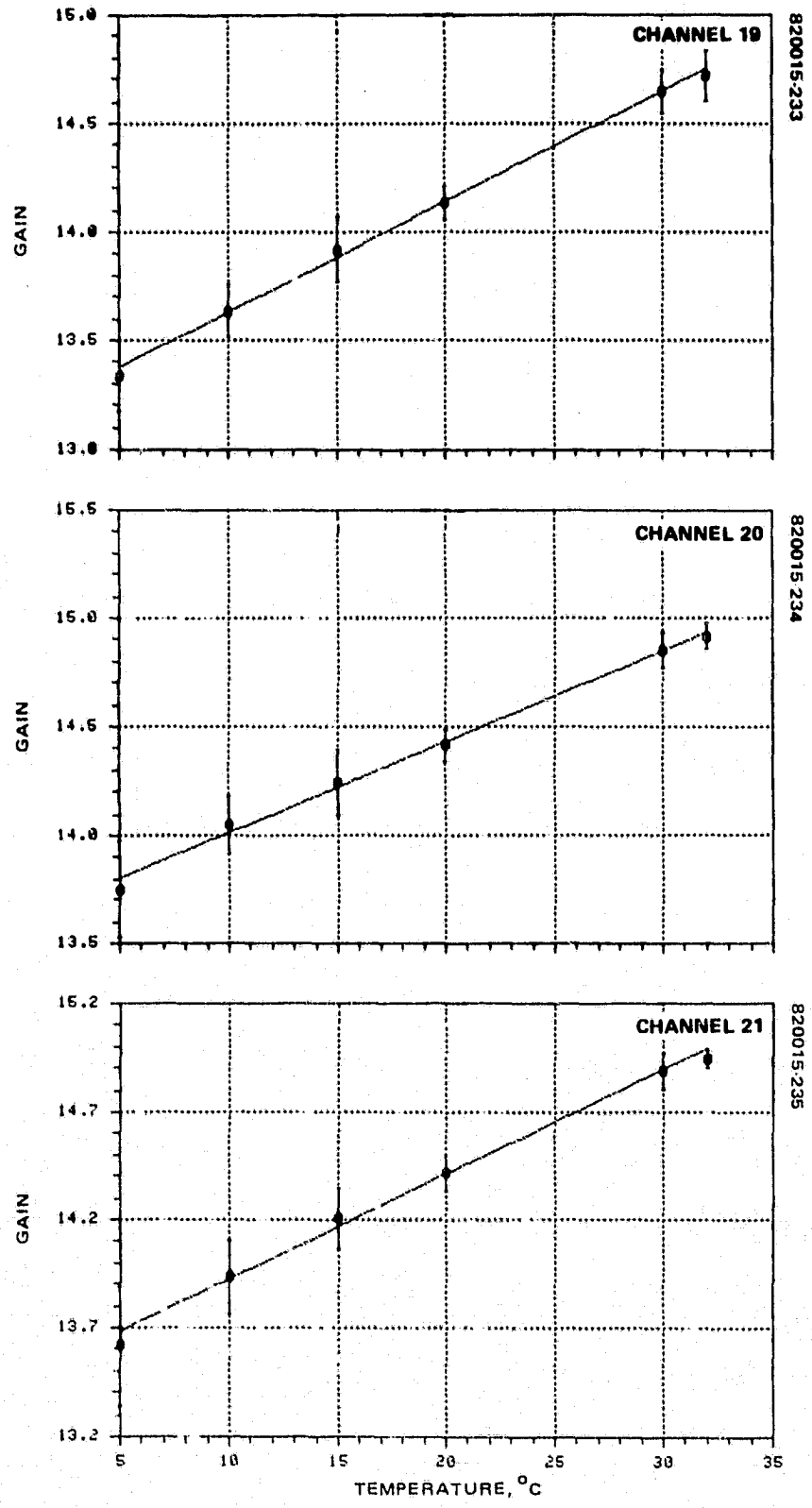

FIGURE 10-14 (CONTINUED). F-1 AVERAGE GAINS VERSUS TEMPERATURE – LINEAR/LOW GAIN MODE

ORIGINAL PAGE IS
OF POOR QUALITY

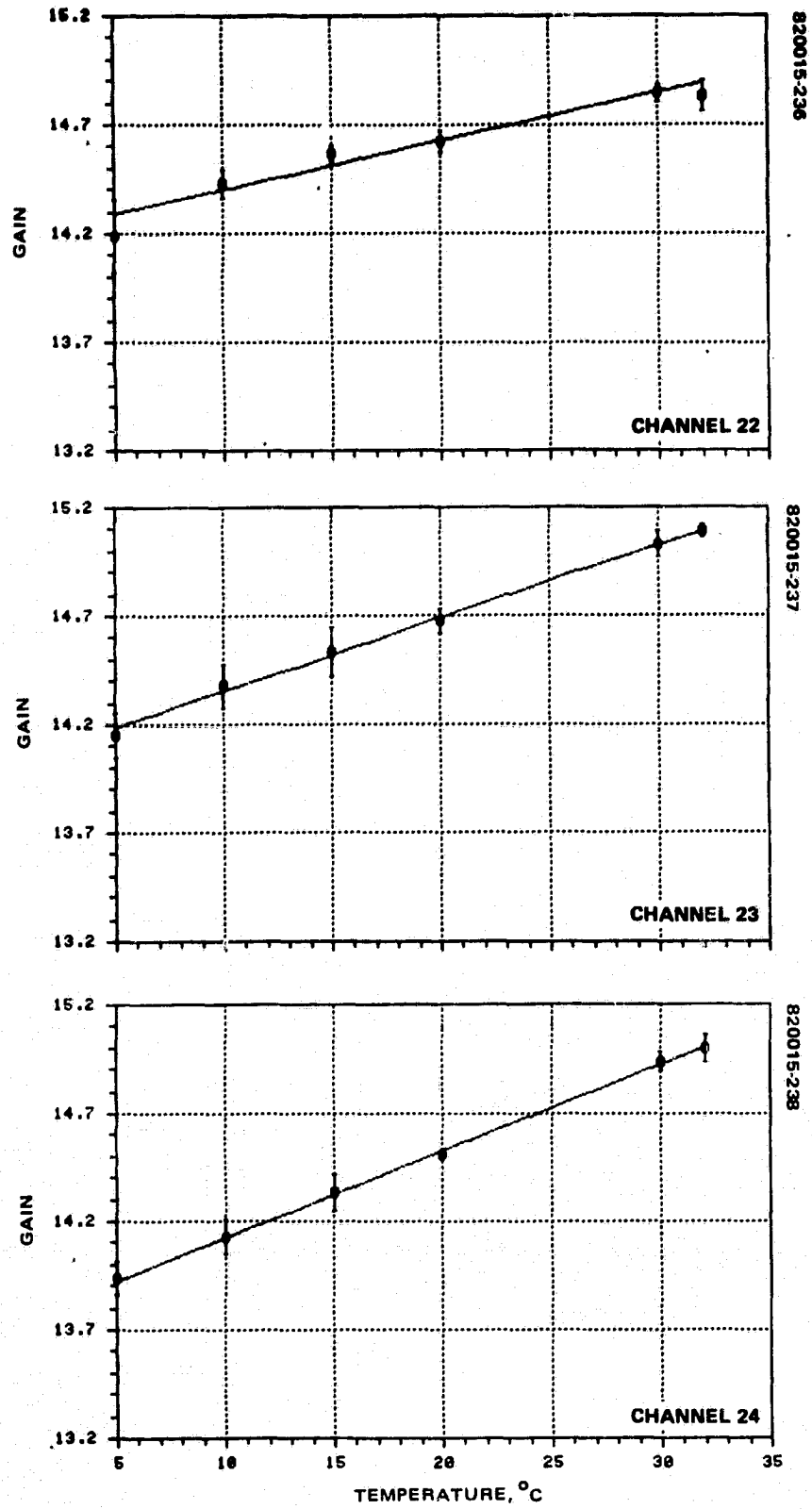

FIGURE 10-14 (CONCLUDED). F-1 AVERAGE GAINS VERSUS TEMPERATURE – LINEAR/LOW GAIN MODE

ORIGINAL PAGE IS
OF POOR QUALITY

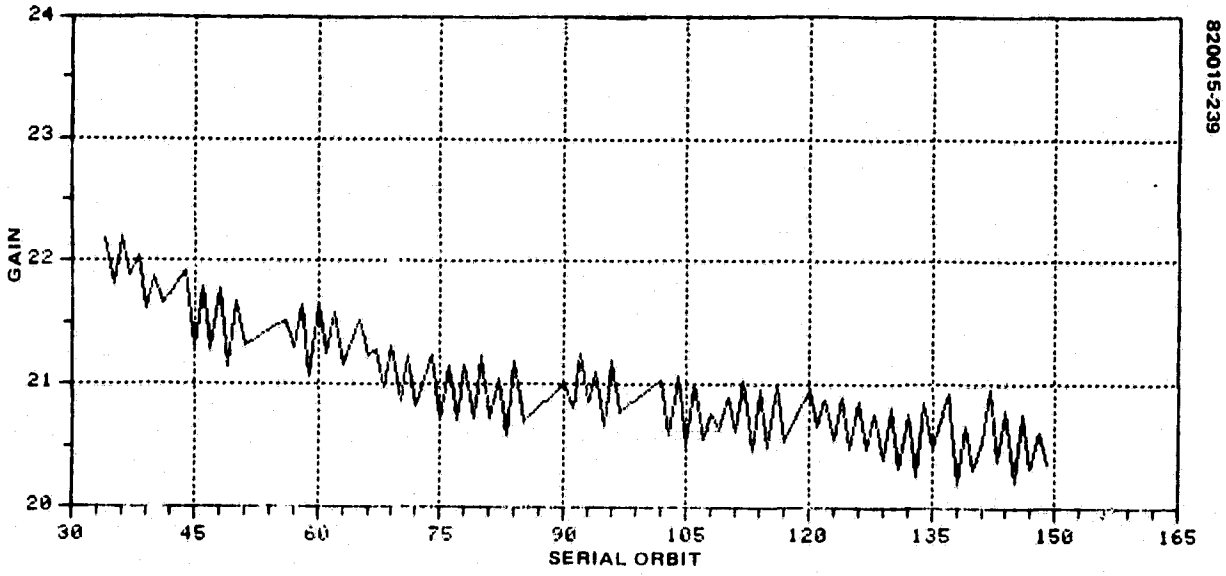

a) CHANNEL 1

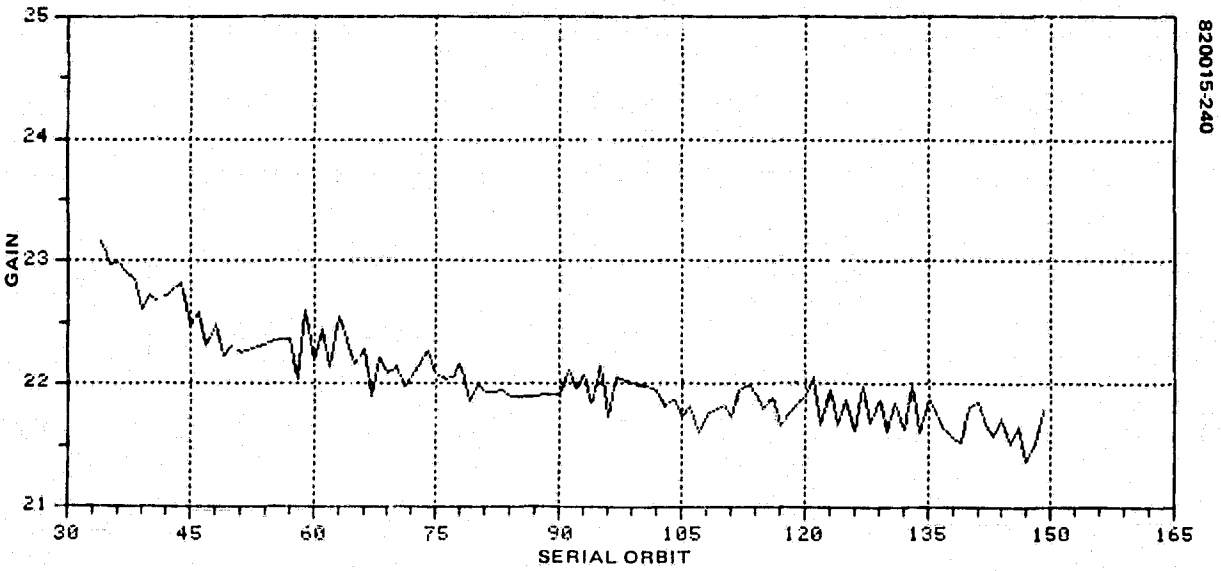

b) CHANNEL 3

FIGURE 10-15. F-1 CHANNEL GAIN WITH TEMPERATURE DEPENDENCE REMOVED -- LINEAR/LOW GAIN MODE

ORIGINAL PAGE IS
OF POOR QUALITY

TABLE 10-8. GAIN CHANGE/°C

Channel	Slope, ΔG/°C	Channel	Slope, ΔG/°C
1	-0.040	13	-0.058
2	-0.068	14	-0.079
3	-0.058	15	-0.109
4	-0.066	16	-0.136
5	-0.071	17	-0.027
6	-0.093	18	-0.097
7	-0.122	19	+0.051
8	-0.146	20	+0.041
9	-0.153	21	+0.048
10	-0.106	22	+0.023
11	-0.155	23	+0.034
12	-0.127	24	+0.040

Table 10-8 is derived from the gain versus temperature plots by extracting the slope of the best fit curve (line; $y = a + b\,x$) through the average gains for each channel.

10.4.3.3 Vacuum Effect on Gain Performance

As indicated above, a long term change in gain was observed throughout thermal-vacuum testing which is not explained by gain versus temperature behavior. To illustrate this change, the channel gain history plots were replotted with the gain temperature dependence removed. Figure 10-15 illustrates the results of that effort for channels 1 and 3. The behavior for these cases is sufficiently well behaved to clearly indicate the exponential-like decay of the gain observed over the entire thermal-vacuum period. It should be noted that although channel 3 is larger in value than channel 1 for the same conditions, the agreement in shape of the curves is excellent. Comparison with other channels in the band (not shown) is very good as well. The other bands show similar comparisons, which further verifies the existence of long time constant gain stabilization component in the data. It indicates that this time constant may be as long as 9 to 10 days.

As a family, the plots for all the channels (not shown) of gain versus orbit number with temperature effects removed was cleaner, better behaved, and more consistently representative of an exponential-like change for F-1 than it was for the proto-flight.

10.4.4 Corrected Signal Level Performance History

The corrected signal level performance for F-1 is presented for all channels in each band in Figure 10-16. In principle, if the calibration system is performing ideally, and if the initial calibrations have been performed perfectly, and if the collimator output is uniform and stable, these plots should be horizontal lines which lie on top of one another; that is, one horizontal line. Clearly from the plots this condition is not realized.

ORIGINAL PAGE IS
OF POOR QUALITY

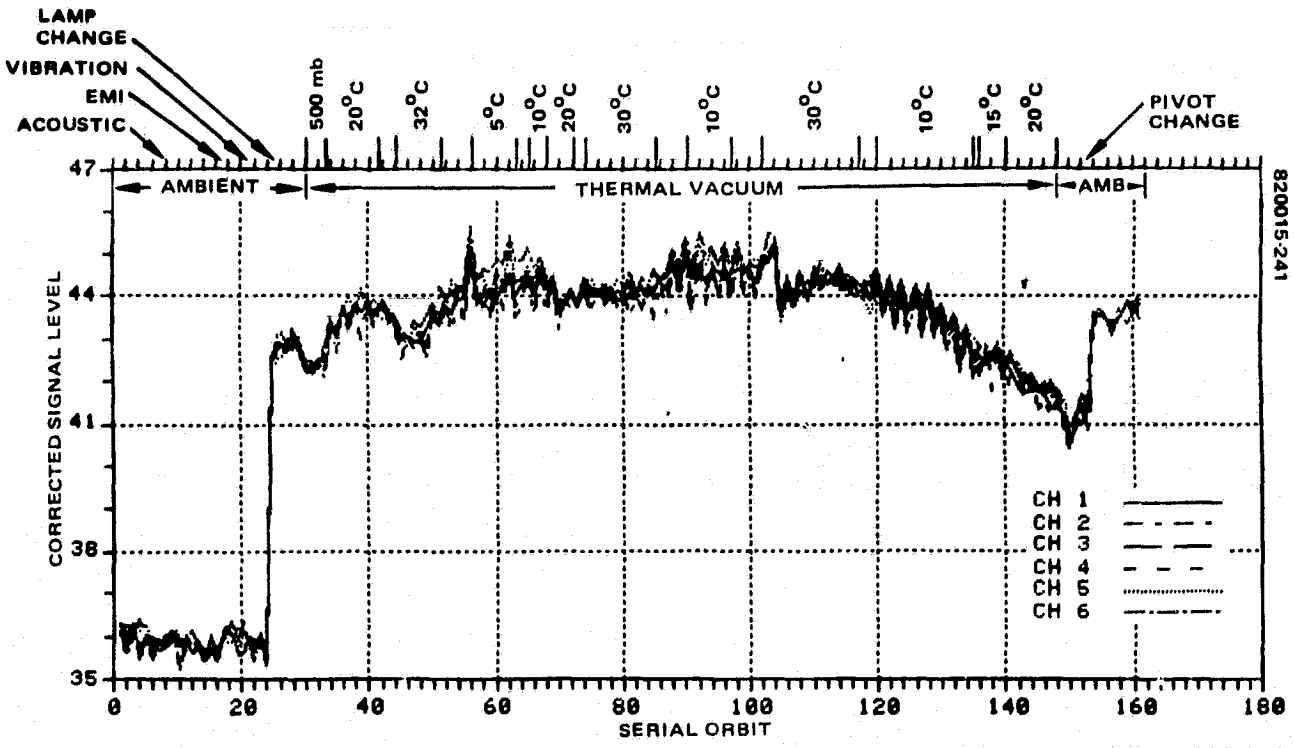

a) BAND 1

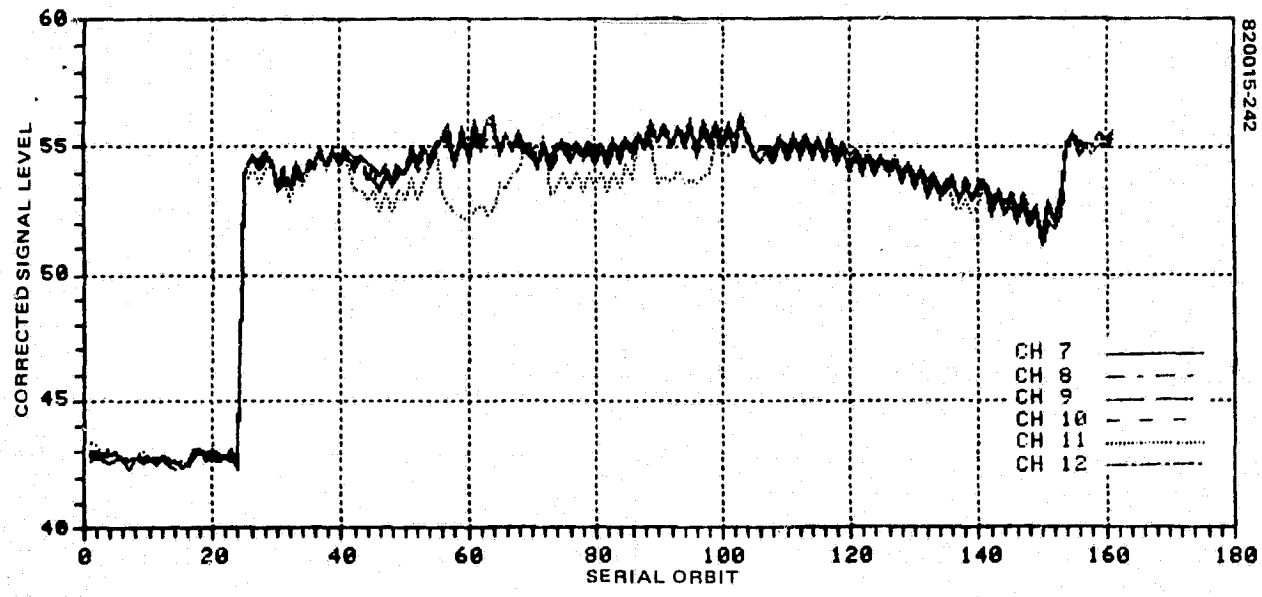

b) BAND 2

FIGURE 10-16. F-1 COSL PERFORMANCE – LINEAR/LOW GAIN MODE

ORIGINAL PAGE IS
OF POOR QUALITY

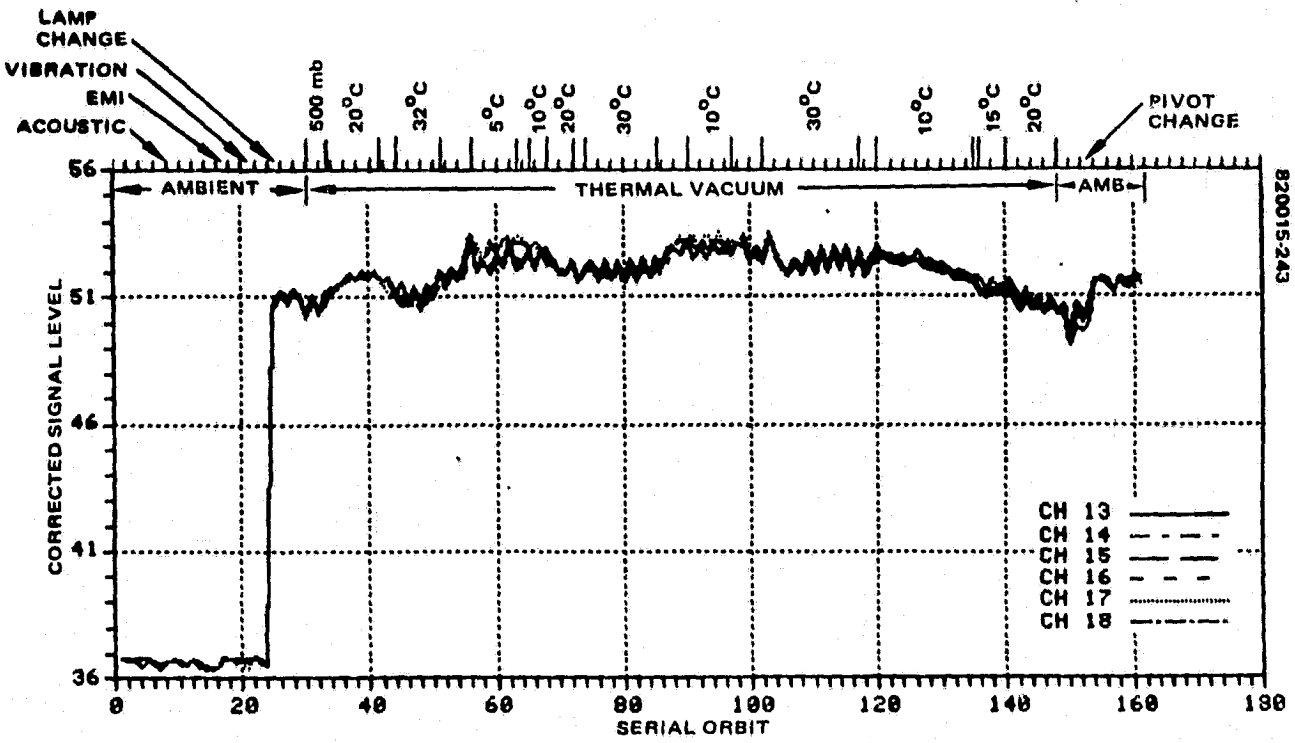

c) BAND 3

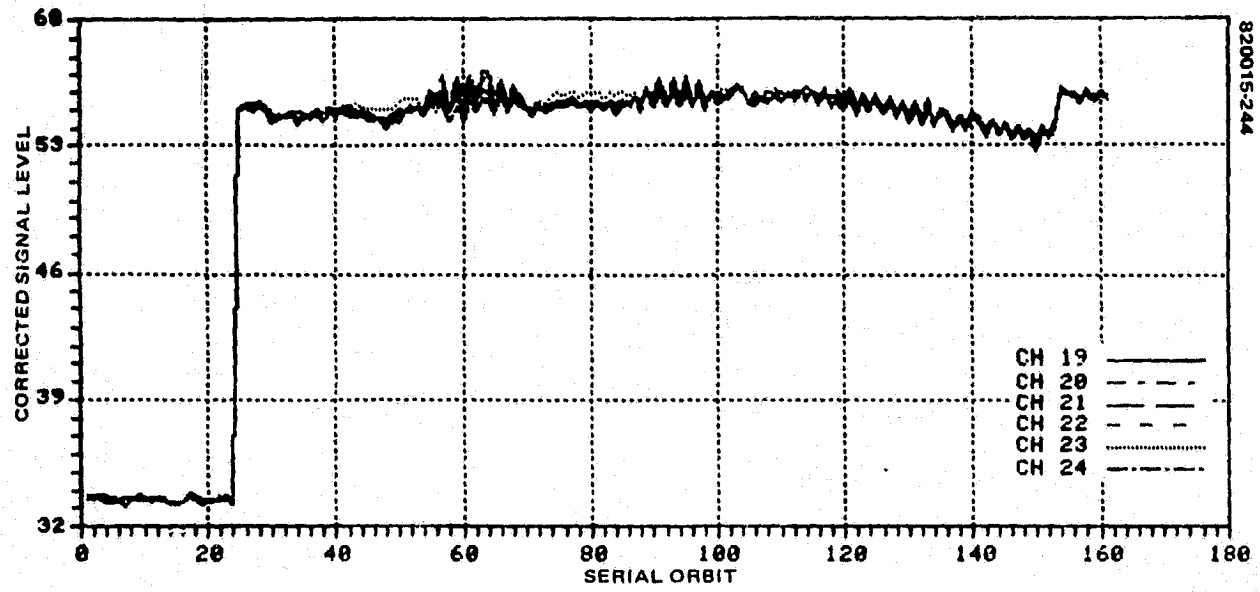

d) BAND 4

FIGURE 10-16 (CONTINUED). F-1 COSL PERFORMANCE – LINEAR/LOW GAIN MODE

More realistically changes will occur in the system which will not be completely sensed and corrected by the internal calibration system. Calibrations of the scanner with the integrating sphere will be subject to errors so that calibration wedge nominals will be approximate, at best. Collimator output will be neither constant nor uniform, and collimator shading will not be stable. Similar comments apply to the internal calibration system. Discovery of the causes of anomalous behavior is complicated by the absence of a suitably accurate, independent, calibrated reference source throughout the entire test period, especially during thermal-vacuum testing.

The features of the COSL performance behavior given in Figure 10-16 that are of principal interest are the following:

1) The width of the envelope of the family of COSL for all the channels in a band. This width (called DCC), the maximum COSL value for all channels in a band at a given environmental condition (serial orbit) minus the minimum COSL value for all channels in that band at the same environmental condition, must have a value less than or equal to 2 percent of the geometric mean value of all of the COSLs for all of the channels in that band during that orbit. Actually, it is the difference in any two COSLs taken as pairs that should have a difference less than 2 percent of the mean COSL for the entire channel. Thus it is possible that problems in COSL performance might exist for channels that are masked by more deviant behavior of some other channel in the band. DCC performance is discussed later in this section.

2) The variation of the mean value of the COSL for all channels in a band, while of lesser importance since it is not directly subject to specification, does give some indication of system test performance relative to DCC. Variations in the mean COSL, which is the systems estimate of collimator radiance will vary with collimator lamp output, of course. Unfortunately it varies also with errors in the gain estimates provided by the internal calibration system. These errors may be due to a faulty or not sufficiently accurate initial calibration using the integrating sphere or the result of instabilities or environmentally induced changes in the calibration system.

The band geometric means are used directly in determining the band-to-band radiometric accuracy (DBB) which is specified to have less than 3 percent deviation relative to its deviation at integrating sphere calibration (see 6.4.2). This performance parameter is discussed at the end of this section.

The change-out of the collimator light source prior to initiating thermal-vacuum testing (between serial orbits 24 and 25) extended the range of these history plots to a degree that only those channels which exhibit severely anomalous behavior (such as channel 11) can be identified. We shall therefore utilize a limited selection of on-line plots to illustrate the MSS-D F-1 COSL performance history.

<u>COSL Ambient Performance</u> (Figure 10-17)

A typical COSL plot (ambient) of Band 1 is shown in Figure 10-17a. It is obvious that the individual channels do not behave in the same way since there is a general spreading of the corrected signal levels.

Band 2 (Figure 10-17b), channels 7 and 11 show occasional deviations from the nominal values. This is the typical band 2 behavior in ambient condition.

SEQ	31	32	33	34	35	36	37	38	39	40	41	42	45	46
STND	27	28	27	28	1	2	3	4	5	6	7	8	1	2
DS	1	1	1	1	1	1	1	1	1	1	1	1	1	1
DATE	07/30	07/30	07/30	07/31	07/31	07/31	07/31	07/31	07/31	07/31	07/31	07/31	08/05	08/05
TIME	9 36	11 21	23 3	6	10 29	12 39	14 6	15 38	17 41	19 9	21 37	23 5	14 9	15 51
TEMP	23.3	24.4	25.5	24.6	23.5	23.0	24.4	24.4	24.6	25.2	24.1	25.2	23 0	23.5

820016-245

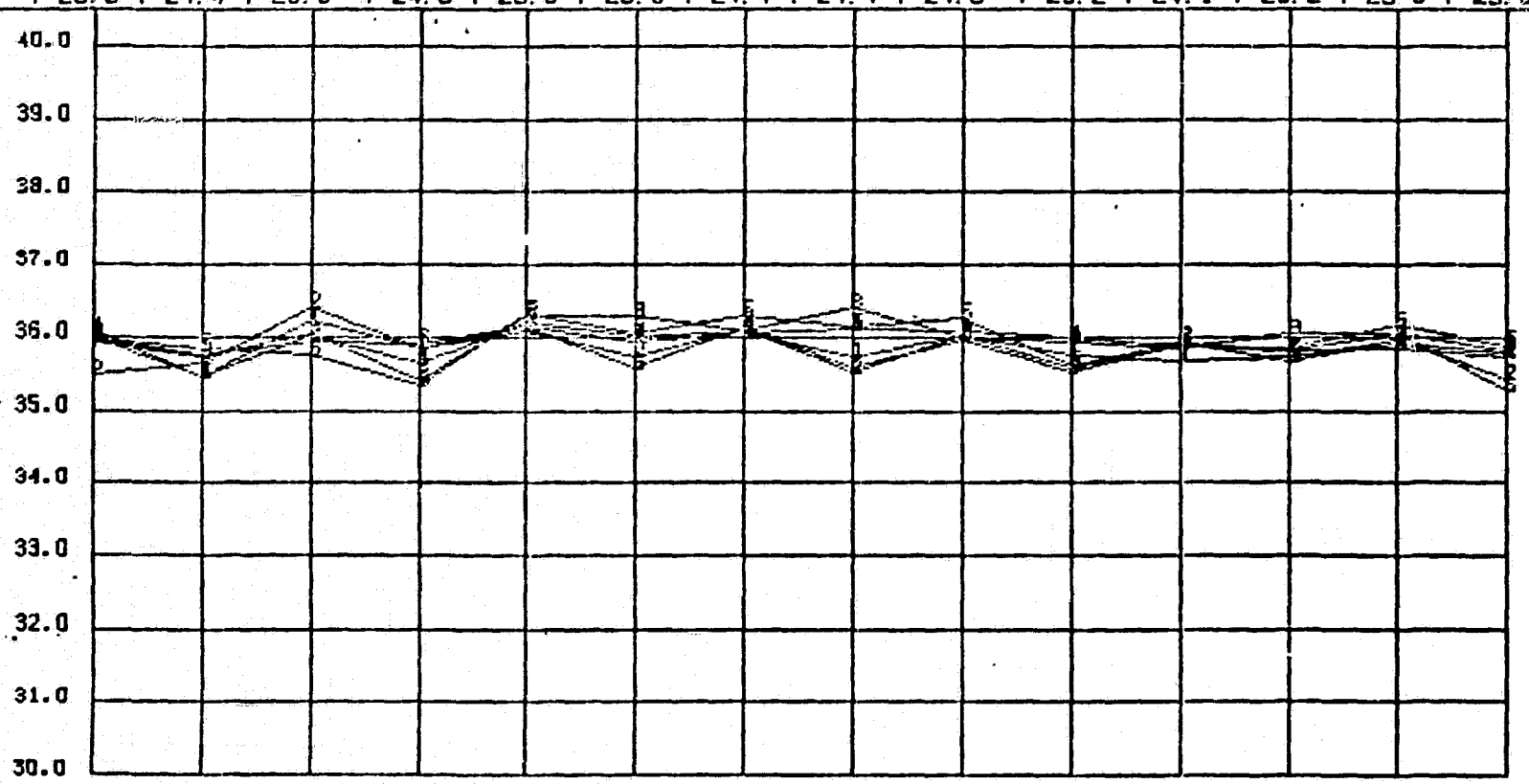

a) BAND 1

FIGURE 10-17. F-1 COSL PERFORMANCE IN AMBIENT

ORIGINAL PAGE IS OF POOR QUALITY

SEQ	31	32	33	34	35	36	37	38	39	40	41	42	45	46
STND	27	28	27	28	1	2	3	4	5	6	7	8	1	2
DS	1	1	1	1	1	1	1	1	1	1	1	1	1	1
DATE	07/30	07/30	07/30	07/31	07/31	07/31	07/31	07/31	07/31	07/31	07/31	07/31	08/05	08/05
TIME	9 36	11 21	23 3	6	10 29	12 39	14 6	15 38	17 41	19 9	21 37	23 5	14 9	15 51
TEMP	23.3	24.4	25.5	24.6	23 5	23.0	24.4	24.4	24 6	25.2	24.1	25.2	23.0	23.5

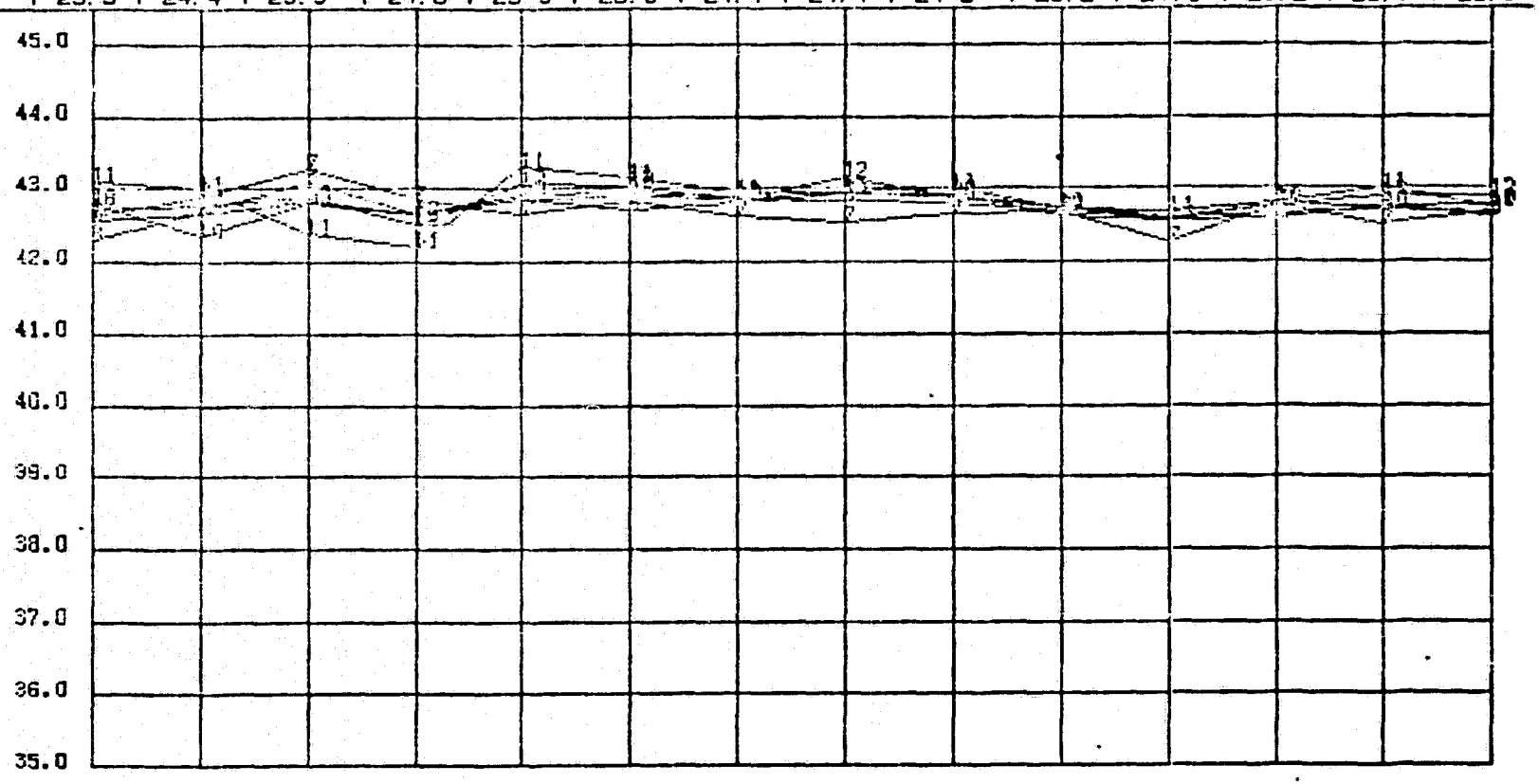

b) BAND 2

FIGURE 10-17 (CONTINUED). F-1 COSL PERFORMANCE IN AMBIENT

820015-246

ORIGINAL PAGE IS OF POOR QUALITY

SEQ	31	32	33	34	35	36	37	38	39	40	41	42	45	46
STND	27	28	27	28	1	2	3	4	5	6	7	8	1	2
DS	1	1	1	1	1	1	1	1	1	1	1	1	1	1
DATE	07/30	07/30	07/30	07/31	07/31	07/31	07/31	07/31	07/31	07/31	07/31	07/31	08/05	08/05
TIME	9 36	11 21	23 3	6	10 29	12 39	14 6	15 38	17 41	19 9	21 37	23 5	14 9	15 51
TEMP	23.3	24.4	25.5	24.6	23.5	23.0	24.4	24.4	24.6	25.2	24.1	25.2	23.0	23.5

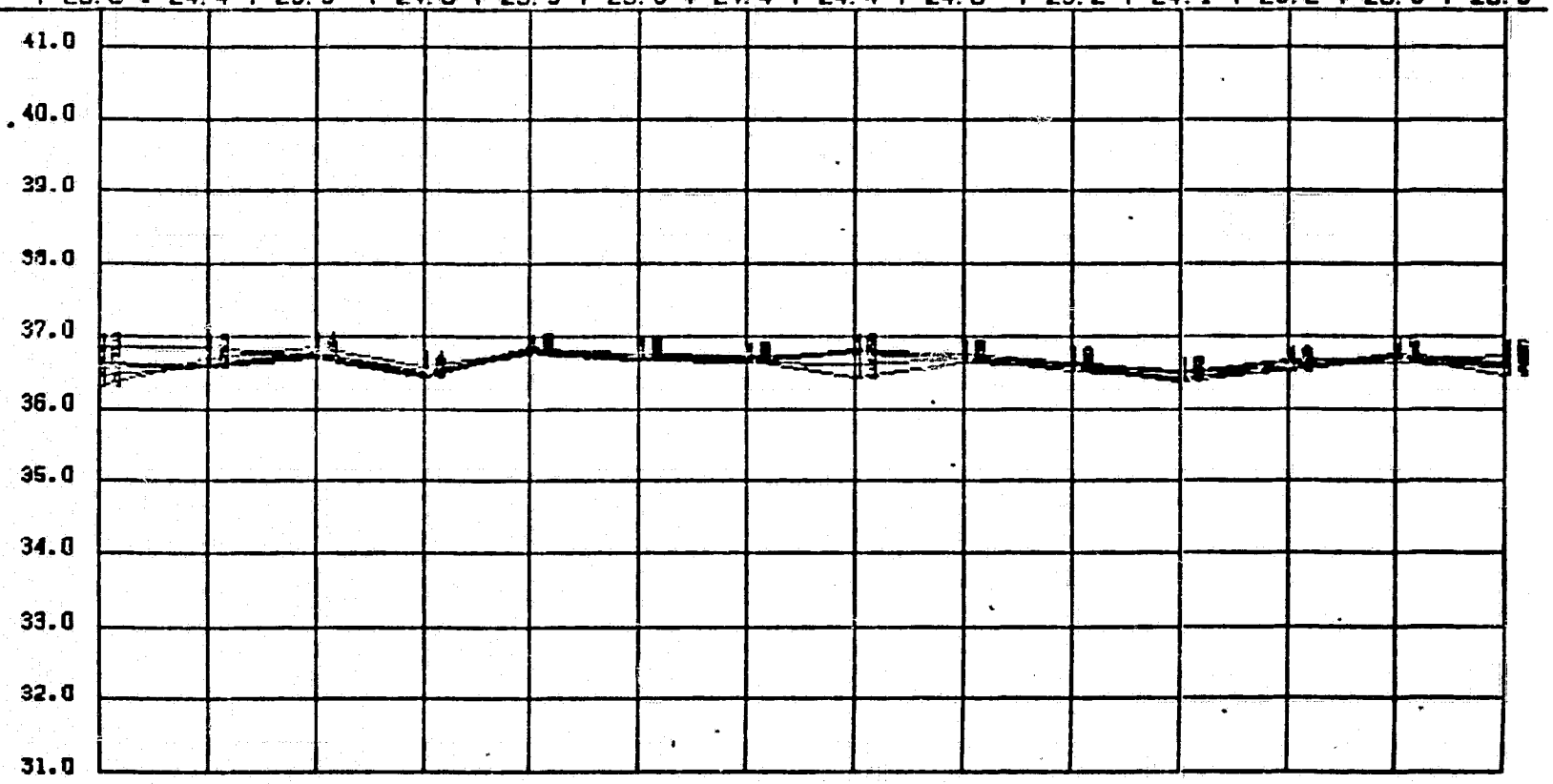

c) BAND 3

FIGURE 10-17 (CONTINUED). F-1 COSL PERFORMANCE IN AMBIENT

820015-247

ORIGINAL PAGE IS OF POOR QUALITY

SEQ	31	32	33	34	35	36	37	38	39	40	41	42	45	46
STND	27	28	27	28	1	2	3	4	5	6	7	8	1	2
DS	1	1	1	1	1	1	1	1	1	1	1	1	1	1
DATE	07/30	07/30	07/30	07/31	07/31	07/31	07/31	07/31	07/31	07/31	07/31	07/31	08/05	08/05
TIME	9 36	11 21	23 3	6	10 29	12 39	14 6	15 38	17 41	19 9	21 37	23 5	14 9	15 51
TEMP	23.3	24.4	25.5	24.6	23.5	23.0	24.4	24.4	24.6	25.2	24.1	25.2	23.0	23.5

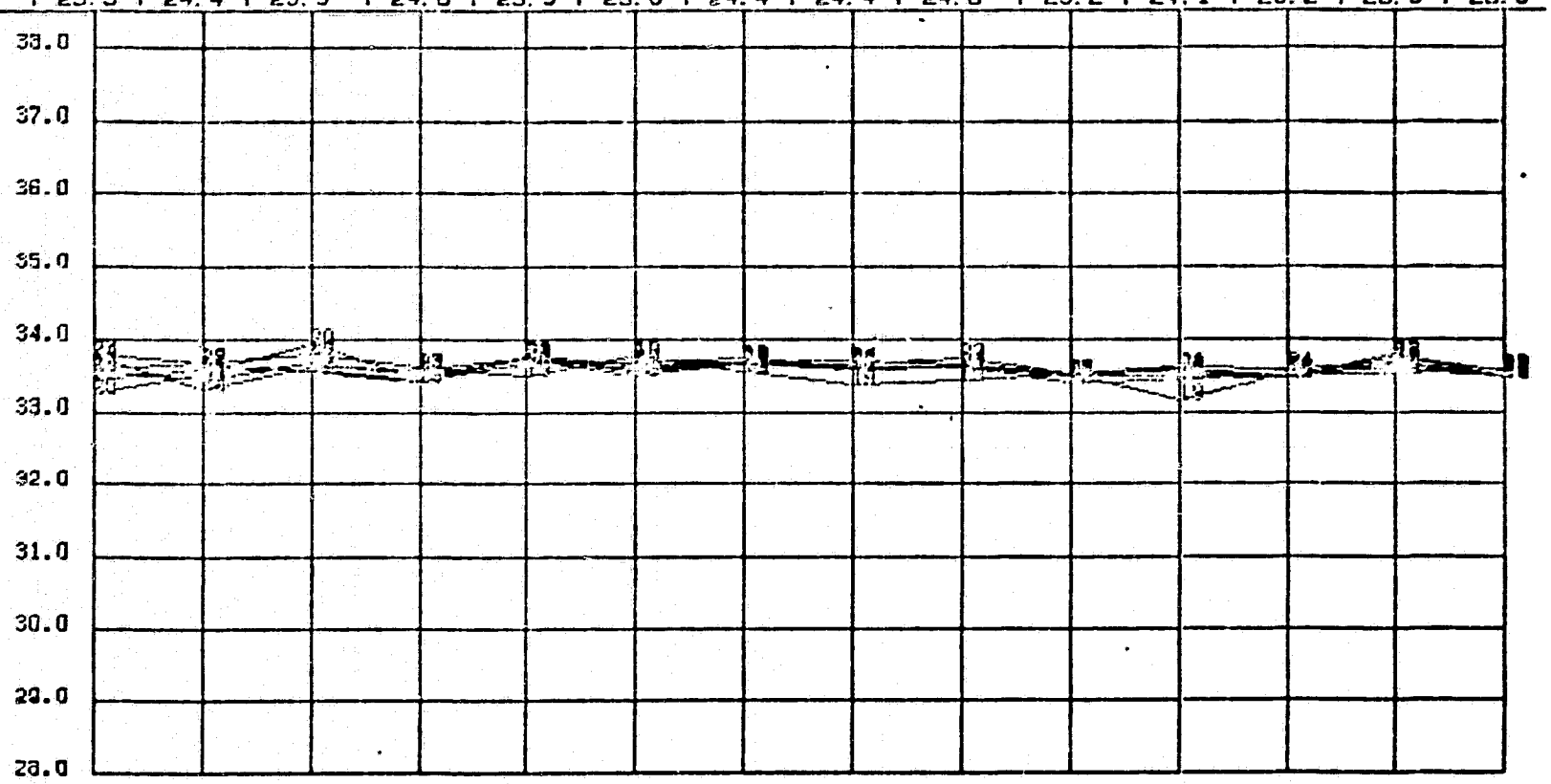

d) BAND 4

FIGURE 10-17 (CONCLUDED). F-1 COSL PERFORMANCE IN AMBIENT

820015-248

ORIGINAL PAGE IS OF POOR QUALITY

Band 3 COSL (Figure 10-17c) behavior is superior to the other bands. The individual channels show a more uniform characteristic in ambient conditions.

Band 4 also shows well-behaved corrected signal levels (Figure 10-17d) in spite of a slight deviation of channel 19 from the nominal values in some orbits.

COSL Thermal-Vacuum Performance (Figure 10-18)

Band 1. In thermal-vacuum, the general spreading of the corrected signal levels became worse, especially at the low temperatures (5° and 10°, Figure 10-18a, orbits 120 to 132). At the other temperature plateaus, the spread of the corrected signal levels is about the same as in ambient conditions.

Band 2. At the extreme temperature (30°, 32°, 5°, and 10°C; Figure 10-18b) channel 11 showed very significant deviation from the other channels. The low temperature (5° and 10°C) have greater effect on channels 11 than the other extreme temperatures (30° and 32°C). The rest of the channels also showed some temperature dependence but not to the same extent as channel 11 does.

Band 3. At 5°C channels (Figure 10-18c, orbits 120 to 128), channels 17 and 18 corrected signal levels, particularly system B, become deviant. The same channels also show slight deviation from the nominal at the 10°C plateau. Other than that, band 3 COSL behavior is consistently normal during thermal-vacuum testing.

Band 4. Greater spreading of the corrected signals occurred at the 5° and 10°C plateaus (Figure 10-18d, orbit 120 to 132) mainly because of the higher sensitivity of channels 21 and 22 (mostly system B) to low temperature. High temperatures (32° and 30°C, Figures 10-18 orbits 113 to 116 and orbits 138 to 140) affect channel 23.

10.4.4.1 Band Average COSL Performance

The history of the band average of the COSLs for all channels in each band is plotted in Figure 10-19. Each band is represented by two plots, one each for data taken when the scanner was in mode A or B, respectively. (See Section 6 for a description of the various scanner modes.)

Plotted above and below the band average COSL are the maximum and minimum COSLs respectively, for all the channels in the band. As is evident in these plots, the envelope width exceeds 2 percent of the band average at a number of test orbits. These DCC specification violations will be discussed later from more illuminating plots where the errant channels are identified. Here band average COSL is emphasized and the envelope behavior provides some insight into the effect of individual channel deviations on the overall average. That is, some pulling of the average results from large deviant behavior of individual channels.

The large difference in band average COSL for prethermal-vacuum orbits (prior to serial orbit 24) from the thermal-vacuum COSL is due to collimator lamp changeout. The range of values which resulted precluded their use in these plots in order that some resolution could be preserved. It should be noted that mode A COSL behavior is generally better than mode B relative to DCC as evidenced by the consistently narrower envelope.

SEQ	113	114	115	116	117	118	119	120	121	122	123	124	125	126
STND	6	7	8	1	2	7	8	1	2	3	4	5	6	7
DS	1	1	1.	1	1	1	1	1	1	1	1	1	1	1
DATE	09/12	09/12	09/12	09/12	09/12	09/13	09/13	09/13	09/13	09/13	09/13	09/13	09/13	09/13
TIME	15	16 24	17 49	21	22 26	1	1 53	6 40	8 18	9 42	12	14 4	15 55	17 10
TEMP	31.9	31.6	32.6	29.9	26.6	19.9	11.6	5.6	6.1	6.5	4.8	4.6	4.6	4.8

820015-249

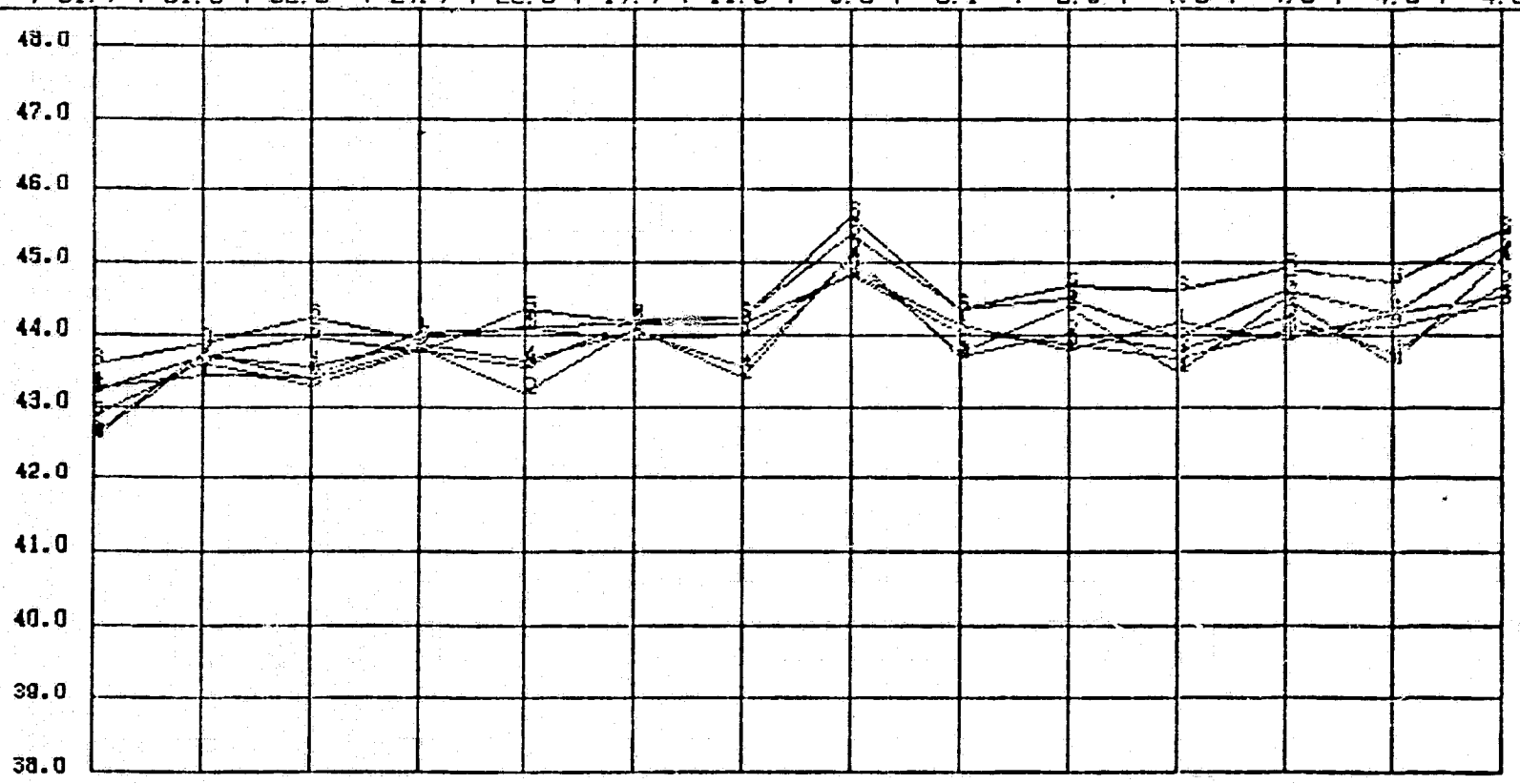

a) BAND 1

FIGURE 10-18. F-1 COSL PERFORMANCE IN THERMAL-VACUUM

ORIGINAL PAGE IS OF POOR QUALITY

SEQ	127	128	129	130	131	132	133	134	135	136	137	138	139	140
STND	8	4	1	2	7	8	1	2	7	8	3	1	2	7
DS	1	1	1	1	1	1	1	1	1	1	1	1	1	1
DATE	09/13	09/13	09/13	09/14	09/14	09/14	09/14	09/14	09/14	09/14	09/14	09/14	09/14	09/14
TIME	19 41	20 53	22 56	21	1 45	3 16	7 34	9 24	11 3	12 54	16 3	18 12	19 36	21 10
TEMP	3.9	5 0	10.4	9.5	11.1	10.4	19.9	20.2	20.2	20.4	27.5	29.3	30.6	30.9

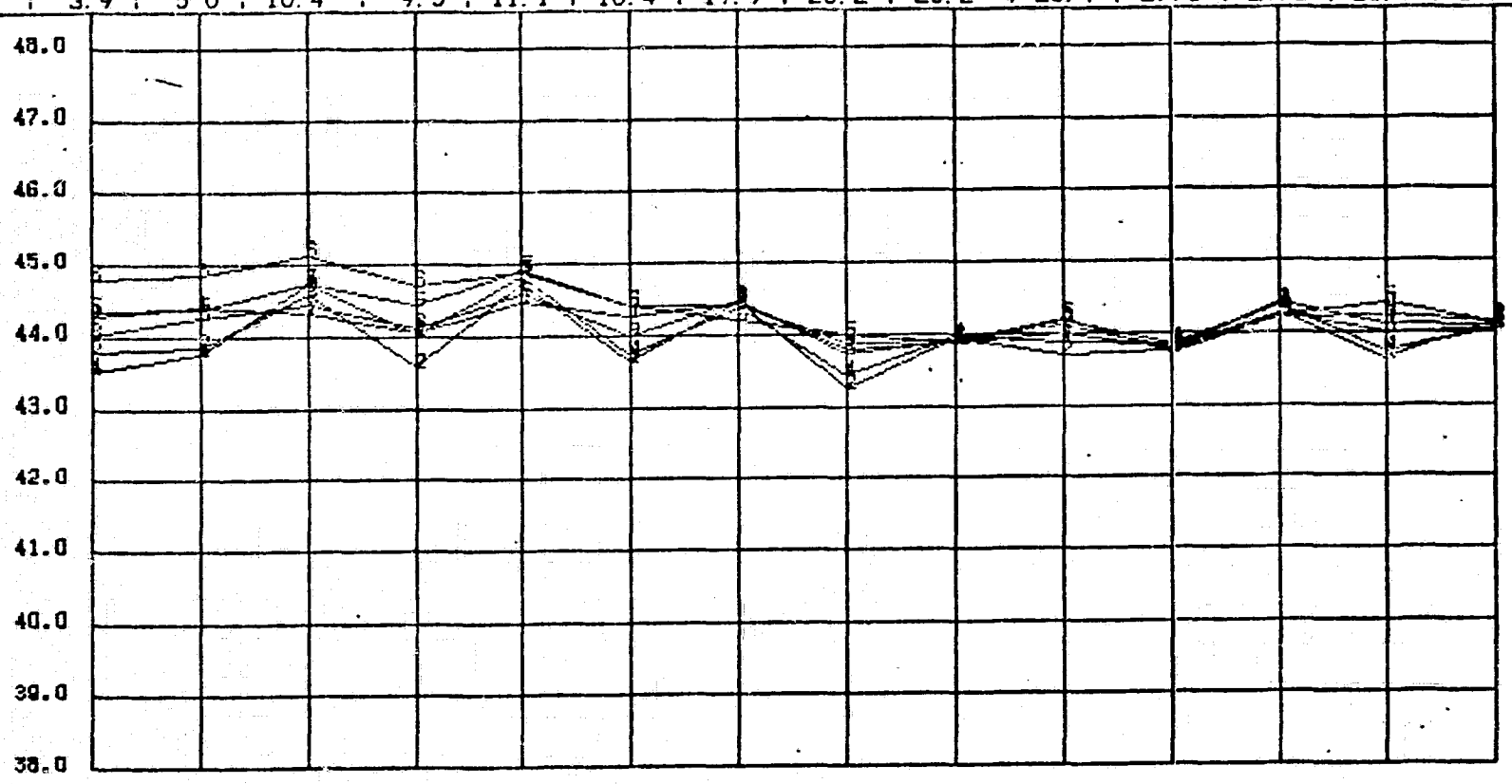

a) BAND 1 CONTINUED

FIGURE 10-18 (CONTINUED). F-1 COSL PERFORMANCE IN THERMAL-VACUUM

820016-250

ORIGINAL PAGE IS OF POOR QUALITY

SEQ	99	100	101	102	103	104	105	106	107	108	109	110	111	112
STND	2	3	4	5	6	7	8	1	2	1	2	3	4	5
DS	1	1	1	1	1	1	1	1	1	1	1	1	1	1
DATE	09/11	09/11	09/11	09/11	09/11	09/11	09/11	09/12	09/12	09/12	09/12	09/12	09/12	09/12
TIME	14 45	15 59	17 10	19 40	20 4	21 36	23 6	1 15	3 2	6 26	8 16	10 16	11 22	13 23
TEMP	21.2	21.2	22.2	21.4	21.4	21.2	21.4	24.6	31.6	31.6	32.9	32.9	32.2	32.2

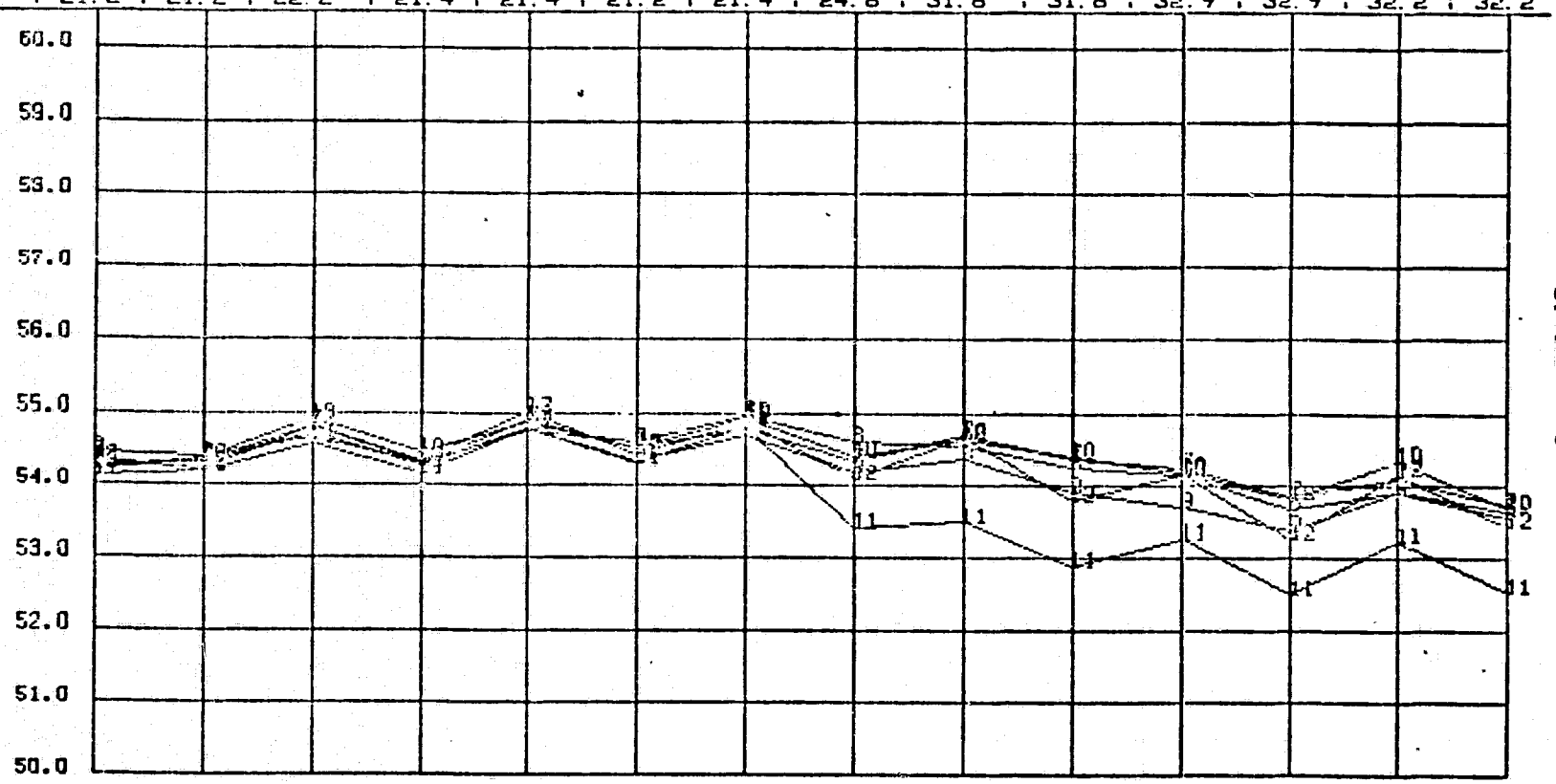

b) BAND 2

FIGURE 10-18 (CONTINUED). F-1 COSL PERFORMANCE IN THERMAL-VACUUM

820015-251

ORIGINAL PAGE IS OF POOR QUALITY

SEQ	113	114	115	116	117	118	119	120	121	122	123	124	125	126
STND	6	7	8	1	2	7	8	1	2	3	4	5	6	7
DS	1	1	1	1	1	1	1	1	1	1	1	1	1	1
DATE	09/12	09/12	09/12	09/12	09/12	09/13	09/13	09/13	09/13	09/13	09/13	09/13	09/13	09/13
TIME	15	16 24	17 49	21	22 26	1	1 53	6 40	8 18	9 42	12	14 4	15 53	17 10
TEMP	31.9	31.6	32.6	29.9	26.6	19.9	11.6	5.6	6.1	6.5	4.8	4.6	4.6	4.8

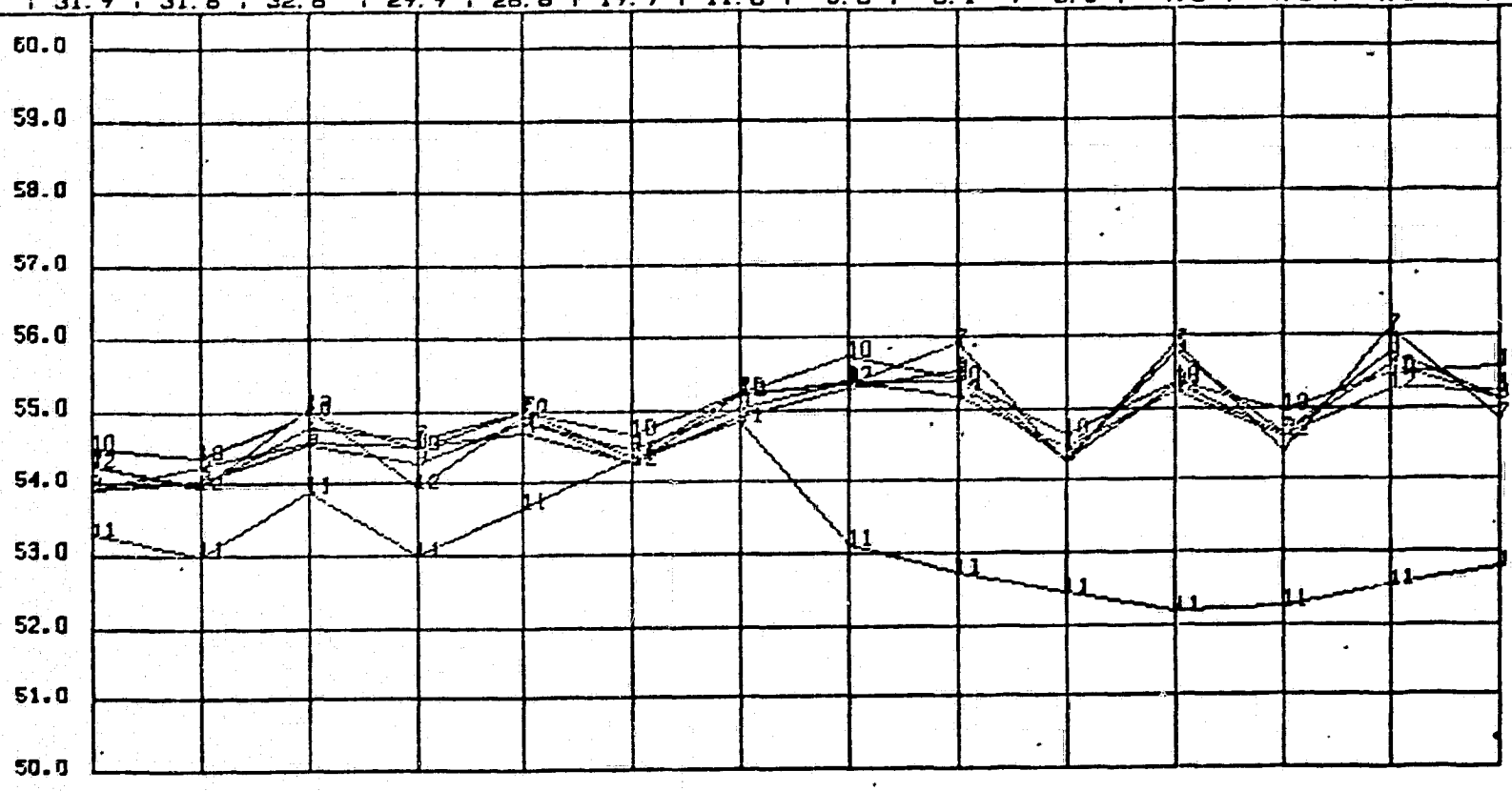

b) BAND 2 CONTINUED

FIGURE 10-18 (CONTINUED). F-1 COSL PERFORMANCE IN THERMAL-VACUUM

820015-252

ORIGINAL PAGE IS OF POOR QUALITY

SEQ	127	128	129	130	131	132	133	134	135	136	137	138	139	140
STND	8	4	1	2	7	8	1	2	7	8	3	1	2	7
DS	1	1	1	1	1	1	1	1	1	1	1	1	1	1
DATE	09/13	09/13	09/13	09/14	09/14	09/14	09/14	09/14	09/14	09/14	09/14	09/14	09/14	09/14
TIME	19 41	20 53	22 56	21	1 45	3 16	7 34	9 24	11 3	12 54	16 3	18 12	19 36	21 10
TEMP	3.9	5.0	10.4	9.5	11.1	10.4	19.9	20.2	20.2	20.4	27.5	29.3	30.6	30.9

820015-253

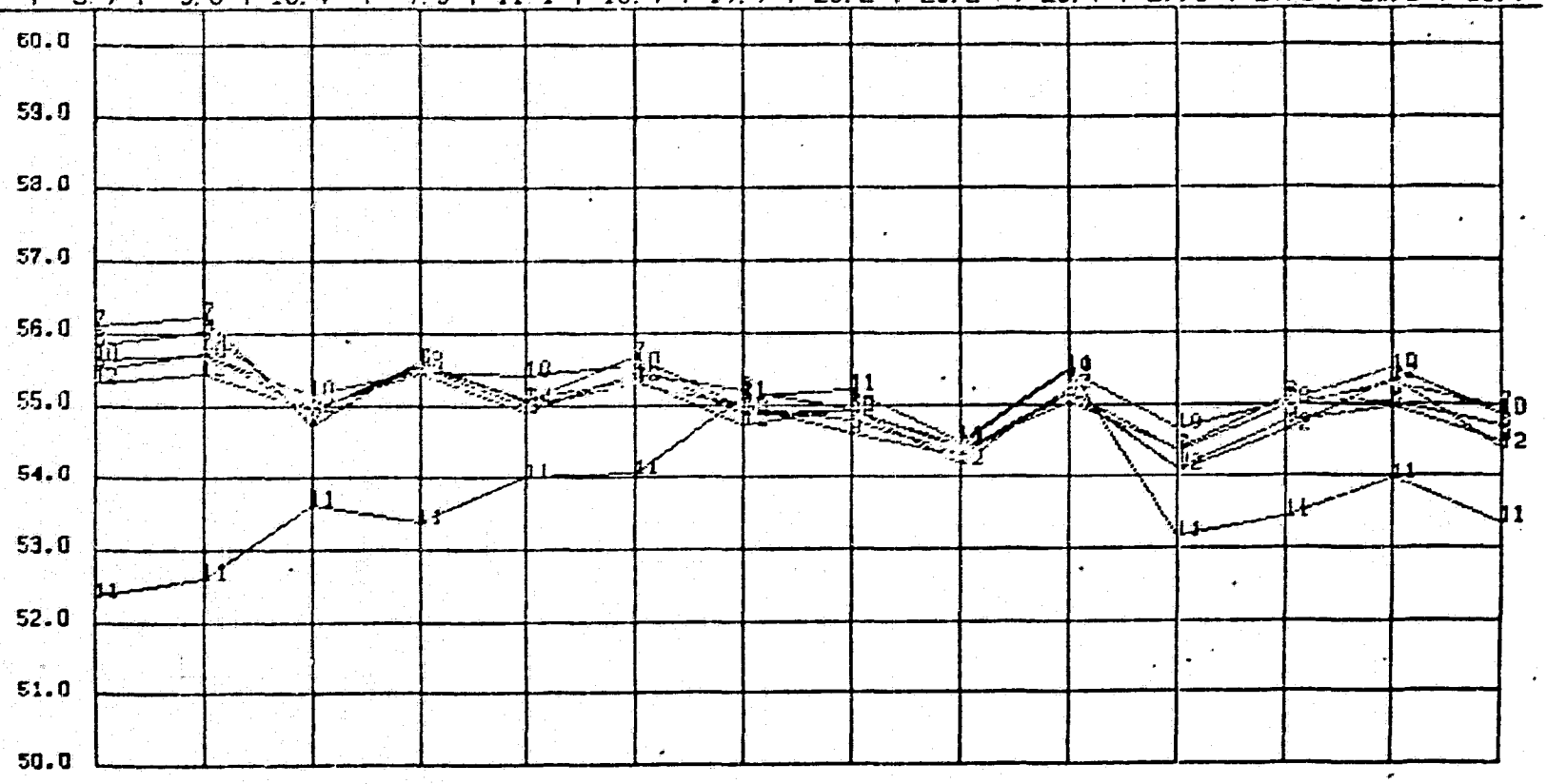

b) BAND 2 CONTINUED

FIGURE 10-18 (CONTINUED). F-1 COSL PERFORMANCE IN THERMAL-VACUUM

ORIGINAL PAGE IS OF POOR QUALITY

SEQ	141	142	143	144	145	146	147	148	149	150	151	152	153	154
STND	8	1	2	3	4	5	6	7	8	1	2	7	8	1
DS	1	1	1	1	1	1	1	1	1	1	1	1	1	1
DATE	09/14	09/15	09/15	09/15	09/15	09/15	09/15	09/15	09/15	09/15	09/15	09/15	09/15	09/15
TIME	22 39	17	1 42	3 16	4 41	6 9	8 25	9 43	11 4	13 7	14 41	16 19	17 39	21 12
TEMP	30.6	30.3	31.3	30.3	30.6	30.9	30.3	31.6	30.3	26.9	20.9	15.9	13.0	10.1

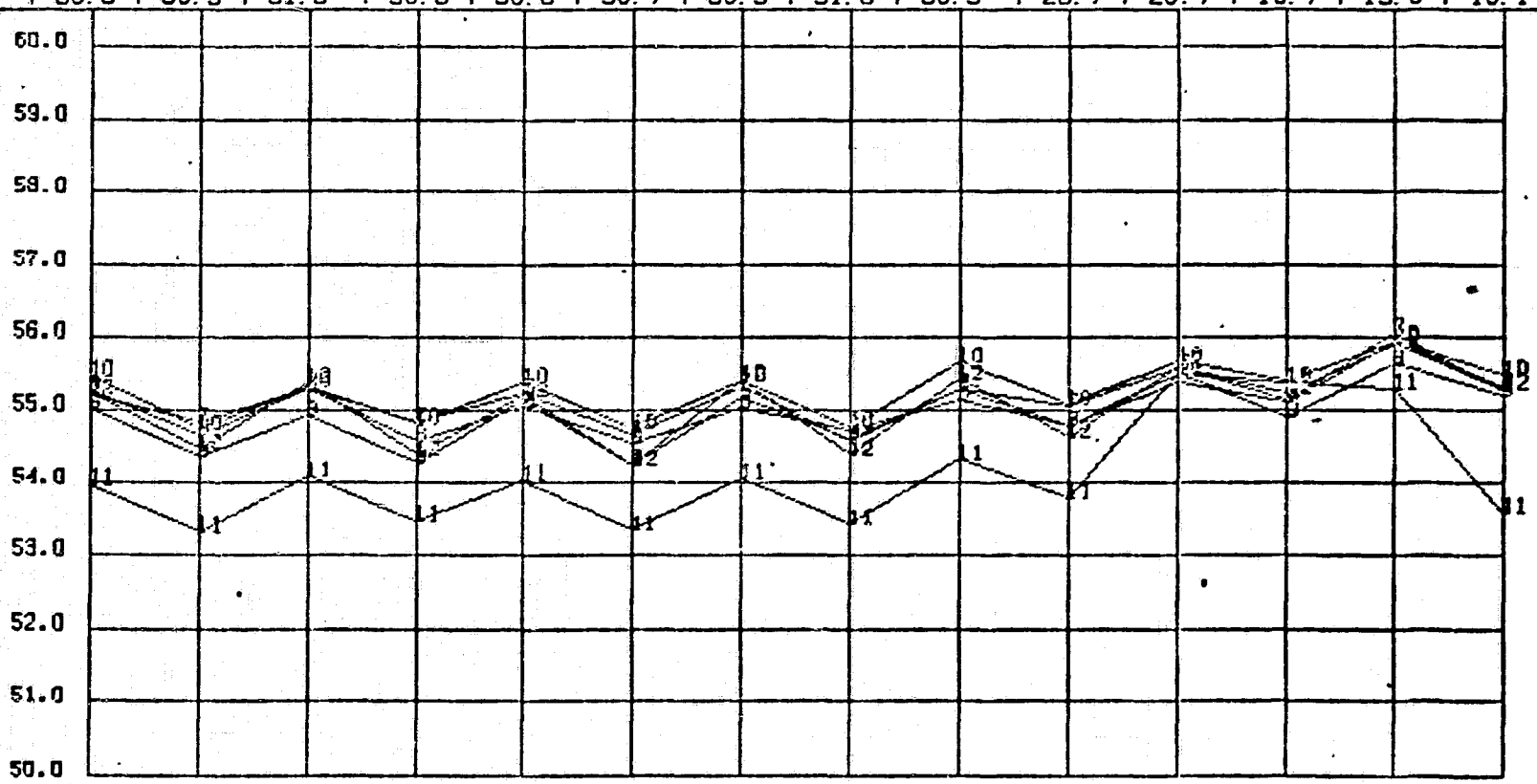

b) BAND 2 CONTINUED

FIGURE 10-18 (CONTINUED). F-1 COSL PERFORMANCE IN THERMAL-VACUUM

820015-254

ORIGINAL PAGE IS OF POOR QUALITY

SEQ	155	156	157	158	159	159	160	161	162	163	164	165	629	630
STND	2	3	4	5	6	6	7	8	1	2	7	8	27	28
DS	1	1	1	1	1	1	1	1	1	1	1	1	1	1
DATE	09/15	09/16	09/16	09/16	09/16	09/16	09/16	09/16	09/16	09/16	09/16	09/16	09/16	09/16
TIME	22 39	51	2 12	3 43	5 18	5 18	6 57	8 39	9 42	11 7	13 1	14 37	17 1	18 34
TEMP	10.8	11.3	11.1	10.8	10.6	10.6	11.3	10.1	11.8	15.4	24.1	28.7	29.9	30.3

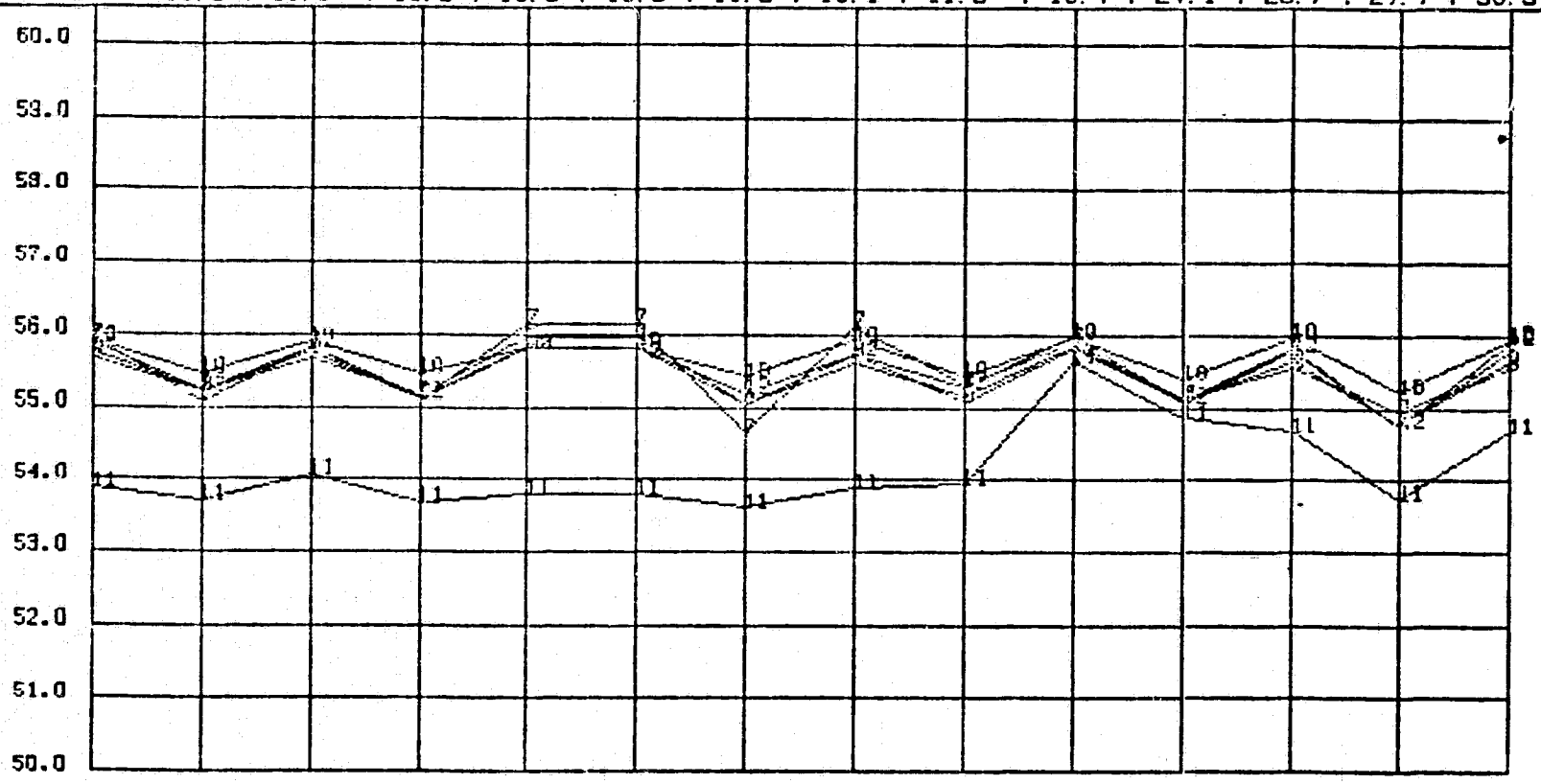

b) BAND 2 CONTINUED

FIGURE 10-18 (CONTINUED). F-1 COSL PERFORMANCE IN THERMAL-VACUUM

820015-255

ORIGINAL PAGE IS OF POOR QUALITY

SEQ	113	114	115	116	117	118	119	120	121	122	123	124	125	126
STND	6	7	8	1	2	7	8	1	2	3	4	5	6	7
DS	1	1	1	1	1	1	1	1	1	1	1	1	1	1
DATE	09/12	09/12	09/12	09/12	09/12	09/13	09/13	09/13	09/13	09/13	09/13	09/13	09/13	09/13
TIME	15	16 24	17 49	21	22 26	1	1 53	6 40	8 18	9 42	12	14 4	15 55	17 10
TEMP	31.9	31.6	32.6	29.9	26.6	19.9	11.6	5.6	6.1	6.5	4.8	4.6	4.6	4.8

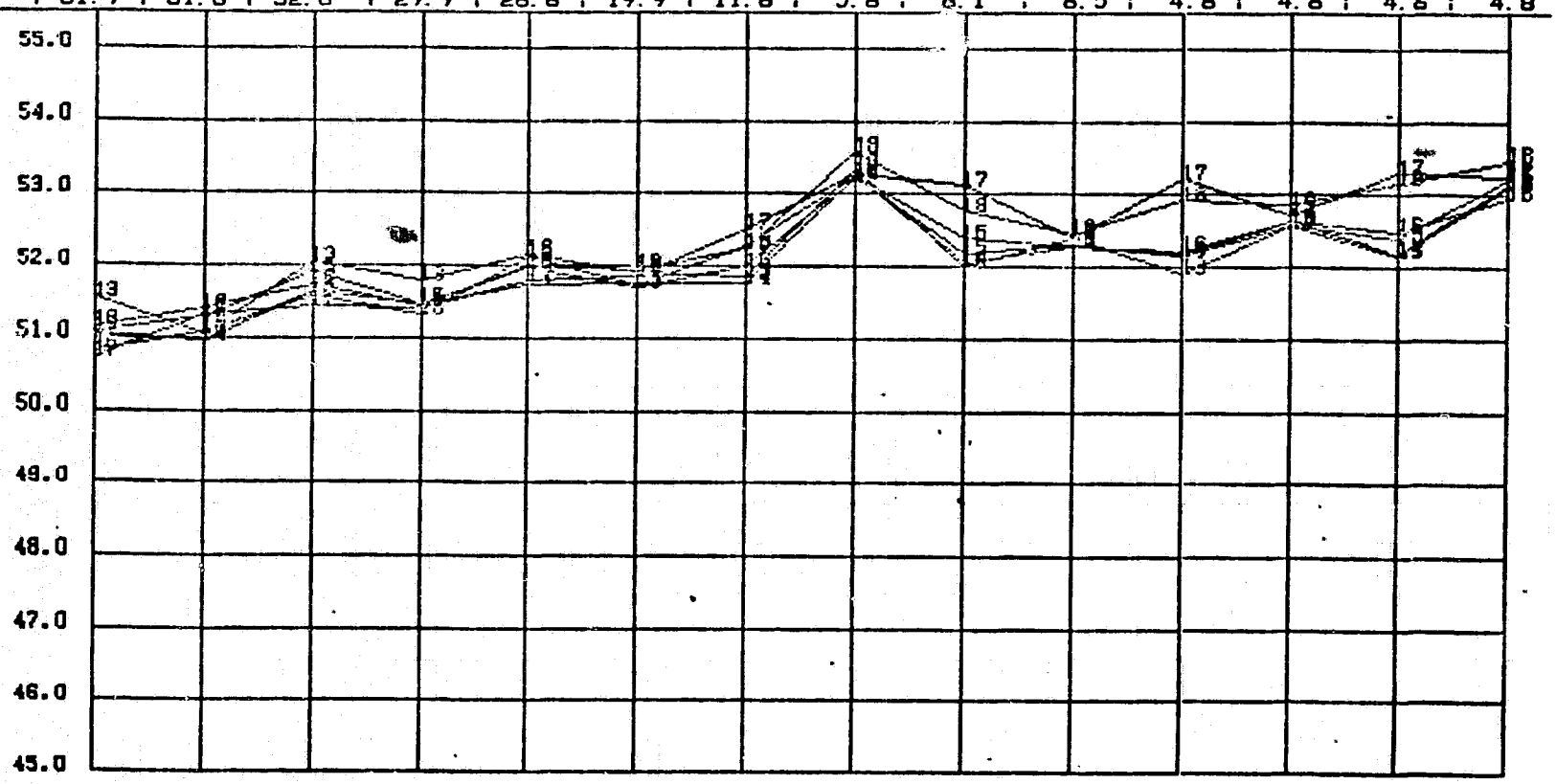

c) BAND 3

FIGURE 10-18 (CONTINUED). F-1 COSL PERFORMANCE IN THERMAL-VACUUM

820015-256

ORIGINAL PAGE IS OF POOR QUALITY

SEQ	127	128	129	130	131	132	133	134	135	136	137	138	139	140
STND	8	4	1	2	7	8	1	2	7	8	3	1	2	7
DS	1	1	1	1	1	1	1	1	1	1	1	1	1	1
DATE	09/13	09/13	09/13	09/14	09/14	09/14	09/14	09/14	09/14	09/14	09/14	09/14	09/14	09/14
TIME	19 41	20 53	22 56	21	1 45	3 16	7 34	9 24	11 3	12 54	16 3	18 12	19 36	21 10
TEMP	3.9	5.0	10.4	9.5	11.1	10.4	19.9	20.2	20.2	20.4	27.5	29.3	30.6	30.9

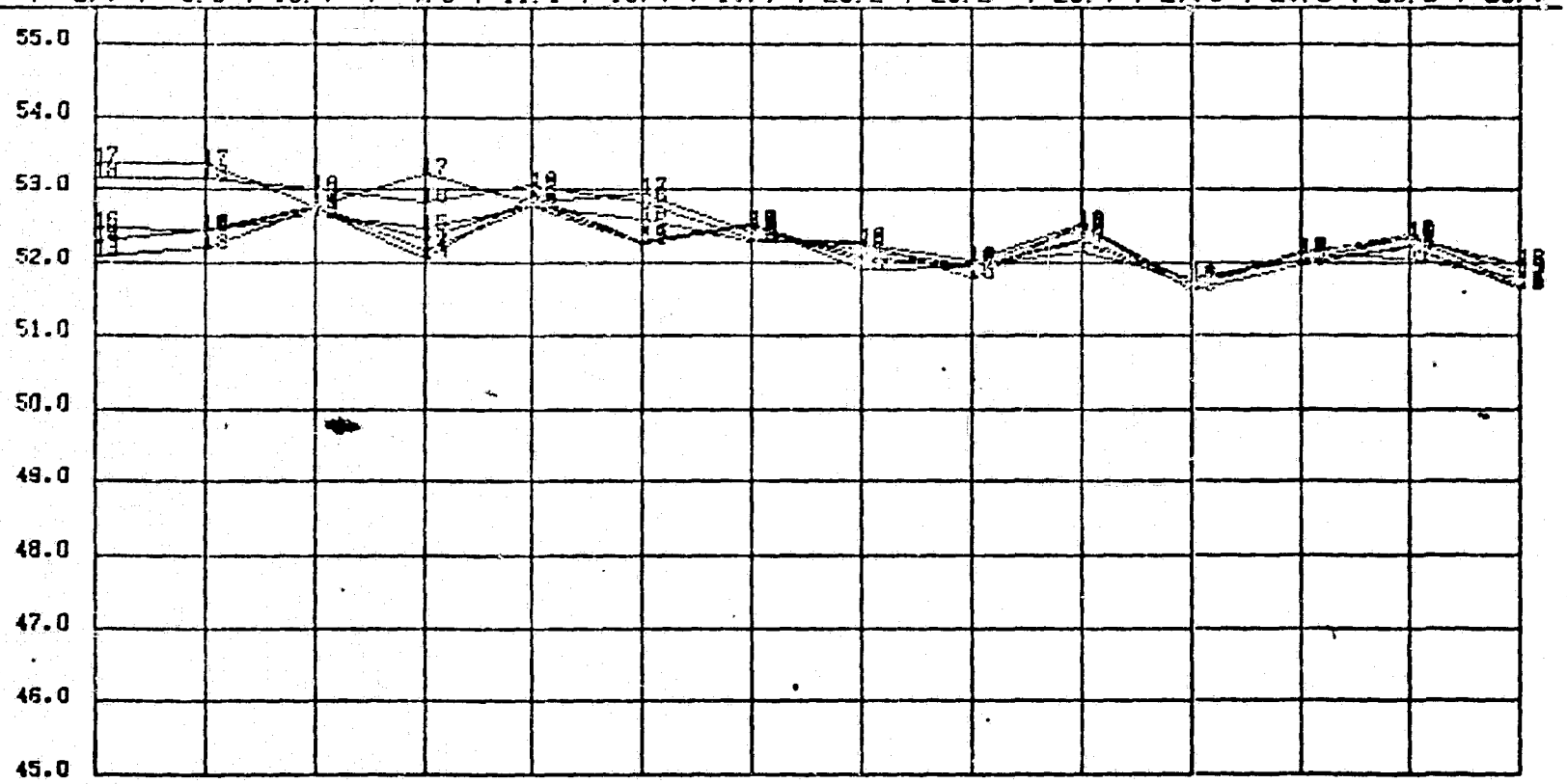

c) BAND 3 CONTINUED

FIGURE 10-18 (CONTINUED). F-1 COSL PERFORMANCE IN THERMAL-VACUUM

820015-257

ORIGINAL PAGE IS OF POOR QUALITY

SEQ	113	114	115	116	117	118	119	120	121	122	123	124	125	126
STND	6	7	8	1	2	7	8	1	2	3	4	5	6	7
DS	1	1	1	1	1	1	1	1	1	1	1	1	1	1
DATE	09/12	09/12	09/12	09/12	09/12	09/13	09/13	09/13	09/13	09/13	09/13	09/13	09/13	09/13
TIME	15	16 24	17 49	21	22 26	1	1 53	6 40	8 18	9 42	12	14 4	15 55	17 10
TEMP	31.9	31.6	32.6	29.9	26.6	19.9	11.6	5.6	6.1	6.5	4.8	4.6	4.6	4.8

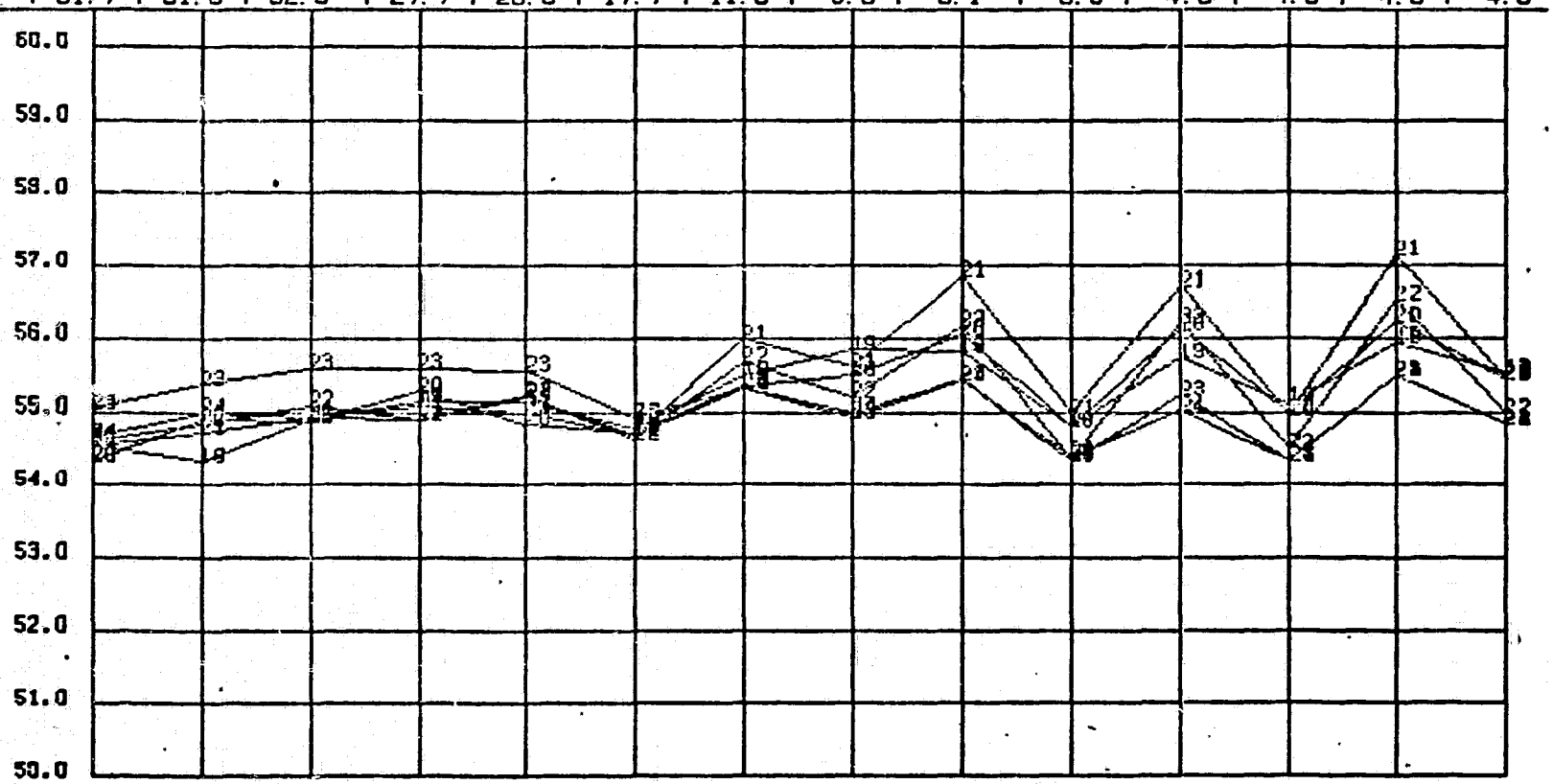

d) BAND 4

FIGURE 10-18 (CONTINUED). F-1 COSL PERFORMANCE IN THERMAL-VACUUM

820015-258

ORIGINAL PAGE IS OF POOR QUALITY

SEQ	127	128	129	130	131	132	133	134	135	136	137	138	139	140
STND	8	4	1	2	7	8	1	2	7	8	3	1	2	7
DS	1	1	1	1	1	1	1	1	1	1	1	1	1	1
DATE	09/13	09/13	09/13	09/14	09/14	09/14	09/14	09/14	09/14	09/14	09/14	09/14	09/14	09/14
TIME	19 41	20 53	22 56	21	1 45	3 16	7 34	9 24	11 3	12 54	16 3	18 12	19 36	21 10
TEMP	3.9	5.0	10.4	9.5	11.1	10.4	19.9	20.2	20.2	20.4	27.5	29.3	30.6	30.9

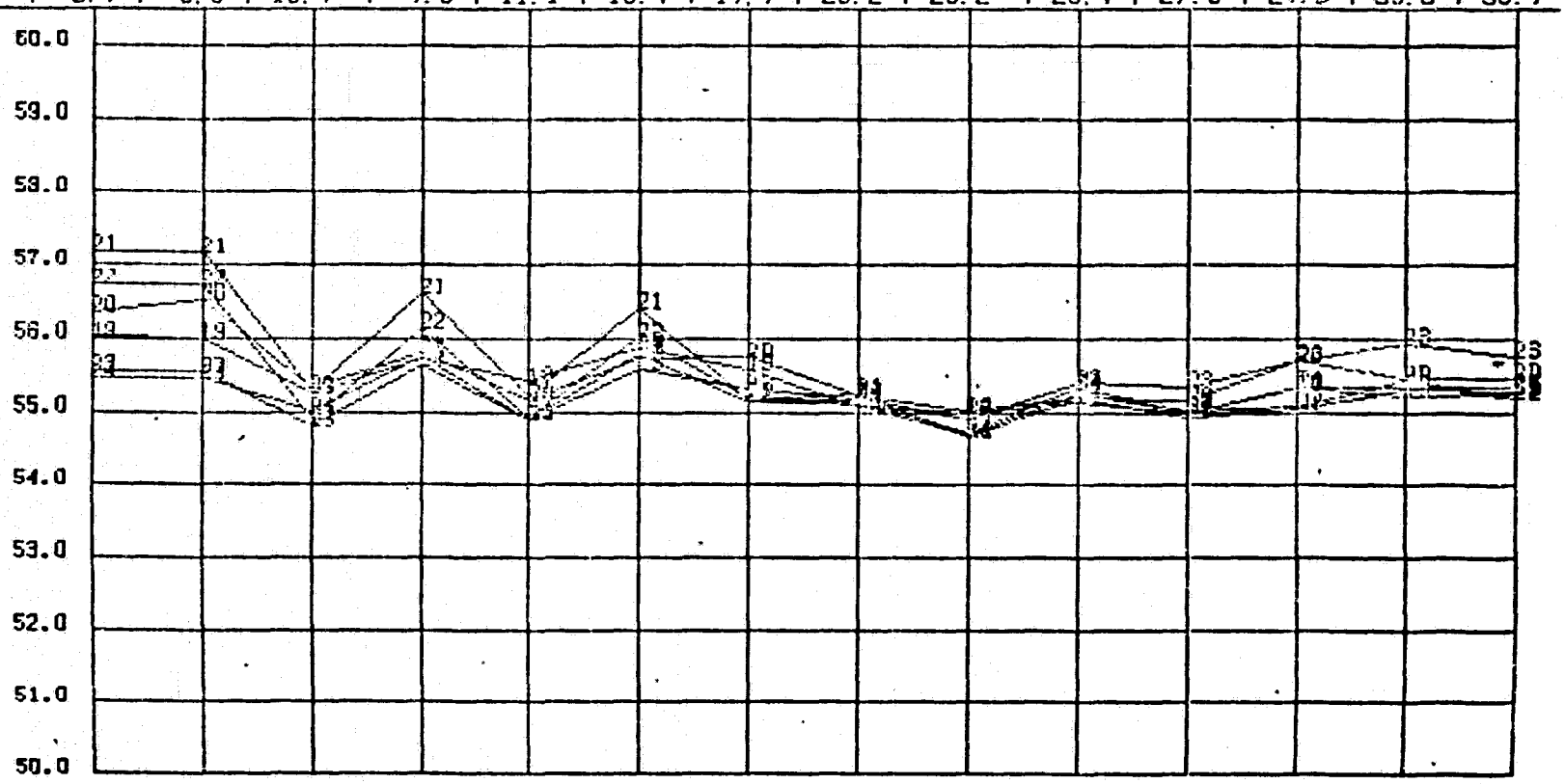

d) BAND 4 CONTINUED

FIGURE 10-18 (CONCLUDED). F-1 COSL PERFORMANCE IN THERMAL-VACUUM

820015-259

ORIGINAL PAGE IS OF POOR QUALITY

ORIGINAL PAGE IS
OF POOR QUALITY

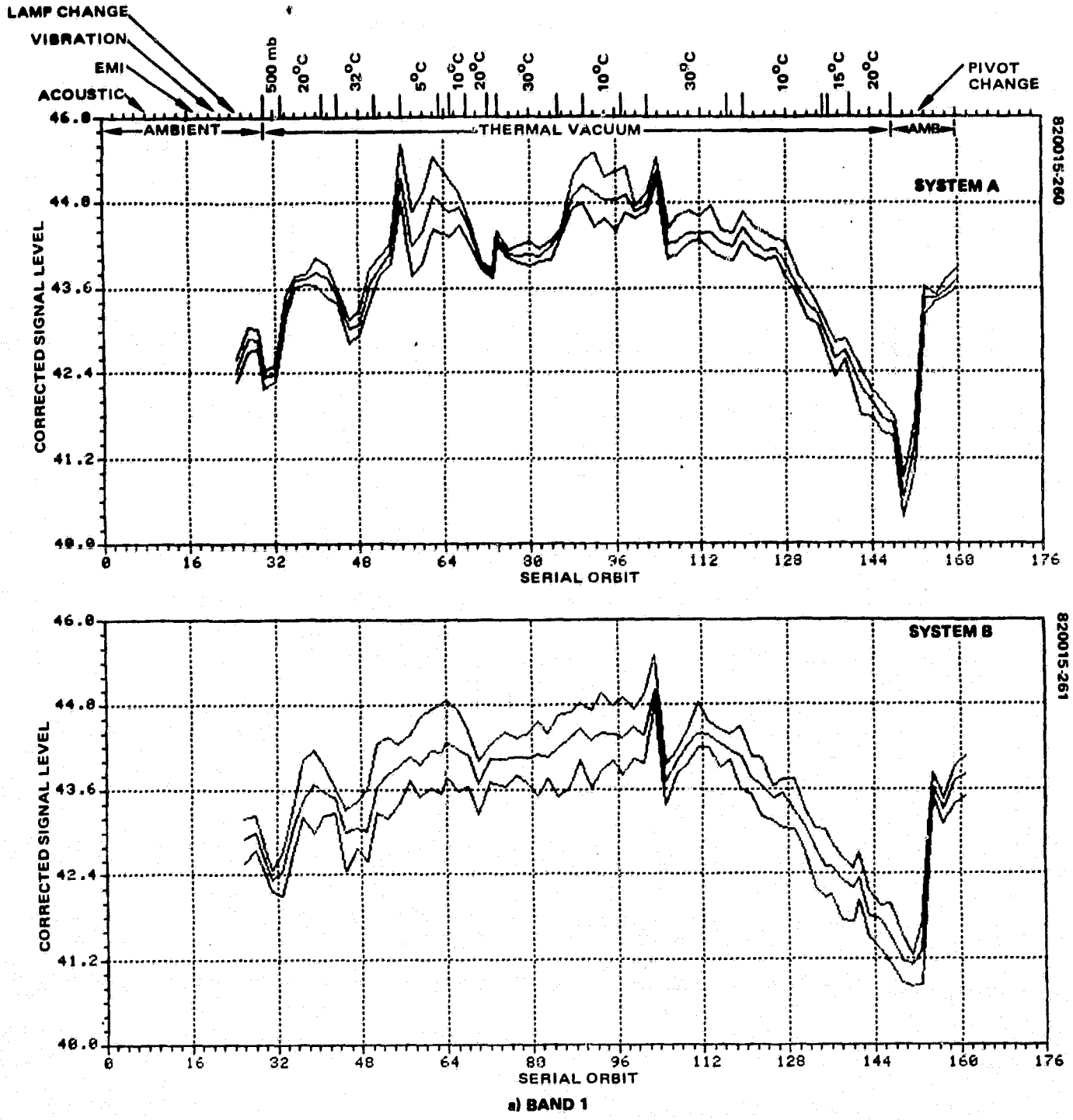

a) BAND 1

FIGURE 10-19. F-1 BAND AVERAGE COSL PERFORMANCE – LINEAR/LOW GAIN MODE

ORIGINAL PAGE IS
OF POOR QUALITY

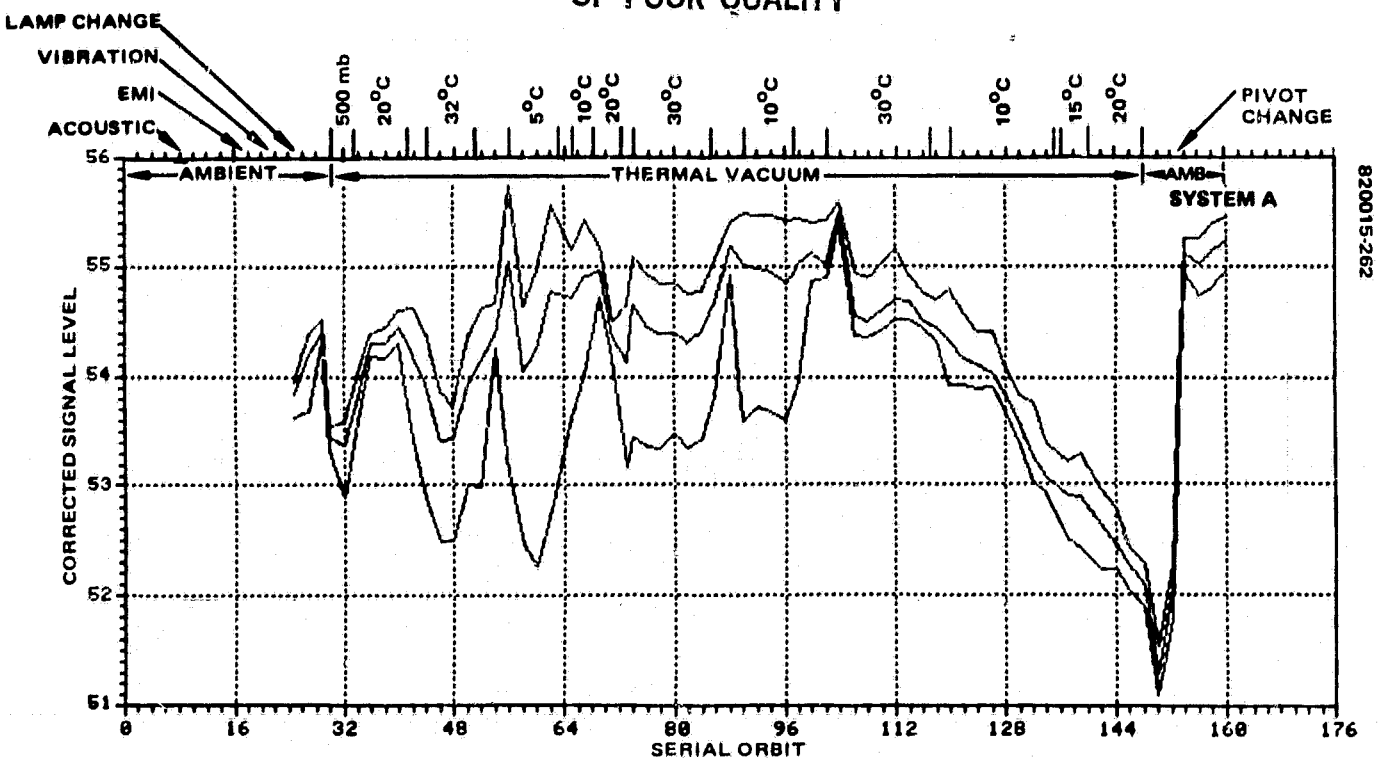

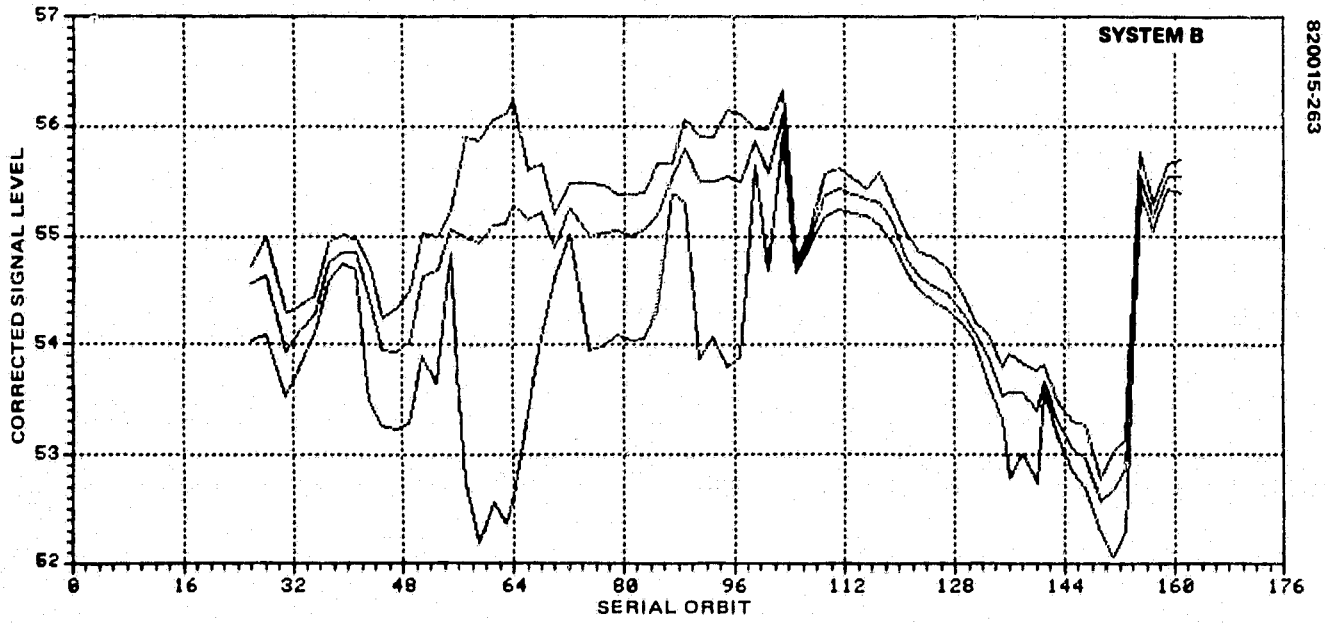

b) BAND 2

FIGURE 10-19 (CONTINUED). F-1 BAND AVERAGE COSL PERFORMANCE – LINEAR/LOW GAIN MODE

ORIGINAL PAGE IS
OF POOR QUALITY

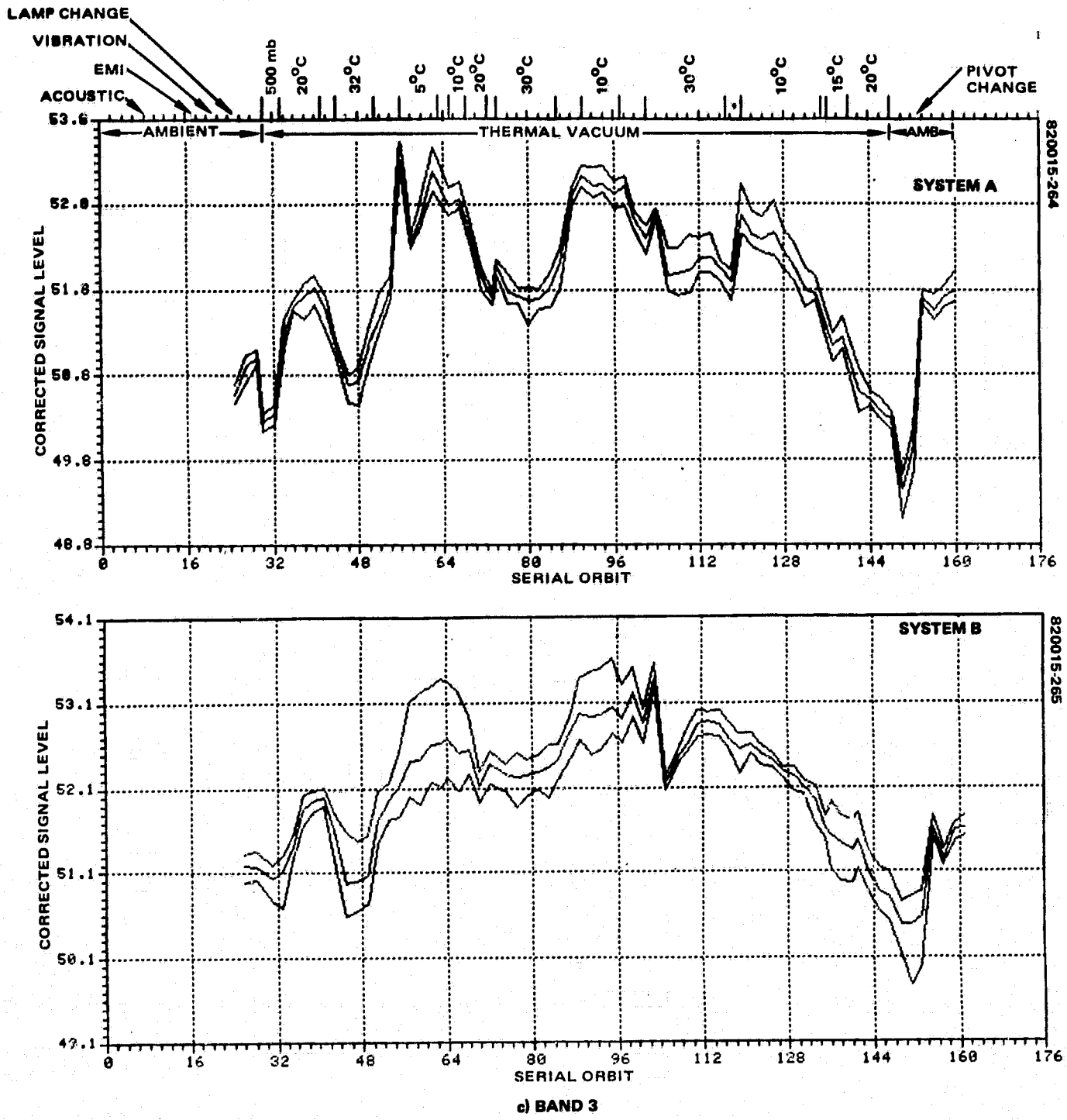

c) BAND 3

FIGURE 10-19 (CONTINUED). BAND AVERAGE COSL PERFORMANCE – LINEAR/LOW GAIN MODE

C-5

ORIGINAL PAGE IS
OF POOR QUALITY

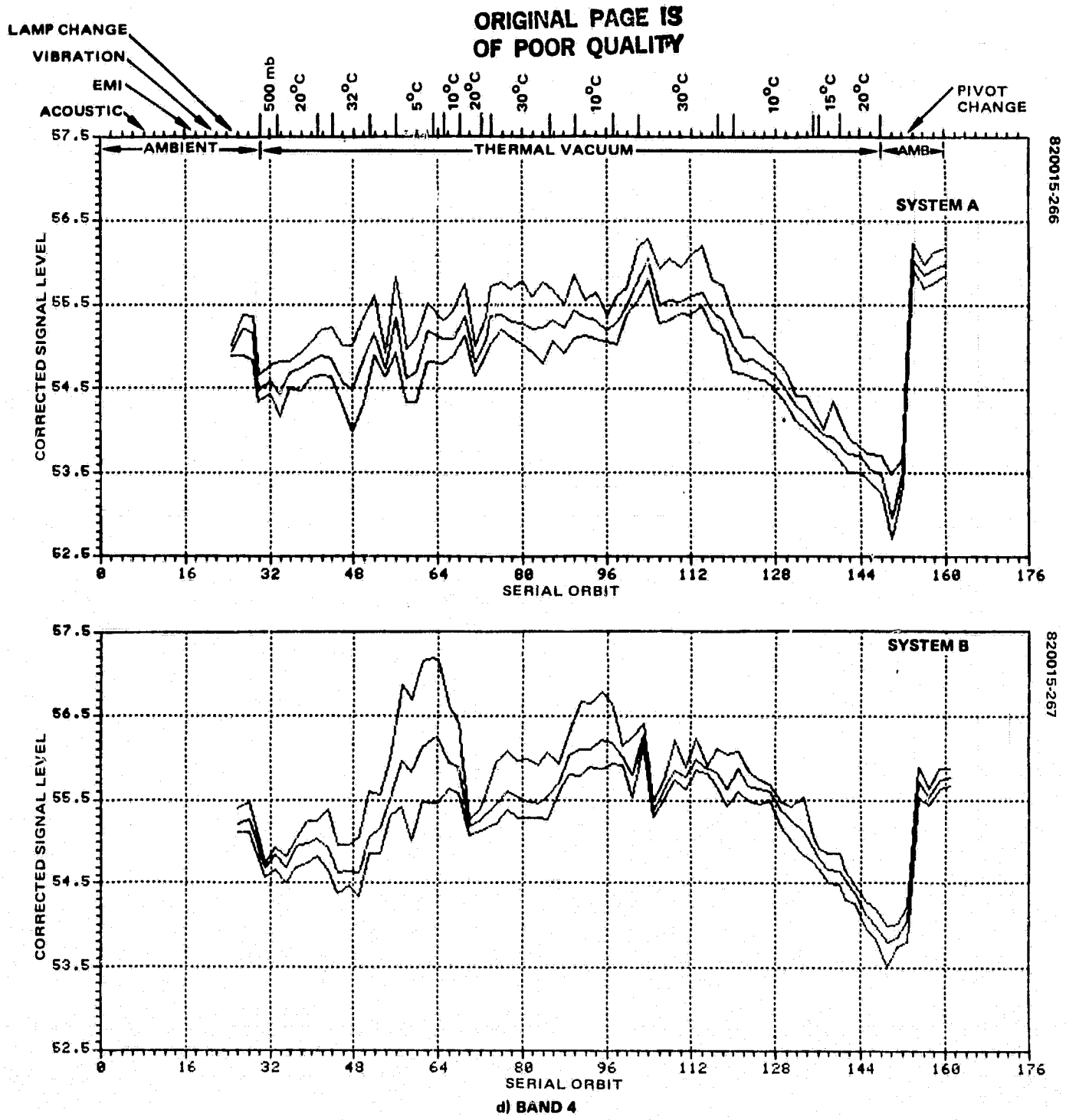

d) BAND 4

FIGURE 10-19 (CONCLUDED). BAND AVERAGE COSL PERFORMANCE – LINEAR/LOW GAIN MODE

10.4.4.2 Deviation Channel-to-Channel (DCC) Performance

DCC is a measure of the internal calibration system stability on a channel-to-channel basis for an individual band in the instrument. DCC is, by definition, the difference between the maximum and minimum calculated COSL in a given band. The specification limits this value to be less than 2 percent of the average COSL over the six channels in the band. (See 6.4.2 for a detailed account of the DCC algorithm.)

The COSL performance history of the MSS-D F-1 is presented in Figure 10-20 in a form very convenient for assessing system DCC performance versus the specification. These plots were generated by dividing the individual COSLs for each channel in a band by the band average COSL for that band. These normalized COSLs are plotted for all of the regular (non-STR) orbits run during MSS-D protoflight acceptance testing. To compare the DCC performance of the scanner using its redundant calibration sources, scanner configurations Mode A and B are plotted separately.

Plotted in this manner the data exhibits readily, regions of test environment during which DCC specification violations occur. The responsible channels can be identified as well. The 2 percent of band average specification requirement with respect to the family of COSLs in a band are converted to a 2 percent envelope width for the normalized COSLs. One need envision the mean at unity (1) and the limits of the specifications to be located at 1.01 and 0.99 for the maximum and minimum respectively. More precisely, the specification is not that the value of the normalized COSL should be between ± 1 percent but rather that the peak-to-peak difference over all the channels in a band must be less than 2 percent.

During F-1 thermal-vacuum testing there were numerous examples (200) of DCC out-of-specification occurrences. The calibration plan for thermal-vacuum was to do a collimator transfer calibration during the first two orbits in hard vacuum and to use this calibration for all of the remaining thermal-vacuum test orbits. Figure 10-21 shows the temperature profile versus sequential orbit number actually followed during thermal-vacuum testing. The two calibration orbits, 96 and 97, are shown as the first two orbits of this sequence. As soon as the scanner temperature was moved to 32°C at orbit 108 (see Figure 10-18b), band 2 started showing consistent out-of-specification DCC conditions, primarily due to the anomalous behavior of corrected signal level in channel 11. Minor out-of-specification conditions were also seen in band 1 due to a general spreading of the corrected signals. At the lowest temperature plateau of 5°C, orbits 120 through 127, the deviant behavior of channel 11 became worse, causing peak-to-peak corrected signal variations as large as 6.93 percent. The maximum allowable variation is 2.0 percent. At the 5°C plateau there were also minor DCC violations in bands 1, 3, and 4. In band 1 peak-to-peak corrected signal level variations were less than 3.31 percent; in band 3 less than 2.54 percent; in band 4 less than 3.18 percent. As the test continued it became apparent that the temperature dependence of the calibration system was such as to cause minor specification violations of DCC in bands 1 and 2 at all temperatures including later orbits run at the temperature at which the reference calibration was done. Bands 3 and 4 DCC violations showed up only at the 5° and 10°C temperature plateaus.

When the test sequence got to the last temperature plateau at 30°C, orbit 164 of Figure 10-20, a recalibration was done for this temperature plateau, and another recalibration was done for the final 10°C plateau, orbit 184. With these recalibrations there

ORIGINAL PAGE IS
OF POOR QUALITY

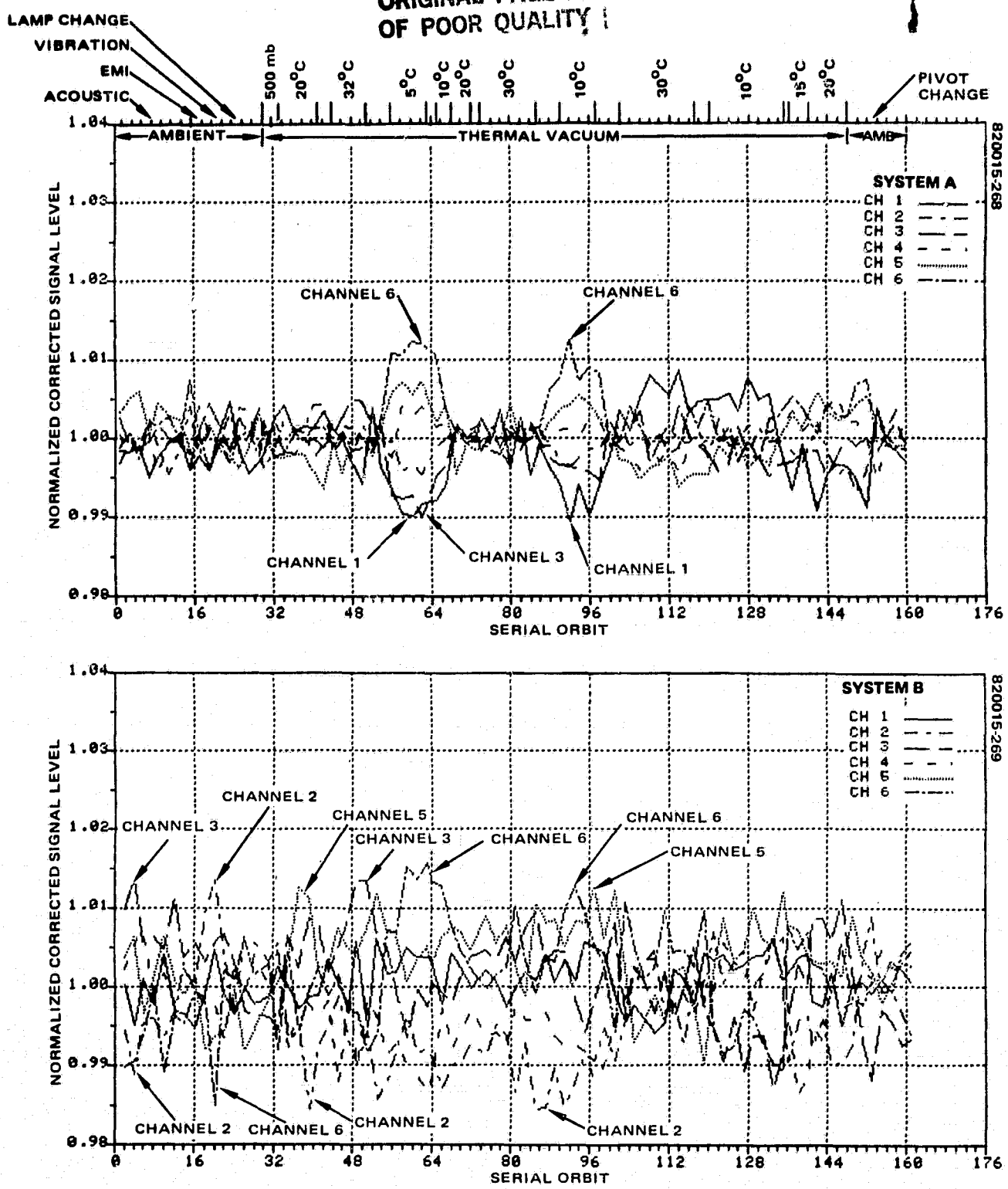

a) BAND 1

FIGURE 10-20. F-1 MEAN-NORMALIZED COSL PERFORMANCE – LINEAR/LOW GAIN MODE

ORIGINAL PAGE IS
OF POOR QUALITY

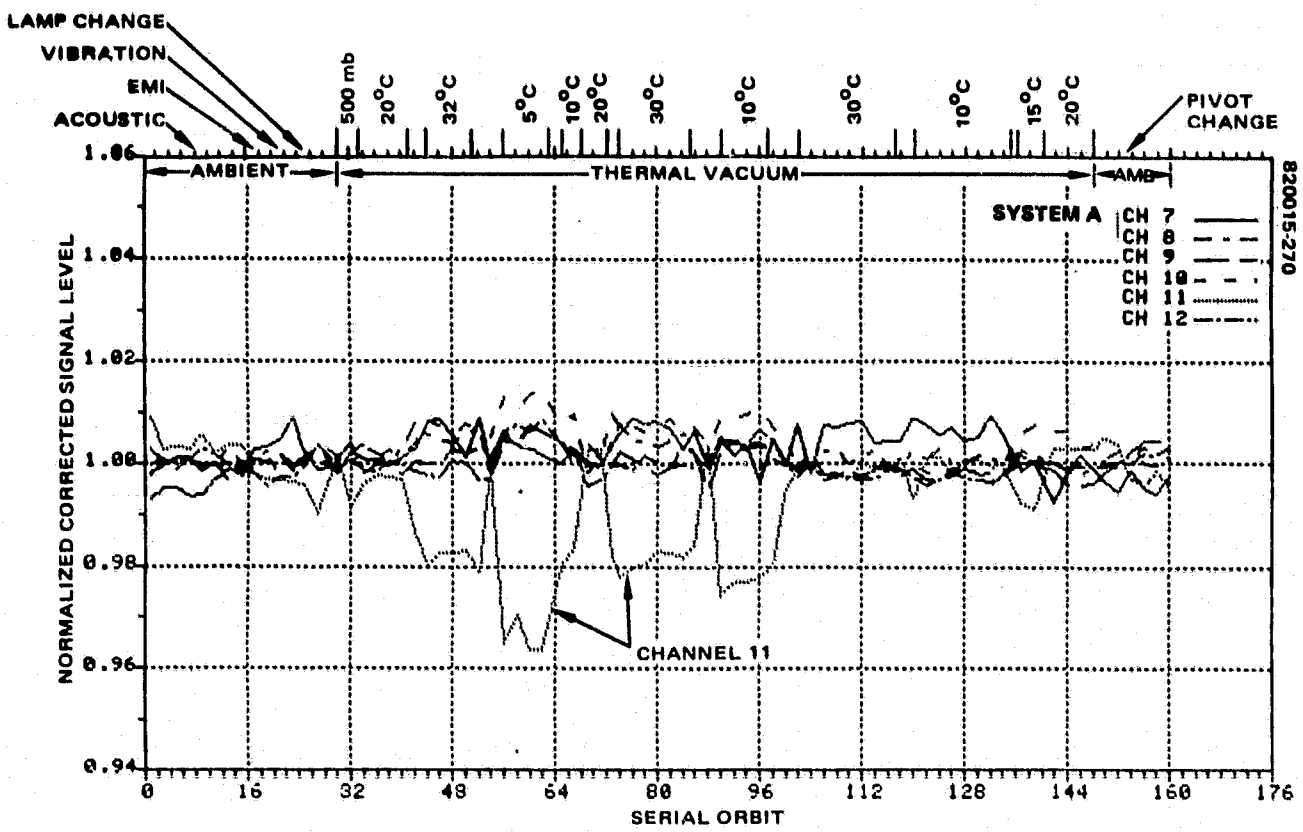

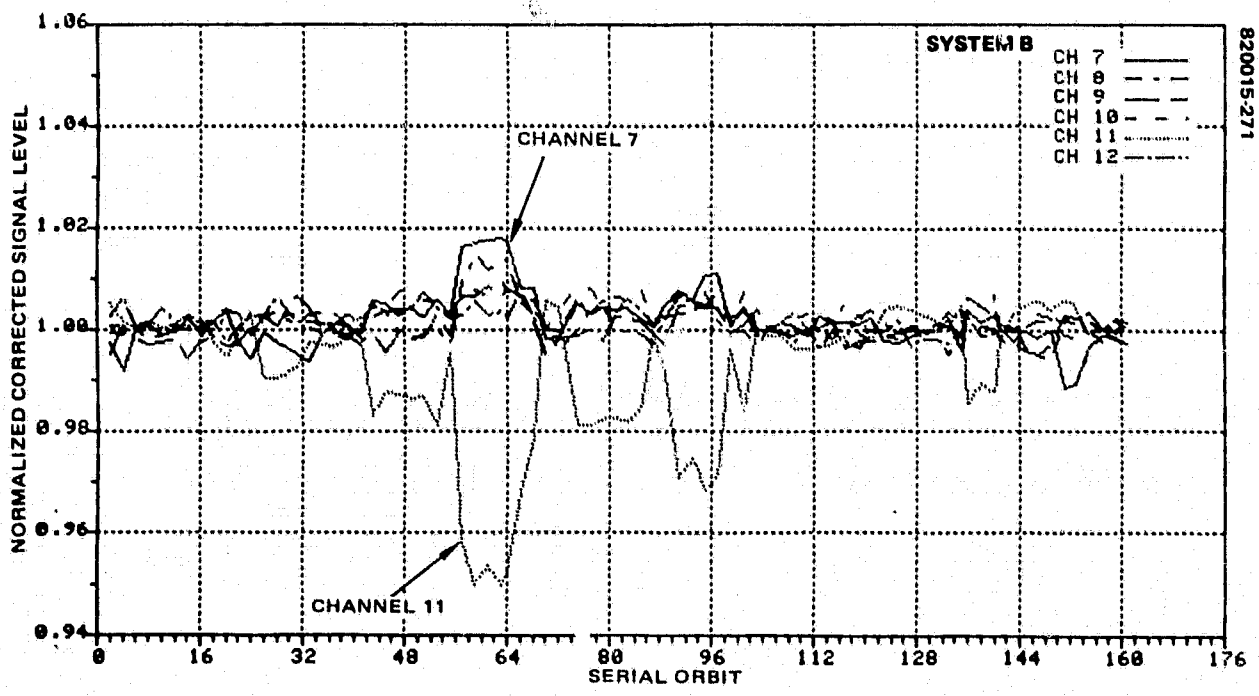

b) BAND 2

FIGURE 10-20 (CONTINUED). F-1 MEAN-NORMALIZED COSL PERFORMANCE – LINEAR/LOW GAIN MODE

ORIGINAL PAGE IS
OF POOR QUALITY

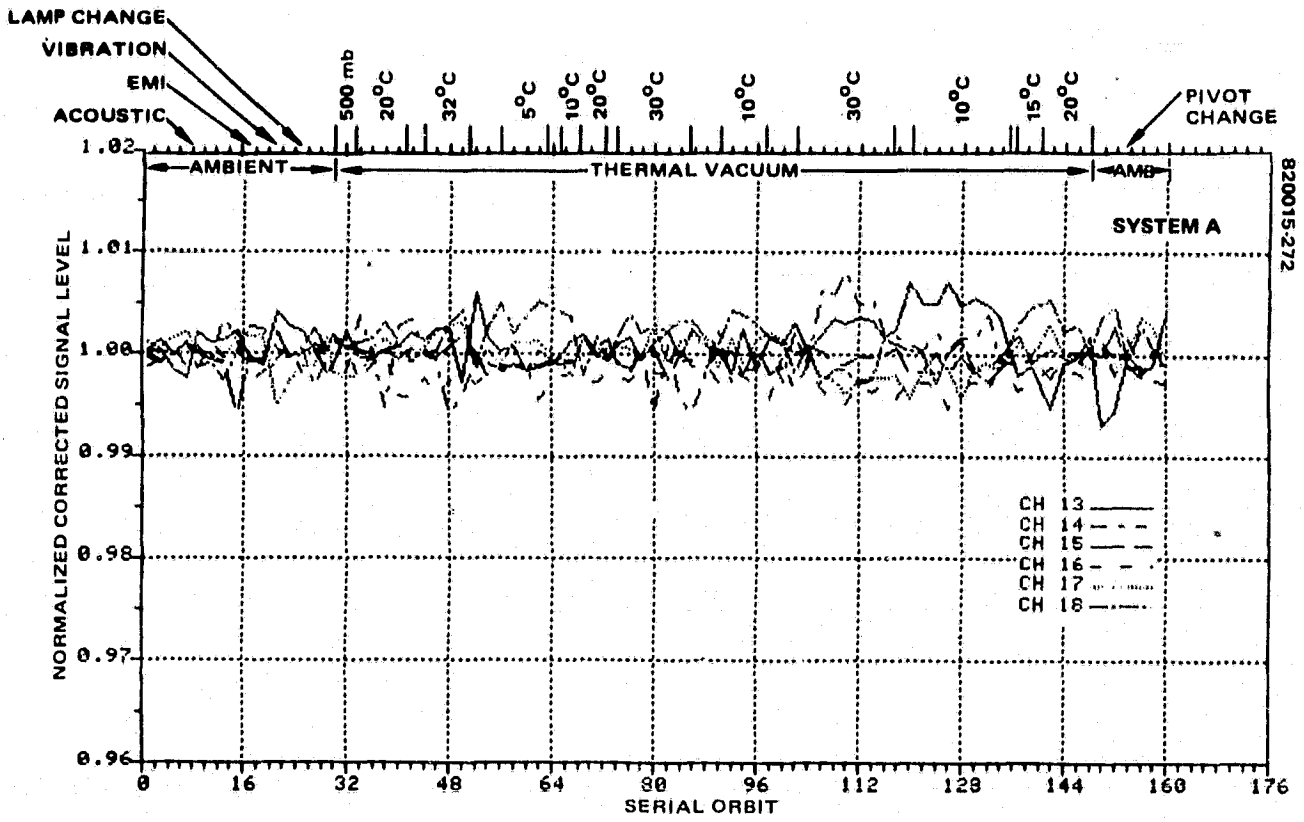

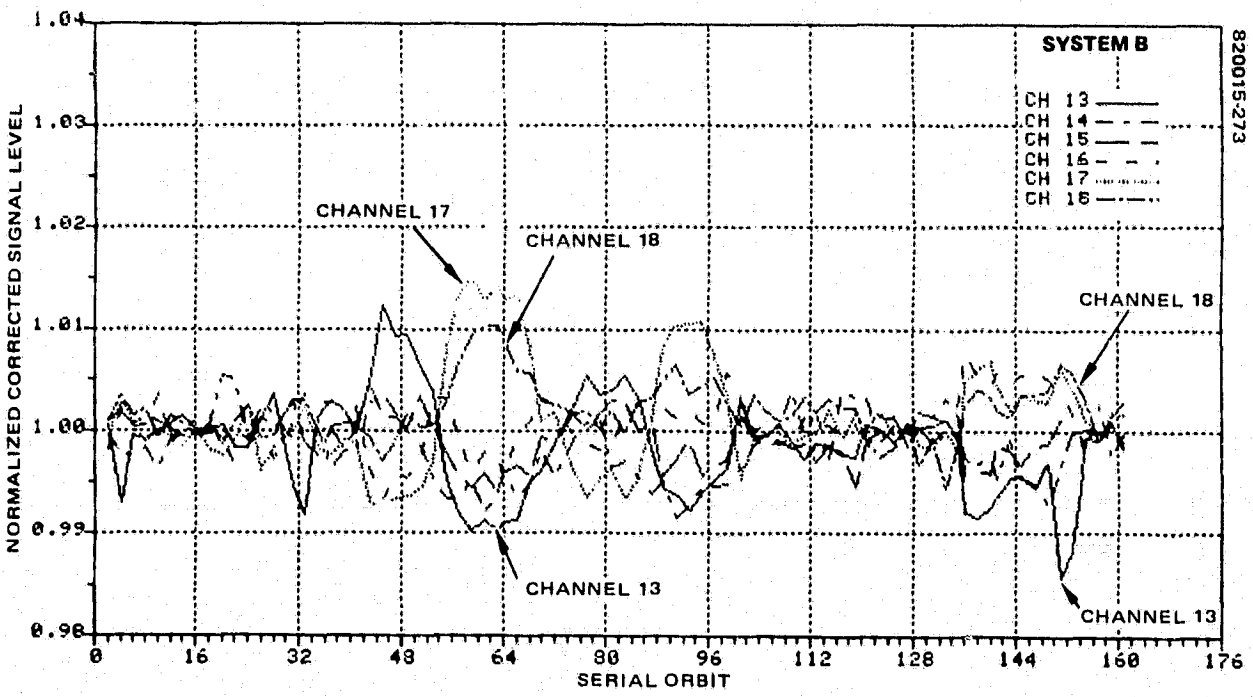

c) BAND 3

FIGURE 10-20 (CONTINUED). F-1 MEAN-NORMALIZED COSL PERFORMANCE — LINEAR/LOW GAIN MODE

ORIGINAL PAGE IS
OF POOR QUALITY

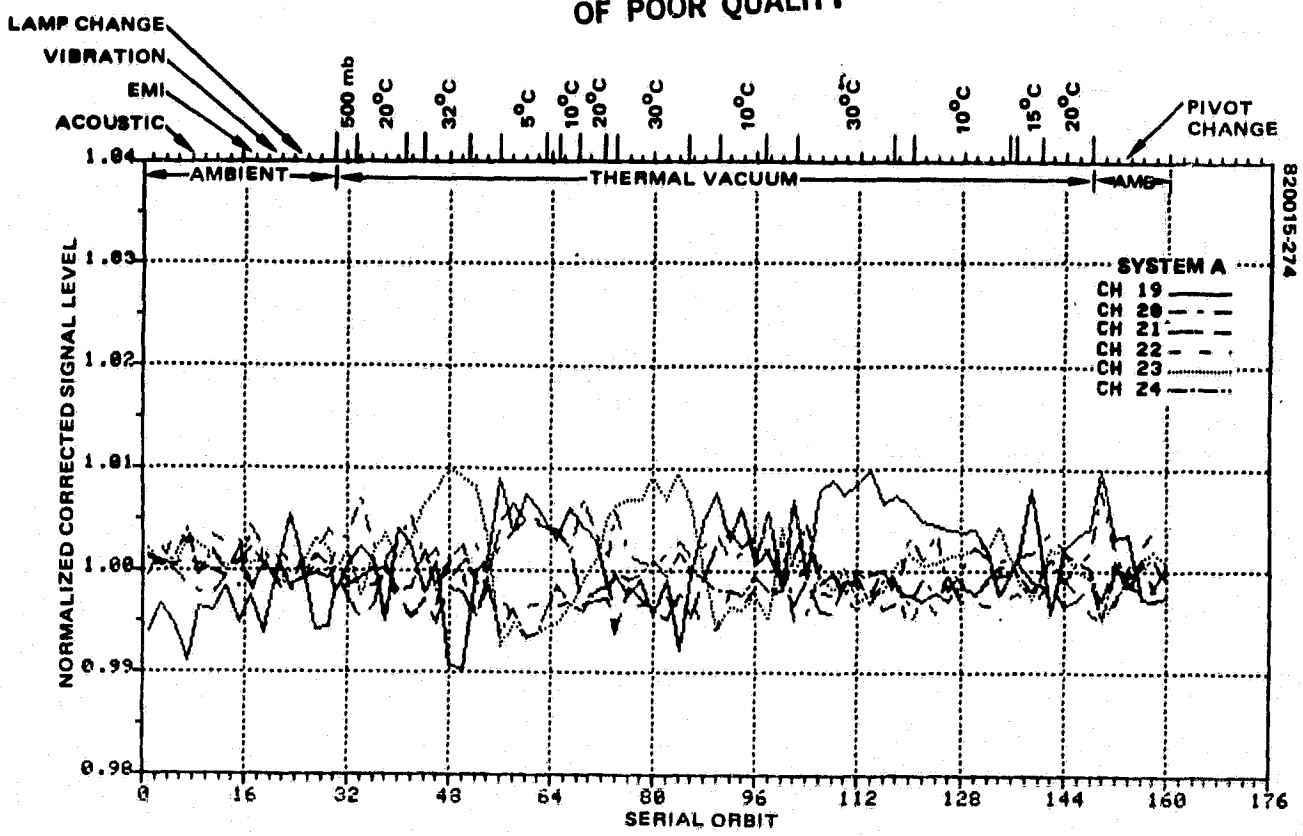

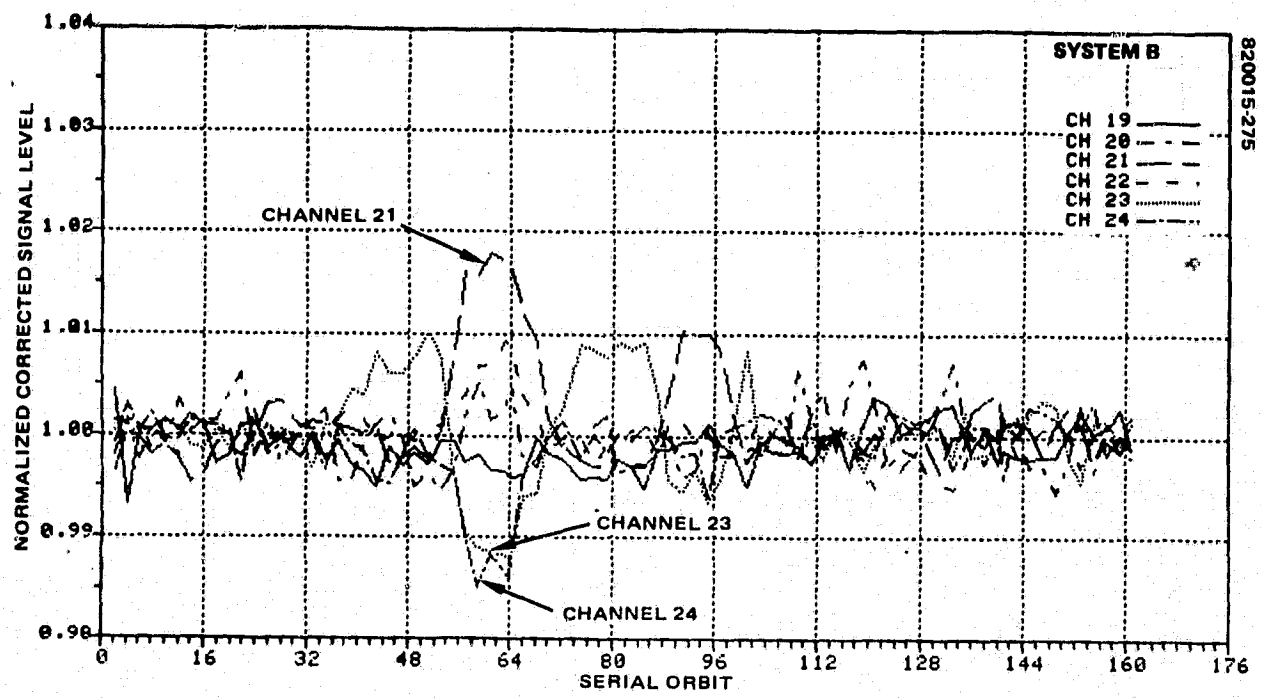

d) BAND 4

FIGURE 10-20 (CONCLUDED). F-1 MEAN-NORMALIZED COSL PERFORMANCE – LINEAR/LOW GAIN MODE

ORIGINAL PAGE IS
OF POOR QUALITY

were no DCC specification violations for the final data at 30° and 10°C. The final two temperature plateaus at 15° and 20°C shown in Figure 10-20 were run with the initial calibration done at orbits 96 and 97.

Table 10-9 is a detailed listing of the DCC specification violations recorded during thermal-vacuum testing. This summary is given in the column labelled Recorded

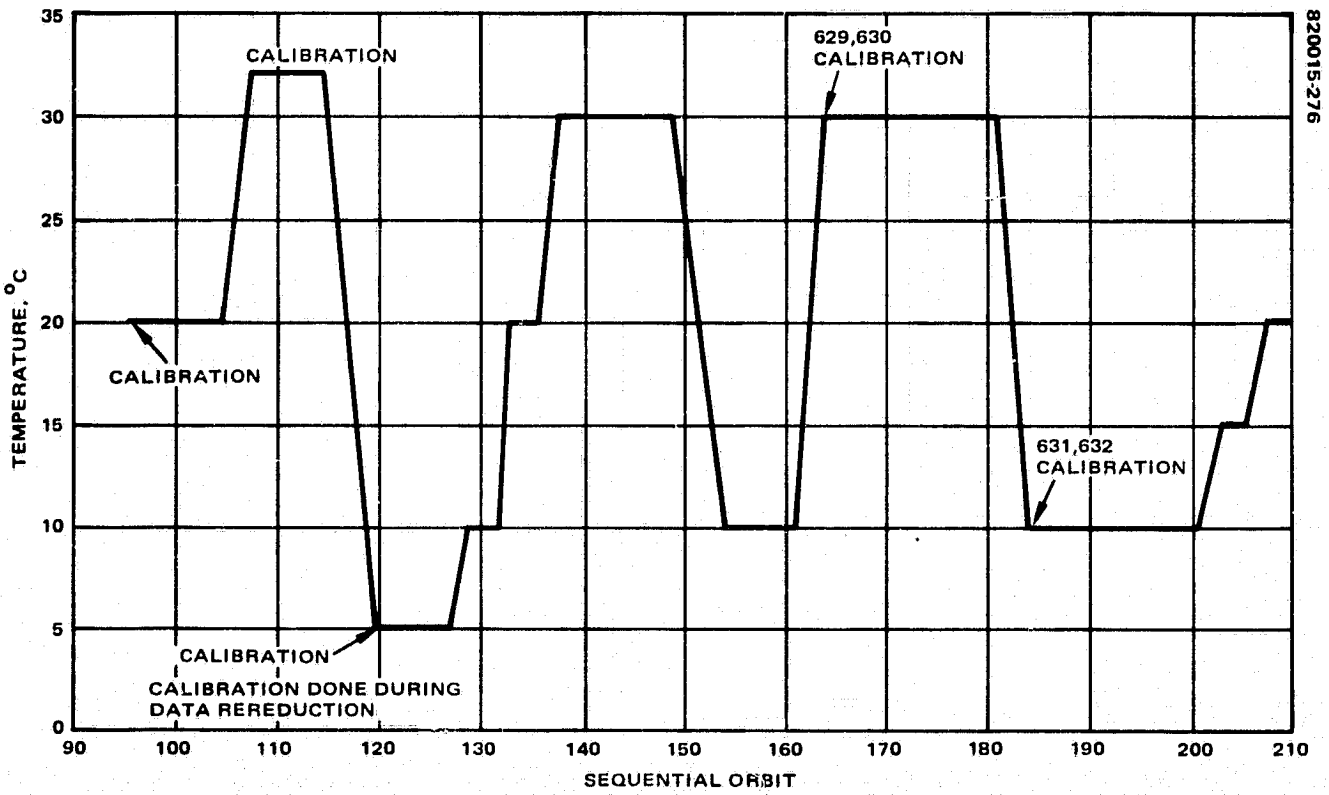

FIGURE 10-21. F-1 THERMAL-VACUUM TEMPERATURE PROFILE

ORIGINAL PAGE IS
OF POOR QUALITY

DCC Violations. The left hand part of the column gives the peak-to-peak corrected signal level deviation from specification; DCC = specification - ($COSL_{max}$ - $COSL_{min}$). The right half of the column gives the peak-to-peak percentage variation of corrected signal level computed from the same data (specification is 2 percent)

$$\text{percent} = \frac{COSL_{max} - COSL_{min}}{COSL_{av}} \times 100$$

A more detailed analysis of the DCC failures in thermal-vacuum was done using the collimator calibration program. The conclusions in this analysis with respect to DCC are:

1) The primary causes of the DCC violations are variations in the effective light output of the internal calibration system in the flight hardware and not test equipment variations.

2) The majority of the variation in the internal calibration system is caused by system temperature changes and it is repeatable.

The most likely cause of the anomalous DCC performance with temperature is a defective bond between the end of the fiber optics and the transfer lens assembly in front of each detector. Numerous experiments have been performed to examine the behavior of these bond interface over temperature. The results are discussed in 12.4. The experiments demonstrated that the optical bond between the fiber end and the transfer lens would break when the fiber plate was cycled to 60°C and back to room temperature. A redesign of this interface would be required to fix this problem.

In reanalyzing the thermal-vacuum DCC data after the completion of the test a separate recalibration was done at each temperature level run in thermal-vacuum. This was done by using the first two orbits of one of the plateaus as calibration orbits and using this calibration information to run all the remaining orbits on that plateau as well as any other plateaus at that temperature during the thermal-vacuum test. By recalibrating at operating temperature the number of DCC specification violations was reduced from 200 with a single calibration for all temperatures to 16 with the calibrations at temperature. Table 10-9 lists DCC results both before and after recalibration.

The orbits used for calibration are indicated in Figure 10-21. In the recorded data collection, orbits 96 and 97 were used for calibration up to orbit 164. Special test request orbits 629, 630 were used for the final temperature plateau at 30°C, orbits 166 to 181. Special test request orbits 631, 632 were used for the final temperature plateau at 10°C, orbits 186 to 201. For the final two temperature plateaus at 15° and 20°C orbits 96 and 97 were again used for calibration. For rereduction of the data, the calibration orbits as marked on Figure 10-21 were used except at 20°C, where orbits 204 and 205 were used instead of orbits 96 and 97.

The system's behavior at 20°C demonstrates yet another phenomenon. Note in Table 10-9 that nearly half the specification violations after rereduction occur in the initial 20°C plateau just after going into a vacuum environment. In the initial recorded

ORIGINAL PAGE IS
OF POOR QUALITY

TABLE 10-9. SUMMARY OF DCC VIOLATIONS

Orbit	Temperature, °C	Data Set	Band	Recorded DCC Violations		Calibration Orbits	Recalibrated DCC Values		Remaining Violations
				DCC	Percent		DCC	Percent	
98/1	20.7	1	1			204, 205	-0.06	2.14	X
		23	2	-0.01	2.07		-0.25	3.75	O
100/3	21.2	23	2				-0.19	3.33	X
		3	1				-0.15	2.35	X
102/5	21.4	23	2				-0.05	2.35	X
		3	1				-0.06	2.14	X
103/6	21.4	1	1	-0.31	2.72		-0.10	2.23	X
104/7	21.2	1	1				-0.02	2.05	X
		23	2				-0.11	2.77	X
105/3	21.4	3	1	-0.05	2.12		0.1		
108/1	31.6	1	2	-0.45	2.83	108, 109	1.04		
		3	2	-0.17	2.31		0.84		
109/2	32.9	3	1	-0.08	2.18		0.21		
		3	2	-0.01	2.02		0.41		
110/3	32.9	1	2	-0.31	2.57		0.93		
		3	2	-0.16	2.30		0.68		
111/4	32.2	1	2	-0.02	2.04		0.62		
112/5	32.2	1	2	-0.14	2.26		0.76		
		23	2				-0.02	2.14	X
113/6	31.9	1	1	-0.15	2.35		0.10		
			2	-0.11	2.20		0.55		
114/7	31.6	1	2	-0.26	2.48		0.56		
		3	2	-0.08	2.15		0.69		
115/8	32.6	1	1	-0.09	2.21		-0.02	2.05	O
		2	2	-0.05	2.09		0.61		
		3	2	-0.07	2.13		0.57		
120/1	5.6	1	2	-1.54	4.85	120, 121	1.04		
		22	1	-0.07	2.61		0.22		
		22	2	-0.28	3.96		0.28		
		23	1	-0.09	2.78		0.21		
		23	2	-0.26	3.82		0.23		
		3	2	-1.51	4.80		0.59		
121/2	6.1	1	2	-2.08	5.85	120, 121	1.04		
		1	3	-0.07	2.14		0.97		
		1	4	-0.36	2.66		1.02		
		22	2	-0.52	5.65		0.28		
		3	1	-0.22	2.51		0.33		
		3	2	-2.17	6.02		0.69		
122/3	6.5	1	1	-0.03	2.07		0.40		
		1	2	-1.11	4.06		0.66		
		22	1	-0.06	2.52		0.16		
		22	2	-0.23	3.61		0.19		
		23	1	-0.10	2.87		0.44		
		23	2	-0.24	3.68		0.20		
		3	1	-0.00	2.00		0.24		
		3	2	-1.34	4.48		0.74		

X = New violations
O = Remaining Violations

ORIGINAL PAGE IS
OF POOR QUALITY

Table 10-9 (continued)

Orbit	Temperature, °C	Data Set	Band	Recorded DCC Violations		Calibration Orbits	Recalibrated DCC Values		Remaining Violations
				DCC	Percent		DCC	Percent	
123/4	4.8	1	1	-0.25	2.58		0.22		
		1	2	-2.60	6.81		0.30		
		1	3	-0.27	2.53		0.70		
		1	4	-0.61	3.12		0.67		
		22	2	-0.52	5.65		0.19		
		23	2	-0.51	5.58		0.15		
		3	1	-0.10	2.23		0.31		
		3	2	-2.10	5.89		0.58		
		3	3	-0.20	2.39		0.71		
124/5	4.6	1	1	-0.11	2.25		0.50		
		1	2	-1.62	5.00		0.81		
		22	1	-0.13	3.13		0.12		
		22	2	-0.32	4.25		0.22		
		23	1	-0.12	3.04		0.16		
		23	2	-0.35	4.46		0.19		
		3	2	-1.53	4.83		0.69		
125/6	4.6	1	1	-0.25	2.58		0.34		
		1	2	-2.43	6.50		0.67		
		1	3	-0.11	2.21		0.74		
		1	4	-0.57	3.05		0.76		
		22	2	-0.57	6.00		0.14		
		23	2	-0.55	5.86		0.18		
		3	1	-0.09	2.21		0.49		
		3	2	-2.58	6.78		0.35		
		3	3	-0.07	2.14		0.76		
126/7	4.8	1	1	-0.13	2.30		0.39		
		1	2	-1.70	5.15		0.75		
		22	1	-0.12	3.04		0.17		
		22	2	-0.32	4.25		0.23		
		23	1	-0.15	3.30		0.14		
		23	2	-0.33	4.32		0.20		
		3	2	-1.50	4.78		0.58		
127/8	3.9	1	1	-0.42	2.97	120, 121	0.18		
		1	2	-2.66	6.93		0.39		
		1	3	-0.24	2.47		0.71		
		1	4	-0.64	3.17		0.59		
		22	2	-0.61	6.28		0.13		
		23	2	-0.58	6.07		0.14		
		3	1	-0.10	2.23		0.51		
		3	2	-2.41	6.46		0.65		
		3	3	-0.08	2.16		0.57		
129/1	10.4	1	2	-0.44	2.81	STR	0.54		
		22	1	-0.01	2.09	631, 632	0.16		
		22	2	-0.07	2.49		0.12		
		23	1	-0.06	2.52		0.18		
		23	2	-0.11	2.77		0.08		
		3	2	-0.53	2.98		0.53		

ORIGINAL PAGE IS
OF POOR QUALITY

Table 10-9 (continued)

Orbit	Temperature, °C	Data Set	Band	Recorded DCC Violations		Calibration Orbits	Recalibrated DCC Values		Remaining Violations
				DCC	Percent		DCC	Percent	
130/2	9.5	1	1	-0.28	2.65		0.26		
		1	2	-1.13	4.09		0.76		
		1	3	-0.14	2.27		0.78		
		22	2	-0.26	3.82		0.12		
		23	2	-0.26	3.82		0.12		
		3	1	-0.10	2.23		0.33		
		3	2	-1.36	4.52		0.86		
131/7	11.1	1	2	-0.34	2.63		0.28		
		22	1	-0.01	2.09		0.15		
		23	1	-0.02	2.17		0.19		
		23	2				-0.01	2.07	X
		3	2	-0.32	2.59		0.33		
132/8	10.4	1	2	-0.53	2.98		0.07		
		22	2	-0.19	3.33		-0.02	2.14	O
		23	2	-0.12	2.84		-0.06	2.42	O
		3	2	-0.74	3.37		0.29		
133/1	19.9	1	1			204, 205	-0.04	2.09	X
		22	2	-0.06	2.42		0.19		
		23	2	-0.02	2.14		0.20		
135/7	20.2	23	2	-0.07	2.49		0.20		
138/1	24.3	1	2	-0.55	3.02	STR	0.55		
		3	2	-0.43	2.80	629, 630	0.78		
139/2	30.6	1	2	-0.43	2.80		0.84		
		22	2	-0.04	2.28		0.26		
		23	2	-0.05	2.35		0.25		
		3	2	-0.27	2.50		0.53		
140/7	30.9	1	2	-0.49	2.91	STR	0.50		
		3	2	-0.20	2.37	629, 630	0.57		
141/8	30.6	1	2	-0.39	2.72		0.72		
		22	2	-0.04	2.28		0.26		
		23	2	-0.01	2.07		0.24		
		3	2	-0.39	2.72		0.88		
142/1	30.3	1	2	-0.42	2.78		0.53		
		3	2	-0.25	2.46		0.61		
143/2	31.3	1	2	-0.20	2.37		0.68		
		22	2	-0.03	2.21		0.24		
		23	2	-0.04	2.28		0.27		
		3	2	-0.26	2.48		1.01		
144/3	30.3	1	1	-0.28	2.52		0.50		
		3	2	-0.24	2.44		0.62		
145/4	30.6	1	1	-0.18	2.42		-0.12	2.28	O
		1	2	-0.25	2.46		0.91		
		23	2	-0.02	2.14		0.25		
		3	2	-0.24	2.44		0.94		
146/5	30.9	1	2	-0.33	2.61		0.66		
		3	2	-0.27	2.50		0.68		

X = New violations.
O = Remaining violations.

ORIGINAL PAGE IS
OF POOR QUALITY

Table 10-9 (continued)

Orbit	Temperature, °C	Data Set	Band	Recorded DCC Violations		Calibration Orbits	Recalibrated DCC Values		Remaining Violations
				DCC	Percent		DCC	Percent	
147/6	30.3	1	2	-0.26	2.48		0.94		
		22	2	-0.05	2.35		0.27		
		23	2	-0.04	2.28		0.26		
		3	2	-0.31	2.57		0.83		
148/7	31.6	1	2	-0.25	2.46		0.81		
		3	2	-0.31	2.57		0.72		
149/8	30.3	1	1	-0.29	2.67		0.27		
		1	2	-0.25	2.46		0.92		
		22	2	-0.04	2.28		0.26		
		23	2	-0.03	2.21		0.27		
		3	2	-0.36	2.67		0.89		
154/1	10.1	1	2	-0.80	3.48	STR	0.64		
		22	1	-0.03	2.26	631, 632	0.16		
		22	2	-0.12	2.84		0.17		
		23	1	-0.02	2.17		0.16		
		23	2	-0.13	2.91		0.16		
		3	2	-0.97	3.80		0.80		
155/2	10.8	1	1	-0.24	2.55	STR	0.56		
		1	2	-0.96	3.78	631, 632	0.63		
		22	2	-0.25	3.75		0.07		
		23	2	-0.23	3.61		0.03		
		3	1	-0.02	2.05		0.29		
		3	2	-0.99	3.83		0.65		
156/3	11.3	1	1	-0.17	2.39		0.53		
		1	2	-0.68	3.26		0.73		
		22	1	-0.05	2.43		0.17		
		22	2	-0.11	2.77		0.17		
		23	1	-0.03	2.26		0.19		
		23	2	-0.06	2.42		0.09		
		3	2	-0.62	3.15		0.56		
157/4	11.1	1	1	-0.25	2.58		0.22		
		1	2	-0.73	3.35		0.33		
		22	2	-0.19	3.33		0.00		
		23	2	-0.17	3.19		0.03		
		3	2	-0.81	3.50		0.03		
		3	3	-0.09	2.18		0.75		
158/5	10.8	1	2	-0.72	3.33		0.63		
		22	1	-0.06	2.52		0.21		
		22	2	-0.11	2.77		0.15		
		23	1	-0.02	2.17		0.16		
		23	2	-0.08	2.56		0.11		
		3	2	-0.68	3.26		0.68		
159/6	10.6	1	2	-1.27	4.35		0.68		
		22	2	-0.21	3.47		0.03		
		23	2	-0.22	3.54		0.02		
		3	2	-1.05	3.94		0.73		

ORIGINAL PAGE IS
OF POOR QUALITY

Table 10-9 (continued)

Orbit	Temperature, °C	Data Set	Band	Recorded DCC Violations		Calibration Orbits	Recalibrated DCC Values		Remaining Violations
				DCC	Percent		DCC	Percent	
160/7	11.3	1	2	-0.73	3.35		0.76		
		22	1	-0.02	2.17		0.17		
		22	2	-0.09	2.63		0.13		
		23	1	-0.04	2.35		0.19		
		23	2	-0.09	2.63		0.12		
		3	2	-0.57	3.06		0.48		
161/8	10.1	1	1	-0.23	2.53		0.03		
		1	2	-1.14	4.11		0.61		
		22	2	-0.26	3.82		0.07		
		23	2	-0.24	3.68		0.03		
		3	2	-1.03	3.91		0.60		
633/1	15.9	22	1	-0.02	2.17	STR 633, 634	0.23		
		23	1	-0.07	2.61		0.16		
634/2	15.9	1	1	-0.03	2.26	STR 633, 634	0.81		
635/7	14.9	22	1	-0.03	2.26		0.18		
		23	1	-0.02	2.17		0.16		
204/1	20.9	22	2	-0.03	2.21	204, 205	0.28		
		23	2	-0.06	2.42		0.23		
206/3	20.2	22	2	-0.02	2.14		0.24		
		23	2	-0.11	2.77		0.17		
208/5	20.7	22	1	-0.00	2.00		0.17		
		22	2	-0.01	2.07		0.24		
		23	2	-0.09	2.63		0.21		
209/6	20.7	1	2	-0.01	2.02		0.35		
210/7	20.7	23	2	-0.09	2.63		0.20		

ORIGINAL PAGE IS
OF POOR QUALITY

data collection there was only one DCC specification violation during the initial 20°C plateau but multiple violation on the second and third 20° plateaus. By using orbits 204 and 205 from the final 20°C temperature plateau, DCC violations were eliminated from the final 20°C plateau and only one minor occurrence was present in the second 20°C plateau. A likely hypothesis for the multiple violations on the first plateau is the ambient to vacuum shift which has occurred on all MSS instruments. This shift is characterized by a changing of gains and channel calibrations going into and out of vacuum. Settling time constants of this process are on the order of a day or perhaps several days. Apparently, at the time of initial calibration, when the system had been in hard vacuum, 10^{-5} Torr, for about 12 hours, sufficient changes were still taking place in the internal calibration system to cause DCC to be out of specification by the time the system was returned to 20°C 2 days later at orbit 133. The truth of the hypothesis that the internal calibration system is changing as a result of the change from ambient to vacuum environment and not merely drifting with time is evidenced by the fact that better DCC performance was obtained from the instrument at the second 20°C plateau by using calibration data from the third 20°C plateau 5 days later than by using the initial 20°C calibration.

Table 10-10 summarized the out-of-specification DCC conditions by band and temperature before and after the recalibration exercise discussed above. The large majority of DCC specification violations occurred in bands 1 and 2 before recalibration, and all of them were confined to bands 1 and 2 after recalibration. The number of violations was reduced from 200 to 16 as a result of recalibration. Of the 16 violations remaining after recalibration, 10 are thought to be related to the long settling time constant of the internal calibration system when it goes from an ambient to a vacuum environment. To achieve the specified DCC performance of the F-1 instrument it will be necessary to calibrate the instrument at its operating temperature and probably make minor adjustments to the calibration once the instrument has stabilized in a vacuum environment.

10.4.4.3 Deviation Band-to-Band (DBB) Performance

The DBB parameter effectively measures relative changes in the apparent band average radiance of the collimator over all four bands. As with DCC, it is ideally zero,

TABLE 10-10. F-1 DCC VIOLATIONS BY BAND AND TEMPERATURE

Baseplate Temperature, °C	Real Time Data Reduction					Re-reduction With Calibration at Temperature				
	Band 1	Band 2	Band 3	Band 4	Total	Band 1	Band 2	Band 3	Band 4	Total
5	19	31	7	4	61	0	0	0	0	0
10	19	46	2	0	67	0	3	0	0	3
15	5	0	0	0	5	0	0	0	0	0
20	4	11	0	0	15	6	4	0	0	10
30	2	35	0	0	37	1	0	0	0	1
32	3	12	0	0	15	1	1	0	0	2
Total	52	135	9	4	200	8	8	0	0	16

ORIGINAL PAGE IS
OF POOR QUALITY

but nonzero values can be expected, if only because of statistical uncertainties in the measurement process. Of course, nonzero values may also be due to real changes in either the collimator or the scanner itself. (Refer to 6.4.2 for detailed explanation on DBB algorithm).

Only three DBB out-of-specifications occurred during the active F-1 system testing period. The out-of-specification DBB happened in EMI at 13 kHz mode A, 9.6 and 12 kHz, mode B. Cause of the violations is still unknown at this time.

10.5 MODULATION TRANSFER FUNCTION (MTF)

10.5.1 Introduction

The modulation transfer function provides an estimate of the spatial frequency response of the MSS system. The function used here is more precisely the square wave response (SWR) of the system, since it is the system response to a square wave input. The square wave radiant input to the scanner results from the use of several rectilinear reticle patterns in the collimator. The reticle pattern spacings correspond to half-cycle (spatial) wavelengths of 236, 450, and 650 feet as measured at the earth's surface. Only the pattern corresponding to 236 feet is subject to the system specification, which states that the square wave response (here MTF) of the instrument at a spatial half-wavelength of 236 feet must be greater than 0.36, for temperatures between 10° and 30°C. The responses may be degraded by 20 percent at temperature extremes of 5° and 35°C. The algorithm developed for making estimates of this parameter is given in 6.4.3. For historical reason, we shall continue to refer to this parameter as the MTF.

The MTF model description is presented in 7.5.2. This section presents the results of the MTF measurements made on the MSS-D flight model (F-1) scanner throughout acceptance testing.

10.5.2 F-1 MTF Measurements

The results of MTF measurements made on the MSS-D F-1 are presented in Figure 10-22. The figure provides the history of MTF performance for all channels in each of the four bands. These plots present all the MTF data taken during regular acceptance testing; data taken during STRs are not shown.

A review of the figure reveals the following features:

1) All of the channels in any given band exhibit the same relative MTF behavior as a function of environment. The significant difference between channels in a band is the spread in measured values. The large spread of MTF values in bands 2 and 3 (Figures 10-21b and c) disappears at serial orbit 13 and beyond.

2) Once the system is in thermal-vacuum testing, the MTF performance is relatively stable and repeatable at the temperature plateaus. It is evident immediately that the temperature dependence for F-1 is different from that for the protoflight when the MTF increases going from system temperatures of 20° to 32°C (serial orbits 42 and 43).

ORIGINAL PAGE IS
OF POOR QUALITY

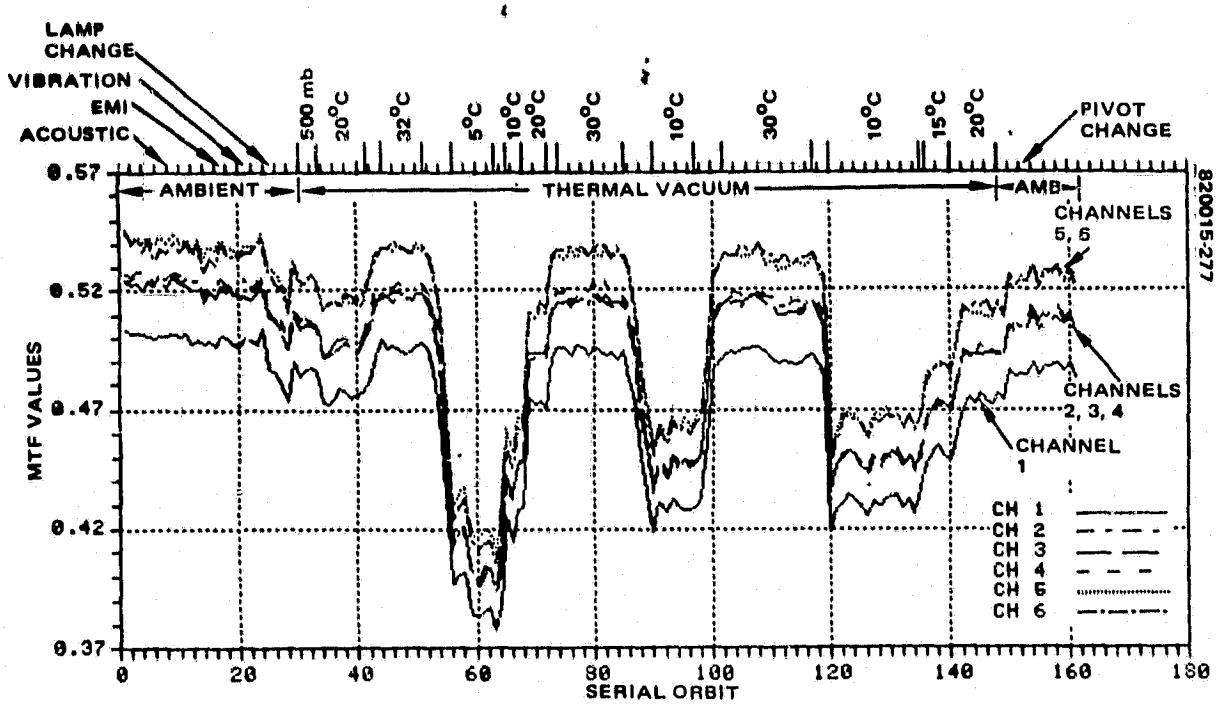

a) BAND 1

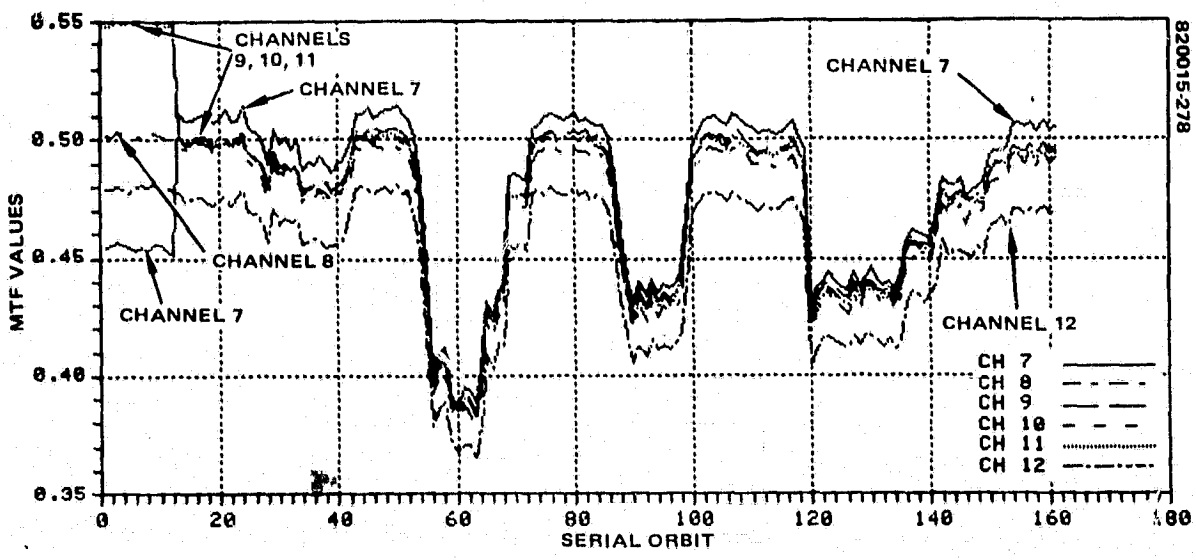

b) BAND 2

FIGURE 10-22. F-1 MTF PERFORMANCE

ORIGINAL PAGE IS
OF POOR QUALITY

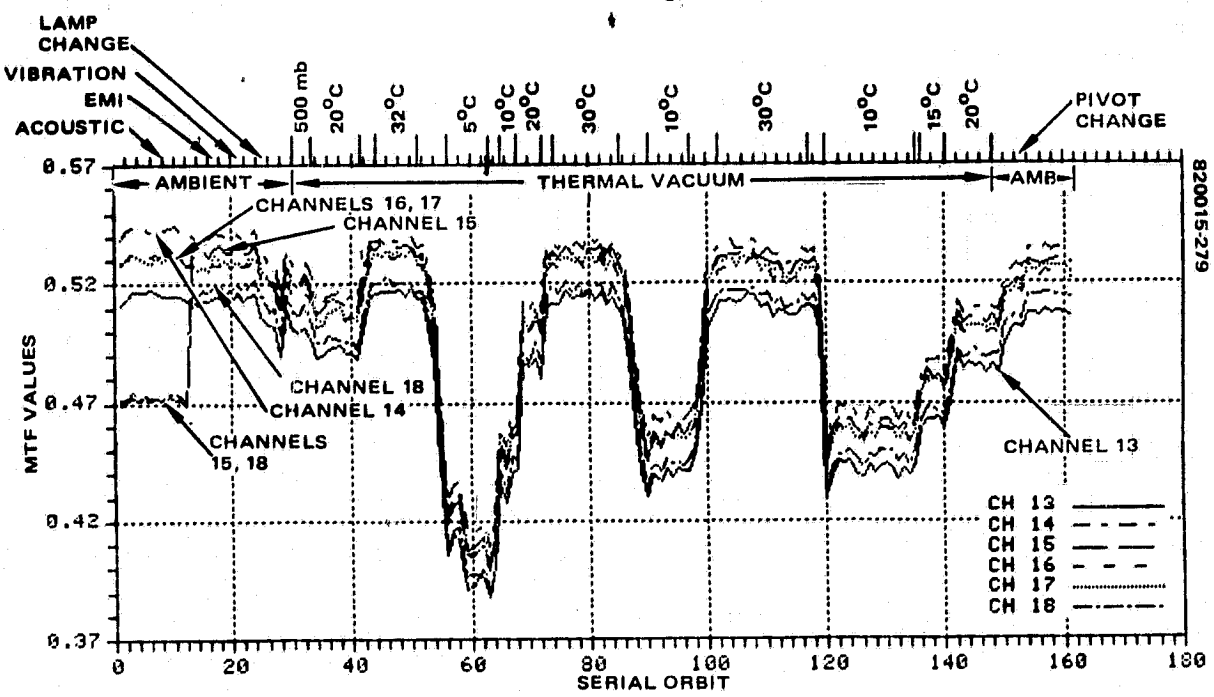

c) BAND 3

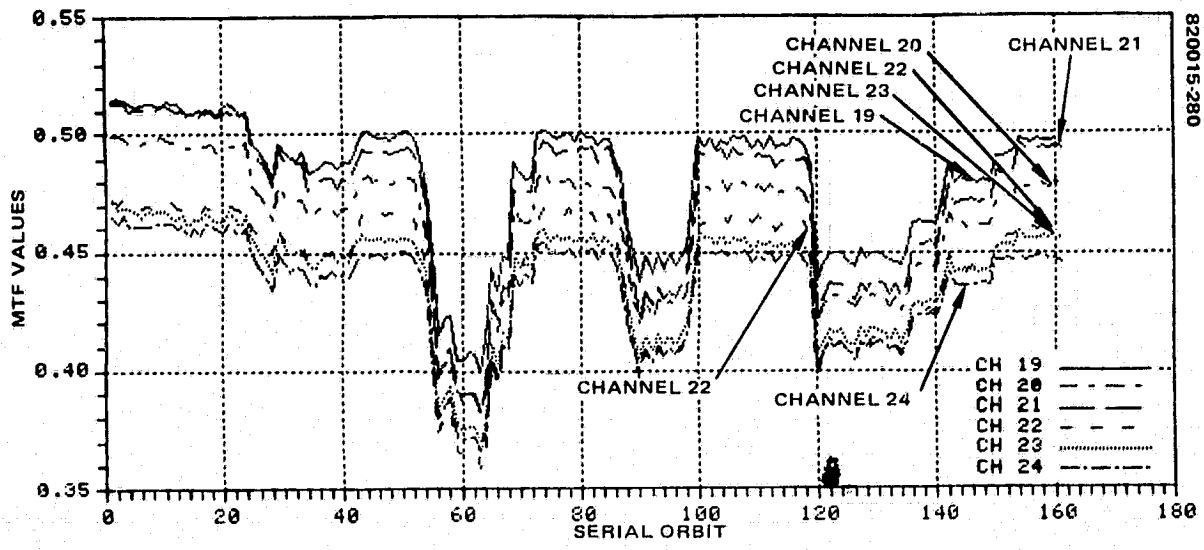

d) BAND 4

FIGURE 10-22 (CONTINUED). F-1 MTF PERFORMANCE

ORIGINAL PAGE IS
OF POOR QUALITY

3) Some change in MTF for all channels in a band occurs going into, and coming out of, vacuum. This change affects the bands differently from the effect of pressure environment change on gains (vacuum shift) (see 10.4.3). This change on entering vacuum is also different from the effect of pressure change on the protoflight. There, MTFs in all bands increased significantly. Here, the MTF change is a slight decrease (see 7.5 for the protoflight MTF discussion).

The following discussion provides a step-by-step explanation of the important features of these data. When the data represent behavior of the system that is typical of a group of data values (e.g., the MTFs for all channels, a subset of all channels in a given band at a specific test environment) we refer to the nominal performance of that group for that condition. Any anomalous behavior (i.e., behavior not characteristic of the group) is discussed separately.

The nominal values of the MTF for each band, as well as the range of the spread of MTF for the channels of each band, are given in Table 10-11 at the end of this subsection.

10.5.2.1 Anomalous MTF Behavior

Since the anomalous MTF behavior occurred during early acceptance testing of the MSS-D F-1 system, these results are discussed first.

During the first long form performance test and the postacoustic testing (serial orbits 1 through 12) several channels in bands 2 and 3 were seen to have anomalously high (and low) MTF values. This is clearly evident in Figure 10-22b in which channels 9, 10, and 11 have MTF much higher than channels 8 and 12. The MTFs for these channels are 10 percent higher than the MTF for channel 8, which is nominal for the band with a value of 0.500. The MTF for channel 7 is 9 percent lower than that for channel 8.

The MTFs for band 3 are plotted in Figure 10-22c. In this band, for these early orbits channels 15 and 18 are 9.5 percent lower than channels 16 and 17, which are nominal for the remainder of the channels in band 3 at a value of 0.525.

These data were suggestive of problems similar to those observed on the MSS-D protoflight (channel 14, high; channel 21, low), which eventually was traced to improper values of capacitors installed on buffer boards which form a part of the Butterworth filter. Subsequent engineering investigation led to direct measurement of the values of the F-1 capacitors installed in boards A1A3 and A1A4 corresponding to the anomalous channels. It was discovered that incorrect values of these capacitors had been installed. Capacitors with the correct values were installed and, as evident from the remaining plot history, the MTFs for these channels with anomalous MTFs were brought closer to the nominal values for the other channels in the respective bands.

For example, in band 2, channel 7 which was 9.0 percent lower than channel 8 became about 2 percent higher, and channels 9, 10, 11 were corrected from 10 percent higher to within 1 percent of channel 8 (Figure 10-22b). Channels 15, 18 of band 3 went from 9.5 percent lower than nominal to falling well within the nominal MTF for that band. (Figure 10-22c.)

ORIGINAL PAGE IS
OF POOR QUALITY

TABLE 10-11. F-1 ACCEPTANCE TEST MTF PERFORMANCE SUMMARY

Date	Test Event, Remarks	Nominal MTFs				MTF Range			
		Band 1	Band 2	Band 3	Band 4	Band 1	Band 2	Band 3	Band 4
7/31/81	LFPT orbits 35 to 42; nominal temperature 24°C	0.526	0.520	0.505	0.475	0.500 to 0.543	0.452 to 0.561	0.470 to 0.542	0.465 to 0.515
8/05/81	Post-acoustic; orbits 45 to 48; nominal temperature 24°C	0.526	0.520	0.505	0.475	0.500 to 0.543	0.452 to 0.561	0.470 to 0.542	0.465 to 0.515
8/07/81	Replaced capacitors in boards A1A3 and A1A4 which correspond to channels 7, 9, 10, 11, 15, and 18								
8/14/81	Pre-EMI; orbits 49 to 52; nominal temperature 24°C	0.525	0.500	0.525	0.480	0.498 to 0.540	0.475 to 0.512	0.512 to 0.541	0.460 to 0.513
8/21/81	Post-EMI; orbits 69 to 72 nominal temperature 24°C	0.525	0.500	0.525	0.481	0.498 to 0.540	0.474 to 0.515	0.513 to 0.540	0.460 to 0.514
8/26/81	Post-vibration; orbits 76 to 79; nominal temperature 24°C	0.525	0.500	0.526	0.480	0.499 to 0.543	0.474 to 0.510	0.513 to 0.543	0.460 to 0.515
8/27/81	Old visible source replaced with new 150 W source								
8/28/81; 8/29/81; 9/04/81; 9/05/81	Realignment and refocus of collimator								
9/08/81	Endbell; (on floor) orbits 86 to 89; 25°C	0.515	0.485	0.515	0.465	0.475 to 0.530	0.460 to 0.505	0.490 to 0.535	0.436 to 0.495
9/10/81	GN_2 backfill; orbits 90 to 93; 25°C	0.515	0.488	0.514	0.465	0.486 to 0.526	0.465 to 0.501	0.499 to 0.528	0.441 to 0.495
9/11/81	Thermal-vacuum orbits 98 to 105; 20°C	0.505	0.480	0.508	0.452	0.490 to 0.515	0.455 to 0.490	0.488 to 0.515	0.435 to 0.487
9/12/81	Orbits 108 to 115; 32°C	0.525	0.500	0.526	0.475	0.490 to 0.540	0.476 to 0.513	0.515 to 0.540	0.449 to 0.501
9/13/81	Orbits 120 to 129; 5°C	0.400	0.390	0.413	0.385	0.380 to 0.436	0.365 to 0.417	0.388 to 0.437	0.360 to 0.425
9/17/81	Orbits 166 to 181; 30°C	0.525	0.500	0.525	0.475	0.490 to 0.540	0.473 to 0.510	0.510 to 0.536	0.443 to 0.500

ORIGINAL PAGE IS
OF POOR QUALITY

Table 10-11 (continued)

Date	Test Event, Remarks	Nominal MTFs				MTF Range			
		Band 1	Band 2	Band 3	Band 4	Band 1	Band 2	Band 3	Band 4
9/18/81	Orbits 186 to 201; 10°C	0.450	0.435	0.460	0.425	0.420 to 0.465	0.405 to 0.441	0.436 to 0.470	0.398 to 0.450
9/19/81	Orbits 633 to 636; 15°C	0.474	0.455	0.475	0.430	0.450 to 0.487	0.432 to 0.461	0.462 to 0.486	0.423 to 0.465
9/19/81	Orbits 204 to 211; 20°C	0.500	0.475	0.500	0.450	0.473 to 0.513	0.450 to 0.485	0.485 to 0.514	0.435 to 0.489
9/21/81	Post-thermal-vacuum; orbits 212 to 215; 22°C	0.513	0.485	0.515	0.460	0.485 to 0.525	0.463 to 0.498	0.495 to 0.528	0.447 to 0.490
9/23/81	Flex pivot changeout								
10/12/81, 10/13/81	Final LFPT, orbits 231 to 238; 24°C	0.515	0.497	0.525	0.475	0.486 to 0.530	0.470 to 0.510	0.510 to 0.535	0.448 to 0.500

10.5.2.2 Nominal MTF Performance

No significant changes of the MTF values occurred after EMI and vibration tests, indicating that the flight system MTF performance was not affected by these environmental exposures.

There was a drop in the MTF values (2 to 3 percent) during the short form test (endbell serial orbits 25 through 28), prior to GN_2 backfill. This drop was probably due to the realignment and refocusing done on the collimator after the visible source changeout. The old visible source was replaced with a new 150 watt source since the old source had neared its expected end of life and might fail during the thermal-vacuum test. A series of realignments and refocusing of the collimator was then performed. For purposes of comparison, the endbell MTF values (serial orbits 25 through 28) will be used as a baseline after the visible source changeout.

During the GN_2 backfill (serial orbits 30 through 33) the MTF in all bands changed very slightly, or there was no change at all. Going into vacuum (20°C), the MTF went down: bands 1 and 2 dropped 2 percent, band 3 dropped 1 percent, and band 4 dropped 3 percent. The shift is due to the temperature change in going from 25° to 20°C. This hypothesis is substantiated by the plot of nominal MTFs versus temperature (for thermal-vacuum orbits) given in Figure 10-23. The MTF behavior was good throughout the thermal-vacuum tests. The values are repeatable at 30° and 10°C. However, there is a difference between the MTF values taken at 20°C during start of thermal-vacuum and those taken at 20°C at the end of thermal-vacuum. The latter values are lower: bands 1 and 2 down by 2 percent, band 3 down by 1 percent, and band 4 down by 3 percent.

ORIGINAL PAGE IS
OF POOR QUALITY

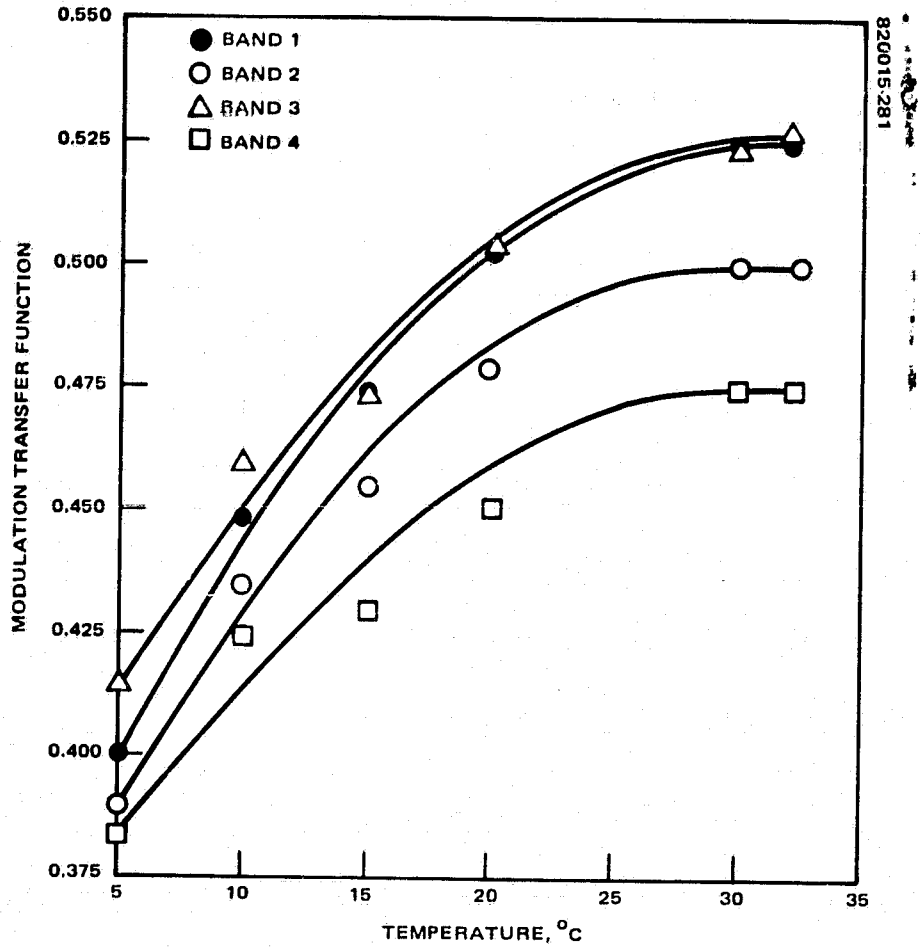

FIGURE 10-23. NOMINAL MTFs VERSUS TEMPERATURE

ORIGINAL PAGE IS
OF POOR QUALITY

In constructing Figure 10-23, the mean values of the 20°C (start thermal-vacuum and end thermal-vacuum) MTF nominals were used. The plot illustrates the MTF behavior throughout thermal-vacuum test and suggests that the system is focused around 30°C.

A comparison between the baseline (endbell) and the post-thermal-vacuum orbits shows that the MTF values are only very slightly different, implying that the exposure of the scanner system to the thermal-vacuum environment did not adversely affect the MTF performance.

After the thermal-vacuum test, the flex pivots were replaced. This operation required that the scan mirror assembly be removed from the scanner. After the flex pivot changeout and scanner reassembly, the system alignment procedure was conducted before the final long form performance test. The MTF values during the final LFPT are different from (in this case, higher) those taken at baseline (endbell).

The F-1 scanner met the MTF specification throughout acceptance testing. Table 10-11 provides a chronological survey of the nominal MTF performances. The range of MTF values for each band is given as well as the nominal values for each major event in the test sequence.

10.6 SCAN PRECISION PARAMETERS

10.6.1 Introduction

The parameters used to evaluate MSS-D scan precision performance are mean line length (MLL), line length variation (VLL), scan repeatability (SRO), and cross-axis repeatability (CXAXO). A discussion of the meaning of these parameters and a description of the algorithms used to compute the measured values of the parameters during testing is given in 6.4.4 and 6.4.5.

This section presents the scan precision performance of the MSS-D F-1 throughout system testing. Each parameter is treated in terms of the effect on the MSS-D F-1 system of the test environment. A summary description of nominal performance, deviation from nominal behavior, data variability, and estimated effects of test environment are given. Anomalous behavior is highlighted, and its potential causes discussed.

10.6.2 Mean Line Length (MLL)

The mean line length, or more accurately, the mean active scan period, is a parameter that is not directly the subject of a system specification. It is indirectly specified by the requirement that the active scan period for each of the individual scans of the 100 scans used in constructing the average mean value lies within the interval from 31.5 to 34.0 ms. Throughout system test this performance parameter was monitored to determine whether the scanner was meeting specification. The maximum scan period, LL_{MAX}, and the minimum scan period, LL_{MIN}, were displayed in the computer printouts and checked to ensure that these values were within the specified limits. The specification is met if $31.5 \text{ ms} \leq LL_{MIN}$ and $LL_{MAX} \leq 34$ ms. It is necesary, but not sufficient, for meeting the specification that the MLL fall within the specified interval.

ORIGINAL PAGE IS
OF POOR QUALITY

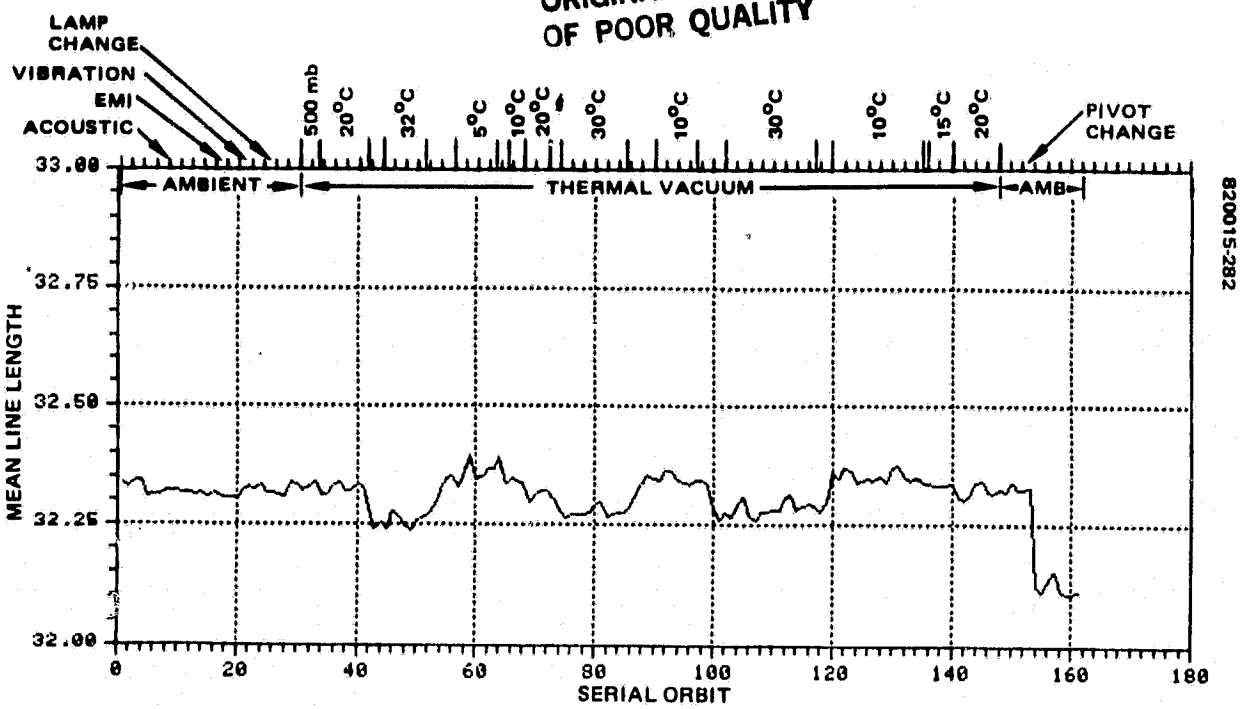

FIGURE 10-24. F-1 MEAN LINE LENGTH PERFORMANCE

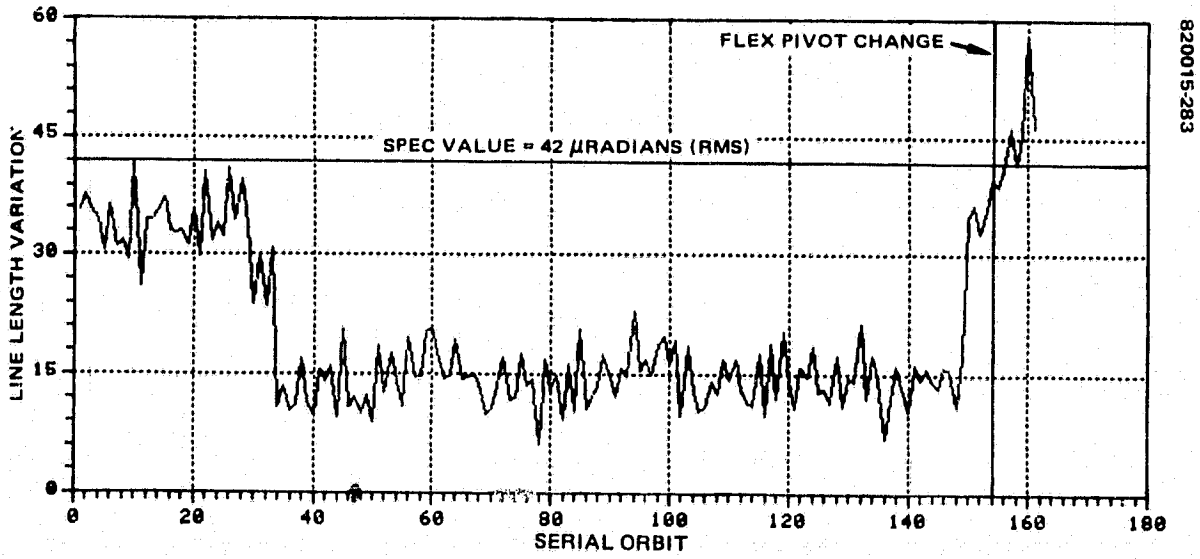

FIGURE 10-25. F-1 LINE LENGTH VARIATION (VLL) PERFORMANCE

ORIGINAL PAGE IS
OF POOR QUALITY

Figure 10-24 provides the values of MLL obtained during F-1 testing. The specification values of LL_{MAX} and LL_{MIN} fall outside the range of the graph. During testing, the measured line length values differed from the MLL values at most in the second decimal place. Thus, it is clear from the MLL values shown in Figure 10-24 that the maximum and minimum values of the individual line lengths did not exceed the specification value at any time during system test.

The abrupt change in MLL which occurs at serial orbit 154 is the result of the removal and replacement of the bumpers during flex pivot changeout following thermal-vacuum testing. The entire range of variation of MLL is less than 1 percent, and is approximately half this value for the initial flex pivot and bumper configuration. Its variation at any given environment is less than 0.2 percent. From the plot it is just barely apparent the the MLL behavior is negatively correlated with temperature, having its largest values at 5°C and lowest at 32°C. The value of MLL goes from 32.24 at 32°C to 32.39 at 5°C prior to the flex pivot changeout. Repeatability on return to temperature appears to be within normal data variability.

The temperature correlation of the MLL is consistent with effect of temperature on bumper coefficient-of-restitution and its concomitant overall effect on scanner "spring constant." That is, as the temperature lowers, the bumper becomes quicker; i.e., the turnaround time at the bumper becomes shorter. Then, since the total round trip of the scan mirror is held constant by the loop dynamics, the active scan period is increased to account for the quicker bumper turnarounds. The effect of temperature on MLL was more evident in the protoflight scanner than on the F-1 scanner.

In summary, the MLL performance of the MSS-D F-1 was predictable and within specification.

10.6.3 Line Length Variation (VLL)

The line length (or, more accurately, active scan period) variation is a measure of the rms scan-to-scan variation in the active scan period. The algorithm used to describe this parameter is given in 6.4.4. Since the definition of VLL involves normalization by MLL, and since the VLL is a function defined on the same parameter values as MLL, the values of these parameters are related. However, as shown in 10.6.2, MLL varies only slightly, so the effect on VLL of MLL changes was minimal for F-1.

The VLL performance history for F-1 is shown in Figure 10-25. The plot gives serially the VLL values measured at each of the standard orbits of system testing. The system was within the 42 μrad (rms) specification throughout all of system testing prior to flex pivot changeout, as indicated by the graph. The only occasion for which the system with the original flex pivots indicated VLL values greater than 42 μrad was during multiplexer integration. This behavior was discovered initially by the appearance of unusual values of the old MTF, MTFO, which is line length sensitive as indicated in 6.4.4. These data were rerun against the VLL algorithm (D.S. #0) and indicated larger than specification values. Engineering investigation failed to isolate the cause, and subsequent examination of the scan mechanism and electronics did not indicate any problem with the system. Attempts to induce the problem in additional tests were unsuccessful. The problem did not occur again throughout the remainder of testing.

ORIGINAL PAGE IS
OF POOR QUALITY

TABLE 10-12. EVENTS SURROUNDING VLL ANOMALY

Event	Date	VLL	Sequential Orbit	Serial Orbit
Post-thermal-vacuum ASPT	9/21/81	OK	212 to 215	150 to 153
Post-thermal-vacuum calibration	9/22/81	OK	216 to 219	–
Remove SMA for flex pivot change	9/23/81	N/A		
Ran postflex pivot calibration	10/1/81	Higher mean and larger σ than 1 and 2	220 to 224	–
Ran STR 35, 2 orbits to establish baseline going into acoustic test	10/6/81	Similar to step 4	735 to 736	–
Acoustic test	10/7/81	N/A		
Ran post-acoustic system calibration	10/9/81	Similar to step 4	225 to 228	–
Ran CSPT	10/12/81 and 10/13/81	High, trending up, very noisy	231 to 238	154 to 161
Ran mass properties	10/14/81	N/A		
Ran STR 38, investigate VLL as function of configuration in clean tent	10/14/81 and 10/15/81	High in all configurations	STR 38	–
STR 41, inspect pivots, check mechanical configuration, Ran electrical tests	10/19/81	High, but non-standard configuration	STR 41	–
STR 42, 24-hr run of system with periodic VLL checks	10/20/81 and 10/21/81	VLL OK	STR 42	–

Following EMI testing, during which the levels of induced susceptibility of VLL to EMI were measured, the MSS-D F-1 scanner was subjected to an acoustic test and sinusoidal vibration testing. No effect of these environments was evident in VLL performance. The remainder of performance with these flex pivots up to sequential orbit 231 (serial orbit 154) is shown in Figure 10-25. As indicated in the figure, VLL is sensitive to changes in the ambient pressure environment. On the floor prior to endbell installation, the VLL value was aproximately 32 μrads with local deviations of ±2 μrad. With F-1 installed on the endbell and prior to intial GN_2 backfill, the VLL value increased to 35 ±4 μrad. This is believed to have been due to a change in the test configuration vibration environment. On backfill with gaseous nitrogen (GN_2) to a pressure of 0.5 atmosphere, VLL dropped to approximately 26 μrad ±4 μrad. On further decrease in pressure during pumpdown to 10^{-5} Torr, VLL dropped to approximately 15 ±5 μrad. The change of VLL as a result of pressure environment is attributed to the effects of turbulent wind loading on the scanning mirror, and the absence of this effect in vacuum. It should be noted that on venting to ambient pressure following the completion of thermal-vacuum testing, VLL returned to the value measured prior to thermal-vacuum testing (serial orbits 150 through 153).

ORIGINAL PAGE IS
OF POOR QUALITY

During thermal-vacuum testing, the VLL was consistently within specification and varied from 10 to 20 μrads. Some negative correlation of VLL with temperature (in vacuum) seemed evident which can be summarized as follows:

$$10\ \mu\text{rad} \leq \text{VLL} \leq 15\ \mu\text{rad at } 30^{\circ}\text{C}$$

$$15\ \mu\text{rad} \leq \text{VLL} \leq 20\ \mu\text{rad at } 5^{\circ}\text{C}$$

During the final complete system performance test (CSPT) following flex pivot changeout and prior to shipment of the MSS-D F-1 system to General Electric (serial orbits 154 through 161), VLL became progressively larger and eventually exceeded specification. This is clearly evident in Figure 10-25. An investigation was instituted to determine the cause of these anomalously high line length variations.

The sequence of events surrounding this investigation was as follows: The system completed thermal-vacuum testing; VLL data looked normal on the endbell and during the subsequent system calibration run in the clean tent in the S1 test area. The first two points of Figure 10-26 were from data taken during the calibration run. All of the data shown were rereduced from 28 track tape. Multiple VLL data sets were run from the recorded data to get a statistical sample of points at each test where VLL is extracted. Table 10-12 gives a chronology of the events thought to be relevant to the VLL anomaly that took place from the end of the thermal-vacuum testing until the end of testing at Hughes. After the post-thermal-vacuum radiometric calibration (sequential orbits 218 and 219 of Figure 10-26), the scan mirror assembly was removed and sent to Culver City for flex pivot changeout. Following the changeout of the flex pivots the average VLL in the data went up by a few microradians and the 1σ spread increased by about 2 μrad (orbits 222, 224, 735, and 736). The acoustic test was completed and the radiometric calibration following (orbits 227 and 228) looked similar to those prior to the acoustic test. The CSPT following (sequential orbits 231-238) was the test which exhibited the out-of-specification conditions. These data displayed even higher 1σ noise values and showed definite trend upward over the eight orbits of the test. Following the CSPT the system underwent mass properties tests, after which a series of special tests (STRs) were begun.

The first STR in the series, STR 38, was run varying the configuration and orientation of the system in the clean tent. The variables were aperture cover on and off, filter bank blowers on and off, and rotational orientation changes of the collimator cart with respect to the filter bank. The data obtained are not given here, but showed no significant changes with any of these variables. Averages were running close to 40 μrad level and had 1σ's similar to the middle orbits of the CSPT. The next test run was STR 41 in which the mechanical and electrical configuration of the system was checked. The sunshield was removed. The flex pivots were examined, and the SMA was inspected for loose bolts, etc. Everything looked normal. The control signals within the scan mirror electronics were carefully examined for noise. No problems were found. Following the completion of STR 41, the sunshield was reinstalled and retorqued.

It was decided to perform a 24 hour run-in of the system to check out the hypothesis that the large line length variations were due to a run-in phenomenon of the scan mirror assembly bumper pads wearing in as a result of the changeout of flex pivots. STR 42 was initiated to perform the run-in. During this test MSS was on continuously for

ORIGINAL PAGE IS
OF POOR QUALITY

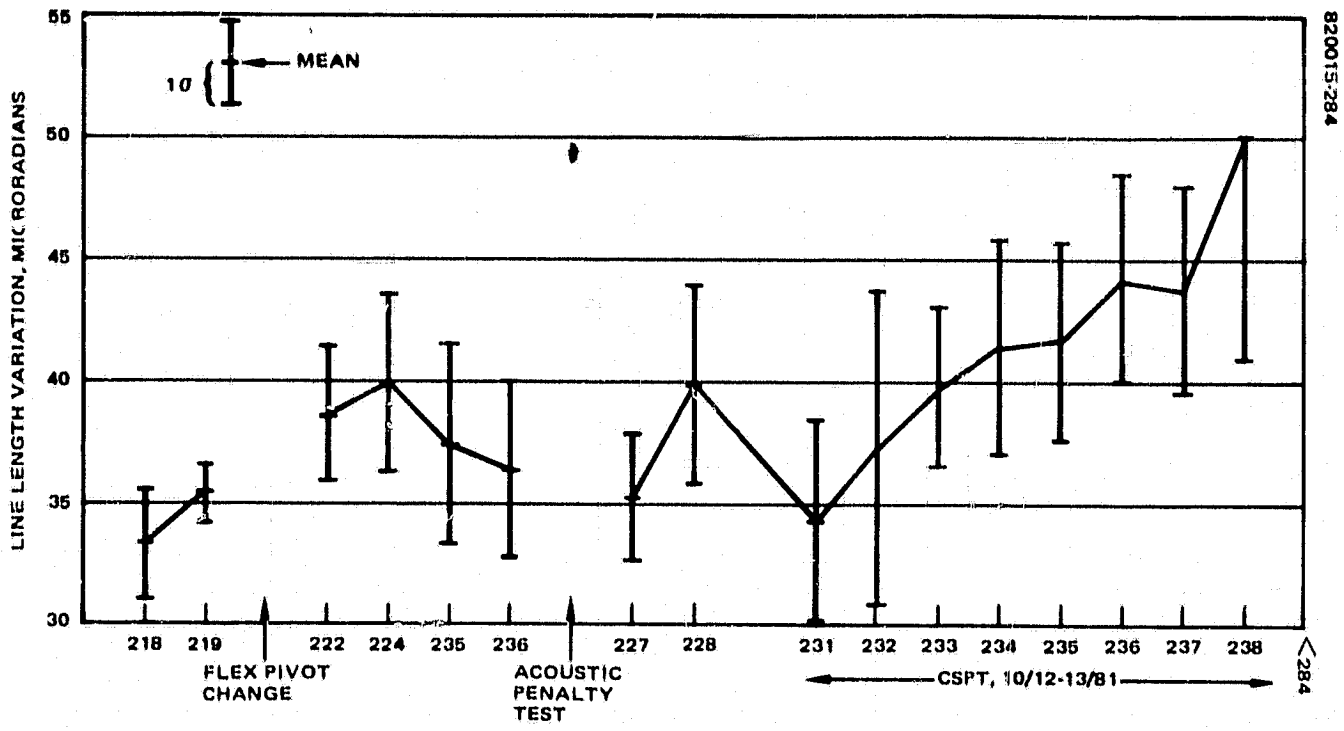

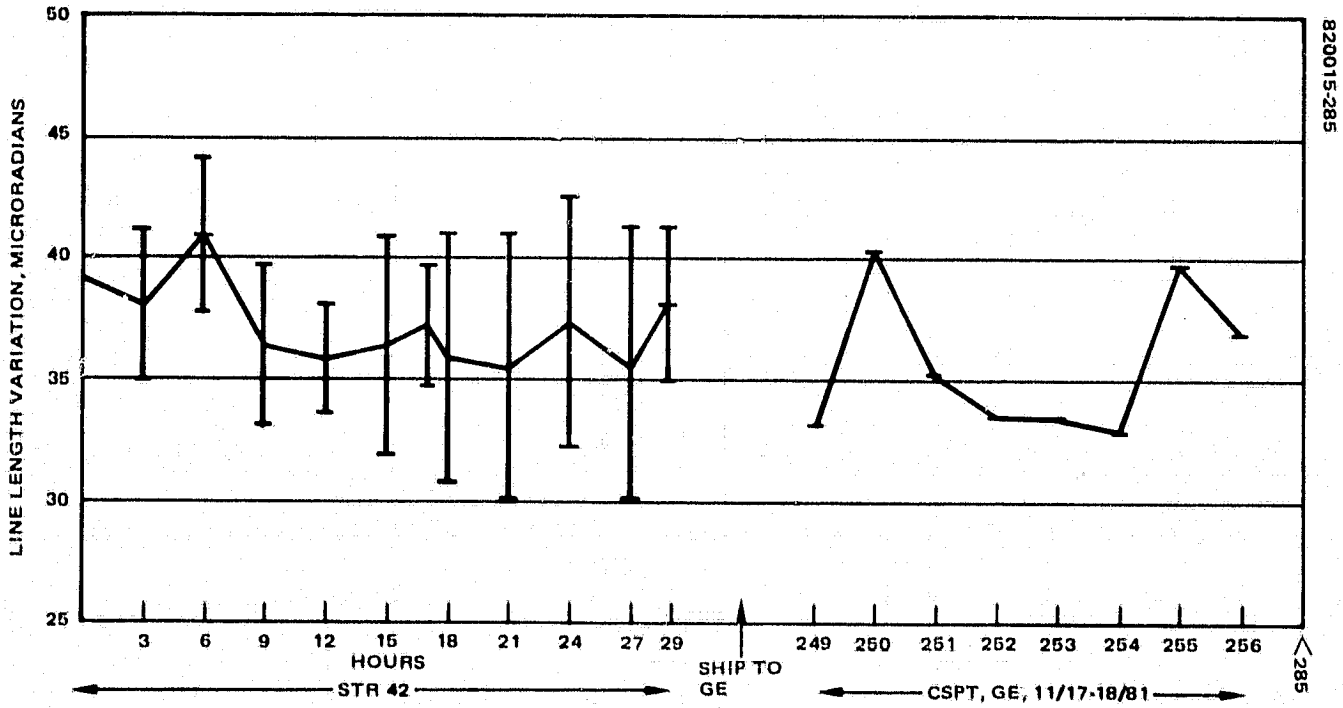

FIGURE 10-26. LINE LENGTH VARIATION HISTORY

ORIGINAL PAGE IS
OF POOR QUALITY

24 hours, and VLL data were collected every 3 hours. The results of this test are shown in Figure 10-26. The VLL points show a slight downward trend over the 24 hour period, but the significant drop in the average took place before the STR started.

Subsequent to STR 42, F-1 was sent to GE, and a CSPT was run there on November 17 and 18, 1981 to verify that the instrument arrived at GE without shipping damage. The results of that testing are presented in Figure 10-26 as well. The data points from GE show that VLL had similar characteristics to those from STR 42, similar means and standard deviations. The raw data from which Figure 10-26 were constructed is given in Table 10-13.

From the foregoing, the following conclusions can be drawn:

1) The cause of the VLL out-of-specification behavior during the CSPT following flex pivot changeout is unknown. A survey of the test history would indicate that the probable cause was a poorly mated electrical connector whose contact was improved as a result of the mating and demating which occurred during the anomaly investigation. A less likely, but possible, explanation is that the problem was mechanically induced and corrected as a result of disassembly and reassembly. The probelm has not recurred.

2) The VLL performance with the new flex pivots has only been measured at ambient pressure. The data indicate that the VLL will be, on the average, within specification. The performance data reveal, however, a significant standard deviation which indicates that during further measurements of VLL at ambient pressure occassional VLL values may exceed the 42 μrad specification. The drop in VLL, which is typical for both the F-1 and protoflight scanner, strongly suggests that the scanner will remain within specification in vacuum.

10.6.4 Scan Repeatability (SRO)

Scan repeatability is a parameter used to measure the ability of the scanner to repeatably (line-to-line) map after scaling out the line length variation of the along-scan position of a target in the scanner field of view. The time variation (scan-to-scan) in the measured value of the time from scan start (SMP 1) to a target (collimator generated video pulse) in the scanner field of view is used to make this estimate. SRO is specified to be less than or equal to 24 μrads. The algorithm used to compute SRO during MSS-D F-1 testing is discussed in 6.4.4.

The SRO performance of the MSS-D F-1 scanner is shown in Figure 10-27. At no time during system testing did the SRO exhibit anomalous behavior. Even during the STR's performed immediately following the VLL specification violations, which occurred after flex pivot changeout and discussed in 10.6.3, the SRO exhibited no associated anomalous behavior.

The measured values of SRO for the MSS-D F-1 were well within specification, nominally 3 to 6 μrad with occasional values of 6 to 12 μrad.

10.6.5 Cross-Axis Repeatability (CXAXO)

The cross-axis repeatability (CXAXO) algorithm and method of measuring cross-axis position using the chevron pattern are discussed in 6.4.5. Cross-axis repeatability is specified to be less than or equal to 33 μrad (rms).

ORIGINAL PAGE IS
OF POOR QUALITY

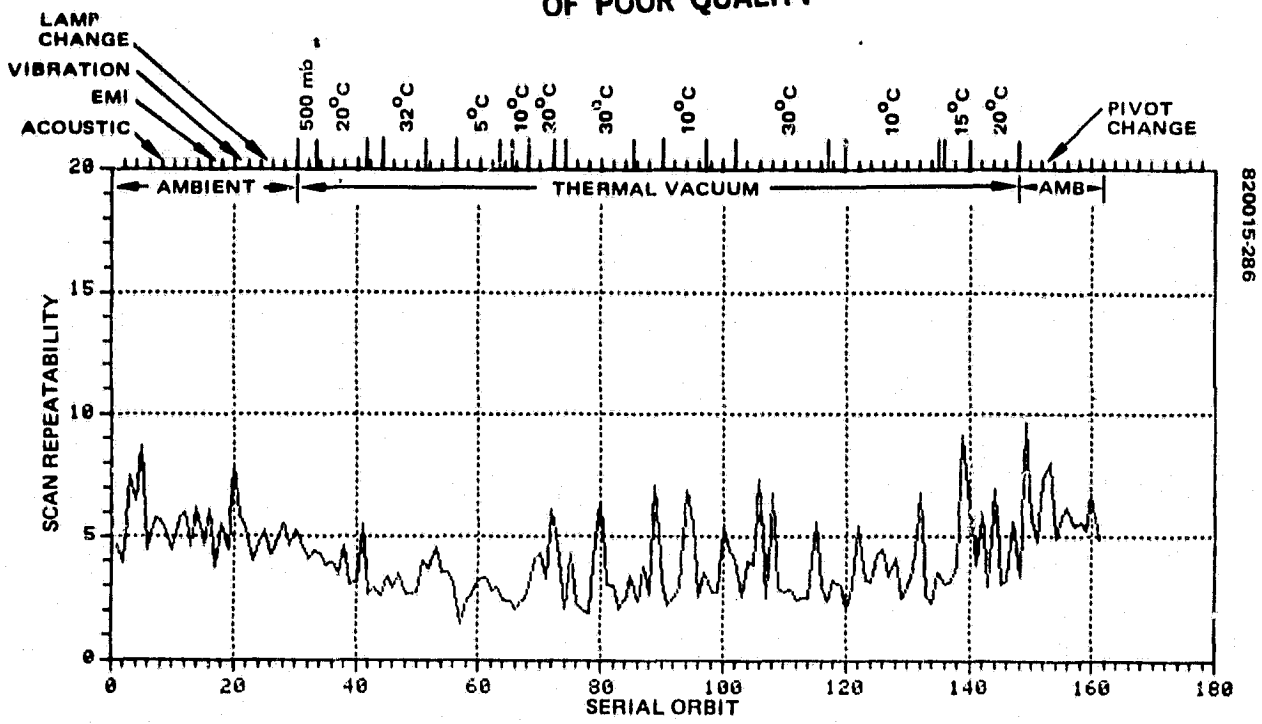

FIGURE 10-27. F-1 SCAN REPEATABILITY PERFORMANCE

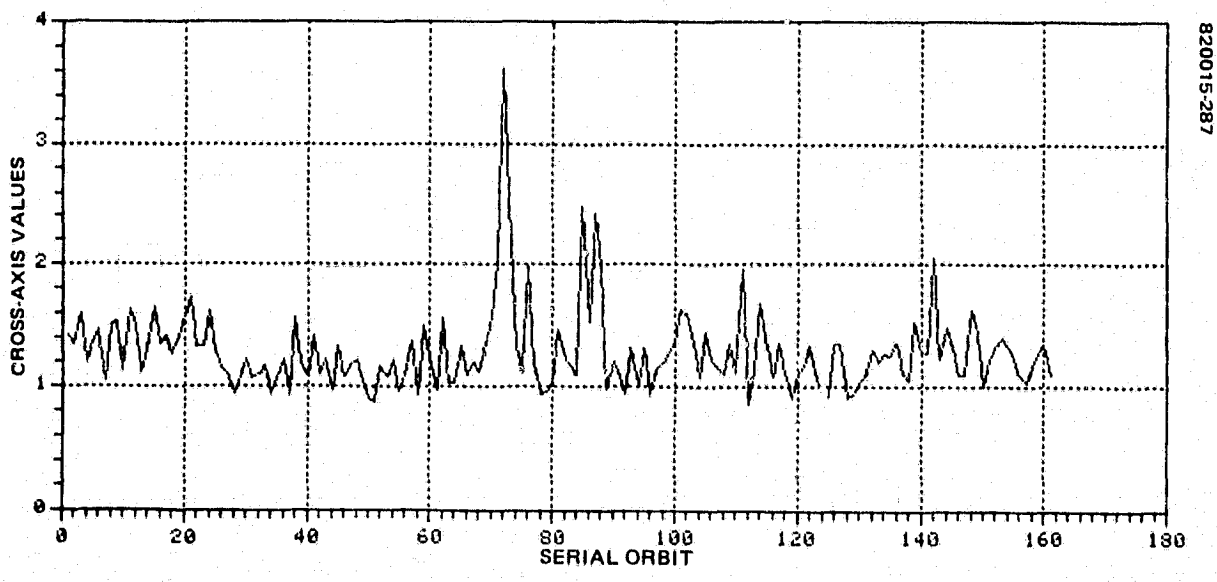

FIGURE 10-28. F-1 CROSS-AXIS REPEATABILITY PERFORMANCE

ORIGINAL PAGE IS
OF POOR QUALITY

During MSS-D F-1 testing the cross-axis performance was always well within specification. As shown in Figure 10-28, this parameter was consistently less than 2μrad. Exceptions to this occurred during temperature transitions in thermal-vacuum, when the measured values of cross-axis occasionally reached values of as much as 3.6 μrad, still well within specification. The sole out-of-specification value recorded for CXAXO throughout MSS-D F-1 testing was the result of a delayed line of data due to the absence of SMP 1 (not shown on plot) and not a true cross-axis problem.

TABLE 10-13. DATA USED TO GENERATE FIGURE 10-26

Test	Date	Orbit	VLL Values	Mean	Sigma
Post-thermal-vacuum calibration	9/22	218/15	29 2, 33.9, 35.7, 33.7, 32.7, 35.6, 33.4, 31.9	33.26	2.09
		219/16	36.3, 35.6, 36.0, 36.6, 34.4, 33.8	35.45	1.11
Post-flex pivot calibration	10/1	222/15	42.7, 39.3, 38.9, 37.8, 34.2, 40.6, 35.3, 39.6	38.55	2.76
		224/16	45 6, 38.6, 42.1, 42.5, 37.6, 41.9, 35.4, 36.0	39.96	3.60
Preacoustic STR for performance	10/5	735/1	39.9, 33.8, 34.4, 35.5, 43.5	37.42	4.15
		736/2	42.2, 32.3, 35.4, 35.7, 36.5	36.42	3.60
Post-acoustic calibration	10/9	227/15	32.2, 37.8, 35.9, 34.6, 46.1, 34.8, 33.3, 34.4	35.39	2.53
		228/16	40.2, 36.1, 40.3, 45.6, 38.1, 42.5, 43.1, 33.1	39.88	4.03
Post-acoustic CSPT	10/12	231/1	30.3, 39.4, 32.8, 31.2, 37.9	34.32	4.09
		232/2	48.0, 34.7, 30.9, 36.1, 36.3	37.2	6.41
		233/3	40.6, 44.6, 37.4, 39.8, 36.2	39.68	3.18
		234/4	45.3, 42.8, 38.7, 35.0, 44.8	41.32	4.39
		235/5	39.3, 46.5, 36.5, 41.0, 44.4	41.54	3.98
		236/6	40.8, 42.9, 45.3, 40.5, 51.0	44.10	4.31
		237/7	47.1, 42.1, 39.6, 49.3, 40.6	43.74	4.24
		238/8	46.8, 50.4, 38.3, 64.0, 51.0	50.10	9.28
Run-in test STR 42	10/20	10:30 am	37.2, 40.6, 39.7, 42.9, 35.8	39.24	2.8
		1:30 pm	41.0, 34.0, 39.9, 35.6, 39.7	38.04	3.05
		4:30 pm	43.7, 37.5, 40.6, 38.7, 44.5	41.00	3.05
		7:30 pm	38.8, 37.8, 31.7, 34.3, 39.7	36.46	3.36
		10:30 pm	35.1, 32.7, 38.6, 36.0, 36.8	35.84	2.18
	10/21	1:30 am	30.1, 33.5, 40.9, 39.1, 38.6	36.44	4.49
		3:30 am	37.8, 41.3, 34.8, 36.3, 36.4	37.32	2.47
		4:30 am	40.3, 29.1, 40.7, 32.1, 37.5	35.94	5.14
		7:30 am	35.3, 40.8, 34.0, 27.2, 40.2	35.5	5.51
		10:30 am	44.7, 38.9, 36.8, 30.4, 36.3	37.42	5.15
		1:30 pm	44.2, 30.0, 32.0, 33.3, 38.3	35.56	5.72
	OFF				
		3:30 pm	41.1, 39.2, 34.8, 34.6, 40.8	38.1	3.19

ORIGINAL PAGE IS
OF POOR QUALITY

11. FLIGHT MODEL PICTURE ANALYSIS

End-to-end evaluation of the MSS flight subsystem and ground equipment was performed by photographic reproduction of images viewed by the flight equipment. Two types of images were produced during the test program for evaluation purposes, the video processor image recorder (VPIR) pictures and the ground processing equipment (GPE) pictures.

The VPIR pictures, made with the video processor working in conjunction with the image recorder, were reproduced in near real time for quick look qualitative assessment of general system performance. Since the VPIR does not reproduce the data in an operational band-by-band format, its use was diagnostic and the flight subsystem performance assessment was confined to the GPE pictures.

The VPIR pictures were, however, very useful in surfacing system problems in a timely manner and in troubleshooting these problems. In particular, microphonics, intensity variations, and channel-to-channel gain variations were enhanced by the VPIR picture presentations. Anomalies associated with scan monitor pulses and line synchronization problems were also quickly diagnosed using VPIR pictures.

The ground processing equipment produces images in a manner similar to that of the operational system. These pictures were the primary tool for assessing overall system performance. The pictures were made under conditions chosen to enhance undesirable interference characteristics which may detract from the scene information. High gain, compression mode, and low light level conditions were thus chosen to overemphasize interference. In addition, the images were produced from the flooding lamp and the collimator simultaneously to provide in-focus detail as well as broad areas of near uniform gray scenes.

11.1 GROUND PROCESSING EQUIPMENT (GPE) PICTURES

The GPE is described in Section 8, along with the picture content and formats used in system test. The following paragraphs describe the F-1 GPE picture evaluation.

11.1.1 Picture Quality Rating

Evaluation of the image quality of the pictures is largely a subjective matter. A rating scale with three incremental levels was developed for each of the interfering phenomena. Table 11-1 gives the value of levels 0 through 2 for each form of interference.

ORIGINAL PAGE IS
OF POOR QUALITY

TABLE 11-1. GPE/VPIR PICTURE RATING SCALE

(Degree of interference caused by microphonics, random, woodgrain, and coherent noise)

Scale	Degree of Interference	Comments
0	Not discernible	No interference to very low level interference
1	Barely discernible	Low level interference, considered acceptable
2	Easily discernible	Marginally acceptable to unacceptable

TABLE 11-2. F-1 GPE EVALUATION SUMMARY*

Ambient							
Problem	Preacoustic	Postacoustic	Pre-EMI	EMI	Post-EMI	Postvibration	Endbell
Microphonics	0	0	0	0	0	0	0
Woodgrain	0	0	0	0	0	0	0
Coherent noise	0	0	0	See Table 11-3	0	0	0
Corona noise	0	0	0	0	0	0	0
Time code error	5	5	5	5	5	No time code error	4,5

Thermal Vacuum														
		Thermal-Vacuum Performance Test 10^5 Torr or Less												
Problems	Pre-thermal-vacuum	Corona and Arcing	20°C	32°C	5°C	10°C	20°C	30°C	10°C	30°C	10°C	20°C	Post-thermal-vacuum	Premass Property
Microphonics	0	0	0	0	0	0	0	0	0	0	0	0	0	0
Woodgrain	0	0	0	0	0	0	0	0	0	0	0	0	0	0
Coherent noise	0	0	0	0	0	0	0	0	0	0	0	0	0	0
Corona noise	0	0	0	0	0	0	0	0	0	0	0	1	0	0
Time code error	5	No time code error	5	No time code error	5	5	No time code error	No time code error	3, 5	5	5	3,5	5	5

*See Table 11-1 and GPE code description.

ORIGINAL PAGE IS
OF POOR QUALITY

Aside from the noise rating, the pictures were also evaluated as to the presence of extra pulses, horizontal image jitter, stray light, MTF bar washout, time code errors, and all other interfering phenomena.

To simplify the summary performance tabulation in Table 11-2, code numbers were assigned for the various problems observed with F-1:

	Code	Comment
Time code error		
Time code error every 6 lines	3	Error in same channel
No time code	4	Missing time code
At least one black and white code missing	5	Time code glitch

11.1.2 EMI Noise Evaluation

As shown in Table 11-3, only the 1 and 9.6 kHz frequencies affected the system. All other frequencies injected into the system during CS01A test had no effect on the system output.

11.1.3 Performance History During Acceptance Test

Table 11-2 shows that F-1's performance throughout the tests was exceptionally good. No noise was detected in any of the GPE pictures except those taken during the EMI test.

There were time code errors, however, which were caused by test equipment anomalies. In one test event, the time code was missing in all bands; it was found the time code cables were somehow dragged, causing the connectors to break. After the connectors were repaired, the time code was back in the pictures. The time code glitch observed in the F-1 GPE pictures was similar to those seen in the protoflight pictures. This time code glitch, where the black time code is grey or missing and two or three words of data were missing, was investigated, and its cause was determined be in the test equipment.

During the final long form test, one orbit (236/6) GPE, dated 13 October 1981, showed a missing start-scan code (SMP1). This is the first occurrence of this anomaly seen throughout the test program, and the cause of the dropout is unknown.

ORIGINAL PAGE IS
OF POOR QUALITY

TABLE 11-3. F-1 GPE CONDUCTED SUSCEPTIBILITY TEST RESULTS

Test	Freq, Hz	System Mode	Result
CS01A at 1.5 V p-p	30	B	No noise apparent
	300	A	No noise apparent
	1000	A	Coherent noise barely discernible in bands 2, 3 and 4
	4350	A	No noise apparent
	9600	B	Coherent noise easily discernible in bands 1, 2, and 3

11.2 VPIR PICTURES

11.2.1 VPIR Picture Quality Rating

The same rating scale was used for F-1 VPIR noise evaluation as for the GPE pictures given in Table 11-1. Table 11-4 summarizes the F-1 VPIR picture analysis.

11.2.2 EMI Noise Evaluation

F-1 performance during the EMI tests from the VPIR picture standpoint is summarized in Table 11-5.

11.2.3 Performance History During Acceptance Tests

Microphonics appeared in channels 3 and 7 during the early part of testing and consistently showed up in the pictures taken throughout the tests. The degree of interference fluctuated from barely to easily discernible and affected the same channels at any test condition. Since there was no trace of microphonics seen in the GPE pictures, the microphonics interference observed in the VPIR pictures was not high enough to degrade the flight system's end product.

Woodgrain noise and coherent noise stayed at the easily discernible level in all test conditions. Random noise is also in easily discernible degree of interference throughout the tests. The fact that GPE pictures do not show any trace of interference indicates that the noise level seen in the VPIR pictures is acceptable.

No scan monitor pulse (SMP) dropouts were observed in any of the test events. Extra white words in the midscan and end of line codes appear in the flight VPIR pictures as expected.

ORIGINAL PAGE IS
OF POOR QUALITY

TABLE 11-4. F-1 VPIR EVALUATION SUMMARY*

Ambient							
Problem	Preacoustic	Postacoustic	Pre-EMI	EMI	Post-EMI	Postvibration	Endbell
Microphonics	1 to 2 channel's 3, 7	1 to 2 channel's 3, 7	1 to 2 channel's 3, 7	See Table 11-4	1 to 2 channel's 3, 7	1 to 2 channel's 3, 7	1 to 2 channel's 3, 7
Woodgrain	2	2	2	See Table 11-4	2	2	2
Coherent noise	2	2	2	See Table 11-4	2	2	2
Random noise	2	2	2	2	2	2	2

Thermal Vacuum														
		Thermal-Vacuum Performance Test 10^{-5} Torr or Less												
Problems	Pre-thermal-vacuum	Corona and Arcing	20°C	32°C	5°C	10°C	20°C	30°C	10°C	30°C	10°C	20°C	Post-thermal-vacuum	Premass Property
Microphonics	1 to 2 channel 3, 5, 7	1 to 2 channel 3, 5, 7	1 to 2 channel 3, 7	1 to 2 channel 3, 7	1 channel 3, 7	1 to 2 channel 3, 7	1 to 2 channel 3, 5, 7	1 to 2 channel 3, 7	1 to 2 channel 3, 5, 7	1 to 2 channel 3, 7	Image recorder out	1 to 2 channel 3, 5, 7	1 to 2 channel 3, 7	1 to 2 channel 3, 7
Woodgrain	2	2	2	2	2	2	2	2	2	2	Infrared out	2	2	2
Coherent noise	2	2	2	2	2	2	2	2	2	2	Infrared out	2	2	2
Random noise	2	2	2	2	2	2	2	2	2	2	Infrared Out	2	2	2

*See Table 11-1.

ORIGINAL PAGE IS
OF POOR QUALITY

TABLE 11-5. F-1 VPIR CONDUCTED SUSCEPTIBILITY TEST RESULTS

Test	Freq, Hz	System Mode	Results
CS01A at 1.5 V p-p	1000	A (+)	Woodgrain noise easily discernible in bands 1, 2; random noise easily discernible in band 4; microphonics in channels 3 and 7; coherent noise in band 3 easily discernible.
	4350	A (+)	Woodgrain noise easily discernible in bands 1, 2; random noise in band 4; microphonics in channels 3 and 7; coherent noise easily discernible in band 3.
	9600	B (+)	Excessive jitter; coherent noise in flooding lamp on some channels in bands 1, 2, 3.
	9600	A (–)	Woodgrain noise easily discernible in bands 1, 2, 3; random noise in band 4; microphonics in channels 3 and 7.
	9600	B (–)	Random noise easily discernible in band 1; woodgrain noise easily discernible in band 3; no microphonics apparent; coherent noise in band 4.
CS02A at 1.5 p-p	110	A (–)	Woodgrain noise easily discernible in bands 1, 2; random noise in band 4; barely discernible microphonics in channel 7; coherent noise easily discernible in band 3.
CS06	60 pps at 56 V p-p for 5 minutes	A(+)/B(–)	Woodgrain noise easily discernible in band 1; random noise in band 4; barely discernible microphonics in channel 7; coherent noise easily discernible in bands 2 and 3.

NOTE: A(+) means system A configuration, interference injected on the +28 V lead of system input power.
B(–) means system B configuration, interference injected on the ground return of system input power.

12. F-1 SPECIAL PROBLEMS

This section focuses on the special problems encountered during the acceptance test program of the F-1 system. Fewer problems were experienced with F-1 due to corrective actions taken for probems identified on the protoflight. Of the uniquely F-1 problems, corrective actions have been taken to eliminate the scan mirror assembly 3/4 mode anomaly (12.1) and the flex pivot corrosion (12.3). Because of cost and schedule constraints, it was not possible to correct the fiber optics plate design deficiency (12.2). A defective optical bond line design in the fiber optics assembly causes the calibration of the affected channels to be temperature dependent. Although first discovered on F-1, the problem exists in both flight systems. This problem presents little, if any, chance of a channel failure, but care must be exercised on both instruments to perform calibrations at or close to the orbital operating temperature of the fiber plate to minimize calibration errors. If proper care is taken in calibration, the problems elaborated below should have no effect on the in-orbit performance of the MSS-D flight model system.

12.1 SCAN MIRROR SUBHARMONIC OPERATION, 3/4 MODE

During the early phase of system integration of F-1, it was found that the scan mirror assembly (SMA) would occasionally start up and remain in stable subharmonic operation. This mode was dubbed a "3/4 mode" because the mirror would go through three more or less complete cycles of operation for every four torque pulses. In normal operation of the mirror one torque cycle is completed each scan cycle. Mathematically, a more precise description of the subharmonic operation would be to call it a 1/4 mode since the mirror position waveform repeated every four torque pulses.

The subharmonic operation is not a new MSS-D phenomenon. A similar problem was encountered during the original mirror development in 1971. The timing of its recurrance on MSS-D was surprising. By the time of its appearance, the engineering model test program was complete, the protoflight and flight model scan mirror assemblies had completed their acceptance tests, and the protoflight MSS-D system was well into acceptance testing. The F-1 SMA was replaced with the engineering model unit, and the F-1 assembly was shipped back for unit level troubleshooting.

The subharmonic operation of the unit was verified on the unit test station. The unique feature of the F-1 SMA was its optical switch setting. The optical switch is the device in the SMA which controls termination of current into the torquer at the end of each torque pulse. On the F-1 the optical switch had been set to cut off torque later in the retrace cycle than it had been for either the engineering or protoflight models. In a

series of tests it was demonstrated that by reducing the optical switch angle setting, the stable subharmonic operation could be eliminated. The optical switch setting was changed from 1.65° to 1.1° after center scan, and the unit was returned to F-1 integration testing. The optical switch boundary for the appearance of subharmonic was about 1.4°.

Subsequent testing on both the engineering and protoflight model SMAs demonstrated that those units would not support a stable subharmonic mode of operation at any optical switch setting. Evidently, there were other parameter differences among the three mirror assemblies other than optical switch setting which allowed only F-1 to show the 3/4 mode.

To investigate these differences and to evaluate margins against stable subharmonic operation, it was decided to refine and update parameters in a digital simulation of the scan mirror assembly. The existing simulation would model only steady state operation and not start-up. Even the steady state simulation agreement with the hardware performance was not very good due to uncertainties in the hardware parameters values in the simulation. Careful measurements were made on the engineering model hardware to update parameters, and the software necessary to model the start-up was transferred into the simulation based on work done by G.F. Banks and B. Johnson of Goddard Space Flight Center in their investigation of the 3/4 mode problem.

A description of the resulting simulation, hardware parameters used, and the estimated margins against subharmonic operation is given in HS248-1437, following this subsection. The results of the simulation were in good agreement with the hardware. The 3/4 mode was simulated on the F-1 SMA with optical switch positions similar to the flight hardware and was absent for reduced optical switch settings. For the engineering model and protoflight model, no 3/4 mode could be induced at any optical switch setting. Other stable subharmonic modes were found, but at operating points far removed from those of any of the three units tested. The margins against 3/4 mode operation are smallest in the F-1 unit, but large enough for safe operation over life. The parameter which makes the F-1 unit susceptible to 3/4 mode operation and not the engineering or protoflight models is torquer efficiency. Both high torquer efficiency and a high optical switch setting are required to induce the problem. After its original acceptance test, the F-1 torquer was carefully reworked to impove efficiency. During this rework particular attention was paid to minimizing the air gap between the torquer armature and pole pieces to maximize torque gain. The result is that the torque gain factor for the F-1 torquer is about 10 percent higher than in the other two assemblies.

The surest way to avoid this problem on any future hardware would be to modify the SMA control loop to control the phasing of the torque pulses relative to mirror position during start-up. With the present hardware one of the torquer control signals (the scan mirror drive signal) comes from the multiplexer and starts or stops the torque pulse independent of mirror position or sign of velocity. Based on the results of the simulation, another way to eliminate the 3/4 mode problem is to drop the drive voltage to the torquer by perhaps 10 percent.

ORIGINAL PAGE IS
OF POOR QUALITY

HUGHES

INTERDEPARTMENTAL CORRESPONDENCE

TO: Robert L. Johnson
ORG: 40-91-30

CC: See Below:

DATE: Sept. 22, 1981
REF. HS248-1437
4091.4/34

SUBJECT: MSS-D Scan Mirror Assembly
Simulation Report:
Three-Quarter Mode Problem

FROM: R.A. Gillmann
ORG. 40-91-40

BLDG. S41 MAIL STA. B322
LOC. ES EXT. 80305

Gillmann 34 3/4 Mode

10 Distribution List

Banks, G.	NASA/Goddard
Brinkman, K.	S1/D335
Ellison, H.E.	S1/D335
Gillmann, R.A.	S41/B332
Johnson, R.L.	S1/D335
Lauletta, A.M.	S1/D335
Malherbe, P. (GE)	S1/D334
Marchant, A.B.	12/W109
Miyagi, M.I.	S41/B323
Norwood, V.I.	12/V129
Paynter, D.D.	S1/D335
Stahura, W.P.	S1/D335
Swarthout, W.	5/B146
Wengler, R.	774/82
Yeagley, J.D.	S1/D335
Zomber, G.L.	S1/D335
Data Bank (3)	S1/D335

MSS-D SCAN MIRROR ASSEMBLY SIMULATION REPORT: THREE-QUARTER MODE PROBLEM

Richard Gillmann
September 18, 1981

ORIGINAL PAGE IS
OF POOR QUALITY

Table of Contents

1 Introduction.....1

2 The Scan Mirror Assembly.....2

3 The Model.....3

4 Parameters of the Model.....5
  4.1 Parameter Definitions.....5
  4.2 Measured Engineering Model Parameter Values.....6
  4.3 Estimated Protoflight Model Parameter Values.....8
  4.4 Estimated Flight Model Parameter Values.....8

5 The Simulation Program.....9
  5.1 Using the Program.....10
  5.2 Moving the Program to Other Computers.....10
  5.3 Sample Data File.....10
  5.4 Sample Listing File.....11
  5.5 Sample Plot.....17

6 Normal Mode Simulation Results.....18
  6.1 Steady State.....19
  6.2 Time Margins.....20
  6.3 Start-Up.....21

7 Three-Quarter Mode Problem.....23
  7.1 Start-Up.....23
    7.1.1 1.65 Degree Three-Quarter Mode.....24
    7.1.2 1.80 Degree Three-Quarter Mode.....24
    7.1.3 1.50 Degree Three-Quarter Mode.....25
  7.2 Steady State.....25
  7.3 Three-Quarter Mode Danger Area Maps.....27
  7.4 Other Secondary Modes.....31

8 Conclusions.....31

9 Bibliography.....32

10 Distribution List.....34

ORIGINAL PAGE IS
OF POOR QUALITY

1 Introduction

The Multi-Spectral Scanner of the LANDSAT-D satellite (MSS-D) generates a raster scan with a rocking scan mirror. This paper discusses a digital computer simulation of the mechanical and electrical characteristics of the Scan Mirror Assembly (SMA).

The purpose of the simulation is to study abnormal scan modes, in particular the so-called three-quarter mode. In normal operation the scan mirror moves in sync with a 13.62 hz clock pulse train. In an abnormal (subharmonic) mode, the scan mirror is in a stable cycle that is not one-to-one with the clock pulses. In three-quarter mode, the scan mirror makes three cycles while the clock covers four cycles.

The simulation program is the latest in a series of simulations over the history of the MSS program [11,12,13]. The first simulation ran on an analog computer. A digital simulation was developed later. Both of these were steady state models only. The current simulation models start-up conditions as well.

The simulation is written in FORTRAN 66 and runs on a PRIME 750 minicomputer. The differential equations of motion and electrical current are integrated using Euler-Cauchy integration of the corresponding difference equations. This method was chosen because of its inherent stability, because it can deal with complicated functions whose derivatives are not known in closed form, and because it makes it easy to add arbitrary boundary conditions and transitions.

The model requires a large number of parameters. The mechanical and electrical parameters of the Engineering Model were measured in the laboratory. Corresponding values for the Protoflight Model and the Flight Model are taken from their specifications where possible. Some of the Protoflight and Flight parameters are subjective estimates based on the perceptions of those who have tested them. Some of them are simply assumed to be the same as for the Engineering Model. Thus the simulations of the Protoflight and Flight Models are less trustworthy than the simulation of the Engineering Model because of uncertain parameter values.

The simulation is able to model normal operation of the Engineering, Protoflight and Flight Models to a reasonable degree of accuracy. Simulation of start-up from time zero until the optical switch is activated is also satisfactory. We do not yet have an accurate model of when the optical switch is enabled, so the transition from start-up to steady state is inadequately modeled.

The simulation will go into three-quarter mode for certain optical switch settings and initial conditions for the Flight Model parameters. We have not found three-quarter mode start-ups for either the Engineering or Protoflight Models. This report includes maps of the three-quarter mode region in the Flight Model parameter space. These maps can be used to judge the distance of the launch parameters from the problem area.

2 The Scan Mirror Assembly

ORIGINAL PAGE IS
OF POOR QUALITY

Mechanically, the SMA consists of an elliptical mirror about ten inches long and half as wide. The mirror is allowed to pivot about its minor axis. Small springs called flex pivots act to move the mirror toward its normal resting position.

The mirror is held within a narrow arc by bumper assemblies, one for each end of the mirror. The bumpers each have two springs in series and a rubber damper in parallel.

The SMA is powered by an inductive torquer, similar to a solenoid. The torquer pulls on one side of the mirror.

The mechanical arrangement of the SMA is shown schematically below.

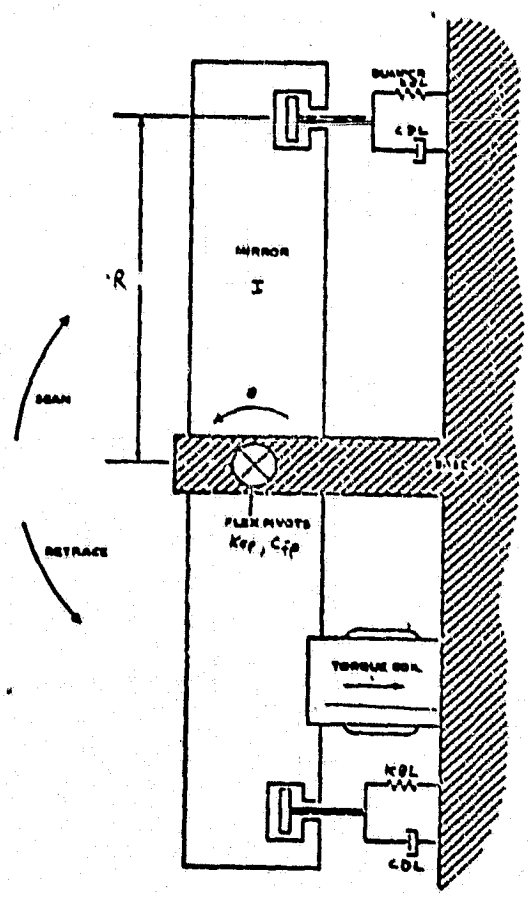

Electrically, the circuit of interest is the one that drives the coil of the inductive torquer. The schematic of this circuit is as follows.

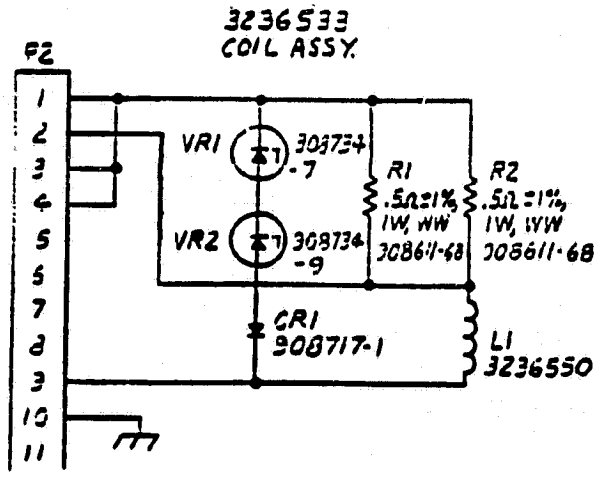

Power is applied according to the system clock and mirror position relative to the optical switch. At start-up the optical switch is ignored. Under normal conditions, after about 0.5 seconds the optical switch is activated. The exact time depends on the number of times the mirror crosses the optical switch. If the mirror is held down, it can be as long as 2 seconds.

3 The Model

The mathematical model used to simulate the SMA is described in detail below. Earlier versions of the model are described in [1] and [8]. The model consists of two differential equations, one describing mirror position and one describing torque coil current. In addition, there are a number of constraints and transient conditions.

Between the bumpers, motion is governed by

```
I*d(dTheta/dt)/dt = - Kfp*Theta - Cfp*dTheta/dt
                    +  K(Current,Theta)*Current**2
```

At bumper impact, an inelastic collision is assumed to take place.

```
dTheta/dt (after impact) = Rho * dTheta/dt (before impact)

Rho = I/(I + 2*Mb*R**2)
```

On the bumpers, motion is governed by

```
(I + 2*Mb*R**2)*d(dTheta/dt)/dt = - Kfp*Theta - Cfp*dTheta/dt
     - 2*Kbl(dTheta/dt)*R**2*sign(Theta)*(abs(Theta) - ThetaB)
     - 2*Cdl(dTheta/dt)*R**2*dTheta/dt
     + K(Current,Theta)*Current**2
```

The following theoretical circuit is used to model the real circuit shown previously.

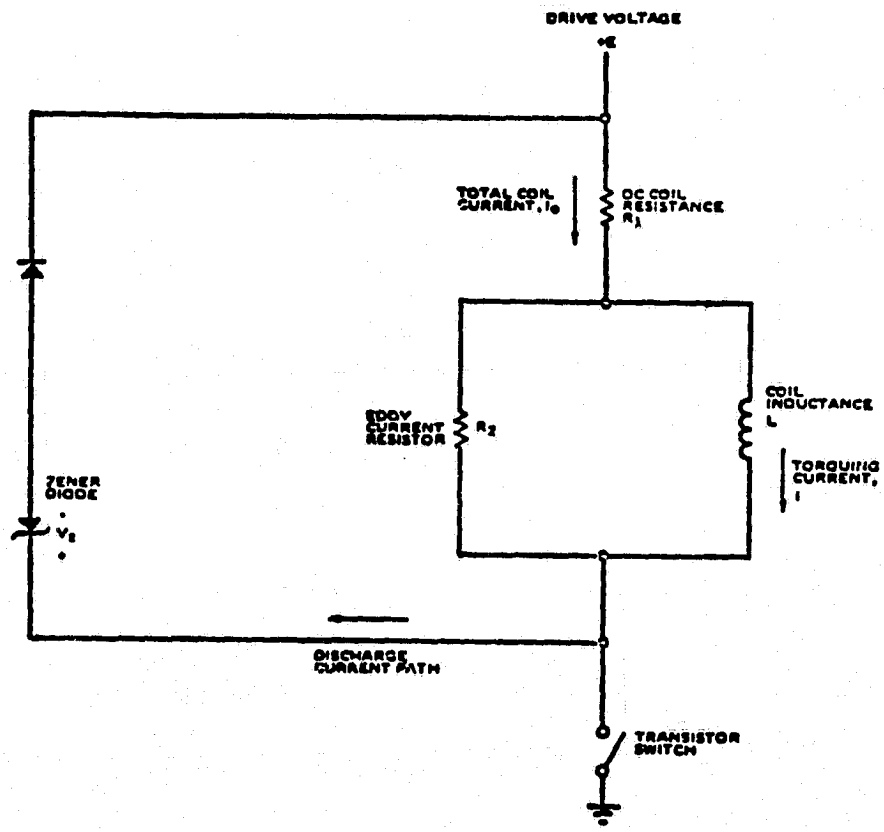

The current flowing through the torque coil is governed by

```
L(Current,Theta)*dCurrent/dt =
     (V(Theta,t) - R1*Current)*R2/(R1 + R2)
     - Q(Current)*Current*dTheta/dt
```

subject to

```
0 <= Current <= IMax
```

because of the cutoff diodes and power supply current limiter.

Drive voltage is governed by

```
V(Theta,t) =
   if sin(2*pi*F*t + Delta)>=0 and (t<TimeS or Theta<=ThetaS)
      then E
      else - Vz
```

4 Parameters of the Model

If an accurate model is to be obtained, then accurate data about the parameters of the model are required. In this section we present the current state of our knowledge about MSS-D parameters.

4.1 Parameter Definitions

The parameters have the following meanings

t	Time
I	Mirror moment of inertia
Theta	Mirror angular position
Kfp	Rotary spring constant of the flex pivots
Cfp	Rotary damping coefficient of the flex pivots
Current	Current through the torque coil
K(Current,Theta)	Torque gain factor
Mb	Mass of one bumper
R	Radius arm from the flex pivots to the bumpers
Kbl(dTheta/dt)	Bumper linear spring constant
Cdl(dTheta/dt)	Bumper linear damping coefficient
ThetaB	Angular position of the bumpers
L(Current,Theta)	Torque coil inductance
R1	Serial (DC) coil resistance
R2	Parallel coil resistance
Q(Current)	Back EMF coefficient
IMax	Power supply current limit
E	Drive voltage
Vz	Zener diode voltage
F	Drive frequency
Delta	Phase angle at startup
ThetaS	Angular position of the optical switch
ThetaM	Angular position of the scan angle monitors
TimeS	Time when the optical switch is enabled

4.2 Measured Engineering Model Parameter Values

Presented here is a table of the parameter values for the Engineering Model. Most of these parameter values are based on laboratory measurements of the Engineering Model in April 1981.

Param.	Value	Units	Reference
I	.089	in-lb-sec**2	[3]
Kfp	2.25	ft-lb/radian	[3]
Cfp	.0072	in-lb-sec/radian	[3]
Mb	.0025	slugs	[5]
R	4.757	inches	[5]
Kbl(nom)	1390.0	lb/inch	[3]
Cdl(nom)	1.50	lb-sec/ft	[3]
ThetaB	3.804	degrees	[3]
R1	5.94	ohms	[2]
R2	120.	ohms	[2]
IMax	1.80	amperes	M.I. Miyagi
E	26.5	volts	G.L. Zomber (w/diode effect)
Vz	27.5	volts	[6] w/diode effect (Zomber)
F	13.62	hertz	[7]
ThetaS	1.55	degrees	W. Swarthout
ThetaM	3.7506	degrees	[3]
TimeS	0.5	seconds	Approximation - see below

The efficiency of the torquer is measured by the torque gain factor K. It is a function of both mirror position and current. The torquer efficiency of the Engineering Model was measured by Zomber and Swarthout [4] in October 1979. Their results are reproduced below. The simulation program uses two-dimensional linear interpolation of the values in this table to obtain arbitrary values of K.

Mirror Position (degrees)	Coil Current (amperes)	Torque Gain Factor (in-lb/amp**2)
-3.82	0.33	21.9
-3.82	0.72	9.2
-3.82	0.98	7.5
-3.82	1.15	7.2
-3.82	1.33	6.8
-3.82	1.50	6.4
-3.82	1.63	6.3
-3.82	1.78	6.0
-3.82	1.94	5.7
-3.82	2.10	5.4
-2.79	0.42	13.6
-2.79	0.77	8.1
-2.79	0.97	7.6
-2.79	1.14	7.4
-2.79	1.32	6.9
-2.79	1.45	6.8
-2.79	1.60	6.5

ORIGINAL PAGE IS
OF POOR QUALITY

-2.79	1.73	6.4
-2.79	1.90	6.0
-2.79	2.10	5.4
-1.76	0.46	11.3
-1.76	0.81	7.3
-1.76	1.02	6.9
-1.76	1.20	6.6
-1.76	1.35	6.6
-1.76	1.52	6.2
-1.76	1.68	5.9
-1.76	1.86	5.5
-1.76	2.10	4.9
-1.76	2.55	3.7
-0.72	0.59	6.9
-0.72	0.81	7.3
-0.72	1.08	6.1
-0.72	1.22	6.4
-0.72	1.42	5.9
-0.72	1.62	5.5
-0.72	1.85	4.9
-0.72	2.28	3.7
0.31	0.64	5.8
0.31	0.89	6.0
0.31	1.10	5.9
0.31	1.31	5.6
0.31	1.53	5.1
0.31	1.88	4.1
1.34	0.70	4.9
1.34	0.95	5.3
1.34	1.18	5.1
1.34	1.44	4.6
1.34	2.03	2.9
2.37	0.75	4.2
2.37	1.03	4.5
2.37	1.31	4.2
2.37	2.08	2.2
2.99	0.80	3.7
2.99	1.10	4.0
2.99	1.50	3.2
3.82	0.96	2.6
3.82	1.80	1.5

If the bumpers were truly linear, the bumper spring constant Kbl and the bumper damping coefficient Cdl would be constant. However, it was found that at low impact speeds (less that 100 degrees/second), the bumper parameters change [3]. We model this low speed behavior as a linear function of impact speed.

```
Kbl = max(1390, 8000 - (8000 - 1390)/100 * Speed)
Cdl = max( 1.5,  40  -  (40  -  1.5)/100 * Speed)
```

where Speed is the absolute value of the impact velocity in degrees/second.

Torque coil inductance and back EMF coefficient values were measured by a method suggested by E.F. Grant [2].

```
L(I,Theta) = - .0209*I**2  - .184*Theta*I**2
             + 1.151*Theta + .326 henrys

Q(I) = 1.151 - .0615*I**2 henrys/radian
```

where the current I is in amperes and the mirror position Theta is in radians.

The time when the optical switch is first allowed to affect the torque pulse (TimeS) is controlled by an RC timing circuit. The details of this circuit have not yet been investigated. It is known that TimeS is longer if the mirror does not cross the optical switch.

4.3 Estimated Protoflight Model Parameter Values

The parameters are assumed to be the same as for the Engineering Model, with the following exceptions:

1. The optical switch is positioned at 1.30 degrees [5,9].
2. The bumper contact angle is set at 3.805 degrees [5].
3. The nominal bumper damping coefficient is set to 2.00 lb-sec/ft. This number was chosen so that the simulated coefficent of restitution would match the measured coefficient of restitution of the Protoflight Model, 0.78 [9].
4. The mirror moment of inertia is estimated at .0906 in-lb-sec**2. This figure is the mean of the moments of inertia of the Engineering and Flight Models.
5. The torque gain factor K was uniformly reduced 10 per cent, to reflect the less efficent torquer of the Protoflight Model [9].

4.4 Estimated Flight Model Parameter Values

The Flight Model parameters are assumed to be the same as the corresponding Engineering Model parameters, with the following exceptions:

1. The optical switch is positioned at 1.10 degrees [5,9].

2. The bumper contact angle is set to 3.785 degrees [5].

3. The nominal bumper damping coefficient is set to 1.33 lb-sec/ft. This figure was chosen to match the measured coefficient of restitution of the Flight Model, 0.82 [9].

4. The mirror moment of inertia is fixed at .0923 in-lb-sec**2 [5].

5. The torque gain factor numbers are all increased by 15 per cent. The Flight Model is known to have a more efficient torquer [9]. This particular value was chosen because it gave the best match between simulated and actual start-ups.

5 The Simulation Program

The simulation program is written in FORTRAN 66 for the PRIME 750 minicomputer. The program uses the Euler-Cauchy method [14] to integrate the difference equations corresponding to the model differential equations. All arithmetic is done in double precision to avert accumulation of round-off error.

To deal with truncation error, the program uses three different step sizes: LARGE, MEDIUM, and SMALL. The LARGE step size is used when the mirror is traveling between the bumpers. When the program finds that the next step would take it past a bumper hit, it backs up and switches to the MEDIUM step size. When it again passes the bumper hit with the MEDIUM step size, the program backs up and switches to the SMALL step size. After the hit, when the mirror is on the bumper, the MEDIUM step size is used to cross the bumper. When the mirror comes off the bumper, the program switches back to the LARGE step size. Likewise, the optical switch is approached in this fashion with successively smaller step sizes.

The LARGE step size is a parameter of the simulation run. The MEDIUM step size is always 1/10 the LARGE step size adn the SMALL step size 1/10 the MEDIUM step size. Basic LARGE step sizes between 10**-4 and 10**-5 seconds are normally used. Long term stability of secondary modes requires a step size of about 2x10**-5 seconds.

ORIGINAL PAGE IS
OF POOR QUALITY

5.1 Using the Program

The program takes one input data file and produces two output files: a listing file and a plot file. The program can produce one of four different plots: start-up, phase plane, steady state, or scope format. The input file contains the simulation parameter settings for those parameters that can be set by a single number. Changing the more complicated parameters, such as the back EMF coefficient function, requires modifications to the program.

5.2 Moving the Program to Other Computers

The simulation program is reasonably portable with a few exceptions. It is written in FORTRAN 66. The plot output requires a traditional Calcomp plotting package and a device that can draw the plot. Opening and closing of files is controlled by special calls unique to the PRIME and these would have to changed on a different computer.

5.3 Sample Data File

```
0.0000D0  PHASE  = CLOCK STARTUP PHASE, IN DEGREES
0.8000D0  TLIMIT = SIMULATION DURATION, IN SECONDS
5.0000D-5 STEP   = BASIC (LARGE) SIMULATION STEP SIZE, IN SECONDS
0.0000D0  THETA0 = INITIAL MIRROR POSITION, IN DEGREES
0.0000D0  DTHET0 = INITIAL MIRROR VELOCITY, IN DEGREES/SECOND
1.5500D0  OPTISW = OPTICAL SWITCH POSITION, IN DEGREES
3.7506D0  SAM    = SCAN ANGLE MONITOR POSITION, IN DEGREES
3.8040D0  BUMPER = BUMPER CONTACT ANGLE, IN DEGREES
2.2500D0  KFP    = FLEX PIVOT ROTARY SPRING CONSTANT, IN FT*LB/RADIAN
0.0072D0  CFP    = FLEX PIVOT ROTARY DAMPING COEFF., IN IN*LB*SEC/RAD
1390.0D0  KBLI   = BUMPER LINEAR SPRING CONSTANT, IN LB/INCH
4.7570D0  ARM    = BUMPER MOMENT ARM, IN INCHES
2.5000D-3 MB     = BUMPER MASS, IN SLUGS
1.5000D0  CDL    = BUMPER LINEAR DAMPING COEFFICIENT, IN LB*SEC/FT
0.0890D0  MOI    = SCAN MIRROR MOMENT OF INERTIA, IN IN*LB*SEC**2
13.620D0  FC     = CLOCK FREQUENCY, IN HERTZ
5.9400D0  R1     = SERIES COIL RESISTANCE, IN OHMS
120.00D0  R2     = PARALLEL COIL RESISTANCE, IN OHMS
26.500D0  DRIVE  = DRIVE VOLTAGE, IN VOLTS
27.500D0  ZENER  = ZENER DIODE VOLTAGE, IN VOLTS
1.8000D0  IMAX   = POWER SUPPLY CURRENT LIMIT, IN AMPERES
1.0000D0  TORQEF = TORQUER EFFICIENCY, EM1 = 1.0
0.5000D0  TIMES  = TIME WHEN OPTICAL SWITCH IS ACTIVATED, IN SECONDS
 0        FLAG   = 0 -> STARTUP, 1 -> PHASE, 2 -> STEADY, 3 -> SCOPE
```

ORIGINAL PAGE IS
OF POOR QUALITY

5.4 Sample Listing File

The simulation program generated the following listing file from the preceeding data file.

```
MSSD SCAN MIRROR ASSEMBLY SIMULATION

0.0000D-01 PHASE  = CLOCK STARTUP PHASE, IN DEGREES
8.0000D-01 TLIMIT = SIMULATION DURATION, IN SECONDS
5.0000D-05 STEP   = BASIC (LARGE) STEP SIZE, IN SECONDS
0.0000D-01 THETA0 = INITIAL MIRROR POSITION, IN DEGREES
0.0000D-01 DTHET0 = INITIAL MIRROR VELOCITY, IN DEGREES/SEC.
1.5500D 00 OPTISW = OPTICAL SWITCH POSITION, IN DEGREES
3.7506D 00 SAM    = SCAN ANGLE MONITOR POSITION, IN DEGREES
3.8040D 00 BUMPER = BUMPER CONTACT ANGLE, IN DEGREES
2.2500D 00 KFP    = FLEX PIVOT SPRING CONST., IN FT*LB/RAD.
0.0072D 00 CFPI   = FLEX PIVOT DAMPING COEFF., IN IN*LB*SEC
1390.0D 00 KBLI   = BUMPER SPRING CONSTANT, IN LB/INCH
4.7570D 00 ARM    = BUMPER MOMENT ARM, IN INCHES
2.5000D-03 MB     = BUMPER MASS, IN SLUGS
1.5000D 00 CDL    = BUMPER DAMPING COEFF., IN LB*SEC/FT
0.0890D 00 MOI    = MIRROR INERTIA, IN IN*LB*SEC**2
13.620D 00 FC     = CLOCK FREQUENCY, IN HERTZ
5.9400D 00 R1     = SERIES COIL RESISTANCE, IN OHMS
120.00D 00 R2     = PARALLEL COIL RESISTANCE, IN OHMS
26.500D 00 DRIVE  = DRIVE VOLTAGE, IN VOLTS
27.500D 00 ZENER  = ZENER DIODE VOLTAGE, IN VOLTS
1.8000D 00 IMAX   = POWER SUPPLY CURRENT LIMIT, IN AMPS
1.0000D 00 TORQEF = TORQUER EFFICIENCY, EM1 = 1.0
0.5000D 00 TIMES  = OPTICAL SWITCH TURNON, IN SEC
         0 FLAG   = 0: NORMAL, 1: PHASE, 2: STEADY, 3: SCOPE
```

ORIGINAL PAGE IS
OF POOR QUALITY

TIME (SEC)	ANGLE (DEG)	VELOCITY (DEG/SEC)	CURRENT (AMP)	TORQUE (FT-LB)	COMMENTS
0.000000	0.0000	0.0000	0.0000	0.0000	
0.000050	0.0000	0.0000	0.0000	0.0000	TORQUER ON
0.005000	0.0012	0.9147	0.3721	0.0694	
0.010000	0.0180	6.9861	0.7181	0.2648	
0.015000	0.0877	22.4859	1.0406	0.5389	
0.020000	0.2620	48.8425	1.3375	0.8271	
0.025000	0.5925	84.0301	1.6030	1.0018	
0.030000	1.1092	122.2335	1.8000	1.0095	
0.033300	1.5523	145.5359	1.8000	0.9278	OPTICAL SWITCH
0.035000	1.8094	156.5500	1.8000	0.8850	
0.036750	2.0930	166.8435	1.8000	0.8379	TORQUER OFF
0.040000	2.6640	182.8248	1.3631	0.5901	
0.045000	3.6096	192.3005	0.8452	0.1748	
0.045750	3.7538	192.3465	0.7781	0.1378	UPPER MONITOR
0.046060	3.8040	173.8861	0.7552	0.1246	HIT UPPER BUMPER
0.047490	3.9878	-2.2133	0.6377	0.0882	SCAN REVERSAL
0.049010	3.8034	-154.9756	0.5289	0.0612	OFF UPPER BUMPER
0.002950	B-TO-B	0.8059	COEFF. OF REST.		
0.049360	3.7491	-155.2120	0.5044	0.0577	UPPER MONITOR
0.003610	SAM-TO-SAM				
0.049960	3.6558	-155.6291	0.4624	0.0508	
0.054960	2.8680	-159.5652	0.1159	0.0045	
0.056660	2.5955	-160.9347	0.0000	0.0000	END TORQUE
0.059960	2.0605	-163.2267	0.0000	0.0000	
0.063110	1.5435	-164.9113	0.0000	0.0000	OPTICAL SWITCH
0.064960	1.2377	-165.6693	0.0000	0.0000	
0.069960	0.4058	-166.8555	0.0000	0.0000	
0.073460	-0.1785	-166.9366	0.0000	0.0000	TORQUER ON
0.074960	-0.4288	-166.7463	0.1217	0.0076	
0.079960	-1.2552	-162.4414	0.5205	0.1957	
0.084960	-2.0320	-146.2815	0.9305	0.5178	
0.089960	-2.6881	-113.0206	1.3438	1.0253	
0.094960	-3.1116	-49.3120	1.7353	2.1562	
0.097560	-3.1748	0.5840	1.8000	2.4264	SCAN REVERSAL
0.099960	-3.1159	47.1653	1.8000	2.3173	
0.104960	-2.6645	127.5622	1.8000	1.6647	
0.109960	-1.8590	192.9752	1.8000	1.5381	
0.110160	-1.8201	194.8358	1.8000	1.5320	TORQUER OFF
0.114960	-0.7696	235.8893	1.0715	0.5955	
0.119960	0.4521	249.1633	0.5159	0.1285	
0.124360	1.5511	249.4986	0.1357	0.0077	OPTICAL SWITCH
0.124960	1.7007	249.2159	0.0898	0.0034	
0.126210	2.0118	248.4994	0.0000	0.0000	END TORQUE
0.129960	2.9385	245.6145	0.0000	0.0000	
0.133310	3.7557	242.1520	0.0000	0.0000	UPPER MONITOR
0.133560	3.8041	218.7449	0.0000	0.0000	HIT UPPER BUMPER
0.135000	4.0420	59.3006	0.0000	0.0000	ON BUMPER
0.135090	4.0448	-0.6991	0.0000	0.0000	SCAN REVERSAL
0.136705	3.8039	-195.3444	0.0000	0.0000	OFF UPPER BUMPER
0.003145	B-TO-B	0.8075	COEFF. OF REST.		
0.137005	3.7452	-195.6836	0.0000	0.0000	UPPER MONITOR
0.003694	SAM-TO-SAM				

TIME (SEC)	ANGLE (DEG)	VELOCITY (DEG/SEC)	CURRENT (AMP)	TORQUE (FT-LB)	COMMENTS
0.139955	3.1633	-198.7330	0.0000	0.0000	
0.144955	2.1589	-202.6984	0.0000	0.0000	
0.146855	1.7727	-203.7771	0.0000	0.0000	TORQUER ON
0.147955	1.5482	-204.3339	0.0806	0.0024	OPTICAL SWITCH
0.149955	1.1388	-204.9658	0.2225	0.0202	
0.154955	0.1167	-202.6847	0.5901	0.1718	
0.159955	-0.8680	-188.6596	0.9789	0.5245	
0.164955	-1.7410	-157.2521	1.3839	1.0339	
0.169955	-2.4009	-103.3944	1.7843	1.5982	
0.174955	-2.7477	-35.5617	1.8000	1.6766	
0.177555	-2.7926	0.4238	1.8000	1.6885	SCAN REVERSAL
0.179955	-2.7508	33.6379	1.8000	1.6776	
0.183555	-2.5397	82.1107	1.8000	1.6447	TORQUER OFF
0.184955	-2.4110	99.8139	1.5676	1.3204	
0.189955	-1.8064	135.9991	0.8843	0.4744	
0.194955	-1.0883	148.4851	0.3441	0.0862	
0.198805	-0.5124	150.1344	0.0000	0.0000	END TORQUE
0.199955	-0.3397	150.2704	0.0000	0.0000	
0.204955	0.4119	150.1605	0.0000	0.0000	
0.209955	1.1600	148.9127	0.0000	0.0000	
0.212605	1.5532	147.7930	0.0000	0.0000	OPTICAL SWITCH
0.214955	1.8990	146.5369	0.0000	0.0000	
0.219955	2.6234	143.0517	0.0000	0.0000	
0.220305	2.6734	142.8078	0.0000	0.0000	TORQUER ON
0.224955	3.3279	138.7890	0.2928	0.0228	
0.228055	3.7542	136.2850	0.4671	0.0485	UPPER MONITOR
0.228471	3.8041	122.9750	0.4869	0.0518	HIT UPPER BUMPER
0.229666	3.9155	-1.4395	0.5516	0.0658	SCAN REVERSAL
0.229996	3.9004	-73.0408	0.5705	0.0704	ON BUMPER
0.230986	3.8035	-106.7557	0.6287	0.0863	OFF UPPER BUMPER
0.002515	B-TO-B	0.7850	COEFF. OF REST.		
0.231486	3.7500	-106.9725	0.6582	0.0961	UPPER MONITOR
0.003431	SAM-TO-SAM				
0.234986	3.3749	-106.8362	0.8664	0.1998	
0.239986	2.8559	-99.0363	1.1680	0.4491	
0.244986	2.4020	-81.1102	1.4727	0.6758	
0.249986	2.0596	-54.9812	1.7757	0.8355	
0.254986	1.8605	-24.6884	1.8000	0.8750	
0.256986	1.8239	-12.5409	1.8000	0.8812	TORQUER OFF
0.259086	1.8119	0.2171	1.5350	0.7883	SCAN REVERSAL
0.259986	1.8144	5.0103	1.4321	0.7347	
0.264986	1.8913	23.0302	0.9222	0.3434	
0.269986	2.0220	27.5475	0.4876	0.0894	
0.274986	2.1567	25.7691	0.1039	0.0042	
0.276436	2.1933	24.8247	0.0000	0.0000	END TORQUE
0.279986	2.2771	22.4106	0.0000	0.0000	
0.284986	2.3803	18.8684	0.0000	0.0000	
0.289986	2.4654	15.1847	0.0000	0.0000	
0.293686	2.5163	12.4223	0.0000	0.0000	TORQUER ON
0.294986	2.5318	11.3965	0.0896	0.0025	
0.299986	2.5804	8.4248	0.4066	0.0547	
0.304986	2.6212	8.5585	0.7049	0.1642	

ORIGINAL PAGE IS
OF POOR QUALITY

TIME (SEC)	ANGLE (DEG)	VELOCITY (DEG/SEC)	CURRENT (AMP)	TORQUE (FT-LB)	COMMENTS
0.309986	2.6750	14.0258	0.9882	0.3378	
0.314986	2.7741	26.5844	1.2575	0.5104	
0.319986	2.9499	44.1303	1.5114	0.6134	
0.324986	3.2229	65.3438	1.7483	0.6984	
0.329986	3.6014	84.5558	1.8000	0.5282	
0.330436	3.6398	85.7138	1.8000	0.5070	TORQUER OFF
0.331736	3.7536	88.9529	1.6289	0.4105	UPPER MONITOR
0.332348	3.8040	81.3852	1.5620	0.3738	HIT UPPER BUMPER
0.333193	3.8472	-0.0405	1.4684	0.3477	SCAN REVERSAL
0.334378	3.8040	-38.1527	1.3514	0.3219	OFF UPPER BUMPER
0.002030	B-TO-B	0.4239	COEFF. OF REST.		
0.334978	3.7813	-37.3717	1.2942	0.3122	
0.335828	3.7500	-36.3475	1.2153	0.2955	UPPER MONITOR
0.004092	SAM-TO-SAM				
0.339978	3.6070	-33.2082	0.8577	0.1792	
0.344978	3.4403	-34.2155	0.4713	0.0582	
0.349978	3.2596	-38.2967	0.1170	0.0040	
0.351728	3.1911	-39.9864	0.0000	0.0000	END TORQUE
0.354978	3.0561	-43.0570	0.0000	0.0000	
0.359978	2.8294	-47.5069	0.0000	0.0000	
0.364978	2.5814	-51.5950	0.0000	0.0000	
0.367128	2.4686	-53.1966	0.0000	0.0000	TORQUER ON
0.369978	2.3140	-55.1953	0.1925	0.0126	
0.374978	2.0329	-56.5995	0.5156	0.0969	
0.379978	1.7568	-52.6746	0.8308	0.2723	
0.384328	1.5488	-41.7742	1.0994	0.5029	OPTICAL SWITCH
0.384978	1.5224	-39.4550	1.1390	0.5381	
0.389978	1.3806	-15.8916	1.4370	0.7853	
0.392628	1.3596	0.0546	1.5886	0.8732	SCAN REVERSAL
0.394978	1.3781	15.4716	1.7182	0.9276	
0.399978	1.5418	49.5908	1.8000	0.9287	
0.400178	1.5519	50.9295	1.8000	0.9271	OPTICAL SWITCH
0.403828	1.7822	74.3880	1.8000	0.8889	TORQUER OFF
0.404978	1.8723	81.6764	1.6381	0.8254	
0.409978	2.3414	103.0023	1.0684	0.4300	
0.414978	2.8759	108.6305	0.6112	0.1198	
0.419978	3.4144	105.9591	0.2269	0.0139	
0.423228	3.7532	102.5112	0.0052	0.0000	UPPER MONITOR
0.423328	3.7635	102.3965	0.0000	0.0000	END TORQUE
0.423775	3.8040	92.1729	0.0000	0.0000	HIT UPPER BUMPER
0.424675	3.8593	-0.4615	0.0000	0.0000	SCAN REVERSAL
0.425000	3.8511	-42.4001	0.0000	0.0000	ON BUMPER
0.425860	3.8038	-52.0812	0.0000	0.0000	OFF UPPER BUMPER
0.002085	B-TO-B	0.5109	COEFF. OF REST.		
0.426910	3.7484	-53.2801	0.0000	0.0000	UPPER MONITOR
0.003681	SAM-TO-SAM				
0.429960	3.5807	-56.6593	0.0000	0.0000	
0.434960	3.2841	-61.8473	0.0000	0.0000	
0.439960	2.9627	-66.5645	0.0000	0.0000	
0.440560	2.9226	-67.0530	0.0000	0.0000	TORQUER ON
0.444960	2.6194	-70.4673	0.2878	0.0270	
0.449960	2.2629	-71.3761	0.6042	0.1286	

ORIGINAL PAGE IS
OF POOR QUALITY

TIME (SEC)	ANGLE (DEG)	VELOCITY (DEG/SEC)	CURRENT (AMP)	TORQUE (FT-LB)	COMMENTS
0.454960	1.9160	-66.0590	0.9165	0.3305	
0.459960	1.6200	-50.6683	1.2245	0.5994	
0.461460	1.5491	-43.9760	1.3155	0.6764	OPTICAL SWITCH
0.464960	1.4276	-25.0165	1.5239	0.8299	
0.468860	1.3786	0.1398	1.7468	0.9377	SCAN REVERSAL
0.469960	1.3831	7.7329	1.8000	0.9548	
0.474960	1.5091	42.1216	1.8000	0.9341	
0.475910	1.5523	48.5060	1.8000	0.9270	OPTICAL SWITCH
0.477260	1.6240	57.1272	1.8000	0.9151	TORQUER OFF
0.479960	1.8020	73.4555	1.4474	0.7454	
0.484960	2.2204	90.8602	0.9177	0.3202	
0.489960	2.6865	93.9032	0.4821	0.0778	
0.494960	3.1492	90.6441	0.1098	0.0037	
0.496610	3.2974	89.0345	0.0000	0.0000	END TORQUE
0.499960	3.5898	85.5123	0.0000	0.0000	
0.501910	3.7544	83.3277	0.0000	0.0000	UPPER MONITOR
0.502558	3.8040	74.7218	0.0000	0.0000	HIT UPPER BUMPER
0.503363	3.8401	-0.2058	0.0000	0.0000	SCAN REVERSAL
0.504513	3.8040	-33.0607	0.0000	0.0000	OFF UPPER BUMPER
0.001955	B-TO-B	0.4001	COEFF. OF REST.		
0.504963	3.7890	-33.5779	0.0000	0.0000	
0.506113	3.7496	-34.8901	0.0000	0.0000	UPPER MONITOR
0.004203	SAM-TO-SAM				
0.509963	3.6068	-39.1773	0.0000	0.0000	
0.514963	3.3974	-44.4776	0.0000	0.0000	
0.519963	3.1624	-49.4387	0.0000	0.0000	
0.524963	2.9034	-54.0231	0.0000	0.0000	
0.529963	2.6226	-58.1962	0.0000	0.0000	
0.534963	2.3220	-61.9267	0.0000	0.0000	
0.539963	2.0040	-65.1864	0.0000	0.0000	
0.544963	1.6708	-67.9508	0.0000	0.0000	
0.546763	1.5477	-68.8206	0.0000	0.0000	OPTICAL SWITCH
0.546813	1.5443	-68.8206	0.0000	0.0000	TORQUER ON
0.549963	1.3253	-70.0348	0.2237	0.0198	
0.550663	1.2762	-70.1647	0.2685	0.0298	TORQUER OFF
0.554113	1.0327	-71.1001	0.0000	0.0000	END TORQUE
0.554963	0.9721	-71.3542	0.0000	0.0000	
0.559963	0.6122	-72.5301	0.0000	0.0000	
0.564963	0.2477	-73.1559	0.0000	0.0000	
0.569963	-0.1185	-73.2271	0.0000	0.0000	
0.574963	-0.4836	-72.7433	0.0000	0.0000	
0.579963	-0.8450	-71.7085	0.0000	0.0000	
0.584963	-1.1998	-70.1307	0.0000	0.0000	
0.587413	-1.3704	-69.1839	0.0000	0.0000	TORQUER ON
0.589963	-1.5451	-67.7594	0.2174	0.0393	
0.594963	-1.8658	-58.7061	0.6225	0.3057	
0.599963	-2.1141	-38.8697	1.0101	0.6027	
0.604963	-2.2272	-3.8461	1.3721	1.0451	
0.605413	-2.2273	0.1676	1.4029	1.0846	SCAN REVERSAL
0.609963	-2.1222	47.8475	1.6929	1.4455	
0.614963	-1.7271	109.7775	1.8000	1.5167	
0.619963	-1.0278	168.4598	1.8000	1.4077	

TIME (SEC)	ANGLE (DEG)	VELOCITY (DEG/SEC)	CURRENT (AMP)	TORQUE (FT-LB)	COMMENTS
0.624113	-0.2348	211.8016	1.8000	1.2709	TORQUER OFF
0.624963	-0.0507	220.2174	1.6545	1.1429	
0.629963	1.1360	249.3170	0.9923	0.4484	
0.631659	1.5501	253.1682	0.8153	0.2725	OPTICAL SWITCH
0.634959	2.3908	255.4029	0.5049	0.0906	
0.639959	3.6614	252.0341	0.1197	0.0036	
0.640359	3.7621	251.5846	0.0924	0.0021	UPPER MONITOR
0.640575	3.8041	227.3105	0.0811	0.0014	HIT UPPER BUMPER
0.642120	4.0556	-0.4336	0.0000	0.0000	SCAN REVERSAL
0.643750	3.8039	-203.0512	0.0000	0.0000	OFF UPPER BUMPER
0.003175	B-TO-B	0.8077	COEFF. OF REST.		
0.644050	3.7429	-203.3901	0.0000	0.0000	UPPER MONITOR
0.003691	SAM-TO-SAM				
0.644950	3.5594	-204.3736	0.0000	0.0000	
0.649950	2.5254	-208.9156	0.0000	0.0000	
0.654600	1.5468	-211.7176	0.0000	0.0000	OPTICAL SWITCH
0.654950	1.4727	-211.8725	0.0000	0.0000	
0.659950	0.4092	-213.2227	0.0000	0.0000	
0.660800	0.2280	-213.2888	0.0000	0.0000	TORQUER ON
0.664950	-0.6562	-212.3388	0.3273	0.0594	
0.669950	-1.6903	-202.6483	0.7381	0.3636	
0.674950	-2.6574	-177.5373	1.1710	0.8205	
0.679950	-3.4176	-116.9261	1.6060	2.3060	
0.684650	-3.7043	0.8594	1.8000	3.4487	SCAN REVERSAL
0.684950	-3.7026	9.1866	1.8000	3.4462	
0.689950	-3.3204	137.5498	1.8000	2.7208	
0.694950	-2.4047	219.8264	1.8000	1.6245	
0.697550	-1.7885	252.4832	1.8000	1.5275	TORQUER OFF
0.699950	-1.1493	277.3229	1.3909	1.0074	
0.704950	0.3094	300.9185	0.7461	0.2782	
0.709091	1.5500	304.0626	0.3508	0.0488	OPTICAL SWITCH
0.709991	1.8236	303.8521	0.2755	0.0298	
0.713691	2.9438	301.3508	0.0000	0.0000	END TORQUE
0.714991	3.3347	300.0840	0.0000	0.0000	
0.716391	3.7537	298.5479	0.0000	0.0000	UPPER MONITOR
0.716609	3.8040	269.7711	0.0000	0.0000	HIT UPPER BUMPER
0.718219	4.1085	-3.5760	0.0000	0.0000	SCAN REVERSAL
0.719909	3.8030	-241.0860	0.0000	0.0000	OFF UPPER BUMPER
0.003300	B-TO-B	0.8081	COEFF. OF REST.		
0.719959	3.7909	-241.1427	0.0000	0.0000	
0.720159	3.7426	-241.3677	0.0000	0.0000	UPPER MONITOR
0.003768	SAM-TO-SAM				
0.724959	2.5725	-245.8826	0.0000	0.0000	
0.729109	1.5463	-248.4012	0.0000	0.0000	OPTICAL SWITCH
0.729959	1.3350	-248.7572	0.0000	0.0000	
0.734259	0.2627	-249.7180	0.0000	0.0000	TORQUER ON
0.734959	0.0879	-249.7427	0.0574	0.0014	
0.739959	-1.1568	-246.9785	0.4570	0.1486	
0.744959	-2.3594	-231.8178	0.8908	0.4928	
0.749959	-3.4356	-191.1695	1.3531	1.6710	
0.751759	-3.7528	-160.1773	1.5193	2.5035	LOWER MONITOR
0.752137	-3.8040	-138.5307	1.5490	2.6974	HIT LOWER BUMPER

ORIGINAL PAGE IS
OF POOR QUALITY

TIME (SEC)	ANGLE (DEG)	VELOCITY (DEG/SEC)	CURRENT (AMP)	TORQUE (FT-LB)	COMMENTS
0.753337	-3.9250	1.9759	1.6496	1.4193	SCAN REVERSAL
0.754632	-3.8038	124.4240	1.7248	3.3435	OFF LOWER BUMPER
0.002495	B-TO-B	0.8121	COEFF. OF REST.		
0.754982	-3.7584	133.8537	1.7430	3.3359	
0.755082	-3.7448	136.5411	1.7482	3.3314	LOWER MONITOR
0.003322	SAM-TO-SAM				
0.759982	-2.7857	242.5743	1.8000	1.6987	
0.764982	-1.4065	306.6997	1.8000	1.4681	
0.769982	0.2646	358.9325	1.8000	1.1804	
0.770932	0.6097	366.7659	1.8000	1.1122	TORQUER OFF
0.773479	1.5501	384.0556	1.3922	0.7347	OPTICAL SWITCH
0.774979	2.1315	390.5382	1.1908	0.5383	
0.779129	3.7701	396.4709	0.7382	0.1238	UPPER MONITOR
0.779264	3.8040	358.4721	0.7302	0.1165	HIT UPPER BUMPER
0.779999	4.0473	285.3165	0.6646	0.0958	ON BUMPER
0.780954	4.2179	-0.0137	0.5874	0.0749	SCAN REVERSAL
0.782724	3.8036	-320.7419	0.4682	0.0479	OFF UPPER BUMPER
0.003460	B-TO-B	0.8090	COEFF. OF REST.		
0.782924	3.7395	-320.8928	0.4551	0.0470	UPPER MONITOR
0.003795	SAM-TO-SAM				
0.784974	3.0801	-322.3436	0.3188	0.0308	
0.789524	1.6068	-325.0691	0.0000	0.0000	END TORQUE
0.789724	1.5418	-325.1599	0.0000	0.0000	OPTICAL SWITCH
0.789974	1.4605	-325.2677	0.0000	0.0000	
0.794974	-0.1690	-326.1282	0.0000	0.0000	
0.799974	-1.7966	-324.5171	0.0000	0.0000	

5.5 Sample Plot

The simulation program produced the following plot for the data file listed above.

ORIGINAL PAGE IS
OF POOR QUALITY

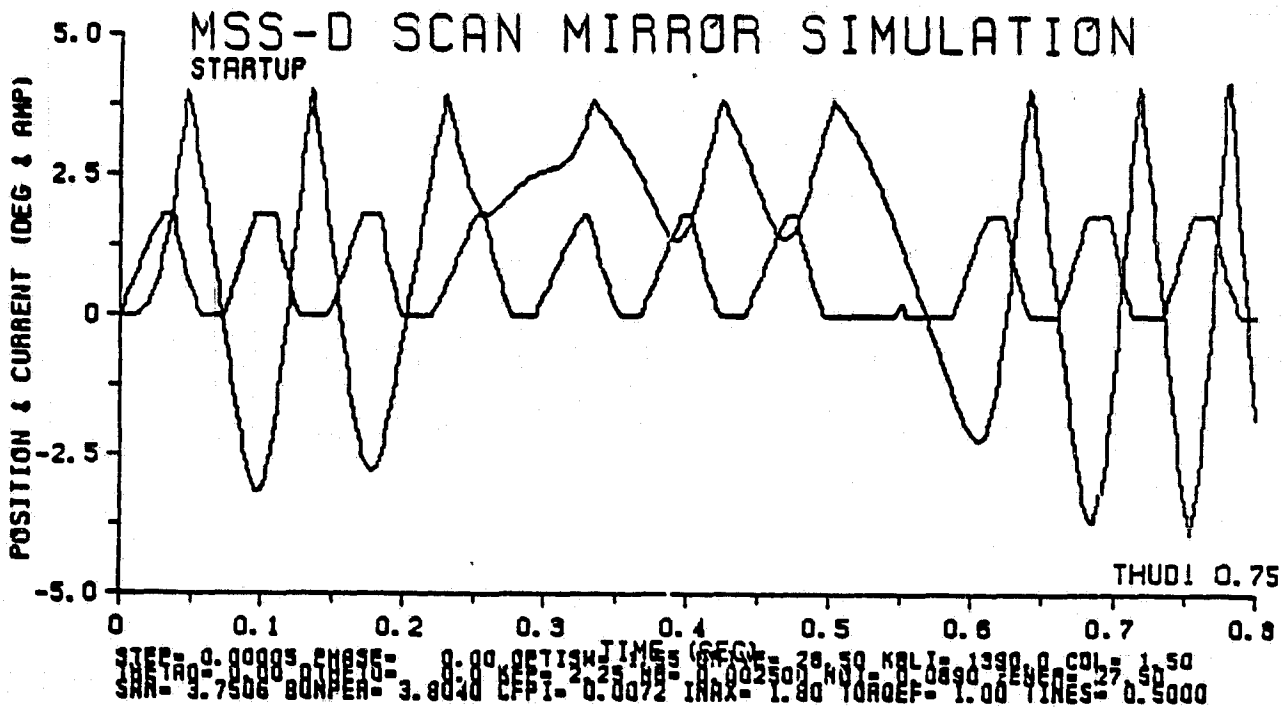

6 Normal Mode Simulation Results

The simulation results have been compared to actual measured results. There are three cases: steady state, start-up, and the optical switch turn-on. The quality of match is usually judged on the basis of phase relationships. Phase relationships are very sensitive measures of the quality of simulation.

ORIGINAL PAGE IS
OF POOR QUALITY

6.1 Steady State

The table below lists steady state measurements of the Engineering Model and the corresponding simulation results. The graph following shows typical steady state operation in the normal mode. This graph is in the normal simulation format, i.e. the torque pulse is in the same direction as its effect on the scan mirror (the reverse of the oscilliscope trace system).

	Engineering Model	Simulation
Time margin, EOS	4.9 ms	7.1 ms
Time margin, BOS	-2.0 ms	-3.8 ms
Peak current	1.32 a	1.35 a
Conduction time	25.0 ms	22.1 ms
Decay time	13.5 ms	15.7 ms
Turnaround, EOS	4.1 ms	4.0 ms
Turnaround, BOS	4.2 ms	4.0 ms
Restitution, EOS	.819	.819
Restitution, BOS	.805	.818

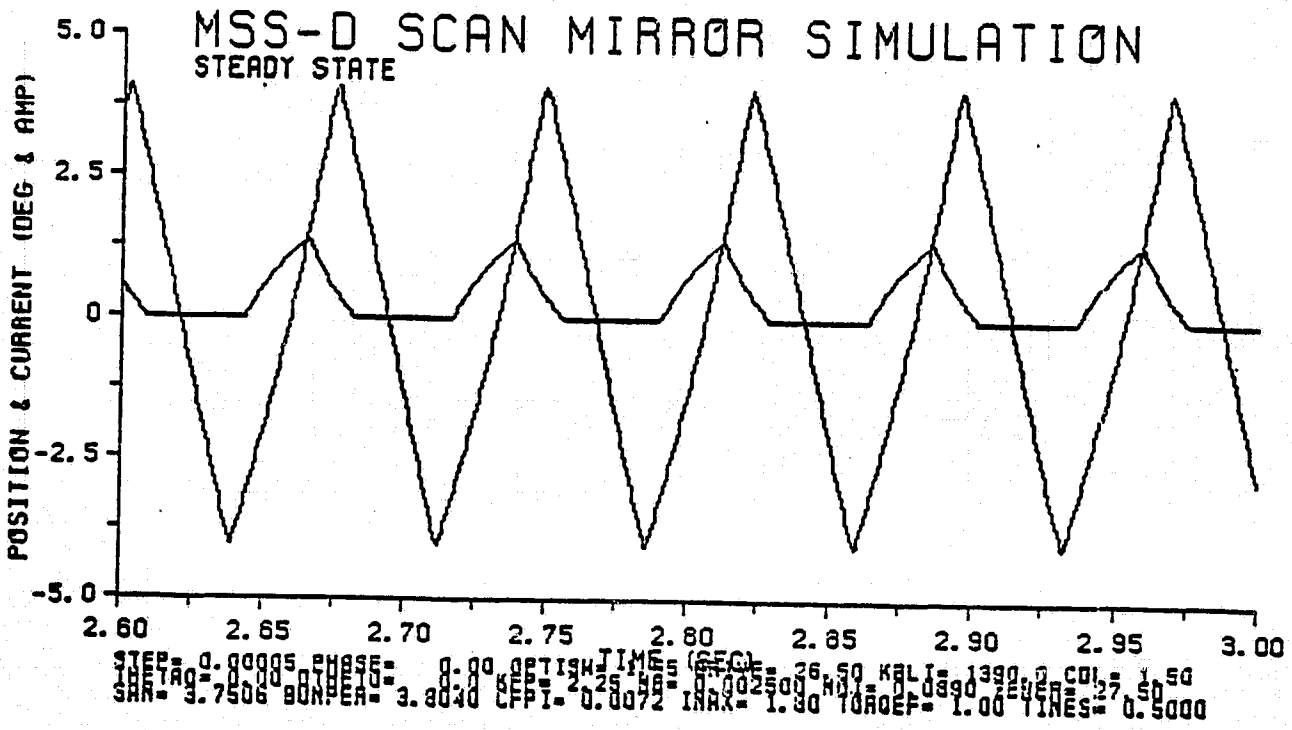

ORIGINAL PAGE IS
OF POOR QUALITY

6.2 Time Margins

The graph below shows simulated BOS and EOS time margins for various optical switch positions, for the Engineering Model. The best setting for the optical switch is 0.2 degrees.

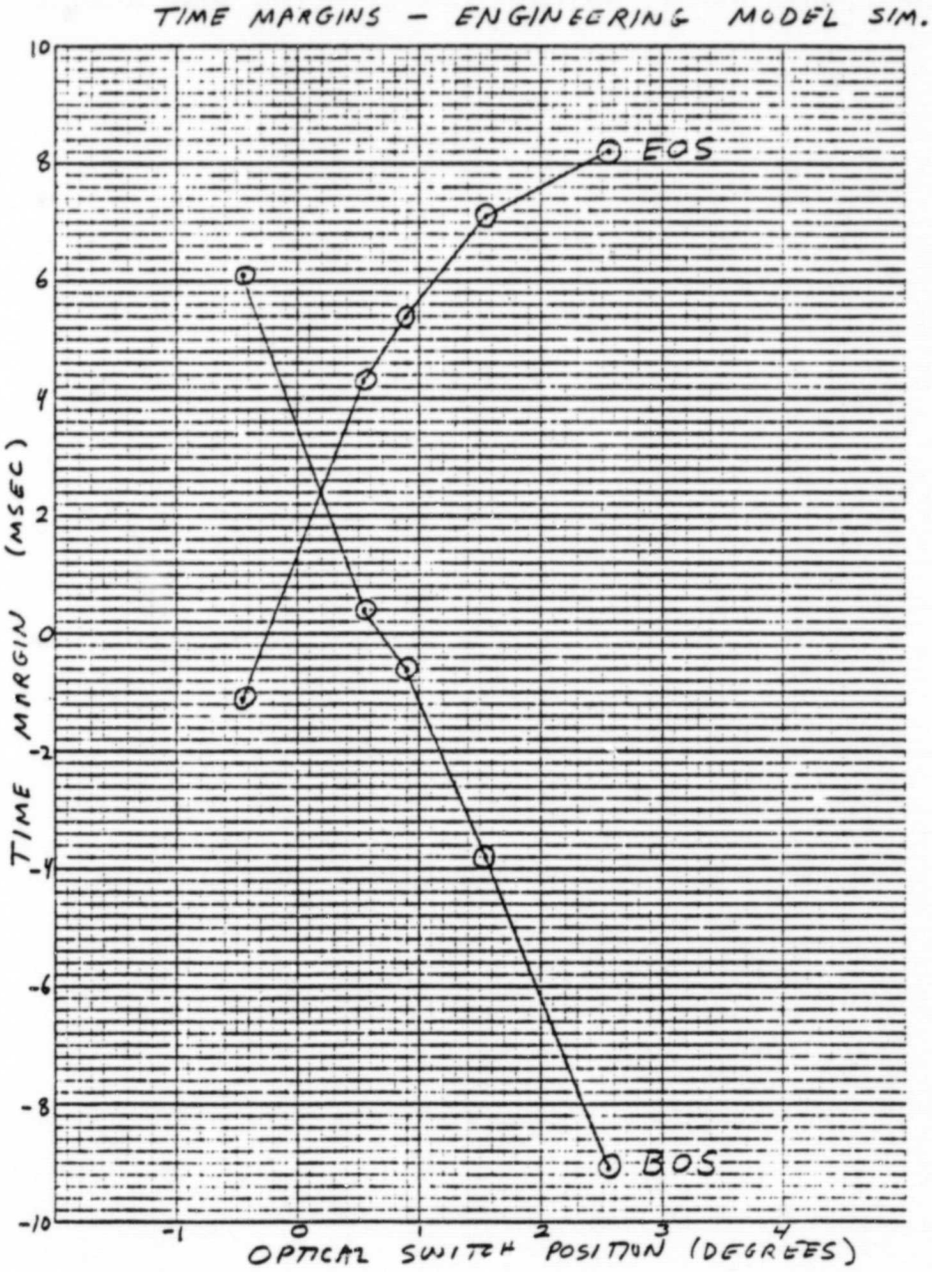

ORIGINAL PAGE IS
OF POOR QUALITY

6.3 Start-Up

In [10] a series of Engineering Model start-ups shown in [9] are compared with simulated start-ups. The notation for startup phase used by [9] is milliseconds of first pulse length. The phase notation used by the simulation program models the applied voltage as E*sign(sin(w*t+phase)), with phase measured in degrees. We show here a startup comparison between an actual scope start-up and a simulated start-up with the phase finely adjusted to give the best match.

ORIGINAL PAGE IS
OF POOR QUALITY

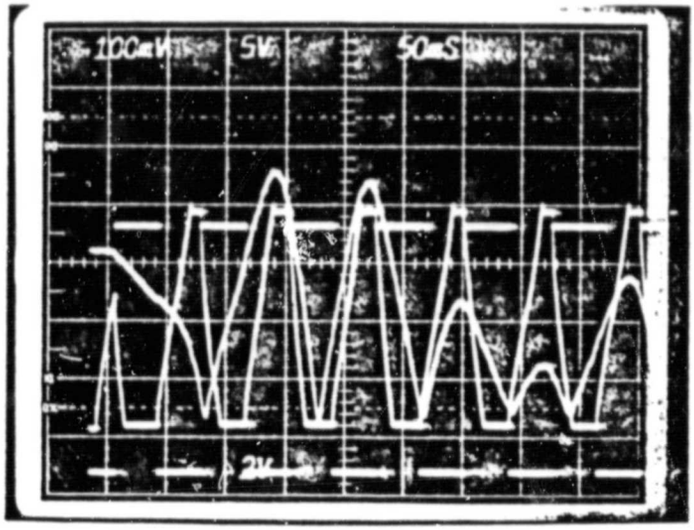

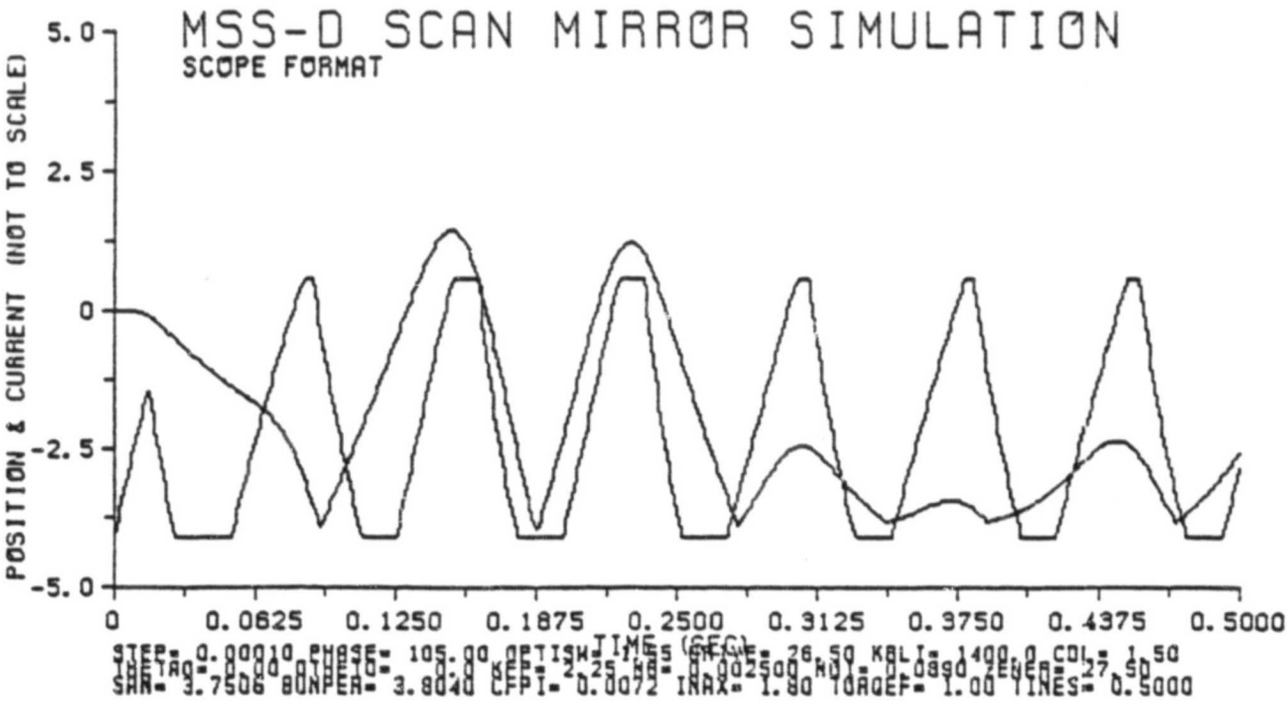

ORIGINAL PAGE IS
OF POOR QUALITY

7 Three-Quarter Mode Problem

Three-quarter mode occurs when the scan mirror makes three cycles in the time taken by four clock cycles. The mode is an unstable equilibrium, like balancing a pencil on its point. The torquer turns on when the mirror is traveling towards the upper bumper. The force of the torquer acts against the mirror motion, turning the mirror around before it can hit the upper bumper. The torquer then turns off and the mirror, now traveling downwards, hits the lower bumper and bounces off it. This pattern repeats two more times. On the third cycle, the torquer is not able to send the mirror downwards as rapidly as it did the first two times. The mirror takes two clock cycles to reach the lower bumper. During the fourth clock cycle, there may be a small torque pulse or none at all, depending on the position of the mirror relative to the optical switch. The entire three on four cycle then repeats.

The mode is an unstable equilibrium in that a small deflection will kick it out of the mode and into normal operation, but once in the mode it will stay there indefinitely if there no outside forces knock it out. Injection into the mode is a delicate process. The start-up phase and optical switch activation time must be precisely chosen; the smallest deviation will fail to inject it into the mode.

The scan mirror may be started at any time; there is no necessary relation to the clock cycle. The first pulse may be of any length up to the length of a full clock pulse. Injection into the mode occurs when the first pulse is a little less then half length. When the next (full) pulse occurs, the scan mirror will be moving out of phase with the torquer. Thus begins the secondary mode. If at any time the mirror should hit the upper bumper, the system will go into its normal mode.

7.1 Start-Up

Simulation start-ups in three-quarter mode have only been found for parameter settings similar to the Flight Model. We have found three sets of parameters that start the mode: the first is the Flight Model parameters with the optical switch at 1.65 degrees, the second is the Flight Model parameters with the optical switch at 1.80 degrees, and the third is the Flight Model parameters with the optical switch set at 1.50 degrees and the drive voltage .55 volts high.

7.1.1 1.65 Degree Three-Quarter Mode

```
116.26D0   PHASE  = CLOCK STARTUP PHASE, IN DEGREES
5.0000D-5  STEP   = BASIC (LARGE) SIMULATION STEP SIZE, IN SECONDS
0.0000D0   THETA0 = INITIAL MIRROR POSITION, IN DEGREES
0.0000D0   DTHET0 = INITIAL MIRROR VELOCITY, IN DEGREES/SECOND
1.6500D0   OPTISW = OPTICAL SWITCH POSITION, IN DEGREES
3.7506D0   SAM    = SCAN ANGLE MONITOR POSITION, IN DEGREES
3.7850D0   BUMPER = BUMPER CONTACT ANGLE, IN DEGREES
2.2500D0   KFP    = FLEX PIVOT ROTARY SPRING CONSTANT, IN FT*LB/RADIAN
0.0072D0   CFP    = FLEX PIVOT ROTARY DAMPING COEFF., IN IN*LB*SEC/RAD
1390.0D0   KBLI   = BUMPER LINEAR SPRING CONSTANT, IN LB/INCH
4.7570D0   ARM    = BUMPER MOMENT ARM, IN INCHES
2.5000D-3  MB     = BUMPER MASS, IN SLUGS
1.5000D0   CDL    = BUMPER LINEAR DAMPING COEFFICIENT, IN LB*SEC/FT
0.0923D0   MOI    = SCAN MIRROR MOMENT OF INERTIA, IN IN*LB*SEC**2
13.620D0   FC     = CLOCK FREQUENCY, IN HERTZ
5.9400D0   R1     = SERIES COIL RESISTANCE, IN OHMS
120.00D0   R2     = PARALLEL COIL RESISTANCE, IN OHMS
26.500D0   DRIVE  = DRIVE VOLTAGE, IN VOLTS
27.500D0   ZENER  = ZENER DIODE VOLTAGE, IN VOLTS
1.8000D0   IMAX   = POWER SUPPLY CURRENT LIMIT, IN AMPERES
1.1500D0   TORQEF = TORQUER EFFICIENCY, EM1 = 1.0
0.4449D0   TIMES  = TIME WHEN OPTICAL SWITCH IS ACTIVATED, IN SECONDS
```

7.1.2 1.80 Degree Three-Quarter Mode

```
116.26D0   PHASE  = CLOCK STARTUP PHASE, IN DEGREES
5.0000D-5  STEP   = BASIC (LARGE) SIMULATION STEP SIZE, IN SECONDS
0.0000D0   THETA0 = INITIAL MIRROR POSITION, IN DEGREES
0.0000D0   DTHET0 = INITIAL MIRROR VELOCITY, IN DEGREES/SECOND
1.8000D0   OPTISW = OPTICAL SWITCH POSITION, IN DEGREES
3.7506D0   SAM    = SCAN ANGLE MONITOR POSITION, IN DEGREES
3.7850D0   BUMPER = BUMPER CONTACT ANGLE, IN DEGREES
2.2500D0   KFP    = FLEX PIVOT ROTARY SPRING CONSTANT, IN FT*LB/RADIAN
0.0072D0   CFP    = FLEX PIVOT ROTARY DAMPING COEFF., IN IN*LB*SEC/RAD
1390.0D0   KBLI   = BUMPER LINEAR SPRING CONSTANT, IN LB/INCH
4.7570D0   ARM    = BUMPER MOMENT ARM, IN INCHES
2.5000D-3  MB     = BUMPER MASS, IN SLUGS
1.5000D0   CDL    = BUMPER LINEAR DAMPING COEFFICIENT, IN LB*SEC/FT
0.0923D0   MOI    = SCAN MIRROR MOMENT OF INERTIA, IN IN*LB*SEC**2
13.620D0   FC     = CLOCK FREQUENCY, IN HERTZ
5.9400D0   R1     = SERIES COIL RESISTANCE, IN OHMS
120.00D0   R2     = PARALLEL COIL RESISTANCE, IN OHMS
26.500D0   DRIVE  = DRIVE VOLTAGE, IN VOLTS
27.500D0   ZENER  = ZENER DIODE VOLTAGE, IN VOLTS
1.8000D0   IMAX   = POWER SUPPLY CURRENT LIMIT, IN AMPERES
1.1500D0   TORQEF = TORQUER EFFICIENCY, EM1 = 1.0
0.4449D0   TIMES  = TIME WHEN OPTICAL SWITCH IS ACTIVATED, IN SECONDS
```

ORIGINAL PAGE IS
OF POOR QUALITY

7.1.3 1.50 Degree Three-Quarter Mode

```
116.29D0   PHASE  = CLOCK STARTUP PHASE, IN DEGREES
5.0000D-5  STEP   = BASIC (LARGE) SIMULATION STEP SIZE, IN SECONDS
0.0000D0   THETA0 = INITIAL MIRROR POSITION, IN DEGREES
0.0000D0   DTHET0 = INITIAL MIRROR VELOCITY, IN DEGREES/SECOND
1.5000D0   OPTISW = OPTICAL SWITCH POSITION, IN DEGREES
3.7506D0   SAM    = SCAN ANGLE MONITOR POSITION, IN DEGREES
3.7850D0   BUMPER = BUMPER CONTACT ANGLE, IN DEGREES
2.2500D0   KFP    = FLEX PIVOT ROTARY SPRING CONSTANT, IN FT*LB/RADIAN
0.0072D0   CFP    = FLEX PIVOT ROTARY DAMPING COEFF., IN IN*LB*SEC/RAD
1390.0D0   KBLI   = BUMPER LINEAR SPRING CONSTANT, IN LB/INCH
4.7570D0   ARM    = BUMPER MOMENT ARM, IN INCHES
2.5000D-3  MB     = BUMPER MASS, IN SLUGS
1.5000D0   CDL    = BUMPER LINEAR DAMPING COEFFICIENT, IN LB*SEC/FT
0.0923D0   MOI    = SCAN MIRROR MOMENT OF INERTIA, IN IN*LB*SEC**2
13.620D0   FC     = CLOCK FREQUENCY, IN HERTZ
5.9400D0   R1     = SERIES COIL RESISTANCE, IN OHMS
120.00D0   R2     = PARALLEL COIL RESISTANCE, IN OHMS
27.050D0   DRIVE  = DRIVE VOLTAGE, IN VOLTS
27.500D0   ZENER  = ZENER DIODE VOLTAGE, IN VOLTS
1.8000D0   IMAX   = POWER SUPPLY CURRENT LIMIT, IN AMPERES
1.1500D0   TORQEF = TORQUER EFFICIENCY, EM1 = 1.0
0.4443D0   TIMES  = TIME WHEN OPTICAL SWITCH IS ACTIVATED, IN SECONDS
```

7.2 Steady State

The following graph shows the steady state three-quarter mode cycle. A small step size is required if the simulation is to stay in the mode indefinitely. The mode has been simulated out to 24 seconds with a basic step size of 2x10**-5, with no signs of kicking out.

ORIGINAL PAGE IS
OF POOR QUALITY

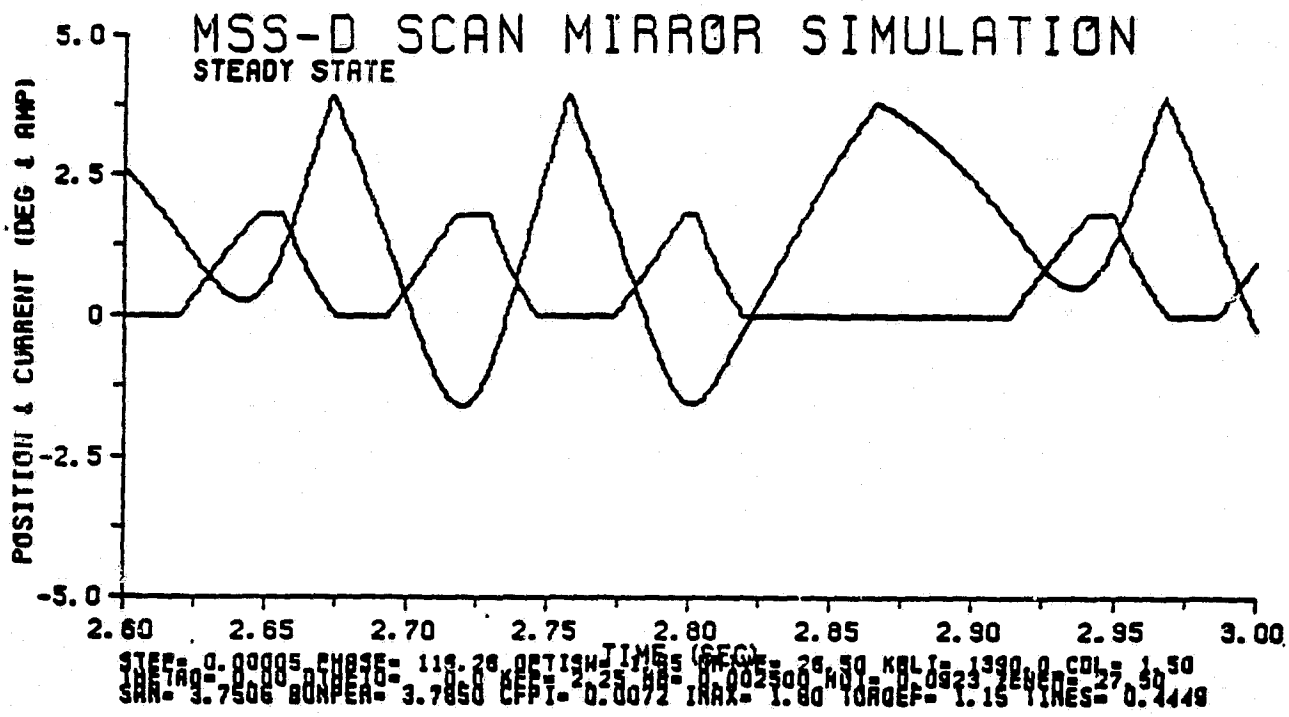

Here is a phase plane plot of the first three seconds of three-quarter mode (1.65 degree start-up).

ORIGINAL PAGE IS
OF POOR QUALITY

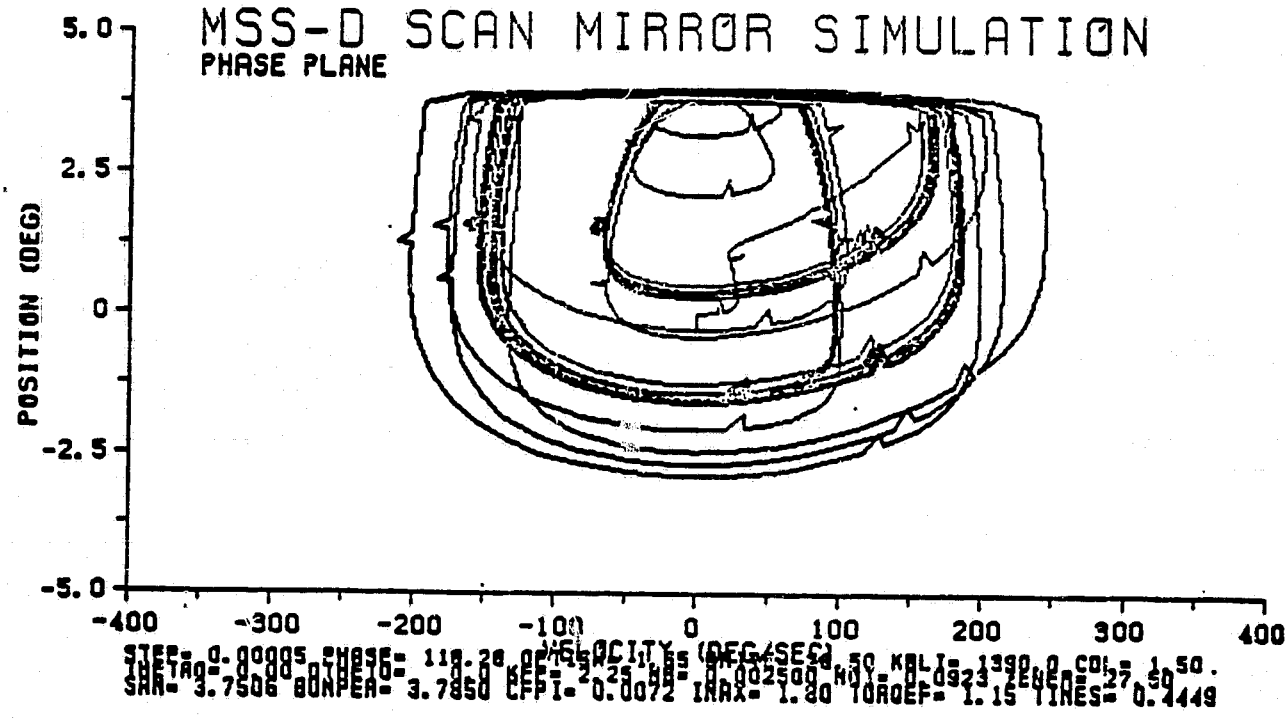

7.3 Three-Quarter Mode Danger Area Maps

The three-quarter mode danger areas have been mapped using a method suggested by Gary Banks of NASA. The simulation is started in three-quarter mode. When it is in the mode, certain parameters are slowly varied until it falls out of the mode. The parameters chosen are optical switch position, drive voltage and bumper coefficient of restitution. In this way a worst-case map of the danger area is formed.

The 1.65 degree three-quarter mode startup was chosen as the nominal starting point. Three graphs of the danger area are mapped, corresponding to each pair of parameters varied. The results are shown below.

ORIGINAL PAGE IS
OF POOR QUALITY

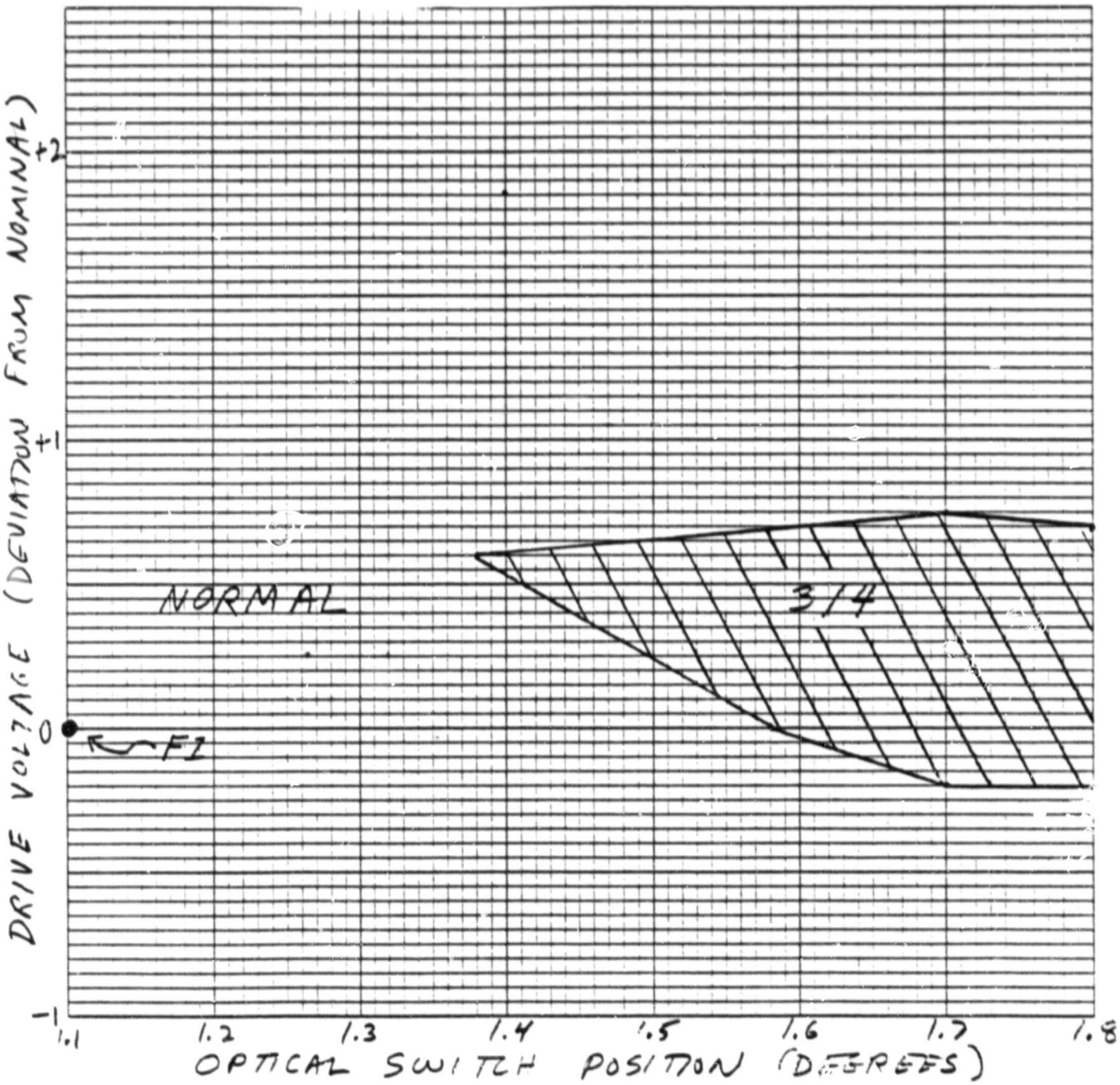

ORIGINAL PAGE IS
OF POOR QUALITY

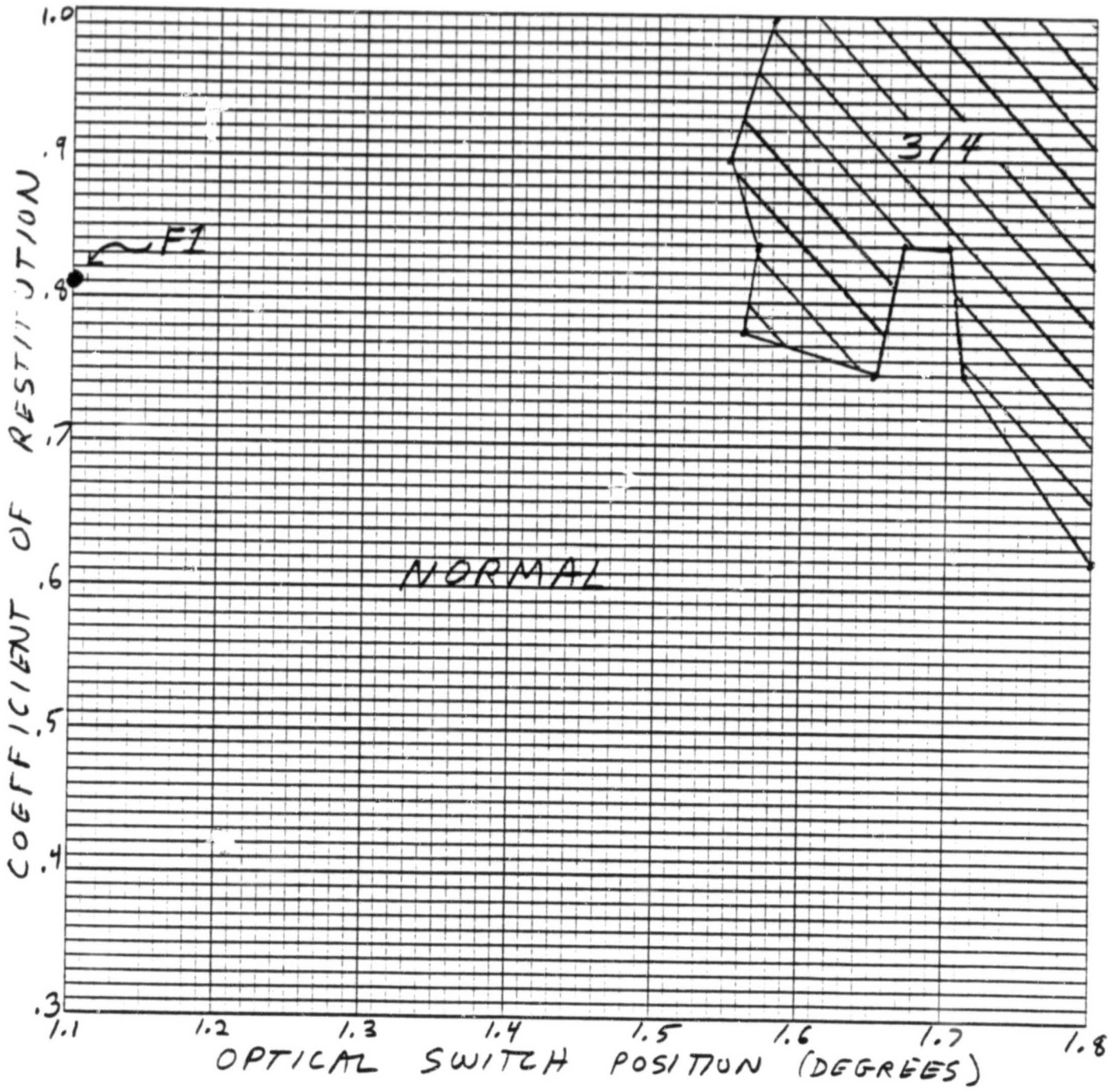

ORIGINAL PAGE IS
OF POOR QUALITY

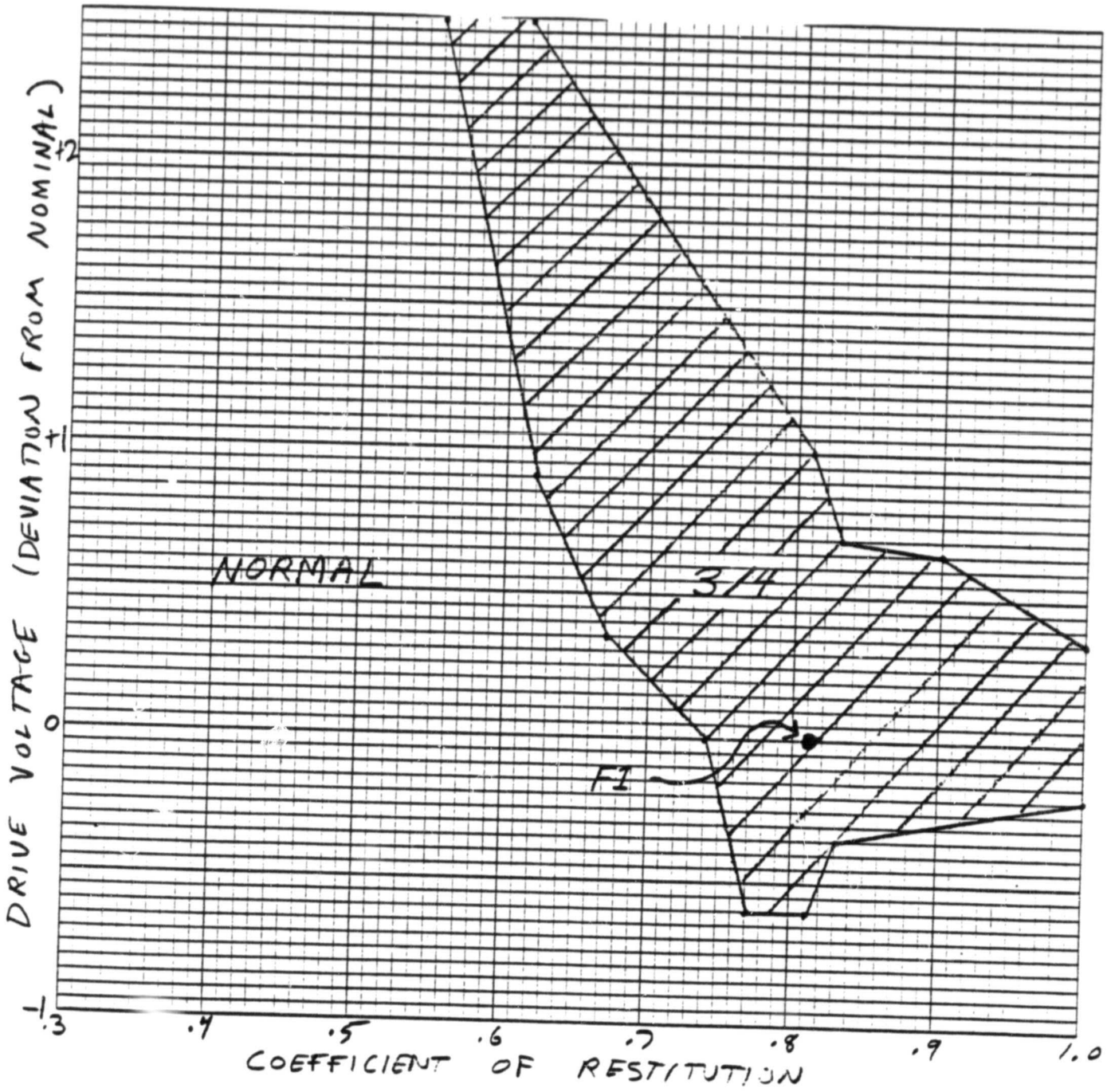

ORIGINAL PAGE IS
OF POOR QUALITY

7.4 Other Secondary Modes

Three-quarter mode is the secondary mode of most concern because it occurs nearest to actual flight parameter settings. There are in addition other secondary stable modes found by the simulation.

"Low voltage modes" occur at drive voltages well below the normal operating range. At very low voltages, several torque pulses are needed to have the same effect as one normal pulse.

Voltage	Mode
5-6	1/5
6-8	1/4
9-11	1/3
12-15	1/2

At drive voltages between 15 and 21 volts, a variety of complex modes between 1/2 and 3/4 exist. In the lower part of this range there is a 5/8 mode and in the upper part a 2/3 mode. A stable start-up in these modes has not been found.

Between 22 and 26 volts, no secondary modes have been observed.

There are "super-harmonic modes" at voltages above the normal operating range. In these modes the scan mirror cycles more often than the clock. A 5/4 mode was observed at about 38 volts. There are also "compound modes" in this region, such as [3/4, 1, 5/4, 1] or [2/3, 1, 3/2, 1]. These modes have a higher level cycle between normal, subharmonic and super-harmonic modes.

8 Conclusions

The simulation program in its current state is able to model the MSS-D SMA reasonably well. If we assume the accuracy of its predictions, what can we say about the danger of secondary stable modes?

1. The critical parameters are optical switch position, drive voltage, and torquer efficiency. Bumper coefficient of restitution is not a significant factor.

2. The dangerous parameter settings are optical switch position over 1.4 degrees, drive voltage 27-29 volts, and high torquer efficiency.

3. The Flight Model comes closest to the mode at nominal parameter settings. Only its low optical switch setting of 1.1 degrees keeps it away from the mode region.

In order for three-quarter mode to occur, a strong torque pulse is required. The torquer must be able to quickly turn the mirror around off bumper. High optical switch position, high drive voltage, and high torquer efficiency all contribute to the strength of the torque pulse. A simple way to increase safety margins would be to lower the drive voltage by 1 or 2 volts. The torquers on all three models, but especially the Flight Model, are stronger than required for normal operation.

If additional MSS scan mirror assemblies are built, the problem should be eliminated entirely by controlling the start-up phase. If the torquer starts with a properly selected fixed length torque pulse, it will go directly into normal operation.

9 Bibliography

[1] "Nondimensional MSS SMA Equations of Motion," M.I. Miyagi, HAC IDC HS248-0476, 20 February 1979.

[2] "Measurements of MSS-D Electrical Parameters," Richard Gillmann, HAC IDC HS248-1351, 16 June 1981.

[3] "Measurements of MSS-D Mechanical Parameters," Richard Gillmann, HAC IDC HS248-1384, 22 July 1981.

[4] "SMA Torquer Measurements," G.L. Zomber and W. Swarthout, HAC IDC HS248-0714, 2 October 1979.

[5] "MSS-D SMA Parameter Values," V. Nocheski, HAC IDC 7732.30/294, 27 April 1981.

[6] "MSS-D Scan Mirror Simulation Status Report," M.I. Miyagi, HS248-0842, 3 March 1980.

[7] "MSS-D SMA Simulation and Analysis Results - Final Report," M.I. Miyagi, HS248-0199, 5 July 1978.

[8] "MSS-D SMA Simulation Model and Parameter Values," R. Gillmann, Hughes IDC HS248-1386, 23 July 1981.

[9] "MSS-D Scan Mirror Assembly Test Report Three-Quarter Mode Problem," W. Swarthout, Hughes IDC HS248-1352, 23 June 1981.

[10] "Agreement between MSS-D SMA Simulation and Engineering Model," R.A. Gillmann, Hughes IDC HS248-1415, 26 August 1981.

[11] "Scan Mechanism Configuration Freeze Report," HS324-3827, 2 September 1970.

[12] "MSS Scan Mechanism Simulation Description," R.H. Bernard, Hughes IDC HS324-4402, 3 June 1971.

[13] "Updated Torquer Model & Parameter Values for MSS-SIM," M.I. Miyagi, Hughes IDC HS248-0112, 9 May 1978.

[14] Analysis of Numerical Methods, E. Isaacson and H.B. Keller, Wiley, 1966.

ORIGINAL PAGE IS
OF POOR QUALITY

12.2 FIBER OPTICS PLATE

A problem that first appeared on F-1, but has subsequently plagued both the protoflight and F-1 models, is a design defect in the fiber optics plate. Although the problem manifests itself in several ways, its most troublesome feature is that, in the video channels affected, one ends up with a radiometric calibration which exhibits temperature dependence. In system performance testing it resulted in out-of-specification conditions of the channel-to-channel calibration within a spectral band. This calibration problem is discussed earlier in 7.4.4 and 10.4.4. As discussed below and in memoranda following this subsection, the problem was diagnosed to be caused by a defective optical bond line between the fiber optics ends and the transfer lenses bonded to them. The problem should be stable over time and the calibration repeatable with temperature cycling.

The first sign of this anomaly came during the gain and offset adjust procedure on the F-1 model during February 1981. When the gains were rechecked after their initial setup, one of the channels in band 4 was out of its allowed ±5 percent tolerance. Subsequent temperature tests on F-1 in ambient confirmed that several of the band 4 channels had departures from their expected gain/temperature relationship. Photos were taken of the focal plane end of the fiber optics array through the optics of the telescope. These photos showed that in some of the channels spurious reflections were occuring in the optical train somewhere downstream of the focal plane, indicating an optical discontinuity between the focal plane and the detectors. Experiments were tried in which only band 4 detectors were swapped among themselves to isolate the anomaly to either the detectors or the fiber array. The problem stayed with the fiber optics. Eventually a decision was made to change out the whole F-1 fiber plate assembly for a spare assembly. Photos of the spare assembly at the time of its installation in F-1 showed no indication of spurious reflections in any channel.

Concurrently with the F-1 effort, photos were taken of the protoflight focal plane which also showed spurious reflections in some of the channels. The protoflight was taken through its thermal-vacuum test during May 1981. During this test the calibration of certain channels exhibited temperature dependance and resulting out-of-specification channel-to-channel calibration performance. The gain versus temperature relationships in these channels were also not the well behaved curves associated with normal MSS video channels. There also was good correlation between channels which exhibited reflectance changes with temperature in the fiber optics photos taken prior to thermal-vacuum testing and the channels showing temperature dependent calibration during the thermal-vacuum test.

Following thermal-vacuum testing on the protoflight, an IDC (HS248-6691) documented what was known about the problem, including a semi-quantitative analysis of the possible causes. The two mechanisms analyzed were a broken fiber and a debonded relay lens.

Subsequent to the protoflight acceptance test, further optical tests were performed on the fiber plate removed from F-1 to determine whether the anomaly experienced on it was due to broken fibers or debonded relay lenses. The tests showed conclusively that relay lenses were debonding and that there were no broken fibers in that assembly. A summary of those tests and their results is given in HS248-6782. Further experimentation would be necessary to understand the bond line failures well enough to avoid this problem in any future fiber optics procurements.

ORIGINAL PAGE IS
OF POOR QUALITY

When the F-1 instrument was taken through its thermal-vacuum test, a similar temperature dependent calibration anomaly was evident. In this case only one channel, number 11, appeared to have the debonding problem.

ORIGINAL PAGE IS
OF POOR QUALITY

SANTA BARBARA RESEARCH CENTER
A Subsidiary of Hughes Aircraft Company

INTERNAL MEMORANDUM

TO: R. Johnson

CC:

DATE: 26 June 1981

REF: HS 248-6691
2221.327

FROM: R. Turtle
R. Turtle

BLDG. 774 MAIL STA. 78
EXT. 4183

SUBJECT: Temperature dependence of corrected signal level and gain and unusual fiber appearance.

Distribution:

L. Barncastle
K. Brinkman
H. Ellison
J. Garcia
G. Gritt
A. Lauletta
G. Lech
T. Sciacca
R. Wengler
J. Yeagley
J. Yuh
J. Zomber
Data Bank(5)
Optics File (1)

ORIGINAL PAGE IS
OF POOR QUALITY

- I -

During thermal-vacuum testing of the MSS-D protoflight instrument, corrected signal level (CSL) varied in an unusual way with temperature in channels 2, 8 and 11 (1B, 2B and 2C). Misbehavior of corrected signal level indicates that there is a problem in the transfer optics that route light from the focal plane of the radiometer telescope to the detector of the channel in question for the following reasons:

Corrected signal level is proportional to $\frac{Rs}{Rc}$, where Rs is the response (or signal) produced when light from the collimator is incident on the detector of a particular channel and Rc is the response when light from one of the calibration sources is incident on the same detector. A prism mounted on the rotating shutter wheel at the focal plane of the radiometer telescope periodically reflects light from one calibration source or the other to all the detectors during intervals between scans of the scene being viewed. For the measurement of corrected signal level, the"scene" is the illuminated focal plane of the collimator. Since many channels produce well-behaved corrected signal level data, it is clear that no factor that would affect all channels (such as a change in the radiometer telescope or in the calibration lamps) can be involved. Detector problems can be ruled out, for the detector of each channel views the collimator and the calibration source alternately in rapid succession. Therefore the cause must lie in the individual transfer optics systems that route light from the radiometer focal plane to the detectors of the channels involved.

ORIGINAL PAGE IS
OF POOR QUALITY

- II -

Before proceding with further analysis, it is necessary to present a summary of all the unusual conditions that have been observed which may have a bearing on the problem. Figure 1 shows these divided into different categories channel by channel.

1. As already discussed, corrected signal level varies with temperature in channels 2, 8 and 11. Typical thermal-vacuum test data showing this are given in Figures 2, 3, and 4. Average signal level (ASL) and gain (G) are also plotted. Corrected signal level (CSL), average signal level and gain are related by

$$CSL \propto R = \frac{ASL - \phi}{G} \qquad (1)$$

where R is the scene radiance and ϕ is the offset, typically about half a quantum level (QL).

2. As the temperature is raised above ambient, the gains measured for channels 2 and 8 begin to vary depending on which calibration source (A or B) is used. This behavior can be seen in Figures 2 and 3. Because of the relationship between corrected signal level and gain shown by Equation 1, the consequences of this effect are apparent in the corrected signal level data for these channels shown in the same figures. At temperatures below ambient, gain and corrected signal level are relatively well behaved in both channel 2 and channel 8. In this respect these channels differ from channel 11, for in this channel an increase in corrected signal level is observed whenever the temperature is raised or lowered relative to ambient. This can be seen in Figure 4, which should be compared with Figures 2 and 3.

ORIGINAL PAGE IS
OF POOR QUALITY

3. When the focal plane fiber termination array was examined by reflected light, channels 2, 8 and 11 all changed appearance as the scanner temperature was gradually raised above ambient. Once again there were differences which suggest that channel 11 falls into a separate category from channels 2 and 8. This investigation was conducted as part of STR 59. The fiber terminations were examined through a spotting telescope focused on the radiometer focal plane. Light from a narrow beam illuminator was incident on the fibers at such an angle that specular reflection from the polished surface of the fiber array would not be seen. However, the beam obliquity was not so great that light could not enter the fibers and be transmitted down them to the detectors. The appearance of a particular channel in the array depended on what the light encountered that would reflect it back toward the observer. During this test the scanner was mounted on the alignment fixture while its temperature was slowly raised to about 40°C by means of resistance heaters. Cooling the instrument was not possible in the clean room environment because of the risk of condensation. Photographs of the focal plan array were made through the spotting telescope at temperatures of approximately 25, 30, 35 and 40°C. These are included here as Figures 5 through 8 and serve as the basis of the following discussion. Note that the scan mirror causes a reversal in channel order from what would be expected based on the channel assignment given in SBRC Drawing 51687.

Figure 5 shows the appearance of the focal plane array at the clean room ambient temperature of approximately 25°C. One would expect all the

ORIGINAL PAGE IS
OF POOR QUALITY

channels in each band to appear nearly the same. Their characteristic colors (red in band 1 and darker shades ranging from blue-green to brown in the other three bands) are due to light reflection at the surfaces of the spectral filters that limit the sensitivity range of each band to the desired wave length interval. For example, Band 1 is meant to detect green light, and red light is excluded by multilayer interference filters that preferentially reflect red light back along the fibers. This accounts for the striking, bright red appearance of the band 1 fibers when the focal plane array is examined by reflected light. In the unusual, brighter-appearing channels there must be optical discontinuities between the focal plane and the detectors that change the character of the light reflected back toward the observer. Many of the unusual appearing channels behaved well during thermal vacuum test: these are channels 9, 16, 17, 22, 23 and 24. It is probably significant that these channels remain about the same in appearance in Figures 6, 7 and 8; in other words, temperature stability of appearance apparently correlates with temperature stability of performance. The converse, it turns out, is also true; note how the hue of the channel 11 fiber termination changes with temperature. At 40°C it is darker than at 25°C, but the violet seen at the higher temperature is strongly suggestive of thin film interference phenomena. Similarly, channels 2 and 8 are almost normal at the two lower temperatures, but both have become much brighter in Figure 7 which was taken at 35° C. The unusual gain behavior of these channels also begins at about 35°C.

ORIGINAL PAGE IS
OF POOR QUALITY

Figure 9 gives a schematic diagram of the relay optics system that transmits light from the focal plane of the radiometer to an individual detector. SBRC documents which can be referred to for additional information are given as References 2 through 8.

The numerical aperture of the optical fibers is about 0.5 in air. That is, the fibers can accept and transmit light from an optical system with a focal ratio as small as f/1 assuming that the axis of the ray cone is properly aligned with the fibers. Appendix I includes information about the properties of the glasses in the optical fibers used for the MSS-D PF radiometer. Note in the optical schematic of Figure 9 that the light from the radiometer telescope (f/3.6) is incident along the axes of the fibers at the focal plane. The calibration sources, on the other hand, are aimed obliquely at the fibers: their optical axes make angles of roughly 14° with the fiber axes at the focal plane. The numerical aperture of the ray cones from the calibration sources incident on the fiber termination array is slightly greater than the numerical aperture of the radiometer telescope. Therefore, some of the rays from the calibration sources are incident on the fiber array at angles approaching the limiting acceptance angle of the fibers.

From the focal plane, the fibers run first through a short, curved gooseneck section. Focusing the radiometer is done by bending this gooseneck. After the gooseneck the fibers pass along epoxy-filled channels in the aluminum fiber optics plate to where they terminate at the positions of the individual detectors. Each fiber termination consists of a stainless steel button that stands clear of the surface of the plate by about .1 inch. The button provides mechanical support during the final process of grinding and polishing flat the end of the fiber it contains.

ORIGINAL PAGE IS
OF POOR QUALITY

Light emerging from the ends of the fibers is focused into the entrance apertures of the detectors by relay lenses. EPO-TEK 301 is used to bond the lenses to the fiber terminations. Because the lenses are mounted in aluminum mounting blocks and because aluminum has a coefficient of thermal expansion greater than that of stainless steel, these bonds are subjected to thermal stresses. EPO-TEK 301 is also used to bond the relay lenses into stainless steel rings which are, in turn, bonded in place in the aluminum mounting blocks with the same adhesive.

The spectral bandpass filters are bonded into the mounting blocks with EPO-TEK 301. Often the bond is to a side of a filter where interference layers were deposited. EPO-TEK 301 is also used to bond the enhancement prisms that couple light into the faceplates of the photomultiplier tube detectors used in bands 1 through 3.

ORIGINAL PAGE IS
OF POOR QUALITY

IV

During the course of analysis, several mechanisms which at first appeared capable of causing the observed problems were considered and tentatively rejected. For example, prism bond failure is probably not involved, for partial prism bond failure would not cause fibers to reflect light in the way that has been observed. Light that might be internally reflected at a prism bond delamination would subsequently be scattered at a ground surface instead of being directed back along the fiber. In addition, such light would be colored or blocked by the spectral filters in a way that is inconsistent with the appearance seen in Figures 5 through 8.

Another failure mode involves the possibility that the spectral transmission properties of some of the bandpass filters were varying to an unusual degree with temperature. As shown in Figure 11, the spectral radiance curves for the collimator earth albedo lamp and the internal calibration sources are distinctly different. Therefore any change in the spectral transmission properties of an individual filter would affect the ratio of the calibration source radiance to the collimator radiance and produce a change in the corrected signal level measured for the channel in question. To test this hypothesis corrected signal level measurements were made as a function of temperature with the calibration sphere substituted for the collimator as part of STR 59. The spectral radiance characteristics of the calibration sphere and collimator are quite different: Figure 11 shows that the spectral radiance of the calibration sphere increases as wave length increases. On the other hand, because of the use of filters, the spectral radiance of the collimator earth albedo source decreases with wave length. Consequently, one would expect corrected signal level to vary differently with temperature with the calibration sphere substituted for the collimator if filter spectral transmission changes were the cause of the problem. However, this turned out not to be the case when the experiment was tried during STR 59. The data obtained are shown in Figures 12 and 13 and are much fewer in number than those generated during

ORIGINAL PAGE IS
OF POOR QUALITY

thermal vacuum test, but, to the extent that comparison is possible, the changes observed in corrected signal level as temperature increases do not appear to depend on whether the collimator or calibration sphere is used.

Another argument against the filters being at the root of the corrected signal level variations is that the most vulnerable parts of a filter are the interference multilayers deposited on its surface. It is unlikely that delamination of these layers could produce an effect that varied reversibly with temperature. Relative spectral response measurements have been repeated for channels 2,8, and 11 at ambient temperature as part of STR 61 without anything unusual about the behavior of the filters being noted.

V

Bond failures between the relay lenses and fiber terminations and/or broken fibers are likely explanations for the unusual conditions that have been observed. These failures would involve portions of the relay optics system which undergo relatively severe stresses.
Analysis by J. Ermlich given in Appendix I is summarized in the following paragraphs:

1. The fibers are subjected to severe bending stresses at each bend between the focal plane and their terminations at the individual detector positions. At the outside of a bend the tension has been calculated to exceed 20,000 pounds per square inch (psi).
2. Because of the difference between the thermal coefficient of expansion of the glass used for the fibers and that of the aluminum from which the fiber optics plate is made, the fibers are subjected to additional stress during thermal cycling. Epoxy fills the channels in the fiber plate and constrains the fibers to follow the motion of the plate as the temperature changes. The glass is consequently subjected to an additional local stress of approximately 130 psi per degree centigrade as the plate temperature is raised above the temperature

ORIGINAL PAGE IS
OF POOR QUALITY

(room ambient) at which the epoxy was cured.

3. The fibers in the gooseneck are subjected to further loads when the gooseneck is bent to focus the radiometer.

4. Because of the difference between the thermal coefficient of expansion of the aluminum used for the relay lens mounts and that of the stainless steel from which the fiber terminations are made, the transparent bonds between the ends of the fibers and the relay lenses are loaded in tension whenever the fiber plate temperature is raised above the temperature (room ambient) at which the lens bonds were cured. However, loads produced in this way should not exceed 20 % of the expected bond strength.

A summary of the environmental stresses to which the fiber optics plate assembly has been exposed is given in Figure 14.

At the present stage of this investigation, stress analysis only points out possible failure modes of the transfer optics assembly that might be responsible for the problems that have been encountered. As will be discussed in the following section, fiber breaks and/or lens delaminations could be what are causing both the temperature dependence of corrected signal level and unusual fiber appearance. However, no single failure mechanism will emerge that accounts for all the observed phenomena in a completely satisfactory manner.

VI

Lens to fiber bond failures or breaks in fibers can be used as hypotheses to explain at least qualitatively changes in fiber appearance and corrected signal level with temperature.

Fiber breaks and/or bond delaminations would reflect light and can account for the bright appearing channels. A situation in which a gap opens as the fiber plate temperature is raised

ORIGINAL PAGE IS
OF POOR QUALITY

above ambient would account for the change in brightness observed in channels 2 and 8 at about 35°C. The fact that colors similar to thin film interference colors appear in the channel 11 fiber as the temperature is raised suggests that in this case a gap width that only changes with temperature is involved.

Optical discontinuities that change with temperature could also explain the variation of corrected signal level with temperature:

1. The coefficient of reflection at an interface between dielectrics is greater for rays incident at a glancing angle than it is for perpendicularly incident rays and can become unity when the conditions for total internal reflection are present. Therefore light rays propagating in a fiber at a large angle to its axis would tend to be more strongly attenuated at a crack or delamination than would more nearly paraxial rays. Also, any thermally-induced change in a discontinuity would consequently have a greater effect on the transmission of oblique rays than on the transmission of paraxial rays.

2. Experiments with a laser show that the magnitude of the angle a ray makes with the fiber axis remains nearly constant along a fiber. The damaged Mss-D F-1 fiber plate was used for this test after it had been removed from the F-1 radiometer. When light was incident of the focal plane termination array along the fiber axes, spots of light were observed on a paper screen held behind the individual fiber terminations. The N.A. of the cones of rays emerging from the individual terminations was about .125. When the laser was swung to an oblique angle of incidence, circles of light with dark centers appeared on the paper screen. The angle subtended by a circle at the exit termination of a fiber was roughly twice the angle the laser beam made with the fiber axes at the focal plane array. This characteristic appearance persisted until the angle of incidence of

ORIGINAL PAGE IS
OF POOR QUALITY

the light exceeded the limiting acceptance angle of the fibers.

3. As shown in the optical schematic of Figure 9, light from both the calibration sources is obliquely incident on the focal plane fiber array, whereas light from the radiometer telescope is paraxially incident on the fibers. Therefore thermally-induced changes in breaks or delaminations anywhere along the fibers could be expected to affect the transmission of light from the calibration sources more than that of light from the radiometer telescope. This process could produce the changes in corrected signal level with temperature that have been observed in channels 2,8, and 11.

At temperatures above 30°C different values for gain are obtained depending on which calibration source is used in both channels 2 and 8. If the angular distribution of light from the two calibration sources differed appreciably, than the same considerations just given in Paragraphs 1 through 3 could also explain this behavior. It is interesting to note, however, that the value for corrected signal level measured for channel 11 does not depend on which calibration source is used.

It does not appear to be possible to distinguish between a fiber break or a relay lens bond delamination as a potential cause of the phenomena that have been observed in channels 2, 8 and 11. Measurements that have been made using the damaged F-1 fiber plate suggest that either a broken fiber or a lens delamination can cause the transmission of a channel to vary with temperature.

VII

Bond failures between the fiber terminations and the transfer lenses may be the cause for the unusual behavior of channels 2,8, and 11 during thermal cycling as well as for the unusual appearance of these and other channels. Breaks in fibers, expecially

ORIGINAL PAGE IS
OF POOR QUALITY

in the highly stressed bend regions, are another possible cause. Both of these failure mechanisms would produce local stress relief that should result in a stable final condition. In the case of a fiber break, the epoxy matrix in which the fibers are imbedded would maintain the broken ends in close proximity. A lens bond delamination would relieve stresses on other bonds that would maintain the lens in position. Temperature changes in the range the instrument is expected to experience should produce only very small, reversible changes in the width of the gap at the position of a break or delamination.

The temperature of the MSS-D radiometer should be kept close to room temperature if possible and certainly not allowed to exceed 40°C if the risk of additional fiber breaks or lens bond failures is to be held to a minimum.

UNUSUAL CHANNELS

HUGHES

CHANNEL	BRIGHTNESS CHANGE	COLOR CHANGE	TEMPERATURE DEPENDENT APPEARANCE	CSL TEMPERATURE DEPENDENT
2	✓		✓	✓
8	✓		✓	✓
9	✓	✓		
11	✓	✓	✓	✓
16	✓			
17	✓			
22	✓			
23	✓	✓		
24	✓			

$$CSL \propto \frac{ASL - d}{G} = RADIANCE$$

Figure 1

ORIGINAL PAGE IS OF POOR QUALITY

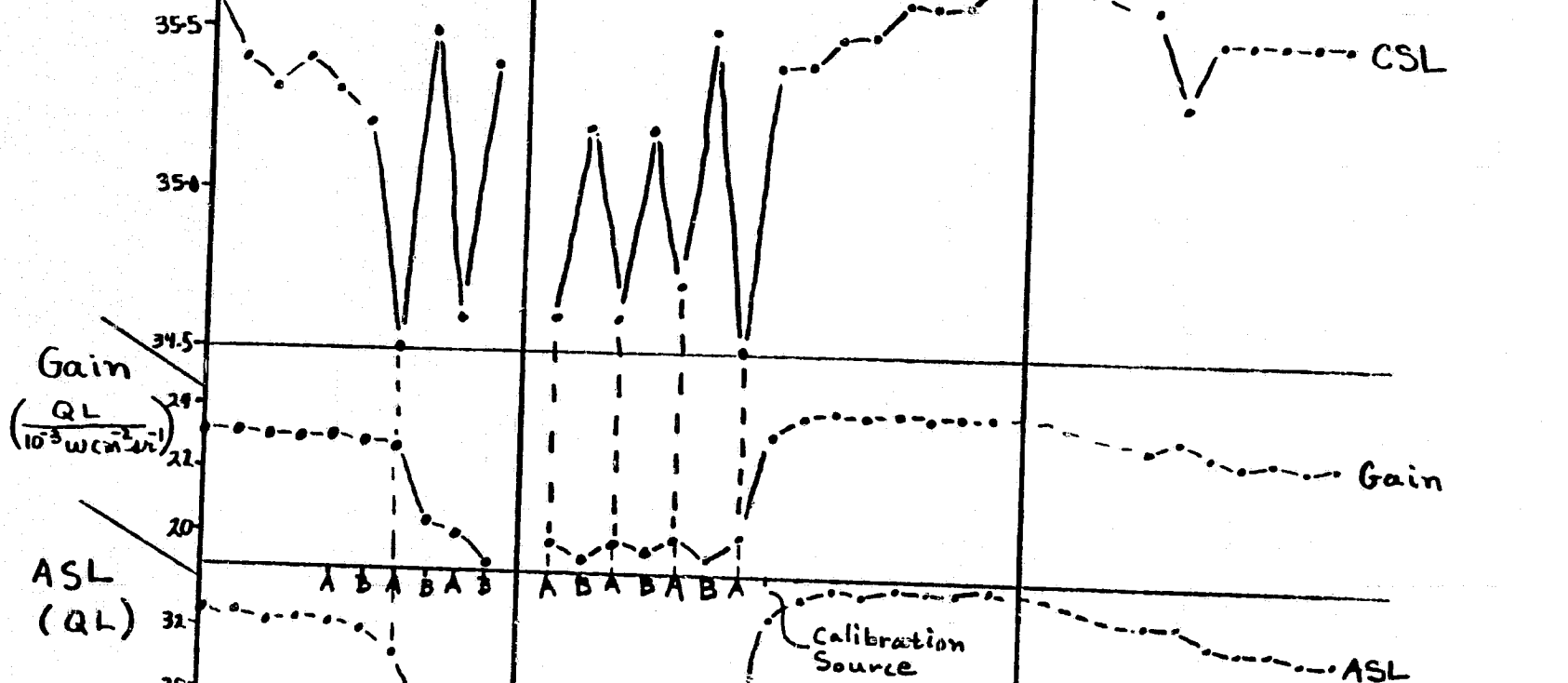

Figure 2. Note suppressed zeros. See Figure 4 for thermal history.

ORIGINAL PAGE IS OF POOR QUALITY

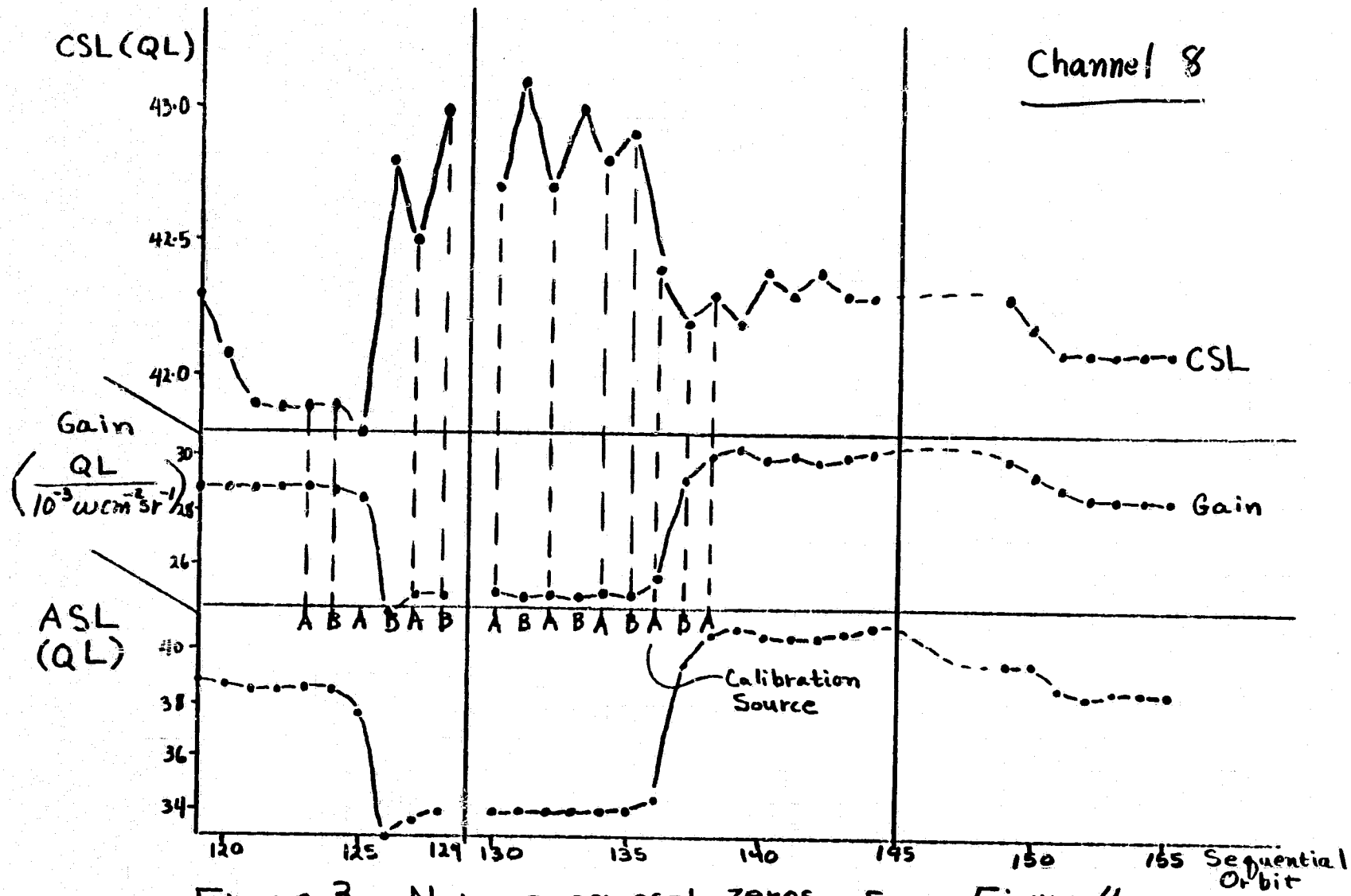

Figure 3. Note suppressed zeros. See Figure 4 for thermal history.

ORIGINAL PAGE IS OF POOR QUALITY

ORIGINAL PAGE IS
OF POOR QUALITY

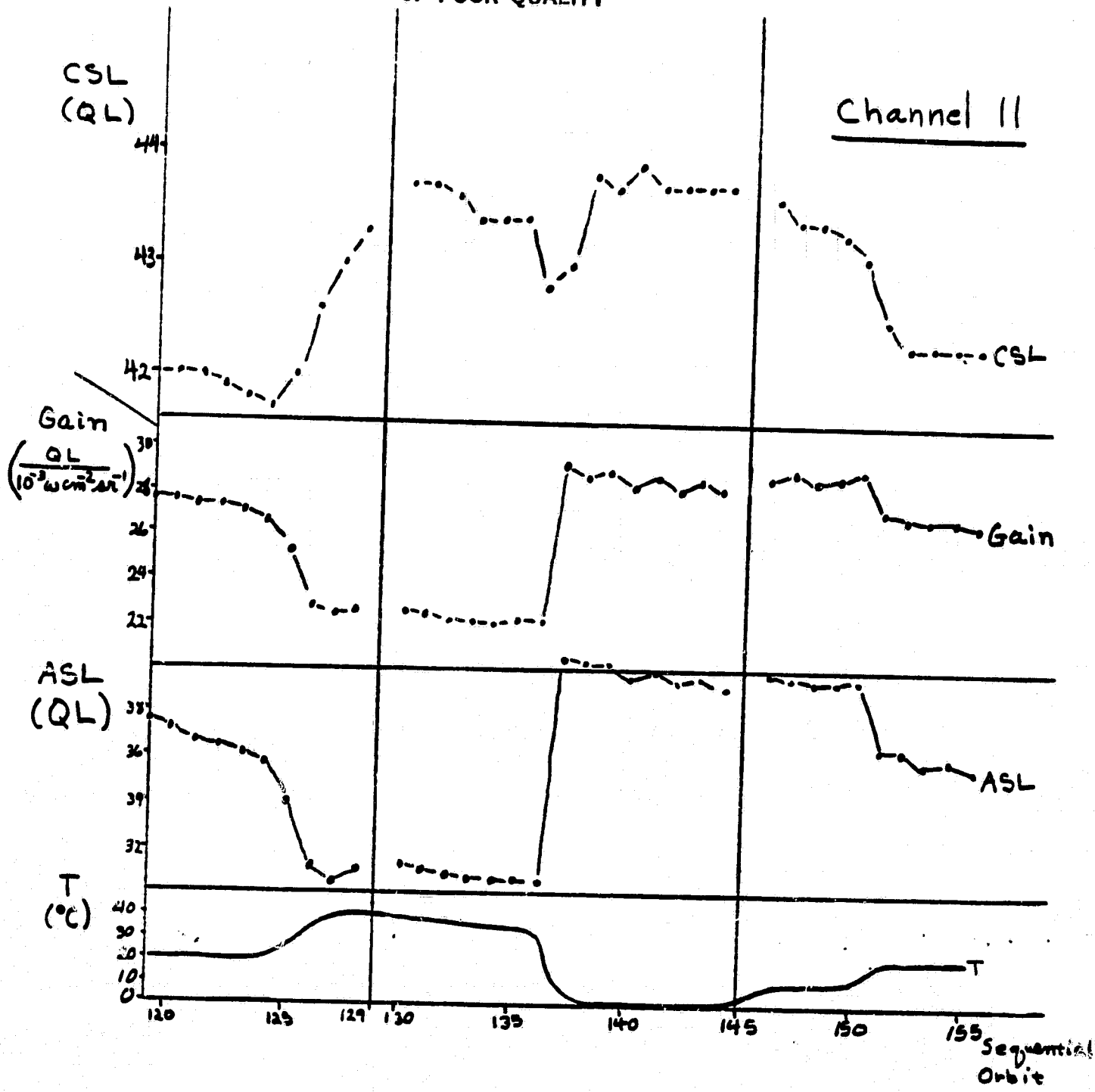

Figure 4. Note suppressed zeros.

ORIGINAL PAGE IS
OF POOR QUALITY

Figures 5 - 8

Photographs showing focal plane array appearance.

Figure	Temperature	SBRC Photo Number
5	ambient	81-5-234
6	30°C	81-5-235
7	35°C	81-5-236
8	40°C	81-5-237

Key:

Band 1	6	5	4	3	2	1	← Red
Band 2	12	11	10	9	8	7	
Band 3	18	17	16	15	14	13	
Band 4	24	23	22	21	20	19	

ORIGINAL PAGE IS
OF POOR QUALITY

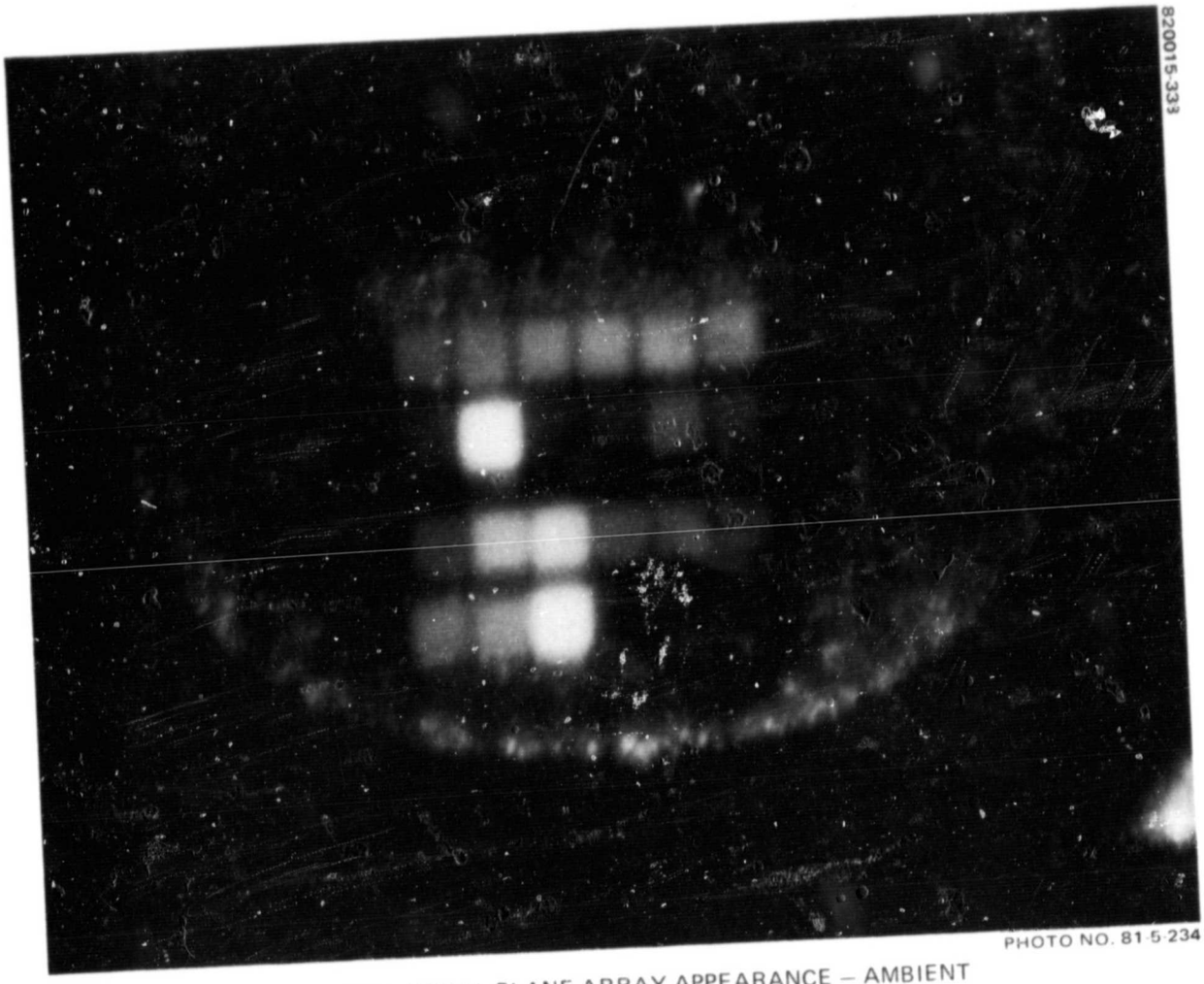

PHOTO NO. 81-5-234

FIGURE 5. FOCAL PLANE ARRAY APPEARANCE – AMBIENT

ORIGINAL PAGE IS
OF POOR QUALITY

PHOTO NO. 81-5-235

FIGURE 6. FOCAL PLAN ARRAY APPEARANCE – 30°C

ORIGINAL PAGE IS
OF POOR QUALITY

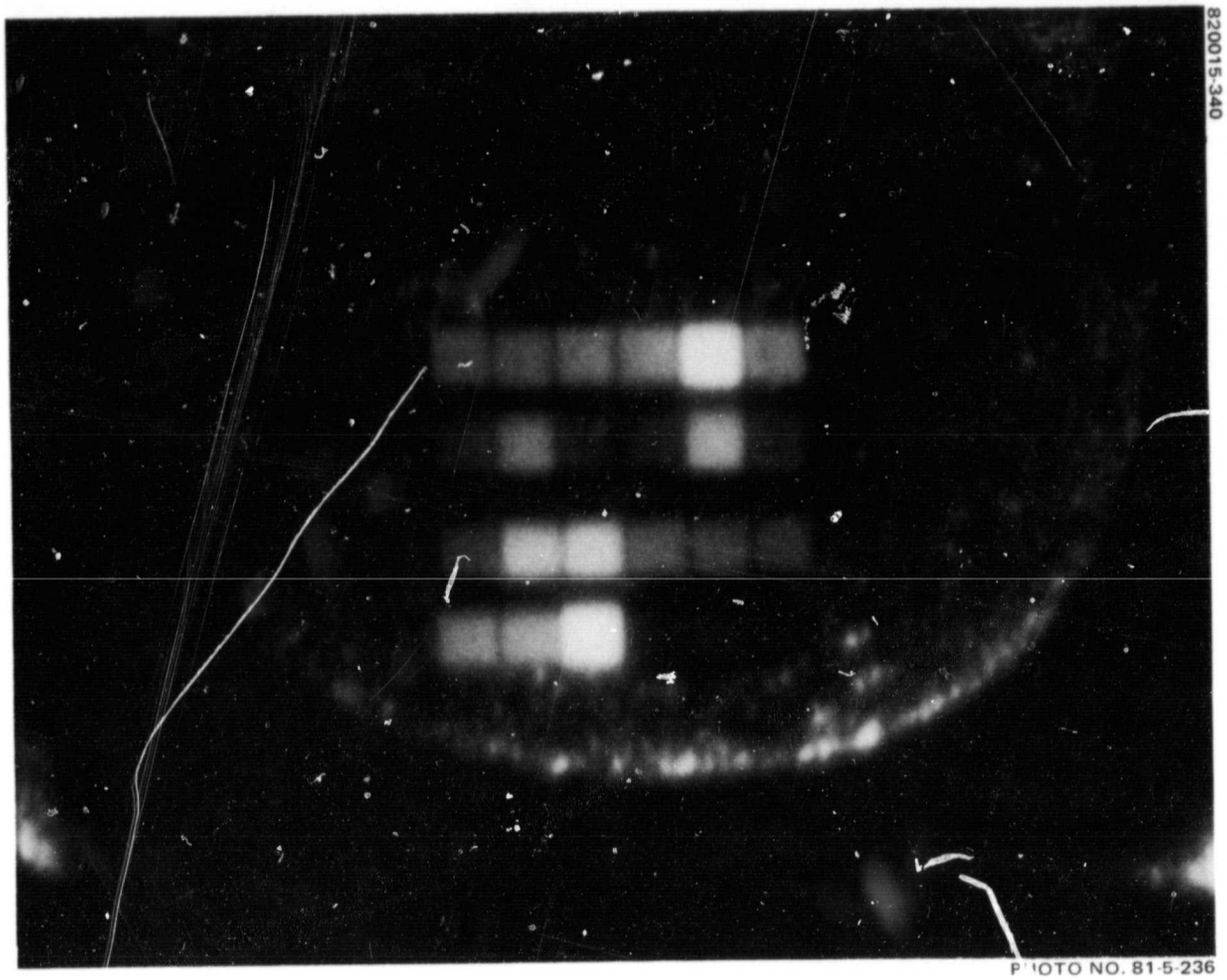

FIGURE 7. FOCAL PLANE ARRAY APPEARANCE – 35°C

C-6

ORIGINAL PAGE IS
OF POOR QUALITY

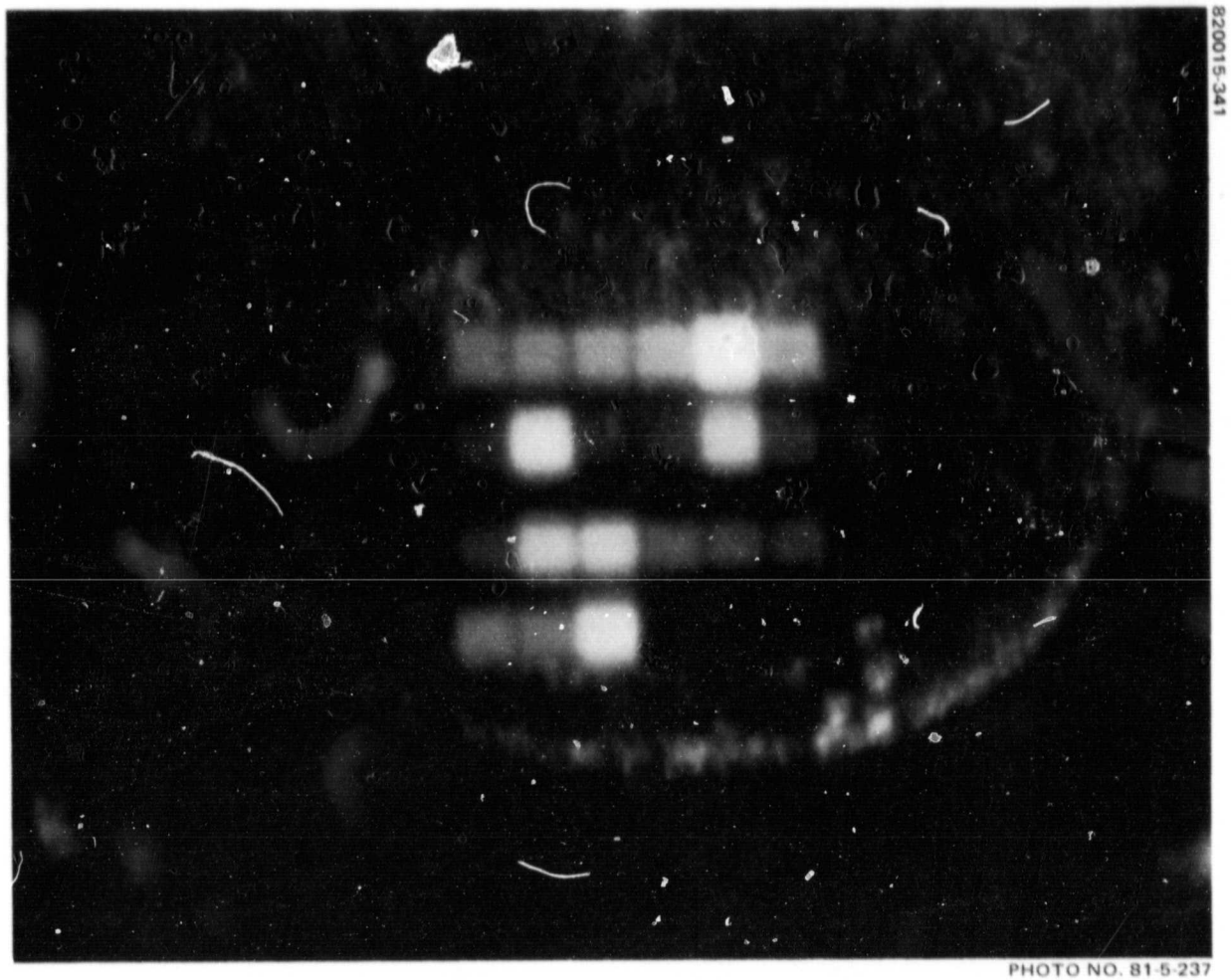

PHOTO NO. 81-5-237

FIGURE 8. FOCAL PLANE ARRAY APPEARANCE – 40°C

OPTICAL SCHEMATIC

HUGHES

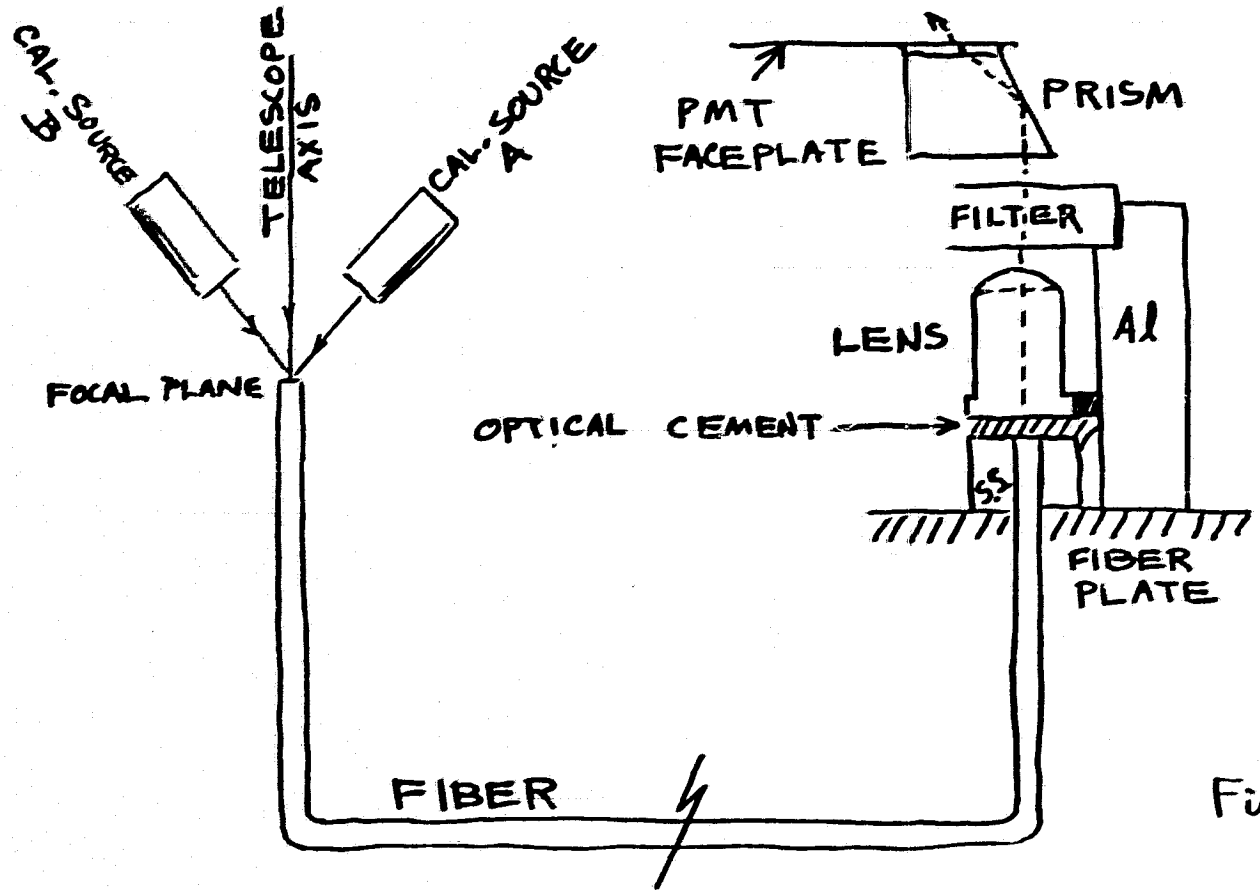

Figure 9

ORIGINAL PAGE IS OF POOR QUALITY

ORIGINAL PAGE IS
OF POOR QUALITY

Figure 10 contained redundant information and has been deleted.

ORIGINAL PAGE IS
OF POOR QUALITY

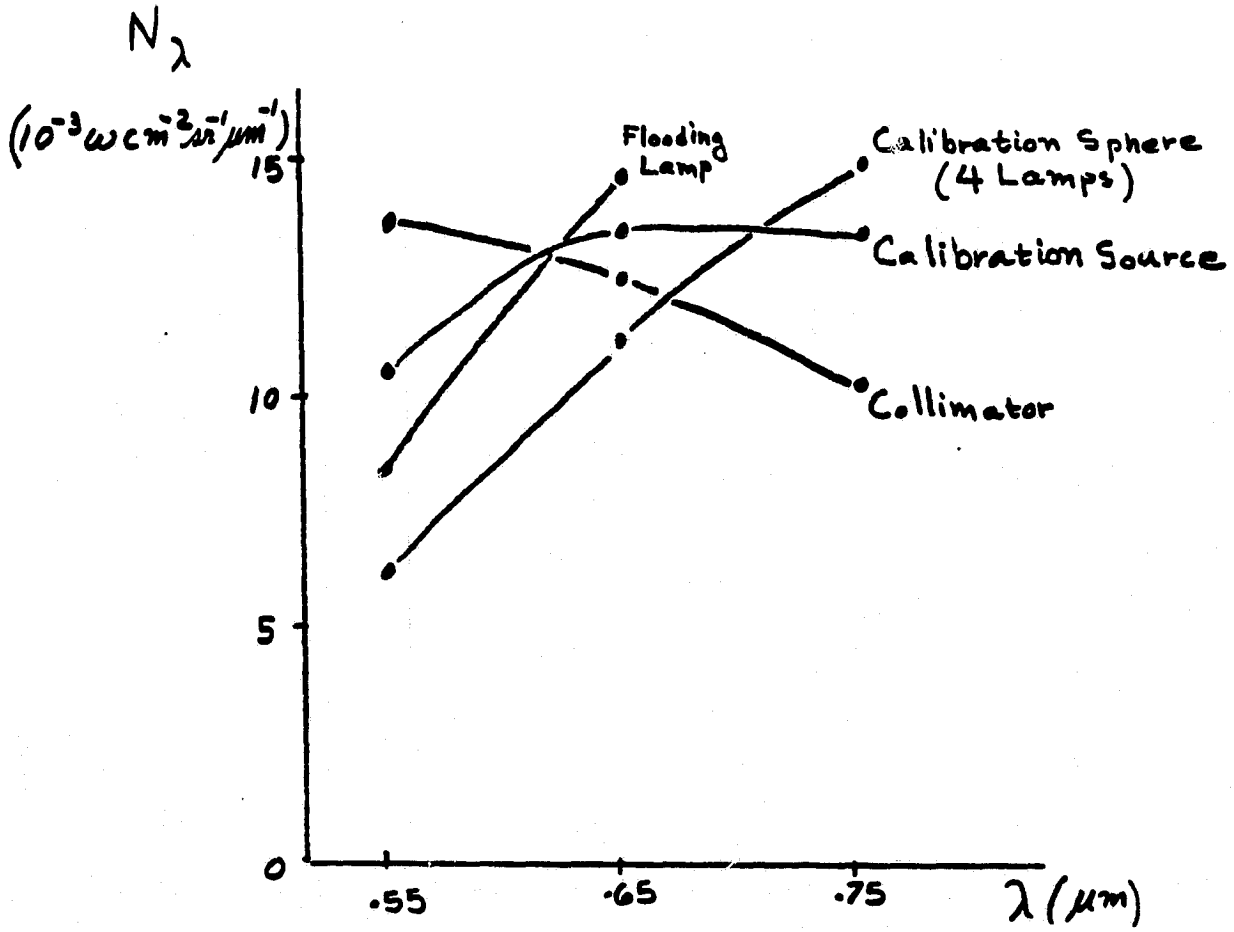

Figure 11

ORIGINAL PAGE IS
OF POOR QUALITY

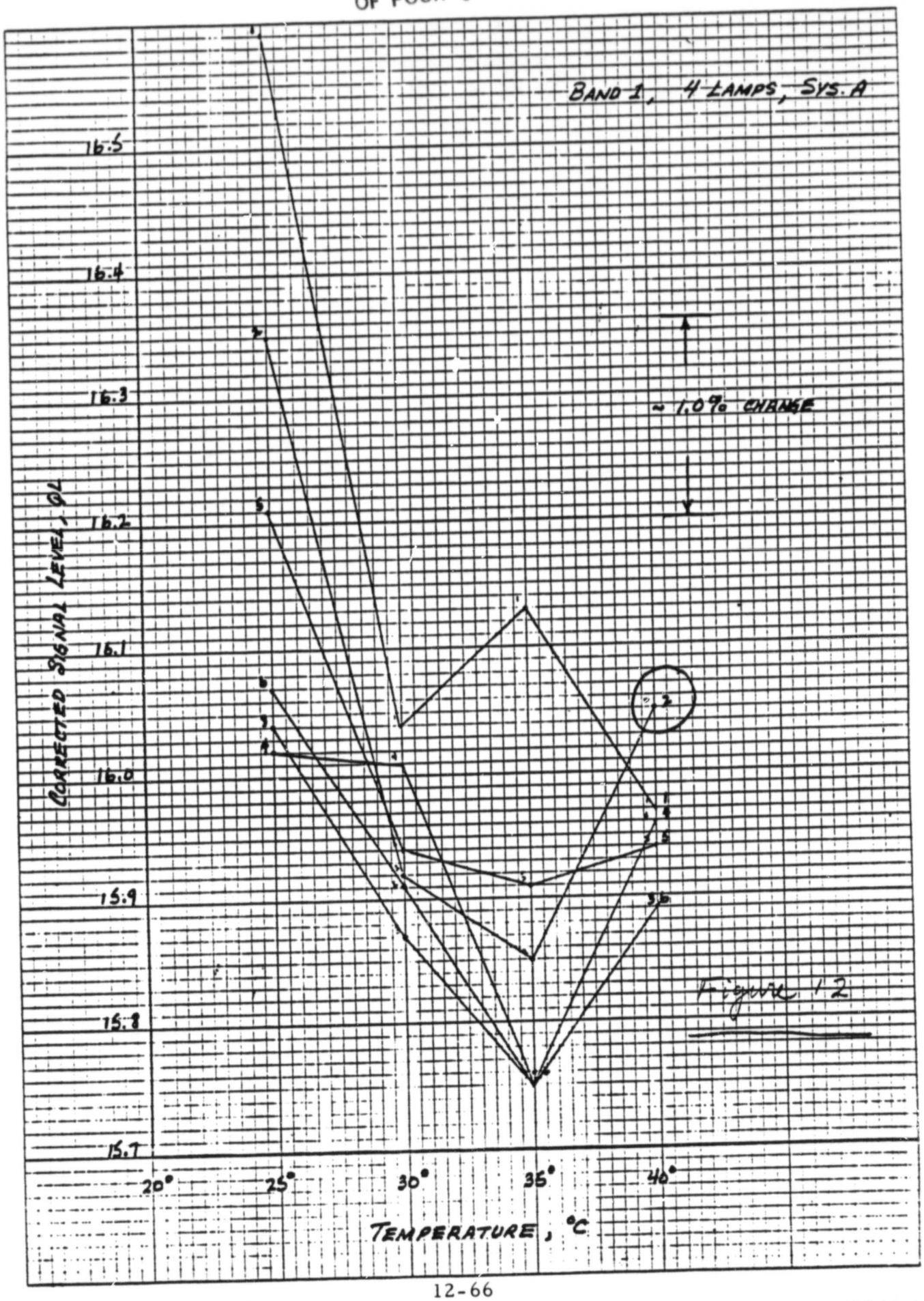

Figure 12

ORIGINAL PAGE IS
OF POOR QUALITY

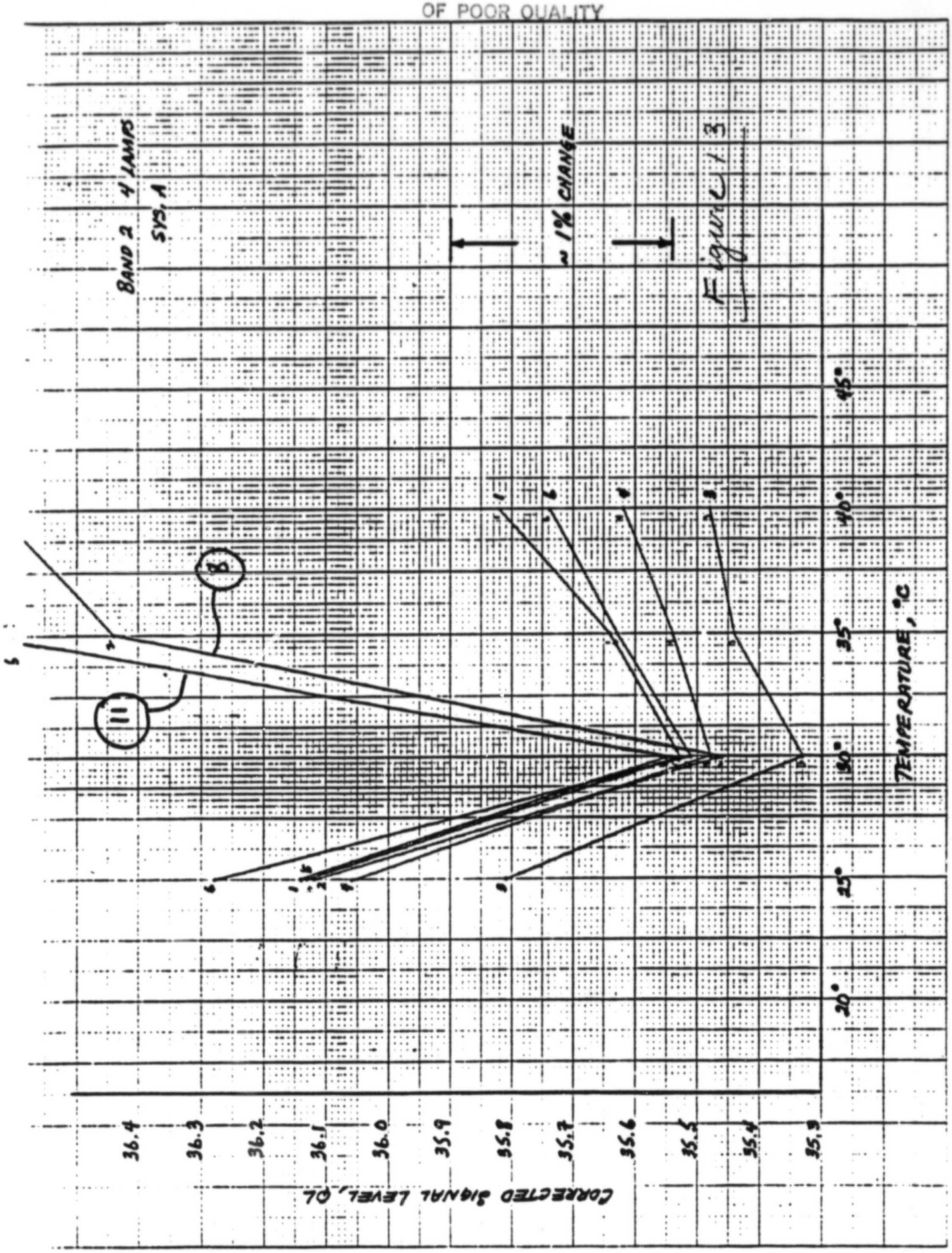

Environmental stresses experienced by the MSS-D PF fiber optics plate assembly.

I. Vendor's tests:

1. -5 to +55°C.
2. 20 g sinusoidal vibration, 5 to 2000 Hz.

II. During assembly:

1. Conformal coat cured at 120°F (49°C) with relay lenses bonded in place.

III. System test:

1. Vibration.
2. Acoustic.
3. Thermal-vacuum.

ORIGINAL PAGE IS
OF POOR QUALITY

Figure 14

ORIGINAL PAGE IS
OF POOR QUALITY

APPENDIX I

TENSILE THERMAL STRESSES ARE INDUCED IN THE GLASS FIBERS AND IN THE FIBER-LENS INTERFACES WHEN THE TEMPERATURES OF THESE COMPONENTS EXCEED THEIR ASSEMBLY TEMPERATURES.

THE THERMAL STRESSES ADD TO WHATEVER OTHER FIBER AND INTERFACE STRESSES MAY BE PRESENT, AND MAY THEREBY CONTRIBUTE TO FIBER BREAKAGE OR INTERFACE BOND FAILURE.

FIBER STRESSES ARISE FROM THE DIFFERENTIAL EXPANSIVITIES OF THE GLASS FIBERS AND THE ALUMINUM FIBER PLATE, WHEREIN THE ARMSTRONG A-12 POTTING ADHESIVE CONSTRAINS THE FIBERS TO ASSUME THE THERMAL STRAIN OF THE PLATE.

WITH E_g AND α_g THE YOUNG'S MODULUS AND COEFFICIENT OF THERMAL EXPANSION FOR GLASS, AND α_p THE TCE FOR THE FIBER PLATE, THE GLASS STRESS FOR A TEMPERATURE ELEVATION ΔT IS

$$S_g = (\alpha_p - \alpha_g) E_g \Delta T$$

APPLYING THE PARAMETERS OF TABLE I, THE TENSILE FIBER STRESS FOR A $\Delta T = 10°C$ IS

$$S_g = (23.2 - 7.4)10^{-6} \times 8.4 \times 10^6 \times 10 = 1330 \text{ psi.}$$

HERE THE CLAD GLASS E_g IS USED, SINCE ANY FAILURE WILL ORIGINATE IN THE CLADDING RATHER THAN CORE, AND AN AREA-WEIGHTED α_g IS EMPLOYED.

MAXIMUM CLAD GLASS BENDING STRESSES OCCUR AT THE GOOSENECK BEND (R=0.75) AND AT THE BEND WHEREIN THE FIBERS ARE DIRECTED THROUGH THE FIBER PLATE (0.75R). THESE STRESSES ARE FOUND FROM $S = \frac{c}{2R} E_g$ WITH C: THE FIBER THICKNESS, AND ARE 22,800 AND 21,300 PSI, RESP.. ADDITIONAL STRESSES AT THE GOOSENECK MAY ARISE FROM FOCUS ADJUSTMENTS, AND OTHER STRESSES OCCUR DUE TO CLAD-CORE CTE DIFFERENCE AND POTTING STRESSES.

THESE ADDITIONAL STRESSES ARE MODEST RELATIVE TO THE BENDING STRESS, BUT COMPARABLE TO 10°C THERMAL STRESSES. THE BENDING STRESSES ARE SUFFICIENT TO ACCOUNT FOR FIBER BREAKAGE IN THE PRESENCE OF MINOR SURFACE FLAWS IN THE CLAD GLASS. SUCH BREAKAGE MAY REASONABLY BE EXPECTED TO OCCUR; DEPENDING ENTIRELY ON FLAW SIZE-FREQUENCY DISTRIBUTION. ANY TENSILE STRESSES OF LONG DURATION (>10 HRS) EXCEEDING 1000 PSI RISK BREAKAGE UNLESS THE SURFACE IS FREE OF MODERATE CHIPS AND SCRATCHES. AT 20,000 PSI, THE SURFACE MUST BE FREE OF SMALL SCRATCHES AND MOISTURE ETCHING IF IT IS TO SURVIVE.

THERMAL STRESSES OF THE MAGNITUDE CALCULATED HERE SIMPLY ADD TO THE RISK. WHEREVER THE BENDING STRESS IS CLOSE TO THE LOCAL FAILURE STRESS, THE ADDED THERMAL STRESS MAY BE SUFFICIENT TO INITIATE A BREAK.

ORIGINAL PAGE IS
OF POOR QUALITY

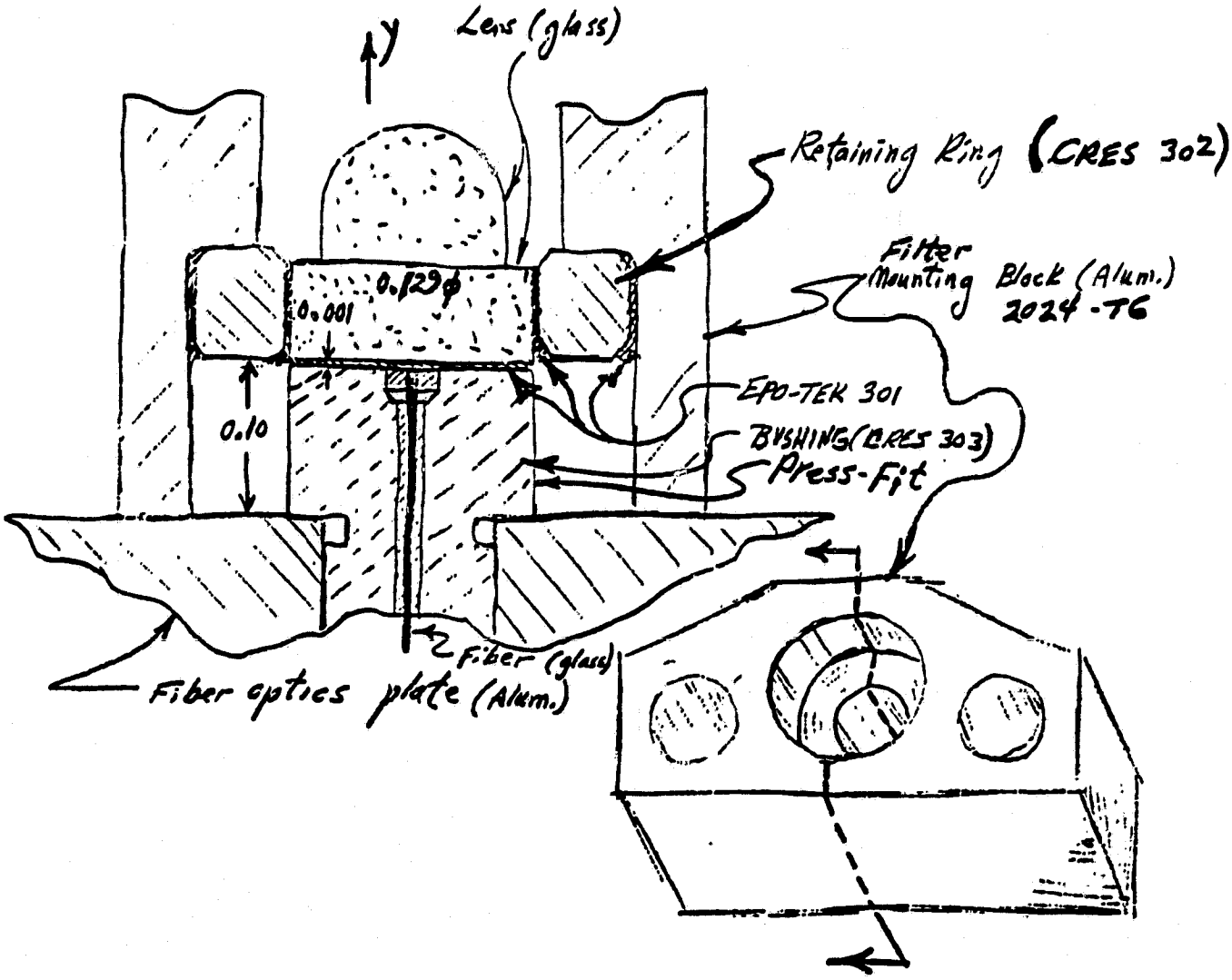

Figure: Glass Fiber/Lens Interface.

ORIGINAL PAGE IS
OF POOR QUALITY

UPON BREAKING, A FIBER END WILL STRAIGHTEN IN THE IMMEDIATE VICINITY OF THE BREAK, AND A SMALL ANGULAR OFFSET BETWEEN BROKEN ENDS WILL OCCUR. THE POTTING MEDIUM PROHIBITS OFFSETS GREATER THAN TENS OF MICROINCHES, OR A FEW HUNDRED MICROINCHES AT MOST. THE BREAKS WILL USUALLY BE REASONABLY CLEAN AND TRANSVERSE TO THE FIBER AXIS. WITH A CORE INDEX OF 1.573, A TRANSMISSION LOSS OF 10% IS EXPECTABLE, BUT OPTICAL INTERFERENCE BEHAVIOR CAN REASONABLY CAUSE LOSSES ANYWHERE FROM 0 TO 20%. THE TRANSMISSION MAY SUBSEQUENTLY BE TEMPERATURE SENSITIVE, AS THE INTERFEROMETRIC GAP AT THE BREAK CHANGES WITH TEMPERATURE.

IT IS EXPECTED THAT ANY SUCH BREAK WILL BE WELL-BEHAVED OVER TIME AND TEMPERATURE, AND WILL BE RELIABLY CALIBRATABLE WITH RESPECT TO TEMPERATURE.

FIBER BREAKS CAN ALSO OCCUR AT LOCATIONS OTHER THAN THE TWO SHARP BENDS, DEPENDING ON FLAW LOCATIONS, BUT THE PROBABILITY IS SHARPLY REDUCED EXCEPT VERY CLOSE TO THE FIBER ENDS. AT THESE TERMINATIONS, FLAWS RESULTING FROM OPTICAL FINISHING MAY INVITE BREAKAGE, BUT STRESS RELIEF BY THE POTTING MEDIA WILL MITIGATE AGAINST EXTERNALLY APPLIED LOADS AT THE GOOSENECK END.

THE LENS-FIBER INTERFACE INTRODUCES AN ADDITIONAL TENSILE STRESS CONDITION:

THE FIGURE ILLUSTRATES THE STRUCTURE, WHEREIN A STAINLESS STEEL BUSHING GUIDES A GLASS FIBER THROUGH THE FIBER OPTICS PLATE AND TO NEAR-CONTACT WITH A PLANO-CONVEX LENS. THE LENS IS MOUNTED ADHESIVELY TO A FILTER MOUNTING BLOCK VIA A MOUNTING RING.

A 0.001 INCH BOND-LINE OF EPO-TEK 301 RIGID EPOXY BONDS THE LENS TO THE FIBER AND BUSHING.

AS TEMPERATURE RISES ABOVE THE ASSEMBLY TEMPERATURE, THE FILTER MOUNTING BLOCK EXPANDS MORE THAN THE CRES BUSHING. THIS DIFFERENTIAL EXPANSION TENDS TO "LIFT" THE LENS FROM THE FIBER AND BUSHING, PLACING THE EPO-TEK EPOXY IN TENSION.

THE RETAINING RING AND ITS BONDS TO LENS AND FILTER MOUNT ARE PLACED IN SHEAR, AS IS THE BUSHING-FIBER PLATE PRESS-FIT INTERFACE.

THE LARGE CROSS-SECTION OF THE FILTER MOUNT (FIGURE) RELATIVE TO THE BUSHING PERMITS THE MOUNT TO ASSUME NEARLY ALL THE STRAIN GIVEN BY $\alpha_p \Delta T$. THE SEPARATION AT THE LENS-BUSHING INTERFACE, IF UNCONSTRAINED BY A BOND, IS THEN

$$\Delta y = y(\alpha_p - \alpha_b)\Delta T$$

FROM FIGURE AND TABLE I, IF $\Delta T = 10°C$, THEN

$$\Delta y = 0.10(23.2 - 17.3)10^{-6} \times 10 = 5.9 \times 10^{-6}$$

OR 6 MICROINCHES FOR A 10°C ELEVATION.

ORIGINAL PAGE IS
OF POOR QUALITY

TREATING THE SEQUENCE OF STRUCTURAL ELEMENTS AS A SERIES OF SPRINGS, THE PARTITION OF THE ΔY DEFORMATION OF THESE ELEMENTS AND THE CONSEQUENT STRESSES WERE CALCULATED. THE Y-DIRECTED FORCE WAS FOUND TO BE (ONLY) 3.8 LBS.

	DEFORMATION $\Delta Y (10^{-7}$ INCH)	COMPLIANCE $\frac{\Delta Y (\text{INCH})}{F \quad lb}$	STRESS (psi)
RETAINING RING TO MOUNTING BLOCK, EPO-TEK (SHEAR)	13.2	3.47×10^{-7}	79
RETAINING RING (SHEAR)	5.8	1.54×10^{-7}	116
RETAINING RING TO LENS, EPO-TEK (SHEAR)	25.5	6.67×10^{-7}	154
BUSHING TO FIBER-PLATE, PRESS FIT (SHEAR)	0	0	105
BUSHING (TENSION)	10.3	2.75×10^{-7}	293
LENS TO BUSHING BOND, EPO-TEK (TENSION)	4.1	1.10×10^{-7}	293

IT IS SEEN THAT THE HIGH CTE FOR THE AUSTENITIC CRES (303) KEEPS THE THERMAL STRAINS AT A MODERATE LEVEL, AND THE SHEAR COMPLIANCE OF THE RETAINING RING AND ITS BONDS ACT AS A MODERATELY EFFECTIVE STRESS RELIEF FOR THE LENS-TO-BUSHING BOND.

EVEN AT $\Delta T = 20^{\circ}C$ THE BOND IS UNDER ONLY ABOUT 600 psi TENSILE LOAD, WHILE A TENSILE STRENGTH OF 4400 MIGHT BE EXPECTED OF THE EPOXY.

ORIGINAL PAGE IS
OF POOR QUALITY

GLASS FIBERS

DIMENSIONS: 0.0038" SQUARE, 25:1 LINEAR CORE-TO CLAD RATIO, OR 12.5:1 AREA RATIO.

	CORE	CLAD
GLASS TYPE	SCHOTT BAK-1	KIMBALL EN-1
YOUNG'S MODULUS (E_g)	10.7×10^6 psi	8.4×10^6 psi
SHEAR MODULUS (G_g)	4.3×10^6 psi	4.7×10^6 psi
THERMAL EXPANSION COEFFICIENT (α_g)	7.6×10^{-6} /°C	4.6×10^{-6}/ °C

FIBER PLATE AND FILTER MOUNTING BLOCK

MATERIAL. ALUMINUM ALLOY 2024-T6.
YOUNG'S MODULUS (E_p) 10.6×10^6 psi.
THERMAL EXP. COEFF. (α_p) 23.2×10^{-6}/ °C.

CRES BUSHING & LENS RETAINING RING

MATERIAL. 303 CRES
YOUNG'S MODULUS (E_b) 28.0×10^6 psi
THERMAL EXP. COEFF (α_b) 17.3×10^{-6}/ °C
SHEAR MODULUS (Gb) 11×10^6 psi (ESTIMATE)

EPO-TEK 301

YOUNG'S MODULUS (Ee)	7×10^5 psi (ESTIMATE)
SHEAR MODULUS	3.6×10^5 psi (ESTIMATE)
LAP SHEAR STRENGTH	1650 psi
TENSILE STRENGTH	4400 psi (ESTIMATE)

TABLE I. MATERIAL PARAMETERS.

ORIGINAL PAGE IS OF POOR QUALITY

WORK SHEET

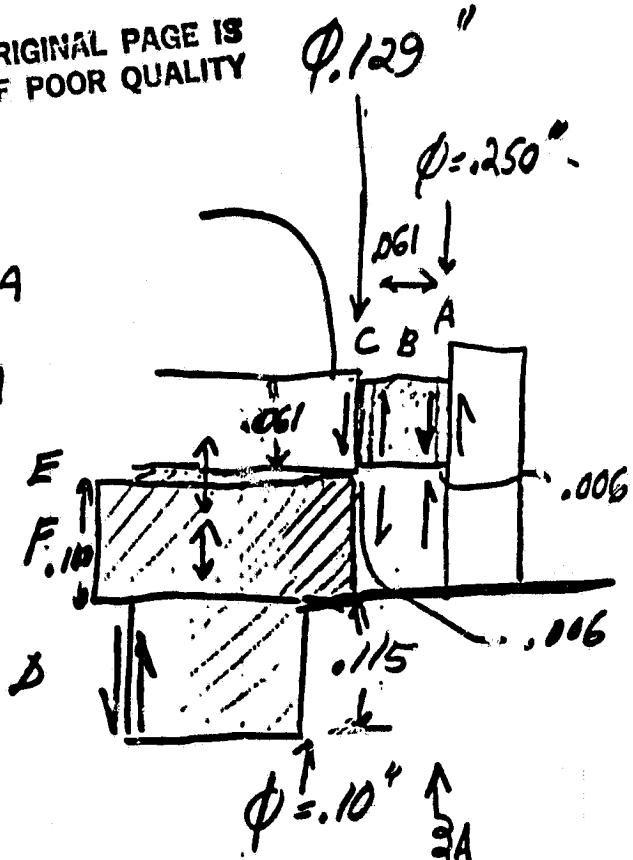

$$F = S_A = \delta E A = \frac{\Delta y}{y} E A$$

$$F = S_s A = \phi G A = \frac{\Delta y}{\Delta x} G A$$

$$\Delta y = (\alpha_A - \alpha_s)\, y \Delta T$$
$$= (23.2 - 17.3)\, .1 \times 10$$
$$= 5.9 \mu in$$

$$\Delta y_A + \Delta y_B + \cdots + \Delta y_F = \Delta y$$
$$F_A = F_B = \cdots = F_F$$

Solve for F:

$$\Delta x_A \overset{3.47\times10^{-7}}{G_A^{-1}} A_A^{-1} + \Delta x_B \overset{1.54\times10^{-7}}{G_B^{-1}} A_B^{-1} + \Delta x_C \overset{6.67\times10^{-7}}{G_C^{-1}} A_C^{-1} + \Delta x_D \overset{0}{G_D^{-1}} A_D^{-1}$$
$$.006/3.6\times10^5 \times .048 + .061/11\times10^6 \times .036 + .006/3.6\times10^5 \times .025 + 0 +$$
$$+ y_E E_E^{-1} A_E^{-1} + y_F E_F^{-1} A_F^{-1} = \Delta y F^{-1}$$
$$.001/7\times10^5 \times .013 + .100/28\times10^6 \times .013 = 1.55\times10^{-6} = 5.9\times10^{-6} F^{-1}$$
$$1.10\times10^{-7} + 2.75\times10^{-7}$$

Then

$$S_A = F/A_A = \frac{3.8}{.0479} = 79 \text{ psi}$$

$$S_C = \frac{3.8}{.0247} = 154 \text{ psi}$$

$$S_D = F/A_D = \frac{3.8}{.0361} = 105 \text{ psi}$$

$$S_E = F/A_E = S_F = 293 \text{ psi}$$

$$S_B = \frac{S_A + S_C}{2} = 116 \text{ psi (Approx)}$$

$$\boxed{F = 3.8 \text{ lbs}}$$

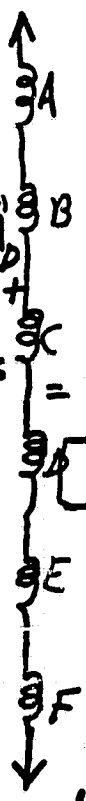

J. Ermlich

$$A_A = \pi .250 \times .061 = .0479$$
$$A_B = \frac{A_A + A_C}{2} = .0363$$
$$A_C = \pi \times .129 \times .061 = .0247$$
$$A_D = \pi \times .10 \times .115 = .0361$$
$$A_E = \pi \times .129^2 = A_F = .0130$$

ORIGINAL PAGE IS
OF POOR QUALITY

List of References

1. STR HS248-1126-59 (STR59) Thermal Test 5/28/81. (Fiber pictures and corrected signal level measurements with the calibration sphere.)

2. SBRC 16347: LAMP AND LENS ASSEMBLY-CALIBRATOR, MSS-D, TEST PROCEDURE FOR.

3. SBRC 52680: LAMP AND LENS ASSY-CALIBRATOR.

4. SBRC 53732: CALIBRATOR, LAMP AND LENS ASSY-OPTICAL SCHEMATIC.

5. SBRC 51687: PLATE ASSEMBLY, FIBER OPTICS-MSSD.

6. SBRC 16201: PROCUREMENT SPECIFICATION FOR MSS FIBER OPTICS ASSEMBLY.

7. SBRC 52731: TRANSFER OPTICS ASSY.

8. SBRC 52003: AFT OPTICS ASSY.

9. HS248-1126-61 (STR61) Protoflight Spectral Test Request - Relative Spectral Response.

ORIGINAL PAGE IS OF POOR QUALITY

SANTA BARBARA RESEARCH CENTER
A Subsidiary of Hughes Aircraft Company

INTERNAL MEMORANDUM

TO: Distribution

CC:

DATE: 2 November 1981

REF: HS248-6782
2221-410

FROM: J. K. Yuh

SUBJECT: Action Item No. 25 of HS248-6724, F1 PATR

BLDG. B11 MAIL STA. 78
EXT. 6289

Reference: HS248-6691, "Temperature Dependence of CSL and Gain and Unusual Fiber Appearance," dated 26 June 1981

Distribution:

	Program Office E.S.	NASA/AF
L. Barncastle		
B. Blomberg		
R. Cline	A. Lauletta	G. Gritt
H. Glenn	H. Ellison	T. Sciacca
G. Lech	R. Johnson	D. Young
J. Scannel	W. Stahura	
R. Turtle	J. Yeagley	
R. Wengler	G. Zomber	
J. Young		
Data Bank (5)		
Optics File		

Series of thermal tests were performed on the damaged F-1 fiber plate in order to isolate the problem area in the transfer optics train that may have caused gain variation in certain channels with temperature during the flight instrument's system testing.

Figure 1 gives a schematic diagram of the test setup. The focal plane fiber termination array was examined by reflected light through a high power microscope, and then photographs were made to record changing appearances of each channel as temperature of the fiber plate was gradually raised above ambient. The appearance of a particular channel depended on the light that would be reflected back toward the observer. For example, the first picture of Figure 2 (top left) shows the appearance of the fiber termination at the room ambient temperature of 23°C. The reason why the channels all appear differently is not only due to the characteristic colors of each band due to light reflected off the band pass filters, but there are also some bright channels due to some type of optical discontinuity, light brown channels due to absence of transfer lenses and finally opaque channels due to absence of any spectral filters. For this test only 14 channels were chosen for observations because of their complete optical trains.

The rest of the pictures of Figure 2 show color changes in some of these 14 channels as temperature of the fiber plate was gradually raised to 60°C. The photographs of Figure 3 were taken as the plate was cooled down to ambient. Figure 4 summarizes the test result: Out of 14 channels, 3 showed no change, 5 showed permanent color changes, and 6 showed color variation during elevated temperature but then returned to original colors when cooled down to ambient. The repeatability of these color changes were confirmed by going through one more complete thermal cycle. (Figures 5 and 6)

Action Item No. 25 of HS248-6724, F1 PATR

From the test it was discovered that the fiber channels experienced two types of color variations: One is that of sudden change to brightness indicating presence of thermally induced optical discontinuities, and the second is, as is the case of channel 3B, a thin film interference type of phenomena indicating a very minute gap width that changes with temperature. Since both of these conditions were most likely caused by bond failures and/or broken fibers, it was decided to do additional tests to isolate the failure mechanism.

I. Rebuild Some Channels

Five channels, 1E, 2E, 3E, 4E, and 2A, were selected as test samples. Their transfer lenses then were removed, cleaned, and reassembled using bond thicknesses (Epotek 301) of 0.002 to 0.004 inch. Figures 7 and 8 show the result of a complete thermal cycle of these channels. As the ambient (23°C) photograph of Figure 7 shows, all five channels started with appearance of very dark-brown color indicating that there was presence of no optical discontinuity anywhere along the fibers or bond interfaces, however, subsequent photos show that they all "popped" between 40°C and 50°C, turning to light brown or brighter-appearance color. Even after the fiber plate was cooled back down to ambient (Figure 8, T = 22.2°C) none of the channels returned to its original dark-brown color suggesting that the weak link in the optical train is the bond interface.

II. Contact Test

Channels 1E and 2F were chosen, and then torque was applied to the mounting screws of transfer lens assembly block. This would cause the gap between the fiber button and transfer lens to vary in proportion to the torque applied. The prupose of this test was to cause minute gap variation to create thin film interference type of phenomena. This should explain the color changes we saw in Channel 11 of the protoflight during thermal cycle. Figure 9 shows the color differences between pre and post tightening of mounting screws of Channels 1E and 2F.

III. Index matching Test

In order to dispel any doubt about the bond interface as the primary reason for this unusual color variation, index matching test was performed. This was done by removing all the transfer lenses from the same five channels, and then applying glycerin solution on the fiber buttons with a piece of dark paper placed behind them. This effectively eliminated light reflection from one end of the fiber, thus only the presence of optical discontinuity such as fiber breaks would make the channels appear bright by reflecting light at the broken interface. Figure 10 shows complete opaque appearance of all five channels after index matching positively indicating no broken fibers.

ORIGINAL PAGE IS
OF POOR QUALITY

2 November 1981
HS248-6782
2221-410

Distribution

Action Item No. 25 of HS248-6724, F1 PATR

Preliminary Conclusions

- Channel 4F gain drift with temperature was entirely due to fractured fiber. Abrasions on fiber termination were prominently noticeable, possibly caused by mishandling during reassembly after gain adjustment.

- On the other hand, the thermal cycles described in this memo and previously performed transmission tests (HS248-6712) both indicate that Epotek-301 bond failure accounted for the thermal anomalies of chanels 4B and 4C.

- Because of the difference between the thermal coefficient of expansion of the aluminum used for the transfer lens mounting blocks and that of stainless steel ferrule from which fiber buttons are made, the Epotek-301 bonds between the lenses and fiber buttons are loaded in tension whenever the fiber plate temperature is raised above ambient. John Ermlich's analysis (Reference 1) showed that tensile loads produced in this way should be well below the expected tensile strength of the bond. However, if other than breaking strength is involved such as peeling due to exudation of water bubble from the bond material (see Figure 2, Channels 3D and 3E, T = 50.4°C, and also Figure 5, Channels 2D and 2E, T = 35.5°C), then the bond failure will occur at substantially lower tensile load.

- Further thermal stress analysis may be needed to determine if there is an inherent temperature limitation on the present design.

Jai K. Yuh

Jai K. Yuh

dz

ORIGINAL PAGE IS
OF POOR QUALITY

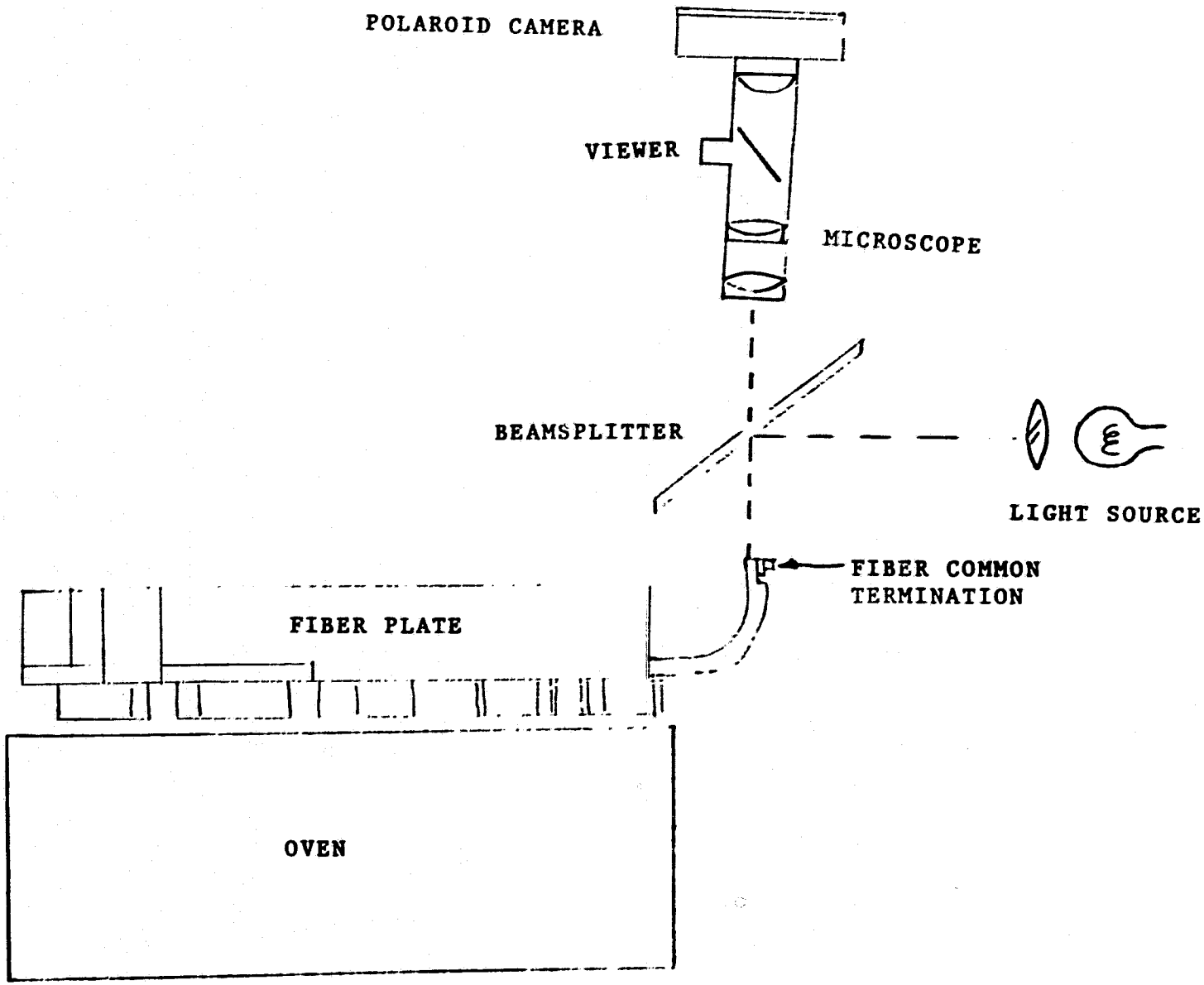

Figure 1 THERMAL CYCLE TEST SETUP

ORIGINAL PAGE IS
OF POOR QUALITY

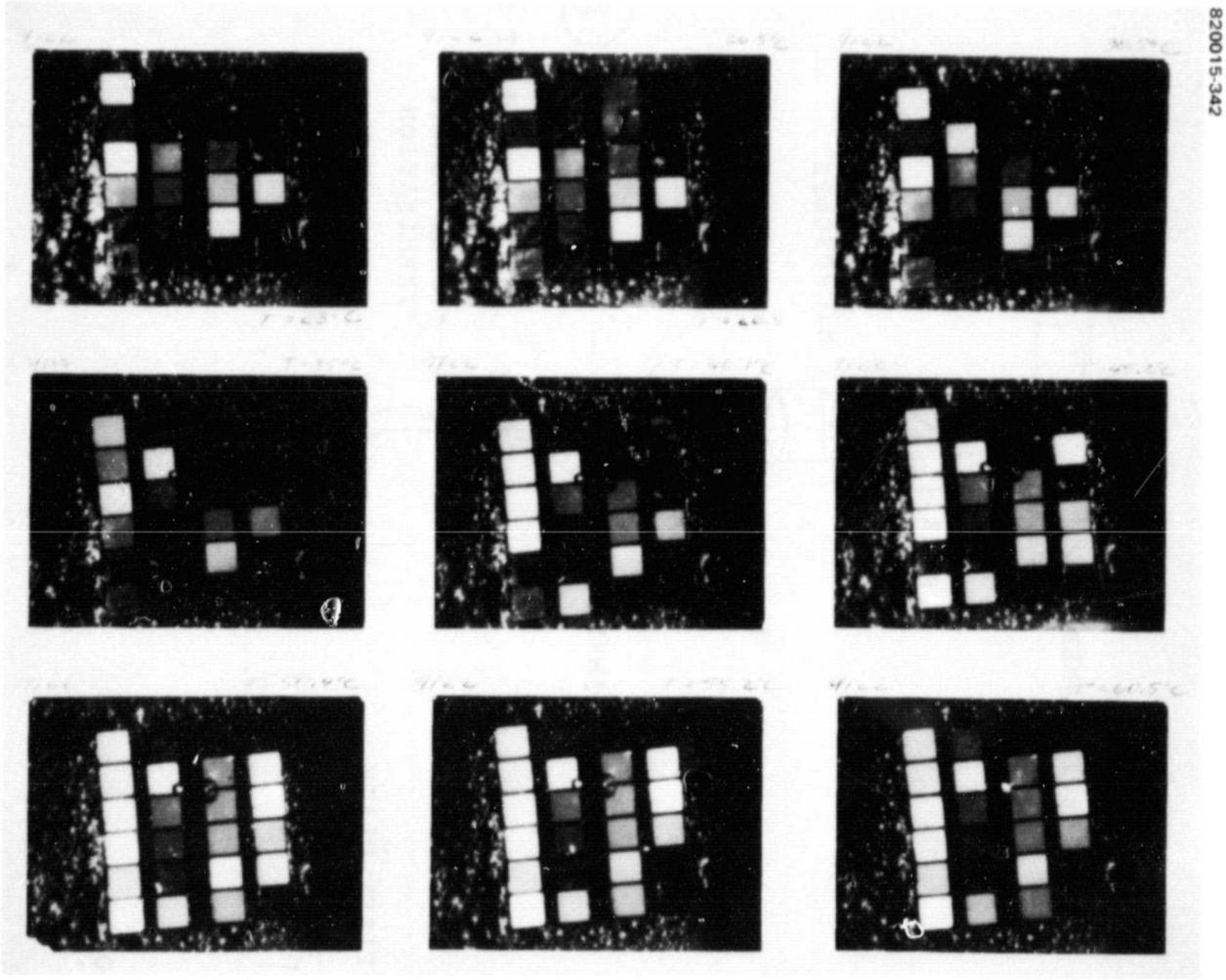

820015-342

PHOTO NO. 81-10-184

FIGURE 2. TYPICAL THERMAL-VACUUM TEST DATA

ORIGINAL PAGE IS
OF POOR QUALITY

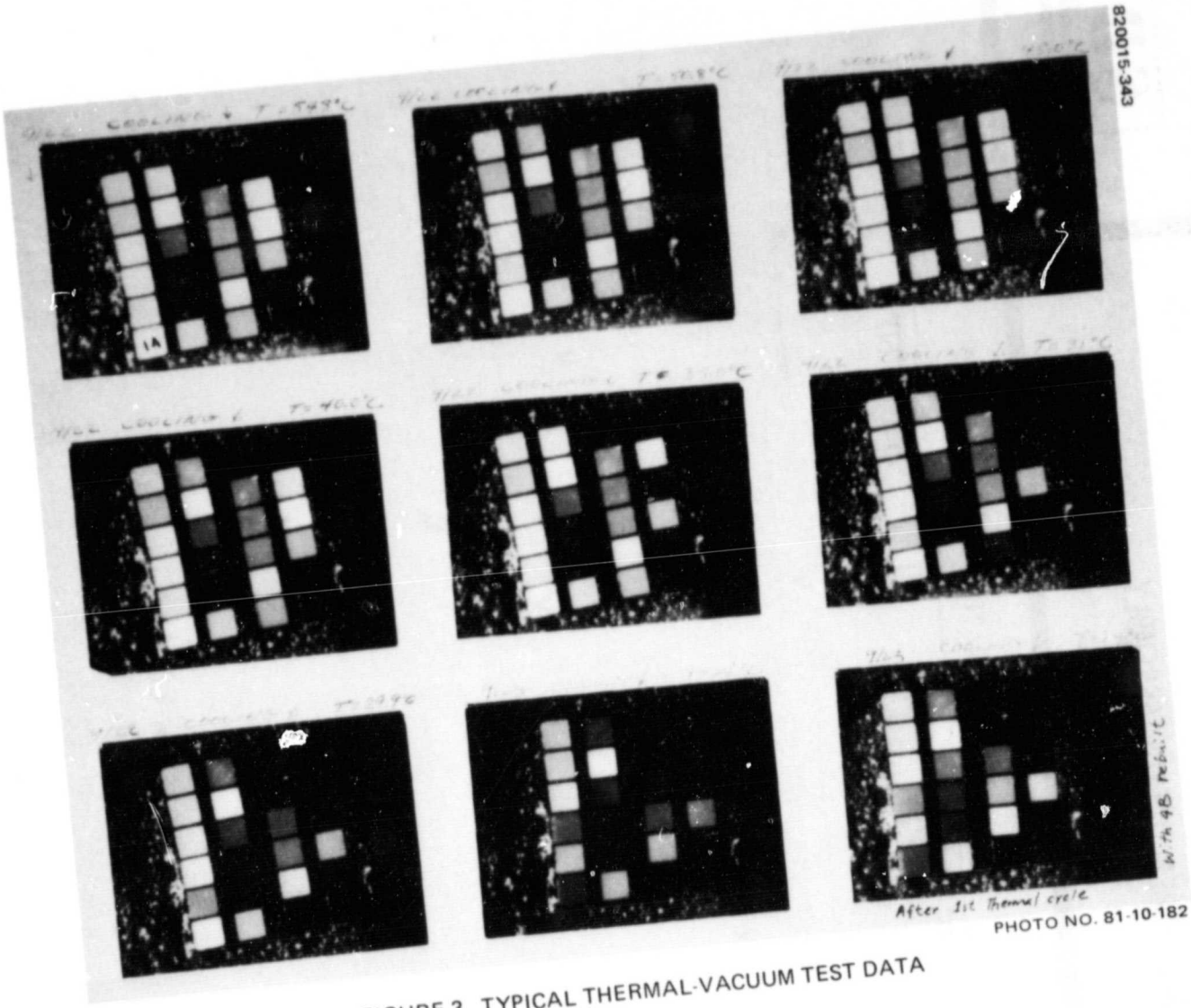

FIGURE 3. TYPICAL THERMAL-VACUUM TEST DATA

DAMAGED F-1 FIBER OPTICS ASSEMBLY

CHANNEL	TEMPERATURE (°C)							
	25	30	35	40	45	50	55	60
1A					V			
1B						V		*
1C				V				
1E			V					*
2A				V				*
2E		V						*
2F								V *
3A						V		
3E					V			
3F	(NO CHANGE)							
4A	(NO CHANGE)							
4B	(NO CHANGE)							
4D						V		
4E					V			

V = STARTED TO SHOW COLOR VARIATION
* = PERMANENT CHANGE

Figure 4

ORIGINAL PAGE IS
OF POOR QUALITY

ORIGINAL PAGE IS
OF POOR QUALITY

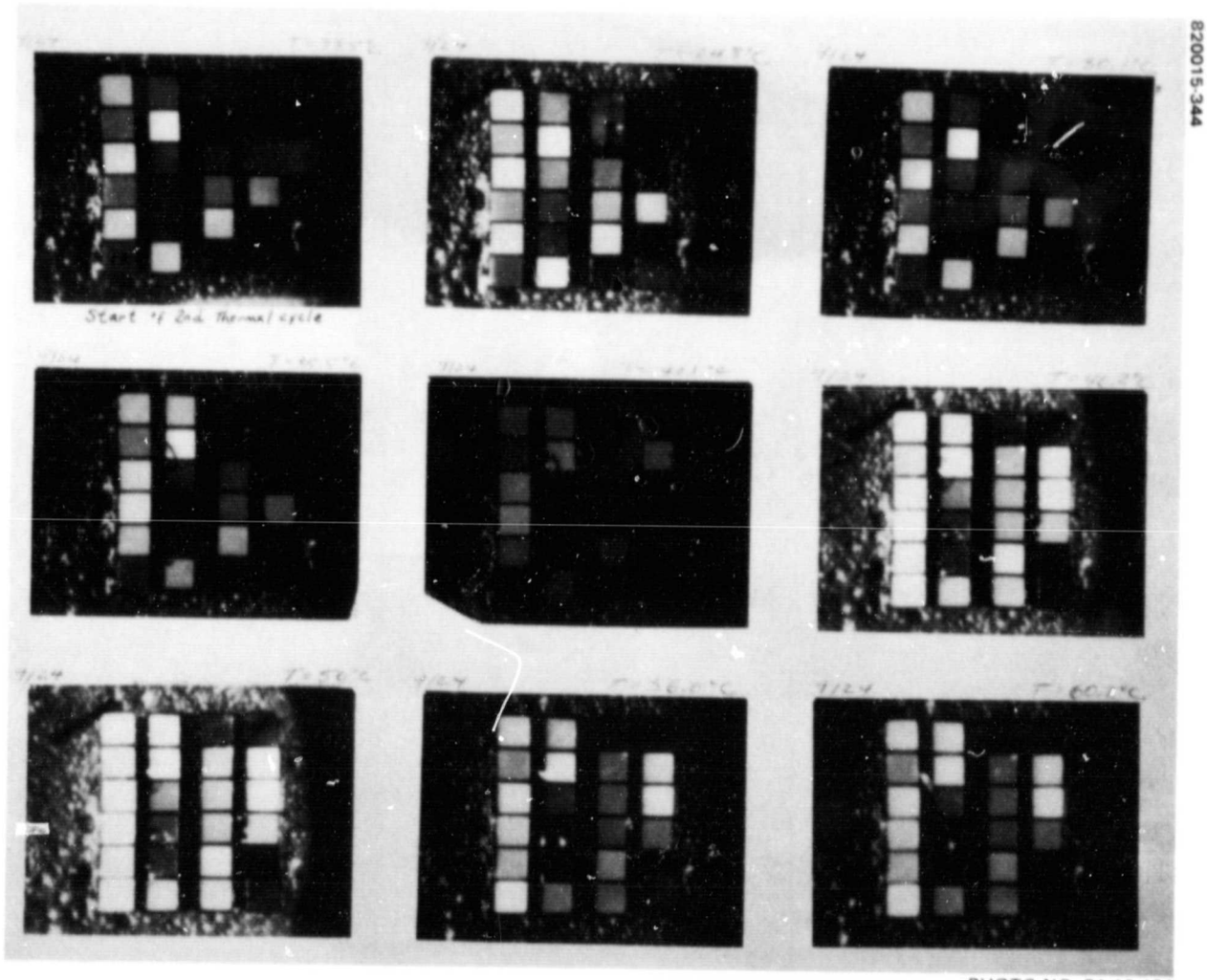

820015-344

PHOTO NO. 81-10-186

FIGURE 5.

ORIGINAL PAGE IS
OF POOR QUALITY

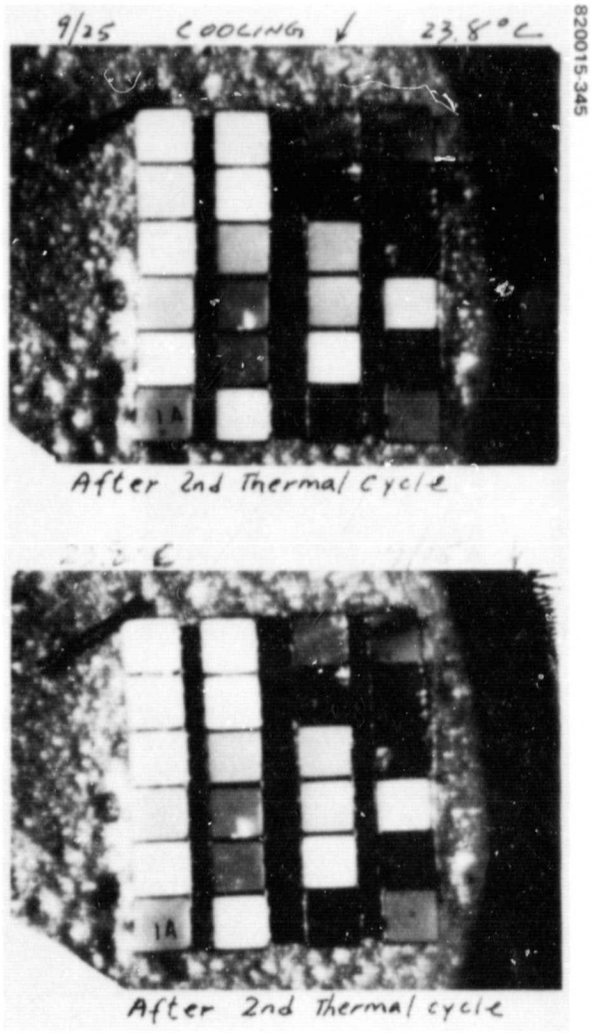

820015-345

PHOTO NO. 81-10-188

FIGURE 6.

ORIGINAL PAGE IS
OF POOR QUALITY

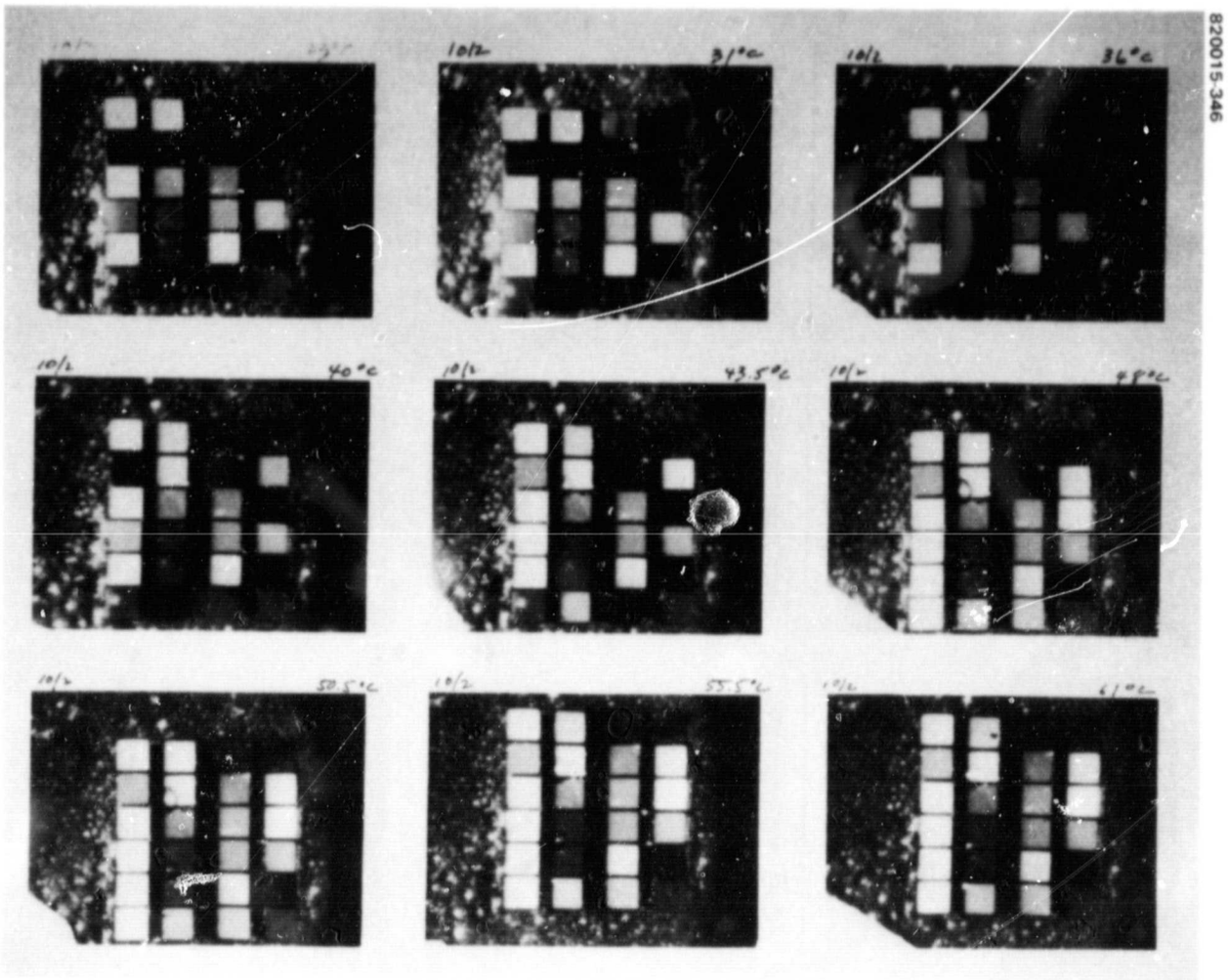

820015-346

PHOTO NO. 81-10-183

FIGURE 7.

ORIGINAL PAGE IS
OF POOR QUALITY

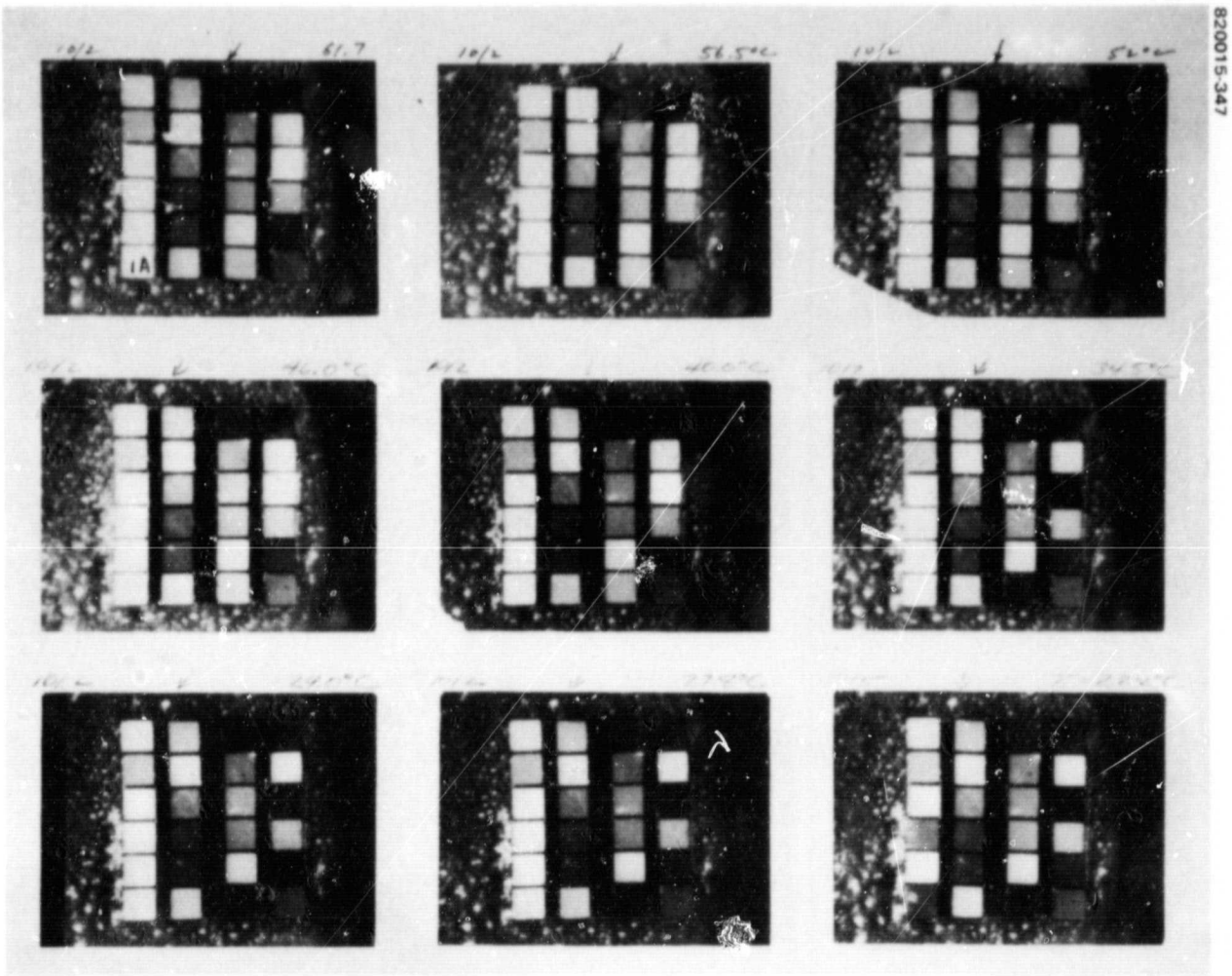

PHOTO NO. 81-10-185

FIGURE 8.

ORIGINAL PAGE IS
OF POOR QUALITY

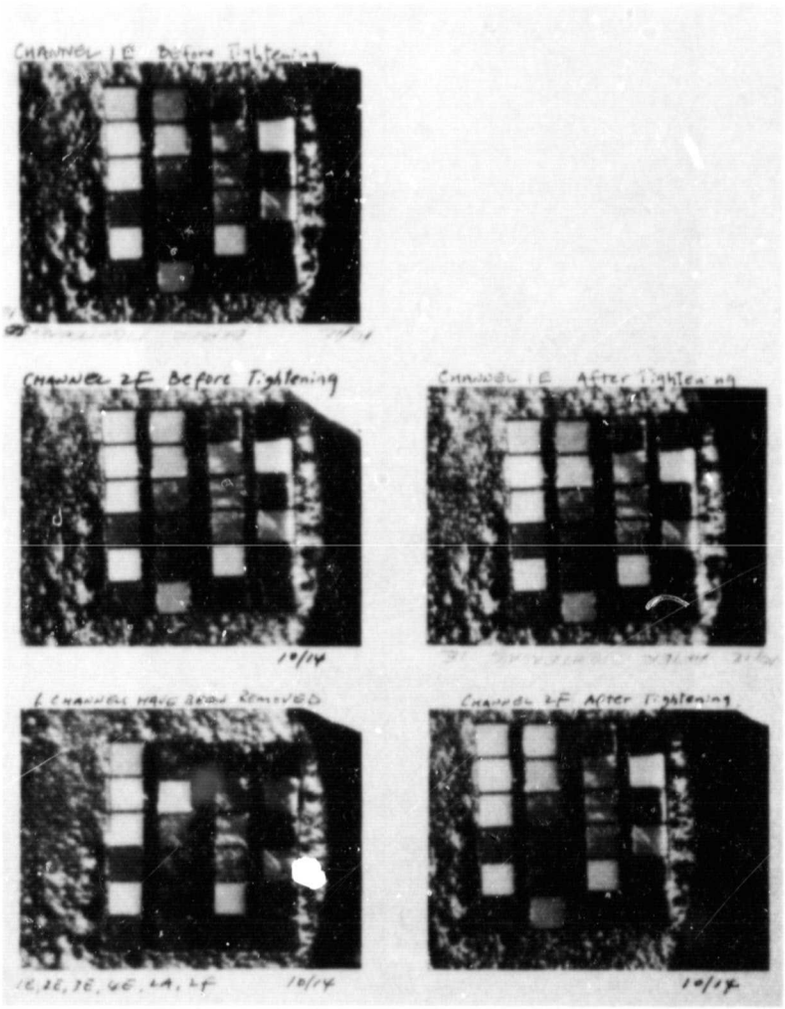

820015-348

PHOTO NO. 81-10-187

FIGURE 9.

ORIGINAL PAGE IS
OF POOR QUALITY

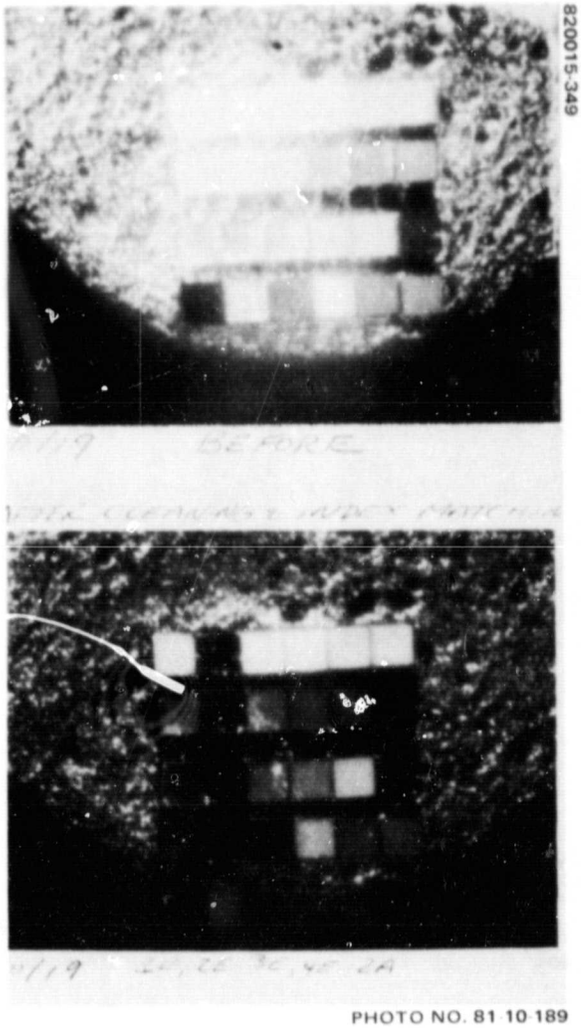

PHOTO NO. 81-10-189

FIGURE 10.

12.3 FLEX PIVOT CORROSION

After the failure of the flex pivots during random vibration of the protoflight system, one of the precautionary measures taken was a series of inspections, before and after environmental exposures, of the flex pivots on both instruments to detect possible cracks or flaws (see section 10.2). During one of these inspections on the F-1 flex pivots, traces of what turned out to be rust were found near the braze joints. Another set of pivots from the same lot, also exhibiting rust deposits, was subjected to analysis to ascertain the source of the rust. In one of these pivots a pocket of intergrannular corrosion was found beneath a pore in a braze joint between the stainless steel web structure and the body of the pivot. Also found in this pocket were traces of chloride ions. An investigation into the manufacturing process of the pivots revealed that they had been subjected to chemical machining in a NaCl solution after the brazing operation. The hypothesis is that traces of this brine solution left in the braze joint after ultrasonic cleaning together with atmospheric humidity were the cause of the intergrannular corrosion in the stainless steel web structure material. The remainder of the lot of pivots in stores was inspected, and the majority of the lot was found to have traces of rust.

At that time prior to vibration and thermal-vacuum testing of the F-1 instrument, a decision was made to proceed into testing without changing out the F-1 flex pivots and to proceed with procurement of a backup lot of pivots with appropriate safeguards to assure the removal of residual brine from the pivots after chemical machining. Continuing inspection to look for possible further corrosion in the flight hardware was instituted. The rationale for the decision not to change pivots was threefold:

1) The rust on the pivots in F-1 was not at a location to endanger their mechanical integrity.

2) The corrosion process would be arrested at the time of launch by the absence of water in an orbital environment.

3) No pivots were available in stores which one could be confident would not exhibit future corrosion problems.

During a flex pivot inspection just prior to thermal-vacuum testing, further evidence of rust was found on the flex pivots. The rust was located on the web structure at a structurally critical place. With this new evidence, a changeout of pivots to those in the newly procured lot was planned following the completion of thermal-vacuum testing. This changeout, plus penalty performance testing and a penalty acoustic test, was successfully completed prior to delivery of the F-1 instrument to General Electric in November 1981. HS248-1496, which follows this subsection, documents the condition of the pivots changed out of F-1.

HUGHES

ORIGINAL PAGE IS
OF POOR QUALITY

INTERDEPARTMENTAL CORRESPONDENCE

TO: A. M. Lauletta
ORG: 44-00

CC: See Distribution

DATE: 21 December 1981
REF. 7621.22/002
HS 248-1496

SUBJECT: F1 S/N 1XX Series
Right Flex Pivot
E523JAA11 - MSS-D

FROM: D. Bronson
ORG. 76-21-22

BLDG. R1 MAIL STA. C325
LOC. ES EXT. 70339

References: 1) AVO Ref. 193 to A. B. Marchant/H. E. Ellison from D. Bronson dated 1 October 1981

2) IDC 7611.42/378, HS-248 1400 to A. B. Marchant from D. A. Demeo dated 4 August 1981

Introduction

Two S/N 1XX series pivots were removed from the F1 Unit on September 23, 1981. Both pivots showed evidence of red discolored deposits when examined on August 11, 1981, see Ref. 1. The intent was to store these pivots on the writer's desk and observe any changes over a one year period.

Discussion

During the second 'desk' visual examination on December 3, 1981 metal separation of the outer flex element, right pivot was discovered. The metal separation was probably present during the first 'desk' visual examination on October 1, 1981 and remained undetected due to its shadow appearance, see Figure 1.

Visual examination of the depression, left after the stainless steel separated, showed it to have a depth of approximately a third of the flex element thickness. The surface of the depression had a granular appearance. Porosity at the braze joint and red discolored deposits were evident adjacent to the depression. It's highly suspected that metal separation occurred as a result of intergranular corrosion caused by entrapped corrosive(s) similar to the condition described in Ref. 2.

Summary

Metal separation was observed on the outer flex element of the right F1 flex pivot. Braze joint porosity and red discolored deposits were evident adjacent to the observed anomaly.

887C.CS.FEB.72

Recommendation

The right F1 S/N 1XX series flex pivot should be metallographically examined to verify the suspected intergranular corrosion.

As planned, the left pivot will be observed for any changes over the remaining year period.

ORIGINAL PAGE IS
OF POOR QUALITY

D. Bronson
Metallurgical Engineer

Approved by: J. M. Keffer
J. M. Keffer, Head
Electronic Assembly Section

DB:lb

ORIGINAL PAGE IS
OF POOR QUALITY

ORIGINAL PAGE IS
OF POOR QUALITY

PHOTO NO. 2181-4155

FIGURE 1. F1 RIGHT FLEX PIVOT

Comments: Optical photograph illustrating metal separation, arrow, adjacent to the braze joint of the outer flex element. Red discolored deposits are evident on the stainless steel surface.

Magnification: Approximately 19X